University of Reading

Going Global: Arabian Palaeoclimate and Human Evolution

Doctor of Philosophy

Department of Archaeology

Samuel Luke Nicholson

Submission date: 8th of April 2020

Declaration

I confirm that this is my own work and the use of all material from other sources has been properly and fully acknowledged.

Samuel L. Nicholson

Abstract

The vast Arabian deserts sit at a crucial interface between Europe and sub-Saharan Africa and acts as a geographical barrier between Afrotropical and Eurasian fauna. However, punctuated increases of rainfall throughout the Pleistocene created "green" deserts that are increasingly related to mammalian dispersals. These "windows of opportunity" were crucial for occupation and dispersal of hominin species and acted as important steppingstones on the way to the global colonisation of *Homo sapiens*. Despite a growing body of palaeoclimate information from marine sediment cores and relict palaeolake deposits, there remain significant gaps in important palaeoclimatological questions. For example, what was the precise timing, duration and frequency of wet events? What precipitation regime delivered precipitation across Arabia? How did precipitation vary within and between pluvial periods? What sorts of environments flourished with increased precipitation? Not only are these pertinent questions for accurately characterising past climates and environments but answering these can identify favourable hominin dispersal windows throughout the Pleistocene.

To elucidate these issues, this thesis aimed to generate new speleothem-based palaeoclimate records from Mukalla (Yemen), Hoti (Oman), Broken-Leg, Star and Surprise (Saudi Arabia) Caves. South Arabian Humid Periods (SAHPs) were identified by U-Pb and ^{230}Th age determinations of stalagmite growth from Mukalla and Hoti Cave. These SAHPs were a result of African and Indian Summer Monsoon incursions during insolation maxima within peak interglacial periods and warm substages up to 1.1 million years ago, as identified by fluid inclusion water δD and $\delta^{18}O$ and calcite $\delta^{18}O$ measurements. This increased annual precipitation to >300 mm yr^{-1} and allowed C_4 vegetation to flourish, as determined by calcite $\delta^{13}C$ measurements. Identification of sub-

annual cycles of $\delta^{13}C$ and $\delta^{18}O$ indicates environments were highly seasonal, characterised by a "wetter" summer and "drier" winter. Additional U-Pb and ^{230}Th dating of stalagmites from Broken-Leg, Star and Surprise Cave reflect these findings, indicating that wet periods occurred during warm periods of the Pliocene and Early-Pleistocene, Together, this information shows that Saharo-Arabian palaeoenvironmental fluctuation – governed by monsoon variability – provided frequent opportunities for hominin occupation of Arabia and dispersal throughout the Plio-Pleistocene.

Acknowledgments

Sir Isaac Newton once said, "if I have seen further, it is by standing on the shoulders of giants". While it would be a false equivalency to compare this thesis to the work of Newton, the sentiment is applicable to my supervisory team; without whom this work would not have come to fruition and whose input has elevated the standard of this thesis. To Rob Hosfield, who – is not only responsible for guiding my interest away from classic civilisation studies and forming my interest in human evolution – has provided excellent guidance and remembering to consider the "human" aspects throughout this project. To Alistair Pike, for providing a wealth of ideas. And, finally, to Dominik Fleitmann, for an extensive amount of time, effort and support given throughout this project. Your enthusiasm and support have not been taken for granted and is much appreciated. Thanks alone are not able to provide the acknowledgement that is deserved to all my supervisors.

Additional recognition is warranted for collaborators, whose contributions have been crucial to the findings and papers produced within this thesis. To Jon Woodhead and Nick Roberts, for the extensive time spent producing U-Pb ages. To Diana Sahy and Hai Cheng, for producing ^{230}Th ages. To Stéphane Affolter and Marcus Leuenberger, for hosting me in Bern and producing fluid inclusion data and teaching me the method. To Stephen Burns and Albert Matter, for providing additional support on bringing the palaeoclimate papers to fruition. To Huw Groucutt, for assisting discussions of human ethnography and the archaeology of Arabia.

Table of Contents

List of Figures

Chapter 1

1) Introduction

1.1 Motivation and aims

The vast Arabian Desert covers over 3 million km^2 of the Earth's surface. Occupying a crucial centre-point of the Saharo-Arabian desert belt, the Arabian Peninsula sits at the interface between Eurasia and Africa (Fig. 1). The interplay between major climate systems means that precipitation does not currently exceed 100-200 mm yr^{-1} over most of Arabia. This hyper-aridity and lack of freshwater forms a geographic barrier between Afrotropical and Eurasian fauna and flora, separating these into two distinct biogeographical zones. Yet, palaeoclimate records show that punctuated migrations of the tropical rain-belt on orbital timescales enhanced Arabian precipitation at various times in the past (Fleitmann et al., 2011; Parton et al., 2015b), allowing grassland environments to flourish (Groucutt et al., 2018). These so-called "green corridors" connected sub-Saharan Africa and Eurasia during peak interglacial periods and warmer sub-stages. A vast body of archaeological evidence indicates these environments facilitated brief human occupation in now arid areas of Arabia during the late Pleistocene and Holocene (Groucutt and Petraglia, 2012; Petraglia et al., 2012, 2020; Groucutt et al., 2015d, 2018). This played a crucial role in facilitating the global distribution of our species, *Homo sapiens* (Petraglia and Rose, 2010; Groucutt et al., 2015a, 2018; Bae et al., 2017). However, the cyclical nature of "Green Arabia" implies that ameliorated conditions should also have occurred on much broader geological timescales. As such,

the paleoclimatic conditions of Arabia could have had a profound impact on hominin demography throughout the evolution of the genus *Homo*.

Fig. 1. The greater landmass of the Arabian Peninsula highlighted in red.

Understanding the distribution and demographic changes of hominin populations is a vital topic within the study of human evolution. The successful dispersal of hominins into novel habitats may inform on the timing of stepped changes in cognition, behaviour, population structure and human-environmental relationships. Moreover, the timings of periods of separation and contact between regional hominin populations can inform on genetic flow/drift, speciation, extinction and other evolutionary events. Specifically, the palaeoclimatic conditions of the Arabian deserts have been used to provide hypotheses

for the timing of human dispersals form Africa (Fleitmann et al., 2011; Groucutt et al., 2015a; Bae et al., 2017), and this has proven to be a valuable approach given the ambiguity of archaeological material, rarity of human fossils and equifinality of genetic data.

1.1.1 Current uncertainties

In spite of a plethora of geological, archaeological and modelling data, there remain substantial gaps in the knowledge of Arabian palaeoclimate and the narrative of human dispersals. For periods beyond the Holocene, palaeoclimate reconstructions often lack robust chronologies, with age uncertainties frequently exceeding 1,000 years (Groucutt et al., 2018; Parton et al., 2018). This means that there is difficulty in establishing the precise timing of "wet" periods and the duration of ameliorated conditions. While statistical modelling has been used to compensate for this (Clark-Balzan et al., 2017; Groucutt et al., 2018), more accurate quantification is required. Furthermore, terrestrial palaeoclimate reconstructions have been limited to ~400-300 ka BP (Blechschmidt et al., 2009; Rosenberg et al., 2013; Roberts et al., 2018) and cannot be used to identify earlier windows of dispersal. It is therefore vital to extend the palaeoclimate record of Arabia, to understand long term influences on human evolution.

There is also some uncertainty concerning which weather system was responsible for increasing precipitation to Saharo-Arabia. Current climates are governed by the Mediterranean frontal system (winter-spring) and the tropical rain-belt (summer-autumn). During ameliorated phases within the Pleistocene, did one of these systems intensify, becoming more dominant? Did both systems intensify? While moisture sources are well documented for the Holocene and model data generally suggests the tropical

rain-belt or monsoon domain was enhanced during the Pleistocene (Otto-Bliesner, 2006; Herold and Lohmann, 2009; Jennings et al., 2015b; Gierz et al., 2017), there is very little quantification (but see Fleitmann et al., 2003). Based on the forcing mechanisms of the tropical rain-belt, it is likely that the African and Indian Summer Monsoons delivered increased precipitation in the Pleistocene. However, current records do not provide explicit evidence of this.

The palaeoenvironments of Arabia are often characterised by an overly-simplistic "wet" or "dry" dichotomy (Parton et al., 2015b). In reality, it is understandable that minor shifts in orbital parameters, solar insolation, local and global climate systems, topography, geology and other factors combined ensure that 'wet' periods differed in intensity. There are also only few areas of Saharo-Arabia that currently receive 0 mm yr^{-1} of precipitation; as such, even 'dry' periods should experience variability in precipitation, both over time and across space. In other words, "how wet is wet?" and "how dry is dry?' are two pertinent questions for the study of Arabian palaeoclimate on long timescales.

1.1.2 Research aims and objectives

Due to these uncertainties, Arabia remains an attractive and important region for palaeoclimate reconstructions. The aim of this research is to extend the palaeoclimate record of Arabia and identify timings for hominin occupation and dispersal. These will be achieved through analysis of cave stalagmites from Arabia. Stalagmites have been used extensively to produce highly resolved and robustly dated palaeoclimate records. Targeted analysis of Arabian stalagmites will aim to fulfil four key research questions and objectives:

1. *Timing of wet periods*

- Question 1: Are substantial increases of precipitation are related to interglacial periods and warm substages throughout the Pliocene and the Pleistocene?
- Objective 1: Renewed Uranium-Thorium (^{230}Th) and Uranium-Lead (U-Pb) dating analyses of speleothem calcite. This can provide precise timing of Arabian pluvial periods relative to glacial-interglacial stages(s).

2. *Past moisture source*
    - Question 2: Can stalagmites confirm whether the African Summer Monsoon and Indian Summer Monsoon become the dominant source of precipitation over Southern Arabia during pluvial periods?
    - Objective 2: measurement of speleothem fluid inclusion Deuterium (δD) and Oxygen ($\delta^{18}O$) and comparison to local meteoric waterlines. Deviation from current waterlines can identify changing moisture source(s).
3. *Nature of wet periods*
    - Question 3: Are there substantial differences in rainfall between pluvial periods? And how does rainfall very within pluvial periods?
    - Objective 3: Measurement of speleothem calcite Oxygen ($\delta^{18}O_{ca}$) can record changes in precipitation intensity. These can be used to detail inter-wet-period variability, for which there is currently very limited information.
4. *Environmental character*
    - Question 4: Can speleothem records serve as a palaeoecological archive by confirming the development of grasslands during pluvial periods?

- Objective 4: Measurement of speleothem Carbon ($\delta^{13}C_{ca}$) can record changing soil (and therefore vegetation) conditions above a cave.

Data produced throughout this thesis must then be combined with current palaeoclimate records in order to identify favourable periods for hominin dispersal and occupation.

1.2 Structure of the thesis

This thesis has been structured around three research papers that have been accepted, are under review or are in preparation. These provide speleothem-based palaeoclimate reconstructions from the Pliocene and into the Holocene, spanning ~4.3 million years.

- Chapters 2 - 4

Chapter 2 provides a background of current climate and environment of the Arabian Peninsula. Chapter 3 provides a review of Arabian palaeoclimate and a broad overview of hominin dispersals since the origin of the genus *Homo*. Chapter 4 discusses how speleothems have been and can be used to produce high-resolution palaeoclimate records. Chapter 4 also introduces the key sites and samples used within this thesis. These chapters have not been submitted for publication.

- Chapter 5

Chapter 5 provides a ~1.1 million-year speleothem-based record of Arabian palaeoclimate, from Mukalla Cave, Yemen. Additional analysis has also been conducted on speleothems from Hoti Cave, Oman. This addresses objectives 1 to 4 by extending the temporal coverage of Arabian palaeoclimate, providing clarification of moisture source, identifying changing monsoon intensity throughout "wet" periods and providing some clarification of environmental conditions. Results are then discussed in regard to hominin

dispersals and occupations of Arabia. This chapter has been accepted and published in *Quaternary Science Reviews* (Nicholson et al., 2020).

- Chapter 6

Chapter 6 provides initial results of Plio-Pleistocene speleothems from the Saudi Arabian deserts. This chapter addresses objectives 1-4, in once again extending the temporal coverage of Arabian palaeoclimate, providing some clarification of past moisture source(s) and identifying changing monsoon intensity throughout the Plio-Pleistocene. Results are then discussed in regard to timings of potential early hominin occupations of Arabia. This chapter is a work in progress manuscript.

- Chapter 7

Chapter 7 provides a high-resolution record of monsoon intensity from Mukalla Cave, Yemen (stalagmite Y99). In this chapter, refined dating and high-resolution stable isotope analysis achieves objectives 1, 3 and 4. This record is then compared to sea-level records to assess the phasing between the onset of pluvial conditions and Bab-al-Mandab width. We found that the onset of pluvial conditions lagged sea-level rise and proposed three models to explain the dispersal of *H. sapiens* during MIS 5e.

- Chapter 8

This penultimate chapter aims to define what is meant by "dispersal" and provide a discussion for how *H. sapiens* societies occupied and dispersed across "Green Arabia". This helps to put findings from chapters 5 and 7 into a "human" perspective and also identifies new research questions. A manuscript has been submitted to the journal *Current Anthropology* for review.

- Chapter 9

This final chapter summarises the main findings of chapters 4-8 and outlines the scope for future work.

The papers that comprise chapters 5, 7 and 8 have been restructured into chapters. The original papers are provided in the appendices, along with the supplementary files and data related to these articles. Author contribution statements and a summary are provided at the beginning of these chapters.

Chapter 2:

2) The Arabian Peninsula: climatic and environmental settings

2.1 The Arabian Peninsula

The Arabian Peninsula occupies the southern extent of the Arabian plate, which is situated between the African plate to the west, Eurasian plate to the east and the Anatolian plate to the north. Arabia is often considered an eastern extension of the Sahara Desert, due to proximity, similar climatic influences and environment. Though some researchers (Groucutt, *pers comm*) consider Arabia as a central point of the desert belt, which, in this view, expands to the Thar desert of India. Arabia can be broadly separated into the "Arabian shield", the highland areas of the west, and the "Arabian platform", a gently sloping plateau that extends from the eastern extent of the Persian Gulf. Arabia has been divided into six topographic regions by Miller and Cope (1996), which are summarised here:

1. The Western coastal plain (the Tihama)

The Tihama plain occupies the western areas of Arabia, running the extent of the Red Sea coast and extending to the escarpment mountains of the Arabian shield. It is at its widest south of Jeddah, where it averages ~30 km, and narrows to the north of Jeddah. It is predominantly comprised of Aeolian sands and fluvial/alluvial deposits, which are washed from the mountains to the east. Low precipitation and high evaporation mean that permanent waterbodies are not maintained, though, flood waters from the mountains can

reach the sea. In Yemen, large areas are characterised by salt flats and sabkhas. Generally, Tihama is defined as a low lying, hot, humid and dry area.

2. Mountains of the south and west

The mountains of the south and west of Arabia form an "L" shaped region, with the broadest arm (the Yemeni Highlands) running ENE to the Dhofar mountains of Oman, and the other running NNW parallel with the Red Sea. The geology is characterised as Precambrian crystalline rocks, overlain by areas of Jurassic limestone and sandstone and extensively overlain by Tertiary volcanic rocks. The southwest escarpment mountains can be subdivided into two sections:

I. The Asir and the Yemeni highlands (Fig. 2): These form a long chain of mostly unbroken escarpments and ridges running from Aden to Makkah. These mostly exceed 2000 m in height, almost rising to 3000 m in the Asir while several peaks exceed 3000 m in the Yemeni highlands. The east and west slopes of the mountain contrast with each other. In the west, the highlands fall abruptly in a series of escarpments towards Tihama; whereas the eastern slopes decline more gradually into the Arabian interior. These highlands are the wettest regions of Arabia. In the Yemeni highlands, precipitation can exceed 500 mm yr^{-1}. The Asir portion is slightly drier. Generally, precipitation declines to the north and to the east. The wettest regions are echoed by being the most floristically diverse areas of Arabia.

II. The Hijaz mountains: these are situated further north, running from Tabak to Makkah on an SSE-NNW transect (Fig. 2). These are more punctuated,

rugged and receive less precipitation than the Asir and Yemeni mountain ranges.

The southern mountains run east, parallel to the Arabian Sea. These can be subdivided into three sections:

I. Jebal al-'Urays: these form the base of the "L" shape that characterises the morphology of the southern and western mountains. These are located ~100 km north of Aden and characterised as an isolated massif comprised of Tertiary volcanic rocks. The north facing-slopes are distinctly dry. Though, the sea-facing slopes are frequently prone to cloud coverage and are generally more humid. This is reflected by denser vegetation cover.

II. The Jol: this is characterised as an "inhospitable limestone plateau" (Miller and Cope, 1996: 5) situated north of Mukalla. The plateau averages 1000 m in height and rises to 2000 m north of Mukalla. It is interrupted by the Wadi Hadramaut. Rainfall is generally less than 120 mm yr^{-1}. Vegetation is sparse but denser on the sea-facing slopes.

III. The Dhofar mountains: this range is comprised of a Tertiary limestone plateau of 800-900 m in height for the majority of its length. In the east, however, this rises to 2100 m. The north facing slopes fall gradually to the plains of the Arabian interior. This contrasts the south-facing slopes, where the mountains fall in steep sea-facing escarpments.

3. Mountains of northern Oman

The mountains of northern Oman are the other major highland area. These are ~700 km in length, extending from Musandam to Ras al Hadd. These are separated from the sea to the east by a flat gravel plain known as the Batinah coast. They are defined by three major ranges: the Musandam mountains, the western Hajar and the eastern Hajar. These typically exceed 1000 m in height and are comprised of dense limestones and dolomites with areas of extensive crystalline rocks.

4. The Western Najd

The Western Najd comprises the area east of the SW mountain escarpments, generally above the 800 m contour. This extends for almost half of the peninsula at its widest point. Extensive lava flows (known as "Harrats") cover the basement crystalline rocks where they are not exposed. Generally, this desertic landscape is comprised of table-lands and plains, from which isolated inselbergs rise. Thin sands and gravels dominate this generally sparsely vegetated (if at all present) region. Precipitation is less than 100 mm yr^{-1} for most of the region. Though annual precipitation can fall below 50 mm yr^{-1} in many areas.

5. The Arabian platform

The Arabian platform lies to the east of the Arabian shield and is comprised mostly of Cambrian to Pliocene sedimentary rocks, which consist of shales limestones and sandstones. Topography varies between plateaux, escarpments, plains and vast sand seas. The sand seas include the Nefud, Rub' al-Khali and the ad Dhana (discussed below).

6. Socotra and the Arabian archipelago

The islands of Socotra, Darsa, Semhah and ‘Abd al Kuri are situated in the Indian Ocean, south of Yemen and east of Somalia. Socotra is the largest of the islands (~3625 km^2), with the others being comparatively much smaller (<400 km^2). Coastal plains (5 km wide), the Haggier mountains and the limestone plateau define the topography of Socotra.

2.2 Current climate of Arabia

2.2.1 Regional climate

In northern Arabia, average precipitation measures less than 100mm yr^{-1} (Fig. 2B). This is mostly derived from north-westerly Winter Mediterranean Cyclones (WMCs) (Glennie and Singhvi, 2002). The Hijaz Asir mountain range exceeds 2000 m in height and consists of uplifted cretaceous igneous rocks (Brown et al., 1989). This orographic barrier restricts the penetration of summer Red Sea and monsoonal rainfall into central Arabia. Temperatures range from 8 to 17°C in the winter months, with temperatures below freezing observed in central and northern Arabia. In the summer months, temperatures vary between 32-35°C, though often exceed 48°C (Glennie and Singhvi, 2002).

In southern Arabia, the highlands of Yemen and Oman receive a maximum annual precipitation of ~200-700 mm yr^{-1} (Fig. 2B). Northern Oman receives most of this precipitation from WMC winds from December to March (Weyhenmeyer et al., 2002). In the Jebel Akhdar mountain range (within the central Hajar mountains) of northern Oman, local thunderstorms (orographic rain) occur during exceedingly hot summers. These are usually brief yet result in heavy rainfall. Every 5-10 years, cyclones driven by the Indian Summer Monsoon (ISM) extend into northern Oman (Pedgley, 1969), resulting in increased rainfall from May to June. These heavy rains may only last for several days but result in highly variable annual precipitation on interdecadal timescales.

This variability means that areas of the southern Oman can receive no rain for several years. Annual temperatures in Oman range from 33-35°C in the summer months, and 20-25°C in the winter months (Glennie and Singhvi, 2002). Current precipitation in the Oman highlands facilitates the growth of some small speleothems, indicating some precipitation is not evaporated from the surface.

In Yemen, average annual precipitation (~120mm yr^{-1}) is derived mostly from Red Sea evaporation and the northern extent of the African Summer Monsoon (ASM) and ISM (Mitchell and Jones, 2005). Up to 700 mm yr^{-1} may fall in the Yemeni highlands (Glennie and Singhvi, 2002), which supports heavily terraced agriculture. Winter temperatures range between 9-30°C, summer temperatures range from 18-46°C (Almazroui et al., 2012). Minimum temperatures are observed in the Hijaz Asir highlands; whereas maximum temperatures are observed in the north-eastern Rub al Khali and coastal lowlands (Almazroui et al., 2012).

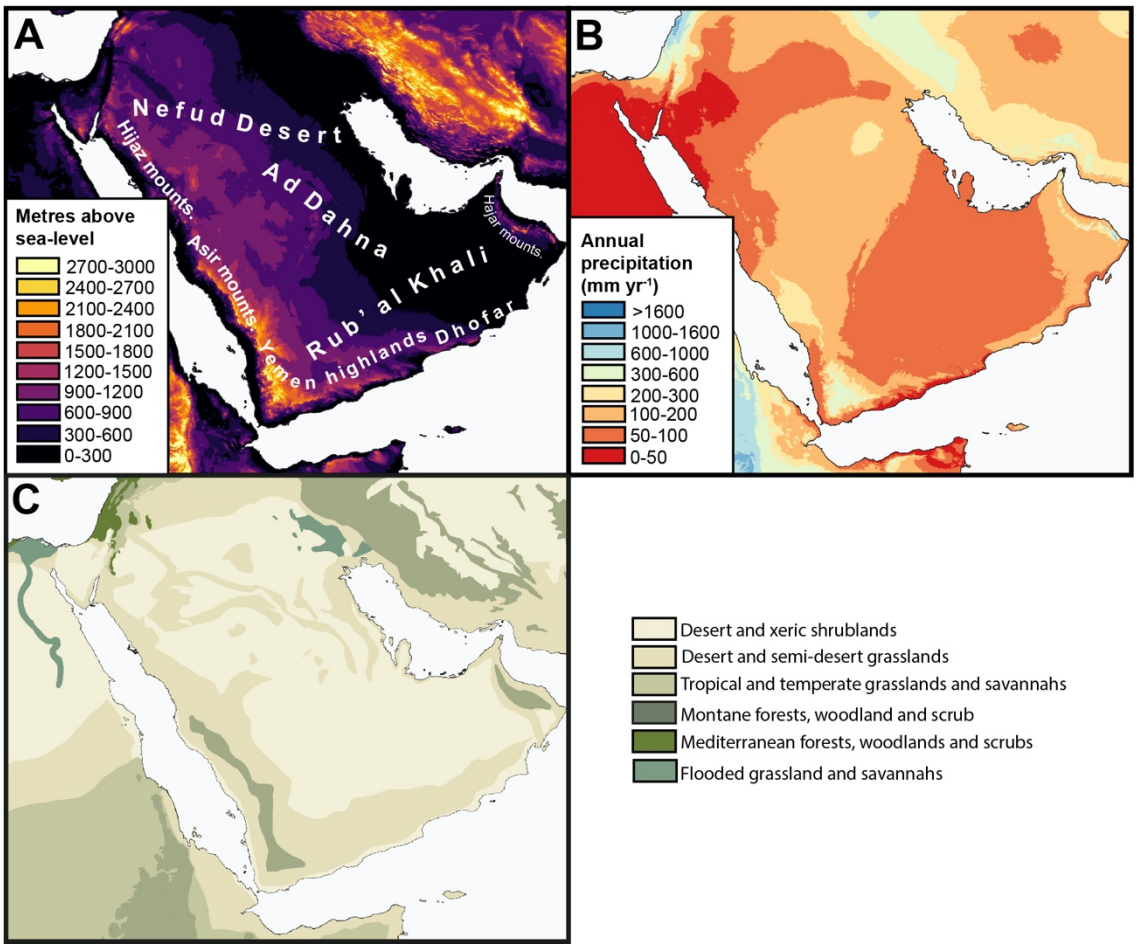

Fig. 2. Elevation (A), average annual precipitation (1970-2000) (B) and vegetation biome maps of the eastern Saharo-Arabian region. Created using the with major deserts and mountain ranges. Data available from A: GMTED2010 dataset from usgs.gov; B: WorldClim V2 bioclimatic variables (Fick and Hijmans, 2017; worldclim.org); C: worldwildlife.org.

2.2.2 Major weather systems

Arabian climates are currently governed by two major weather systems: The North Atlantic/Siberian weather system in winter and spring, and the tropical rain-belt (comprised of the African [ASM] and Indian Summer Monsoons [ISM]) in summer.

The tropical rain-belt

The tropical rain-belt is responsible for delivering monsoonal rains to the tropical areas of Africa, the southern-most points of the Sahara Desert, the southern tips of the Arabian Peninsula, and summer rains to India and the northern Indo-Pacific and East Asia. Though, in its (boreal) winter phase, it also delivers precipitation to the northern areas of Australia, southern Africa and the southern Indo-Pacific region. The ASM, ISM and East Asian Summer Monsoon (EASM) are linked to the position of the Intertropical Convergence Zone ("ITCZ" hereafter. But see Nicholson (2009, 2018) for discussion on the ITCZ). The ITCZ is the confluence of the rising arms of the northern and southern Hadley cells. In boreal winter, the ITCZ is situated close to the equator. In boreal summer, the ITCZ migrates northward. This is caused by increased interhemispheric pressure gradients of the Hadley cells (Basha et al., 2015) in response to increased northern hemisphere insolation and Asian monsoon dynamics (Beck et al., 2018). In boreal summer, increased insolation leads to reduced pressure of the northern Hadley cell and northward migration of the sub-tropical westerly jet (Zhu, 2012; Chiang et al., 2015). The extent of this is regulated by complex atmospheric and ocean circulation mechanisms. During boreal summer, heating of the Tibetan Plateau drives onshore air mass transport, in which convective and monsoon circulation is established due to sensible heating from latent heat release in the mid-troposphere. The subtropical westerly jet also migrates to the north of the Tibetan Plateau, strengthening the Tibetan High. As such, outflow from

the Tibetan High towards the South Indian Ocean Subtropical High (SISH) increases. Simultaneously colder (austral winter) SSTs (Sea Surface Temperatures) of the Indian Ocean increase the anticyclone of the southern Indian Ocean, which in turn increases the outflow of the Tibetan High to the SISH. Combined, these enhance Hadley Circulation. This results in stronger trade winds and Somali Jet in the Indian Ocean, which increase the strength of the ISM and brings precipitation to Arabia (Weyhenmeyer et al., 2002; Fleitmann et al., 2011; Beck et al., 2018). Adversely, reduced insolation and pressure gradients strengthen Tibetan High outflow towards the North Pacific Subtropical High, which leads to dominance of the Western North Pacific Summer Monsoon (WNPSM) and retraction of the Indian monsoon domain (Beck et al., 2018). Therefore, stronger summers (characterised by greater Northern Hemisphere Insolation [NHI]) are echoed by strengthened monsoons and wet conditions across the northern Indo-Pacific rim (Fig. 3A); whereas weaker summers (reduced NHI) result in weakened monsoons and drier conditions across the northern Indo-Pacific rim (Fig. 3B).

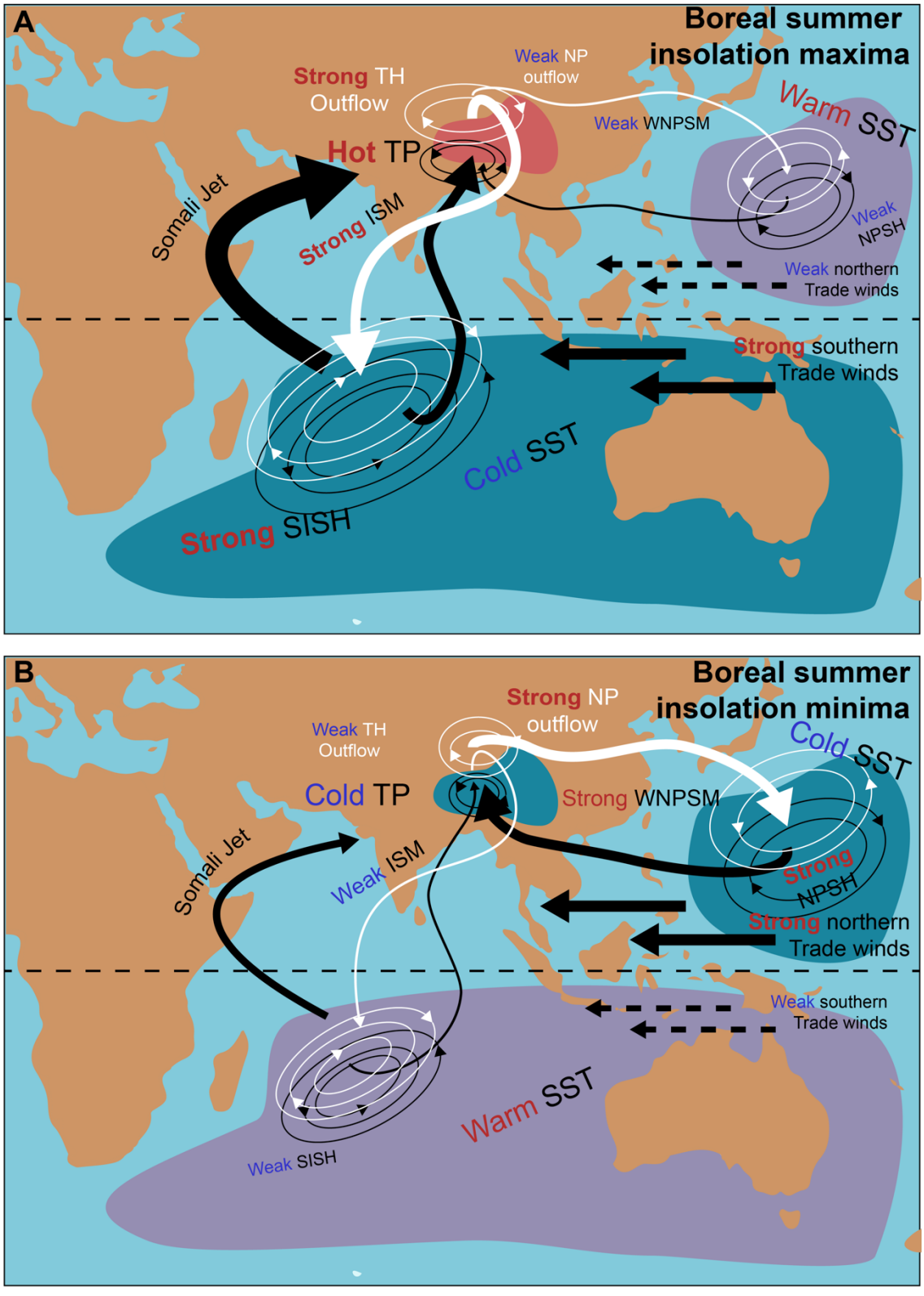

Fig. 3. Tropospheric circulation over the Indo-Pacific during boreal summer insolation maxima (A) and minima (B). During boreal summer maxima (A), heating of the TP and

cold South Indian Ocean SSTs lead to enhanced TH outflow to the SISH. This increases the South Indian Ocean anticyclone, strengthens the southern trade winds and enhances the Somali Jet and ISM/EASM. In boreal summer minima (B), cold northern Pacific SST enhances the Northern Pacific Subtropical High (NPSH), weaker TH outflow is diverted towards the Pacific and increases the northern trade winds and enhances the West Northern Pacific Summer Monsoon (after Beck et al., 2018).

The strength of the Indian Summer Monsoon and northward migration of the tropical rain-belt are strongly influenced by low-latitude insolation, which is controlled by ~100,000-year and ~21,000-year orbital eccentricity and precession cycles. Combined, these enhance NHI, with maxima associated to periods of aligned eccentricity maxima and precession minima. The influence of NHI maxima on the ISM and EASM is clearly recorded in Chinese speleothem $\delta^{18}O$ (Cheng et al., 2009a, 2016) and CLP ^{10}Be (Beck et al., 2018). While Chinese speleothem $\delta^{18}O$ is dominated primarily on the 21 kyr band, CLP ^{10}Be shows a clear enhancement of monsoon strength during eccentricity paced maxima.

This low-latitude forcing of SISH intensity is coupled to high-latitude climates, particularly northern hemisphere ice-sheet extent, via the Atlantic Meridional Overturning Circulation (AMOC). AMOC is crucial to the transport of oceanic heat to the North Atlantic. This is influenced by the Agulhas current leakage of high-salinity waters from the Indian Ocean into the Atlantic. This has a large impact on the production of North Atlantic Deep Water, which is a critical component of AMOC. Recent observations have shown that an intensified SISH was matched by enhanced southern westerlies and trade winds (Backeberg et al., 2012). This resulted in greater wind stress

coupled to the sea surface and led to a strengthened South Equatorial Current and enhancement of the Agulhas western boundary current system (Backeberg et al., 2012). Thus, periods of greatest SISH intensity (eccentricity maxima NHI peaks) may have had profound effects in reducing northern hemisphere ice-sheet extent (Beck et al., 2018). Though, it must be considered that northern hemisphere ice-sheet extent is also linked to high-latitude insolation (Tzedakis et al., 2017), global atmospheric CO_2 concentrations (Raymo, 1997; Berger et al., 1999; Hodell and Venz-Curtis, 2006; Martínez-Garcia et al., 2011; Maslin and Brierley, 2015), regolith erosion (Clark et al., 2006), sea-ice switch mechanisms (Tziperman and Gildor, 2003) and the Nordic Heat Pump (Berger and Jansen, 1994).

The Mediterranean Frontal System

Winter Mediterranean Cyclones are currently responsible for delivering precipitation across the eastern Mediterranean, southern Iran and the northern Arabian Peninsula. These north-westerly Mediterranean winds track south as far as northern Oman (Weyhenmeyer et al., 2002) and constitute approximately 40-50% of rainfall in northern Arabia (Fisher and Membery, 1998). Mediterranean climate is highly seasonal, characterised by wet and stormy winters and dry summers. The Mediterranean basin is located at the transition between the high-pressure subtropical belt over northern Africa and the temperate westerlies over western Europe, resulting in this high seasonality as these domains expand and contract (Lolis et al., 2002).

In (boreal) winter, polar/continental airmasses over Europe bring cold and dry air to the Gulf of Lions, the Adriatic Sea and the Aegean Sea. This induces evaporation and cooling

of the sea surface, forming depressions. The northerly airflow into the western and eastern Mediterranean is governed by the low pressure that develops over warm eastern and central surface waters in the Mediterranean and the eastward extent of the Azores High.

The European westerlies are strongly influenced by the North Atlantic Oscillation (NAO), which describes the pressure gradient between the Azores High (AH) and the Icelandic Low (IL). Positive phases (enhanced AH and IL) see increasing strength of Atlantic trade winds, which directs moisture away from the Mediterranean basin (Fig. 4A). Whereas negative phases (weakened AH and IL) decrease the strength of the trade winds, resulting in greater transport of Atlantic moisture into the Mediterranean basin (Fig. 4B) (Hurrell et al., 2001; Visbeck et al., 2001). These phases are regulated by the strength of the Gulf Stream into the Northern Atlantic, which is influenced by SSTs and ice coverage of the Labrador Sea. When the Labrador Sea experienced warm temperatures and low ice conditions, warm waters from the Gulf Stream advance north while decreasing in the east Atlantic (Kvamstø et al., 2004). Warmer water in the north enhances the Icelandic Low, whereas reduced input into the east Atlantic enhances the Azores High (Fig. 4A). The warm and humid north westerlies are thus directed further north, towards the Icelandic Low and northern Europe. An enhanced Azores High also increases the strength of the trade winds, increasing humidity (especially in the form of Hurricanes) to eastern north America. During periods of increased ice coverage in the Labrador Sea, warmer Gulf Stream waters are predominantly directed into the East Atlantic (Kvamstø et al., 2004). Low SSTs in the north Atlantic reduce the strength of the Icelandic Low, whereas warmer waters reduced the Azores High. This directs the north westerlies towards the Mediterranean basin, while also reducing trade wind strength

(Fig. 4B). Furthermore, the relatively cold and dry polar easterlies expand into northern Europe, reducing winter temperatures here.

On long orbital time-scales, the strength and direction of the westerlies are regulated by glacial-boundary conditions and, for Arabia, are often juxtaposed to the monsoon domain. In other words, increased glacial-boundary conditions forces the westerlies to a more equatorial position in both northern and southern hemispheres; whereas, during periods of reduced ice-sheet extent, the westerlies are diverted towards the poles, while the monsoon domain expands (Blome et al., 2012; Fig. 5).

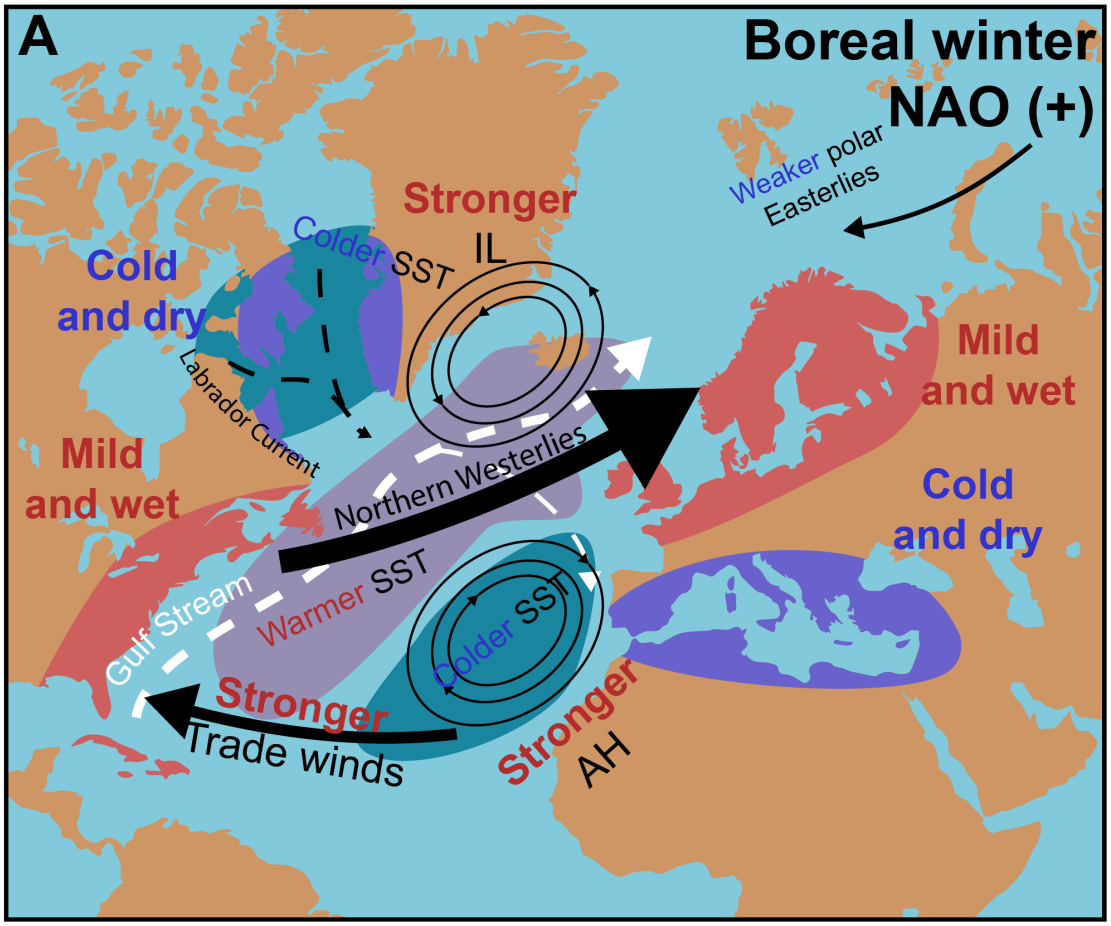
A
Boreal winter
NAO (+)
Weaker polar
Easterlies
Stronger
IL
Colder SST
Cold
and dry
Labrador Current
Mild
and wet
Northern Westerlies
Mild
and wet
Cold
and dry
Gulf Stream
Warmer SST
Colder SST
Stronger
Trade winds
Stronger
AH

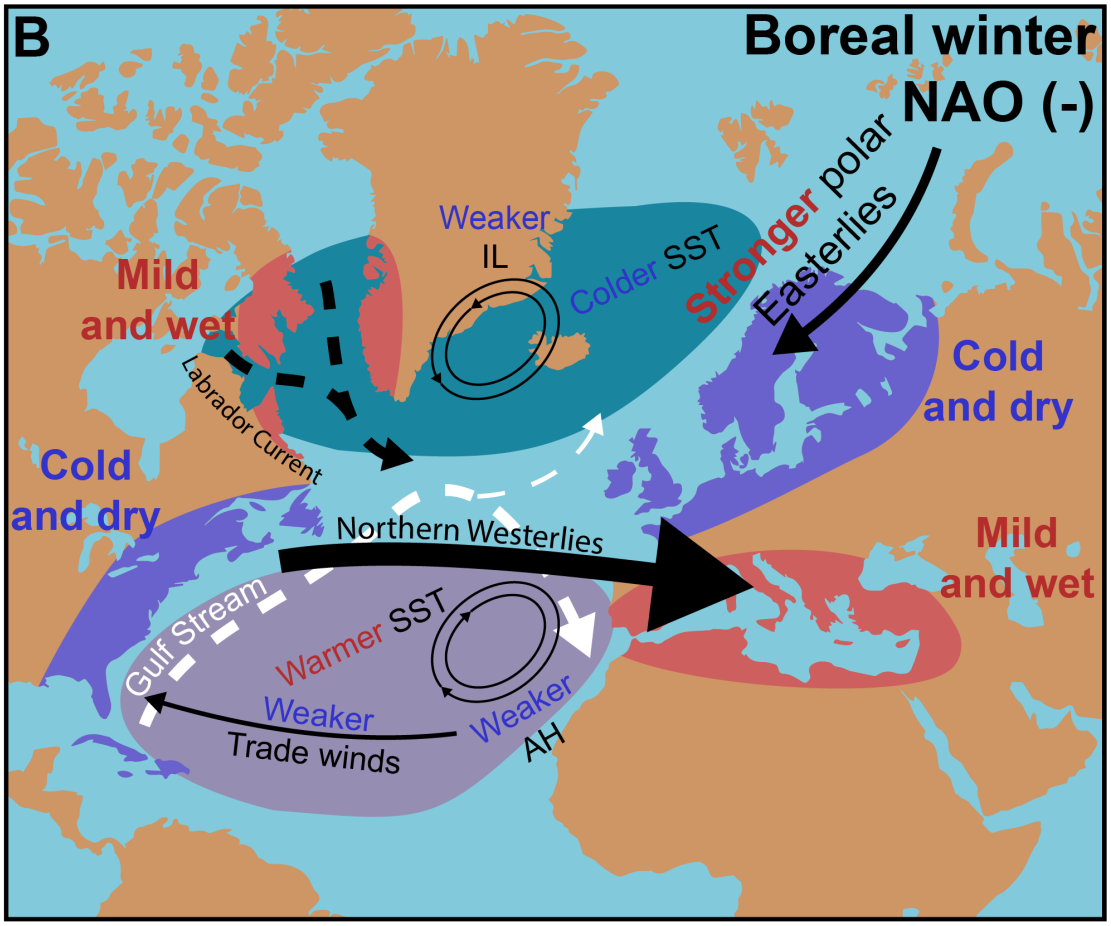
B
Boreal winter
NAO (-)
Weaker
IL
Colder SST
Stronger polar
Easterlies
Mild
and wet
Cold
and dry
Labrador Current
Cold
and dry
Northern Westerlies
Mild
and wet
Gulf Stream
Warmer SST
Weaker
Trade winds
Weaker
AH

Fig. 4. The North Atlantic Oscillation in positive (A) and negative (B) modes.

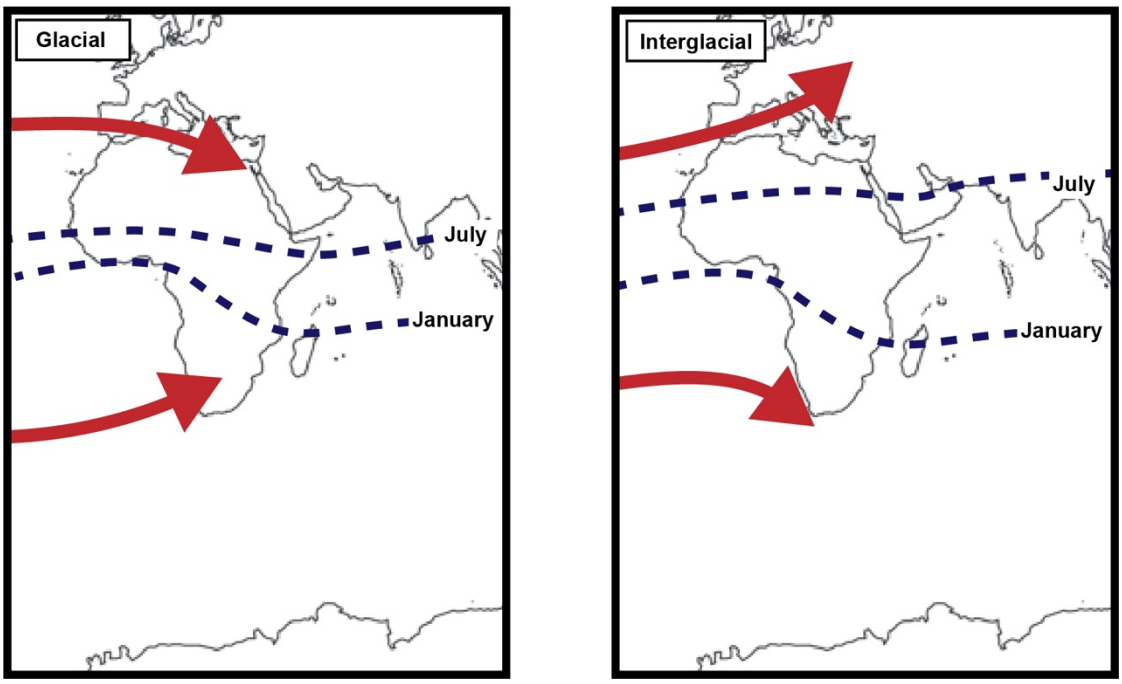

Fig. 5. Direction of westerlies (red arrows) and latitudinal extent of the tropical rain-belt (blue lines) between glacial and interglacial periods (after Blome et al. 2012a, but see Nicholson, 2018).

The main source of climatic variability in the Mediterranean is the "Mediterranean Oscillation" (MO), a west-east pressure seesaw which is active at the surface and at 500 hPa, predominantly in winter and spring (Lolis et al., 2002). There is a statistical correlation between the MO and the NAO, whereby a low (or "negative") NAO index is matched by wet western Mediterranean conditions (Lolis et al., 2002; Dünkeloh and Jacobeit, 2003). Though, the relationship between the eastern Mediterranean and the NAO is less well established (Dünkeloh and Jacobeit, 2003).

The next main source of climatic variability in the Mediterranean is the Mediterranean Meridional Circulation (MMC). This has strong influence on the cyclogenesis in the basin and resultant precipitation in the north eastern and south-central sectors (Dünkeloh and Jacobeit, 2003). The Aegean Sea to Cyprus is a key area for the formation of cyclogenesis, as well as the Gulf of Genoa and the Ligurian Sea in the western Mediterranean. The depressions that form over the Gulf of Genoa and Ligurian Sea track south-eastwards, down the coast of Italy, then north-eastwards or eastwards across the Aegean and the north Levantine Sea. The movement of these depressions causes the winter precipitation regime that characterises Mediterranean climates. As such, most of this precipitation is evaporated from the Mediterranean basin itself. This dominance of source water over the eastern Mediterranean allowed a distinct meteoric waterline (Mediterranean Meteoric Waterline) to be established from cave drip water $\delta^{18}O$ and δD values (Matthews et al., 2000). Geological records, particularly speleothem $\delta^{18}O$ and δD, have shown that evaporated water from the Mediterranean has been the dominant source of precipitation on interglacial-glacial timescales (Matthews et al., 2000; Vaks et al., 2006, 2010; Grant et al., 2012, 2016).

2.2.3 Minor weather systems

Further winter precipitation in Arabia is delivered by the Red Sea Trough (RST). These winds extend northwards from the African Monsoon domain over the Red Sea, bringing infrequent precipitation during the autumn months (Marcos, 1970; Almazroui, 2011; De Vries et al., 2013; Parton et al., 2015b). Another important wind pattern is the “Shamal”, occurring in both summer and winter. A semi-permanent high-pressure cell develops an anticyclonic system over northern Arabia. This combined with cyclonic circulation around the Asian low-pressure system blows winds across the Persian Gulf and into the

Rub' al Khali (Edgell, 2006; Fig. 6), known as the Shamal. These winds are at their most intense during summer.

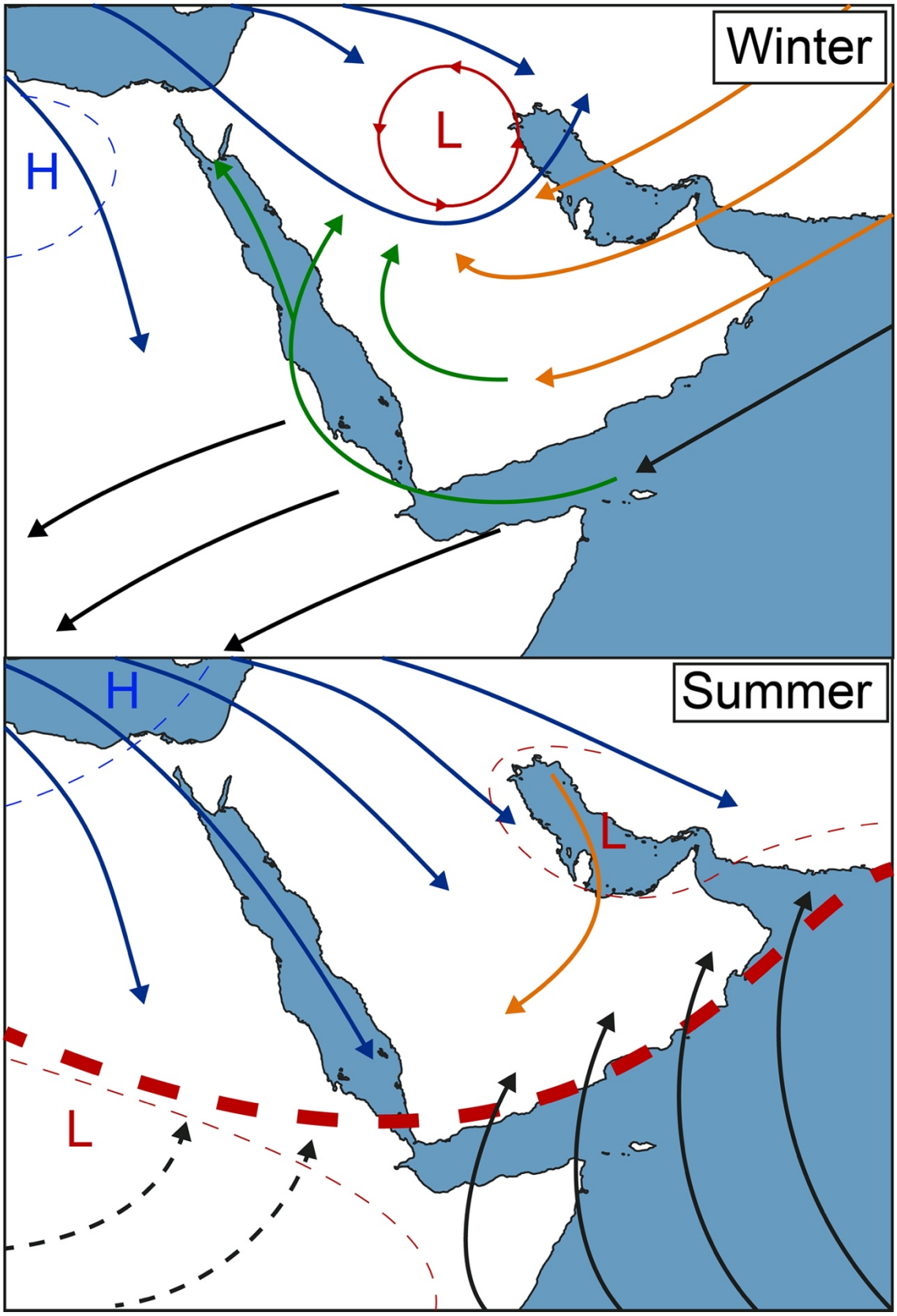

Fig. 6. Wind patterns and pressure systems of Arabia (after Edgell, 2006; Parton et al., 2015b). Lines mark direction of winds (black: Indian Ocean and tropical Atlantic; blue: Mediterranean; green: RST winds and orange: Shamal winds. The summer position of the tropical rain-belt is represented by the dashed red line.

2.3 Environmental settings

Arabian environments are currently characterised mostly by deserts/semi-deserts (Fig. 2C). This applies to areas in which vegetation only covers ~15% of the surface, leaving most of the substrate exposed. In deserts, the vegetation is mostly confined to depressions or wadis, where precipitation can be stored underground. Though, vegetation in the semi-deserts is more randomly distributed on the surface. Generally, deserts receive less than 100 mm yr^{-1}; whereas the semi-deserts are present between the 100 and 250 mm yr^{-1} isohyets (Miller and Cope, 1996). However, the gradual transition from desert to semi-desert means these distinct boundaries are not clear. Deserts can be subdivided into the sand deserts and gravel deserts.

Five major sand deserts are present on the Arabian Peninsula:

I. Rub al Khali, or "the empty quarter" (Fig. 7), sand sea (the Earth's largest sand desert: ~600,000km^2) dominates the southern extent of the Arabian Peninsula. Only the plains at the edge of the sands or between sand dunes are devoid of vegetation. Vegetation is comprised of xerophytic shrubs and herbs, such as *Cornulaca monocantha*, *Cyperus conglomeratus*, *Dipterygium glaucum*, *Lineaum Arabicum*, *Calligonum crinitum* and *Haloxylon persicum* (Miller and Cope, 1996). Annuals are mostly absent

and may only occur after heavy rainfall. Apart from marginal woodlands, comprising of *Acacia sp*. and *Prosopis cineraria*, trees are absent.

II. The ad Dhana sand belt forms between the Rub al Khali to its south and the Nefud to the north and forms a boundary between eastern and central Arabia. *Atermisia monosperma* and *Calligonum comosum* are the most characteristic species within the ad Dhana. After rains, annuals flourish in the northern part of the ad Dhana.

III. The Nefud dominates northern to central Arabia Fig. 8. This area consists of sand dunes, sheets of deep undulating sands and hollows with very thin sand. Dwarf shrublands consisting mainly of *Atermisia monosperma*, *Calligonum comosum*, *Haloxylon persicum*, *Stipagrotis drarii*, *Scrophularia hyoericifolia*. Following the winter rains, vegetation generally increases to a greater extent than in the Rub al Khali in the south.

IV. The Eastern coastal sands form along the Persian Gulf in eastern Saudi Arabia to Kuwait. Vegetation is characterised as dwarf shrubland containing *Panicum turgidum*, *Calligonum comosum* and *Leptadenia pyrotechniva* bushes.

V. The Wahiba sands are a small isolated sand desert in north eastern Oman. Mostly vegetation is dominated by *Dipterygium glaucum*, *Cyperus conglomeratus*, *Calligonum crinitum* and *Panicum turgidum*. Woodlands, comprising mostly of *Prosopis cineraria*, form at the margins.

Fig. 7. The Rub al Khali in Yemen. By Ljuba brank - Own work, CC BY-SA 3.0, https://commons.wikimedia.org/w/index.php?curid=47156426.

Fig. 8. The Nafud desert. By Charles. T.G. Clarke - CC BY-SA 4.0, https://commons.wikimedia.org/w/index.php?curid=52956489.

The rock and gravel deserts dominate the topography of Arabia. Though, these are mostly present in the north and central regions, while the Rub' al-Khali dominates in the south. Generally, these are less well vegetated than the sand deserts. Gravel deserts can be separated into rock and stone deserts (*hamadas*) and gravel deserts (*regs*). Hamadas are distinguished by a lack of fine material, which has been removed by the wind. Regs are more heterogenous, comprising of alluvium and areas lacking fine material. Vegetation is largely restricted to drainage channels, wadis and rock crevices, in which sand and soil can accumulate. "Meadows" can form in areas in which soils develop after rains. Any trees and shrubs are restricted to wadis.

The plains and lower slopes of Hijaz and the Yemeni highlands (Fig. 9) are dominated by drought-deciduous *Acacia-Commiphora* bushlands (Miller and Cope, 1996). This bushland is replaced by semi-evergreen and thicket bushland as altitude increases. Small forests are present in the valleys. *Juniperus* woodlands are present in the Asir mountains of Saudi Arabia, the thickets and bushlands of Socotra, the valley forest of the Yemeni highlands, the Jebel Akhdar mountains of northern Oman and the escarpments of Dhofar.

Fig. 9. The Yemeni Highlands. By Rod Waddington from Kergunyah, Australia - Yemeni Highlands, CC BY-SA 2.0, https://commons.wikimedia.org/w/index.php?curid=33168032.

2.4 Summary

Currently, Arabia climates are influenced by the Mediterranean frontal system and the Summer Monsoons (ASM and ISM). Precipitation across most of the peninsula is delivered during winter by cyclones that develop over the Mediterranean. However, precipitation to the southernmost points are delivered by the ASM and the ISM. While the landscape is highly heterogenous and environments have different responses to precipitation changes, low precipitation currently restricts vegetation growth over much of Arabia (Nemani, 2003). In the Rub' al Khali, Ad Dahna and Nefud deserts, vegetation density is increased following rainy periods. Providing records of increased precipitation may therefore inform when 'green' landscapes formed throughout the Pleistocene.

Chapter 3

3) Arabian palaeoclimate and human dispersals

3.1 Introduction

Saharo-Arabian is currently dominated by desert and semi-desert environments. Over most of the Arabian Peninsula, current precipitation is insufficient to overcome the highly evaporative conditions to form widespread permanent waterbodies and sustain dense vegetation. However, periods of increased precipitation during peak interglacial periods, facilitated formation of grassland, savannah-like environments (Fleitmann et al., 2011; Rosenberg et al., 2013; Jennings et al., 2015b; Parton et al., 2015b; Beck et al., 2018). These are becoming increasingly related to *H. sapiens* occupations of the now arid areas of Arabia and demographic shifts in Eurasia. The clear relationship between the timing of Arabian pluvial periods, high low-latitude northern hemisphere insolation and glacial boundary conditions means that incursions of the monsoon should have occurred on much broader timescales. In this case, the palaeoclimate conditions of the Arabian Peninsula could have had significant impact on hominin distribution throughout the evolution of the *Homo* genus. This chapter reviews the current understanding of Arabian palaeoclimate from the late Miocene to termination of the last glacial maximum. A broad overview of hominin dispersals and occupation of the Arabian Peninsula is then provided to identify the impact that ameliorated Arabian environments may have had on the distribution of the genus *Homo*.

3.2 Saharo-Arabian Palaeoclimate

3.2.1 Formation of the Saharo-Arabian Deserts

It is clear that the Arabian plate uplifted during the late Eocene to early Oligocene (40-25 Ma BP: Allen and Armstrong, 2008; Liu et al., 2019); however, the timing of formation of the Saharo-Arabian deserts are less clear. Understanding the formation of these deserts is crucial to understanding the evolution of the monsoon systems. Model simulation data shows the African Summer Monsoon systems (northern and southern hemisphere) and the equatorial tropical domain had existed since the Palaeocene (Liu et al., 2019). As Arabia uplifted during the Eo-Oligocene, the ASM system delivered precipitation to the south of the Peninsula. Throughout the Oligocene, formation of subtropical arid regions in northern Africa were related to the position of the continents and the scale of mean annual subtropical high pressure systems; whereas the formation of subtropical arid regions in the Arabian Peninsula and west Asia were related to ongoing uplift and reduction of the Paratethys Sea (Liu et al., 2019). Beyond this, there is currently little information on precise timing of aridification in Eo-Oligocene; however, it is probable that this was a time progressive processes, spanning millions of years as atmospheric and ocean circulation were reorganised in response to uplift and Paratethys shrinkage.

Incursion of the monsoon reduced throughout the Miocene to the present day, where only the tips of the ASM and Indian Summer Monsoon (ISM) affect the southernmost points of the Arabia Peninsula (Weyhenmeyer et al., 2002). A recent palaeoclimate model – based on the hypsodonty index of Neogene Eurasian and African mammalian teeth – found that, by the late Miocene, arid conditions had been established within the Saharo-

Arabian region (Kaya et al., 2018). However, compared to today's climates the southern margins of the Sahara and Arabia received an additional ~1-2 mm day^{-1} of rainfall (Fig. 10). Aeolian sand accumulations act as a more definitive proxy for terrestrial aridity. In the eastern Djurab, sand accumulations were dated to the late Miocene and used to provide a *terminus ante quem* for aridification of the southern Sahara (~7 Ma: Schuster et al., 2006). This age was established on the basis that these sandstones underly the Anthracotheriid unit of the Toros-Menalla locality, with no independent direct ages for the aeolian sediments themselves. The Anthracotheriid unit was dated to 7.2-6.8 Ma (Lebatard et al., 2008) and contains *Sahelanthropus tchadensis* and large mammals, suggesting greater annual rainfall and perhaps forested environments (Brunet et al., 2002, 2005; Geraads et al., 2008; Peigné et al., 2008; Novello et al., 2017). However, the burial context of these fossils is uncertain (Beauvilain, 2008) (and they may have been reburied) and it is possible that the Toros-Menalla fossils are of an earlier Miocene age, prior to the onset of widespread aridification. Despite this, formation of argillaceous sandstones, diatomites and argillaceous pelites in local geological units show punctuated periods of increased rainfall occurred throughout the Miocene (Lebatard et al., 2008; Novello et al., 2015, 2017). Similarly, the mid-late Miocene Barzaman Formation in eastern UAE, and potentially Oman, represents widespread alluvial fan activation (Styles et al., 2006; Lacinska et al., 2014). Reworking of the fan, in the form of erosional and incisional processes, suggests that later reactivation phases had occurred, probably throughout the late Miocene and Pliocene. As rainfall Saharo-Arabian climates are linked by the tropical rain-belt, it may be speculated that these were caused by incursions of the monsoons. However, the source of moisture requires further clarification.

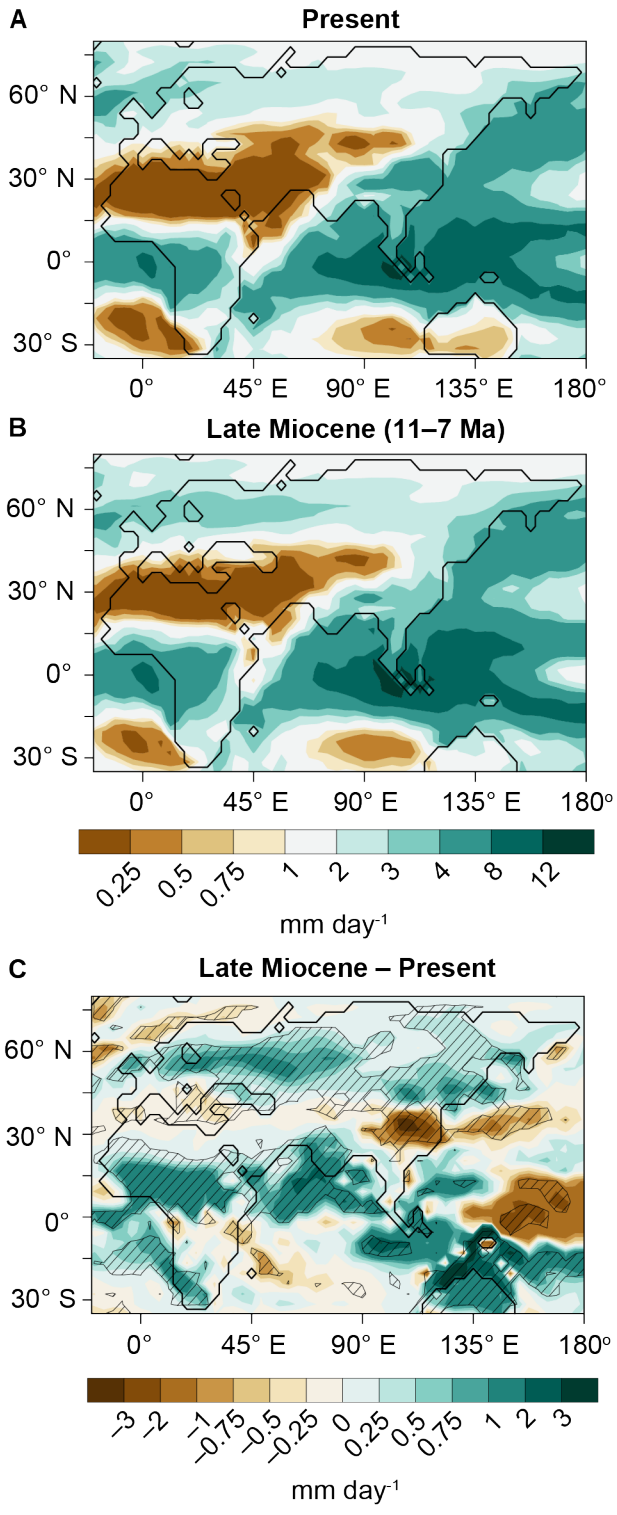

Fig. 10. Present (A) and the late Miocene (B) average daily precipitation (mm day^{-1}). (C) Miocene — present precipitation (after Kaya et al., 2018).

The cause of late Miocene aridification is currently debated. Two climate model simulations indicate that eastern Saharo-Arabian aridification ensued ~7.2 Ma, as constriction of the Tethys Sea led to a reorganisation of atmospheric and ocean circulation and reduced penetration of the African Summer Monsoon (Zhang et al., 2014; Liu et al., 2019). However, it must also be considered that the late Miocene is characterised by global cooling and aridification, expansion of northern and southern hemisphere ice-sheets and expansion of mid-latitude deserts (Zachos et al., 2001; Hartley and Chong, 2002; Jordan et al., 2014; Wang et al., 2015; Ao et al., 2016). The increased ice-sheet extent and phased uplift Tibetan Plateau (TP) enhanced meridional thermal contrast, restricting the extent of the tropical domain and would have led to contraction of green environments in the Sahara. Additionally, cooler global conditions reduced global atmospheric vapour content, meaning that precipitation at a macro-scale was reduced. Thus, when taken into a broader context, the formation of the Saharo-Arabian deserts could have been part of a global transition to mid-latitude aridity in response to cooling and ice sheet expansion. However, further chronological data is required to link regional climate responses to global climate change versus regional events (and/or the competing effects of both).

Interestingly, an adverse effect of global cooling was the enhancement of monsoon circulation within a more restricted area. A recent EASM intensity record (derived from magnetism of the Chinese loess Red Clay sequence) highlights the role of southern-hemisphere glaciation in enhancing monsoon circulation in the late Mio-Pliocene (Ao et al., 2016). At ~8 Ma the EASM was particularly weak but intensified throughout the Mio-Pliocene as southern-hemisphere glaciation increased (Ao et al., 2016). Southern-hemisphere glaciation throughout the Miocene and Pliocene intensified the SISH and

subtropical high cell above Australia during boreal summer. Reduced South Indian Ocean SSTs would enhance the anticyclone that develops during boreal summer, which would intensify the Somali Jet (Beck et al., 2018). Additionally, phased TP uplift throughout the Mio-Pliocene (25-22, 16-14, 10-7, 4-2.6 Ma) enhanced interhemispheric pressure gradients and increased outflow from the Tibetan High to the South Indian Ocean Subtropical High, strengthening the EASM and ISM (see chapter 2 for details; An et al., 2006; Liu et al., 2019). This highlights the role of numerous factors underlying monsoon formation, strength and variability.

3.2.2 The Pliocene

The Pliocene (5.3-2.7 Ma) was the last time when global atmospheric CO_2 and global temperatures exceeded modern values (Pagani et al., 2010). Two distinctly warm periods are frequently discussed within the literature, defined here as the Early Pliocene Warm Period (EPWP) and the Mid Pliocene Warm Period (MPWP). Despite a paucity of data from Arabia, climate models and data from elsewhere indicate mid-latitude deserts underwent dramatic increases in precipitation during these periods. The Pliocene may therefore be an important analogue for determining future mid-latitude desert environments within a high CO_2 world.

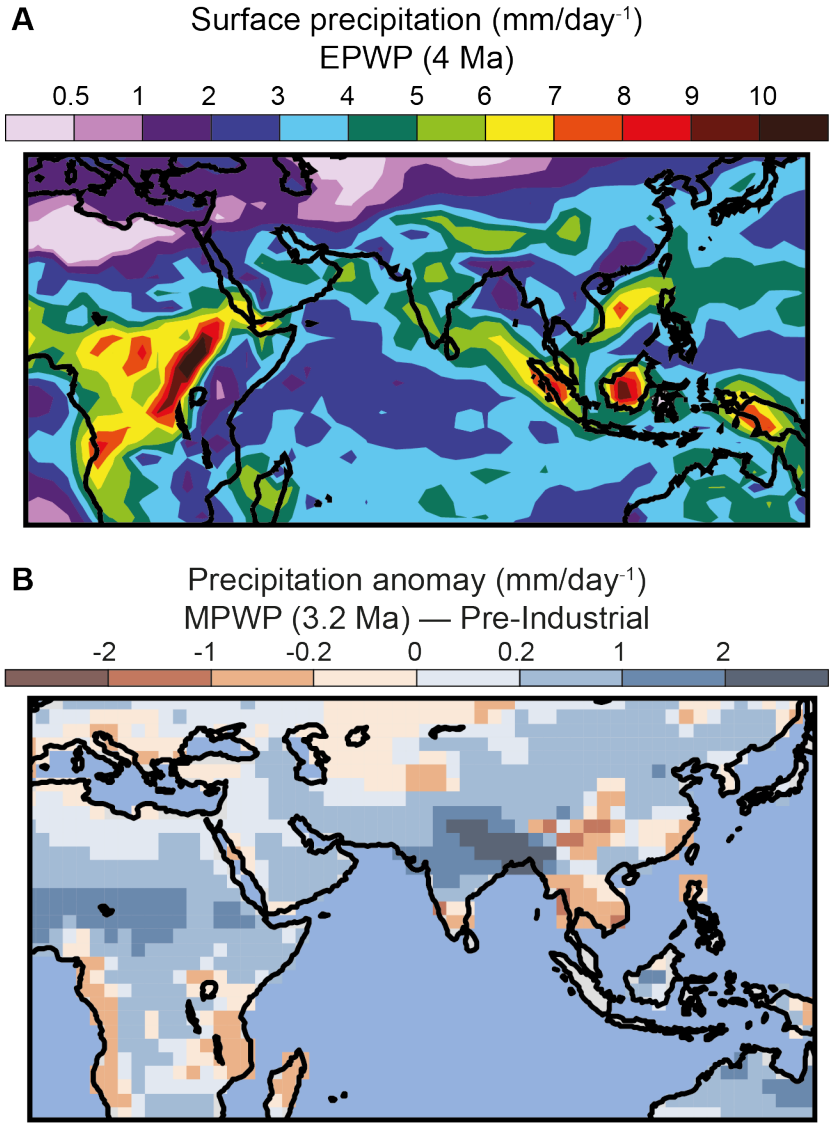

Fig. 11. (A) modelled EPWP precipitation (mm day^{-1}) at 4 Ma (after Brierley et al., 2009). (B) Mixed modelled ensemble of global land monsoon during the MPWP (3.2 Ma) minus Pre-industrial precipitation (mm day^{-1}) (Li et al., 2018).

3.2.2.1 The Early Pliocene Warm Period (EPWP)

The EPWP is broadly defined as a period ~4.2-4 Ma. Major climatic and geological events throughout this period include reduced Antarctic ice-sheet, with Antarctic SST of -1.8°C (winter) and ~5°C (summer), collapse of the western ice-sheet and no summer eastern ice-sheet (Golledge et al., 2017); phased uplift of the Tibetan Plateau (An et al., 2006); high global temperatures and reduced interhemispheric temperature gradients (Brierley et al., 2009); weak Hadley and Walker circulation, leading to a wider but weaker ITCZ (Brierley et al., 2009); weaker tropical atmospheric subsidence, which lead to greater convective precipitation over continents due to enhanced atmospheric water-vapour concentration (Brierley et al., 2009; Sniderman et al., 2016). An EPWP climate simulation suggest precipitation increased over the Saharo-Arabian deserts (Fig. 11A), reaching 730-2190 mm yr^{-1}. This may be confirmed by formation of an argillaceous pelite dated to 3.96 ± 0.48 Ma at Koro Toro. Additionally, two further pelites were dated to 3.58 ± 0.27 Ma and 5.26 ± 0.23 Ma in nearby sedimentary units at Kollé and Kossom Bougoudi, respectively (Lebatard et al., 2008), showing punctuated phases of increased precipitation throughout the Pliocene. A phytolith record from nearby Lake Chad showed that grasslands flourished within these phases (Novello et al., 2015, 2017), highlighting the terrestrial impact of these periods of increased precipitation. In the Horn of Africa, a period of decreased $\delta^{13}C_{leaf\text{-}wax}$ (increased vegetation density) from DSDP 231 (Gulf of Aden) occurred from ~4.3-3.8 Ma, indicating both precipitation and vegetation density increased in the horn of Africa (Liddy et al., 2016; Fig. 12). As precipitation in Lake Chad and the Horn of Africa are influenced by the ASM, this correlation is expected. Transition to warmer climates during the EPWP may therefore have had a profound influence on the climate and environments of Arabia.

The mechanisms that brought increased precipitation to these areas are poorly understood. While it is possible that precipitation over Arabia was derived from a southern source (Brierley et al., 2009), the interhemispheric pressure gradient were reduced between the northern and southern Hadley cell. This suggest monsoon circulation would have been weakened. Prescribed SSTs from northern (ODP 1012: 32°N), southern (ODP 846: 03°S) and equatorial records (ODP 806 and ODP 847) showed that a reduced meridional temperature gradient widened the intertropical convergence zone (ITCZ), yet resulted in decreased precipitation intensity (Brierley et al., 2009; Fig. 11A). Weak SST gradient (leading to reduced localised wind convergence) and increased atmospheric water-vapour content (as a consequence of increased global temperatures) resulted in enhanced convective precipitation over land (Brierley et al., 2009). Similarly, a collapsed western Antarctic ice-sheet and reduced austral winter ice-sheet (Golledge et al., 2017) would have reduced the interhemispheric pressure gradient during boreal (austral) summer (winter), facilitating a widening of the tropics. In other words, precipitation increased overland as a result of increased atmospheric vapour and was not necessarily related to an enhancement of monsoon circulation. However, phased uplift of the TP 4-2.6 Ma could have increased outflow to the SISH and led to enhancement of summer monsoon circulation (An et al., 2006). Moreover, $\delta^{18}O_{ca}$ (Ji et al., 2017), pollen records (Wang et al., 2006) and a recent EASM stack (derived from magnetism of the Red Clay sequence: Ao et al., 2016; Fig. 12) from the Chinese Loess Plateau (CLP) confirm that precipitation over land was enhanced ~4.2-4 Ma. This is in conflict with the aforementioned model, which shows precipitation over the CLP was similar as today (Fig. 11B).

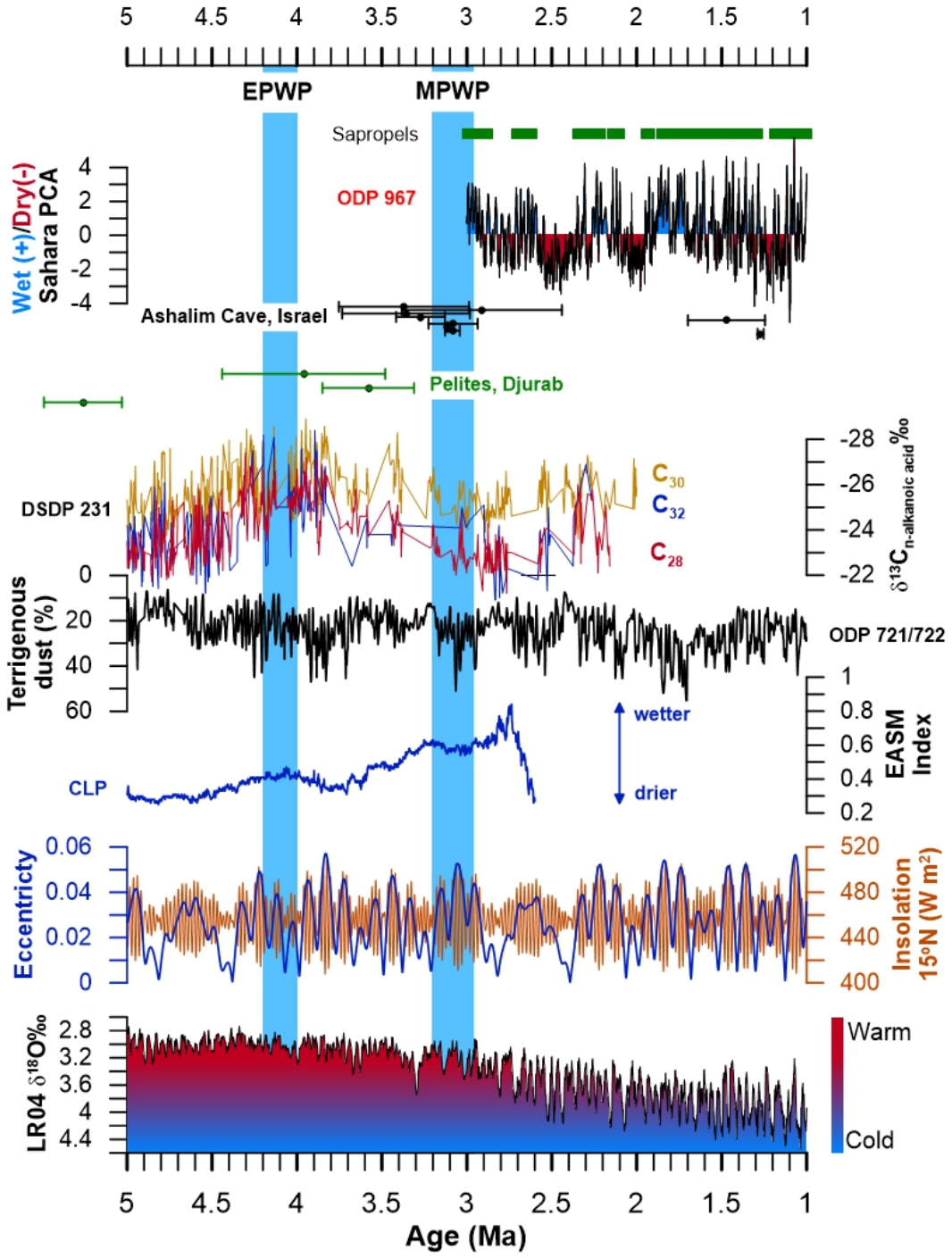

Fig. 12. Monsoon influenced Pliocene palaeoclimate records (ODP 721/722: deMenocal, 1995; Djurab pelites: Lebatard et al., 2008; Ashalim Cave speleothems: Vaks et al., 2013; CLP EASM index: Ao et al., 2016; DSDP 231 $\delta^{13}C_{leaf\text{-}wax}$ ‰: Liddy et al., 2016; ODP 967 PC2 (wet/dry index) and sapropels: Grant et al., 2017) compared to

eccentricity (Berger and Loutre, 1991, 1999) and global (LR04) $\delta^{18}O_{benthic}$ values (Lisiecki and Raymo, 2005). Blue bars mark the EPWP and MPWP, respectively.

3.2.2.2 The Mid Pliocene Warm Period (MPWP)

The MPWP is defined as a global warm period that persisted between ~3.2 to 3 Ma. Within this time period, atmospheric CO_2 reached ~415 ppm and global temperatures were 1-2°C greater than modern climates (Pagani et al., 2010). As such, the MPWP is frequently used as a potential analogue for future climates under high greenhouse gas conditions. This has resulted in greater research into the global climatic settings of this period when compared to the EPWP, especially from the climate modelling community (e.g., Salzmann et al., 2011; Haywood et al., 2013; Tindall and Haywood, 2015; Li et al., 2018). The MPWP was characterised by expansion of the monsoon domain and tropics, as a result of reduced meridional thermal contrast in the mid-to-upper troposphere, variation of vertical moisture advection and increased evaporation (Li et al., 2018). Four periods (G17: 2.95 Ma; K1: 3.06 Ma; KM3: 3.15 Ma and KM5c: 3.2 Ma) of decreased precession have been the subject of recent efforts to understand MPWP monsoon variability (e.g., Prescott et al., 2018, 2019). These periods are characterised by high orbital eccentricity, low orbital precession and low LR04 $\delta^{18}O_{benthic}$ (Lisiecki and Raymo, 2005; Prescott et al., 2018). The lowest precession and greatest eccentricity values occurred within K1 (3.06 Ma), resulting in a greater short wave radiation flux anomaly compared to modern conditions (Prescott et al., 2018). While all of these periods were marked by an expanded monsoon domain, precipitation over Arabia during KM5c (3.2 Ma) was less intense; whereas, K1 (3.06 Ma) saw the largest increase in Arabian precipitation (Prescott et al., 2018). Together, this variability shows that precession and

insolation forcing remained a vital component for monsoon area and strength throughout the MPWP (Prescott et al., 2019).

In order to understand the environmental response to increased precipitation, simulations have also included vegetation outputs. The PRISM3 reconstruction shows that increased subtropical precipitation caused a retraction of the mid-latitude deserts (Fig. 13). In Arabia, most of the current arid and semi-arid mid-latitude climate zones were replaced by tropical xerophytic shrublands (Salzmann et al., 2011). PRISM3, however, may have overpredicted the extent of this change, with BIOME4 simulations showing that, while tropical xerophytic shrubland did expand, northern Saharo-Arabia remained a desert during MPWP interglacials (G17: 2.95 Ma; K1: 3.06 Ma; KM3: 3.15 Ma and KM5c: 3.2 Ma) (Prescott et al., 2018). This is consistent with evidence from MIS 5e, which shows the desert did not entirely disappear in the most northern areas of Saharo-Arabia (Scerri et al., 2014a). Terrestrial records, however, are required to test these simulations.

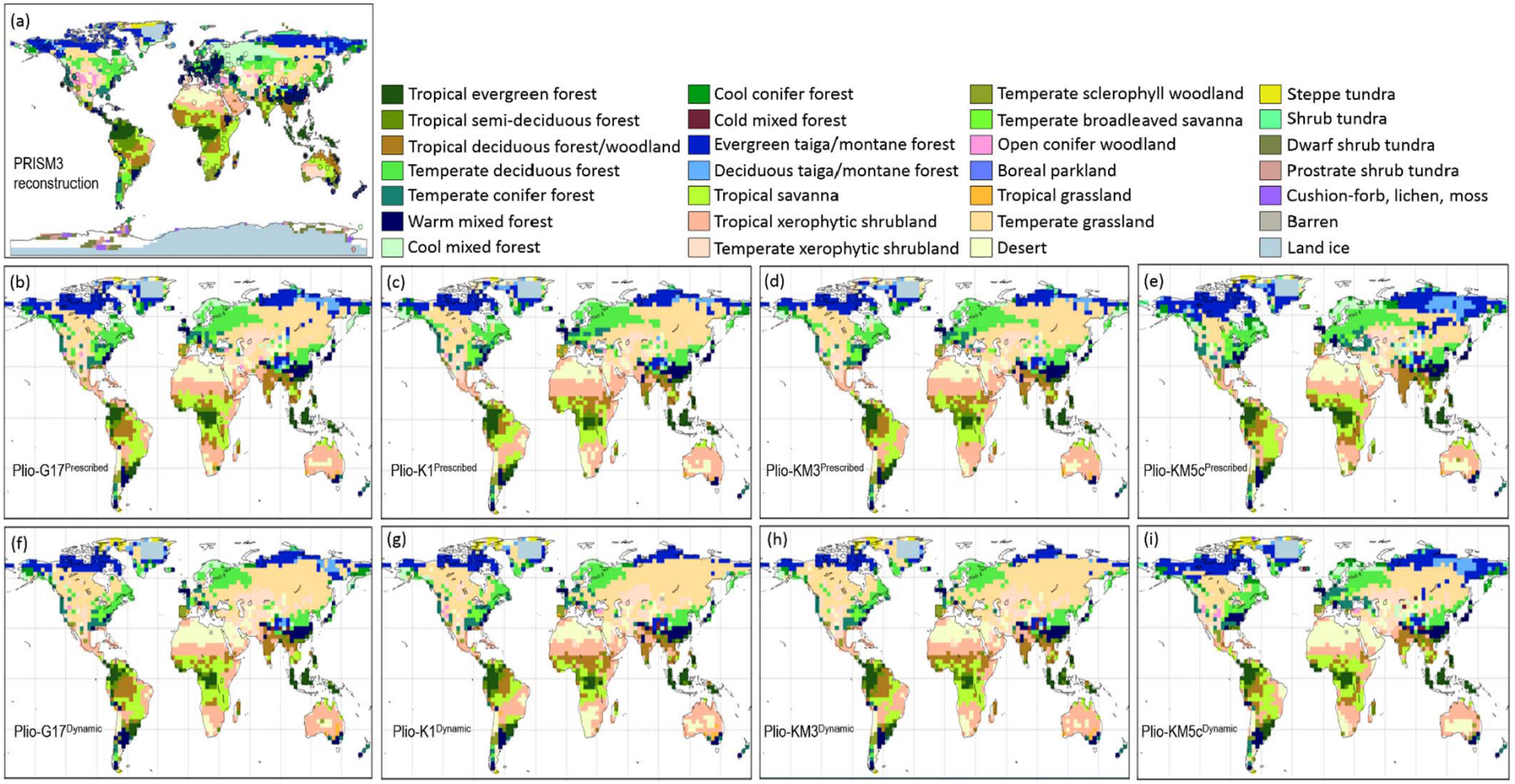
(a)
PRISM3 reconstruction
Tropical evergreen forest
Tropical semi-deciduous forest
Tropical deciduous forest/woodland
Temperate deciduous forest
Temperate conifer forest
Warm mixed forest
Cool mixed forest
Cool conifer forest
Cold mixed forest
Evergreen taiga/montane forest
Deciduous taiga/montane forest
Tropical savanna
Tropical xerophytic shrubland
Temperate xerophytic shrubland
Temperate sclerophyll woodland
Temperate broadleaved savanna
Open conifer woodland
Boreal parkland
Tropical grassland
Temperate grassland
Desert
Steppe tundra
Shrub tundra
Dwarf shrub tundra
Prostrate shrub tundra
Cushion-forb, lichen, moss
Barren
Land ice
(b)
Plio-G17Prescribed
(c)
Plio-K1Prescribed
(d)
Plio-KM3Prescribed
(e)
Plio-KM5cPrescribed
(f)
Plio-G17Dynamic
(g)
Plio-K1Dynamic
(h)
Plio-KM3Dynamic
(i)
Plio-KM5cDynamic

Fig. 13. (a) PRISM 3 vegetation reconstruction (Salzmann et al., 2011). (b-e) BIOME4 land vegetation reconstruction using prescribed vegetation with HadCM3 and land surface scheme MOSES1 for MPWP interstadials (G17: b; K1: c; KM3 d; KM5c: e; Prescott et al., 2018). (f-i) BIOME4 experiments run with HadCM3 coupled to TRIFFID vegetation model and MOSES2 land surface scheme for MPWP interstadials (G17: f; K1: g; KM3 h; KM5c: i; Prescott et al., 2018).

Few terrestrial records provide an insight in MPWP precipitation regimes and environmental settings. The lake Chad phytolith record shows expansion of grassland environments at ~3.2-3 Ma (Novello et al., 2015, 2017), which is in good agreement with the aforementioned models. Further north, speleothem growth in the Negev Desert was dated to 3.5-.2.9 Ma (Vaks et al., 2013; Fig. 12). Here, $\delta^{18}O_{ca}$ was not dissimilar from younger Pleistocene samples. Based on current isohyet boundaries and the spatial distribution of modern speleothem growth, Pleistocene speleothem growth was taken to represent precipitation of ≥300 mm yr^{-1} in the southern Negev (Vaks et al., 2010). Similar $\delta^{18}O_{ca}$ between these samples suggest precipitation reached 300 mm yr^{-1} in the southern Negev with the Pliocene (Vaks et al., 2013). ODP 967 wet/dry index and sapropel formations are also in good coherence for enhanced MPWP precipitation in now arid areas of the Saharo-Arabian desert belt (Grant et al., 2017; Fig. 12). A recent $\delta^{18}O_{ca}$ CLP record showed that relatively weak precipitation occurred at 3.2-3 Ma compared to the EPWP (Ji et al., 2017). Similarly, reduced arboreal pollen from Xifeng indicates that precipitation was lower during the MPWP than the EPWP (Wang et al., 2006). The EASM stack, however, shows the MPWP monsoon was more intense than during the EPWP (Fig. 12), though this is inconsistent between the records that comprise the stack,

with some showing the EPWP and MPWP monsoons were of similar intensity (Ao et al., 2016).

Current terrestrial records are sparsely distributed, and few records are available from mid-latitude deserts – particularly Arabia. Thus, model data is often supplemented by Pleistocene records or records that may span the entire Pliocene (e.g, Salzmann et al., 2011; Tindall and Haywood, 2015; Li et al., 2018), which cannot be strictly confined to the MPWP. It is therefore vital that new palaeoclimate records, with robust chronologies, are developed to test and mitigate uncertainties within palaeoclimate models. While current evidence is fragmented, and more specific examples of Pliocene age should be identified on the Arabian Peninsula, the emerging picture suggests increased Pliocene precipitation was echoed by an expansion of semi-arid grasslands.

Desert expansion resumed during the Pleistocene, as global climates cooled, and the northern hemisphere ice-sheet expanded (Zachos et al., 2001). Over the past 500 ka BP, desert environments predominantly characterised the majority of the Sahara and Arabian Peninsula. However, a growing evidence from numerous palaeoclimate archives demonstrates Arabian precipitation substantially increased during peak interglacials and warm substages throughout the Middle and Late Pleistocene, and the Holocene (Burns et al., 2003; Fleitmann et al., 2003a, 2007, 2011; Rosenberg et al., 2013). These saw the expansion of ephemeral grassland biomes into the now arid interiors of the Saharo-Arabian desert belt (Stimpson et al., 2016; Groucutt et al., 2018; Roberts et al., 2018). Yet very few terrestrial palaeoclimate records extend beyond 350 ka BP. Initial studies of speleothems recovered from the Saudi Arabian deserts also suggest periods of enhanced precipitation throughout the Plio-Pleistocene. While some samples provide

^{230}Th ages within the Pleistocene (SA 'B': 484.4 ± 82 ka BP/MIS 13.1; SA 15.778 ± 153 ka BP and SC1-1: 377.93 ± 26.855 ka BP/~MIS 11/10), many samples fell beyond the range of ^{230}Th dating (Fleitmann et al., 2004b). These samples possess ^{234}U/^{238}U ratios close to 1, which likely indicates ages over 1 Ma. Furthermore, speleothem δ^{18}O was utilised to calculate past precipitation δ^{18}O values (-5.8 to -10.9 ± 1 ‰), which were more negative than modern precipitation (~-2‰ to 2‰) (Fleitmann et al., 2004b). These initial findings demonstrate that precipitation increased in the Arabian interior sometime before 1 Ma. U-Pb dating of these samples has the potential to expand the terrestrial palaeoenvironmental record of Arabia beyond lake records.

3.2.3 The Pleistocene

During the Pleistocene, the arid environments of the Saharo-Arabian desert belt were punctuated by increases of rainfall during interglacial maxima and warm substages. Currently, there is strong evidence to show these pluvial phases occurred up to 350 ka BP; however, there is currently a paucity of palaeoclimate records that extend beyond 350 ka BP. Records that do extend beyond 350 ka BP often contain dating uncertainties too large to assign to specific interglacial/glacial stages (e.g., Rosenberg et al., 2013). In order to understand the environments of Pleistocene Arabian pluvial periods, this section explores the last 350 ka BP of climatic conditions in Arabia, where age uncertainties are more precise and palaeoclimate records are more numerous. It should be noted that, while it is highly likely that wet periods persisted throughout the Pleistocene, the Early-Middle Pleistocene Transition (EMPT) witnessed a dramatic reorganisation of global climates in terms of interglacial-glacial amplitude and cyclical frequency. Therefore, Arabian climates within the last 350 ka BP should not necessarily be seen as a direct analogue for all potentially earlier wet periods.

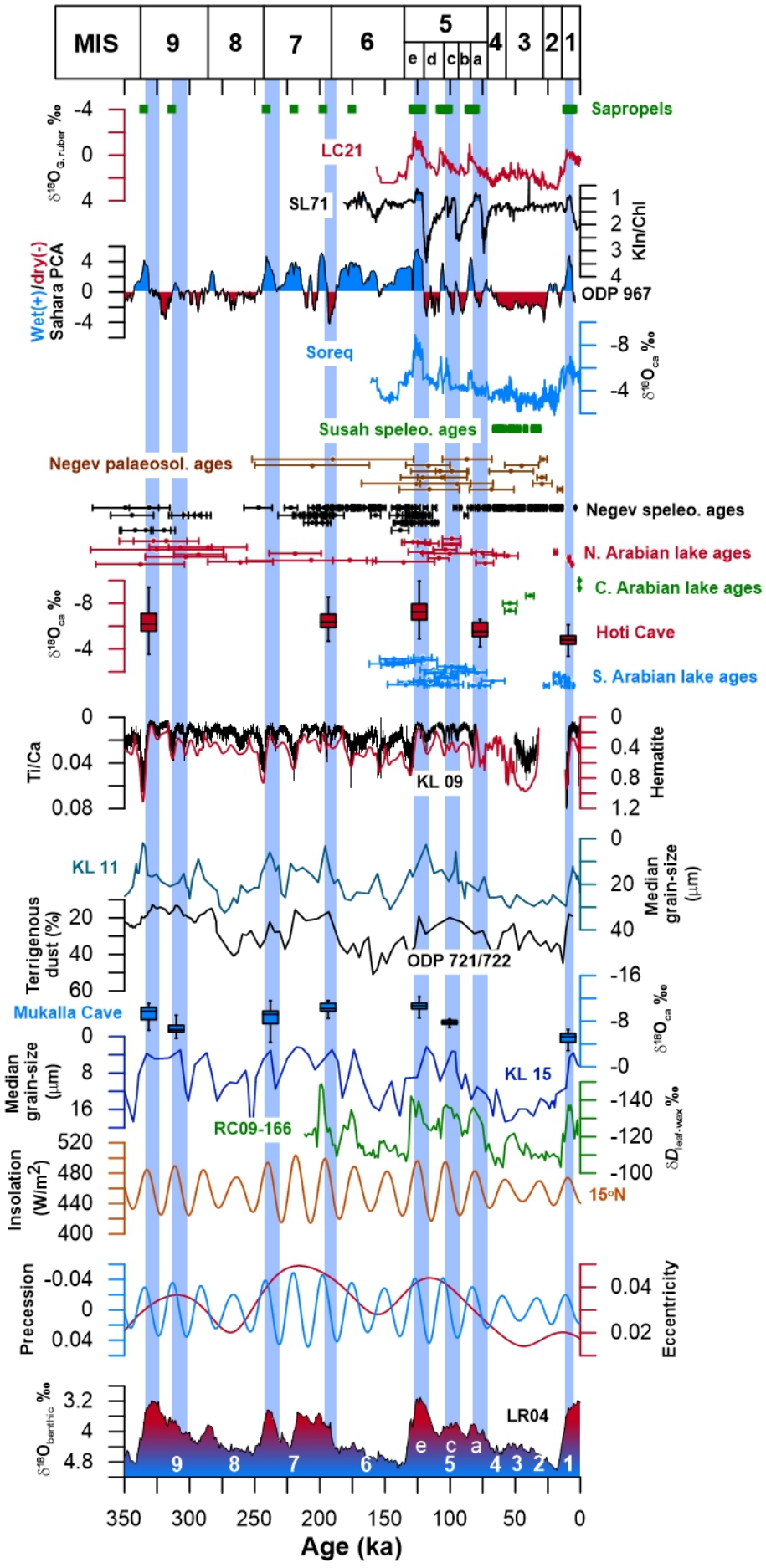
MIS
9
8
7
6
5
e d c b a
4
3
2
1
Sapropels
LC21
SL71
KIn/Chl
ODP 967
Wet(+)/dry(-) Sahara PCA
Soreq
Susah speleo. ages
Negev palaeosol. ages
Negev speleo. ages
N. Arabian lake ages
C. Arabian lake ages
Hoti Cave
S. Arabian lake ages
Ti/Ca
KL 09
Hematite
KL 11
Terrigenous dust (%)
ODP 721/722
Median grain-size (μm)
Mukalla Cave
KL 15
RC09-166
15°N
Insolation (W/m²)
Precession
Eccentricity
LR04
Age (ka)

Fig. 14. Current palaeoclimate records from the eastern Saharo-Arabia region. All continuous records aligned so that precipitation increases upwards.

3.2.3.1 MIS 9 (337-270 ka BP)

MIS 9 is characterised as an interglacial period. The precise duration of MIS 9 is unclear due to a reversal of glaciation at 280 ka BP. Some taxonomic systems classify this as MIS 9a/9.1 (Tzedakis et al., 1997; Railsback et al., 2015), whereas other systems classify this as 8e/8.5 (Bassinot et al., 1994) and some do not specifically assign sub-stages (e.g., Lisiecki and Raymo, 2005). The former system (Tzedakis et al., 1997) is used here, as, between 300-280 ka, LR04 $\delta^{18}O$ did not reach the positive values exhibited in later glacial periods. Thus, MIS 9 is tentatively defined here between ~337-270 ka BP.

Marine records generally show that the interglacial conditions of MIS 9 saw increased humidity in the broader Saharo-Arabian region. At this time, sapropel formation (Mediterranean), reduced grainsizes (KL 11: Red Sea; KL 15: Gulf of Aden) and decreased terrigenous dust (ODP 721/722) indicate increased soil humidity, Nile outflow and Saharan run-off (deMenocal, 1995; Fleitmann, 1997; Grant et al., 2017). Yet very few terrestrial climate records can be confidently dated to this period. Despites some age offsets, Mukalla Cave and Hoti Cave stalagmite $\delta^{18}O$ records are in good coherence with KL 11, KL 15 and ODP 721/722 records, and sapropel formation (S10: ~334.82 ka BP; and S*1: ~313.33 ka BP). The $\delta^{18}O_{ca}$ of these stalagmites is more negative than Holocene and modern values, suggesting precipitation was comparably greater. However, $\delta^{18}O$ is more positive than succeeding interglacial periods (MIS 5e, 7a and 7e), suggesting somewhat drier conditions. Nevertheless, fluid inclusion δD of Hoti Cave speleothems

was closely aligned to δD of current groundwaters recharged by the ISM (Fleitmann et al., 2003b), indicating that the monsoon domain was enhanced during MIS 9. This is in good coherence with a plethora of climate data which indicates interglacial conditions were echoed by enhancements of the monsoon domain through the Pleistocene.

Speleothem formation in southern Arabia matches speleothem formations in the Negev desert during NHP 4 and 3 (Negev Humid Period) (Vaks et al., 2010). The height and width of speleothems from both southern Arabia and the Negev were taken to represent that precipitation increased to >300 mm yr^{-1} at these times (Vaks et al., 2010; Fleitmann et al., 2011). More intense deposition in the southern Negev compared to the central Negev was taken to be indicative of a southern, monsoonal, source of palaeo-precipitation (Vaks et al., 2010), differing from the inferred WMC source for NHP 2 (MIS 7) and NHP 1 (MIS 5e). Yet, the more positive Mukalla and Hoti $\delta^{18}O_{ca}$ suggests a somewhat weaker monsoon during MIS 9 than MIS 7 and MIS 5e. This discrepancy highlights an issue when using speleothem deposition alone to infer moisture source. MIS 9 stalagmites from the Negev may benefit from fluid inclusion δD and $\delta^{18}O$ analysis to verify the source of palaeo-precipitation. Nevertheless, combining these records suggest that precipitation was greatly increased in both the now arid northern and southern margins of the Saharo-Arabian desert belt during MIS 9 interstadials.

Lake activation ages in the Nafud show that the interiors also saw increased precipitation. While age uncertainties are large, and often exceed >10 ka BP, central ages cluster close to interglacial maxima (Rosenberg et al., 2013; Parton et al., 2018). The stratigraphic position and more precise dating of stalagmites has been used to temporally confine these wet periods to MIS 9 (e.g., Rosenberg et al., 2013). However, more precise dating of

these should be conducted to provide independent age assignments. Nevertheless, the palaeontological remains derived from sediments from the Ti's al Ghadah palaeolake (318 ± 24 to 328 ± 26: Rosenberg et al., 2013) offer a unique insight into the environmental conditions of the MIS 9 wet periods. Crayfish, fish >155 cm, zebra, tortoise, hippopotamus, horse, panther, ostrich, grebe, sandgrouse, kite, wagtail, mallard, lizard, vulture, oryx, *Palaeoloxodon* sp., mustelids, fox, African wolf and spotted hyena were present in these sediments (Rosenberg et al., 2013; Stimpson et al., 2016; Roberts et al., 2018). A mixture of Eurasian and African taxa indicates fauna dispersed from both northern (Levant) and southern sources (Stimpson et al., 2016). $\delta^{18}O$ and $\delta^{13}C$ isotopic signatures attained from ungulate teeth fall into the range of grassland environments, which were characterised by seasonal climates (Roberts et al., 2018). Similarly, presence of fish and tortoise bones indicates that perennial waterbodies were present, showing that seasonal precipitation was sufficient to maintain permanent waterbodies within these highly evaporative environments. While the extent of these grassland environments is not clear, current data from the Nafud indicates that precipitation during MIS 9 was sufficient to sustain large bodied fauna.

3.2.3.2 MIS 8 (270-243 ka BP)

MIS 8 is a glacial period characterised by increased northern hemisphere ice-sheets and aridity in the Saharo-Arabia desert belt. Between 270-243 ka BP, the ODP 967 PC2 record shows 'dry' conditions prevailed in the Sahara (Grant et al., 2017). Additionally, absence of sapropel formations in the Mediterranean indicate Nile outflow and Saharan run-off were relatively weak. Similarly, lack of speleothem growth in both the northern and southern Negev suggest rainfall was reduced compared to modern climates. Further

south, grain size data of marine records from the Red Sea (KL 11) and Gulf of Aden (KL 15) again indicate conditions were dry in Arabia and the eastern Sahara, with grain sizes comparable to the last glacial maximum (MIS 2). Terrigenous dust of ODP 721/722 is also high, showing the Horn of Africa was perhaps drier than modern climates (Fig. 14).

Terrestrial records also show that desert conditions prevailed. While some ages of lacustrine episodes fall into MIS 8 (e.g., Rosenberg et al., 2013), these are considered to be related to MIS 9 or 7 based on speleothem growth at Mukalla or Hoti caves (Fleitmann et al., 2011). Absence of speleothem growth at Mukalla or Hoti caves indicate the tropical rain-belt did not expand into Arabia during MIS 8.

While these data indicate the tropical rain-belt was supressed, it is often regarded that the Atlantic westerlies should have increased precipitation in northern Saharo-Arabia during glacial periods (Blome et al., 2012). A reduced Icelandic Low – Azores High pressure contrast and glacial boundary conditions is frequently regarded to push the northern and southern hemisphere westerlies into lower latitudes (e.g., Blome et al., 2012). This, however, does not appear to be the case for Arabia, as palaeoclimate records from around the Saharo-Arabian regions characterise MIS 8 as a period of increased aridity.

3.2.3.3 MIS 7 (243-191 ka BP)

The MIS 7 interglacial is characterised by eccentricity values and NHI peaks greater than both MIS 9 and MIS 5. Early (~ 245-235 ka BP: MIS 7e) and later (205-195 ka BP: MIS 7a) substages are well represented in marine and terrestrial records as periods of increased

rainfall. There is evidence to suggest that rainfall also increased ~220-210 ka BP during MIS 7c, however this less consistent between records.

Sapropel formations in the Mediterranean marine records occurred at 241.35 ka BP (S9: MIS 7e), 220.22 ka BP (S8: MIS 7c) and 197.53 ka BP (S7: MIS 7a) (Grant et al., 2017). Similarly, the wet/dry PCA model of Saharan palaeoclimate suggests that humid conditions prevailed throughout most of MIS 7, with few short-lived punctuated 'dry' conditions (Grant et al., 2017). Evidence of wet periods in this record suggest enhanced monsoonal intensity within the Ethiopian highlands due to rain-belt migration, which is corroborated by negative $\delta D_{leafwax}$ ‰ RC09-166 showing increased humidity in the Horn of Africa (Fig. 14). Good coherence is observed with KL 11 and KL 15, where punctuated decreases in median grain-sizes indicate more humid soils (Fleitmann, 1997; Fig. 14) and matches a more recent $\delta^{18}O_{G.\ ruber}$ ‰ record from KL 11 (Siddall et al., 2003). A similar trend is observed in ODP 721/722 terrigenous dust, though is only slightly reduced during MIS 7c (Fig. 14).

While there is a paucity of Arabian terrestrial records from this period, available records provide good evidence for increased humidity. Speleothem growth is observed both at Mukalla and Hoti Cave within MIS 7. ^{230}Th ages from Y99 growth phase III generally cluster within MIS 7e, though some also fall within MIS 8 and MIS 7d-c. Similarly, growth phase II ^{230}Th ages generally cluster within MIS 7a, however some ages also fall within MIS 6e and MIS 7c (Fleitmann et al., 2011). Average stalagmite $\delta^{18}O_{ca}$ from Mukalla Cave is slightly more positive (drier conditions) during MIS 7e (-8.49‰) than MIS 7a (-10.62‰) (Fleitmann et al., 2011; Fig. 14), which reflects median grainsize records from KL 11 and KL 15 showing slightly larger measurements (Fleitmann, 1997).

Together, these indicate precipitation was slightly less during MIS 7e than MIS 7a. Fluid inclusion water δ*D* from Hoti Cave stalagmites plot on the southern Oman meteoric waterline, representing an increase of ISM precipitation during MIS 7a (Fleitmann et al., 2003b). While there is no evidence of speleothem growth from Hoti Cave during MIS 7e, this provides good evidence that the tropical rain-belt migrated northwards during MIS 7.

Further north, palaeolake sediments from the Nafud also show increased humidity during MIS 7 (Petraglia et al., 2012; Rosenberg et al., 2013; Parton et al., 2018). While large age uncertainties restrict these from being assigned to specific interstadial periods, the good coherence with speleothem growth and sapropel formation may be used as a tentative method to confine lake activity (e.g., Rosenberg et al., 2013). Abundant burrows were identified by Rosenberg et al. (2013) and were taken to represent the presence of crayfish.

Enhanced humid conditions are also detailed in the Negev by a clustering of speleothem ages within MIS 7c and 7a (Vaks et al., 2006, 2010), defined as NHP 2 (220-190 ka BP). A clear north-south gradient shows that precipitation was derived from intensified WMCs, which is in good agreement with increased arboreal pollen from Yammouneh, Lebanon throughout MIS 7 (Gasse et al., 2015). However, reduced occurrence of speleothem growth in the southern-most Negev suggests that the 300 mm yr^{-1} isohyet did expand into northern Arabia. A single age from northern-central Negev falls into MIS 7e (247.4 ± 10.8 ka BP: Hol Zakh). Absence of widespread speleothem deposition, particularly in the central Negev, suggests MIS 7e precipitation may have been short-lived and restricted to the northern Negev. There is some overlap in MIS 7 Negev speleothem growth with the Mudawwara palaeolake in Jordan, though the central age

falls within MIS 6e (Petit-Maire et al., 2010). Mudawwara is situated south of the current 300 mm yr^{-1} isohyet and the Negev Desert cave sites. The large catchment area extends into the southern Jordan highlands and may therefore be influenced by both WMC and monsoonal rainfall during peak interglacials (Petit-Maire et al., 2010). Given this, Parton et al. (2015) suggest this could show increased precipitation across both the northern and southern Arabian deserts during MIS 7. In summary, there is good confidence that MIS 7 was characterised by increased precipitation in Arabia; however, current dating cannot always strictly confine the timing of increased rainfall to specific substages.

3.2.3.4 MIS 6 (191-130 ka BP)

The transition from MIS 7 to MIS 6 saw a sharp decline in global climates ~180 ka BP (Fig. 14). A reversal at ~175 ka BP (MIS 6e) may have been a time of increased precipitation in the Saharo-Arabian region. However, the evidence for enhanced humidity during MIS 6e is equivocal and variable between different records. There is also some evidence for punctuated periods of increased precipitation throughout MIS 6. However, the varied appearance between records may suggest some temporal and spatial variability or perhaps less substantial rainfall when compared to preceding and succeeding interglacial periods.

In the Mediterranean, sapropel deposition was dated to 175.63 ka BP (S6), suggesting that Nile outflow, Saharan run-off and (by corollary) Ethiopian highland precipitation increased at this time (Grant et al., 2017). This is corroborated by speleothem records from the Levant, which show decreased $\delta^{18}O_{ca}$ values at ~178 and 152 ka BP (Ayalon et al., 2002; Bar-Matthews et al., 2003). $\delta^{18}O_{ca}$ from Levantine speleothems is highly

dependent on the composition of Eastern Mediterranean Sea sea-water on glacial-interglacial timescales, which is governed by Nile outflow and sea-level (Bard et al., 2002; Grant et al., 2012, 2016; Rohling et al., 2015). The correlation between sapropel deposition and $\delta^{18}O_{ca}$ does support an increase of Saharan runoff and Nile outflow at this time. However, it should also be considered that 1) MIS 6e is a period of increased sea-level height, which also influenced sapropel deposition (Rohling et al., 2015; Grant et al., 2016), and 2) the Ethiopian highlands sit within the monsoon domain; therefore, less substantial changes of monsoon precipitation could be reflected here and not be apparent elsewhere in Saharo-Arabia. For example, while SL71 Kln/Chl ratios do show a slight trough followed by a slight and rapid increase (which is characteristic of increased soil humidity; e.g., Ehrmann et al., 2017), this increase is not comparable to MIS 5e, 5c and 5a. This indicates that MIS 6e soil humidity did not reach equivalent levels, which may suggest MIS 6e rainfall increase was perhaps less intense and/or short-lived. Additionally, a comparably weak MIS 6e pluvial period is observed by slightly reduced RC09-166 $\delta D_{leaf\text{-}wax}$ values in the Gulf of Aden (Tierney et al., 2017), which again, do not reach levels of the MIS 7 and MIS 5 warm substages (Fig. 14). This would suggest a slight, but not substantial, change in the position of the tropical rain-belt. This is again corroborated by absence of speleothem growth at Mukalla or Hoti caves during MIS 6e. As these sites are sensitive recorders of tropical rain-belt position it is unlikely that the tropical rain-belt expanded into Arabia for a protracted period.

There is also little evidence for increased precipitation during MIS 6e from northern Saharo-Arabia. While speleothems continued to grow in the northern Negev (Vaks et al., 2006; Fig. 14), no speleothem growth was dated to MIS 6e within the southern Negev

(Vaks et al., 2006, 2010), indicating WMC intensity was not greatly enhanced when compared to MIS 7 or MIS 5 interstadials. This suggests that the 300 mm yr^{-1} isohyet remained in its current position, or, at the very least, precipitation to Saharo-Arabia did not exceed 300 mm yr^{-1} for a prolonged period.

Alluvial fan formation in the Hajar Mountains (Oman) provide evidence for enhanced rainfall at ~160-150 ka BP (Parton et al., 2015a). Phytoliths recovered from these sediments included a mixture of C_3 and C_4 grassland taxa, though pedogenic $\delta^{13}C_{ca}$ was closely aligned to C_4 signatures (Parton et al., 2015a). This record of increased precipitation is out of phase with speleothem growth at Hoti Cave (Fleitmann et al., 2011). Current precipitation (~180 mm yr^{-1}) facilitates the growth of rare and small stalagmites (Burns et al., 1998, 2001; Fleitmann et al., 2011). Therefore, any prolonged enhancement of precipitation above modern values should be represented in Hoti Cave speleothems. However, >20 m of aggradation of fine-grained alluvial sediments, including a shallow channel, sheetflood and an extensive palaeosol deposit (>3 m thick) at Al Sibetah, UAE, points to prolonged (though perhaps less intense) rainfall during mid MIS 6 (155 ka BP: Parton et al. 2015a). As previously mentioned, RC09-166 $\delta D_{leaf\text{-}wax}$ values do show enhanced precipitation in the Horn of Africa between 160-150 ka BP. This discrepancy between these records may be explained by less intense incursions of ISM storms which activated alluvial fans but have been insufficient to lead to speleothem deposition. Unfortunately, there is not currently a method to use alluvial fan data to clarify moisture source, and, as speleothems did not grow, this cannot be clarified by available methods.

Some records also suggests further wet periods throughout MIS 6. While some of these records point to increased humidity at ~155-150 ka BP (Ayalon et al., 2002; Parton et al.,

2015a; Grant et al., 2017), many terrestrial point to increased humidity at the glacial termination and MIS 6/5 transition or overlap with MIS 5e (Smith et al., 2007; Geyh and Thiedig, 2008). Other records, such as Soreq and Peqiin are difficult to relate specifically to precipitation amount changes due to their relationship with the isotopic composition of Mediterranean sea-water (Bar-Matthews et al., 2003; Rohling et al., 2015).

3.2.3.5 MIS 5 (130-71 ka BP)

The palaeoclimatic and palaeoenvironmental conditions of Arabia during MIS 5 has been increasingly related to the dispersals of *H. sapiens*. Due to the rarity of fossil finds, equifinality of genetic data and ambiguity of archaeological material, palaeoclimatic data have been used to offer timings for when the Saharo-Arabian deserts were traversable (e.g., Fleitmann et al., 2011; Bae et al., 2017; Groucutt et al., 2018). Furthermore, MIS 5 was the last time in which peak interglacial conditions occurred, prior to the Holocene Climatic Optimum. It is therefore useful as a comparative period, to detail changes in interglacial conditions throughout the Upper Pleistocene. As such, there is a growing body of palaeoclimatic and palaeoenvironmental data provided by both archaeological and palaeoclimate research initiatives. Three distinctly humid periods occurred during the interstadial conditions of MIS 5: MIS 5e (130-120 ka BP), MIS 5c (104-91 ka BP) and MIS 5a (85-71 ka BP). Current evidence shows that precipitation regimes in the Saharo-Arabia region underwent a dramatic intensification, forming vast lake and river systems (Breeze et al., 2015). The broader northern Indo-Pacific rim also shows a transition to increased rainfall (Blinkhorn et al., 2013; Beck et al., 2018; Chen et al., 2019), most likely related to northward migration of the tropical rain-belt (Fleitmann et al., 2003b, 2011; Beck et al., 2018).

Speleothems grew at Mukalla and Hoti caves during the MIS 5 interstadials. ^{230}Th ages of speleothems from both caves fall into MIS 5e, while Y97 (Mukalla) fell into MIS 5c and H4 fell into MIS 5a (Fleitmann et al., 2011). The excellent coherence of speleothem growth at these caves and small dating uncertainties means that the timing of wet periods can be precisely constrained to MIS 5e, 5c and 5a. $\delta^{18}O_{ca}$ of stalagmites from both caves also showed that MIS 5e was particularly intense when compared to preceding interglacials and the later Holocene wet period (Fleitmann et al., 2003a; Rosenberg et al., 2011; Fig. 14). The Holocene was a time in which large palaeolakes formed in the now arid interior and human societies expanded into these areas (Rosenberg et al., 2011, 2012, 2013; Jennings et al., 2013). δD_{FI} from H13 is consistent with previous findings, showing that the ISM and tropical rain-belt were situated further north than present climates (Fleitmann et al., 2003b). The height and width of Y99 and H13 was used to estimate that precipitation exceeded 300 mm yr^{-1}. This is in good agreement with more recent palaeoclimate simulations, in which 300-600 mm yr^{-1} of precipitation was estimated for southern Arabia (Jennings et al., 2015b).

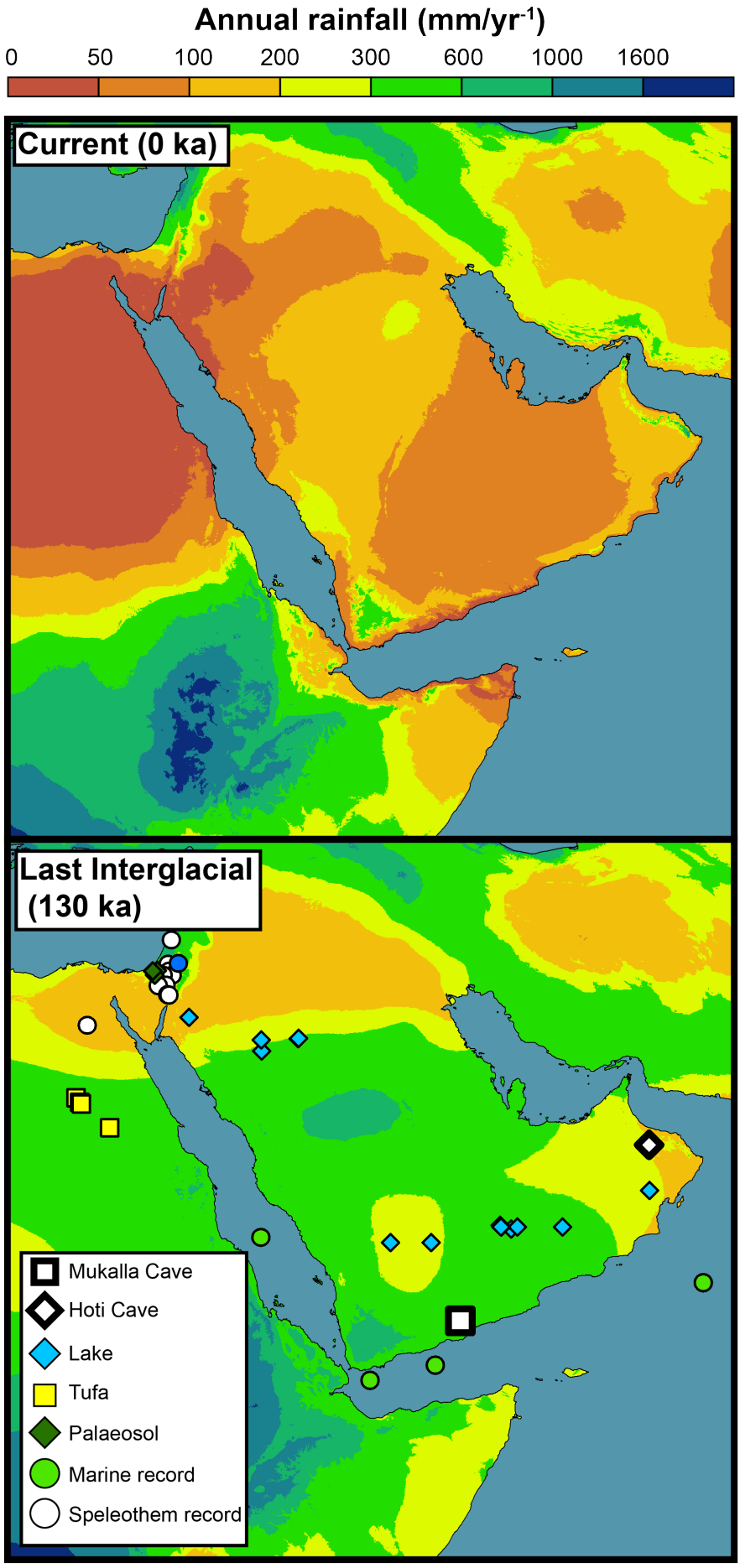
Annual rainfall (mm/yr-1)
0
50
100
200
300
600
1000
1600
Current (0 ka)
Last Interglacial (130 ka)
Mukalla Cave
Hoti Cave
Lake
Tufa
Palaeosol
Marine record
Speleothem record

Fig. 15. Current (1970-2000; Fick and Hijmans, 2017) and MIS 5e (Otto-Bliesner, 2006; Jennings et al., 2015b) *climate models of Arabian annual precipitation.*

Soreq Cave $\delta^{18}O_{ca}$ shows a transition to more negative values between 128.3 ka BP and 127.6 ka BP to 120.8 ka BP (Grant et al., 2012). Soreq Cave $\delta^{18}O_{ca}$ is frequently used as a precipitation record for the Levant. However, there is a strong association with compositional changes in Mediterranean Sea water $\delta^{18}O$, as seen in LC21 (Fig. 14). These are primarily governed by Saharan run-off and Nile outflow (where increased negative $\delta^{18}O$ is due to enhanced monsoonal precipitation), and Sea Surface Temperatures (Frumkin et al., 1999; Grant et al., 2012, 2016; Rohling et al., 2015). While Soreq Cave $\delta^{18}O_{ca}$ can therefore be used to show timing of tropical rain-belt migration, it is much more difficult to use it as a precipitation record for the northern Saharo-Arabian margins. Thus, independent precipitation records are required to understand hydrological changes in the Levant. Speleothems from the arid Negev desert offer a unique opportunity to show changes in precipitation intensity. Here, speleothem formation in the Negev matches findings of increased humidity during MIS 5. In particular, a clustering of ^{230}Th ages is observed during MIS 5e (Vaks et al., 2010), which show humidity increased in both the northern and southern areas of the Negev. These samples also show a clear $\delta^{18}O_{ca}$ gradient on a north-south transect, indicating that increased humidity was derived from intensified WMCs (Vaks et al., 2010). Using modern day distribution of active and inactive stalagmite deposition in the Levant and rainfall data, it was suggested that 300-350 mm yr^{-1} of annual rainfall was required for speleothem growth (Vaks et al., 2010). The

evidence for increased precipitation during later interstadials is less clear, with only a single ^{230}Th age (87.7 ± 1.4 ka BP – Even-Sid-Ramon mini-cave) falling within MIS 5b.

Further south, formation of palaeolake Mudawwara provides good evidence of the extent of MIS 5 humidity. During MIS 5e, Mudawwara covered an area of ~2000 km^2 and exceeded 40 m in depth (Petit-Maire et al., 2010), in an area which is now desert. ^{230}Th ages obtained from *Cerastoderma* shells show lacustrine environments were present during MIS 5e, 5c and 5a (Petit-Maire et al., 2010). Though, the origin of palaeo-precipitation is uncertain. The researchers argue that the size and depth indicate Mudawwara must have been supplied by moisture from both Mediterranean and monsoonal sources. The large catchment of Mudawwara extends into the southern Jordan highlands, where precipitation is estimated to have increased to 100-300 mm yr^{-1} (Jennings et al., 2015b). Though, could this alone have facilitated such a large lake in a highly evaporative environment? As mentioned, a clear north-south gradient observed in Negev stalagmites suggests the 300 mm yr^{-1} isohyet did not extend beyond southern Negev (Vaks et al., 2010). More recent models have estimated that a brief expansion of the WMC domain occurred at the onset of MIS 5e; although, these have also shown that summer rains contributed most to annual precipitation over Arabia until 120 ka BP (Gierz et al., 2017). Perhaps increased evaporation from the Red Sea and the development of synoptic troughs brought additional summer precipitation to the southern Levant (Waldmann et al., 2010)?

Arabian fluvio-lacustrine and alluvial fan formations are consistent with evidence of enhanced humidity within MIS 5e interstadials. Within MIS 5e, age uncertainties are generally more precise than preceding interglacials and allow these records to be more

accurately assigned to interstadial periods. In the Nafud there is a clear clustering of (TT)OSL ages centring within MIS 5e, MIS 5c and MIS 5a (Petraglia et al., 2012; Rosenberg et al., 2013; Parton et al., 2018; Fig. 14). In southern Arabia, ages tend to also cluster close to or prior to these periods (Rosenberg et al., 2011, 2012; Matter et al., 2015). However, age uncertainties do fall into these periods and speleothem evidence may therefore be used to confine these ages to the MIS 5 interstadials (e.g., Rosenberg et al., 2011, 2012).

Lacustrine microfauna/flora in palaeolake deposits detail conditions of the palaeolake environment. MIS 5e palaeolake sediments from the Nafud contain diatoms (*Stephanodiscus* cf. *rotula*, *Aulacoseira granulata*, *Fragilaria brevistriata*, *F. construens*, *F. construens v. venter*), which indicate deep freshwater lakes. MIS 5c (~105-100 ka BP) diatom assemblages reflect somewhat drier conditions (*Anomoeoneis sphaerophora, Campylodiscus clypeus, Mastogloia* spp, *A. crenulata* and *Meridion circulare*) (Rosenberg et al., 2013). More recent findings from the Jubbah basin are consistent with this, in which shallower and more brackish conditions were reported during MIS 5a compared to MIS 5e (Parton et al., 2018). Nevertheless, these diatom assemblages indicate lakes were perennial features of interglacial Arabian environments (Rosenberg et al., 2011, 2012). In the Rub al Khali, ostracods *Darwinula stevensoni* and *Unio* sp. demonstrate conditions with fresh, open running water within MIS 5e (Rosenberg et al., 2011). Additionally, the presence of *Unio* is indicative of well stratified faunal communities, which would have included large freshwater fish (Rosenberg et al., 2011, 2012; Matter et al., 2015). A key finding of both ostracod and diatom assemblages from these study areas confirms speleothem data which indicates MIS 5 wet phases were more intense than the Holocene wet phase.

Recent excavations from Al-Wusta have provided an insight into the palaeoecological conditions of northern Arabia during late MIS 5. Marlstone absent of $\delta^{18}O$ and $\delta^{13}C$ covariance and diatom flora including *Aulacoseira italica* and *Aulacoseira granulate* show a perennial shallow, alkaline lake with freshwater input formed (Groucutt et al., 2018). Palaeontological remains included *Hippopotamus*, *Kobus*, *Varanus*, *Struthio* and *Pelorovis*, which were taken to infer a grassland environment with perennial standing waterbodies (Groucutt et al., 2018). Perhaps most importantly, the presence of a *H. sapiens* phalanx demonstrates that humans could inhabit Arabia during MIS 5a. As mentioned previously, lake diatoms (Rosenberg et al., 2013) and speleothem $\delta^{18}O_{ca}$ (Fleitmann et al., 2011) demonstrates that MIS 5c/a was a relatively 'weak' monsoon period when compared to MIS 5e. This leads to two important points: 1) MIS 5a environmental amelioration was sufficient for *H. sapiens* occupation. These conditions may therefore be used to benchmark the environmental settings necessary for *H. sapiens* occupation of Arabia. 2) If a comparatively 'weak' monsoon was sufficient for *H. sapiens* occupation, what may this tell us about the comparatively 'strong' monsoon periods and their habitability?

Alluvial fan formations at Al Sibetah, Oman, are in good coherence with palaeolake formations. Three phases of stream channel activation occurred within MIS 5e, 5c and 5a (Parton et al., 2015a). MIS 5e sediments contained the greatest Panicoid values (13%) and were highest in woody taxa. While $\delta^{13}C_{ca}$ values between –3.45‰ and +0.58‰ suggest a dominance of C_4 taxa, Parton et al. (2015a) explained that the higher proportion of clastic and detrital material may convolute an environmental signal. A common issue with using $\delta^{13}C_{ca}$ as a vegetation proxy is that $\delta^{13}C_{ca}$ can be influenced by numerous

factors that are difficult to account for (e.g., temperature, atmospheric $\delta^{13}C$ contribution, soil humidity and porosity, and vegetation density). These dilute the environmental signal of $\delta^{13}C_{ca}$ and, in this case, may underestimate the vegetation signature and could explain the disparity with phytolith data. Nevertheless, the geological and environmental records detail more mesic conditions within MIS 5e and 5c, with more xeric conditions in MIS 5a (Parton et al., 2015a).

Phytolith analysis from the Jabal Faya archaeological site offers insight into terrestrial floral communities between 127-95 ka BP in Arabia. Sediments of the archaeological horizons (assemblage C) are high in organic matter and silt – indicating humid conditions (Bretzke et al., 2013). Pooids range between 10-40% of the assemblage, Panicoids range between 5-20%, Chloridoids range between 2-20% and long grasses between 10-20%. Cyperaceae, Asteraceae, Palmae and other grasses are also present within assemblage C in small quantities – evincing mixed C_3/C_4 grassland. These taxa are repeated in lower quantities in the younger assemblage B (90-40 ka BP); however, absence of Pooid phytoliths indicates slightly warmer conditions (Bretzke et al., 2013). Large disparities of phytolith quantities are present in assemblage B; none are present in the later phases which can be attributed to the arid conditions of MIS 4.

The emerging picture is that increases of precipitation during MIS 5 led to formation of "green" environments. However, there have been two competing models that aim to describe the environments of Arabia. One suggests that the desert of the Sahara disappeared completely (Larrasoaña et al., 2013). While Arabia was not included in this study, the close proximity and similar controls on precipitation suggest disappearance of the desert in the Sahara should have been echoed in Arabia. Another model, however,

suggests that continued deposition of marine dust records and the biogeography of fauna uncovered in northern Africa indicates arid to semi-arid areas remained components of the northern Saharo-Arabian landscapes (Scerri et al., 2014a). This model is consistent with simulated MIS 5e rainfall, in which areas of northern Arabia received less than 300 mm yr^{-1} of rainfall (Fig. 15). Current Arabian environments that receive <300 mm yr^{-1} are frequently characterised by desert to semi-desert flora (Miller and Cope, 1996), which suggests that these northern areas were not necessarily "green". These findings highlight a degree of environmental heterogeneity; whereas past Arabian environments have often been broadly characterised as "grasslands" or "savannahs".

3.2.3.6 MIS 4 (71-57 ka BP)

MIS 4 is characterised by widespread aridity in Arabia (Fleitmann et al., 2011; Rosenberg et al., 2013; Parton et al., 2015b) and the broader northern Indo-Pacific rim (Beck et al., 2018; Chen et al., 2019). This follows this transition to glacial conditions after MIS 5a. Due to the erosive nature of hyper-arid deserts, very few terrestrial archives are available from this period.

Marine records from the Mediterranean (ODP 967 and LC21) do not record decreased hematite dust (ODP 967: Larrasoana et al., 2003), sapropel deposition (ODP 967: Larrasoana et al., 2003; Grant et al., 2017; LC21: Grant et al., 2012, 2016)(Larrasoana et al., 2003; Grant et al., 2017, LC21: Grant et al., 2012, 2016) or decreased $\delta^{18}O_{G.\ ruber}$ (LC21: Grant et al., 2012, 2016), suggesting that Nile outflow and Saharan run-off reduced following MIS 5a. This is corroborated by a rapid influx of Kln into the Mediterranean, following desiccation of MIS 5a soils (Ehrmann et al., 2017). A rise of

Kln/Chl to normal (desert) input occurred throughout MIS 4 (Ehrmann et al., 2017). On the contrary, a major phase of speleothem growth at Susah Cave, Libya, was recorded between 65-61 ka BP (Hoffmann et al., 2016) and could be a result of an enhancement of the Atlantic westerlies during winter. However, there are few very records available to corroborate these findings.

In the northern Levant, a decline of arboreal pollen and rise of steppic taxa at Yammouneh conforms to the trend of global aridity (Gasse et al., 2015). This is corroborated by the Lake Van arboreal pollen and deciduous oak records, which indicate reduced precipitation during MIS 4 (Pickarski et al., 2015). Adversely, a recently published marine record (MD-9509) shows that coniferous pollen was low when compared to MIS 3 and approximates to MIS 5a levels (Langgut et al., 2018). With all pollen records, however, it is necessary to consider the taphonomy of the pollen and record formation processes. MD-9509 is situated in the Mediterranean Sea, and therefore has 1) has a larger catchment than the lake records and, 2) pollen transport will be determined by both atmospheric and ocean currents. Terrestrial pollen records, such as Yammouneh, may therefore provide more localised environmental signals.

In the southern Levant, speleothems continued to form in the northern Negev, suggesting that there was no significant reduction in MIS 4 WMC intensity compared to modern records (Vaks et al., 2006). No speleothem growth in the southern margins was recorded (Vaks et al., 2010), suggesting that WMCs were not significantly enhanced within MIS 4. While palaeosol formation on the Sinai Peninsula was dated to 68 ± 17 ka BP (Roskin et al., 2013), these large uncertainties also overlap with MIS 5, where there is more secure

evidence of further palaeosol formations (Roskin et al., 2013) and generally enhanced interregional rainfall.

Further south, marine records from the Red Sea, Arabian Sea and Gulf of Aden conform to the arid trend. RC09-166 $\delta D_{\text{leaf-wax}}$ is high and ODP 721/722 terrigenous dust input is enhanced, showing arid conditions in the Horn of Africa (deMenocal, 1995; Tierney et al., 2017). Similarly, KL 11 (Red Sea) shows larger median grain sizes (Fleitmann, 1997). KL 15 does show a peak in smaller grain sizes, though, this is not comparable to MIS 5 peaks (Fleitmann, 1997). While a Red Sea marine sediment core record (KL 09) shows a peak minima in hematite and Ti/Ca ratios (70-65 ka BP; Roberts et al., 2011), this is not corroborated by the aforementioned records. On land, no speleothem deposition was recorded at Mukalla or Hoti caves (Burns et al., 2001; Fleitmann et al., 2003b, 2011; Fleitmann and Matter, 2009). Taken together, this shows that the monsoon domain was suppressed during MIS 4 and that arid conditions prevailed in Arabia.

Low sea-levels during MIS 4-3 extended the Arabian coast, exposing now submerged landscapes (Ghoneim, 2008; Parker and Rose, 2008; Bailey, 2010). Faure et al. (2002) argued that low sea-level stands led to seepage of aquifers – due to alleviation of seawater mass – which formed springs and coastal wetlands (or mangroves) with diverse ecologies (Faure et al., 2002; Ghoneim, 2008; Parker and Rose, 2008; Erlandson and Braje, 2015). Groundwater seepage currently occurs in the coastal areas of the Sahara and northern coast of the UAE (Ghoneim, 2008). These so called “coastal oases” were speculated to have been present between ~115 ka BP and ~6 ka BP – after the sea-level high-stand of MIS 5e (Parker and Rose, 2008). A favourable period of enhanced precipitation at ~70-

65 ka BP (based on KL 09) was argued to have made the landscapes of the horn of Africa and southwestern Arabia attractive for dispersal (Rohling et al., 2013). However, 1) the southern Arabian Peninsula is a highly evaporative and karstic landscape, with groundwater aquifers that requires long term precipitation to remain active. Speleothem records, excellent records of groundwater conditions, have shown that aquifers can dry rapidly as a result of shifting precipitation in less than 100 years (Fleitmann et al., 2007). Without significant increases in rainfall, it is unlikely that any such oases could be supported. And, 2) evidence for enhanced monsoon precipitation at 70-65 ka BP observed in KL 09 is yet to be corroborated by other marine sediment core records (e.g., KL 11, KL 15 and RC09-166) or speleothem data (Mukalla and Hoti caves).

3.2.3.7 MIS 3 (57-29 ka BP)

Another Arabian "green" period is considered to have occurred during MIS 3. However, the evidence of this is inconsistent between records, showing some spatial and temporal variability and perhaps a much less substantial increase in precipitation. MIS 3 is a time of highly variable climates at a global level. Orbital eccentricity is reduced compared to peak interglacials and insolation does not see the same high amplitude variations. Though, Greenland ice-cores show large variations in $\delta^{18}O$ (Grootes et al., 1993; Svensson et al., 2008), known as Dansgaard-Oeschger cycles. Similarly, Heinrich events H5-3 also fall into MIS 3 (Bond and Lotti, 1995). These are detectable in numerous global records, showing they had significant impact on global climate regimes.

RC09-166 $\delta D_{leafwax}$ ‰ shows a negative peak when compared to MIS 4 and MIS 2; however, this peak is not comparable to the negative peaks of MIS 5e, 5c, 5a, the Holocene and the most recent values. Similarly, ODP 721/722 also records somewhat

reduced terrigenous dust. Taken together, this may suggest enhanced precipitation in the Horn of Africa compared to glacial periods, though absence of speleothem growth and high $\delta D_{leaf\text{-}wax}$ suggests precipitation was lower than today. LC21 $\delta^{18}O_{G.\ ruber}$ ‰, however, shows insufficient evidence of increased Saharan run-off or Nile discharge during MIS 3 (Grant et al., 2012). This is also evidenced by lack of clear sapropel (S2) formation in ODP 967, despite XRF scanning to identify invisible sapropels (Grant et al., 2017). Similarly, SL71 does not show the distinct troughs in Kln/Chl values that represent increased Saharan soil humidity (Ehrmann et al., 2017). KL 11 and KL 15 median grainsizes are also larger during MIS 3 than within MIS 5 and the Holocene (Fleitmann, 1997).

Conversely, speleothem growth in the northern Negev is continuous throughout MIS 4 and MIS 3 (Vaks et al., 2006). This has recently been matched by speleothem growth from Susah Cave, Libya (Hoffmann et al., 2016). Main growth phases at Susah were recorded at 65-61, 52.5-50.5 and 37.5-33 ka BP, with shorter-lived growth phases occurring throughout MIS 4 and into MIS 3 (Hoffmann et al., 2016). Similarly, palaeosol formation on the Sinai Peninsula was dated to 45 ± 13 ka BP and 53 ± 17 ka BP (Roskin et al., 2013; Fig. 14). Though, increased humidity is not observed in the southern Negev (Vaks et al., 2006, 2010), suggesting that the 300 mm yr^{-1} isohyet did not expand to the southern MIS 5e position.

The evidence for enhanced precipitation in Arabia is variable between records. Early radiocarbon dating of palaeolakes in the Rub' al Khali (McClure, 1976, 1984) and Nafud (Garrard et al., 1981) suggested a prolonged wet period from 35-20 ka BP. Recent redating of these sediments using OSL and TT-OSL techniques has provided ages falling

within MIS 5 (Rosenberg et al., 2011, 2012, 2013). The younger radiocarbon ages were interpreted to have been a result of contaminating material. However, further evidence of enhanced rainfall during MIS 3 is becoming available. Three fluvial deposits at Al-Quwaiayh, Saudi Arabia, were OSL dated to 53.9 ± 4.2 ka BP, 54.0 ± 5.4 ka BP and 38.8 ± 3.1 ka BP (McLaren et al., 2009). Though, unlike the MIS 5 units, no clearly laminated sediments were recorded, suggesting MIS 3 wet phases may represent high energy floods.

Further evidence of MIS 3 rainfall was recorded in southern Arabia (Parton et al., 2013; Hoffmann et al., 2015). Playa-like sediments from Wadi Mistral formed within a dammed ephemeral lake in Oman, between 53.0 ± 5.7 and 44.7 ± 6.5 ka BP (Hoffmann et al., 2015). Based on the geomorphological similarities with modern aggregated sediments, Pleistocene sediments were considered to have resulted from brief and intense storms in the Omani Highlands. Rather than showing any significant changes in precipitation regimes, it was considered that climates were not dissimilar from modern (Hoffmann et al., 2015). Age uncertainties overlap with grassland and lake formation at Jabal Aqabah, Saudi Arabia. Aeolian sands between lake sediments were dated to 61 ± 8.3 ka BP, 58 ± 15.8 ka BP and 57 ± 8.8 ka BP (Parton et al., 2013), suggesting the MIS 4-3 transition was characterised by punctuated increases in humidity in southern Arabia. At Jabal Faya, increased Panicoid and Chloridoid (C_4 taxa) were present within assemblage A (~40-38 ka BP). Compared to preceding MIS 5 assemblages, this suggests more arid environments during MIS 3 (Bretzke et al., 2013).

However, no speleothems from Mukalla or Hoti caves were dated to MIS 3. As demonstrated above, speleothem growth at Mukalla and Hoti caves are sensitive records of tropical rain-belt position. Though, speleothem growth was recorded at Moomi Cave

on Socotra Island from 55-42 ka BP (Burns et al., 2003). Two-thirds of $\delta^{18}O$ variation of M1-2 could be related to precipitation amount, showing that precipitation was enhanced during D/O 13-9 (Burns et al., 2003). Yet, lack of speleothem formation at both Mukalla and Hoti cave indicates that any precipitation was not sufficient to recharge the aquifers above these more northern caves on the mainland of the Arabian Peninsula. Current annual precipitation of ~180 mm yr^{-1} facilitates infrequent growth of small stalagmites at Hoti Cave. Absence of speleothems dated to MIS 3 suggests precipitation may have been less than current amounts. As speleothem growth at these caves records long term regional changes in precipitation, increased MIS 3 precipitation may be undetectable in these records. In this case, low-level but sustained (or conversely, sudden and short-lived storms) may explain why MIS 3 precipitation is only detected in more sensitive records (Parton et al., 2013, 2015a, 2015b; Hoffmann et al., 2015).

In northern Arabia, recent findings from the Jubbah palaeolake (Nafud) has shown MIS 3 precipitation was sufficient to form standing waterbodies (Parton et al., 2018). These formations were dated to 66.3 ± 8.0 (MIS 5a-3) and 56.2 ± 8.3 ka BP (MIS 4-3). Bivalves from these sediments included *Cerastoderma* sp., *Mytilopsis* sp., *Hyddrobia* cf. *lacteal* and *Cyprideis forosa*, indicating more brackish conditions than MIS 5 (Parton et al., 2018). This suggests precipitation was less than within MIS 5 interstadials, as has previously been argued (Parton et al., 2015b). Similarly, a relict lake deposit was uncovered further south at Al Marrat (Jennings et al., 2016). While OSL dating was inconsistent between single grain and multigrain analyses, a shallow palaeolake with grassland surroundings has been dated to ~60-50 ka (single grain). Jennings et al. (2016) related palaeolake formation to an intensification of the monsoon domain; however, there are currently no terrestrial records that can establish an MIS 3 moisture source. If an

enhanced monsoon brought increased precipitation to northern Arabia, surely this would be conspicuous within Mukalla and Hoti cave speleothem records (see below)? And if the WMC domain was enhanced, surely greater speleothem deposition would have occurred in the southern Negev (Vaks et al., 2006, 2010)? To establish potential moisture source, analysis of palaeolake gypsum ($CaSO_4 \cdot 2H_2O$) fluid inclusion $\delta^{18}O$ and δD values could be compared to local meteoric lines to establish changing precipitation regimes (e.g., Fleitmann et al., 2003b; but following the methods outlined by Koehler and Wassenaar, 2012).

In summary, the evidence of enhanced rainfall during MIS 3 is inconsistent between palaeoclimate records. While enhanced rainfall is recorded within MIS 3 in some marine records, this is not comparable to modern day climates. Similarly, lack of speleothem growth at Mukalla or Hoti cave indicates increased MIS 3 precipitation did not substantially increase precipitation to southern Arabia. Although evidence of palaeolake formation in the Nafud may suggest an increase of the WMC domain, this is not corroborated by speleothem growth in the southern Negev. As speleothem activation in the southern Negev and at Mukalla Cave required ≥300 mm yr^{-1} of precipitation, it is unlikely that MIS 3 precipitation breached this threshold for a prolonged period.

3.2.4 Limitations of current palaeoclimate records

3.2.4.1 Marine records

Marine sediment cores from the Gulf of Aden, Red Sea and Mediterranean Sea have provided long continuous palaeoclimate records of the Saharo-Arabian deserts, spanning almost 8 million years (e.g., deMenocal, 1995). Differing methods of analysis (i.e., the measurement of grain size, terrigenous dust percentage, hematite dust concentration and

elemental composition) have been applied to these cores. The underlying assumptions of all these methods suggest differing levels of humidification of soils will lead to material differences within the cores. During wet phases, hematite (Fe_2O_3) dust decreased in the Mediterranean (ODP 967, Larrasoana et al., 2003) and Red Sea (KL 09, Roberts et al., 2011), median grain sizes decreased in the Red Sea and Gulf of Aden (KL 11 and KL 15, Fleitmann, 1997), and terrigenous dust increased in the Arabian Sea (OPD 721/722: deMenocal, 1995, 2004). There is good coherence between many of these archives, showing increased humidity during peak interglacial periods. Though, low resolution of these records means high-resolution climatic variability cannot be studied at length. Another issue is that marine sediment cores can be influenced by numerous non-linear factors. For example, wind strength can influence mobilisation of dust; changing wind direction can affect deposition within a specific record; productivity/erosion can influence dust quantities and particle size; large catchment areas and ocean current strength can distort local signals. For example, clear 'arid' periods are not statistically distinct within ODP 721/722 (Trauth et al., 2009) and this record has also been used to identify broader East African and Arabian climates (deMenocal, 1995; Clemens and Prell, 2003). Thus, independent terrestrial records are required to mitigate these uncertainties.

Sapropel layers of Mediterranean ocean cores have been used to identify periods of increased Nile outflow and Saharan run-off (Larrasoana et al., 2003; Rohling et al., 2015; Williams et al., 2015; Grant et al., 2016, 2017). This means that sapropel formations may be used to show periods of increased monsoonal rainfall over the Ethiopian highlands and the Sahara (Grant et al., 2017), which is linked to Arabia through the dynamics of the tropical rain-belt. Sapropel formations generally centre within the peak interglacial

periods and are coetaneous to the hematite dust minima and negative Mediterranean $\delta^{18}O$ (Larrasoana et al., 2003; Grant et al., 2016). Long records of sapropel formations means these may detail periods of Saharo-Arabian wet periods into the Pliocene. However, as marine records, sapropel formations can also be influenced by broader Mediterranean conditions (Atlantic input, glacial ice-melt, riverine input, black sea input). Furthermore, sapropels are also affected by post-depositional alterations (such as oxidisation), which may hinder identification within an ocean core.

3.2.4.2 Fluvio-lacustrine/alluvial records

Fluvio-lacustrine and alluvial sediments are one of the most widely studied palaeoclimate archives from the Arabian Peninsula. As well as detailing the timing of wet periods, they can also preserve archaeological remains, meaning they have been studied by both geological and archaeological surveys. Palaeolake cores from the Nafud desert provide the longest terrestrial record of rainfall, with interglacial humid periods up to ~500 ka BP (MIS 13) (Rosenberg et al., 2013; Stimpson et al., 2016). Yet, there are uncertainties when using palaeolake sediments alone as reorders of regional changes in rainfall. For instance, in comparison to speleothems, these are much more sensitive recorders of precipitation, which may be useful to identify local flooding events (e.g, McLaren et al., 2009). However, the high porosity of dune sands in Arabia does not facilitate storage of rainwater, which facilitates ephemeral lake formations between dunes following brief storms under current climates. The sudden occurrence and brief nature of these rains does not provide sufficient time for soil generation, such that large scale 'green deserts' do not form. Similarly, recent dating of Saharan scarp and scarp-foot depression sediments has shown that groundwater may discharge after thousands of years following wet periods

(Abotalib et al., 2019). This could be represented within sensitive hydrological records, despite no apparent changes in precipitation regimes. Thus, careful consideration must be taken when using fluvial/lacustrine/alluvial deposits alone to determine regional 'green' periods.

Another potential short coming is that palaeolake sediments are dated via Optically Stimulated Luminescence (OSL) techniques, applied to underlying and overlying aeolian sediments. This means that direct ages for the lakes are not attained. When applied to underlying sediments, the working assumption is that these sands become stabilised by increased precipitation. While for some palaeolakes this holds true (e.g., Groucutt et al., 2018), this is not always the case. Another issue is that OSL dating can contain large uncertainties and age inversions are common. For MIS 5 sediments, age uncertainties are >1 ka BP (Rosenberg et al., 2011, 2012, 2013), and may be subjected to Bayesian statistical modelling in order to reduce uncertainties (Clark-Balzan et al., 2017; Groucutt et al., 2018). Thus, precisely plotting these to palaeoclimate datasets and specific interglacial stages is not always straightforward (e.g., Groucutt et al., 2018). The large age uncertainties and absence of direct ages through a sequence means that high-resolution palaeoclimate records are not always easy to produce.

3.2.4.3 Speleothems

Subterranean cave stalagmites provide a terrestrial palaeoclimate record protected from the erosive nature of desert environments. Compared to OSL dating of lake sediments, ^{230}Th dating of speleothems (e.g., Cheng et al., 2013) provide precise onset and termination dates of humid periods (Fleitmann et al., 2011), with uncertainties of <1%.

Moreover, as precipitation must significantly outweigh evaporation, these can be used to detail prolonged and dramatic increases in regional precipitation. Though, traditional analyses of speleothem $\delta^{18}O$ and $\delta^{13}C$ are influenced by numerous factors, meaning their palaeoclimatic interpretation is not necessarily straightforward. For example, the *amount effect* has significant control of $\delta^{18}O_{precipitation}$ in Arabia (Burns et al., 2001; Fleitmann et al., 2004a, 2011; Cheng et al., 2009b); however, $\delta^{18}O_{precipitation}$ is also dependent on moisture source $\delta^{18}O$ (which can be altered over time: Herold and Lohmann, 2009; Tindall and Haywood, 2015; Gierz et al., 2017) and airmass history (Lachniet, 2009; Beck et al., 2018). Moreover, It is also not always possible to relate $\delta^{13}C_{ca}$ to a vegetation signature, as $\delta^{13}C_{ca}$ is also influenced by 1) density of vegetation, (2) soil thickness and moisture, (3) biological activity within the soil, (4) recharge conditions, (5) prior calcite precipitation, and (6) kinetic fractionation during calcite precipitation; the latter factor is influenced by cave air PCO_2 and drip rate (Baker et al., 1997; McDermott, 2004; Wong and Breecker, 2015; Breecker, 2017; Mickler et al., 2019). Recently developed techniques in trace-element analysis (particularly Sr/Ca and Mg/Ca values) are showing potential as independent palaeoclimate proxies (e.g., Fairchild et al., 2000; Fairchild and Treble, 2009; Häuselmann et al., 2015; Treble et al., 2015). Combination with traditional $\delta^{18}O_{ca}$ analysis may therefore help to distinguish between local changes in precipitation regimes and changes of airmass history. Whereas, combination with $\delta^{13}C_{ca}$ analysis can provide additional information on soil processes (Badertscher et al., 2014; Häuselmann et al., 2015).

Analysis of speleothem fluid inclusion δD from Hoti Cave (northern Oman) allowed comparison to modern local meteoric waterlines from northern Oman (mostly WMC) and

southern Oman (mostly ISM) (Fleitmann et al., 2003b). Findings showed that ISM precipitation became the dominant source of moisture during past interglacial periods. Yet, in this study, only δD_{FI} was analysed. $\delta^{18}O_{FI}$ was calculated through global precipitation δD and $\delta^{18}O$ relationships, as at the time of publication, there were ongoing discussions concerning the post-depositional alteration and exchange between $\delta^{18}O_{FI}$ and the parent $CaCO_3$ Oxygen. Also, contemporary methods of O_{FI} extraction resulted in large analytical fractionation and required significant correction. More recent findings have shown that only negligible interaction takes place between O_{FI} and carbonate O_{ca} (Meckler et al., 2015). Recent advances in the extraction of O_{FI} have also reduced the analytical fractionation (Affolter et al., 2014, 2015; Meckler et al., 2015), meaning no correction is required.

3.2.5 Summary

The emerging picture provided by palaeoclimate records is that Arabia was subjected to increased precipitation during peak interglacials and warm substages. This establishes a clear relationship between low glacial boundary conditions, peaks in orbital eccentricity and precession forced NHI maxima. However, the relationship between peaks in NHI during periods of relatively high glaciation (e.g., throughout MIS 8, 6 and 3) and Arabian wet periods is less well established. However, there remain significant gaps in the palaeoclimate record of Arabia, including: (1) while marine records extend to 8 Ma, terrestrial archives are currently limited to 500 ka BP (Rosenberg et al., 2013) and are not particularly well confined beyond 130 ka BP. This means that palaeoclimate reconstructions for older periods are currently based on marine sediment records; however, extended terrestrial records are required to test and mitigate the uncertainties of marine records. (2) There are disagreements on which moisture source brought increased

precipitation to Arabia during peak interglacials, especially the Holocene (Fleitmann et al., 2003b; Rosenberg et al., 2013; Enzel et al., 2015; Engel et al., 2017). This means there is limited information concerning seasonal changes of the 'green' environments. (3) The intensity differences between interglacials have not been studied at length (but see Fleitmann et al., 2011). This means the current understanding of Arabian palaeoclimate is limited to "wet" and "dry" periods. Furthermore, there are few high-resolution records available from terrestrial archives, thus variability throughout pluvial periods is largely unknown.

3.3 Hominin dispersals

3.3.1 Appearance of the genus *Homo* and the earliest dispersals

Hominins (defined here as all members of the tribe *Hominini* excluding *Pan*) appeared in Africa ~4.37-4.2 Ma (White et al., 2006; Wood and Boyle, 2016). One of the earliest hominins and the putative ancestor to *Homo*, *Australopithecus*, is considered to have evolved from either *Ardipithecus*, *Sahelanthropus* or *Orrorin* (or successively: *Sahelanthropus – Orrorin – Ardipithecus – Australopithecus*). Not only does poor chronological control, low sample size, taxonomical definitions and the challenges of the theoretical approaches to evolution convolute the ancestral position of *Ardipithecus*, *Sahelanthropus* and *Orrorin*, but their statuses as hominins is also debated (Wolpoff et al., 2002; Suwa et al., 2009; White et al., 2009; Wood and Boyle, 2016). The emergence of *Homo* is equally unclear, due to similar issues (Kimbel and Villmoare, 2016; Villmoare, 2018). That, however, is beyond the scope of this project. What may be said is that the earliest candidates of the *Homo* genus appeared in Africa between 2.7 and 2.2 Ma (Villmoare et al., 2015; Wood and Boyle, 2016), and a "modern" anatomy

(facultative bipedal morphology, low inter-membral index) had appeared by 1.6-1.4 Ma (Brown et al., 1985; Walker and Leakey, 1993; McDougall et al., 2012).

Fossil finds from Dmanisi, Georgia, demonstrate that by 1.8 Ma, early *Homo* species had dispersed from Africa (Gabunia et al., 2000; Lordkipanidze et al., 2005, 2013; Messager et al., 2011). The complicated relationship of early *Homo* species (*H. habilis*, *H. georgicus*, *H. erectus*, *H. rudolfensis* and *H. ergaster*) (Spoor et al., 2007; Wood and Boyle, 2016) means it is uncertain if the Dmanisi fossils represent a *H. habilis* or an early *H. erectus/ergaster* dispersal. Some have argued the Dmanisi fossils represent a dispersal of *H. habilis*, which was subsequently overprinted by a *H. erectus sensu lato* (assuming *H. ergaster* is not distinct) dispersal (Palombo, 2013). Others have argued that, following a *H. habilis* dispersal, *H. erectus* developed within Asia (Dennell and Roebroeks, 2005); whereas *H. ergaster* developed within Africa (Dai et al., 2016). An extremely linear evolutionary view suggests the Dmanisi fossils can be lumped into a group combining *H. erectus* and *H. ergaster* (*Homo erectus ergaster georgicus*) (Lordkipanidze et al., 2013), though this is not widely accepted (e.g., Spoor, 2013).

The earliest dispersal of hominins has seldom been discussed in terms of Saharo-Arabian climatic optima. Environmental considerations have primarily focussed on either climate conditions in East Africa (as "push" factors) (deMenocal, 1995, 2004; Shultz and Maslin, 2013; Maslin et al., 2014; Maslin and Brierley, 2015) or Eurasia (as "pull", or facilitative, factors) (Dennell, 2008; Bettis et al., 2009; Messager et al., 2010b, 2010a; Muttoni et al., 2010; Kahlke et al., 2011; Dennell and Petraglia, 2012; Blain et al., 2014). For example, Maslin et al. (2014) argued increased precipitation in East Africa facilitated expansions of species that fell within the hominin food chain, thus leading to hominin population

explosions and dispersal through competition pressure. Alternatively, presence of warm temperate grasslands of Eurasia was argued to support occupation of savannah-type species, including early *Homo* (Dennell, 2010; Blain et al., 2014). While both of these models provide valuable insights into the palaeoclimate context for how dispersal could be initiated and facilitated, they do not consider whether the Saharo-Arabian deserts were occupiable and traversable. In other words, there may have been push factors in East Africa at time period x, but how was dispersal possible if no synchronous pull factors prevailed in the Saharo-Arabian desert? And, in turn, how could dispersal into Eurasia have been facilitated?

Other approaches to understanding early *Homo* dispersal have focussed on the anatomical and cognitive adaptations. In particular, the appearance of "modern" postcranial morphologies (as observed on the Narioktome WT-15000 and Dmanisi specimens) was considered to have increased locomotor efficiency and the potential for long distance travel, thereby leading to range expansion and dispersal of early *Homo* (Walker and Leakey, 1993; Lordkipanidze et al., 2007; Pontzer et al., 2010). Prior to this, it was argued that larger cranial capacities of *H. erectus* and the development of Acheulean (hand-axe) technologies – as well as social and other behavioural adaptations related to brain-size – could have facilitated dispersal by increasing the adaptive response to novel environments (Potts, 1996, 1998a, 1998b). As the earliest archaeological sites outside of Africa contain mode-1 (Oldowan) tool assemblages (Mgeladze et al., 2011; Zhu et al., 2018; Scardia et al., 2019), this argument was later revised to suggest that dispersals may have been facilitated by the development of Oldowan technologies (Agustí and Lordkipanidze, 2011). Yet, inconsistent first appearance datum (FAD) between Oldowan technologies and the earliest evidence of hominins outside of Africa convolutes this

relationship. Conversely, the growing evidence that the much later *H. sapiens* dispersal was facilitated by ameliorated conditions of the Saharo-Arabian deserts (discussed below) – despite arguable being more behaviourally flexible and technologically complex – suggests that early *Homo* dispersals were regulated by changes in Saharo-Arabian environmental conditions.

Arabia possesses a surprisingly rich Lower Palaeolithic record (Fig. 16). Oldowan tool typologies have been reported from sites across north-western, western and southwestern Saudi Arabia, Yemen and Oman (Groucutt and Petraglia, 2012 and references therein). Moreover, an Oldowan site from Perin Island raises questions about the possibility of Lower Palaeolithic dispersals across the Bab el Mandeb straits – despite no evidence for land bridges between East Africa and Arabia since the Miocene (Fernandes et al., 2006). However, no precise absolute dating has been applied to the Oldowan record. This uncertainty is exacerbated by the presence of Oldowan-like artefacts mixed with Holocene artefacts (Groucutt and Petraglia, 2012), and some similarities with MSA artefacts (Whalen and Schatte, 1997). Moreover, many of these artefacts are made from quartzite (Whalen and Schatte, 1997) which may have played a role in artefact form (Groucutt and Petraglia, 2012), condition the perceived sophistication and influence the notion of industry affiliations. If, however, this data is taken at face value, it highlights the role of Arabia as a key area for hominin dispersals from Africa.

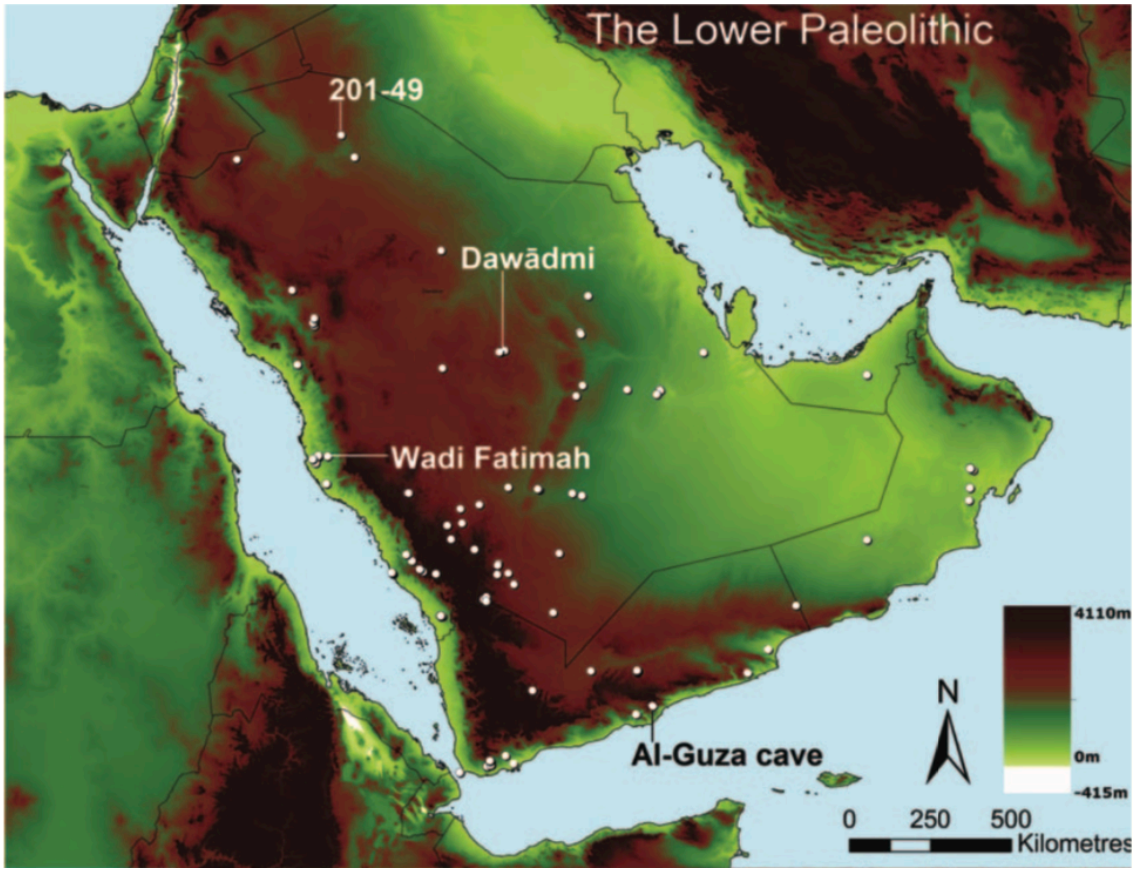

Fig. 16. Lower Palaeolithic archaeological sites in Arabia (after Groucutt and Petraglia, 2012).

If hominin dispersal was dependent on favourable climatic conditions of the Saharo-Arabian desert belt, there is no reason to doubt that hominins could disperse during potentially earlier ameliorated states prior to 1.8 Ma (Dennell and Roebroeks, 2005). Recent archaeological finds from China (Zhu et al., 2018) and the Levant (Scardia et al., 2019), point to hominin occupation of Eurasia between 2.5 and 2.0 Ma. Dispersals during this time may have been related to broader dispersals of African fauna. Appearances of non-migratory African fauna – such as *Propotamochoerus provincialis* and *Kvabebihyrax kachethicus* – in the Levant ~2.6 Ma (Kahlke et al., 2011) suggest green corridors connected sub-Saharan African and the Levant. These could have provided

windows for hominin dispersals, which may have resulting in hominin occupation in the Levant soon after 2.5 Ma (Scardia et al., 2019); however, there is poor chronological control for the timings of these windows and limited archaeological/fossil data for earlier hominin dispersals (Ronen, 2006; Dennell, 2008; Zhu et al., 2018). Yet, the identification of earlier possible dispersal windows prior to 1.8 Ma has the potential to stimulate new hypotheses for human evolution. For example, if *Australopithecus* or earlier *Homo* dispersals occurred, to what extent did some later derived *Homo* traits developed outside of Africa (e.g., Dennell and Roebroeks, 2005; Dennell, 2011)?

3.3.2 Later Early and Middle Pleistocene dispersals

Another under-discussed topic within palaeoanthropology is the influence of later dispersals – throughout the Early Pleistocene – on human evolution. While there is a general research bias to provide timings of when the *earliest* possible dispersals occurred, there is no reason to doubt that hominins could repeatedly disperse throughout the Early Pleistocene. Discussions of the Lower Palaeolithic record in Europe have suggested occupation may not be continuous, but punctuated (Dennell, 2011; Hosfield, 2016; Hosfield and Cole, 2018). This model argues that local extirpations were frequent during the Lower Palaeolithic (particularly, mode-1 'Oldowan' bearing populations), and populations may have repeatedly re-entered Europe during periods of favourable conditions. Whether this can be related to dispersals from Africa is unclear, as mode-2 occurrences in Africa (~1.8 Ma; Lepre et al., 2011), the Levant (1.6-1.2 Ma; Bar-Yosef, 1994; Belmaker et al., 2002; Bar-Yosef and Belmaker, 2011; Belmaker, 2011; Moncel et al., 2015) and later appearance in Europe (~0.8 Ma) occludes direct techno-cultural links between European and African populations at 1.8 to 0.8 Ma. Moreover, it must be established whether the persistence of Levantine mode-2 tools represent frequent

dispersals into the Levant, at an archaeologically invisible level, or population continuity after the initial *Homo* dispersals. Yet, the resolution and homogeneity of the hominin fossil and archaeological records means analysing local extinctions, population turnovers or population continuity is not straight forward. The palaeontological record, however, shows that grassland conditions in the Apennine and Iberian Peninsulas supported taxa of African influence throughout the Lower Pleistocene and may indicate frequent connections to Africa (Kahlke et al., 2011). These are coetaneous to the earliest fossil finds in Europe (Bermúdez de Castro et al., 2011; Toro-Moyano et al., 2013), which could suggest a relationship between these fauna and hominin dispersals during the Lower Pleistocene, which could have been reflected in Arabia.

As previously discussed, there are few terrestrial Arabian palaeoclimate records that extend beyond 500 ka BP. This is in part due to the preservation issues related to desert environments and limitations of current dating methods. Detailed dating and environmental analysis must be obtained from a new archive, in order to extend the environmental record of Arabia. Doing so will allow determinations of when hominins could have possibly occupied and dispersed across the Arabian Peninsula.

3.3.3 Early Middle Pleistocene

A potentially later dispersal is related to the appearance of *H. heidelbergensis* and Acheulean tool industries in Europe ~800-500 ka BP (Maslin et al., 2014; Hosfield and Cole, 2018). The fossil records of Europe and Africa share a shift towards slightly enlarged cranial capacities, reduced facial prognathism and a more vaulted cranium within this period (Stringer, 2012; Profico et al., 2016). Shared and heterogenous traits

with *H. erectus*, *H. neanderthalensis* and *H. sapiens*, and the fact that these are heterogenous between fossils, means the taxonomic validity of *H. heidelbergensis* is not always clear (Stringer, 2012). For example, the cranial fossils from Ceprano (Italy), Arago (France), Bodo (Tanzania) and Sima de los Huesos (Spain) are currently considered to be fairly contemporaneous, dating to ~500-400 ka BP (Clarke, 1990; Falguères et al., 2004, 2015; Manzi et al., 2010; Demuro et al., 2019); yet, there is considerable intraregional variability in trait expression (Fig. 17). Thus, compared to the Late Pleistocene dispersal of *H. sapiens* (discussed below), using the fossil record alone to detect major Middle Pleistocene demographic changes is not straightforward.

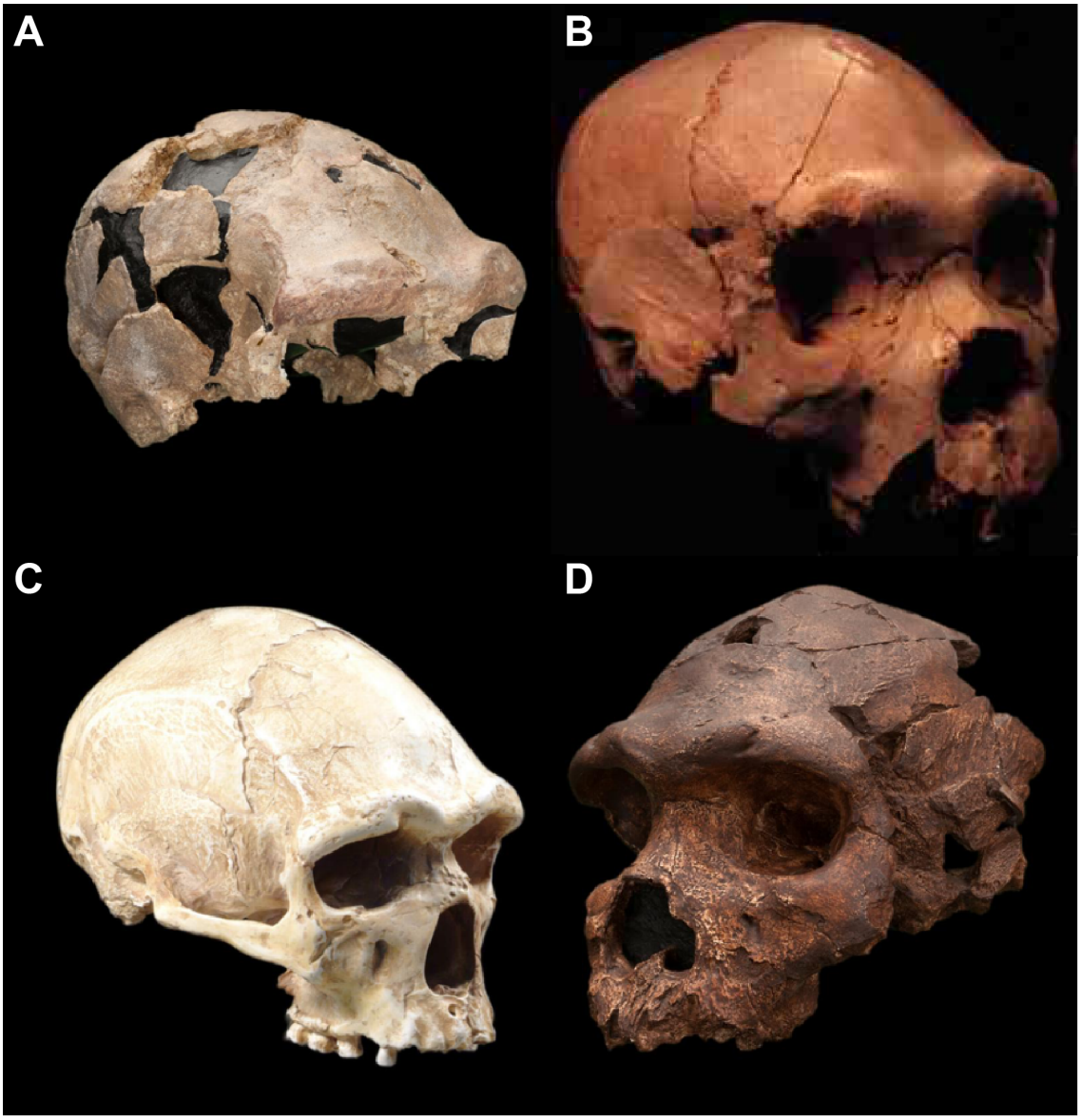

Fig. 17. Fossil Homo heidelbergensis crania: (A) Ceprano (Ascenzi et al., 1996), (B) Sime de los Huesos VI (Arsuaga et al., 1997), (C) Arago XXI (de Lumley, 1981, 2015) and (D) Bodo (Clark, 1976; Mturi, 1976; Clarke, 1990). Images attained from Smithsonian, human origins (http://humanorigins.si.edu/).

A technological shift observed by Moncel et al. (2015) is coincident with inferred African dispersion. Increased East African precipitation was argued to have forced population expansion and dispersal of *H. heidelbergensis* into Europe ~800-700 ka BP (Shultz and

Maslin, 2013; Maslin et al., 2014), though this is perhaps an over simplistic model. Adversely, Muttoni et al. (2010) argued that MIS 22 (900-866 ka BP) glacial conditions and increased aridity may have stimulated dispersal from Africa. However, neither of these models considers whether the Saharo-Arabian deserts were traversable. The faunal composition of the Levant demonstrates an ongoing African influence between 0.9 and 0.7 Ma (Kahlke et al., 2011), indicating the presence of green landscapes between Africa and the Levant. However, there are no specific examples of "green landscapes" from Saharo-Arabia. Terrestrial evidence of ameliorated Saharo-Arabian climatic/environmental conditions must be obtained to identify and refine the timing of potential faunal (including human) dispersals at this time.

Dispersals are seldom discussed again until the late Middle Pleistocene and early Late Pleistocene (Groucutt et al., 2015a; Hershkovitz et al., 2018; Harvati et al., 2019). If, however, wet Saharo-Arabian interglacial conditions persisted, there is no reason to question why dispersals should not have occurred in punctuated episodes throughout the entire Middle Pleistocene. The lack of discussion regarding dispersal may be related to the so called 'muddle in the middle': the uncertainty of regionally and chronologically distinct morphological trends in Europe and Asia throughout the Middle Pleistocene. Only towards the later Middle Pleistocene are distinct 'African' and 'Eurasian' morphologies accepted (White et al., 2003; Stringer, 2012; Hublin et al., 2017). The absence of distinct regional morphological trends means there is considerable difficulty in identifying the movement of populations throughout the Middle Pleistocene.

There is currently a paucity of (and conflicting) indirect evidence to support Middle Pleistocene dispersals. For example, faunal turnover in the Levant sees increased

Eurasian influence and a disappearance of African-type species, suggesting less connectivity between sub-Saharan Africa and the Levant (Kahlke et al., 2011). However, marine sediment records (e.g., ODP 967 and ODP 721/722) and the appearance of African and Eurasian fauna in Arabia suggests 'green periods' occurred during peak interglacials and warm substages (deMenocal, 1995; Larrasoana et al., 2003; Roberts et al., 2011; Rosenberg et al., 2013; Stimpson et al., 2016; Grant et al., 2017; Stewart et al., 2019b). Archaeological finds also indicate these wet periods may have been occupied by hominins. The earliest dated stone artefacts in Arabia have ages of 0.8 ± 0.3 Ma and 0.44 ± 0.26 Ma (Dabbagh et al., 1984; Bailey et al., 2015) and were uncovered in southwestern Saudi Arabia. While these age uncertainties are large and cannot be ascribed to a distinct pluvial period, they do indicate hominin occupation of Arabia during the Middle Pleistocene (or perhaps the later Early Pleistocene). Additionally, flint scatters dated to MIS 9 or 13 have also been uncovered from sediments of the Ti's al Ghadah palaeolake in northern Saudi Arabia (Stimpson et al., 2016; Roberts et al., 2018). Palaeontological remains uncovered from these sediments also showed signs of anthropogenic modification (Stimpson et al., 2016; Stewart et al., 2019a); however the authenticity of these cut marks is not entirely clear (Stewart et al., 2019a). Further "Acheulean" Middle Pleistocene stone artefacts have been uncovered as surface scatters (Jennings et al., 2015a; Groucutt et al., 2017; Roberts et al., 2018; Shipton et al., 2018). While these could represent occupations throughout the Middle Pleistocene, the broad temporal range of Acheulean industries (1.8 Ma onwards) means it is not currently possible to provide a time-specific occupation age from these artefacts. This issue is exacerbated by the fact that currently dated Acheulean assemblages from Arabia date to as late as MIS 7(e.g., Scerri et al., 2018). Furthermore, broad typological definitions (i.e., ESA/EP; Bailey et al., 2015) means these provide limited demographic information. Thus, improving the

terrestrial palaeoclimate record of Arabia could provide new evidence of when occupation of Arabia (and dispersals) may have occurred.

3.3.4 Later Middle Pleistocene (MIS 7 and MIS 6)

Genetic and fossil data suggest that early *H. sapiens* had appeared somewhat variably throughout Africa during the Middle Pleistocene, prior to MIS 5 (White et al., 2003; McDougall et al., 2012; Hublin et al., 2017; Richter et al., 2017; Hershkovitz et al., 2018; Scerri et al., 2018b, 2019). Recently, there has been increased efforts to determine the distribution of these early populations within and outside of Africa (Breeze et al., 2016; Hershkovitz et al., 2018; Scerri et al., 2018b, 2018a; Harvati et al., 2019). Breeze et al. (2016) reviewed that palaeohydrological conditions of north-eastern Africa, Sinai, the Negev desert and the Nafud desert, concluding that enhanced precipitation during MIS 7 (~243-190 ka BP) could support *H. sapiens* dispersals. Indeed, the palaeoclimate evidence (discussed above) and recent archaeological findings indicate that ameliorated conditions of Saharo-Arabia could have had a profound impact on the distribution of early *H. sapiens* during the late Middle Pleistocene.

Acheulean tools recovered from Saudi Arabia have recently been dated to MIS 7 (Scerri et al., 2018a). Scerri et al. (2018a) argued these were morphologically aligned to East African Acheulean industries (such as Meiso, Ethiopia), as opposed to the Levantine Acheuleo-Yabrudian industry (although they shared some characteristics). Scerri et al. (2018a) continue to explain that later (undated) archaeological horizons should fall into MIS 6e, overlapping the reputed age of the Misliya Cave fossil (discussed below). Yet, there is only equivocal evidence for enhanced precipitation during MIS 6e (Fleitmann et

al., 2011; Rosenberg et al., 2013), questioning whether occupation of Arabia could be facilitated at this time. Nevertheless, whilst these findings do not explicitly demonstrate *H. sapiens* occupied Arabia, they do indicate Arabia was inhabited by *a* hominin species during MIS 7.

The evidence for *H. sapiens* dispersion beyond Arabia at this time is even less clear due to dating uncertainties. A fossil *H. sapiens* maxilla uncovered at Misliya Cave, Israel, was used to argue *H. sapiens* dispersed during early MIS 6 (190-170 ka BP) (Hershkovitz et al., 2018). However, dating of this fossil was inconsistent across methods, with total ages ranging from 227 to 68.6 ka BP. Two indirect ages were obtained for the Misliya Cave mandible via ^{230}Th analysis of a calcite crust overlying the I^2 (185 ± 8 ka BP) and cumulative TL ages of Tabun "type D" industries (179 ± 48 ka BP). Yet, the calcite crust was heavily contaminated by ^{232}Th, suggesting post-depositional mobilisation of Th (see supplementary file provided by Hershkovitz et al., 2018). Two direct ages were obtained via ^{230}Th dating of I^2 dentine (70.2 ± 1.6 ka BP) and combined US-ESR dating of the same tooth (174 ± 10 ka BP); however, these ages are largely inconsistent. One reason for this may be that combined US-ESR dating was conducted after X-Ray scanning. X-Ray dose given during scanning scan be highly variable, and thus obscures the final US-ESR age (Sharp and Paces, 2018). The least controversial date attained provided an age of 70.2 ± 1.6 ka BP, suggesting a much younger age than the proposed 194-177 ka BP age (Hershkovitz et al., 2018). If the 70.2 ± 1.6 ka BP age is considered more accurate, this would suggest *H. sapiens* presence in the Levant during early MIS 4. Alternatively, the age disparity between sediment and fossil ages could indicate the mandible was deposited later than the archaeological material and that Misliya cave has an extensive occupation history.

More recently, *H. sapiens* cranial fragments were identified at Apidima Cave, Greece, dated to MIS 7 (Harvati et al., 2019). However, both taxonomical and dating issues have led to scepticism as to whether *H. sapiens* were present in southeast Europe at this time (Wade, 2019). Firstly, based on the size of the sample (a fragment of an occipital bone), it has been argued that it is not possible to assign a species designation. This issue is exacerbated by the range of cranial variation among coetaneous European fossils (such as Steinheim, which was not analysed during this study). Secondly, while an age of >210 ka BP was reported based on averages of clustered ages, individual ages were highly variable, suggesting some post-depositional mobilisation of U and/or Th. In fact, 19 out of 25 ages of breccia sample 3754 were rejected due to U leaching. Such leaching can lead to older than expected ages (Borsato et al., 2003; Bajo et al., 2016). Ages from breccia sample 3755 also showed a high amount of leaching. ^{230}Th Ages that were used to produce the final (average) age ranged from 334.8 ± 131.9 to 77.5 ± 10 ka BP. This cannot be used to unequivocally assign *H. sapiens* occupation in Greece to MIS 7.

While palaeoclimate data shows that it was possible for *H. sapiens* to have dispersed during MIS 7 (e.g., Fleitmann et al., 2011; Breeze et al., 2016), there is currently no unequivocal archaeological or fossil evidence to support this.

3.3.5 Late Pleistocene

The dispersal of *H. sapiens* from Africa is a key event in our evolutionary history, and thus a controversial topic. Until recently, it was considered that initial *H. sapiens* dispersals during MIS 5 (127-71 ka BP) were limited to the Levant (e.g., Shea, 2008).

These, however, failed, due to the onset of glacial conditions, competition with Neanderthals, and behavioural and morphological primacy (Mellars, 2006a; Shea, 2008). *H. sapiens* once again dispersed from Africa during MIS 3, reappearing in the Levant as morphologically and behaviourally modern, and utilising Upper Palaeolithic tool kits (Mellars, 2006a; Shea, 2008; Mellars et al., 2013). This hypothesis argued that *H. sapiens* populations dispersed by following the coasts of Arabia and the Persian Gulf (Stringer, 2000; Mellars, 2006a, 2006b; Mellars et al., 2013).

The 'successful' Upper Palaeolithic dispersal hypothesis was challenged on the grounds that *H. sapiens* fossils and Middle Stone Age (MSA) typologies were present in India and Asia throughout MIS 5 and into MIS 3 (Petraglia et al., 2007; Groucutt et al., 2015b, 2015a; Liu et al., 2015). This revised model favours an eastward dispersal during the MIS 5 interstadials, in which mid-latitude deserts underwent transitions to "green" deserts, including Arabia and Thar, which facilitated occupation of these now arid areas (as indicated by Middle Stone Age/Middle Palaeolithic stone tool assemblages: Fig. 18). This led to introduction of *H. sapiens* into India, southeast Asia and east Asia (Dennell and Petraglia, 2012; Groucutt et al., 2015a; Liu et al., 2015; Petraglia et al., 2015). A later MIS 3 expansion then occurred into the Levant and Europe, though the origin is unclear (e.g., Groucutt et al., 2015a). Moreover, this revised model suggests that cognitive capacities of MIS 5 *H. sapiens* did not substantially differ from MIS 3 *H. sapiens*.

A more recent model, however, combines and synthesises these arguments with genetic data, suggesting multiple dispersals occurred during MIS 5, which were 'overprinted' by a subsequent MIS 3 dispersal (Mallick et al., 2016; Pagani et al., 2016; Bae et al., 2017; Rabett, 2018). This model stresses MIS 5 dispersals did not necessarily 'fail' in Asia and

suggests that these populations may have been long-lived throughout MIS 4 and MIS 3 (Rabett, 2018). Additionally, the relatively arid (compared to MIS 5 interstadials) climates across Saharo-Arabia during MIS 3 perhaps suggests different dispersal processes.

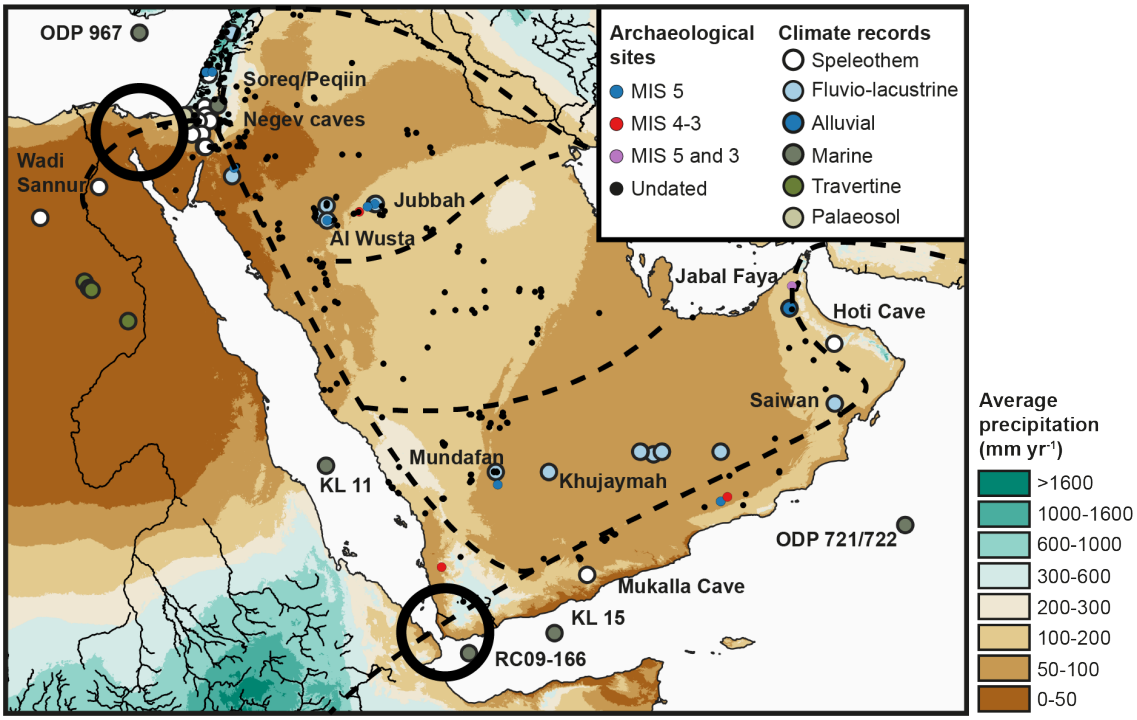

Fig. 18. Map of modern average annual rainfall (1970-2000. mm yr^{-1}; Fick and Hijamns, 2017) and distribution of palaeoclimate records and archaeological sites in the eastern Sahara, Arabia and the Near East (Rose et al., 2011; Petraglia et al., 2012; Bailey et al., 2015; Groucutt et al., 2015a, 2015b; Jennings et al., 2015a; Breeze et al., 2016). Points of entry into Arabia via the Sinai Peninsula and the Bab-al-Mandab strait are marked by hollow circles. Dispersal corridors (Rosenberg et al., 2011; Petraglia et al., 2019) are marked by dashed lines.

3.3.5.1 MIS 5 (130-71 ka BP)

Due to the scarcity of fossils in Arabia, archaeological finds comprise almost the entirety of the human record of Arabia. Middle Palaeolithic (MP) assemblages predominate the main human record of Arabia, most of them uncovered in the now-arid interior (it should be noted, that, based on qualitative assessment, some researchers refer to these as Middle Stone Age (MSA) assemblages). Many of these are surface finds, lacking any contextual association; however, of those that have been excavated, most have been derived from fluvio-lacustrine sediments, or close to fluvial channels, due to their favourable preservation biases. The rock shelter of Jabal Faya, UAE, is a notable exception. The Stratum C archaeological horizon (OSL dated to ~127 ± 16, 123 ± 10 and 95 ± 15 ka BP, though the former age was considered problematic) contained ~500 stone artefacts of a variety of reduction strategies including the production of volumetric blades and Levallois debitage, bifaces, and retouched forms. Armitage et al. (2011) recorded similarities to tools recovered from Muguruk, Kenya (McBrearty, 1988). Alternatively, Groucutt and Petraglia (2012) have proposed that this assemblage could represent an autochthonous development or be related to a dispersal from the Indian subcontinent. Stratum B and A, however, lack bifacial reduction and Levallois flaking. Assemblage A was OSL dated to 40.2 ± 3.0 and 38.6 ± 3.1 ka BP, indicating hominin occupation during MIS 3 (Armitage et al., 2011), thus stratum B may be related to later MIS 5 or MIS 4. The assemblage from stratum B contains little evidence of bifacial and Levallois reduction, with the exception of a few convergent flakes, which are similar to Levallois points.

Aybut al Auwal, Oman, a fluvial channel containing artefacts, could be contemporaneous to Jabal Faya. OSL dates of 107 ± 9 and 106 ± 9 ka BP provided a weighted mean date

of 106.6 ± 6.4 ka BP for the archaeology-bearing fluvial sediments (unit 3) from Aybut Al Auwal, Oman (Rose et al., 2011). This falls within 5d and 5c. Based on the palaeoclimate record of Arabia (see above), an MIS 5c age is perhaps most likely. Unit 3 was described by Rose et al. (2011) as homogeneous, accumulating in a single, continuous phase. 859 artefacts from a ~2,500m^2 surface, 10 artefacts from unit 3 and 11 desilicified artefacts eroding from a nearby channel were collected for analysis. 79% of Levallois cores were classified as Nubian; of these, 10 % were type 2 Nubian; whereas 60% were type 1 Nubian (Rose et al., 2011). Blades, flakes and points were collected in conjunction with cores, displaying *chapeau de gendarme*, faceted and dihedral striking platforms. Rose et al. (2011) argued that the similarities between the archaeological industries of Dhofar and the northeast Africa 'Nubian' industries implied demographic connections between these regions. However, the archaeological industries of Arabia are highly heterogenous (Groucutt and Petraglia, 2012), weakening this association. Additionally, it is possible that these remains were washed out from an earlier burial (or perhaps surface) context and redeposited during MIS 5c. Rose et al. (2011) described the stratigraphy: "This unit represents the lateral accretion of suspended fluvial sediments that have been eroded from the surrounding bedrock and deposited downstream, along with lithic artifacts and chert debris that slumped in from the surface as the terrace was undercut". Current working models suggest that Arabian populations were locally extirpated following a return to arid conditions. As such, if these tools were washed from earlier sediments, this may imply that the Aybut al Auwal stone tool assemblages could date to MIS 5e.

The archaeology of the Nafud has been extensively studied by the Palaeodeserts project. The archaeological sites of the Jubbah palaeolake were the prime focus of archaeological

investigations. A tool bearing layer (stratum H) from Jabal Katefeh (JKF-1) was dated via OSL analysis of quartz to 90-85 ka BP (Petraglia et al., 2012). A total of 1,222 Levallois stone artefacts have been recovered from Jabal Katefeh (JKF-1 and JKF-12), displaying a mixture of Nubian (median-distal ridge, a triangular shape of the core and faceted platforms) and Levallois characteristics (Petraglia et al., 2012; Groucutt et al., 2015b). Another site, Jabal Umm Sanman, consists of surface and stratified material produced from a distinctive yellow quartzite (Petraglia et al., 2012; Scerri et al., 2014b). A total of 88 (11 surface, 77 buried) stone tools have been recovered (JSM-1), exhibiting more centripetal reduction than JKF-1 (Scerri et al., 2014b). Retouch, again, is extremely rare (Scerri et al., 2014b). Four OSL samples were taken from two archaeological layers found beneath a colluvium and aeolian sands: stratum B (20cm below the surface) and stratum C (42cm below the surface). Stratum C yielded burial ages of 140 ± 14 and 61 ± 8 ka BP; stratum B provided ages of 96 ± 9 and 42 ± 9 ka BP (Petraglia et al., 2012). Petraglia et al. (2012) explain that ~60% of grains in stratum B provided the former age and thus assert that younger grains had been mixed into stratum B. A burial age of 100-60 ka BP was therefore preferred. Jabal Qattar, 24 km away from Jabal Katefeh, is another important site of the Jubbah palaeolake. Palaeosols were identified and dated to MIS 7 (OSL: 211 ± 16 ka BP), MIS 5e (based on stratigraphic position), MIS 5c (OSL: 95 ± 7 ka BP) and MIS 5a (OSL: 75 ± 5 ka BP) (Petraglia et al., 2012). The palaeosol suggested to represent the MIS 5e interstadial is characterised by greater magnetic values (indicating fluvial influx) and organic content, reflecting palaeoclimate studies' findings that MIS 5e saw greater rainfall than subsequent MIS 5 interstadials (Fleitmann et al., 2011; Rosenberg et al., 2011). 114 stone artefacts were recovered from the MIS 5a palaeosol. Cores include discoidal and both recurrent centripetal and preferential centripetal Levallois types (Petraglia et al., 2012). These were produced from ferruginous

quartzite (77%), quartz (12%), rhyolite (4%) and other materials (7%). The presence of rhyolite tools is important, as local outcrops had not been located and may suggest some long-distance transfer of material. Overall, the tools from Jubbah were described as having some derived morphological characteristics but retained similarities to the MSA of north-eastern Africa and the MP of the Levant (Petraglia et al., 2012).

Claims of the relationship between African and Arabian tool assemblages have been crucial to dispersal models; however, these are often based on qualitative assessment (e.g., Armitage et al., 2011; Rose et al., 2011). Scerri et al. (2014b) aimed to elucidate the issues of how typology may or may not be related to MIS 5 *H. sapiens* dispersal through morphometric and statistical (ANOVA) studies of assemblages from Jubbah. Results indicated core reduction at Jubbah was distinct from African assemblages; where preferential flake reduction, core shaping and preparation were derived from the African assemblages (Scerri et al., 2014b). JFK-12 repeatedly exhibited no statistical difference from African sites; however, the JSM-1 assemblage was not similar to African or Arabian assemblages. Scerri et al. (2014b) concluded similarities between Arabian and African assemblages demonstrate that interactions had occurred between northeast African and Arabian populations during MIS 5, though autochthonous development and techno-cultural heterogeneity were key characteristics of Arabian populations. The qualitative assessment of Jubbah highlights high levels of technological variation which does not support a simple interpretation of the archaeology, in which single populations (reflected by single techno-cultural complexes) dispersed into Arabia. Instead, this data suggests multiple populations, reflected by techno-cultural heterogeneity, were present in Arabia at different times.

Until recently, no fossil evidence was available to clarify whether stone tools from Arabia could be unequivocally related to *H. sapiens*. A phalanx recently recovered from Al Wusta (Nafud desert, Saudi Arabia) fell into the range of variation of *H. sapiens* and could be distinguished from Neanderthal specimens (Groucutt et al., 2018). Sediments were dated from late MIS 5c to early MIS 5a. Neither MIS 5c nor MIS 5a were the "wettest" pluvial phases (Fleitmann et al., 2011), which may show that the peak interglacial conditions of MIS 5e could have been even less challenging to human populations. The finding of this fossil lends support to the hypothesis that ameliorated conditions in Arabia facilitated *H. sapiens* occupation, which were the creators of these stone tools. However, this fossil is only one isolated remain and dating to an individual green Arabia period. There are still no human remains dated to MIS 5e or in southern Arabia. Further fossil evidence is required to 1) relate archaeological evidence from all green periods to *H. sapiens*, and 2) determine whether *H. sapiens* occupied and dispersed beyond Arabia during earlier green periods.

Despite a growing body of evidence highlighting the crucial role that green deserts had for dispersal (Dennell and Petraglia, 2012; Groucutt et al., 2015a and references therein), the methods of *H. sapiens* dispersal across Arabia remain a contentious topic. These include the 'route' (a northern route across the Sinai Peninsula, or southern route across the Bab-al-Mandab straits) and the timing of dispersal (either prior to and after interglacial/warm substages, or during interglacial/warm substages). Some researchers have argued for stadial and glacial dispersals (Mellars, 2006a, 2006b; Parker and Rose, 2008; Rohling et al., 2013) via the Bab el Mandeb strait. This is considered likely due to both its geographical proximity to the horn of Africa and the "East African" influence on the Jabal Faya assemblage. An enhanced monsoon (inferred by KL 09 Ti/Ca and

Hematite content) and low Red Sea sea-level between 145-140 ka BP was argued to have provided a window of opportunity for dispersal across the Bab el Mandeb strait (Rohling et al., 2013). There are, however, three issues with this hypothesis. Firstly, lack of a land-bridge (Fernandes et al., 2006) indicates that swimming, rafting and maritime navigation would have been vital for crossing the Bab el Mandeb strait. Whether sea-faring capabilities were part of the behavioural repertoire of *H. sapiens* prior to 65 ka BP is a highly contentious topic (Erlandson and Braje, 2015; Leppard and Runnels, 2017). Secondly, the inferred period of increased monsoon strength between 145-140 ka BP is yet to be corroborated by records from the Red Sea and Gulf of Aden region (Fleitmann, 1997; Fleitmann et al., 2011; Tierney et al., 2017). Finally, current terrestrial records from Arabia lack the precise dating required to compare the timing of increased rainfall to reconstructed sea-levels.

Alternatively, a northward migration of sub-Saharan fauna is argued to have been facilitated by the widespread interglacial formation of vast rivers and palaeolakes in the Sahara Desert (Drake et al., 2011, 2013). Once *H. sapiens* populations crossed the Sanai Peninsula, palaeohydrological corridors facilitated the southward movement of populations in Arabia (Breeze et al., 2016), with further dispersals into the Levant (Shea, 2008a). Subsequent dispersals then occurred into the Persian Gulf and India (Petraglia et al., 2007; Dennell, 2013; Blinkhorn et al., 2015). This hypothesis does not depend upon the uncertainties of MSA seafaring (Drake et al., 2011; Breeze et al., 2016). Yet, lack of precisely dated records with detailed evidence of the onset and termination of pluvial conditions means it is uncertain for how long this route was viable for dispersal, especially on a north-south transect. Understanding the duration of increased rainfall on a meridional transect could be vital for understanding the dynamics of dispersal: if we

can estimate how long sub-Saharan Africa, Arabia and the Levant were connected by palaeohydrological corridors, we may be able to infer dispersal rates, which can lead to further questions concerning how hominins occupied these landscapes. For example, within the Holocene wet period, human societies were able to expand into the Saharan desert interior ~8 ka BP, which also facilitated the introduction of sedentism and pastoralism into sub-Saharan Africa (Drake et al., 2011; Kuper and Kropelin, 2015). Aridification on a north-south transect onset at ~6 ka BP – as the tropical rain-belt retreated to its current position (Fig. 19) – led to a gradual decline of habitable areas and human societies retracted towards refugia and the Nile (Kuper and Kropelin, 2015). This analogue could provide a crucial insight into the earlier demographic changes in 'green Arabia', in which the habitability of northern Arabia could have been truncated compared to southern Arabia.

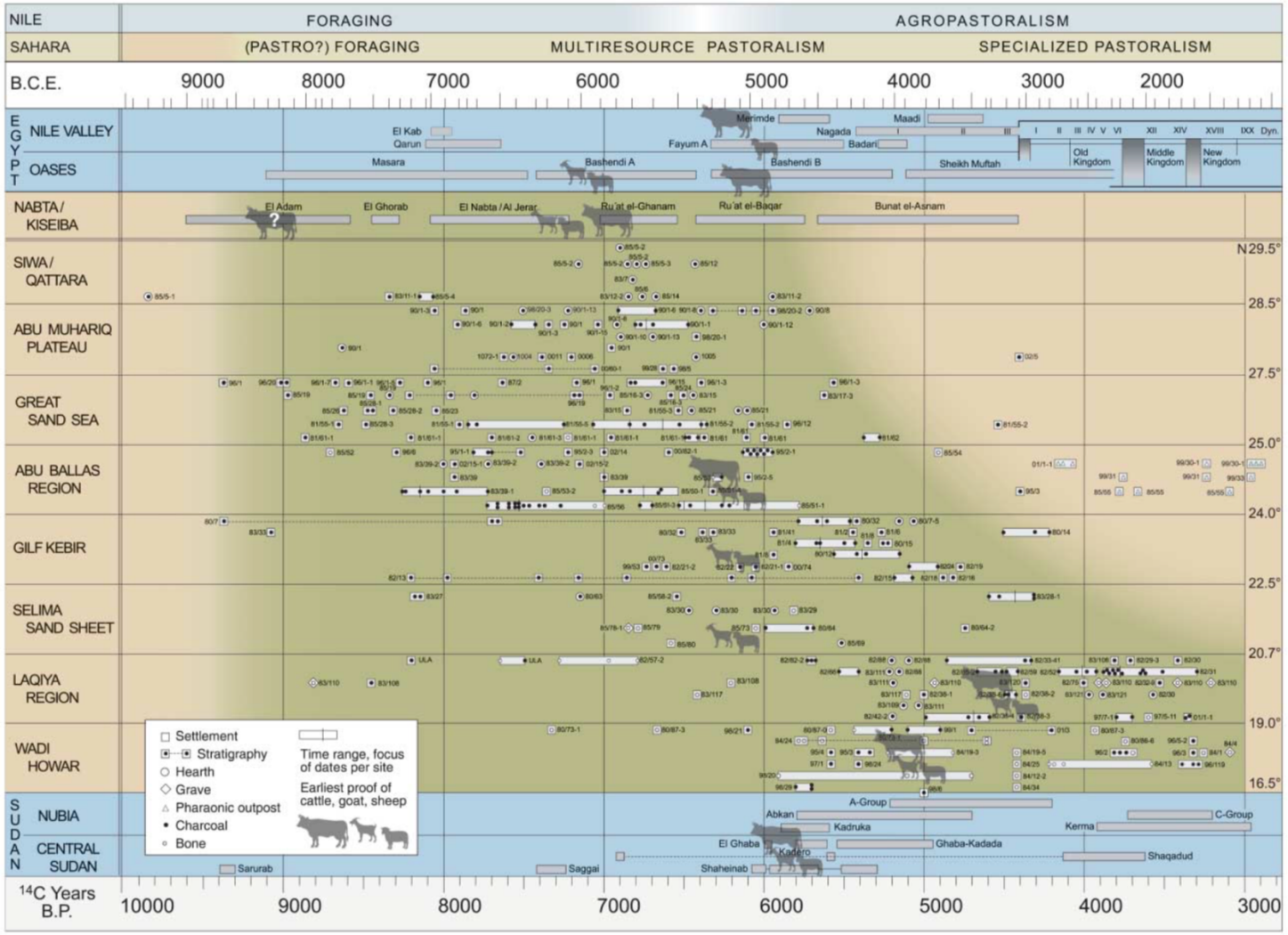

Fig. 19. human occupation of the Sahara Desert during the Holocene Green Period (Kuper and Kropelin, 2015).

One fundamental aspect for the dispersal of humans into and through Arabia is the formation of so called "green corridors" or "palaeohydrological corridors". These are defined as areas of focussed availability of both freshwater and vegetation linking Africa and Eurasia, which would have created habitable areas for *H. sapiens* to occupy and traverse. The coastal regions of the Red Sea and southern Arabia, the "Tabuk corridor" and inland palaeorivers crossing the peninsula from west-east have been identified as potential corridors (Erlandson and Braje, 2015; Breeze et al., 2016; Petraglia et al., 2019). The availability of these corridors is time variable. For example, some authors suggest that the southern corridor may have been favourable during sea-level low-stands (glacial or colder substages), when the enhanced hydraulic head facilitated freshwater seepage onto emerged shelves from groundwater reservoirs (Parker and Rose, 2008; Rohling et al., 2013), potentially creating areas of high-resource availability. Whereas others have suggested that the northward incursions of the monsoon during interglacials and warmer substages transformed larger areas of southern (and northern Arabia) into habitable areas (Fleitmann et al., 2011; Rosenberg et al., 2011; Parton et al., 2015a). In the north, the availability of corridors is again considered dependent on the formation of palaeo-lake and river systems spread across the Arabian interiors. These formed during interglacials and warm substages (Breeze et al., 2016; Petraglia et al., 2019) and were perhaps more attractive than surrounding areas due to the permanent availability of water. As such, the rivers acted as a method to disperse across Arabia. In either case, current hypotheses stress that *H. sapiens* occupations and dispersals were dependent on freshwater availability and abundant vegetation resources.

While green corridors may have indeed provided more optimal areas of habitation, there are few limitations to their applicability. 1) while MP sites across Arabia are closer to

rivers and lakes than would be expected by a random distribution (Breeze et al., 2015), many archaeological sites a) are not dated, and b) typically located away from the traditional "corridors" (fig.). 2) our understanding of environmental homogeneity and heterogeneity during "green phases" is limited. As has been discussed in chapter two, the current environments of Arabia should not be simplistically defined as "desert", as there is great variability even today. While the densest vegetation and biodiversity is typically located in areas of greater water availability (such as streams and valleys of the highlands), vegetation blooms and activation of lakes occur following brief rainfall events even in the desert interior (Miller and Cope, 1996). However, under and enhanced precipitation regime, it is quite possible that vegetation biodiversity and density was increased in the now arid areas. Simply put, it is not currently possible to fully discern what environments surrounded these green corridors (i.e., how did "corridors" differ from the surrounding landscape?) and there is little information of the spatial extent of the corridors. Indeed, evidence of large herbivorous fauna (e.g., Stewart et al., 2019b, 2020) likely suggests that increased bio-productivity was not exclusive to riparian zones. 4) there is an implication of transience to these corridors (as well as discussions of dispersal "routes"). In other words, they imply a rather simplistic point A to point B directionality (and perhaps intentionality) of *H. sapiens* movements across Arabia – this is rather unlikely. It is perhaps more likely that *H. sapiens* were reacting to a mixture of push and pull factors related to patch quality and population pressures (this is covered in greater detail in Chapter 8). While "green corridors" are useful constructs and certainly aid our understanding for how humans occupied and traversed Arabia, it is important to note that there remain many uncertainties as to environmental homogeneity/heterogeneity and the dynamics of *H. sapiens* dispersals.

While the details of human occupation in Arabia have become increasingly well studied, there are still significant gaps in knowledge. For example, there is little discussion of 'lived experiences' of *H. sapiens* in Pleistocene Arabia, and the methods used to survive these landscapes. Indeed, as the palaeoenvironmental data demonstrates that 'savannah-type' landscapes formed, it has been argued that there was no need for adaptation (Roberts et al., 2018). While, from a broader perspective this is likely to be true, it dissuades research into understanding how hominins may have reacted to seasonal environments at latitudes greater than East Africa, or how they reacted/adapted to the mixed Eurasian and African fauna (Stimpson et al., 2016), or at what speed range expansion took place across these landscapes. Moreover, due to current low resolution of palaeoclimate archives, there is little discussion of climatic extremes and variability within pluvial phases, which may have affected human societies and dispersal. Another issue that is not considered is the precise timings of the onset of humid conditions, north-south precipitation gradients and for how long "green corridors" were traversable.

An increasing body of evidence shows that the dispersal of *H. sapiens* during MIS 5 expanded beyond Arabia (Tab. 1). Stone artefacts present in the Levant (Groucutt et al., 2019) and India (Petraglia et al., 2007, 2009; Haslam et al., 2012; Blinkhorn et al., 2013, 2019) with similarities to Arabian and Northeast African industries have been taken to represent demographic connections between these regions (Dennell and Petraglia, 2012; Groucutt et al., 2015a). While occupation may have been short-lived in the Levant (Shea, 2008), it may have had a much longer history in the northern Indo-Pacific rim (Rabett, 2018). Dating of archaeological horizons at Jwalapuram (Petraglia et al., 2007; Clarkson et al., 2009), Katoati (Blinkhorn et al., 2013) and the broader distribution of pre-Upper Palaeolithic sites across Southeast Asia (Rabett, 2018) shows that these techno-

complexes endured until 32 ka BP prior to a shift to Upper Palaeolithic and microlithic technologies. This has been attributed to a survival of dispersal populations from MIS 5 (Rabett, 2018). Technological convergence between Northeast African (*H. sapiens*) and "archaic" (*H. erectus*) populations has been offered as an alternative explanation (Mellars et al., 2013). However, when considering the apparent spread of MSA traits and human fossils along equatorial regions from Africa into Arabia, Thar, China and southeast Asia during MIS 5 (Petraglia et al., 2007; Blinkhorn et al., 2013; Scerri et al., 2014a; Liu et al., 2015; Groucutt et al., 2018; Rabett, 2018), technological convergence is perhaps not the most likely explanation of tool morphology. Yet, it must be remembered that the data for *H. sapiens* dispersals and lengths of occupations are poorly understood (few precisely dated sites) and based on qualitative assessment (e.g., tool morphology). To adopt a cautious position, just because *H. sapiens* were present in China, it does not mean that all archaeological sites between Fuyan Cave and Arabia should be attributed to *H. sapiens*. Indeed, current evidence suggests that there could have been at least three different human species present in eastern Asia during the Late Pleistocene (the "denisovans", *H. floresiensis*, *H. sapiens* and perhaps *H. erectus* and *H. neanderthalensis*: Bae et al., 2017). While the emerging picture currently favours *H. sapiens* occupation in Asia from MIS 5 onwards (with some demographic shifts: Bae et al., 2017), further fossil and archaeological data is required to corroborate these views.

Region	Site	Type	FAD	Method	Reference
Levant	Qafzeh	Fossil and archaeology	120 ± 8 ka BP	ESR	Grün and Stringer, (1991)

	Skhul	Fossil and archaeology	98^{+19}_{-10} ka BP	ESR	Grün et al. (2005); Groucutt et al. (2019), but see Millard (2008)
India (Thar)	Katoati site	MSA archaeological sediments (S8)	95.6 ± 13.1 ka BP	OSL	Blinkhorn et al. (2013)
		(S4)	48 ± 11 ka BP	OSL	
			>57.9 and >62 ka BP	^{14}C	
India	Jwalapuram	MSA archaeological sediments	>74 ka BP	OSL	Petraglia et al. (2007)
China	Fuyan Cave	Fossil teeth	130-80 ka BP	Calcite floor ^{230}Th and palaeontology	Liu et al. (2015)

Tab. 1. Key H. sapiens palaeontological and archaeological records related to Middle Stone Age dispersals.

3.3.5.2 MIS 4-3 (71-29 ka BP)

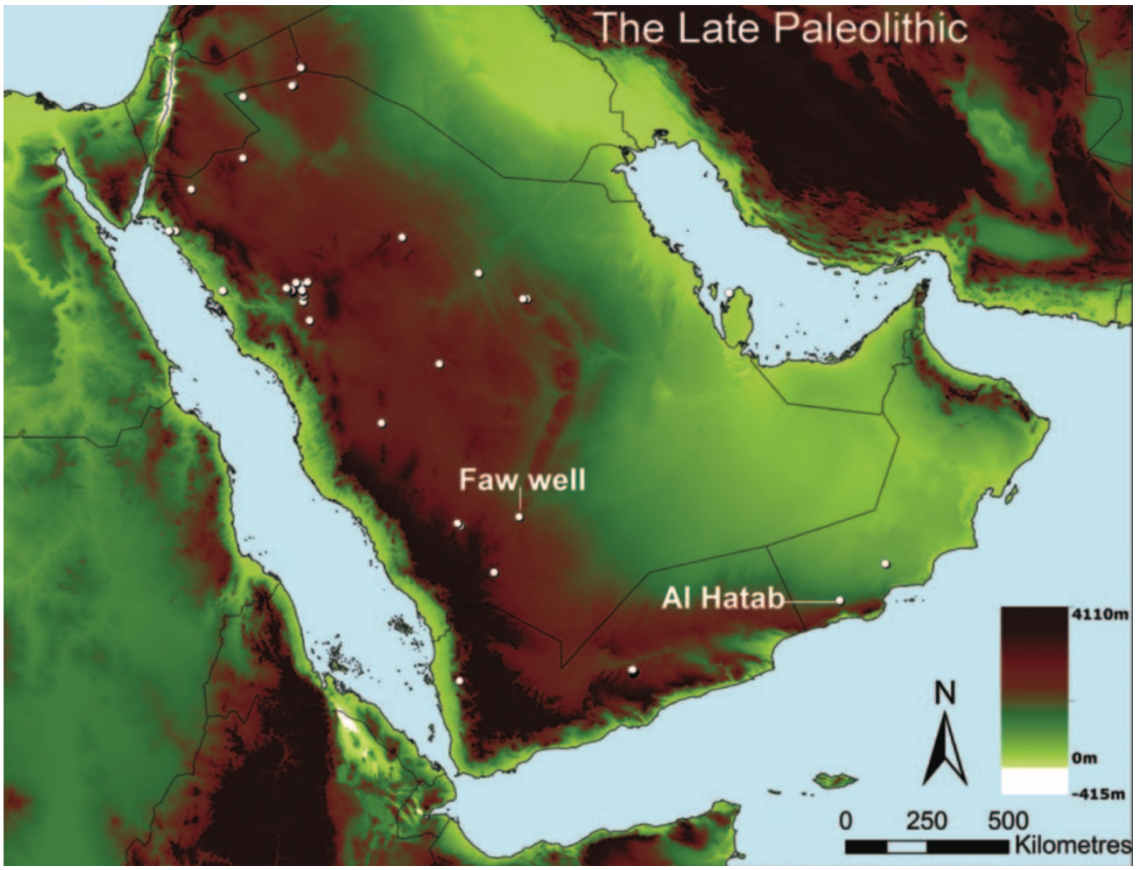

Fig. 20. "Late Palaeolithic" archaeological sites in Arabia (after Groucutt and Petraglia, 2012).

An appearance of Upper Palaeolithic (or Late Stone Age) tool assemblages and fossils with more modern cranial morphologies (parietal bossing, rounded occipital, flat sagittal area) from Africa into Eurasia suggests a secondary dispersal occurred ~60-50 ka BP (Stringer, 2000; Shea, 2008; Hershkovitz et al., 2015; Bae et al., 2017). Similarly, genetic data (discussed later) has also shown that the first Eurasian genetic structures had appeared at 60-50 ka BP (Mallick et al., 2016; Pagani et al., 2016), and may suggest a limited impact of earlier *H. sapiens* dispersals on modern human demography. It has been hypothesised that the reduced sea-levels during MIS 5 stadials and MIS 4-3 led to

enhanced hydraulic head and seepage onto newly exposed continental shelves (Faure et al., 2002). This seepage created habitable "coastal oases" (Faure et al., 2002; Parker and Rose, 2008) or vast mangrove (Erlandson and Braje, 2015) environments (but see above). Lower sea-levels have also been considered to have assisted dispersal across the Bab-al-Mandab strait leading to occupation of Arabia, with favourable periods of enhanced precipitation at ~145-140 ka BP and, in particular, ~70-65 ka BP (Rohling et al., 2013).

While there are some Arabian archaeological sites that include "Upper Palaeolithic" assemblages, many of these are surface scatters and cannot be absolutely dated (Fig. 20). One particular site from southern Saudi Arabia, Faw Well, is characterised by blade and microblade production (Edens, 2003) which perhaps suggests occupation between 60-30 ka BP. However, within the last decade, a growing number of dated Upper Palaeolithic sites have been reported from Arabia. Assemblage A from Jabal Faya, UAE, was OSL dated to 40.2 ± 3.0 and 38.6 ± 3.1 ka BP, indicating hominin occupation during MIS 3 (Armitage et al., 2011). A diverse range of reduction strategies included production of denticulates, retouched pieces, side scrapers, end scrapers, and burins. Flakes were produced from platform cores, which contrasts the apparent absence of prepared platforms from assemblage C (discussed previously in 3.3.5.1). Similarly, neither assemblage A nor B possess a substantial retouch component, which contrasts with assemblage C (Armitage et al., 2011). Another assemblage (SD-1) from the wadi Surdud site Shi'bat Dihya in the Yemeni highlands has been OSL dated to ~55 ka BP (Delagnes et al., 2012). The lithic assemblage here include blades, pointed blades, Levallois-like flakes and pointed flakes, which contrasts with the Jabal Faya assemblage A. Though, very few tools were uncovered, and none were assigned to a formal type. Interestingly, the burial context of these artefacts indicates that the local environment was semi-arid to

arid between 63-44 ka BP (based of the presences of gypsums and groundwater calcretes), with running freshwater (based on the presence of silts and clays). This could suggest a crucial role for the highlands of Arabia as a 'refugia' during the more arid periods. This disparity between Jabal Faya assemblage A and C, Faw Well and Shi'bat Dihya has been suggested to represent some local developments – due to regional isolation and segregation – following a return to arid conditions (Armitage et al., 2011; Delagnes et al., 2012; Groucutt and Petraglia, 2012).

Another MIS 3 assemblage was uncovered at Al Marrat (AM-3), Saudi Arabia. Calcrete sediments containing the artefacts were dated between 56.2 ± 6.5 and 53.9 ± 4.1 ka BP via OSL analysis (Jennings et al., 2016). Unlike Shi'bat Dihya, the phytolith assemblage was characterised by low C_4 and high C_3 content, showing grasslands were present in the local vicinity. Interestingly, tools uncovered from the archaeological units were described as 'Levallois', while synchronous Arabian archaeological assemblages are characterised by a reduced Levallois component (e.g., Jabal Faya; Armitage et al., 2011). While further data is required (especially fossils directly associated with the archaeological finds), the variability of stone tool assemblages shows populations in Arabia were techno-culturally heterogenous. Combined with the absence of widespread grasslands across Arabia, this could show a degree of isolation and independent technological developments within MIS 3, as has been previously suggested (Armitage et al., 2011; Delagnes et al., 2012; Bretzke and Conard, 2017). Additionally, it has also been considered that Levantine Neanderthals may have tracked southwards (Groucutt, *pers comm.*). Regardless of the creator, the morphological heterogeneity of Al Marrat continues to highlight demographic variability in Arabia during MIS 3.

Recently, an archaeological site dated to MIS 3 has been uncovered in a tributary of Wadi Ghadun, on the west-central Nejud Plateau of southern Oman (Rose et al., 2019). Luminescence dating of the Matafah fluvial gravels GU 5a, in which Archaeological Horizon (AH) III was identified, provided ages of 33.3 ± 2.1 and 30.3 ± 2.0. These ages are consistent with respective pIR-150 ages of 21.8 ± 2.9 ka and 29.8 ± 2.0 ka. 159 chert artefacts were recorded from AH III, though almost half of the assemblage comprised of debitage < 2 cm in maximum dimension. The authors take this to suggest AH III was not altered by post-depositional transport. 41% of the assemblage was comprised of debitage; whereas 10% included retouched tools. The retouched tools included a distal fragment of a Nubian Levallois point, eight geometric microliths, a dihedral burin and burin snap on, a denticulate and a perforator (Rose et al., 2019). The authors related the occupation of Matafah to a weak pluvial period during MIS 3. Interestingly, this is ~30-20 kyrs later than other terrestrial indicators for increased MIS 3 rainfall, suggesting that multiple limited expansions of the monsoon domain occurred throughout MIS 3, perhaps on D-O cycles (e.g., Burns et al., 2003). Nevertheless, the presence of *H. sapiens* in southern Oman was taken to suggest that "glacial refugium"

Outside of Arabia, the appearance of Upper Palaeolithic technologies in Eurasia and Australasia has been crucial to the hypothesised later dispersal. In particular, the first appearance datum of *H. sapiens* in Australia has been of great interest in determining timing of dispersal and also the cognitive capacities of dispersing hominins (Groucutt et al., 2015a; Tierney et al., 2017; O'Connell et al., 2018; Rabett, 2018). Current evidence shows no hominin colonised Australia prior to *H. sapiens*. The earliest archaeology may therefore inform when *H. sapiens* had reached Australia – providing a *terminus ante quem* for dispersal. In order to colonise Australia, *H. sapiens* populations had to disperse

across the islands of Southeast Asia and Oceania. Seafaring and navigating capabilities were required to do this, as the distances between islands meant they were not easily visible, even when glacial low-stands of 60 ka BP are considered (Kealy et al., 2017; Norman et al., 2018). Therefore, advanced planning and exploration skills were required in order to make such crossings possible. This has been used to support arguments of coastal dispersals from Africa, around the Indo-Pacific rim, during MIS 4-3 (Stringer, 2000; Mellars, 2006b, 2006a; Erlandson and Braje, 2015). Yet, there is considerable variation in ages of putative FAD for *H. sapiens* in Australia (Tab. 2). Many of these ages have been highly contested on stratigraphic and methodological grounds with very little cross-method consensus (Roberts et al., 1994; Simpson and Grün, 1998; Thorne et al., 1999; Grün et al., 2000; Turney et al., 2001; Bowler et al., 2003; O'Connell and Allen, 2004; Allen and O'Connell, 2014; O'Connell et al., 2018).

Determining timings of African dispersals using an Australian FAD and seafaring is also problematic. Primarily, the evolution of seafaring in the Pleistocene is poorly understood and highly contested (Leppard and Runnels, 2017). Maritime dispersal from Africa and around the Arabian Peninsula is favoured by the late dispersal hypothesis (Stringer, 2000; Mellars, 2006b, 2006a; Mellars et al., 2013), yet current evidence suggests the earliest long-distance maritime activity took place within southeast Asia (Kealy et al., 2018). This is not to say that these technologies could not have developed in Africa, but that the most secure evidence of seafaring so far, is not found in Africa. It is therefore not self-evident that an Australian FAD approximates African dispersion times and/or validates a seafaring dispersal around the Indo-Pacific rim (e.g., Stringer, 2000; Mellars, 2006a).

A final issue of using Australian FAD is the close match between genetic date for a dispersal at 65-50 ka BP and the first Australian genetic structures (Mallick et al., 2016). This means, for populations to have reached Australia by 65 ka BP, dispersal across the Indo-Pacific rim must have been extremely rapid (not to mention having to cross an arid Arabia and Thar desert). The unlikeness of such a scenario – combined with similarities in morphology and assemblage characteristics – has led to the suggestion that archaeological industries from Sahul and Australia sites dated to ~65-45 ka BP represent a continuation of earlier MSA *H. sapiens* populations (Petraglia et al., 2009; Rabett, 2018). Such a suggestion is consistent with a delayed (<35 ka BP) appearance of Upper Palaeolithic industries in India (Petraglia et al., 2007, 2009; Clarkson et al., 2009; Haslam et al., 2012), China (Zhang et al., 2011; Qu et al., 2013) and the possibility that introgression can distort the Mt-DNA 'dispersal' age (Groucutt et al., 2015a).

In summary, the Arabian palaeoclimatic and archaeological record during MIS 3 poses interesting questions for the changing nature of *H. sapiens* dispersals. As discussed, absence of speleothem growth at both Mukalla and Hoti cave suggest that rainfall was perhaps less substantial than during MIS 5 green periods. However, fluvio-lacustrine, alluvial and archaeological records (Parton et al., 2015a, 2018; Jennings et al., 2016; Rose et al., 2019) all indicate there was, at times, increased precipitation that was sufficient to allow movement of *H. sapiens* into the now desert interiors (Jennings et al., 2016; Parton et al., 2018). If we accept that MIS 3 was "drier" compared to MIS 5 green periods, what could this mean for the changing nature of human dispersals? Were MIS 5 green periods more amenable to massive population expansions, whereas MIS 3 may have favoured more limited groups? If MIS 3 was drier, did mobility patterns differ from MIS 5 populations? (I.e., were MIS 3 populations comparably mobile). Or did MIS 3

populations possess a technological/behaviour advantage that made occupation possible? Indeed, Bretzke and Conrad (2017) have previously suggested that differences in the Jabal Faya assemblages likely reflect "distinct differences in spatial behaviour"; whereas Rose et al. (2019) implied that the geometric microliths from Matafah indicate a hafted projectile technology, which could have assisted occupation in challenging regions… If MIS 4 was too hostile for successful populations, did *H. sapiens* re-enter Arabia during MIS 3? If not, what were the conditions that facilitated *H. sapiens* survival during the more arid climates of MIS 4? Many of these questions go beyond the scope of this thesis, however, the records shows us that, at least by MIS 3, *H. sapiens* were able to maintain an occupation on the Arabian Peninsula outside of a major "wet" period.

Region	**Site**	**Type**	**FAD**	**Method**	**Reference**
Levant	Manot cave	Fossil	54.7 ± 5.5 or 51.8 ± 4.5 ka BP	Calcite crust ^{230}Th	Hershkovitz et al. (2015)
India	Jwalapuram	Sediments containing Upper Palaeolithic and microlithic archaeology	38 ± 2 ka BP	OSL	Petraglia et al. (2007)
Europe	Kents' cavern	Fossil	44.2 – 41.5 ka BP	^{14}C	Higham et al. (2011)

Australia	Mungo III	Grave cut	42 ± 3 ka BP	OSL	Bowler et al. (2003)
		Grave seal	38 ± 2 ka BP	OSL	Bowler et al. (2003)
		Fossil	50.7 ± 0.9 ka BP	U-Th	Simpson and Grün (1998)
			82 ± 7 ka BP	U-Pa	Simpson and Grün (1998)
		Tooth enamel	63 ± 6 ka (early uptake) and 78 ± 7 ka (linear uptake)	ESR	Simpson and Grün (1998)
			62 ± 6 ka BP	U-series ESR	Thorne et al. (1999)
	Mungo B	Silcrete flakes	50.1 ± 2.4 ka BP	ESR	Bowler et al. (2003)
	Nauwalabila I	Archaeological horizons	60.3 ± 6.7 ka and 53.4 ± 5.4 ka BP	OSL	Roberts et al. (1994)

	Madjabebe	Archaeological horizons	60-50 ka BP	OSL	Roberts et al. (1990, 1998)
			65.0 ± 3.7/5.7 ka BP	^{14}C, OSL and Bayesian modelling	Clarkson et al. (2017)

Tab. 2. Key archaeological and palaeontological records related to the "Upper Palaeolithic" dispersal.

3.3.5.3 H. sapiens *dispersals and genetics*

Palaeogenetics has become an increasingly important field within Palaeoanthropology. Identification of lineage divergences have been used to determine dispersal dates of *H. sapiens*, particularly the evolution of genomic structures absent from African lineages (Soares et al., 2012; Mallick et al., 2016). Early genetic studies supported the Recent African Origins model (also known as "Out of Africa II"), indicating an African origin of *H. sapiens* and concluding that no genetic interaction took place between Middle Pleistocene hominin species (Currat and Excoffier, 2004). Differing estimated dates for the Out of Africa events were dependent on the DNA analysed. Templeton (2002) combined mtDNA and Y-DNA distributions to estimate that a recent African expansion took place between 80 and 150 ka BP. Moreover, potentially earlier African range expansions were predicted to have occurred at around 420 and 840 ka BP (Templeton, 2002). Since then, the study of genetics has increased and has been refined to provide smaller dating uncertainties; yet, there is still controversy concerning the correct mutation rate to be utilised (Scally and Durbin, 2012).

Recently, the Simons Genome Diversity Project published a study of 300 genomes from 142 populations (Mallick et al., 2016). The authors concluded that the oldest genomic structures outside of Africa are approximately 50,000 years old – evincing modern populations are related to a later, probably MIS 4/3 dispersal (Mallick et al., 2016). Interestingly, substantial separation of non-African populations from the southern African Khoesan and central African Mbuti pygmies took place at 131 and 112 ka BP, respectively. While divergence ages from this study are large, spanning from MIS 6 to MIS 5 (Khoesan–non-African separation: 173-82 ka BP; Mbuti 171-66 ka BP), the findings remain consistent with a plethora of palaeo-genetic data, which favour a later expansion ~60-50 ka BP.

A recent study, however, provides some genetic evidence for an earlier dispersal (Pagani et al., 2016). Papuan and Philippine Negrito genomes possess more short haplotypes assigned as African than other non-African individuals (~2%). A median genetic split between Papuan and Yoruban (Nigeria) populations is estimated to have occurred at ~90 ka BP; predating the mainland Eurasian-Yoruban split at ~75 ka BP (Pagani et al., 2016). Furthermore, when introgressed Denisovan haplotypes were identified and removed, the estimated divergence between Papuan and African populations was corrected to 120 ka BP (Pagani et al., 2016). While the more ancient 2% signature has not been replicated in other studies (Malaspinas et al., 2016; Mallick et al., 2016), the divergence indicates an earlier dispersion of *H. sapiens*, potentially during MIS 5.

Broader issues with genetic datasets cause issues for the study of human dispersals. Primarily, the assumed 'tree-like' genealogical structures used by these studies simply

does not represent human demography and population genealogy. Another assumption used is that lineages are static in the landscape, which, again, is simply not the case. Modern DNA groups are utilised and projected into the deep past, as they assume the modern lineage distribution is autochthonous (e.g., Chan et al., 2019). The historical record, however, shows that dispersal waves, conflict, extirpations and colonisations are common features of human societies.

Another issue is the role of introgression between 'dispersed' and autochthonous populations. Groucutt et al. (2015a) provided an excellent example, in which the dispersal of haplogroup L3 could provide an equifinal age of 80 ka BP under three models with differing introgression. In the first model, no introgression and dispersal at 50 ka BP was assumed. Within the remaining models, a dispersal datum of 120 ka BP and introgression into and out of Africa were assumed. This is supported by a more recent study, in which divergences of populations within Africa (Mbuti and Biaka, Mbuti and west African Yoruba, Yoruba and San, San and both Biaka and Mbuti) and between these groups and non-African were inconsistent with clear genetic splits (Bergström et al., 2020). Instead, genetic divergence of many of these lineages could have been a long process spanning tens of thousands of years. These findings highlight the potential issues of using genetic data alone to establish a dispersal age for *H. sapiens*. In order to mitigate these uncertainties, recent studies have aimed to extract aDNA from dated ancient individuals to understand past genetic structures (Kuhlwilm et al., 2016; Meyer et al., 2016; Welker et al., 2016; Loosdrecht et al., 2018). While this new data is revealing more than once previously believed possible, data remains geographically and chronologically sparsely distributed.

3.3.6 Summary

While genetic data is currently providing limited evidence of earlier *H. sapiens* dispersals, palaeoclimate, palaeontology and archaeology of Arabia, the Indo-Pacific rim, China and Sahul are demonstrating a more complex picture than previously considered (Groucutt et al., 2015a; Bae et al., 2017; Rabett, 2018). The palaeoclimatic conditions of Arabia therefore could provide a unique opportunity to determine null hypotheses for terrestrial dispersal timings from sub-Saharan Africa. Current palaeoclimate evidence shows the potential for peak interglacial conditions of MIS 5 to have facilitated these dispersals, and perhaps also MIS 3, although this is less clear. However, there remain a number of uncertainties. For example, did *H. sapiens* disperse across the Bab el Mandeb strait, or via the Sinai Peninsula (or both)? To what extent did precipitation during MIS 3 impact the environments of Saharo-Arabia? Understanding the precise timings of increased rainfall could mitigate some of these current uncertainties, by comparison with independently dated records (such as sea-level).

3.4 Conclusion

Throughout the duration of the *Homo* genus, dispersals Out of Africa have occurred multiple times, though the precise timings of these is unclear. For early *Homo* dispersals, there is mounting evidence that dispersal took place prior to the earliest fossils finds outside of Africa, potentially indicating hominins occupied Eurasia as early as 2.5 Ma BP. Yet, it cannot be said whether dispersals at this time were frequent events, or whether one major dispersal was followed by long periods of isolation between Eurasian and African hominins. As Saharo-Arabia currently acts as a vast biogeographic barrier between sub-Saharan Africa and Eurasia, the paleoclimate conditions of the Saharo-Arabian desert belts can offer null hypothesis for these dispersals. Current data shows

that periods of increased rainfall in Saharo-Arabia can be associated to insolation maxima over the last 350 ka BP. This was reflected by activation of fluvio-lacustrine systems and formation of habitable "green" environments. During MIS 5 interstadials, environmental amelioration facilitated hominin occupation of now arid areas of the Arabian Peninsula and provided opportunities for dispersal into Eurasia. While the phases of increased rainfall can be attributed to insolation maxima, there are currently conflicting data on 1) the timing and duration of pluvial periods, 2) the source of precipitation during these wet periods, 3) the nature of wet periods (at both an inter-pluvial period level, but also within pluvial phases), and 4) the type of environments that formed within pluvial phases.

1. Taphonomical and chronological uncertainties of palaeoclimate and archaeological material means that it is more difficult to determine the influence of monsoon variability on hominin distribution over 130 ka BP. While indeed there is good evidence for periods of increased rainfall up to 350 ka BP, many terrestrial records currently contain large dating uncertainties, making precise assignment to interglacial (and interstadial periods) difficult. Additionally, there is very limited evidence for timing of enhanced precipitation prior to 350 ka BP. However, given the clear relationship between an enhanced monsoon domain, increased NHI and interglacial maxima and warm substages within the mid-late Pleistocene (Fleitmann et al., 2011; Parton et al., 2015b), it is likely that incursions of the tropical rain-belt continued throughout the Pleistocene. Further palaeoclimate records with robust chronologies may therefore inform on the potential timings of hominin occupation of Arabia prior to 130 ka BP.
2. While evidence currently favours a southern, monsoonal source of precipitation during these wet periods (e.g., Fleitmann et al., 2003b), this was established using

only speleothem δD_{FI} values; whereas $\delta^{18}O_{FI}$ was estimated using the temperature dependent calcite-water fractionation equation. New methods now allow precise measurement of fluid inclusion $\delta^{18}O$, which could be used to refine these earlier findings. Additionally, this original analysis was performed on speleothems from Hoti Cave. Mukalla Cave speleothems are yet to undergo this analysis, where the African Summer Monsoon is considered to have been responsible for delivering increased precipitation (Rosenberg et al., 2013). This hypothesis could be tested by comparison of renewed isotope analysis of fluid inclusion water from Mukalla and Hoti Cave speleothems.

3. There is currently limited data from terrestrial records that allow comparison between the intensity of pluvial phases. This means discussions of Arabian palaeoclimate are often limited to a wet-dry dichotomy, with little discussion of 1) changing annual rainfall on a continuum, 2) comparison of intensity between so called "wetter" phases and 3) high-resolution changes of precipitation during wetter phases. Gaining insight into these topics is key for understanding palaeoclimatic variability and feasibility of dispersal windows.
4. Definitions of past Arabian palaeoenvironments are frequently limited to "green" or "savannah" environments. Current evidence restricts clarification of environments beyond these broad and woolly definitions; however, it is important that further environmental data is produced to identify landscape variability within "green" phases.

Resolving these issues is of prime importance to understanding the timings of hominin occupation of Saharo-Arabia and demographic shifts in Eurasia. Throughout this thesis, points 1-4 were addressed as follows:

1. A novel 1.1 million-year speleothem-based palaeoclimate record was developed from Mukalla Cave, Yemen. South Arabian Humid Periods (SAHPs) were restricted to precession forced NHI maxima during interglacial periods. Preliminary work on stalagmites from Broken-Leg Cave, Star Cave and Surprise Cave, Saudi Arabia, also suggests wet periods occurred in Arabia during punctuated periods during the Pliocene and Early Pleistocene.
2. Speleothem fluid inclusion $\delta^{18}O$ and δD measurements were obtained from Mukalla and Hoti Cave (Oman) stalagmites, finding that both the ASM and ISM became the dominant source of precipitation during SAHPs.
3. Analysis of speleothem $\delta^{18}O_{ca}$ showed that there was considerable variability in precipitation intensity between SAHPs. One key finding is that all Pleistocene SAHPs were wetter than the Holocene SAHP.
4. Speleothem $\delta^{13}C_{ca}$ measurements showed that mixed C_3/C_4 grasslands flourished above Mukalla Cave during SAHPs. Additionally, ultra-high-resolution analysis of $\delta^{18}O_{ca}$ and $\delta^{13}C_{ca}$ from an annually limited stalagmite (H13, Hoti Cave), showed that environments were characterised by a wetter (summer) and drier (winter) seasonality.

Chapter 4

4) Speleothems in palaeoclimatology: materials and methods

4.1 Introduction

In the previous chapter the use of speleothems for reconstructing Arabian palaeoclimate was briefly discussed. In particular, the ability to precisely date speleothems via U-Pb and ^{230}Th techniques and provided a plethora of palaeoclimate information via stable isotope analyses has the potential to provide timings of hominin dispersal windows. The stalagmite records from Hoti Cave, Oman, and Mukalla Cave, Yemen, grew exclusively within interglacial periods and warm substages back to MIS 9 (Burns et al., 1998; Fleitmann et al., 2003b, 2011). One stalagmite, Y99 (Mukalla Cave), was only analysed at the top ~60 cm, out of a total of 3.2 m. Y99 is therefore an excellent sample to extend the palaeoclimate record of Arabia. Additionally, a stalagmite from Hoti Cave (H13) possesses annual visible laminations, which could be used to provide records of sub-annual climates during pluvial periods. Further stalagmite samples had also been collected from across Saudi Arabia during 2001 (Fleitmann et al., 2004b). Initial findings suggest these samples are older than 1 million years and could provide crucial information of the Saharo-Arabia deserts during the early Pleistocene. This thesis therefore aims to extend the palaeoclimate record of Arabia based on these stalagmites. In this chapter, the formation of speleothems and palaeoclimate information they can provide is discussed.

4.2 Formation

Approximately 80% of dissolution caves are formed by the downward percolation of meteoric water with elevated CO_2 concentrations. This dissolves the relatively soluble host rock of the cave, which are typically carbonate aquifers with little to no water drainage (Fairchild et al., 2006). Speleothems (flowstones, stalagmites and stalactites) are secondary calcium carbonate deposits formed in solution caves from drip-waters These are formed by complex interactions between CO_2, H_2O and Ca in three zones: the soil zone, the karst zone and the cave environment.

4.2.1 The soil zone

Within the soil zone, the primary reaction is that between precipitation H_2O and soil CO_2 (Fig. 21). Soil CO_2 is derived mostly from microbial and plant respiration and decaying plant matter (Clark and Fritz, 1997). Percolating H_2O equilibrates with soil CO_2 to form carbonic acid. This process is known as carbonation (Bar-Matthews et al., 1991):

$$H_2O_{rainwater}(l) + CO_{2\ soil}(g) \rightarrow\ H_2CO_3(aq)$$

Carbonation typically takes place within minutes to hours from the introduction of water. Carbonic acid then dissociates in two steps, and both steps release a hydrogen ion:

$$H_2CO_3(aq) \leftrightarrow\ HCO_3^-(aq) + H^+(aq)$$

$$HCO_3^-(aq) \leftrightarrow\ H^+(aq) +\ CO_3^{2-}(aq)$$

The dissolved carbonic acid reacts with calcium carbonate ($CaCO_3$) in the soil and cave limestone to form aqueous calcium bicarbonate ($Ca(HCO_3)_2$):

$$H_2CO_3(aq) + CaCO_3 \leftrightarrow Ca^{2+} + 2HCO_3^-$$

The ratio of soil CO_2 to host rock carbonate of cave drip-water is dependent on soil PCO_2 concentration. Soil CO_2 concentration is influenced by soil productivity and organic matter degradation, which are determined by plant productivity, vegetation, rainfall amount and temperature (Clark and Fritz, 1997). Where temperatures and plant activity are high, increased soil CO_2 equilibrates with $H_2O_{precipitation}$, leading to increased dissolution of host rock carbonate. Moreover, atmospheric CO_2 that infiltrates porous soils can reduced soil CO_2 contribution of groundwaters (Baker et al., 1997; Wong and Breecker, 2015; Breecker, 2017).

If the cave system is "open", constant equilibrium occurs between the water and reservoir of soil CO_2, thus the dissolved CO_2 reflects the isotopic composition of the soil. In a closed system, however, seepage water is isolated from soil CO_2. As shown above, CO_2 is consumed in the carbonate reaction; thus, limestone dissolution is limited by the finite CO_2; whereas an open system possesses an almost limitless source of CO_2.

4.2.2 The karst zone

After mixing in the soil zone, the solution is transported into the karst zone. Mostly, waterflow is vertical, moving through fracture, conduit and seepage flow. Water is predominantly directed through fractures, which transport the faster flowing waters (Fig. 21). Conduits tend to be the most variable flow path, which usually activate only after

heavy rainfall and deluge (Fairchild and McMillan, 2007). Seepage water enhances when evapotransportation decreases. Flow through the karst system can range from hours to years. ^{14}C measurements from Belgian and Slovenian stalagmites have been utilised to estimate a 5-10 year lag between carbonation and speleothem precipitation (Genty et al., 1998); however, groundwater mixing may have led to overestimated residence times. Nevertheless, long residence times should not be expected to be issues for stalagmites from caves below thin soils, such as those found in hyper-arid regions (e.g., the deserts of Arabia).

4.2.3 The cave system

Speleothem precipitation occurs within the cave system when nucleation occurs (Fig. 21). This is achieved by rising supersaturation of the drip-water. Degassing of drip-water facilitates supersaturation by removing CO_2 from the solution:

$$Ca^{2+} + 2HCO_3^- \leftrightarrow CaCO_3(s) + CO_2(g) + H_2O(l)$$

The pressure difference between cave atmosphere PCO_2 and soil PCO_2 drives the degassing of drip-water. Soil PCO_2 ranges 0.1-3.5%, whereas cave atmosphere CO_2 is typically 0.06-0.6%. CO_2 in drip-water is present in molecular form, thus, when the higher PCO_2 of the drip-water meets the low PCO_2 of the cave air, molecular diffusion occurs (Dreybrodt, 2011). This process is rapid, resulting in degassing of water films of <0.02cm in tens of seconds (Dreybrodt, 2011). This creates equilibrium between PCO_2 drip-water and cave air, leading to supersaturation of drip-water $CaCO_3$, which in turn promotes the precipitation of speleothems. “Synchronous crystallisation” enables speleothem growth (Stepanov, 1997). This is the process by which each successive

growth layer of calcite crystals precipitates at almost the same time as the preceding layer. If, however, equilibrium of PCO_2 is not reached, the drip-water will continue to travel until equilibrium occurs (Dreybrodt, 2011).

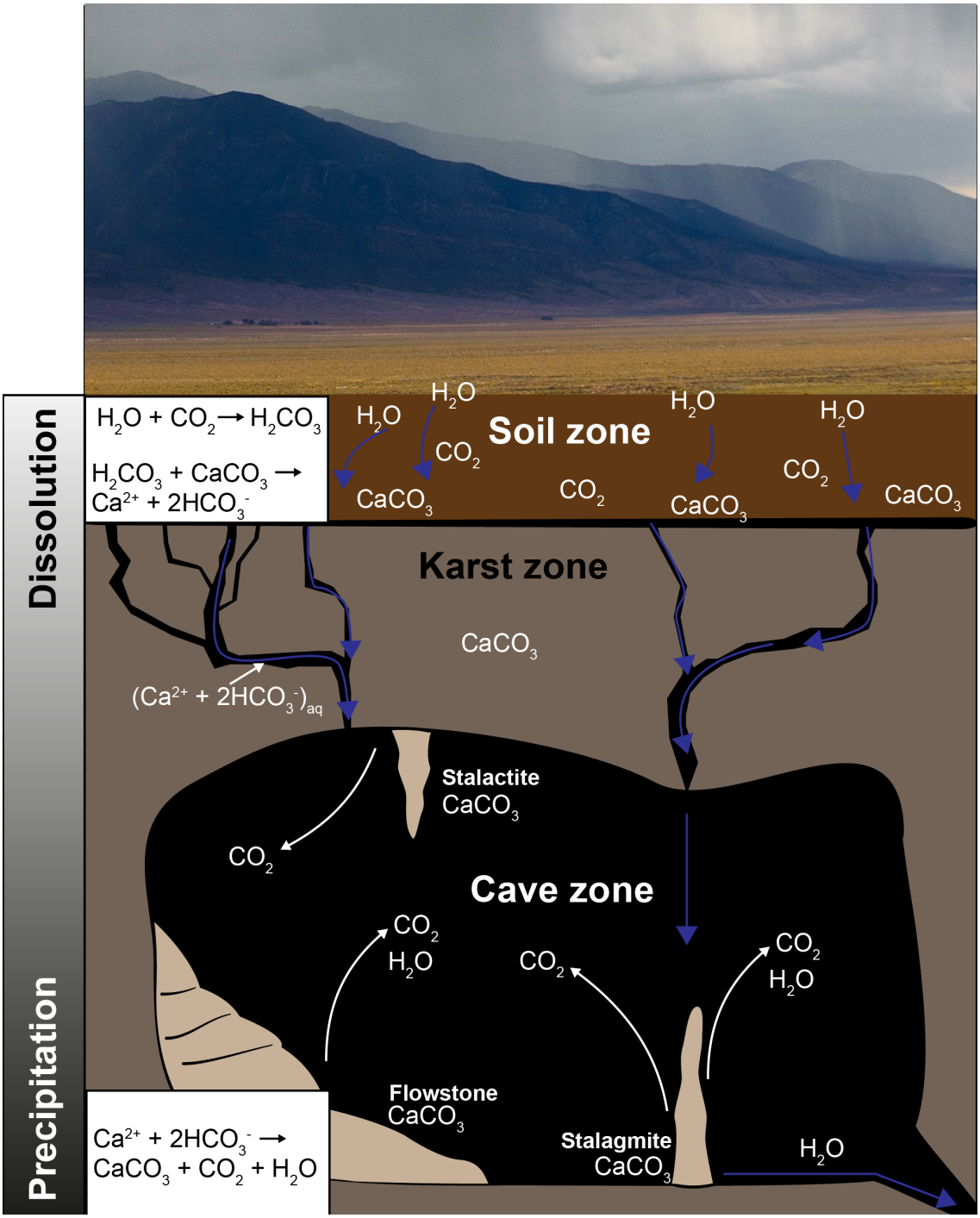

Fig. 21. Conceptual illustration of the formation of speleothems (stalagmites, stalactites and flowstones) and zone-specific processes.

4.3 Types of speleothem

4.3.1 Stalagmites

Stalagmites grow vertically from the cave floor – usually from a dripping stalactite – and have a growth axis perpendicular to the substrate (Fig. 21). These are cylindrical to conical in shape with more candle-like shapes associated with highly effective $CaCO_3$ precipitation. Stalagmites are preferred for palaeoclimate reconstructions, as they often have only one associated drip water source and possess a relatively simple growth pattern. When cut open, calcite stalagmites often present clearly laminated growth layers, similar to tree-rings. These allow a clear stratigraphy to be developed. When combined with accurate ^{230}Th ages (discussed below) and high-resolution analysis of stable isotopes, this can be used to create palaeoclimate records with robust chronologies. Furthermore, some stalagmites possess annual laminations. When ^{230}Th ages are combined with the couniting of annual laminations, palaeoclimate records can be produced at annual or even sub-annual resolution (e.g., Asrat et al., 2018). Another feature of speleothems is that their growth can be activated multiple times. Within a stalagmite, cessation of growth can be identified macroscopically by clear white layers or shifts in the growth axis. These may also be identified isotopically by distinct shifts in $\delta^{18}O_{ca}$ or increased prevalence of trace-elements (e.g., Ti; discussed below). These growth hiatuses can provide timing of reduced rainfall (Fleitmann et al., 2011), changes in the flow path and tectonic activity (Asrat et al., 2018).

4.3.2 Stalactites

Stalactites grow downward from cave ceilings (Fig. 21). These are similar to stalagmites in being conical or cylindrical in morphology. Soda straw stalactites are cylindrical and hollow on the inside. These form downward at seepage zones on cave ceilings, with very little outward growth. Conical stalactites form from soda straws, where a soda straw is gradually filled by sparite crystals, leading to the redirection of waterflow to the outside of the straw. This directs calcite precipitation to the side of the straw, which then forms a cone. The irregular evolution of stalactites means these are often undesirable for creating high-resolution palaeoclimate records, unlike stalagmites.

4.3.3 Flowstones

Flowstones are laminated deposits that grow on cave floors and cave walls (Fig. 21). These develop from films of $CaCO_3$ supersaturated waters or relatively strong fissure/conduit flows. As such, these can be extremely thick and long and extend far beyond the water source. These are frequently associated to high energy flooding events; though flowstones can be frequent in caves with high annual precipitation. The large extent means that they can be cored repeatedly; however, the irregularity of growth (and irregular stratigraphy), increased potential of detrital input and impurities means that dating flowstones can be problematic.

4.4 Mineralogy

The minerology of speleothems can provide critical details on the formation processes, which can be linked to conditions of the cave environment and climate outside of the cave. Calcite and aragonite are the two most common speleothems that are used within

palaeoclimate science. Whereas aragonite speleothems can be related to extreme events (aridity or flooding), calcite speleothems are related to more stable conditions. However, both aragonite and calcite can be present within a single speleothem and can influence the ability to construct reliable palaeoclimate records.

4.4.1 Calcite

Calcite is a trigonal mineral and the most stable polymorph of calcium-carbonate. Typically, calcite contains less than 0.5% mole of $MgCO_3$ (Lippmann, 1973; Borsato et al., 2003). Though, low magnesium calcite (LMC) and high magnesium calcite (HMC) are used to distinguish calcite in which magnesium concentrations are either less than or greater than 5% mole, respectively (Scoffin, 1987). Under earth surface pressures and temperatures, LMC with <4% mole $MgCO_3$ are the most stable forms of calcite (Lippmann, 1973). Calcite speleothems are the most abundant carbonates due to the dominance of limestone in carbonate host rocks (Lippmann, 1973).

Calcite is rhombohedral, with a Ca atom surrounded by six CO_3 groups with oxygen being situated closest to Ca atoms (Lippmann, 1973). In a pure form calcite is colourless; however, in natural systems, impurities can turn calcite a colourful mineral, ranging from white, yellow, hues of greens, light to dark brown and red (White, 1981). Colour is given to calcite via the inclusion of detrital materials, oxides, organic matter or organic molecules. Calcite can be shinier and brighter than aragonite. Generally, calcites have more visible banding than aragonite.

4.4.2 Aragonite

Aragonite is another polymorph of calcium carbonate. Aragonite crystals are orthorhombic, in which Ca^{2+} is bonded to nine oxygen atoms from six CO_3 groups (Lippmann, 1973). Three CO_3 groups bond to Ca^{2+} with two oxygen atoms. The remaining CO_3 bonds to Ca^{2+} with one oxygen atom. This gives aragonite the structural formula of $A^{IX}C^{III}O^{iV}_3$ (Lippmann, 1973). Aragonite crystals appear more fibrous than calcite and are oriented parallel to the growth axis (Fairchild et al., 2006), they also tend to fan from a single point of origin.

Aragonite and calcite can occur in the same caves and even in the same speleothem (Wickens, 2013). Aragonite stalagmites usually form from more seasonal drip waters, whereas calcites often form from more continuous drip waters. Larger stalagmites are often comprised of calcite due to the greater amount of drip water required to form these. Additionally, extremely high flow rate can lead to dissolution of aragonite due to insufficient residence time to allow efficient $CaCO_3$ precipitation from the cave waters. Within a stalagmite, fluctuating calcite/aragonite layers can be used to identify periods of increased/decreased rainfall.

The usefulness of aragonite speleothems as palaeoclimate indicators is varied. As aragonite is less stable than calcite, it is much more sensitive to changing hydrological, temperature and pressure conditions in the cave, which can lead to phase change and recrystallisation to calcite (Fairchild et al., 2006). Whereas studies from Hulu cave have shown that aragonite speleothem $\delta^{18}O$ was in equilibrium with drip water $\delta^{18}O$, it is much more complicated to draw palaeoclimate interpretations from aragonite $\delta^{13}C$ (Hopley et al., 2009). Another study of South African speleothems with calcite and aragonite fabrics

found $\delta^{18}O$ was invariable between primary and secondary materials, yet $\delta^{13}C$ was more negative in primary fabrics (Hopley et al., 2009). Thus, drawing conclusions from aragonite $\delta^{13}C$ may not be straightforward. Yet, when aragonite is dissolved during recrystallisation, the $CaCO_3$ $\delta^{18}O$ equilibrates with the water $\delta^{18}O$, meaning that the precipitated calcite can take on this signature (Perdikouri et al., 2011). As such, recrystallised areas are often avoided during analysis of speleothem stable isotopes ($\delta^{18}O/\delta^{13}C$).

Another issue is that recrystallisation can lead to problematic ^{230}Th ages. Loss of Uranium (U) during recrystallisation can occur as the UO_2^{2+} cation is soluble, whereas the Thorium (Th) Th^{4-} anion is insoluble in aqueous environments. Therefore, U can be mobilised and leached from the speleothem (Bajo et al., 2016). This can lead to older ^{230}Th ages than the true age of the speleothem. However, if closed system conditions prevail, the integrity of ^{230}Th ages should not be compromised.

4.5 Stable Isotopes of Speleothems

The most commonly analysed stable isotopes within speleothem based palaeoclimate reconstructions are O, C and H (Tab. 3). These occur in abundance in the natural environment, and (as above) are present throughout the dissolution and deposition of speleothems. It is the difference of isotopic composition of the elements which is crucial to palaeoclimate research. Between isotopes, the proton and electron quantity remain consistent, however, the number of neutrons within the nuclei differs and influences the overall atomic mass.

	Isotopic abundance (%)	**Measurement**

Oxygen	^{18}O: 0.1995	^{17}O: 0.0375	^{16}O: 99.763	$\delta^{18}O$ ($^{18}O/^{16}O$)
Carbon	^{13}C: 1.11	^{12}C: 98.89		$\delta^{13}C$ ($^{13}C/^{12}C$)
Hydrogen	^{2}H (*D*): 0.0156	^{1}H (*P*): 99.9844		δD (*D*/*P*)

Tab. 3. Isotopic abundances of Oxygen, Carbon and Hydrogen.

The isotopic composition does not affect the chemical behaviour of these elements but causes distinct fraction between physical phases. The differences in atomic mass influence the differences in mobilisation of the heavy isotope relative to the lighter isotope. For O and H, this is particularly relevant during the temperature dependent evaporation and condensation of water. However, differences of mobilisation and preferential incorporation are present throughout the formation of speleothems (Lachniet, 2009). The difference between two phases is measured by a fractionation factor (α). This is calculated as the ratio between isotope ratios (R) of the reactant and product:

$$a = \frac{R_{reactant}}{R_{product}}$$

or, for example: $$a\mathrm{D}(\mathrm{water} - \mathrm{vapour}) = \frac{\frac{D}{P}water}{\frac{D}{P}vapour}$$

The delta (δ) notation is the current method used to report stable isotope data. This value represents the isotopic ratios of heavy to light isotopes between a sample and a standard. This is defined as:

$$\delta = \frac{R_{sample} - R_{standard}}{R_{standard}} \times 1000$$

In the case of $\delta^{18}O$:

$$\delta^{18}O = \frac{\frac{^{18}O}{^{16}O}sample - \frac{^{18}O}{^{16}O}standard}{\frac{^{18}O}{^{16}O}standard}$$

The standard is an internationally used material of known composition. For calcite ($\delta^{18}O$ and $\delta^{13}C$), the V-PDB (Vienna – Pee Dee Belemnite) scale is utilised; whereas water-isotope (δD and $\delta^{18}O$) measurements are reported relative to the V-SMOW (Vienna – Standard Mean Ocean Water) scale.

4.5.1 Oxygen isotopes as climate indicators

Oxygen-18 (^{18}O), or heavy oxygen, is a stable isotope of oxygen, containing 8 protons and 10 neutrons in the nucleus; whereas oxygen-16 (^{16}O), light oxygen, contains 8 protons and 8 neutrons in the nucleus. Oxygen $^{18}O/^{16}O$ ratios stored in speleothem $CaCO_3$ are derived from surface runoff rainwater which percolates into conduits and fractures of the epikarst (Fig. 21 and Fig. 22). Oxygen isotopes are incorporated into the $CaCO_3$ and in small fluid inclusions (discussed in 4.6) of the stalagmite. The fractionation of $\delta^{18}O$ from the moisture source and final incorporation into a stalagmite can provide a plethora of palaeoclimate information.

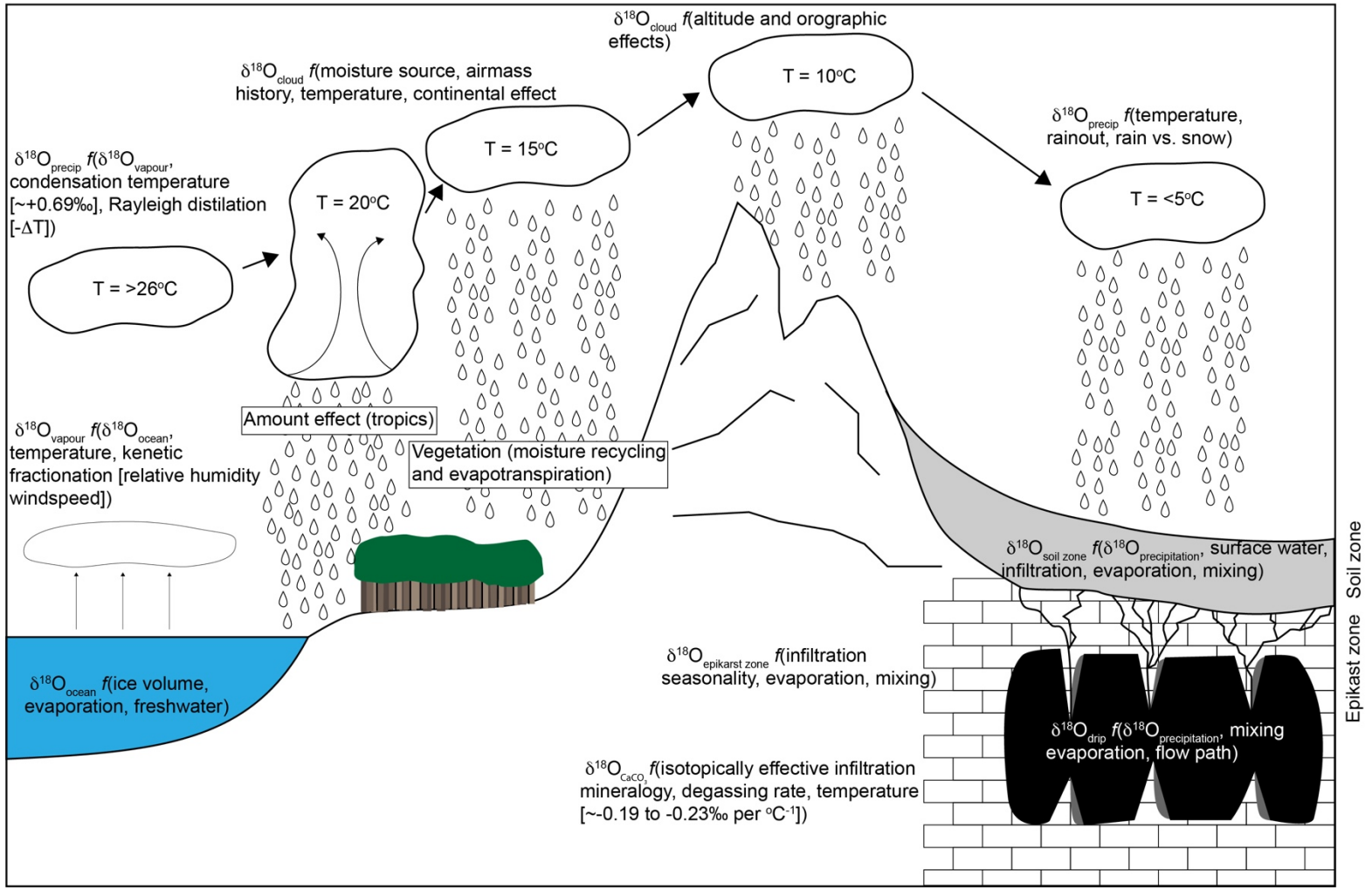

Fig. 22. Fraction effects on precipitation $\delta^{18}O$ (after Lachniet, 2009)

4.5.1.1 The source effect

The source effect is the observation that air masses derived from different moisture sources possess distinct $\delta^{18}O$ values (Lachniet, 2009). $\delta^{18}O$ values differ between oceans and seas: higher ocean $\delta^{18}O$ values are present in equatorial and subtropical zones, where evaporation is greater; whereas more negative $\delta^{18}O$ values are associated with freshwater input from ice-melt and high-latitude regions (LeGrande and Schmidt, 2006). The evaporated $\delta^{18}O_{vapour}$ therefore is reflected by the source. The evaporation of source water is also temperature dependent:

$$1000 \ln a(liquid - vapour) = 1.137(10^6 T_k^2) - 0.4156\left(\frac{10^3}{T_k}\right)$$

where T is Kelvin (Clark and Fritz, 1997), and dependent on relative humidity:

$$\Delta_\varepsilon {}^{18}O(liquid - vapour) = 14.2(1 - h)‰$$

where h is relative humidity (Clark and Fritz, 1997). Thus, highly evaporative or high relative humidity environments influence the resulting $\delta^{18}O_{precipitation}$. Rainfall $\delta^{18}O$ values are thus reflective of the source.

Stalagmite $\delta^{18}O_{ca}$ of a composite Chinese record was interpreted to show 21 ka cycles of monsoon intensity (Cheng et al., 2016). However, recent studies of $^{10}Be_{loess}$ indicates that ESAM (East Summer Asian Monsoon) precipitation intensity matched global glacial-interglacial cyclicity (increased precipitation during interglacial periods) (Beck et al., 2018). Speleothem $\delta^{18}O_{ca}$was subsequently reinterpreted to represent changing dominance of the ESAM and WNPSM (Western North Pacific Summer Monsoon) (Wang et al., 2001; Beck et al., 2018).

It must also be considered that the source water can be altered by various influences, which will be reflected in $\delta^{18}O_{precipitation}$. On glacial-interglacial timescales, the LR04 stack $\delta^{18}O_{benthic}$ record shows changes in sea-ice coverage are reflected by changes in $\delta^{18}O_{ocean}$ (Lisiecki and Raymo, 2005). Additionally, changes of precipitation regimes can also influence source water $\delta^{18}O$. Mediterranean Sea $\delta^{18}O$ was altered during interglacial maxima (Rohling et al., 2015; Grant et al., 2016). This was caused by increased sea-level and Sahara runoff of monsoonal rainfall into the Mediterranean, reducing $\delta^{18}O_{ocean}$ (Bar-Matthews et al., 2003; Rohling et al., 2015; Grant et al., 2016). Evaporated precipitation from the Mediterranean was thus negative in $\delta^{18}O$ compared to glacial periods and resulted in more negative $\delta^{18}O_{ca}$ within the long Soreq Cave speleothem record (Bar-Matthews et al., 2003; Grant et al., 2016). Similarly, $\delta^{18}O_{ca}$ from Kanaan Cave (Nehme et al., 2015) and Peqiin Cave (Bar-Matthews et al., 2003) was influenced by decreased Mediterranean $\delta^{18}O_{precipitation}$.

4.5.1.2 Rayleigh distillation

Rayleigh distillation explains the progressive condensation and distillation of $\delta^{18}O_{precipitation}$ (Fig. 23). This is a fundamental concept for the application of $\delta^{18}O$ as a palaeoclimate indicator. After evaporation from the moisture source, the removal of ^{18}O from an airmass is temperature dependent. The condensation of vapour to liquid is an equilibrium process. However, ^{18}O is preferentially incorporated into the condensed state, meaning that the $\delta^{18}O_{precipitation}$ is greater than $\delta^{18}O_{vapour}$. In order to condense more moisture, temperature must decrease. This may be achieved by orographic lifting, frontal cooling and/or convection. The processes described by Rayleigh distillation are key for

understanding the temperature effects, altitude effects and the continental effect (discussed below).

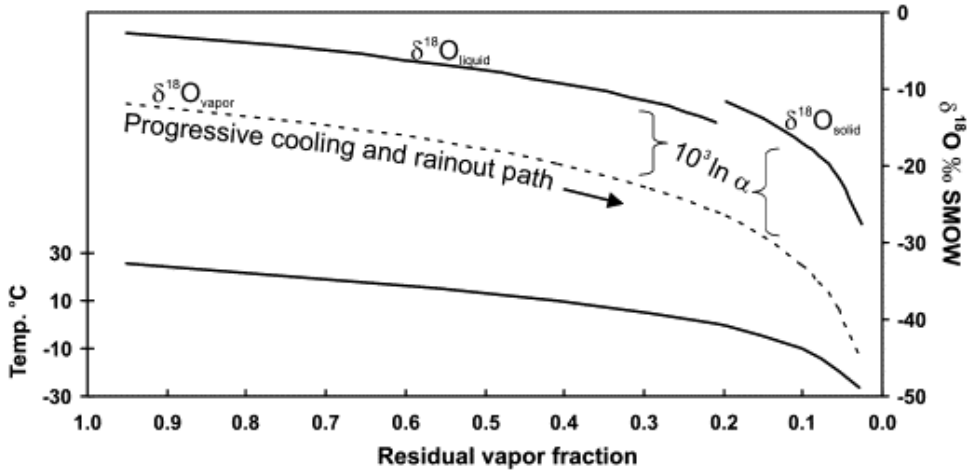

Fig. 23. Rayleigh distillation of $\delta^{18}O_{precipitation}$. Cooling and rainout is a function of increasing latitude, altitude and reduced temperature (Lachniet, 2009).

4.5.1.3 Temperature effects

The temperature effect in precipitation

The temperature effect is the observed positive correlation between the MAT (mean annual temperature) of a site and rainfall $\delta^{18}O/\delta D$ (Dansgaard, 1964; Lachniet, 2009). The global relationship was expressed as:

$$\delta^{18}O = 0.69(MAT) - 13.6‰SMOW$$

(Dansgaard, 1964)

This is present in mid to high latitudes. In low latitudes (discussed below), however, the gradient of this relationship is site dependent and temporally variable (Dansgaard, 1964; Rozanski et al., 1993). Temperature changes may also affect seasonal precipitation $\delta^{18}O$ values (Lachniet, 2009). The temperature dependent fractionation of $\delta^{18}O_{precipitation}$ posits

greater ^{16}O during winter months relative to summer months. This has been exhibited in rainfall values from Kentucky (Harmon, 1979) and Israel (Ayalon et al., 1998).

The cave air temperature effect

Once precipitation reaches that cave as groundwater, temperature continues to control the final $\delta^{18}O_{ca}$ value. The fractionation of $\delta^{18}O_{drip\text{-}water}$ and precipitated $\delta^{18}O_{ca}$ is temperature dependent. This results in greater ^{18}O within a stalagmite relative to the drip-water due to stronger ^{18}O bonds (Sharp, 2007). An equilibrium fractionation factor was formulated by the study of synthetic calcite (Kim and O'Neil, 1997):

$$1000\ ln\ \alpha(calcite - water) = 18.03(10^3 T^{-1}) - 32.42$$

1000 ln α (calcite – water) is the fraction between calcite and water, and T is temperature measured in Kelvin. The resulting 1000 ln α values range from 33.62‰ to 26.12‰. When converted to a $\delta^{18}O/T^{o}C$ equation, the resulting $\delta^{18}O/T$ slope ranges -0.18 to -0.23‰ per $^{o}C^{-1}$ for temperatures between 35°C to 5°C. Thus, increased cave temperatures lead to decreased $\delta^{18}O_{ca}$. As cave temperatures typically reflect the average annual temperature outside of the cave, the cave temperature effect should not be expected to influence stalagmite $\delta^{18}O$ at a sub-annual level. Though, seasonal temperature variations exerted on $\delta^{18}O_{precipitation}$ before entry into the cave may be detected at sub-annual level.

4.5.1.4 The altitude effect

The altitude effect describes the relationship between decreased $\delta^{18}O_{precipitation}$ with increased altitude. This is influenced by the decreased temperature of $\delta^{18}O_{vapour}$ and Rayleigh distillation as the airmass is lifted by an orographic barrier (Fig. 22 and Fig.

23). Typically, the altitude effect influences $\delta^{18}O$ by ~2 to 3‰ km^{-1} (Gonfiantini et al., 2001; Poage and Chamberlain, 2001; Lachniet and Patterson, 2006). Orographic lifting over a mountain range can also cause an isotopic rain shadow, where $\delta^{18}O_{precipitation}$ is more negative on the leeward side.

4.5.1.5 The continental effect

The continental effect is the observation that rainfall $\delta^{18}O$ values decrease with distance from the ocean (Dansgaard, 1964; Rozanski et al., 1993; Clark and Fritz, 1997; Lachniet, 2009). The isotopic composition of clouds is dependent on temperature; heavy ^{18}O is preferentially precipitated at lower altitudes and higher temperatures (Lachniet, 2009). As clouds prevail inland, orographic lifting, frontal cooling and convection lifts lead to distillation of the airmass and decreased $\delta^{18}O_{vapoir}$ (Lachniet, 2009). Thus, an airmass will be comprised of greater $\delta^{18}O_{vapour}$ at the coast, whereas more negative $\delta^{18}O_{vapour}$ will occur further inland. This may, however, be counteracted by recycled $\delta^{18}O$ from surface evaporation of soil water, rivers and lakes (Lachniet, 2009).

4.5.1.6 The amount effect

The amount effect is the observed negative correlation of $\delta^{18}O_{precipitation}$ with increased rainfall (Dansgaard, 1964; Rozanski et al., 1993; Risi et al., 2008); occurring predominantly in tropical regions, where deep vertical convection is common, prompted when sea surface temperatures exceed 27.5°C (Graham and Barnett, 1987; Lachniet, 2009). Rainfall quantity has the largest influence on $\delta^{18}O$ values of tropical moisture sources, attenuating or overprinting the temperature effect (Fleitmann et al., 2003b, 2004a, 2011). Previous analyses of speleothems from the Arabian Peninsula have shown

seasonal $\delta^{18}O_{precipitation}$ values vary by ~2‰ due to rainfall amount (Fleitmann et al., 2003b, 2004a).

4.5.2 Carbon isotopes as environmental indicators

Carbon-13 (^{13}C), or heavy Carbon, is a stable isotope of carbon, with a nucleus comprising of 6 protons and 7 neutrons. Carbon-12 (^{12}C), or light carbon, another stable isotope of carbon, has a nucleus consisting of 6 protons and 6 neutrons. Calcite $\delta^{13}C$ values provide information of vegetation and soil CO_2 compositions above the cave. Uptake of atmospheric carbon by plants leads to a significant depletion of Carbon-13, as the lighter ^{12}C isotope is preferentially absorbed for photosynthesis. During this process, CO_2 is converted to Carbohydrate (CH_2O) through a process known as carboxylation. As plants die and accumulate within the soil, aerobic bacteria convert plant CH_2O back to CO_2 with a similar $\delta^{13}C$ value. Microbial activity is largely dependent on temperature and soil humidity (derived from precipitation), increased temperature and soil humidity lead to lower $\delta^{13}C$ values.

The photosynthesis pathway of vegetation (C_3, C_4 or CAM) influences the fractionation of ^{13}C during carboxylation. The Calvin (C_3) cycle operates in ~85% of plant species, fixing CO_2 with the Rubisco enzyme, which catalyses CO_2 respiration with oxygen. This results in a ^{13}C depletion of 22%. The Hatch-Slack (C_4) pathway adds a preceding step in which the PEP carboxylase enzyme increases the quantity of carbon to Rubisco for fixation, resulting in reduced $\delta^{13}C$ fractionation, and $\delta^{13}C$ values of -16 to -10‰; with more negative values associated with xeric environments, and more positive values associated with mesic conditions (Clark and Fritz, 1997). C_3 vegetation dominates

temperate, high latitude regions, and tropical rainforests – ~85% of plant species utilising this pathway; whereas C_4 plants flourish in tropical and temperate grasslands – representing 5% of floral species. Crassulacean acid metabolism (CAM) operates in ~10% of plant species, distributed in desert biomes, such as cacti. The CAM system utilises the C_3 pathway at day and the C_4 pathway during night. As a result, $\delta^{13}C$ values are intermediate.

During the transportation of soil CO_2, some is hydrated and dissociated into HCO_3^- (bicarbonate) and CO_3^{2-} (carbonate). Fractionation is determined by temperature, and results in $\delta^{13}C$ enrichment of 11‰ for a soil CO_2 value of -23‰ at 25°C (Clark and Fritz, 1997). Cave limestone $\delta^{13}C$ (≈0‰) is close to the international VPDB calcite standard value and is approximately 15‰ more positive than carbon from the soil zone (Clark and Fritz, 1997). The dissolution of cave limestone increases $\delta^{13}C$ values of dissolved carbonate and bicarbonate in cave drip waters, the extent to which depends on the "openness" of the system and the soil PCO_2 (discussed below). However, C_3 vegetation are typically be reflected by $\delta^{13}C_{ca}$ values of -14 to -6‰; whereas C_4 vegetation is typically reflected by $\delta^{13}C_{ca}$ values of -6 to +2‰ (Clark and Fritz, 1997; McDermott, 2004).

While speleothem $\delta^{13}C$ provides vegetation information, it is also influence by other factors. Atmospheric CO_2, vegetation density, soil thickness, effective moisture, residence time, drip rate and degassing all impart significant influences on speleothem $\delta^{13}C$ (Clark and Fritz, 1997; McDermott, 2004; Wong and Breecker, 2015). For example, a recent study has shown that degassing and dissolved inorganic carbon (DIC) loss along the drip water flow path can increase $\delta^{13}C_{ca}$ by 1‰ to 4‰, (Mickler et al., 2019). A 4‰

increase is sufficient to distort C_3 vegetation signatures into the C_4 range. This study may have a pertinent impact for the understanding of $\delta^{13}C_{ca}$ in speleothem studies, as this shows cave specific influences for the evolution of $\delta^{13}C_{ca}$. Thus, careful monitoring of DIC_{soil} and $DIC_{drip\text{-}water}$ may be required to truly understand the vegetation signature of $\delta^{13}C_{ca}$.

Deluge of thin soils (during periods of intense humidity) can lead to more positive $\delta^{13}C_{ca}$. Rapid flow of water leads to reduced interaction with soil CO_2 and comparatively increased interaction with host-rock carbonate (Bar-Matthews et al., 2000, 2003). Thus, during transitional phases of desert-savannah environments, a vegetation signal may not be achieved until residence time increases either through reduced precipitation or thickening of soils.

High-resolution $\delta^{13}C_{ca}$ records may also detail changes of effective moisture (precipitation-evaporation). If good soil conditions are present, $\delta^{13}C_{ca}$ will be more negative during humid periods; whereas drier periods will be reflected by increased $\delta^{13}C_{ca}$ (Vaks et al., 2010). The variation is driven by changes in the soil humidification, drip rate of cave water and rate of degassing (Vaks et al., 2010). Soil humidity influences the quantity of photosynthetic discrimination. Dry/hot climates (with low soil water content) results in increased $\delta^{13}C_{ca}$ (Wong and Breecker, 2015). Thus, an effective-moisture signal can be identified by positive correlation with $\delta^{18}O_{ca}$ (when $\delta^{18}O_{ca}$ is controlled by the *amount effect*). Alternatively, within dry/hot climates, atmospheric $\delta^{13}C$ (high compared to soil $\delta^{13}C$) can infiltrate belowground pore spaces, leading to elevated soil and epikarst $\delta^{13}C$ (Wong and Breecker, 2015).

Some attempts have been made to convert speleothem $\delta^{13}C_{ca}$ values into percentage of C_3/C_4 cover above the cave (Hopley et al., 2007). This can be achieved by using speleothem organic matter $\delta^{13}C$ to correct for host rock contribution. Alternatively, a typical host rock dilution (~15 ± 5%) and $\delta^{13}C$ value of -0.9‰ can be used to correct vegetation end members (C_3 = -8.0‰; C_4 = +1.3‰). $\delta^{13}C_{ca}$ can then be converted to a percentage of C_4 or C_3 plant converge (Veizer et al., 1992; Genty et al., 2001; Hopley et al., 2007). This method has been used to detail Plio-Pleistocene high-resolution changes of C_4 cover in South Africa (Hopley et al., 2007). However, organic matter may be related to host rock organic matter and/or the soil organic matter at the time of speleothem formation. Moreover, this assumes a constant ratio between water interaction of soil CO_2 and the host rock, which may not always be the case.

A more direct method of environmental analysis is the extraction of trapped pollen in speleothems (McGarry and Caseldine, 2004; Caseldine et al., 2008). These methods have been successful in identification of pollen within speleothems and can provide a species level vegetation identification. This has the potential to analyse palaeoenvironmental change at greater detail than $\delta^{13}C_{ca}$. However, speleothems typically contain 1-5 grains g^{-1} calcite (McGarry and Caseldine, 2004). To ensure a representative environmental signal, palynological studies require 150-300 per sample. Thus, the minimum material required for a single sample is 150 g and much more destructive than the 0.2 mg of powder required for $\delta^{13}C_{ca}$ analysis. Alternatively, new methods permit the extraction and analysis of ancient DNA preserved in stalagmites to detail past fauna and flora communities above the cave (Stahlschmidt et al., 2019).

4.5.2.1 Open and closed system conditions

The "openness" of the pathway between soil CO_2 and speleothem formation influences the reliability of $\delta^{13}C$ as an environmental indicator. The *Open system* and *closed* system model describe how waters become saturated with calcium carbonate.

The open system model predicts that constant interaction takes place between groundwater and an infinite soil CO_2 supply. This leads to a steady increased of bicarbonate as groundwater travels through the unsaturated zone. The dissolved $\delta^{13}C$ thus reflects the soil CO_2, with little influence of host-rock carbonate (Clark and Fritz, 1997). If a closed system prevails, groundwaters equilibrate with a limited CO_2 reservoir prior to interaction with the calcium carbonate bedrock. The groundwater is then separated from the reservoir prior to calcium carbonate dissolution (Clark and Fritz, 1997). Limestone dissolution is limited by this finite reservoir:

$$H_2O + CO_2 \rightarrow H_2CO_3$$

The dissolved CO_2 then reacts with bedrock $CaCO_3$, explained by the equation:

$$H_2O + CO_2 + CaCO_3 \rightarrow Ca^{2+} + 2HCO_3^-$$

In contrast to open system conditions, the CO_2 is largely contributed by the host-rock (McDermott, 2004). In a fully closed system, model data has indicated up to 50% of speleothem CO_2 may be derived from the host-rock (Hendy, 1971). Under open system conditions, C_3 vegetation with a $\delta^{13}C$ value of -23‰ and C_4 vegetation with a $\delta^{13}C$ value of 9‰ will result in speleothem $\delta^{13}C$ values of -16.8‰ and -4.9‰, respectively. Whereas,

under closed system conditions, the same vegetation $\delta^{13}C$ values would be reflected by speleothem $\delta^{13}C$ values of -12.1‰ and -2.9‰, respectively (Clark and Fritz, 1997).

4.5.3 Calcite Oxygen and Carbon isotope analysis (Gasbench)

Samples are collected from speleothems at designated intervals to attain the desired resolution. Two different methods are utilised: a handheld drill (with a 0.8 mm diameter tip) is used to drill ~5 mm horizontal trenches on the growth axis of the speleothem at ≥1 mm intervals; alternatively, a micro mill drill may be used to collect samples at <1 mm intervals. In this case, a continuous 1.5 mm wide trench is drilled along the vertical axis, excavated dust is collected after the desired advancements. Once dust has been collected following either method, it is weighed between 0.19-0.22 mg, placed into a vial and sealed with an airtight lid.

Calcite $\delta^{18}O$ and $\delta^{13}C$ values are analysed by Gas Isotope Ratio Mass Spectrometry of stalagmite CO_2. Firstly, Helium is introduced to the samples, flushing the air (with CO_2 and O_2) out of the vial. Once complete, phosphoric acid (H_3PO_4) is introduced to the test tube, reacting with the calcite ($CaCO_3$) to form CO_2, H_2O, and $Ca_3(PO_4)_2$ (Tricalcium Phosphate):

$$3CaCO_{3\,(S)} + 2H_4PO_{4\,(aq)} \rightarrow Ca_3(PO_4)_{2\,(aq)} + H_2O_{(l)} + CO_{2\,(g)}$$

The reacted gases are then transported into a Finnigan Delta V Advantage Isotope Mass Spectrometer (IRMS), which is coupled to an automated carbonate preparation system (Gasbench II). Precision (1σ) is ≤0.2‰ for $\delta^{18}O$ and ≤0.1‰ for $\delta^{13}C$.

4.5.4 Oxygen and Deuterium in fluid inclusions

Deuterium (^{2}H, or *D*), or heavy hydrogen, is a stable isotope of hydrogen, containing 1 proton and 1 neutron in the nucleus; whereas the other stable isotope of hydrogen, protium (^{1}H), or light hydrogen, contains a solitary proton in the nucleus. The δD isotopic composition of water is determined by the same fractionation processes as $\delta^{18}O$, thus, δD and $\delta^{18}O$ values are highly correlated, with a slope of ~8 (Sharp, 2007; Lachniet, 2009). The GMWL (global meteoric water line) is the linear correlation of δD and $\delta^{18}O$ in global precipitation, originally defined as $\delta D = 8 \times \delta^{18}O + 10$ (Dansgaard, 1964). This is now revised to $\delta D = (8.20 \pm 0.07) \times \delta^{18}O + (11.27 \pm 0.65)$ for the weighted mean of annual precipitation (Rozanski et al., 1993). The "deuterium excess" is the intercept of a line with a slope of 8. However, the slope and intercept of δD and $\delta^{18}O$ varies at a regional level and reflects the δD and $\delta^{18}O$ of the water source. Comparison of rainwater δD and $\delta^{18}O$ to regional meteoric waterlines can therefore be used to show shifting dominance of rainfall regimes.

Speleothem fluid inclusions are natural repositories of cave drip water (Fig. 24), accounting for 0.05 – 0.5% weight of a speleothems weight (Scheidegger et al., 2010). After formation, there is no interaction between the *D* (and minimal interaction of ^{18}O) of trapped water and host calcite (Meckler et al., 2015); thus, fluid inclusion δD and $\delta^{18}O$ are unaffected by the degassing of speleothems. δD and $\delta^{18}O$ values of the fluid inclusions therefore provide direct information of palaeogroundwaters and past rainfall. This can be utilised to determine source water (Fleitmann et al., 2003b) and calculate palaeotemperatures when combined with $\delta^{18}O_{ca}$ (McGarry et al., 2004) using the palaeotemperature equation (Epstein et al., 1953):

$$T(°C) = 15.75 - 4.3(\delta^{18}O_{calcite-PDB} - \delta^{18}O_{water-SMOW}) + 0.14(\delta^{18}O_{calcite-PDB} - \delta^{18}O_{water-SMOW})$$

Two methods have traditionally been utilised to extract trapped water from speleothem fluid inclusions. The crushing method releases the trapped water by zinc reduction and vacuum crushing linked to a cold trap. Analysis of water is conducted by pyrolysis with an IRMS and gas chromatography; this method has been applied and adapted to measure the water composition of speleothem fluid inclusions (Vonhof et al., 2006; Dublyansky and Spötl, 2009). The thermal decrepitation method heats the sample to 550°C to extract water (Yonge, 1982); however, large fractionations (of up to 30‰ for δD) are observed in comparison to cave drip waters (Matthews et al., 2000; McGarry et al., 2004). A recent method developed by Affolter et al. (2014), however, combines a heating and crushing to liberate fluid inclusion water then analyse this via WS-CRDS (wavelength scanned cavity ring down spectroscopy). A sample is placed into a copper tube and attached onto a continuous flow line under humid conditions (using water of known isotopic composition). This sample is then heated to 140°C and then crushed, instantaneously vaporising the water and transported (under humid conditions to prevent kinetic isotope fractionation) to a Picarro L2401-i. Laser absorption spectroscopy is utilised, opposed to traditional IRMS techniques, as it is precise and practical. The method provides a precision of <1.5‰ for δD and 0.2‰ for $\delta^{18}O$ (Affolter et al., 2014, 2015) and is utilised in this thesis.

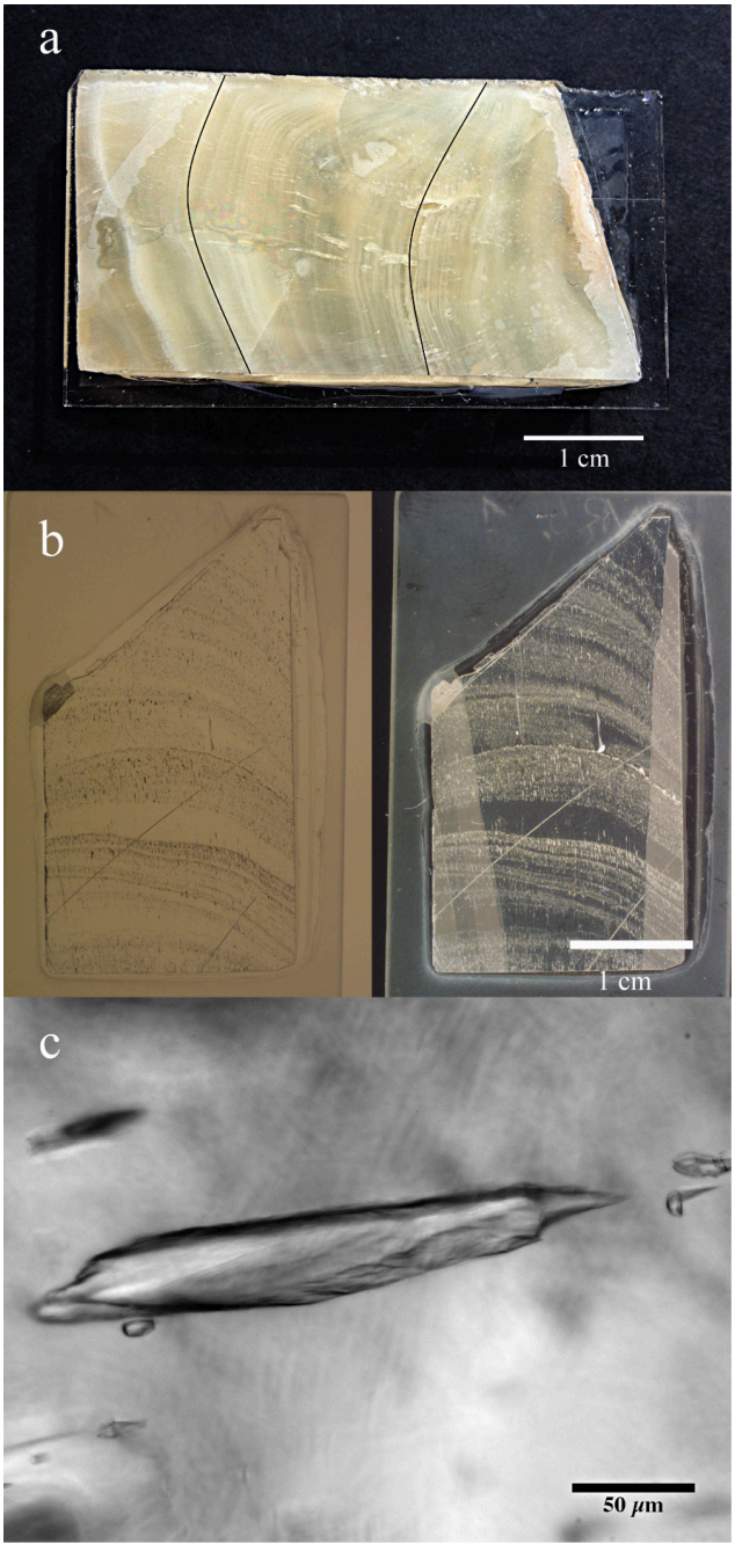

Fig. 24. A) speleothem sample prior to conditioning. Growth laminae are clearly visible. B) thin section of speleothem. Fluid inclusions are visible under cross-polarised (black)

and bright flied view (white). C) Enlarged image of a speleothem fluid inclusion. (after Affolter et al., 2014).

4.6 Trace elements in Speleothems

As detailed above, speleothem $\delta^{18}O_{ca}$ has been widely used as a palaeoclimate proxy for past precipitation changes (Fleitmann et al., 2003a, 2011; Cheng et al., 2006; Shakun et al., 2007). Though, determining the correct control on high resolution $\delta^{18}O_{ca}$ records is not necessarily straightforward, especially for past climates, where modern observation data may not provide appropriate models (e.g., Gierz et al., 2017; Beck et al., 2018). Thus, high resolution $\delta^{18}O_{ca}$ records should be tested against independent records.

Pioneering work has revealed that speleothem trace elements can provide numerous environmental records (Huang et al., 2001; Fairchild and Treble, 2009; Badertscher et al., 2014). These are incorporated into cave drip waters from precipitation, dust, sea-spray, volcanism and soil/bedrock leaching. Concentrations may be modified later by hydrological flow paths (Fairchild et al., 2000) and biogeochemical processes (Hartland et al., 2012; Wynn et al., 2013). In combination with traditional $\delta^{18}O_{ca}$ and $\delta^{13}C_{ca}$ analyses, these can provide independent multi-proxy climate records.

4.6.1 Strontium and Magnesium

Strontium (Sr) and Magnesium (Mg) are among the most widely studied trace elements, as these are strongly influence by palaeo-precipitation and may be used to mitigate uncertainties of speleothem $\delta^{18}O_{ca}$. Sr and Mg are readily substituted for Ca in the carbonate lattice and behave in a predictable manner (Fairchild and Treble, 2009),

meaning they are ideal for constructing speleothem derived palaeoclimate records. Their uptake is defined by a partition coefficient:

$$K_{Mg} = \left(\frac{Mg/Ca\ calcite}{Mg/Ca\ fluid}\right)$$

In particular, increased concentration relative to Ca can determine the extent of prior calcite precipitation (PCP hereafter). PCP is defined as "the calcite precipitated from a solution before it reaches the stalagmite" (Treble et al., 2015). This occurs during periods of lower recharge (generally arid periods), when water residence time along a flow path increases. As such, heavier Ca ions are precipitated from the solution before reaching the stalagmite, caused by equilibration with lower PCO_2 along the flow path (Fairchild and Treble, 2009; Treble et al., 2015). This leads to increased concentrations of Sr and Mg relative to Ca in the resultant stalagmite. Therefore, analysis of speleothem Sr/Ca and Mg/Ca ratios can provide an independent record of past changes in rainfall (e.g., Asrat et al., 2018).

However, when Sr/Ca and Mg/Ca values are not correlated they may serve as independent climate proxies. Sr/Ca can detail speleothem growth rate and other soil processes (e.g., soil thickness and composition) (Treble et al., 2003); whereas Mg/Ca can indicate changes in soil residence time (particularly when correlated with $\delta^{13}C_{ca}$) (Hellstrom and McCulloch, 2000; McDonald et al., 2004; Häuselmann et al., 2015). For example, high Sr values in Tasmanian speleothems have been related to detrital material and dust within the drip water (Goede et al., 1998). And low Mg/Ca ratios of Alpine Schafsloch Cave (Switzerland) were related to high infiltration of meltwater following the MIS 6 termination (Häuselmann et al., 2015).

4.6.2 Other trace elements

Other commonly analysed trace elements include Phosphorous (P), Sulphur (S), Beryllium (Be), Uranium (U), Titanium (Ti), Aluminium (Al), Yttrium (Y) Bromine (Br) and Molybdenum (Mo). S, Br and Mo are released into the atmosphere during volcanic eruptions, these are incorporated into speleothems directly from contaminated precipitation or through secondary uptake from plant respiration (Badertscher et al., 2014). Br, S and Mo have been used to provide precise timing of the 3.2 ka Santorini eruption (Badertscher et al., 2014). Higher concentrations of U can be used in combination with Mg to indicate periods of increased soil residence times of groundwater (Häuselmann et al., 2015). P is related to vegetation conditions above a cave, with higher concentrations reflecting greater vegetation cover, which is also linked to precipitation and temperature (Borsato et al., 2007). Ti is elevated within detrital material due to its low solubility, and thus could be used to identify hiatuses within speleothems (Häuselmann et al., 2015); whereas Y can be used to identify both detrital input and as a precipitation proxy (Schimpf et al., 2011). Al is also incorporated into fine grained detrital material that is deposited on speleothems during flooding events (Borsato et al., 2007). Together Ti, Y and Al can thus be used to identify periods of high input events associated with mobilisation of particles and colloids above a cave. These form so called "impulse laminae" within speleothems (Fairchild and Treble, 2009; Häuselmann et al., 2015)(Fairchild and Treble, 2009; Häuselmann et al., 2015).

4.6.3 Measuring trace elements

In recent years, there has been a growing interest in the palaeoclimatic significance of speleothem trace elements. Currently, three methods are commonly used to analyse speleothem trace elements.

The non-destructive X-Ray Florescence (XRF) technique can be used to collect information of trace elemental composition with no damage to the sample. Ultra-high resolution can be achieved using synchrotron-radiation based micro X-Ray Florescence (SR-μXRF). The SR-μXRF technique allows simultaneous collection of multiple trace elements (at ppb- ppm-scale concentration) excited by a set maximum energy at the ppb and ppm scales (Frisia et al., 2005; Badertscher et al., 2014). This method benefits from the fact that virtually no background is incorporated into the analysis, meaning no corrections have to be applied (Frisia et al., 2005).

Laser-ablation inductively coupled plasma mass spectrometry (LA-ICP-MS) is also widely used as it can achieve a resolution at the 10-100 μm scale (Jochum et al., 2012). While destructive, only (≥1 μg) of material is required per sample (Jochum et al., 2012). Additionally, this technique is rapid, allowing a sample to be measured for 90 isotopes from 50 elements in 1.5 secs (Jochum et al., 2012). This method can therefore produce a wealth of ultra-high-resolution isotope data at a currently unparalleled rated.

Another, less commonly used, method is the inductively coupled plasma optical emission spectroscopy (ICP-OES) and/or atomic emission spectroscopy (ICP-AES) technique (McMillan et al., 2005; Fairchild and Treble, 2009). While this technique offers the

greatest analytical precision for most elements, a greater amount of material is required (100-5000 μg; Fairchild and Treble, 2009). Additionally, sample preparation is much more laborious, requiring collection of the powder by hand-drill, weighing of the powder, preparation of the solvent and standards and combing the solvent and powder at the correct masses.

4.7 Uranium series dating of speleothems

Uranium (U) is an actinide element with three unstable isotopes present in nature (^{234}U, ^{235}U and ^{238}U) and two common oxidation states (U^{4+} and U^{6+}). U is present in waters and soils above a cave, where the hexavalent U ion (U^{6+}, in the form of uranyl [UO_2^{2+}]) is mobile with carbonate ions (Langmuir, 1978), allowing its incorporation into speleothems. It is considered that the large size and shape of uranyl (O = U = O) does not promote substitution for Ca^{2+}. This is supported by studies which showed U^{6+} in calcite has a partition coefficient less than unity (Meece and Benninger, 1993); however, once incorporated into the calcite structure, it has a stable position in the lattice (Kelly et al., 2003), where the axial uranyl ions substitute for CO_3 groups (Kelly et al., 2003, 2006). This allows the structure to take on a calcite-like form and become more stable over time (Kelly et al., 2003, 2006; Woodhead et al., 2012). In speleothems U frequently follows P, which has led to the suggestion that increased solubility of uranyl-phosphate complexes promote the transport of the uranyl ion (Treble et al., 2003). As the natural U isotopes are unstable and their decay is well known, they allow accurate dating of speleothems. The Uranium-Lead and the Uranium-Thorium methods are commonly used to establish the ages of speleothems.

4.7.1 Uranium-Lead (U-Pb) dating analysis

The decay of U-Pb is increasingly used to provide ages for speleothems beyond the range of ^{230}Th analysis (discussed below) and has the potential to date speleothems to millions of years-old (Woodhead et al., 2006; Vaks et al., 2013; Sniderman et al., 2016). This technique uses both the ^{238}U-^{206}Pb (Fig. 25) and ^{235}U-^{207}Pb parent-daughter isotope pairs to construct separate ages (Woodhead et al., 2006). Good agreement between these ages demonstrates closed system conditions with isotopic equilibrium; whereas disagreement can show the system opened during stalagmite deposition (Woodhead et al., 2006). However, U-Pb dating can be hindered by introduction of common Pb into the calcite. The origin of Pb and its incorporation into calcite are poorly understood (Woodhead et al., 2012). Pb salts are slightly soluble, with an average concentration in river waters of <100 ppt (Gaillardet et al., 2013). As such, Pb in speleothems should be incorporated into speleothems in relatively low quantities (Rasbury and Cole, 2009). Additionally, Pb can be introduced into speleothems with sub-micron colloids or detrital particles (Fairchild and Treble, 2009). Alternatively, anthropogenic Pb can be introduced during analysis and handling of speleothems (Woodhead et al., 2012). As such, the variability of Pb in speleothems means samples must be screened for common Pb prior to analysis (Woodhead et al., 2012).

There are multiple methods of measuring speleothem U-Pb ratios. Here, MC-ICPMS (Multi Collector Isotope Coupled Plasma Mass Spectrometry) will be conducted following the method of Woodhead et al. (2006). A second method, LA-ICP-MS (Laser Ablation Isotope Coupled Plasma Multi Spectrometry: following the analytical protocol of Coogan et al., 2016), is also utilised to provide cross-laboratory and cross-method comparisons of speleothem ages.

4.7.2 Uranium-Thorium (^{230}Th) dating analysis

Speleothems are predominantly dated through the known isotopic decay rate of ^{234}U to ^{230}Th. The naturally occurring Uranium parent isotopes ^{238}U ($\lambda = 4.47 \times 10^9$ yr) and first decay daughter ^{234}U ($\lambda = 2.48 \times 10^5$ yr) are abundant in rocks. While Thorium is insoluble in groundwaters, uranium concentrations measure 0.1 to 3 ppb (parts per billion). Furthermore, ^{238}U/^{230}Th values are low, thus, freshly deposited speleothems contain almost no Thorium. Uranium is transported in cave water as a series of uranyl ions (UO^{2+}_2), with sulphate, carbonate and dissolved organic ions. After deposition of a speleothem, ^{234}U starts the decay process to ^{230}Th, until the rate of decay comes into equilibrium with production from ^{234}U (Fig. 25).

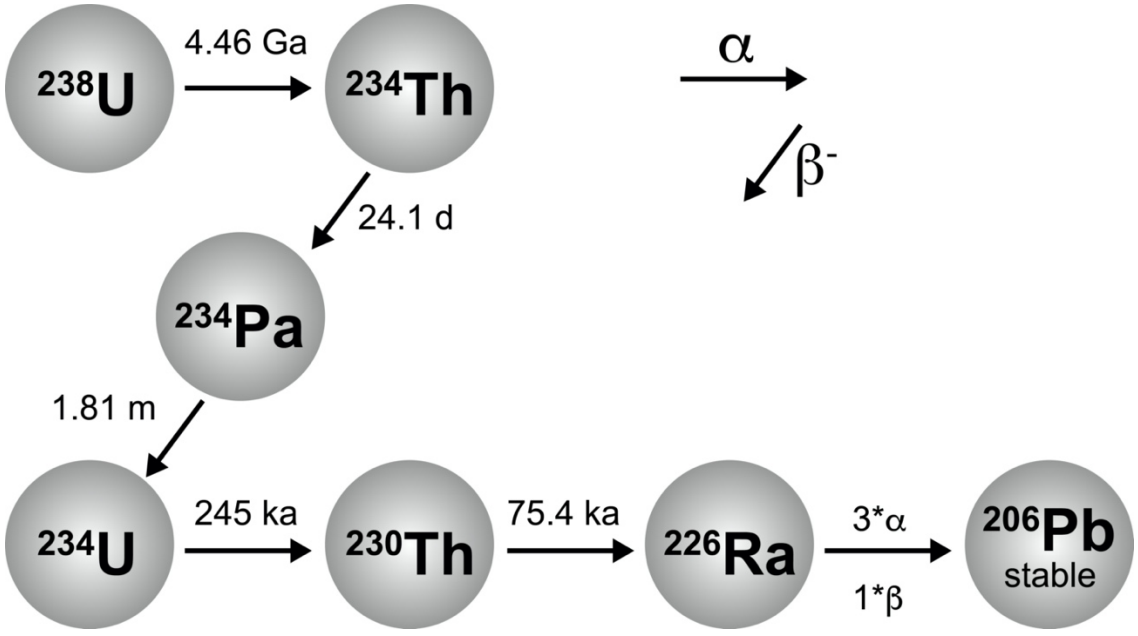

Fig. 25. Decay of ^{238}U to ^{206}Pb and associated daughter isotopes.

Accurate rates of decay are vital for accurate age calculations of speleothems. The half-lives of the three nuclides used in U-Th dating are $4.4683 \pm 0.0048 \times 10^9$ yr for ^{238}U (2σ, Jaffey et al., 1971), 245.250 ± 490 yr for ^{234}U (2σ, Cheng et al., 2000) and 75.690 ± 230

yr for ^{230}Th (2σ, Chang et al., 2000). Speleothems can be dated to ~600,000-500,000 years using the U-Th method.

However, the accuracy of dating a stalagmite via ^{230}Th ages can be compromised by post-depositional mobilisation of U or Th (or "open system" behaviour), incorporation of ^{230}Th absorbed onto organic acids and small-scale dissolution and reprecipitation of calcite (Borsato et al., 2003; Scholz et al., 2014). Post depositional mobilisation (or leaching) of U can lead to older ages, which can be caused by introduction of younger drip water into microscopic fractures in the speleothem (Bajo et al., 2016). Alternatively, reprecipitation of calcite can lead to younger ages than the true age of the speleothem.

4.8 Speleothem summary

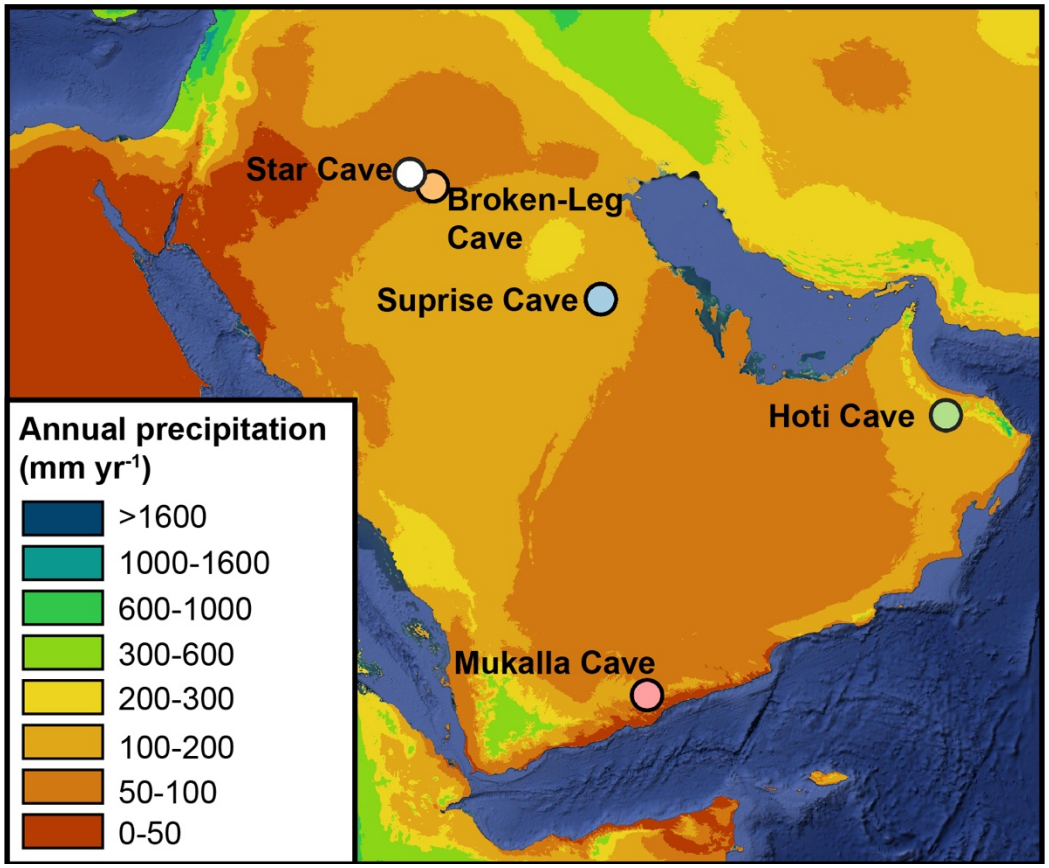

Fig. 26. Map of average annual rainfall (1970-2000; mm yr^{-1}; Fick and Hijmans, 2017) and location of stalagmite cave sites studied within this thesis: Mukalla Cave (pink circle), Hoti Cave (green circle), Surprise Cave (blue circle), Broken-Leg Cave (orange circle) and Star Cave (white circle).

4.8.1 Mukalla Cave

Mukalla cave (14°55'02"N; 48°35'23" E; ~ 1500m asl; Fig. 26) is situated in the hyper-arid desert of Yemen, approximately 70km North of Al Mukalla, Hadhramaut. Thickness of the bedrock above the cave is approximately 30m, and soil above the cave is mostly absent. Current rainfall to southern Yemen is predominated by the annual northward migration of the monsoonal rainfall belt. Annual precipitation is highly variable, yet averages ~120 mm yr^{-1}, mostly delivered in the spring and summer months (Mitchell and Jones, 2005). No actively growing stalagmites were found when stalagmites Y99, Y97-4 and Y97-5 were collected in 1997 and 1999 (Fleitmann et al., 2011).

Y99 is a fossil speleothem measuring 3.20 metres in length (Fig. 27). Fleitmann et al. (2011) provided ^{230}Th analysis of the top 60 cm (Tab. 4), finding growth phases occurred exclusively within interglacial periods up to MIS 9. Y99 is therefore a perfect candidate for extending the palaeoclimate record of Arabia. Initial $\delta^{18}O_{ca}$ analyses found that MIS 5e was the most intense period of increased rainfall. However, as high-resolution analyses were not published, variability throughout growth phases cannot be attained. Moreover, $\delta^{13}C_{ca}$ results were not published, meaning there is currently no evidence of vegetation signals above Mukalla Cave.

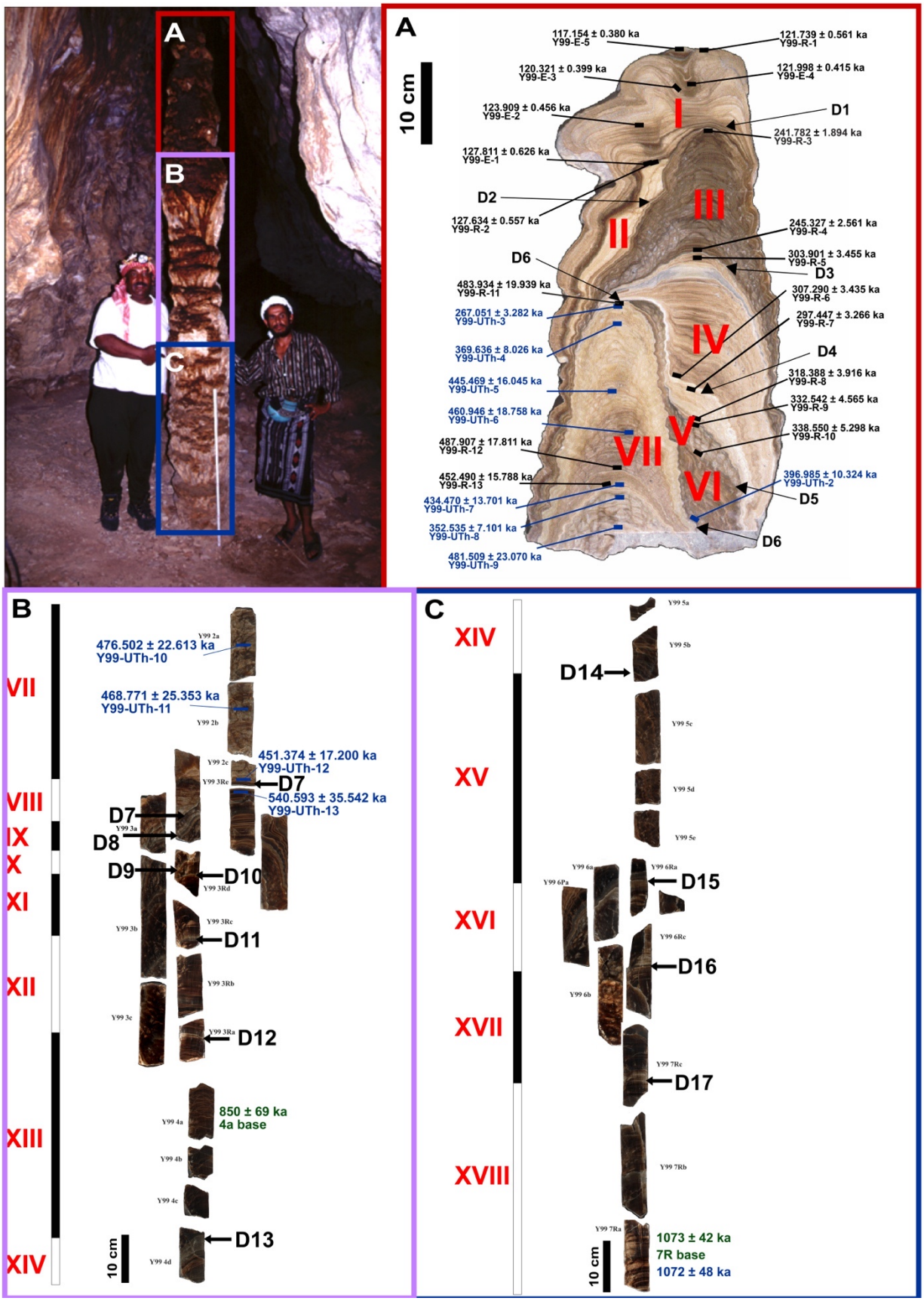
A
B
C
10 cm
117.154 ± 0.380 ka
Y99-E-5
121.739 ± 0.561 ka
Y99-R-1
120.321 ± 0.399 ka
Y99-E-3
121.998 ± 0.415 ka
Y99-E-4
123.909 ± 0.456 ka
Y99-E-2
D1
241.782 ± 1.894 ka
Y99-R-3
127.811 ± 0.626 ka
Y99-E-1
D2
127.634 ± 0.557 ka
Y99-R-2
I
II
III
IV
V
VI
VII
245.327 ± 2.561 ka
Y99-R-4
303.901 ± 3.455 ka
Y99-R-5
D3
D6
483.934 ± 19.939 ka
Y99-R-11
307.290 ± 3.435 ka
Y99-R-6
267.051 ± 3.282 ka
Y99-UTh-3
297.447 ± 3.266 ka
Y99-R-7
369.636 ± 8.026 ka
Y99-UTh-4
D4
445.469 ± 16.045 ka
Y99-UTh-5
318.388 ± 3.916 ka
Y99-R-8
460.946 ± 18.758 ka
Y99-UTh-6
332.542 ± 4.565 ka
Y99-R-9
487.907 ± 17.811 ka
Y99-R-12
338.550 ± 5.298 ka
Y99-R-10
452.490 ± 15.788 ka
Y99-R-13
396.985 ± 10.324 ka
Y99-UTh-2
434.470 ± 13.701 ka
Y99-UTh-7
D5
352.535 ± 7.101 ka
Y99-UTh-8
D6
481.509 ± 23.070 ka
Y99-UTh-9
B
VII
VIII
IX
X
XI
XII
XIII
XIV
476.502 ± 22.613 ka
Y99-UTh-10
Y99 2a
468.771 ± 25.353 ka
Y99-UTh-11
Y99 2b
451.374 ± 17.200 ka
Y99-UTh-12
Y99 2c
Y99 3Rc
D7
540.593 ± 35.542 ka
Y99-UTh-13
D7
Y99 3a
D8
D9
D10
Y99 3Rd
Y99 3Rc
Y99 3b
D11
Y99 3Rb
Y99 3c
Y99 3Ra
D12
850 ± 69 ka
4a base
Y99 4a
Y99 4b
Y99 4c
10 cm
D13
Y99 4d
C
XIV
XV
XVI
XVII
XVIII
Y99 5a
Y99 5b
D14
Y99 5c
Y99 5d
Y99 5e
Y99 6a
Y99 6Ra
Y99 6Pa
D15
Y99 6Rc
D16
Y99 6b
Y99 7Rc
D17
Y99 7Rb
Y99 7Ra
1073 ± 42 ka
7R base
1072 ± 48 ka
10 cm

Fig. 27. Y99 sections. The top section (A: red) was previously analysed by Fleitmann et al. (2011). All sections (A: red; B: purple; C: blue) have been analysed within this thesis. ^{230}Th ages presented by Fleitmann et al. (2011) are given in black. ^{230}Th ages provided in this thesis are given in blue. U-Pb presented in this thesis are given blue (BGS Keyworth) and green (Melbourne).

4.8.2 Hoti Cave

Hoti Cave (23°05'N; 57°21'E: ~ 800m asl, Fig. 26) is located in the hills of the northern Oman mountains. The cave is hosted in cretaceous limestone of the Natih Formation, with two entrances and is a subsurface wadi (4.5km long) (Fleitmann et al., 2003b). Outside temperatures range 33-35°C during summer months and 20-25°C during winter months. Annual cave air temperature is around 26°C and annual precipitation ranges between 50 and 255mm yr^{-1} (station AI Hamra, 700 m above sea level, 1974–1997). Precipitation is variable and mainly derived from three sources: the Mediterranean frontal system (December-March: Weyhenmeyer et al., 2002); orographic rain produced over the Jebel Akhdar Mountains during hot summers; and tropical cyclones, originating in the south-eastern Arabian Sea and the Bay of Bengal, every 5 to 10 years (Pedgley, 1969). Stalagmites from Hoti Cave have been extensively studied (Burns et al., 2001; Neff et al., 2001; Fleitmann et al., 2003b, 2003a, 2004a; Cheng et al., 2009b).

H13 is a ~3 metre long speleothem (Fig. 28), U-Th dated to MIS 5e, MIS 7e, MIS 9 and MIS 11 (Burns et al., 2001). A fragment from the top 30 cm was U-Th dated 134-124 ka (Burns et al., 2001; Fleitmann et al., 2003b). Previous analysis of fluid inclusion δD suggested the ISM enhanced precipitation to Oman during Pleistocene interglacials

(Fleitmann et al., 2003b). However, fluid inclusion $\delta^{18}O$ was not attained, and was estimated using the temperature dependent calcite-water fractionation equation ($10^3 \ln \alpha = 2.78(10^6 T^2)$-2.89). New fluid inclusion water extraction methods now allow accurate measurement of $\delta^{18}O$ (Affolter et al., 2014). Thus, further analysis of this sample can refine previous interpretations (e.g., Fleitmann et al., 2003b).

Fig. 28. H13 being collected from Hoti Cave.

Stalagmites situated close to H13 (e.g., H14) possess clearly limited annual growth layers. Similar layers appear within the fabric of H13, likely indicating that this sample is also annually laminated. Application of $\delta^{18}O_{ca}$ and $\delta^{13}C_{ca}$ analyses at sub-annual level has the potential to reveal climate variation which is yet to be attained for MIS 5e. Combined with fluid inclusion analyses, this could reveal distinct wet and dry seasons. This approach can therefore test palaeoclimate models (Kutzbach et al., 2014; Enzel et al., 2015; Jennings et al., 2015b; Gierz et al., 2017). H13 3a was selected for this purpose.

H5 is a Holocene sample U-Th dated between 10.5 ka and 6.2 ka (Burns et al., 2001; Fleitmann et al., 2003b) selected for isotopic analysis of fluid inclusion water δD and $\delta^{18}O$. Previous $\delta^{18}O$ analyses of H5 have focussed on reconstructing Holocene precipitation. Indeed, a decrease of $\delta^{18}O$ occurs at ~8 ka, simultaneously to decreased $\delta^{18}O_{ca}$ of a speleothem record from Qunf Cave (southern Oman). This was interpreted to show a strengthening of the Indian Summer Monsoon on a south-north transect (Fleitmann et al., 2003a, 2007).

4.8.3 Saudi Arabian Caves

Current precipitation is less than 100 mm yr^{-1} in Saudi Arabia, with the exemption of the southern Asir province. Mean monthly temperatures vary between 8 and 17°C. In winter months, the temperature drops below freezing in central and northern Arabia. Whereas in the summer months, temperatures typically vary between 32 and 35°C, though frequently exceed 48°C.

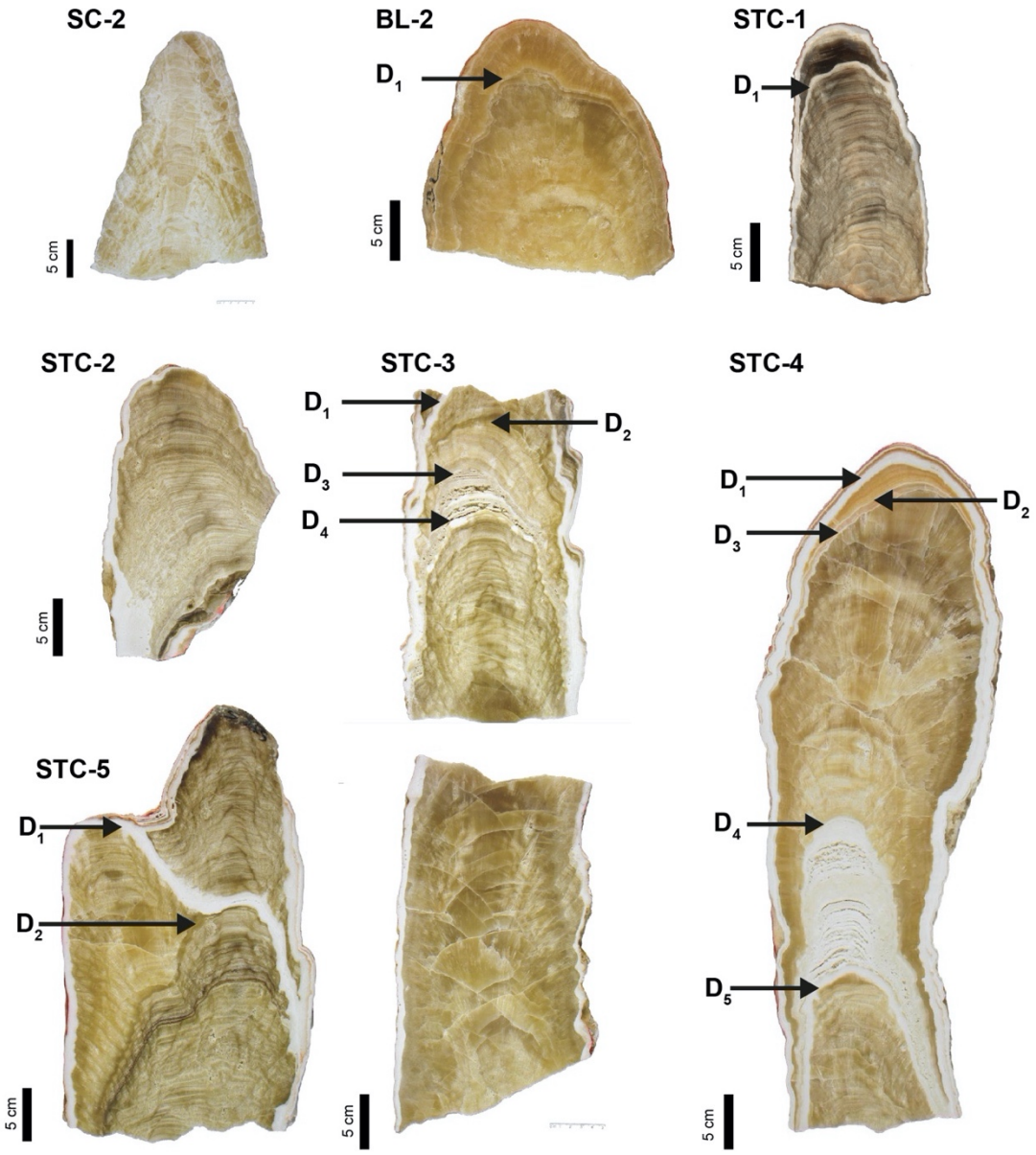

Fig. 29. Speleothem samples from Surprise Cave (SC), Star Cave (STC) and Broken-Leg Cave (BL) (after Fleitmann et al., 2004b).

4.8.3.1 Star Cave

Star Cave is located in the Nefud desert of Saudi Arabia (30°6'36"N., 41°37'48"E Fig. 26). The cave is located on the Aruma Formation. The Aruman formation is roughly 125 m thick composed of late cretaceous white, crystalline and nodular limestone, which is

typical of open-platform domains (SGS, 2007). The top of the formation becomes clayey and then dolomitic (SGS, 2007). Two entrances were located in a 6.22 m diameter depression (Fig. 30). A smaller entrance measured 2.8 m wide and 0.8 m in height. A larger entrance measured 3.8 m wide and 2.6 m in height. The total recorded length of the cave was 43 m, with a vertical difference of ~13 m. Two rooms were identified. The first room measured 32.5 m long and 11 m wide, with an average height of 1 m. A 1 m wide, flowstone coated passage was identified at the south end of the cave, which leads to a low room. A variety of stalagmites and bones were found in the cave (Fleitmann et al., 2004b; SGS, 2007).

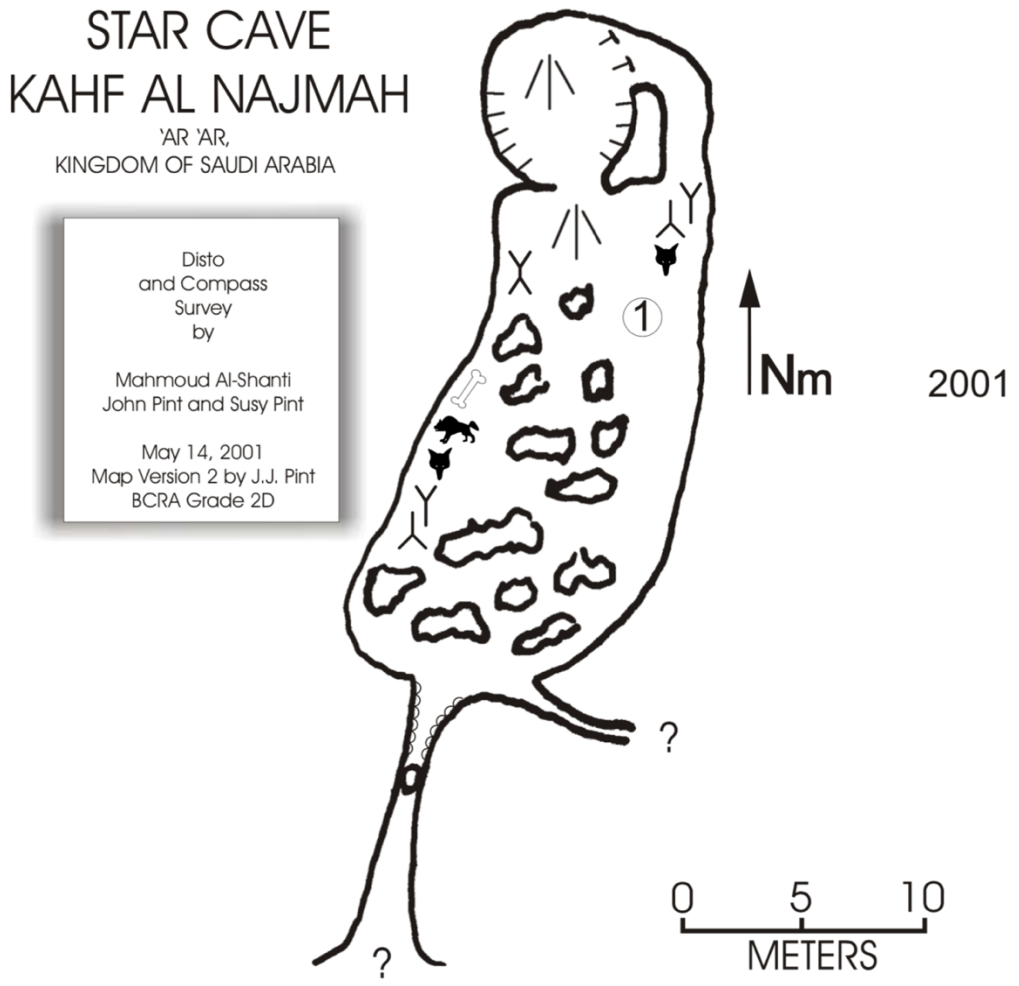

Fig. 30. Schematic diagram of Star Cave (after SGS, 2007)

Five speleothems were collected from Star Cave (Fig. 29). Attempts to date these via the U-Th method were unsuccessful, and $^{234}U/^{238}U$ values measured ~1. Preliminary U-Pb analyses have suggested dates of 4.17-4.08 Ma (STC 2), 4.1-4.02 Ma (STC 3), 3.5-3.1 Ma (STC 4) and 4.21-4.03 Ma (STC 5). Calcite values of STC 1 ranged -13.64 to -12.27‰ ($\delta^{18}O_{ca}$) and -9.02 to -6.74‰ ($\delta^{13}C_{ca}$). $\delta^{18}O_{ca}$ values of -14.71 to -6.95‰ and $\delta^{13}C_{ca}$ values of -7.4 to -2.7‰ were achieved for STC 4. STC 5 exhibited $\delta^{18}O_{ca}$ values of -9.24 to -5.67‰ and $\delta^{13}C_{ca}$ values of -6.38 to -5.2‰.

4.8.3.2 Broken-Leg Cave

Broken leg Cave (29°45'36"N., 42°18'36"E.; Fig. 26), northern Saudi Arabia, is located on the Umm er Radhuma Formation, which consists of white to light grey foraminifera bearing, fine-grained, calcarenitic limestone, dolomitic limestone and dolomite (SGS, 2007). Gypsum layers of a few meters in thickness are interbedded with the limestone. A single vertical entrance to the cave measures 5.85 x 4.5 m. The floor lies 11 m below the surface, though a large, steep-sided mound is 6.98 m below the entrance (Fig. 31).

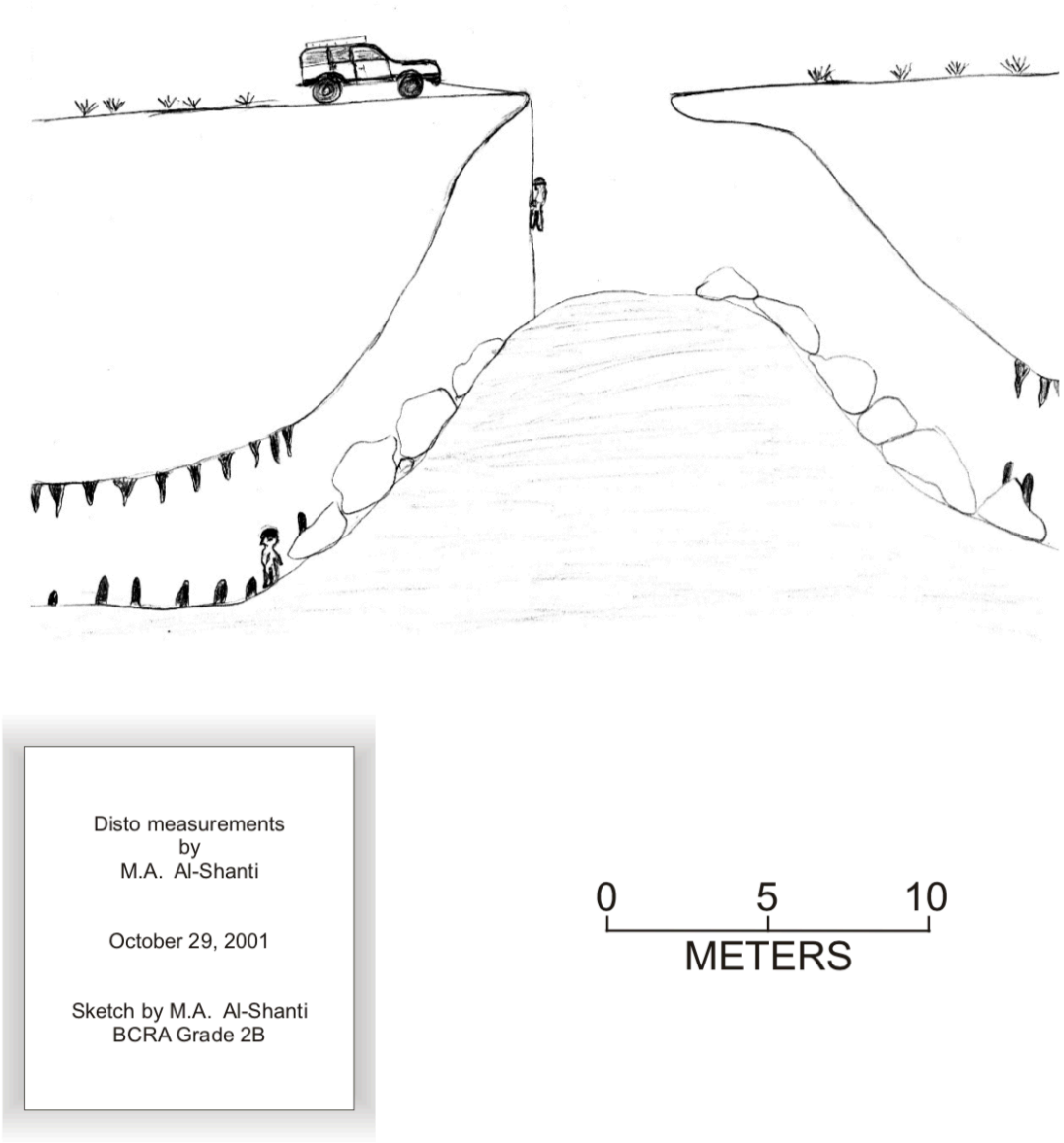

Fig. 31. Schematic diagram of Broken-Leg Cave (after SGS, 2007).

Two speleothems (Fig. 29) from Broken-Leg Cave, northern Saudi Arabia, underwent dating analysis via U-Th method. A date was not obtained as $^{234}U/^{238}U$ values were ~1, and it is considered these will date in excess of 1 Ma. $\delta^{18}O_{ca}$ values range -11.14‰ to -8.82‰ and $\delta^{13}C_{ca}$ values range -6.85‰ to -5.31‰ for BL-1. Carbonate analysis are yet to be performed on BL-2.

4.8.3.3 Surprise Cave

Surprise Cave (26°28'12"N., 47°13'48" E.; Fig. 26) is located within central western Saudi Arabia, ~200 Km NE of Riyadh. Surprise cave was located on the As Sulb Plateau, which encompasses the Umm er Radhuma Formation (a Palaeocene-early Eocene deposit) and a younger Miocene-Pliocene unit. This younger unit is comprised of calcareous clastic rocks, which contain calcareous sandstone, limestone and marl (Schyfsma et al., 1978; SGS, 2007), which is referred to as the Tertiary sandstone and marl (Tsm) formation. Two entrances were recorded during survey, though the report suggests other entrances exist (SGS, 2007). Entrance 1 (Fig. 32) is a 14 m vertical shaft, located below a 90 cm diametre hole. Entrance 2 is an openining located in a horziontal wall in a gully southwest of entrance 1. The explored areas of the cave range from 6 to 0.5 m in height and 15 m wide. Cave debris, loess, sand and mud are frequently found in the cave. Stalactites are frequent within this cave, including both fossil stalagmites and active drips. Stalagmites, flowstones and draperies are also present. Some gypsum speleothems were also found in the cave (SGS, 2007). Current temperature was reported as 25°C and humidity was 85%.

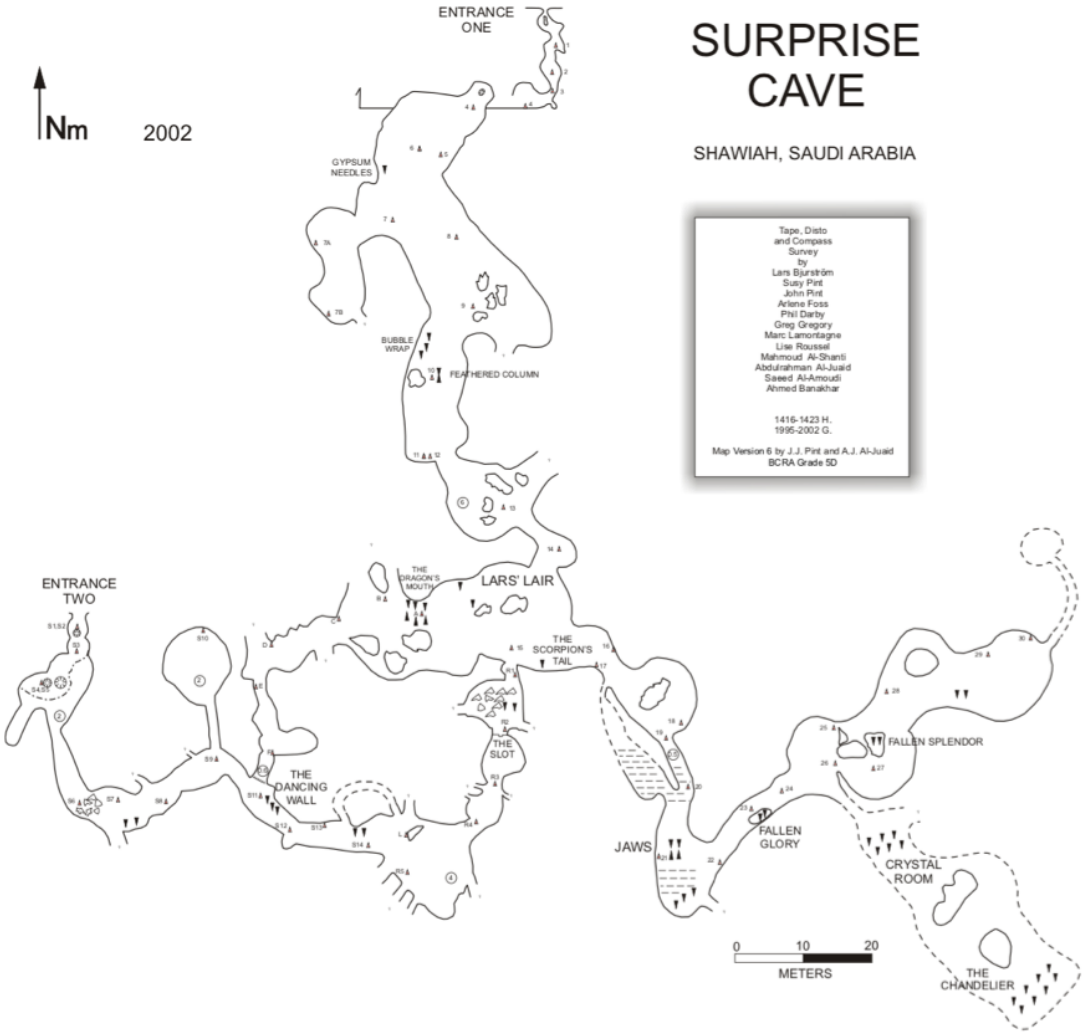

Fig. 32. Schematic diagram of Surprise Cave (after SGS, 2007).

Three stalagmites were collected in October 2001 (Fleitmann et al., 2004b; Fig. 29 and Fig. 33). SC3 has been cut, the lower section is not pictured here. Speleothems from Surprise Cave were beyond the range of U-Th dating analysis, with $^{234}U/^{238}U$ values of ~1. Preliminary U-Pb analysis has yielded dates of 2.57 ± 0.43 Ma (SC-2) and 5.3 ± 2.9 Ma (SC-3). Initial carbonate analyses were conducted by Fleitmann et al. (2004b). SC-1 measured -13.62 to -10.68‰ for $\delta^{18}O_{ca}$ and 0.23 to 5.07‰ for $\delta^{13}C_{ca}$. SC 2 measured -13.7 to -11.12‰ for $\delta^{18}O_{ca}$ and -4.93 to -1.69‰ for $\delta^{13}C_{ca}$.

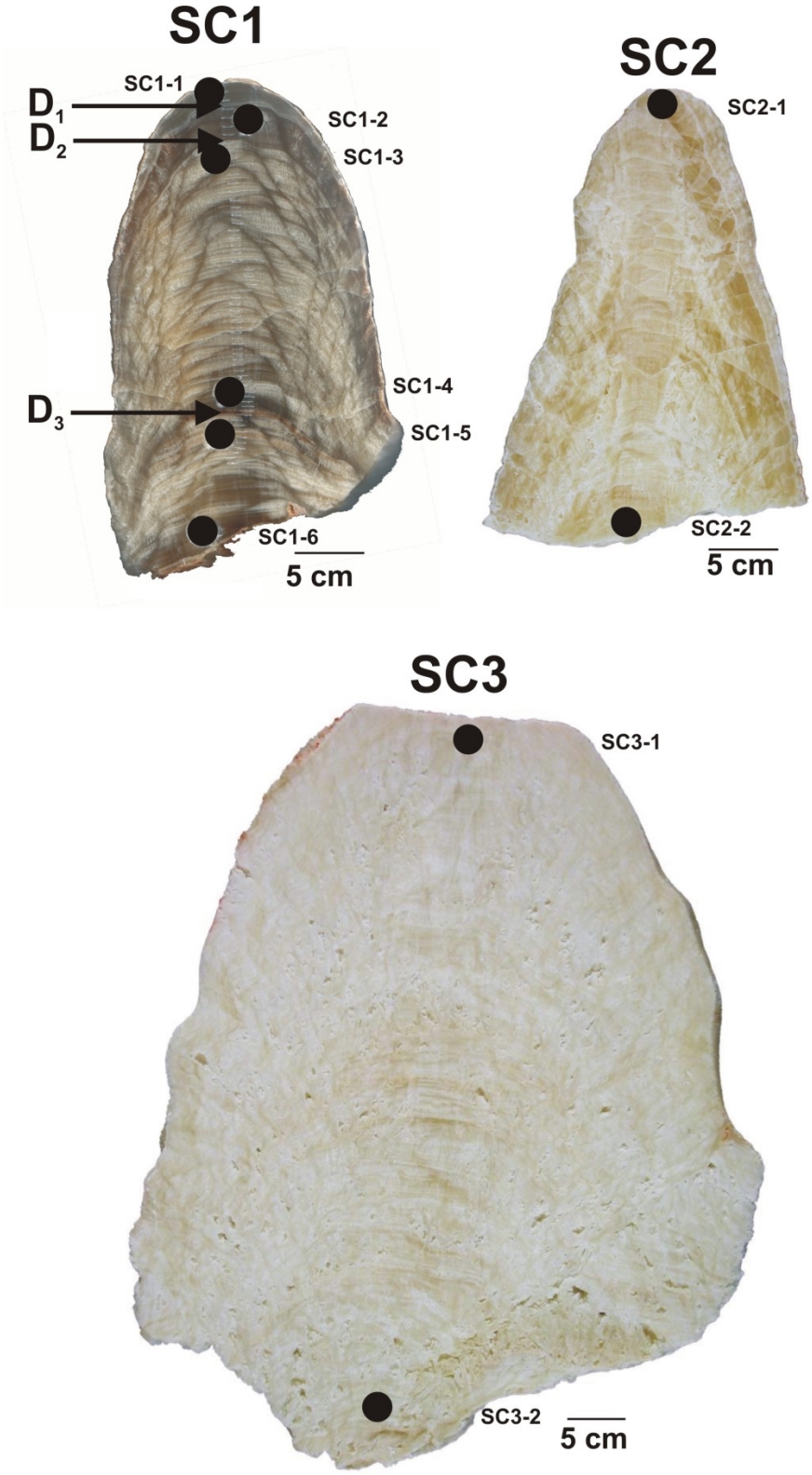

Fig. 33. Stalagmite sample cross sections from Surprise Cave. Growth discontinuities are marked by D numbers (e.g., Fleitmann et al., 2004b).

Country	Cave	Stalagmite sample	Previous analysis	Refs.	This thesis
Yemen	Mukalla (14°55'02''N., 48°35'23''E.)	Y99	U-Th ages (MIS 5e to 9e) and calcite $\delta^{18}O$ from GI I to V.	Fleitmann et al. (2011)	Additional calcite $\delta^{18}O$ and $\delta^{13}C$ from GI II to XVIII. Conducted by S. Nicholson under the supervision of D. Fleitmann (University of Reading) Fluid inclusion $\delta^{18}O$ and δD from GI I-IV . Conducted by S. Affolter (University of Bern) Additional U-Th samples from GI I to VIII. Conducted by D. Sahy (BGS, Keyworth) U-Pb from GI XIII and XVIII. Conducted by J. Woodhead (University of Melbourne) and N. Roberts (BGS, Keyworth). Preliminary Sr/Ca and Mg/Ca from GI I to VII. Conducted by S. Nicholson under the supervision of D. Fleitmann (University of Reading).
			U-Th ages (MIS 5e) and high-resolution calcite $\delta^{18}O$ and $\delta^{13}C$ from GI I.	Nicholson (2015). Unpublished undergraduate dissertation.	
			High-resolution calcite $\delta^{18}O$ and $\delta^{13}C$.	Bearfield (2016). Unpublished Master' thesis.	
			High-resolution calcite $\delta^{18}O$ and $\delta^{13}C$ from GI V-VIII.	Bruce (2015). Unpublished dissertation.	
		Y97-4	U-Th ages (Holocene, MIS 5c and 7a) and calcite $\delta^{18}O$.	Fleitmann et al. (2011)	N/A
		Y97-5	U-Th ages (Holocene, MIS 5c and 7e) and calcite $\delta^{18}O$.	Fleitmann et al. (2011)	N/A
Oman	Hoti (23°05'N., 57°21'E.)	H1	U-Th ages (MIS 5a) and calcite $\delta^{18}O$.	Burns et al. (2001)	N/A
			U-Th ages (MIS 5a) and fluid inclusion δD.	Fleitmann et al. (2003b)	
		H4	U-Th ages (MIS 5e) and calcite $\delta^{18}O$.	Burns et al. (1998)	N/A
			U-Th ages (MIS 5e) and calcite $\delta^{18}O$.	Burns et al. (2001)	

			U-Th ages (MIS 5e) fluid inclusion δD.	Fleitmann et al. (2003b)	
		H5	U-Th ages (Holocene) and calcite $\delta^{18}O$.	Burns et al. (1998)	Fluid inclusion $\delta^{18}O$ and δD analysis. Conducted by S. Affolter (University of Bern).
			U-Th ages (Holocene) and calcite $\delta^{18}O$.	Burns et al. (2001)	
			U-Th ages (Holocene) and high-resolution calcite $\delta^{18}O$.	Neff et al. (2001).	
			U-Th ages (Holocene) and fluid inclusion δD.	Fleitmann et al. (2003b)	
			U-Th ages (Holocene) and high-resolution calcite $\delta^{18}O$ and $\delta^{13}C$.	Fleitmann et al. (2007)	
		H10	U-Th ages (Holocene) and calcite $\delta^{18}O$.	Burns et al. (2001)	N/A
			U-Th ages (Holocene) and fluid inclusion δD.	Fleitmann et al. (2003)	
		H11	U-Th ages (Holocene) and calcite $\delta^{18}O$.	Burns et al. (2001)	N/A
			U-Th ages (Holocene) and fluid inclusion δD.	Fleitmann et al. (2003a)	
		H12	U-Th ages (Holocene – modern) and fluid inclusion δD.	Fleitmann et al. (2003a)	N/A
			U-Th ages (Holocene – modern) and high-resolution calcite $\delta^{18}O$ and $\delta^{13}C$.	Fleitmann et al. (2007)	
		H13	U-Th ages (MIS 5e to 9) and calcite $\delta^{18}O$ of entire stalagmite.	Burns et al. (2001)	Fluid inclusion $\delta^{18}O$ and δD analysis from MIS 5 section. Conducted by S. Affolter (University of Bern) Ultra-high-resolution calcite $\delta^{18}O$ and $\delta^{13}C$ analysis of annual layers from MIS 5 section. Conducted b S. Nicholson under
			U-Th ages throughout stalagmite (MIS 5e to 9) and fluid inclusion δD from MIS 5-9 sections.	Fleitmann et al. (2003)	
			U-Th ages and high-resolution calcite $\delta^{18}O$ and	Holzkampfer (2004). Unpublished Master's thesis.	

			$\delta^{13}C$ of MIS 5 section.		the supervision of D. Fleitmann (University of Reading).
		H14	U-Th ages. Calcite $\delta^{18}O$.	Burns et al. (2001)	N/A
			U-Th ages. Fluid inclusion δD.	Fleitmann et al. (2003)	N/A
			U-Th ages and high-resolution calcite $\delta^{18}O$ and $\delta^{13}C$ of Holocene section.	Cheng et al. (2009)	
Saudi Arabia	Broken-Leg (29°45'36"N., 42°18'36"E.)	BL-1	U-Th ages (>1 Ma) and calcite $\delta^{18}O$ and $\delta^{13}C$.	Fleitmann et al. (2004b)	N/A
		BL-2	U-Th ages (>1 Ma).	Fleitmann et al. (2004b)	Additional calcite $\delta^{18}O$ and $\delta^{13}C$ analysis. Conducted by S. Nicholson under the supervision of D. Fleitmann (University of Reading). Fluid inclusion $\delta^{18}O$ and δD analysis. Conducted by S. Affolter (University of Bern) Preliminary U-Pb age analysis. Conducted by J. Woodhead (University of Melbourne).
		BL-3	Initial description.	Fleitmann et al. (2004b)	N/A
	Star (30°6'36"N., 41°37'48"E.)	STC-1	U-Th ages. Calcite $\delta^{18}O$ and $\delta^{13}C$.	Fleitmann et al. (2004b)	Additional caclite $\delta^{18}O$ and $\delta^{13}C$ from sections studied by Fleitmann et al. (2004). Conducted by S. Nicholson under the supervision of D. Fleitmann (University of Reading). Fluid inclusion $\delta^{18}O$ and δD analysis. Conducted by S. Affolter (University of Bern).

					Preliminary U-Pb age analysis. Conducted by J. Woodhead (University of Melbourne).
		STC-2	U-Th ages.	Fleitmann et al. (2004b)	Preliminary U-Pb age analysis. Conducted by N. Roberts (BGS, Keyworth).
		STC-3	U-Th ages.	Fleitmann et al. (2004b)	Additional calcite $\delta^{18}O$ and $\delta^{13}C$ from sections studied by Fleitmann et al. (2004). Conducted by S. Nicholson under the supervision of D. Fleitmann (University of Reading). Fluid inclusion $\delta^{18}O$ and δD analysis. Conducted by S. Affolter (University of Bern). Preliminary U-Pb age analysis. Conducted by N. Roberts (BGS, Keyworth).
		STC-4	U-Th ages. Calcite $\delta^{18}O$ and $\delta^{13}C$.	Fleitmann et al. (2004b)	N/A
		STC-5	U-Th ages. Calcite $\delta^{18}O$ and $\delta^{13}C$.	Fleitmann et al. (2004b)	Additional calcite $\delta^{18}O$ and $\delta^{13}C$ analysis from sections studied by Fleitmann et al. (2004). Conducted by S. Nicholson under the supervision of D. Fleitmann (University of Reading). Preliminary U-Pb age analysis. Conducted by N. Roberts (BGS, Keyworth).
	Surprise (26°28'12"N., 47°13'48" E.)	SC-1	U-Th ages. Calcite $\delta^{18}O$ and $\delta^{13}C$.	Fleitmann et al. (2004b)	Preliminary U-Pb age analysis. Conducted by N. Roberts (BGS, Keyworth).

					Additional calcite $\delta^{18}O$ and $\delta^{13}C$ analysis from sections studied by Fleitmann et al. (2004). Conducted by S. Nicholson under the supervision of D. Fleitmann (Unversity of Reading).
		SC-2	U-Th ages. Calcite $\delta^{18}O$ and $\delta^{13}C$.	Fleitmann et al. (2004b)	Preliminary U-Pb age analysis. Conducted by N. Roberts (BGS, Keyworth).
	Gecko (26°26′N., 47°15′E.) and B32 (26°27′N., 47°14″E.)	SA "A"	Initial description.	Fleitmann et al. (2004b)	N/A
		SA "B"	Initial description.	Fleitmann et al. (2004b)	N/A
		SA "C"	Initial description.	Fleitmann et al. (2004b)	N/A

Tab. 4. List of previous and new analyses conducted on sites and samples used throughout this thesis.

4.9 Summary

Speleothems can be used to provide a plethora of highly resolved palaeoclimate records including rainfall, temperature, vegetation and moisture source. Due to their subterranean location, they are also protected from desert weathering and offer an excellent opportunity to extend the palaeoclimate record of Arabia. Previous analyses of Arabian speleothems have found that $\delta^{18}O_{ca}$ is determined by both the *source effect* and the *amount effect*, overprinting and attenuating other effects (such as temperature: Fleitmann et al., 2003a, 2007, 2011). These studies found that more negative $\delta^{18}O_{ca}$ is a result of increased precipitation delivered by the ISM (Oman) and either the ASM or ISM in Yemen (Fleitmann et al., 2003b, 2011; Cheng et al., 2009b). Using this information and the samples described above, it is possible to extend the palaeoclimate record of Arabia and identify climatically optimal periods for hominin dispersals. In addition to renewed

δD_{FI} and $\delta^{18}O_{FI}$ analyses, comparison of $\delta^{18}O_{ca}$ values could establish both the source of precipitation and the relative rainfall intensity between "green" periods. $\delta^{13}C_{ca}$ is yet to be studied from these speleothems; however, if a vegetation signature can be identified, analysis of $\delta^{13}C_{ca}$ could be used to compare and contrast the vegetation conditions during "green" periods. Additionally, high-resolution analysis of $\delta^{18}O_{ca}$ and $\delta^{13}C_{ca}$ from Mukalla and Hoti Cave stalagmites could produce the first Pleistocene sub-centennial or even sub-annual rainfall and vegetation records from Arabia. Such records can be used to show climatic variability during "green" periods, which, combined with ethnographic data could provide new hypotheses for human-environment interactions.

Chapter 5:

5) Pluvial periods in southern Arabia over the last 1.1 million-years

This chapter has provided a new speleothem derived palaeoclimate record of southern Arabia, spanning ~1.1 million years. This chapter addresses research questions 1-4; providing information on the timing of Arabian climatic optima, past moisture source, evidence of climatic variability between and address whether speleothems can be used as a palaeoenvironmental archive.

This chapter has been adapted (citation style and figure numbers) from a research paper published in *Quaternary Science Reviews* with the following citation:

Nicholson, S.L., Pike, A.W.G., Hosfield, R., Roberts, N., Sahy, D., Woodhead, J., Cheng, H., Edwards, R.L., Affolter, S., Leuenberger, M., Burns, S.J., Matter, A., Fleitmann, D., 2020. Pluvial periods in Southern Arabia over the last 1.1 million-years. *Quaternary Science Reviews 229*: 106112

The author contributions are as follows: S.L.N conducted the stable isotope analysis and acted as primary author for the paper with the guidance of D.F., R.H., A.W.G.P. U-Pb dating analyses were performed by N.R. and J.W. and U-Th dating analyses were conducted by D.S. and H.C.. Laser absorption spectroscopy of speleothem fluid inclusions were performed by S.A. under the supervision of M.L. All authors contributed to the ongoing editing and refinement of the manuscript.

Submitted to *Quaternary Science Reviews*: 31st of May 2019.

Under review: 10th June 2019

Accepted by *Quaternary Science Reviews*: 26th November 2019

Published in *Quaternary Science Reviews*: 19th of December 2019

Abstract

Past climates and environments experienced by the Saharo-Arabian desert belt are of prime importance for palaeoclimatic and palaeoanthropological research. On orbital timescales transformations of the desert into a savannah-like landscape in response to higher precipitation provided "windows of opportunity" for hominin dispersal from Africa into Eurasia. On long timescales, palaeoenvironmental reconstructions for the region are predominantly derived from marine sediments and available terrestrial records from the Arabian Peninsula are limited to 450 ka before present (BP). Here, we present a new stalagmite-based palaeoclimate record from Mukalla Cave in Yemen which extends back to ~1.1 million years BP or Marine Isotope Stage (MIS) 31, as determined by Uranium-lead dating. Stalagmite Y99 grew only during peak interglacial periods and warm substages back to ~1.1 Ma. Stalagmite calcite oxygen isotope ($\delta^{18}O$) values show that every past interglacial humid period was wetter than the Holocene, a period in which large lakes formed in the now arid areas of southern Arabia. Carbon isotope ($\delta^{13}C$) values indicate habitable savannah-like environments developed during these pluvial periods. A total of 21 pluvial periods with precipitation of more than 300 mm yr^{-1} occurred since ~1.1 Ma and thus numerous opportunities for hominin dispersals occurred throughout the Pleistocene. New determinations of hydrogen (δD_{FI}) and oxygen ($\delta^{18}O_{FI}$) isotopes in stalagmite fluid inclusion water demonstrates that enhanced precipitation in Southern Arabia was brought by the African and Indian Summer Monsoons. When combined with

sub-annual calcite analysis of $\delta^{18}O$ and $\delta^{13}C$, these data reveal a distinct wet (summer) and dry (winter) seasonality.

5.1 Introduction

The Saharo-Arabian desert belt is a key-area for both palaeoclimatic and palaeoanthropological research. On orbital timescales, changes in the intensity and spatial extent of the African (ASM) and Indian Summer monsoons (ISM) transformed the Saharo-Arabian desert belt into a "green" landscape with abundant lakes (Drake et al., 2011; Fleitmann et al., 2011; Rosenberg et al., 2011, 2012, 2013; Matter et al., 2015; Breeze et al., 2016; Drake and Breeze, 2016). The timing and duration of these humid periods were pivotal "windows of opportunity" for hominin dispersals from Africa into Eurasia ("out-of-Africa"), which caused substantial demographic shifts during the last 130 ka (Timmermann and Friedrich, 2016; Bae et al., 2017). Knowledge of the "permeability" of the Saharo-Arabian desert belt on longer timescales could therefore be linked to potentially earlier hominin dispersals (e.g., Hershkovitz et al., 2018; Harvati et al., 2019). To date, two dispersals routes into Eurasia are favoured, the Levantine corridor (the northern route) and the narrow strait of Bab-al-Mandab (the southern route) (Fernandes et al., 2006; Fleitmann et al., 2011; Lambeck et al., 2011; Grant et al., 2012; Rohling et al., 2013; Breeze et al., 2016).

Marine sediments from the Mediterranean (ODP 967, Larrasoana et al., 2003; Grant et al., 2017), the Red Sea (KL 11, Fleitmann, 1997) Gulf of Aden (KL 15, Fleitmann, 1997; RC09-166, Tierney et al., 2017) and Arabian Sea (ODP 721/722, deMenocal, 1995; Clemens and Prell, 2003) provide long and continuous records of climate changes in the

Saharo-Arabian desert belt, with a few extending back to the Pliocene. The majority of these records use terrigenous dust as a proxy for continental wetness, where reduced dust input and grain size data are related to enhanced vegetation cover during periods of higher precipitation (Fleitmann, 1997; Larrasoana et al., 2003). However, mobilisation, transport and deposition of dust is determined by multiple non-linear factors, such as production of dust, transport paths (wind direction), wind strength, erosion and vegetation density (Zabel et al., 2001). Terrestrial archives are thus required to test and mitigate uncertainties within marine dust records.

Terrestrial records from the main dispersal routes (Fig. 34) are primarily based on lacustrine sediments and speleothems (Burns et al., 2001; Armitage et al., 2007; Vaks et al., 2010; Fleitmann et al., 2011; Petraglia et al., 2011; Rosenberg et al., 2011, 2012, 2013; Jennings et al., 2015b), which cover only the last 350 to 450 ka before present (BP) (Rosenberg et al., 2013; Parton et al., 2018). While lake records provide information on the timing of these pluvial periods, it is much more difficult to use them for characterizing the climatic conditions at the time of their formation (Rosenberg et al., 2011, 2012, 2013). Palaeolake formations currently only provide limited “wet” or “dry” environmental information; comparison of climates among interglacial periods is much more challenging. Moreover, the nature of the lakes is the subject of debate, i.e. whether seasonal "wetlands" or perennial lakes existed (Enzel et al., 2015; Engel et al., 2017; Quade et al., 2018). Furthermore, palaeolake records from Arabia cannot currently be used to determine the source of moisture; a contentious issue within palaeoclimate research (Fleitmann et al., 2003b; Rosenberg et al., 2013; Kutzbach et al., 2014; Jennings et al., 2015b; Torfstein et al., 2015). Thus, an independent archive of continental wetness is required to elucidate these issues.

Speleothems (stalagmites, stalactites and flowstones) from the Arabian Peninsula and Middle East have great potential to deliver more comprehensive climatic records as they are protected from erosion. In addition, they can be used to extend the terrestrial palaeoclimate record beyond 600 ka using the Uranium-Lead (U-Pb hereafter) chronometer (Woodhead et al., 2006, 2012; Vaks et al., 2013, 2018). In arid regions such as Arabia, speleothem growth is dependent on both availability of moisture and vegetation respired CO_2 in soils (Burns et al., 1998; McDermott, 2004). The amount and source of precipitation are important controls on speleothem calcite $\delta^{18}O_{ca}$ values (Dansgaard, 1964; Fleitmann et al., 2003a, 2011); whereas carbon isotopes ($\delta^{13}C_{ca}$) can provide information on the type (C_3/C_4 plants) and density of vegetation above the cave (McDermott, 2004; Cerling et al., 2011; Rowe et al., 2012). Finally, δD_{FI} and $\delta^{18}O_{FI}$ values of water trapped in speleothem fluid inclusion provide direct evidence of moisture sources when compared to modern isotopes in precipitation and regional meteoric waterlines (Bar-Matthews et al., 1996; Dennis et al., 2001; Meckler et al., 2015).

Previously published stalagmite records from Mukalla Cave in Yemen and Hoti Cave in Northern Oman (Fig. 34) extend back to ~330-300 ka BP, or Marine Isotope Stage (MIS) 9 (Fleitmann et al., 2011). The unique geographical position of Mukalla cave means speleothem growth occurs only when the northern limit of the monsoon rain belt passes ~14°N. Stalagmite Y99 (Mukalla Cave) is therefore an ideal specimen to track both meridional and zonal movements of the monsoon rain belt in southern Arabia and eastern Africa. Here, we present new Uranium-Thorium (^{230}Th) and Uranium-Lead (U-Pb) dates for stalagmite Y99, which allows us to expand the Arabia terrestrial palaeoclimate record back to ~1.073 Ma, or MIS 31. Additional isotope measurements performed on Mukalla

and Hoti Cave stalagmite calcite and fluid inclusion water allow us to track changes in the amount and source of rainfall.

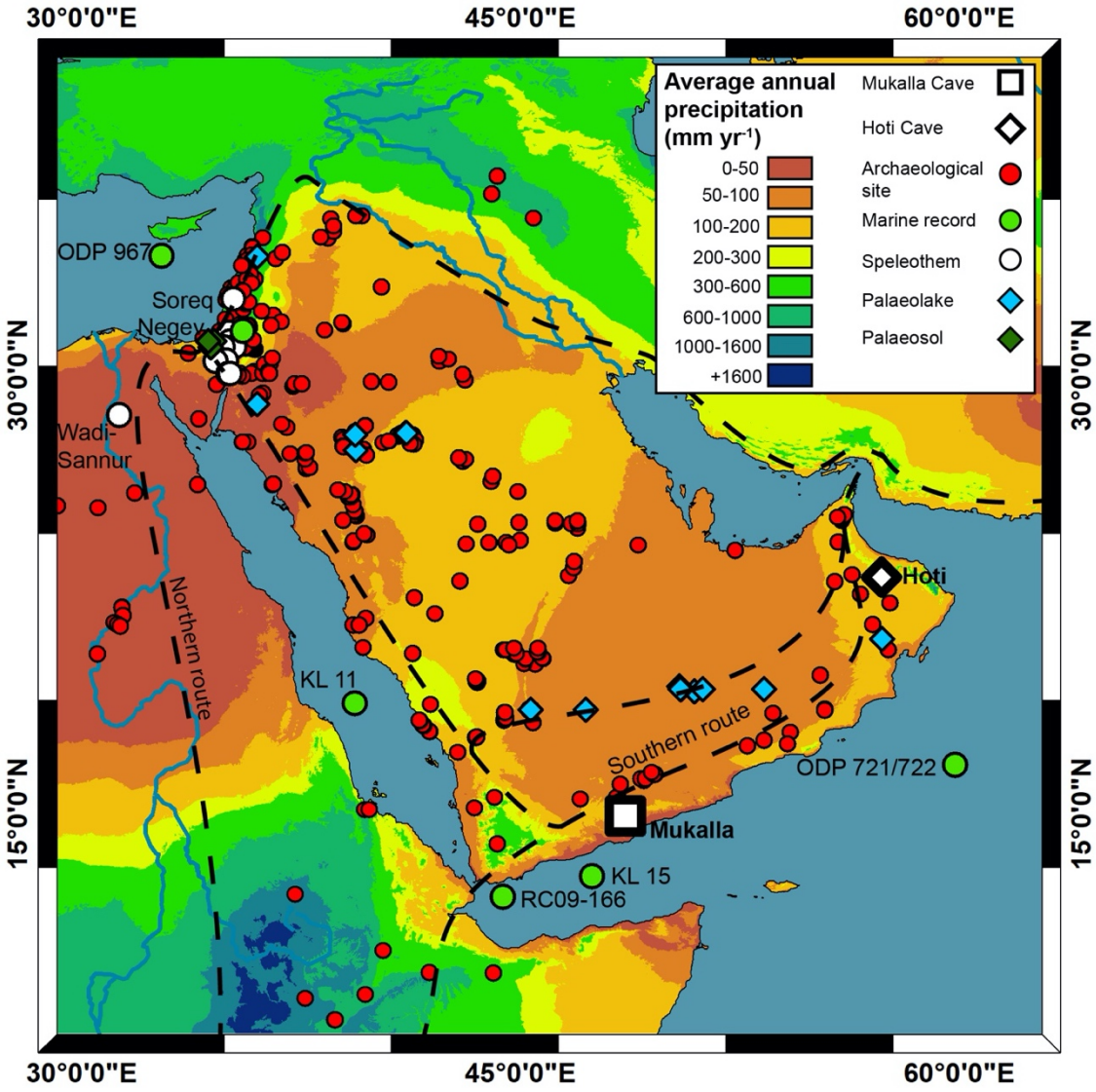

Fig. 34. Map of the Arabian Peninsula with present day (1970-2000) annual precipitation (accessible at: WorldClim, 2015; Fick and Hijmans, 2017). Red circles denote Middle Palaeolithic archaeological sites (red circles; Petraglia et al., 2011; Rose et al., 2011; Bailey et al., 2015; Breeze et al., 2015; Groucutt et al., 2015a, 2015b; Jennings et al., 2015a). Dashed lines show potential hominin dispersal routes (Rosenberg et al., 2011). Also shown are caves (white cirlces; Frumkin et al., 1999; Bar-Matthews et al., 2003; Vaks et al., 2010; El-Shenawy et al., 2018); palaeolake sites (blue diamonds; Rosenberg

et al., 2011, 2012, 2013; Petraglia et al., 2012; Matter et al., 2015), marine records (deMenocal, 1995; Fleitmann, 1997; Almogi-Labin et al., 2000; Larrasoana et al., 2003; Tierney et al., 2017), lake records (blue circles; Torfstein et al., 2015) and Mukalla and Hoti caves (hollow square and diamond, respectively; Burns et al., 1998, 2001; Fleitmann et al., 2003b, 2011).

5.2 Climatic and Cave settings

Stalagmites presented in this study were collected from Mukalla Cave in Yemen and Hoti Cave in Northern Oman (Burns et al., 2001; Fleitmann et al., 2003b, 2011). Present-day climate in Southern Arabia is strongly governed by two major weather systems: The North Atlantic/Siberian pressure system in winter/spring and the ASM/ISM in summer (Fleitmann et al., 2003b). At present, hyper-arid to arid climate conditions prevail on the Arabian Peninsula and only the southernmost parts, such as the Yemen Highlands and Dhofar Mountains, are affected by the ASM and ISM.

5.2.1 Mukalla Cave, Yemen

Mukalla Cave (14°55'02"N; 48°35'23" E; ~ 1500 metres above sea level, masl) is situated in the arid desert of Yemen, approximately 70 km North of Al Mukalla, Hadhramaut (Fig. 34). The current climate of Southern Yemen is dependent on the annual northward movement of the Intertropical Convergence Zone (ITCZ) and associated monsoonal rainfall belt. Annual precipitation is highly variable, yet averages ~120 mm yr^{-1}, mostly delivered in the spring and summer months (Mitchell and Jones, 2005). Bedrock thickness above the cave is approximately 30 m, and soil above the cave is mostly absent. No actively growing stalagmites were found when stalagmites Y99, Y97-4 and Y97-5

were collected in 1997 and 1999 respectively (Fleitmann et al., 2011), indicating that modern rainfall is too low to recharge the aquifer above Mukalla Cave. Based on these samples, Fleitmann et al. (2011) produced an environmental record up to MIS 9 (~330 ka), identifying four distinct growth intervals (GI I-IV) within stalagmite Y99. However, only the top section (collected in whole; Fig. 35B and S1) of a 3.2m sample (Y99) was analysed. Here, remaining growth intervals from the lower part of Y99 (which was cored in several overlapping sections; Fig. 35C, S2 and S3), was dated to expand the terrestrial palaeoclimate record of Arabia. Calcite isotope measurements were performed throughout these growth intervals to characterise the climatic and environmental conditions during stalagmite growth. Additional calcite isotope measurements were performed at greater resolution in the top section of Y99.

5.2.2 Hoti Cave, Oman

Hoti Cave (23°05'N; 57°21'E: ~ 800 masl, Fig. 34) is located in the northern Oman mountains, where annual precipitation ranges between 50 and 255 mm yr-1 (station AI Hamra, 700 masl, 1974–1997). Precipitation is highly variable and mainly derived from three sources: the Mediterranean frontal system (December-March: Weyhenmeyer et al., 2002); orographic rain produced over the Jabal Akhdar Mountains during summer; and tropical cyclones, originating in the south-eastern Arabian Sea and the Bay of Bengal, every 5 to 10 years (Pedgley, 1969).

Stalagmites from Hoti Cave have been extensively studied (Burns et al., 2001; Neff et al., 2001; Fleitmann et al., 2003b, 2007). Several stalagmites cover the Holocene (samples H5, H12 and H14) and beyond (samples H1, H4, and H13). Stalagmite H13 is

a ~3 m tall stalagmite covering MIS 5e, MIS 7e and MIS 9. Further details on the chronology and sampling location of Hoti Cave were presented in previous publications (Burns et al., 1998, 2001; Neff et al., 2001; Fleitmann et al., 2003b, 2007, 2011).

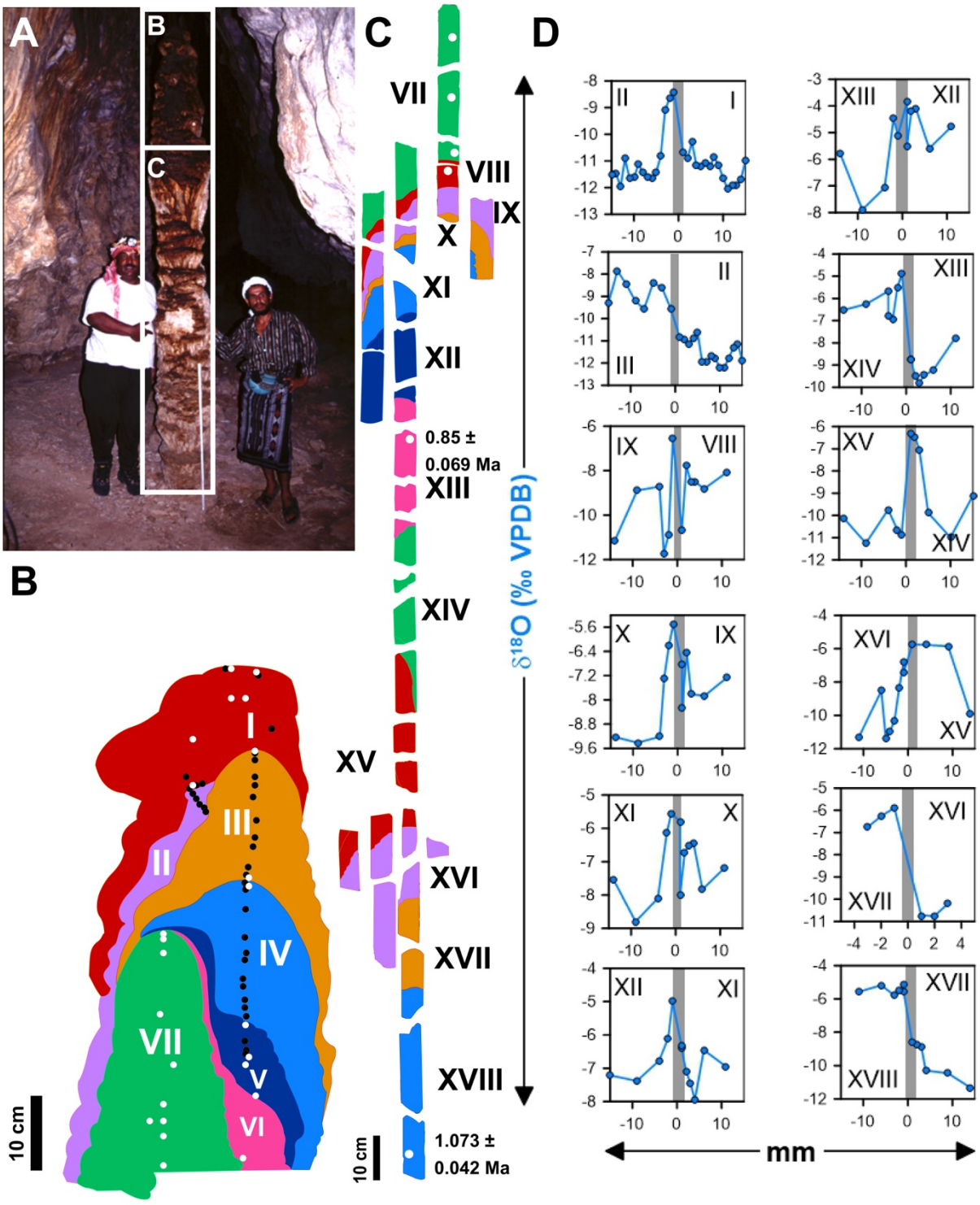

Fig. 35. (A) Stalagmite Y99 in situ in Mukalla Cave. (B and C) Y99 consecutive growth intervals (Fig. S1-S3). Location of ^{230}Th and U-Pb ages marked by black (Fleitmann et

al., 2011) and white (this study) circles. (D) Plots show $\delta^{18}O_{ca}$ shifts over discontinuities between GIs (Tab. S6 and S7).

5.3 Methods

5.3.1 Dating

Stalagmites presented in this study were dated using the ^{230}Th dating method back to ~550 ka and the U-Pb method for older samples (Woodhead et al., 2006; Cheng et al., 2013). The ^{230}Th ages for Hoti Cave stalagmites are reported in (Fleitmann et al., 2003a, 2007). For stalagmite Y99 (Mukalla Cave), a total of seventy ^{230}Th ages were determined back to approx. 550 ka BP (Tab. S1-S3). Nineteen samples were analysed at the University of Minnesota (following the methods outlined by Cheng et al., 2013) and twelve additional samples were analysed at the British Geological Survey, Nottingham, UK (following the methods by Crémière et al., 2016). Dates were calculated using the decay constant of Cheng et al. (2013), and a correction for the presence of initial ^{230}Th was applied assuming a detrital U-Th isotope composition of (^{232}Th/^{238}U) = 1.2 ± 0.6, (^{230}Th/^{238}U) = 1 ± 0.5 and (^{234}U/^{238}U) = 1 ± 0.5. The ages for GI XII and GI XVIII were determined via U-Pb methods. U-Pb ages for the lower part of Y99 were produced using both traditional solution-mode multi-collector inductively coupled plasma mass spectrometry (MC-ICP-MS) (following the methods detailed in: Woodhead et al., 2006) analysis (University of Melbourne, Australia) along with the recently developed Laser ablation (LA) method (BGS) (Tab. S4 and S5). For LA-ICP-MS, the methods and analytical protocol follows that described by Coogan et al. (2016); U/Pb ratios were normalised to WC-1 carbonate (Roberts et al., 2017) and Duff Brown carbonate (Hill et al., 2016) was run as a check on accuracy.

5.3.2 Calcite oxygen and carbon isotope analysis

A total of 910 samples were collected along the main growth axes of stalagmite Y99 GIs for stable isotope analysis. Samples were collected at resolutions of ~1mm for growth phase I and II, ~2 mm for growth phases III-VII and ~5 mm for growth phases VII-XVIII (Tab. S6). Due to the variable size, visibility and direction of independent growth layers, it was not possible to produce Hendy tests. To provide addition support for our Growth Interval assignments, additional samples were collected across visible growth discontinuities at 1 mm resolution within the lower sections of Y99 (Tab. S7; Fig. 35C). Furthermore, H13 (Hoti Cave) was selected for sub-annual isotopic analysis to examine seasonality, due to its annual laminations. Samples were collected at 0.1mm resolution (Tab. S8).

Isotope measurements were performed using a Finnigan Delta V Advantage Isotope Mass Spectrometer (IRMS) coupled to an automated carbonate preparation system (Gasbench II). Precision (1σ) is ≤0.2‰ for $\delta^{18}O$ and ≤0.1‰ for $\delta^{13}C$. Measurements were performed at the Chemical Analysis Facility (CAF), University of Reading, UK, and the Institute of Geological Sciences, University of Bern, Switzerland. Isotope values are reported relative to the Vienna Peedee Belemnite (VPDB) standard.

5.3.3 Fluid inclusion deuterium and oxygen isotope analysis

Deuterium (δD_{FI}) and oxygen ($\delta^{18}O_{FI}$) isotopes of speleothem fluid inclusion water were analysed at the Physics Institute, University of Bern, Switzerland, using a recently developed extraction method (Affolter et al., 2014, 2015). Sixteen calcite blocks of ~25

x 5 x 5 mm (L, W, H) for fluid inclusion analysis were collected from Y99, H13 and H5. Samples were placed into a copper tube and connected to the measuring line, heated to ~140°C and crushed, the liberated water was then transported to a wavelength scanned cavity ring down spectroscopy system (Picarro L2401-i analyser) under humid conditions (with standardised water of known isotopic composition) to prevent fractionation and minimize memory effects. The crushing of samples released, on average, ~1 µl of water. Precision is 1‰ for δD_{FI} and 0.2‰ for $\delta^{18}O_{FI}$. Fluid inclusion values are reported on the Vienna Standard Mean Ocean Water (V-SMOW) scale (Tab. S9).

5.4 Results and Discussion

This section is divided into two parts. In the first part we focus on rainfall variability during the last 350 ka. We provide additional and more precise ^{230}Th ages for Y99 (Mukalla Cave), as well as stable isotope analysis of calcite and fluid inclusion water from Y99 (Mukalla Cave), H5 and H13 (Hoti Cave). We combine these ages with previously published Mukalla and Hoti Cave speleothem data to discuss the timing and environmental conditions of South Arabian Humid Periods (SAHPs) since 350 ka BP. By comparing our multiproxy records with marine and terrestrial palaeoclimate records from the African and Asian monsoon domains, we show that periods of enhanced rainfall and speleothem growth in Southern Arabia are related to a strengthening and greater spatial extent of the ASM and ISM during peak interglacials and interstadials. Within the second section, we provide an extended chronology and $\delta^{18}O_{ca}$ and $\delta^{13}C_{ca}$ stable isotope data for the lower portion of Y99 (Fig. 35C) in order to characterise humid periods in Southern Arabia back to ~1.1 Ma BP, making the stalagmite Y99 record one of the longest continental records from Southern Arabia.

5.4.1 Timing and Nature of SAHPs during the last 350 ka

5.4.1.1 Chronology of Y99 GI I to V

The chronology of Y99 growth phase I to V is based on a total of 53 ^{230}Th ages (Fig. 36). These include 38 ages presented in Fleitmann et al. (2011) and 15 additional more precise ^{230}Th ages analysed for this study (Tab. S1 and S2). Stalagmite Y99 GIs I-V coincide with peak interglacial periods and interstadials corresponding to MIS 5e, 7a, 7e, 9c and 9e (Fig. 36) when Southern Arabia was affected by the ASM and ISM (Fleitmann et al., 2011; Rosenberg et al., 2013). While age reversals are observed in GI IV and V, kernel probability density plots of all ^{230}Th ages obtained from Mukalla Cave (Y99, Y97-4.-5) and Hoti Cave (H1, H4, H5, H10, H11 and H14) indicates Y99 growth was more likely to occur within MIS 9c and 9e (Fig. 36).

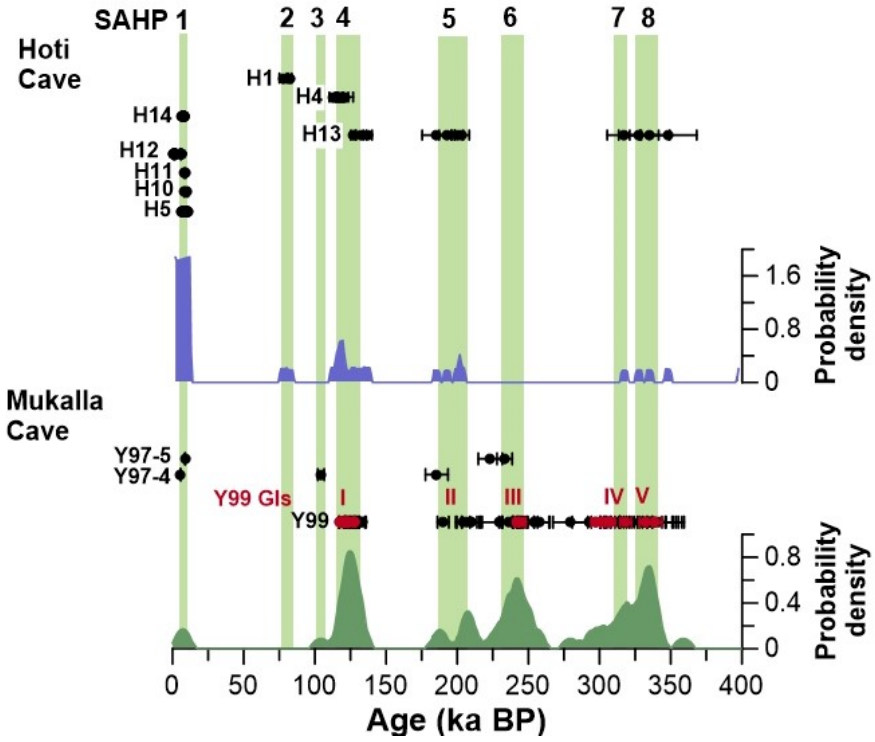

Fig. 36. ^{230}Th ages of Hoti Cave and Mukalla Cave speleothems. Red dots denote new Y99 ^{230}Th ages determined for this study. Age kernel probability density plots of Hoti (blue; 5 pt. moving average) and Mukalla (green) and green bars show periods of most likely speleothem deposition. These were used to assign South Arabian Humid Periods (SAHP) 1-8.

5.4.1.2 SAHPs in Oman and Yemen during the last 350 ka

Growth intervals of stalagmites from Mukalla and Hoti Caves mark climatic intervals when effective precipitation was high enough to recharge the aquifers above both caves (Burns et al., 2001; Fleitmann et al., 2003b, 2011; Fleitmann and Matter, 2009). At present, total annual rainfall averages ~120 mm yr^{-1} and ~180 mm yr^{-1} at Mukalla and Hoti Cave respectively, and actively growing stalagmites are either absent (Mukalla Cave) or very rare (Hoti Cave) (Burns et al., 2001; Fleitmann et al., 2003a, 2007, 2011). Thus, the existence of very tall and large diameter stalagmites such as H13 and Y99 (Fig. 35) in both caves is clear evidence that precipitation was considerably higher than today when they were formed (Vaks et al., 2010; Fleitmann et al., 2011; El-Shenawy et al., 2018). Based on the spatial distribution of actively growing stalagmites in the Levant and Negev – areas with very similar climatic conditions compared to Yemen and Oman – precipitation should have been around 300 mm yr^{-1} or greater to recharge the groundwater and trigger growth of stalagmites (Vaks et al., 2010, 2013). Considering the height and diameter of stalagmites Y99 and H13 (Fig. 35), precipitation was most likely considerably higher than 300 mm yr^{-1}. Intervals of speleothem growth at both cave sites are therefore a first indicator for continental wetness in Southern Arabia. An important feature of stalagmites Y99 and H13 is that their growth was reactivated multiple times,

suggesting that the long-lasting cessations of stalagmite growth are related to arid climatic conditions (Burns et al., 2001; Fleitmann et al., 2011).

Over the last 350 ka BP, stalagmite growth in Mukalla and Hoti Caves occurred during peak interglacial periods and warmer substages corresponding to the early and mid-Holocene, MISs 5a, 5c, 5e, 7a, 7e, 9c and 9e (Fig. 37; Burns et al., 2001; Fleitmann et al., 2003a, 2003b; Fleitmann and Matter, 2009). SAHPs were related to intensified African and Indian summer monsoon circulation and a northward displacement of the tropical rain-belt and ITCZ at times of high boreal summer insolation and low ice volume (LR04 stack) (Burns et al., 1998; Fleitmann et al., 2011; Beck et al., 2018). Both the timing and frequency of SHAPs over the last 350 ka are in excellent agreement with other marine and terrestrial hydroclimate records from the Saharo-Arabian desert belt (Fig. 37). In the Gulf of Aden, low $\delta D_{leafwax}$ values in Core RC09-166 (Fig. 37) indicate greater rainfall in the Horn of Africa and Afar regions during the early to mid-Holocene (SAHP 1), MIS 5a, 5c, 5e (SAHPs 2-4) and MIS 7a (SAHP 5) (Tierney et al., 2017). Two aeolian dust records from the Gulf of Aden (KL 15) and central Red Sea (KL 11) show generally lower median grain size values during peak interglacial periods when erosion and mobilization of dust was significantly reduced as a result of a denser vegetation cover in North Africa and Arabia (Fleitmann, 1997). Similarly, speleothem growth in Southern Arabia and Northern Egypt (Wadi Sannur Cave) are in good agreement, occurring at MIS 5e, MIS 7c and MIS 9c and 9e (El-Shenawy et al., 2018). Absence of speleothem growth in Northern Egypt during relatively warm substages (MIS 5c and 5a and MIS 3) suggests that ASM rainfall did not reach far into Egypt, highlighting a degree of regional and temporal variability. Sapropel layers in the Eastern Mediterranean are an additional proxy for ASM and ISM intensity and were mainly deposited during periods of increased

Mediterranean rainfall and significantly higher monsoon precipitation in the Ethiopian highlands and resultant higher Nile discharge (Fig. 37; summarised in Rohling et al., 2015; Grant et al., 2016). The timing of SAHPs 1 to 8 is in excellent agreement with sapropels records, with the exception of the "ghost sapropels" 2 and 6 which are most likely not associated with higher Nile discharge (Rohling et al., 2015). Further north, the Soreq and Peqiin Cave $\delta^{18}O_{ca}$ records from the Levant are also sensitive recorders of changes in $\delta^{18}O$ of eastern Mediterranean surface seawater related to Nile discharge (Bar-Matthews et al., 2003; Rohling et al., 2015), with more negative $\delta^{18}O_{ca}$ values indicating higher Nile discharge during peak interglacial and interstadial periods (Fig. 37). Likewise, speleothem-based Negev Humid Periods (NHPs; based on speleothem ages) 1-4 are synchronous to SAHPs (Fig. 37), with the exemption of SAHP 6 (~245-241 ka), in which there is only limited evidence of speleothem deposition (Vaks et al., 2010). Also, SAHPs 1-8 correlate to phases of lake formation in the Nafud desert in Northern Arabia related to enhanced ASM rainfall (Rosenberg et al., 2011; Jennings et al., 2015b). SAHPs are therefore in phase with wet intervals in Northern Arabia. One notable discrepancy, however, is the lack of evidence for stalagmite growth in Mukalla and Hoti Caves during MIS 7c (Fig. 37); whereas increased precipitation is observed in Wadi-Sannur Cave, Peqiin and Soreq $\delta^{18}O_{ca}$ records, KL-15 grain size and Mediterranean sapropels (S8) (Fig. 37). MIS 7c is also reflected by a less substantial enhancement of the monsoon in Asia (Beck et al., 2018) and KL-11 (Fleitmann, 1997) (Fig. 37). The reason of lack of evidence for an SAHP during MIS 7c remains unknown. Furthermore, we acknowledge that some fluvio-lacustrine deposition and alluvial aggradation occurred in Arabia during MIS 6 and 3 (e.g., McLaren et al., 2009; Parton et al., 2013, 2015a, 2018). Previous analyses have shown that that only 200 mm yr^{-1} is required to activate alluvial

systems in Arabia (Parton et al., 2015b); whereas more than 300 mm yr^{-1} required to active the growth of tall stalagmites (Vaks et al., 2010; Fleitmann et al., 2011).

The influence of precessional and glacial boundary forcing on Asian monsoon intensity remains controversial, as some monsoon records suggest dominant precession-driven monsoon maxima during Northern hemisphere summer insolation maxima (Cheng et al., 2016) while others show evidence for a dampening effect of glacial boundary conditions on monsoon strength during glacial periods (Neff et al., 2001; Fleitmann et al., 2003a; Beck et al., 2018). A recently published East Asian summer monsoon (EASM) reconstruction based on ^{10}Be-flux from Chinese loess shows highest summer monsoon rainfall during peak interglacial periods (Fig. 37). The ^{10}Be-flux rainfall EASM record is closely linked with global ice volume, which is consistent with the timing of SAHPs 1-8 in our speleothem record (Fig. 37).

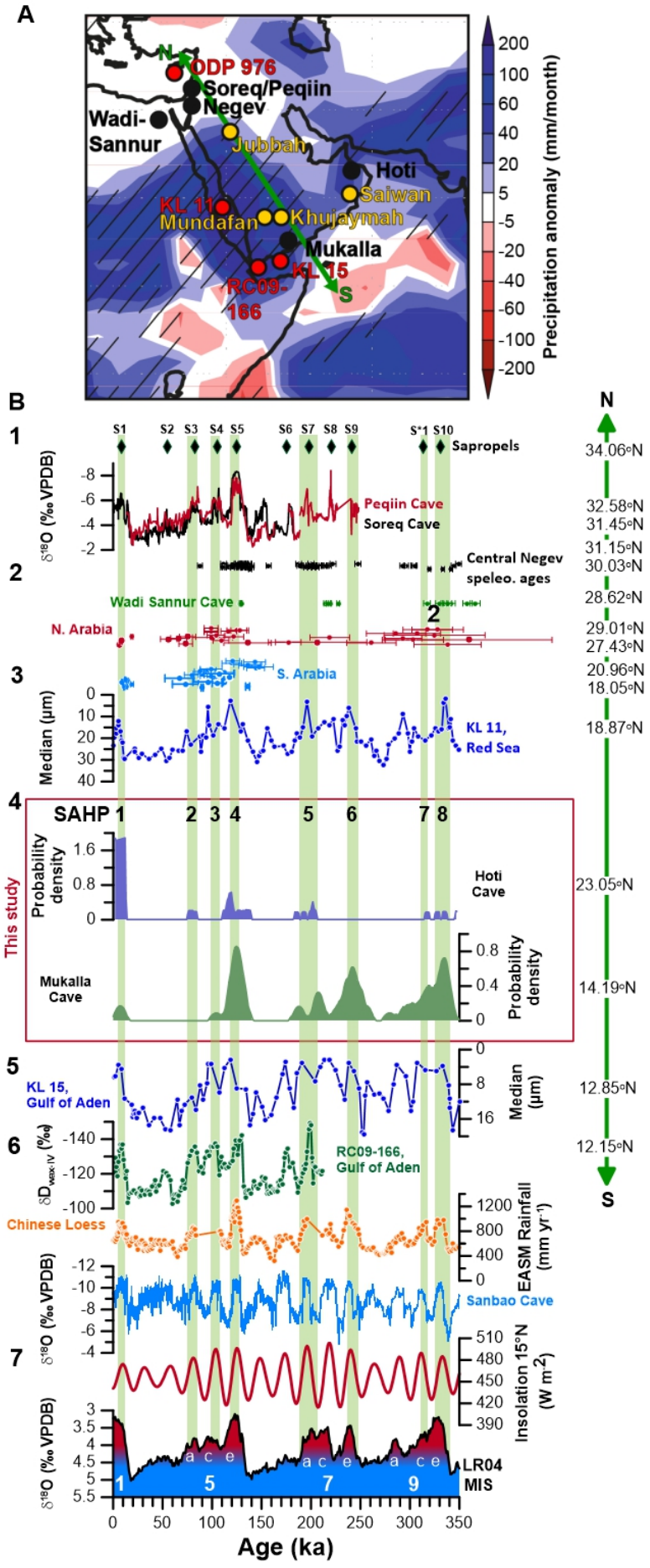
A
N
ODP 976
Soreq/Peqiin
Negev
Wadi-
Sannur
Jubbah
Hoti
Saiwan
KL 11
Mundafan
Khujaymah
Mukalla
KL 15
RC09-
166
S
200
100
60
40
20
5
-5
-20
-40
-60
-100
-200
Precipitation anomaly (mm/month)
B
N
34.06°N
32.58°N
31.45°N
31.15°N
30.03°N
28.62°N
29.01°N
27.43°N
20.96°N
18.05°N
18.87°N
23.05°N
14.19°N
12.85°N
12.15°N
S
1
S1 S2 S3 S4 S5 S6 S7 S8 S9 S*1 S10
Sapropels
δ18O (‰ VPDB)
Peqiin Cave
Soreq Cave
2
Central Negev
speleo. ages
Wadi Sannur Cave
N. Arabia
2
3
S. Arabia
Median (μm)
KL 11,
Red Sea
4
SAHP 1 2 3 4 5 6 7 8
This study
Probability
density
Hoti
Cave
Mukalla
Cave
Probability
density
5
KL 15,
Gulf of Aden
Median
(μm)
6
δDwax-IV (‰)
RC09-166,
Gulf of Aden
Chinese Loess
EASM Rainfall
(mm yr-1)
Sanbao Cave
δ18O (‰ VPDB)
7
Insolation 15°N
(W m-2)
δ18O (‰ VPDB)
LR04
MIS
1 5 7 9
Age (ka)

Fig. 37. (A) Location of speleothems (black circles), palaeolakes (yellow circles) and marine sediment cores from the eastern Saharo-Arabian deserts compared to simulated precipitation anomalies (MIS 5e – pre-industrial: Herold and Lohmann, 2009). (1) Sapropel layers in the Eastern Mediterranean Sea (green diamonds; Williams et al., 2015; Grant et al., 2017) vs Peqiin Cave (red) and Soreq Cave (black; Bar-Matthews et al., 2003) $\delta^{18}O$ records; (2) Central Negev (black; Vaks et al., 2010) and Wadi Sannur (green; El-Shenawy et al., 2018) speleothem deposition periods compared to north (red; Petraglia et al., 2012; Rosenberg et al., 2013; Parton et al., 2018) and South Arabian lakes (blue; Rosenberg et al., 2011, 2012; Matter et al., 2015); (3) Red Sea median grain size (Fleitmann, 1997); (4) age kernel density plots of Hoti Cave (blue; 5pt moving average) and Mukalla Cave (green) stalagmites; (5) Gulf of Aden median grain size (Fleitmann, 1997) and $\delta D_{leafwax}$ ‰ (Tierney et al., 2017); (6) Chinese reconstructed rainfall (Beck et al., 2018) vs Sanbao Cave composite speleothem $\delta^{18}O_{ca}$ record (Cheng et al., 2016); (7) Northern hemisphere June insolation at 15°N (Berger and Loutre, 1991, 1999) vs global marine $\delta^{18}O_{benthic}$ (Lisiecki and Raymo, 2005). Marine Isotope Stages follow the taxonomy of (Railsback et al., 2015).

In summary, there is excellent agreement between SAHPs and low latitude northern-hemisphere insolation, glacial boundary conditions and African and Asian (Indian) monsoon records. This adds confidence that the Mukalla and Hoti Cave speleothems are an accurate recorder of changes in ASM and ISM intensity and extent in north-eastern Africa and Southern Arabian Peninsula.

5.4.1.3 Source of moisture in Southern Arabia during SAHPs 1 to 8

Current climate reconstructions derived from lacustrine sediments and dune deposits are unable to identify the source of precipitation during Arabian pluvial periods (Fleitmann et al., 2003b; Kutzbach et al., 2014; Enzel et al., 2015; Torfstein et al., 2015; Engel et al., 2017). This has triggered controversial debates about the origin of rainfall at the time of their formations. Enzel et al. (2015), for instance, questioned the paradigm that enhanced precipitation in Arabia was related to an amplification of the ASM and ISM and northward displacement of the summer ITCZ. Instead, Enzel et al. (2015) proposed two other potential sources of precipitation in Oman during the early and mid-Holocene humid period (SAHP 1): more frequent Arabian Sea cyclones or enhanced advection of moisture from the Gulf of Oman in winter. Direct measurements of hydrogen and oxygen isotope values in speleothem fluid inclusions from Hoti and Mukalla Caves provide direct information on drip water isotopic composition and palaeoprecipitation respectively (Fleitmann et al., 2003b). Stalagmite δD_{FI} and $\delta^{18}O_{FI}$ values enable us to determine the origin (e.g., Mediterranean or Indian Ocean) and transport of moisture to Southern Arabia during pluvial periods. Furthermore, they also permit a direct comparison with isotope-enabled climate model simulations, to benchmark the models (Herold and Lohmann, 2009) and also help to settle current debates about the origin and seasonality of precipitation in Southern Arabia.

At present, a large proportion of moisture in Yemen derives from the northern reach of the ISM (Fleitmann et al., 2011) with additional moisture originating from Africa (by the ASM) and the Red Sea (mainly in winter/spring) (e.g., Al-ameri et al., 2014). The isotopic composition of modern precipitation (collected between 2008 and 2010) from sampling sites between 500 and 1700 meters asl in Yemen ranges from around -40 to 40‰ and -4

to 8‰ in δD and $\delta^{18}O$ respectively, and rainfall plots along the Global Meteoric Waterline (GMWL; $\delta D=8\ \delta^{18}O + 10$; Fig. 38A; Al-ameri et al., 2014). In contrast, stalagmite Y99 fluid inclusion isotope values for MISs 5e (SAHP 4) and 7e (SAHP 6) are more negative and range from -64.5‰ to -35.0% and -8.6 and -4.5‰ in δD and $\delta^{18}O$ respectively (Fig. 38A; Tab. S9). Like modern rainfall, Y99 fluid inclusion isotope values plot close to the GMWL, whereas some samples appear to be slightly affected by evaporation as they plot below the GMWL. Stalagmite Y99 MIS 5e and MIS 7e δD_{FI} and $\delta^{18}O_{FI}$ values are more negative than isotope values in modern summer monsoonal rainfall (June to September) in Addis Ababa, Ethiopia, where moisture is delivered by the African and Indian summer monsoons. This suggests that enhanced rainfall at Mukalla Cave during MIS 5e (SAHP 4) and MIS 7e (SAHP 6) resulted from an amplification of the ASM and/or ISM (Fig. 38C). Our assumption is also supported by climate model data for MIS 5e (Herold and Lohmann, 2009; Jennings et al., 2015b), which indicate a more zonal transport of moisture from Africa to the Arabian Peninsula during MIS 5e (SAHP 4). Y99 $\delta^{18}O_{FI}$ values of around -7.2 ± 1.5‰ during MIS 5e are within the range of modelled summer precipitation $\delta^{18}O$ values of between -6 and -7‰ in Yemen (Fig. 38C). Finally, significant contributions of rainfall from a Mediterranean source can be excluded as Y99 δD_{FI} and $\delta^{18}O_{FI}$ values plot below the Mediterranean Meteoric Waterline (MMWL; $\delta D = \delta^{18}O + 22$; Fig. 38A).

In Northern Oman, present-day rainfall originates predominantly from a northern (Mediterranean) and a southern (Indian Ocean) moisture source. As a result, two distinctly different local meteoric waterlines exist, the Northern Meteoric Waterline (N-LMWL; $\delta D = 5.0\ \delta^{18}O +10.7$) and the Southern Local Meteoric Waterline (S-LMWL; $\delta D = 7.1\ \delta^{18}O -1.1$) (Fig. 38B; Weyhenmeyer et al., 2002; Fleitmann et al., 2003b).

Precipitation originating from a northern moisture source ranges from -4.5 to 1.0‰ in $\delta^{18}O$ and from -25 to 5‰ in δD, whereas precipitation from a southern moisture source is more negative, with $\delta^{18}O$ values varying from -10 to -2‰ and δD values from -75 to -15‰ (Weyhenmeyer et al., 2002; Fleitmann et al., 2003b). Modern groundwater in Northern Oman (N-OGL: $\delta D = 5.3\ \delta^{18}O + 2.7$) and cave drip water in Hoti Cave is intermediate between both sources, indicating that both contribute to groundwater recharge (Weyhenmeyer et al., 2002; Fleitmann et al., 2003b; Fig. 38B). The isotopic composition of fluid inclusion water extracted from the Holocene stalagmite H5 (SAHP 1: 10.9 ka-6.2 ka; Neff et al., 2001; Fleitmann et al., 2007) ranges from -21.4‰ to -13.2‰ in δD_{FI}, and -3.2‰ to -0.7‰ in $\delta^{18}O_{FI}$. Fluid inclusion water extracted from the MIS 5e (SAHP 4) section of stalagmite H13 is more negative and measured -41.7‰ for δD_{FI} and -7.8‰ to -4.2‰ for $\delta^{18}O_{FI}$. Both H5 and H13 fluid inclusion values plot closer to the S-LMWL (Fig. 38B), indicating the ISM was the primary moisture source in Oman during peak interglacials (Fleitmann et al., 2003b). One sample, however, plots above the S-LMWL, yet this remains more closely aligned to modern southern groundwater values. Overall, Hoti Cave δD_{FI} and $\delta^{18}O_{FI}$ values show clear evidence that enhanced rainfall during the early to middle Holocene (SAHP 1) and MIS 5e (SAHP 4) was related to an intensification of the ISM. This is in stark contrast to suggestions that enhanced frontal depressions from the Persian Gulf and/or Mediterranean increased precipitation during the early to mid-Holocene wet period (SAHP 1) (Enzel et al., 2015).

When compared to isotope-enabled climate model simulation, the measured isotope $\delta^{18}O_{FI}$ values at both caves for SAHP 4 (MIS 5e) are in good agreement with modelled $\delta^{18}O$ of summer precipitation (Fig. 38C). Furthermore, the distinct isotopic gradient across Southern Arabia is also supported by the Y99 and H13 $\delta^{18}O_{FI}$ values, with more

negative modelled summer rainfall $\delta^{18}O$ values prevailing in the west due to a greater moisture supply from the African summer monsoon (Herold and Lohmann, 2009). Thus, growth intervals and isotope values in stalagmites from Mukalla Cave are excellent proxies for the intensity of the ASM in eastern Africa, whereas stalagmites from Hoti Cave are more closely connected to intensity changes of the ISM and, to a lesser extent, ASM. This is also in agreement with climate model simulations for MIS 5e, which indicate that higher precipitation in Northern Oman was associated with the ASM and ISM, with negligible and fairly stable contribution of rainfall from Mediterranean westerlies (Jennings et al., 2015b).

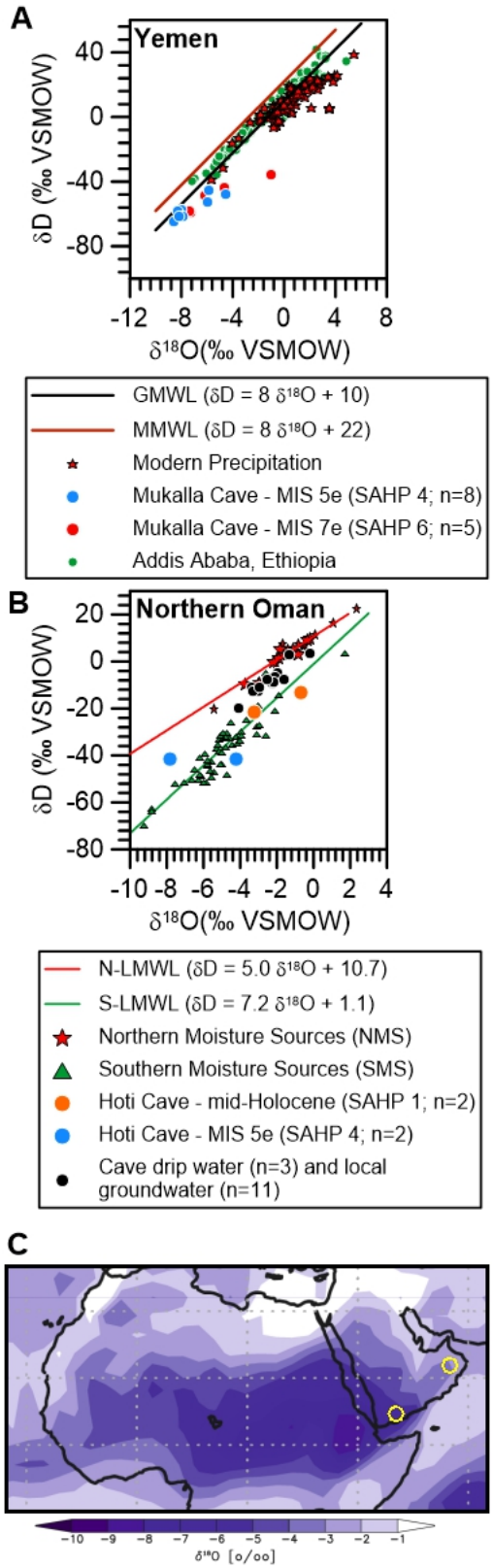

Fig. 38. Water isotope (δD_{FI} and $\delta^{18}O_{FI}$) values from stalagmites from Mukalla and Hoti Caves (Tab. S9). (A) Stalagmite Y99 δD_{FI} and $\delta^{18}O_{FI}$ values in comparison to δD and

$\delta^{18}O$ in modern precipitation in Yemen (Al-ameri et al., 2014) and Ethiopia (IAEA/WMO, 2019. Global Network of Isotopes in Precipitation. The GNIP Database. Accessible at: https://nucleus.iaea.org/wiser). Black line denotes the Global Meteoric Waterline (G-MWL: $\delta D = 8\ \delta^{18}O + 10$). Brown line denotes the Mediterranean Meteoric Waterline ($\delta D = 8\ \delta^{18}O + 22$) (Gat and Carmi, 1970; Matthews et al., 2000; McGarry et al., 2004). (B) δD_{FI} and $\delta^{18}O_{FI}$ values H5 and H13 compared to regional precipitation values and meteoric waterlines from Oman for northern (N-LMWL: $\delta D = 5.0\ \delta^{18}O + 10.7$; Weyhenmeyer et al., 2000, 2002) and southern moisture sources (S-LMWL: $\delta D = 7.2\ \delta^{18}O + 1.1$; Weyhenmeyer et al., 2000, 2002). (C) Locations of Mukalla Cave and Hoti Cave relative to modelled $\delta^{18}O_{precipitation}$ values for boreal summer precipitation during MIS 5e (modified after Herold and Lohmann, 2009). Yellow circles mark the location of Mukalla and Hoti Caves.

5.4.1.4 Comparison between pluvial conditions in Southern Arabia during the last 350 ka

$\delta^{18}O_{ca}$ values of stalagmites from Southern Arabia are primarily controlled by two effects: i.e. the amount and source of rainfall (Fleitmann et al., 2003b, 2004a, 2007, 2011). $\delta^{18}O_{ca}$ values of Mukalla Cave stalagmites are generally more negative than those of stalagmites from Hoti Cave (Fig. 39A), with a west-east (Mukalla-Hoti) isotopic gradient of between 2 and 4 ‰ during SAHPs 1-7. This gradient is also evident in δD_{FI} and $\delta^{18}O_{FI}$ values from both caves and in simulated MIS 5e $\delta^{18}O$ in summer precipitation across Southern Arabia (Fig. 38A). This adds further confidence in the palaeoclimatic significance of $\delta^{18}O_{ca}$ values from Mukalla and Hoti Caves. Furthermore, $\delta^{18}O_{ca}$ values from both cave sites reveals marked and consistent differences in the amount of rainfall between among the

SAHPs (Fig. 39). The most striking feature of the Mukalla and Hoti Cave records is the fact that least negative $\delta^{18}O_{ca}$ values were obtained from early to mid-Holocene stalagmites, indicating that monsoon rainfall during SAHP 1 was the lowest in the last 350 ka. On the other hand, monsoon precipitation was highest at both caves during SAHP 4 (MIS 5e). When we combine our fluid inclusion data with the relatively consistent $\delta^{18}O_{ca}$ between SAHPs, we can show that the moisture source was likely consistent throughout SAHPs. Modern $\delta^{18}O_{ca}$ values from Hoti Cave (derived from the winter Mediterranean precipitation source) are more positive than SAHP values (Fig. 39A). SAHP 1 (early to middle Holocene), 4 (MIS 5e) and 6 (MIS 7e) FI data allows us to confidently state that $\delta^{18}O_{ca}$ of these periods represents a monsoon rainfall signature. Thus, we can use the more positive $\delta^{18}O_{ca}$ values (Mediterranean signature) of modern and more negative $\delta^{18}O_{ca}$ values (monsoon signature) of past precipitation to posit that monsoon precipitation was the dominant source of preceding SAHPs. This isotopic relationship has also been observed in previously published high-resolution $\delta^{18}O_{ca}$ profiles of H5 and H12 (Fig. 39B), where an abrupt shift from more negative values (increased precipitation from the ISM) to more positive values (reduced precipitation delivered by Winter Mediterranean Cyclones (WMCs)) occurred at the termination of the early Holocene pluvial period (SAHP 1) (Fleitmann et al., 2007).

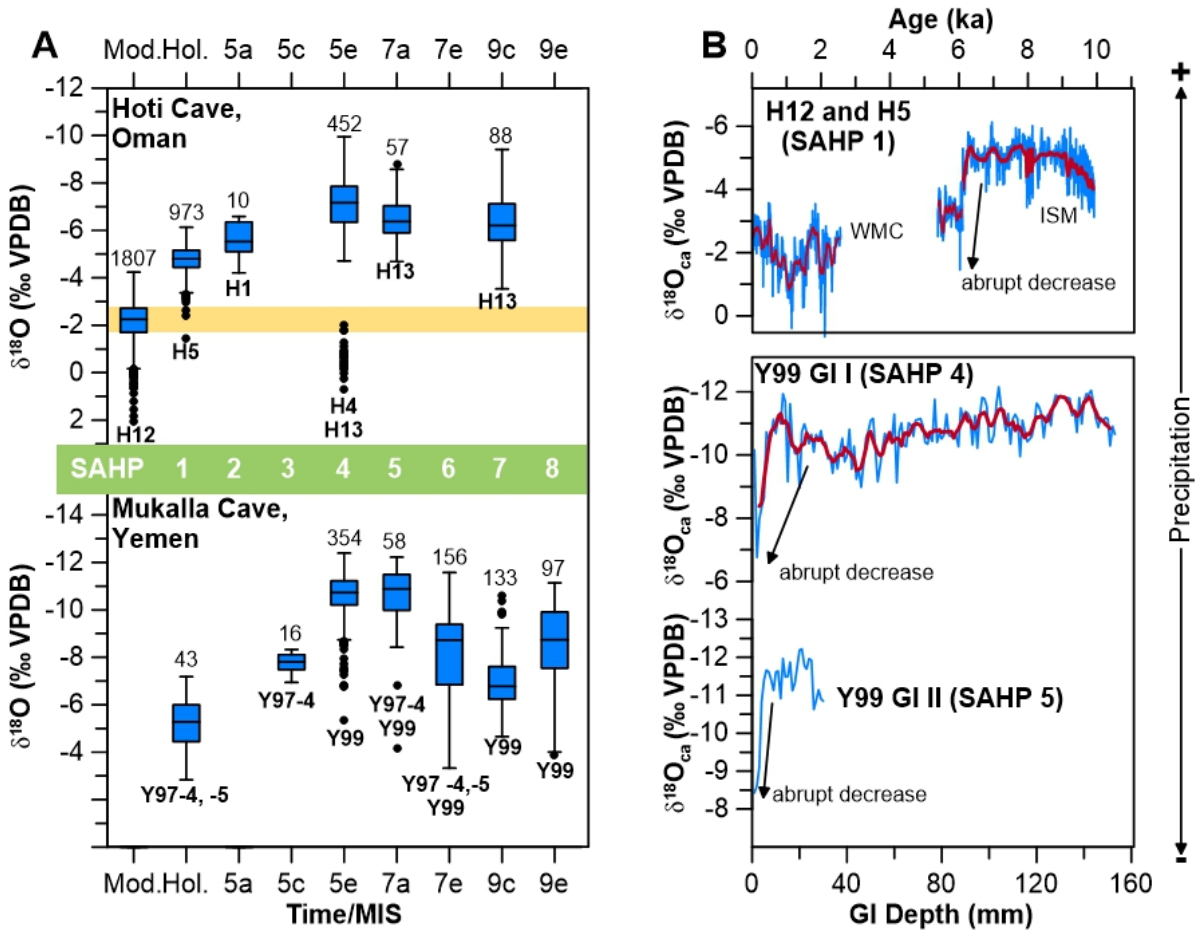

Fig. 39. (A) $\delta^{18}O_{ca}$ whisker-boxplot of Mukalla Cave and Hoti Cave composite records (new Y99 $\delta^{18}O_{ca}$ values combined with data from Fleitmann et al., 2011: Tab. S10). Numbers below whiskers denote sample labels and number of $\delta^{18}O_{ca}$ measurements Statistically extreme values marked as black circles. (B) $\delta^{18}O_{ca}$ profiles of Holocene (H5 and H12) and MIS 5e (Y99 GI I) and MIS 7a (Y99 GI II) stalagmites.

5.4.1.5 Environmental conditions

Mukalla Cave speleothem $\delta^{13}C_{ca}$ values vary between -8 and 2‰ (VPDB) (Fig. 40; Tab. S11). Such a wide range in $\delta^{13}C_{ca}$ is quite common in speleothems as $\delta^{13}C_{ca}$ depends on a variety of environmental, partly counteracting, parameters, including: (1) type and density of vegetation, (2) soil thickness and moisture, (3) biological activity within the

soil, (4) recharge conditions and (5) kinetic isotope fractionation during calcite precipitation, the latter factor is influenced by cave air PCO_2 and drip rate (e.g., Baker et al., 1997). At times of high precipitation and short soil-water residence times, equilibration between soil CO_2 and percolating water may be incomplete. Under such a scenario, seepage water would have a stronger atmospheric CO_2 component and thus speleothem $\delta^{13}C_{ca}$ values would be more positive. In addition, CO_2 degassing within the cave can lead to more positive speleothem $\delta^{13}C_{ca}$ values and thus blur the biogenic signal. Overall, speleothem $\delta^{13}C_{ca}$ values can be difficult to interpret, which is one reason why the Hoti Cave $\delta^{13}C_{ca}$ records were never used for palaeoenvironmental reconstructions. This is also related to the fact that Hoti Cave has two entrances and therefore strong ventilation, leading to fluctuations in cave air PCO_2 and strong kinetic fractionation of $\delta^{13}C$ during calcite precipitation. In contrast, Mukalla Cave has only one narrow entrance and ventilation within the cave is therefore low. Mukalla Cave stalagmite $\delta^{13}C_{ca}$ values are therefore more closely related to surface vegetation and biological soil activity, provided that complete equilibration ("open system conditions") between soil CO_2 and soil water has occurred. Under such conditions, $\delta^{13}C_{ca}$ values of a stalagmite growing under a C_3 plant dominated environment vary between -14 and -6‰ (VPDB) and -6 to +2‰ under C_4 plants (Clark and Fritz, 1997; McDermott, 2004). Assuming open system conditions, Mukalla Cave speleothem $\delta^{13}C_{ca}$ values fall into the range of C_4 plant dominated vegetation with occasional C_3 plants (Fig. 40), indicating herbaceous semi-desert grassland environment above the cave during SAHPs 1-8.

Our data also shows that C_4 environments were present during the warm substages of MIS 5. This is in good coherence with phytolith data from the Jabal Faya archaeological site, UAE, showing denser and more diverse vegetation was present during MIS 5 than

succeeding substages (Bretzke et al., 2013). Grassland taxa (*Kobus, Hippopotamus, Pelovoris*) and *H. sapiens* were uncovered from MIS 5a palaeolake sediments in the Nafud showing that grasslands were present in northern Arabia (Groucutt et al., 2018). In particularly, *Hippopotamus* is not a long-distance migratory species, and requires year-round access to water. Similarly, the MIS 5e speleothem $\delta^{13}C_{ca}$ values from Ashalim Cave, Negev, range from -8‰ to -2‰ (Vaks et al., 2010), suggesting comparable environments existed in the northern and southern extent of the Saharo-Arabian desert. Archaeological and fossils finds have demonstrated that *H. sapiens* were present in Arabia during MIS 5 interstadials (Groucutt et al., 2018). Furthermore, Mukalla Cave $\delta^{13}C_{ca}$ values are coherent with palaeontological evidences from older pluvial periods. Faunal assemblages from the Ti's al Ghadah palaeolake (MIS 9-13) exhibit large mammals from African and European sources (Thomas et al., 1998; Rosenberg et al., 2013; Stimpson et al., 2016), showing these wet periods were sufficient to sustain fauna that required a perennial water supply. Overall, our data adds to the growing evidence that the formation of widespread 'green' environments formed across Arabia during peak interglacial periods, which facilitated *H. sapiens* occupation and movement across the now desert areas of Arabia.

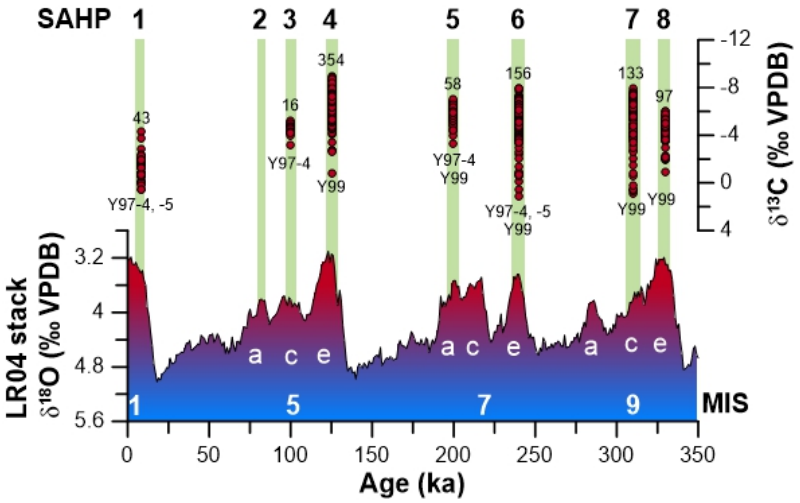

Fig. 40. $\delta^{13}C_{ca}$ values of Mukalla Cave speleothems during SAHPs I-V (Tab. S11) compared to the LR04 stack $\delta^{18}O$ record (Lisiecki and Raymo, 2005).

5.4.1.6 Seasonality of precipitation during SAHPs

Some stalagmites from Hoti Cave exhibit distinct annual layers, with a thickness varying between 0.1 and 1.2 mm (e.g., stalagmite H14; Cheng et al., 2009b). Such layers are also visible un the MIS 5e section of stalagmite H13, composed of a white porous laminae and dense translucent laminae. Their presence suggests distinct seasonal changes in the drip rate in response to surface precipitation. Nearly monthly resolved $\delta^{18}O_{ca}$ and $\delta^{13}C_{ca}$ profiles over 4 years (Fig. 41B; Tab. S8) show seasonal variations of more than 1 ‰, where denser layers display more negative $\delta^{18}O_{ca}$ and $\delta^{13}C_{ca}$ values. We suggest that these denser layers were formed during the monsoon seasons, at times of higher drip rate, slower CO_2 degassing and lower evaporation of cave drip waters (Fleitmann et al., 2004a). In. contrast, the more porous white layers display more positive $\delta^{18}O_{ca}$ and $\delta^{13}C_{ca}$ due to a reduced drip rate, resulting in greater CO_2 degassing and evaporation. Combined with δD_{FI} and $\delta^{18}O_{FI}$ values from H13, the presence of annual layers during SAHP 1 (early to mid-Holocene Cheng et al., 2009b) and SAHP 4 (MIS 5e; this study) and seasonal changes in $\delta^{18}O_{ca}$ and $\delta^{13}C_{ca}$ indicates that Southern Arabia experienced a rainy (monsoon) season during boreal summer and a drier season during boreal winter. This is in good agreement with climate simulations for MIS 5e, with simulations at 130, 125 and 120 ka BP (Gierz et al., 2017). These simulations show a strong increase in summer (JJA) precipitation at 130 and 125 ka BP, whereas no significant increase in winter (DJF) is observed in Southern Arabia (Fig. 41C). We can therefore exclude that increased precipitation was provided by enhanced Mediterranean cyclone activity in winter/spring

as suggested Enzel et al. (2015). Taken together, there is clear evidence that climatic conditions during SAHPs were still characterized by a strong seasonality with wet summers and rather dry winters.

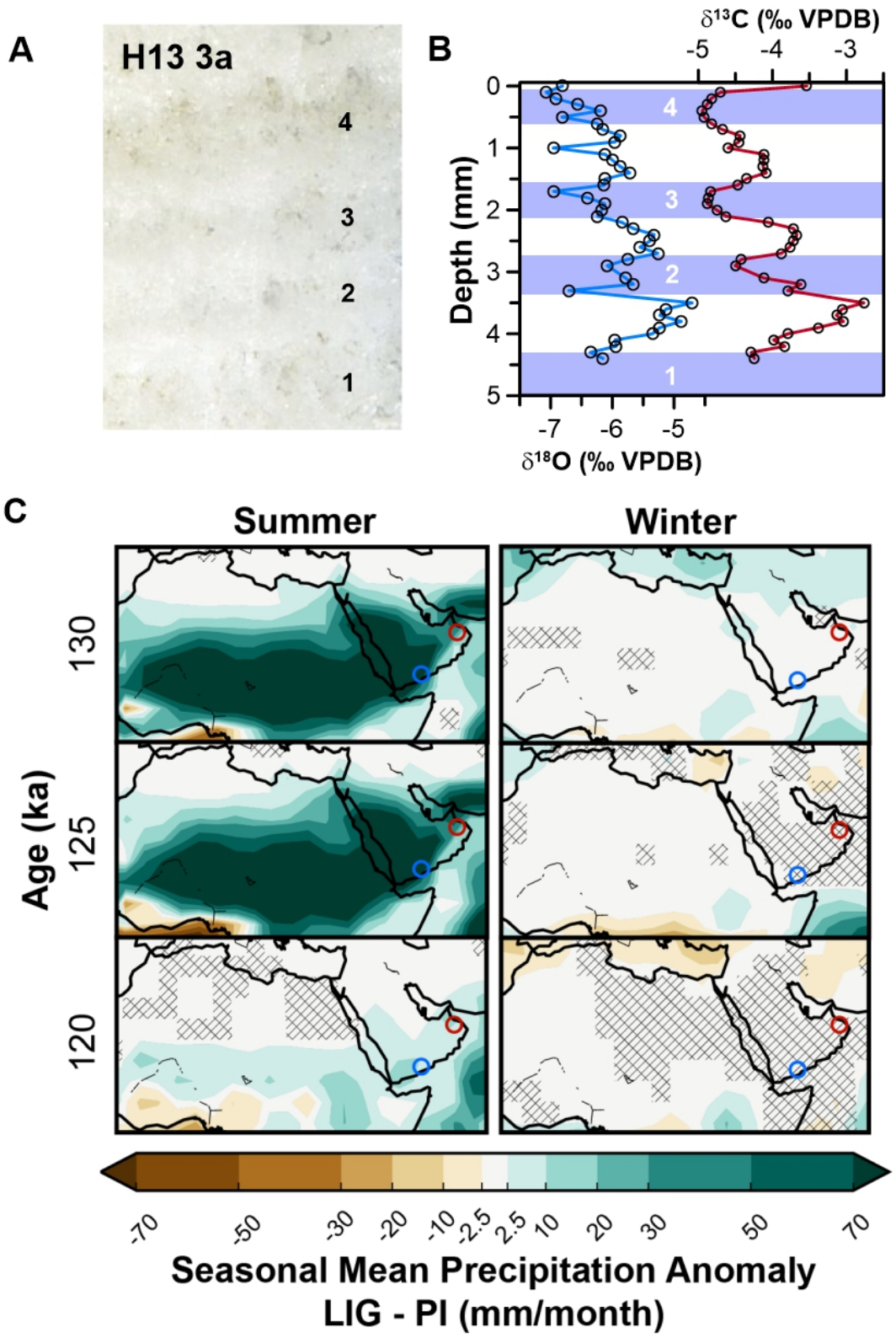
A
H13 3a
4
3
2
1
B
δ13C (‰ VPDB)
-5
-4
-3
0
1
2
3
4
5
Depth (mm)
4
3
2
1
-7
-6
-5
δ18O (‰ VPDB)
C
Summer
Winter
Age (ka)
130
125
120
-70
-50
-30
-20
-10
-2.5
2.5
10
20
30
50
70
Seasonal Mean Precipitation Anomaly
LIG - PI (mm/month)

Fig. 41. (B) Sub-annual $\delta^{18}O_{ca}$ and $\delta^{13}C_{ca}$ values from a MIS 5e section of stalagmite H13 (A) from Hoti Cave (Tab. S8). Shaded blue areas and numbers mark the monsoon seasons. (C) Mukalla Cave (blue circle) and Hoti Cave (red circle) mapped to modelled MIS 5e winter and summer precipitation anomaly (compared to pre-industrial) (Gierz et al., 2017).

5.4.2 Timing and Nature of SAHPs beyond 350 ka

5.4.2.1 Chronology of stalagmite Y99 beyond 350 ka

The identification of Y99 GIs beyond 350 ka BP is based (1) on thirty-one ^{230}Th and three U-Pb ages (Tab. S1, S2 and S4), (2) macroscopic evidence for major discontinuities (e.g., abrupt changes in colour of the fabric, abrupt changes in the frequency of laminae, finely defined and bright laminae and lateral displacements of the growth axis), and (3) abrupt shifts in $\delta^{18}O_{ca}$ over potential discontinuities (Fig. 35D). The latter are strong evidences for the termination of a SAHP, as they occur immediately before the cessation of stalagmite growth, when annual precipitation dropped below 300 mm yr^{-1} (Burns et al., 2001; Fleitmann et al., 2003b). Positive shifts in $\delta^{18}O_{ca}$ are also observed in stalagmites from Hoti Cave, where they mark a weakening and termination of pluvial monsoon periods within a few decades. This is particularly evident ~6.2 ka BP (Neff et al., 2001; Fleitmann et al., 2007; Fig. 39B). Using these criteria, we identified 12 further GIs (VI to XVIII) in stalagmite Y99. However, it is slightly more challenging to assign absolute ages to these GIs, as it becomes increasingly difficult to obtain accurate and precise ages ^{230}Th ages beyond 400 ka BP. While the chronology of Y99 GIs VI-XVIII is supported by thirty-one ^{230}Th and three U-Pb ages, ^{230}Th ages for GIs VI to VIII are not in perfect stratigraphic order, with several age reversals occurring between 400 and 550 ka BP. This

is not related to analytical problems but rather caused by post-depositional mobilisation of U and Th, potential small-scale dissolution and re-precipitation of calcite or incorporation of ^{230}Th adsorbed to organic acids (Borsato et al., 2003; Scholz et al., 2014). These effects can imply localized open-system behaviour (Bajo et al., 2016). While post-depositional leaching of U would lead to older ages, re-precipitation of calcite or incorporation of ^{230}Th would result in younger ages as observed in some GIs. All these effects are critical for very old samples that are close to the ^{230}Th-dating limit of ~500-600 ka as even minute post-depositional alterations and several phases of dissolution and/or re-precipitation can have significant effects on the age. The higher porosity and micro-voids make in the upper section of stalagmite Y99 (Fig. 35A and B) more prone to post-depositional loss or addition of radionuclides. In contrast, the lower part of Y99, comprising GIs IX to XVIII, is composed of very dense calcite but too old for the ^{230}Th-dating method. Nevertheless, two U-Pb ages determined in different laboratories are consistent and date the base of stalagmite Y99 to 1.07 ± 0.04 Ma (GI XVIII; MIS 31). One additional U-Pb age of 0.85 ± 0.07 Ma BP for GI XII serves as an additional tie point for the chronology of the lower part of stalagmite Y99. Based on the consistent pattern of high-monsoonal rainfall and stalagmite growth during interglacial intervals during the last 350 ka BP (Fig. 37), we used orbital tuning to the LR04 stack (Lisiecki and Raymo, 2005) to assign absolute ages for Y99 GIs VI to XIII and XIV to XVII (Fig. 42). The good match between the number of identified GIs and peak interglacial periods gives credence to the Y99 chronology.

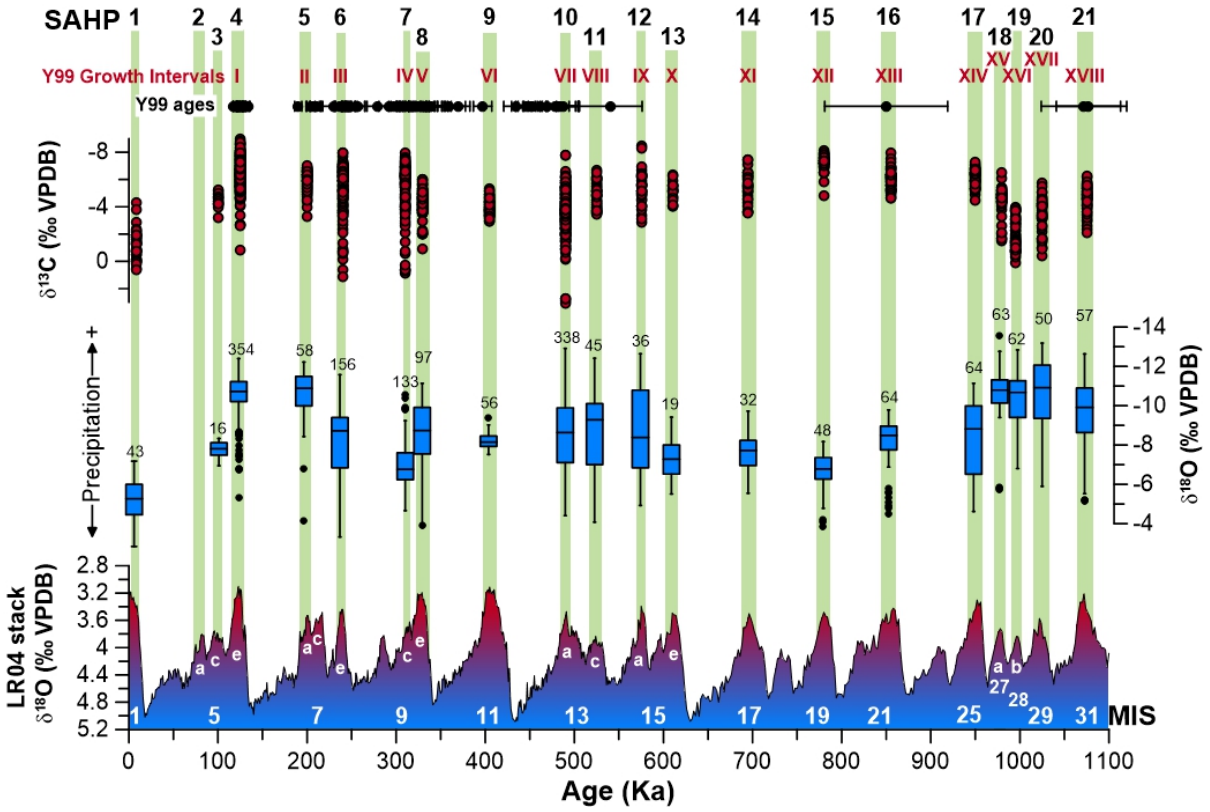

Fig. 42. ^{230}Th (Tab. S1-S3) and U-Pb (Tab. S4 and S5) ages for stalagmite Y99 compared to the LR04 stack $\delta^{18}O$ record (Lisiecki and Raymo, 2005) and extended $\delta^{18}O_{ca}$ and $\delta^{13}C_{ca}$ records of Mukalla Cave stalagmites (Y97-4, Y97-5 and Y99). Undated Y99 growth intervals were assigned to intermediate interglacials and warm substages. Green bars denote timing of SAHPs (South Arabian Humid Periods). Marine Isotope Stages follow the taxonomy of Railsback et al. (2015).

5.4.2.2 Climate and environmental conditions in Southern Arabia over the last 1.1 Ma

At least 21 SAHPs occurred over the last 1.1 Ma at times when low ice volume and high summer insolation strengthened both the ISM and ASM. AS mentioned previously, there is a general scarcity of terrestrial records covering more than 400 to 500 ka BP in Northern Africa and the Arabian Peninsula, and marine sediments are the only source of information. Two dust records from the Eastern Mediterranean (ODP 967; Grant et al.,

2017) and Arabian Sea (ODP 721/722; deMenocal, 1995) extend beyond 500 ka BP and are interpreted to reflect continental wetness in the wider northeast African region and the Arabian Peninsula. The ODP 967 PCA index of rainfall and aridity (PC2; Fig. 43) is based on trace element content (e.g., titanium) and sapropels and shows distinct fluctuations in the strength and spatial extent of the ASM. The ODP 967 record thus provides evidence for multiple "Green Sahara Periods". When compared to the stalagmite record of SAHPs, some wet periods in the ODP 967 record coincide with SAHPs, such as during the early to middle Holocene, MIS 5e, 7a, 9e and 13a (Fig. 43). There are also notable differences and wet climatic phases in the ODP 967 PC2 record are not always consistent with SAHPs, such as MIS 6 or MIS 16. Adversely, between 950-650 ka BP, the ODP 967 rainfall index is typically in a 'dry' mode while at least three SAHPs occurred within MIS 17, 19 and 21. Likewise, the association between SAHPs and low dust content in the ODP 721/722 core is not always evident. For instance, dust content is relatively low and constant between MISs 12 and 16, suggesting rather humid climatic conditions between 425 and 675 ka BP. The discrepancy between dust and stalagmite records has been observed before (Fleitmann et al., 2011) and could be related to regional variability, availability of dust and changes in wind direction and strength.

Stalagmite Y99 $\delta^{18}O_{ca}$ values of all GIs are very similar and typically range from -7 to -11 ‰ (Fig. 42), indicating that the ASM was the dominant source of precipitation during all SAHPs. There are, however, differences in the degree of wetness between SAHPs as more negative $\delta^{18}O_{ca}$ values indicate higher ASM and ISM rainfall in Yemen and Oman. The boxplot (Fig. 42) of $\delta^{18}O_{ca}$ values of all Mukalla Cave stalagmites show that SAHPs 4, 5, 18, 19 and 20 exhibit the most negative $\delta^{18}O_{ca}$ values and are thus characterized by the highest monsoonal rainfall.

Y99 $\delta^{13}C_{ca}$ values range 2 to -8‰ (Fig. 42) and differences are apparent between SAHPs. As stated above, these ranges are typical of C_4 environments above the cave assuming 'open system' conditions. However, $\delta^{13}C_{ca}$ values can be influenced by various parameters such as vegetation type and density, soil thickness and moisture, as well as atmospheric and other processes (McDermott, 2004; Rowe et al., 2012). Moreover, deluge of thin soils at times of very high rainfall can lead to more positive speleothem $\delta^{13}C_{ca}$ values due to rapid infiltration into the karst system and reduced interaction with soil CO_2 (e.g., Bar-Matthews et al., 2003). Increased rainfall during SAHP 19-20 could have led to more positive $\delta^{13}C_{ca}$ values. In contrast, reduced rainfall and increased interaction of percolating water with soil CO_2 may have had the opposite effect, contributing to more negative $\delta^{13}C_{ca}$ values during SAHP 14-17. Due to the numerous controls on speleothem $\delta^{13}C_{ca}$, alterations of the principal determinant can be expected over such a long period of time. Despite this, the overall range of $\delta^{13}C_{ca}$ values indicates C_4 grasslands were present during SAHP VI-XVII. This shows that interglacial periods routinely saw vegetation form in the now desert areas of southwestern Arabia.

5.4.3 Hominin migrations

5.4.3.1 Early-Middle Pleistocene

Estimates for the potential timing of hominin dispersals during the last few hundred thousand years are mostly modelled on palaeoclimate conditions of East Africa (deMenocal, 1995; Shultz and Maslin, 2013; Maslin et al., 2014) or Eurasia (Muttoni et al., 2010; Kahlke et al., 2011). These models do not consider whether and when the Saharo-Arabian desert was traversable. Yet the formation of so called "green corridors"

between sub-Saharan Africa, northern Africa and Eurasia created "windows of opportunity" that would have been critical for hominin occupation and dispersal. Though, it is surely more apt to consider these areas as "green landscapes" in which hominin populations inhabited – rather than a route to the 'other' side. Based on the timing of SAHPs and their close connection to humid intervals in Northern Africa, we suggest that the Saharo-Arabian grasslands could facilitate occupation and dispersal during MIS 31 (~1080 ka: SAHP 21), MIS 29 (~1014 ka: SAHP 20), MIS 28b (~1000 ka: SAHP 19) MIS 27a (~982 ka: SAHP 18) MIS 25 (~955 ka: SAHP 17), MIS 21 (~850 ka: SAHP 16) and MIS 19 (~760 ka: SAHP 15) (Fig. 43). Frequent windows of opportunity take place between SAHP 21 to SAHP 17 (MIS 31 to MIS 25), varying between 40-10 ka intervals. SAHP 21 to 18 are also marked as some of the most negative $\delta^{18}O_{ca}$ values in Y99 (Fig. 42), indicating intense monsoon periods. Succeeding this, SAHPs reduced in frequency, with ~100-70 ka intervals between SAHPs 17-13 (MIS 25-15e). These are also marked by increased $\delta^{18}O_{ca}$ values – indicating somewhat drier periods – and reduced occurrence of Mediterranean sapropels (Fig. 43). This shift echoes the transition from ~40 ka to ~100 ka glacial interglacial cycles, known as the Middle Pleistocene Transition (MPT) (Lisiecki and Raymo, 2005; Railsback et al., 2015; Tzedakis et al., 2017). Thus, it is likely that the pattern of hominin occupation of Arabia shift in line with this transition, with longer gaps between occupations phases. However, we must emphasise that direct ages have not been attained for SAHPs 20-17 and 19-13, meaning this argument is currently somewhat tentative. Attaining direct ages for these SAHPs should be a target of future analysis.

The early appearance of *H. heidelbergensis* at Melka Kunture (Ethiopia) soon after ~875 ± 10 ka (MIS 21; Profico et al., 2016) and subsequent appearances in Eurasia is a key

event in Early-Middle Pleistocene hominin evolution. SAHPs within this period provide potential timings for *H. heidelbergensis* dispersal, assuming an African origin for this species. While there is a paucity of absolute dating, Oldowan and Acheulean tool typologies have been uncovered in Southern Arabia (Chauhan, 2009; Groucutt and Petraglia, 2012 and references therein; Bailey et al., 2015; Bretzke et al., 2018). This suggests an additional behavioural adaptation was not required for Mode-1 or Mode-2 bearing hominins to occupy Arabia, at least as represented by the lithic record, but occupation was likely dependent on periods of ameliorated climatic conditions. Here, we have provided timings in which the Arabian Peninsula was occupiable and traversable.

SAHPs during MIS 17 (~700 ka: SAHP 14), MIS 15e (~600 ka: SAHP 13), MIS 15a (~675 ka: SAHP 12), MIS 13c (~530 ka: SAHP 11) and MIS 13a (~480 ka: SAHP 10) may have facilitated dispersals from Africa. Y99 $\delta^{18}O_{ca}$ have positive (SAHP 14 and 13) and variable (SAHP 12, 11 and 10) values, indicating somewhat drier or more variable climates, respectively. Nevertheless, these values are more negative than Holocene values, demonstrating the climate was significantly wetter. As stated above, Oldowan and Acheulean sites are distributed across western and Southern Arabia (Groucutt and Petraglia, 2012), most likely representing Lower Palaeolithic occupation. In particular, flint scatters from the Nafud – found in conjunction with grassland fauna – indicates hominin occupation of Arabia during MIS 13 or 9 (Rosenberg et al., 2013; Stimpson et al., 2016; Roberts et al., 2018). While these SAHPs facilitated occupation of Arabia, it is difficult to relate these to demographic changes in Eurasia due to the persistent presence of Acheulean typologies since ~1.4 Ma (Moncel et al., 2015; Gallotti, 2016). Nonetheless, future studies of Middle Pleistocene population dynamics in Eurasia may benefit from consideration of SAHP timings.

5.4.3.2 Early H. sapiens dispersal

H. sapiens emerged as a distinct species in Africa during the Middle Pleistocene (Hublin et al., 2017; Richter et al., 2017; Scerri et al., 2018b). Behavioural and anatomical modernity evolved gradually throughout the later Middle Pleistocene and into the Upper Pleistocene (Mcbrearty and Brooks, 2000). Whilst *H. sapiens* dispersals during the Upper Pleistocene led to colonisation of Eurasia, it has been suggested that *H. sapiens* may also have dispersed within the Middle Pleistocene (Breeze et al., 2016). This may be validated by *a H. sapiens* maxilla from Misliya Cave, Israel, dated between 194 and 177 ka (Hershkovitz et al., 2018, but see Sharp and Paces, 2018). Hershkovitz et al. (2018) suggested a dispersal may have occurred during MIS 6e (~191-170 ka). Similarly, the recent identification of *H. sapiens* at Apidima, Greece, ~210 ka (MIS 7) provides further support for earlier dispersals (Harvati et al., 2019, but see Wade, 2019).

Travertine deposition in the Negev (Waldmann et al., 2010), increase rainfall in the Levant and Dead Sea catchment (Frumkin et al., 1999; Bar-Matthews et al., 2003; Gasse et al., 2015; Torfstein et al., 2015), decreased RC09-166 $\delta D_{leafwax}$ (Tierney et al., 2017), and increased Saharan run-off (Williams et al., 2015) indicate ameliorated conditions which may have facilitated *H. sapiens* dispersal within MIS 6e (~191-170 ka) (Breeze et al., 2016; Garcea, 2016). Lack of speleothem growth at Mukalla and Hoti Cave and absence of lake formations (Rosenberg et al., 2011, 2012, 2013) indicate the tropical rain belt did not migrate past 14°N during MIS 6. Moreover, absence of speleothem growth in the central Negev (Vaks et al., 2010) also demonstrates that winter Mediterranean precipitation regimes were not substantially enhanced during MIS 6e. Without these

widespread changes in regional precipitation, it is unlikely that green landscapes and inter-regional range expansion could have been sustained.

We therefore suggest dispersals may have occurred during SAHP 5 and 6 (MIS 7a and 7e). Y99 $\delta^{18}O_{ca}$ reveals SAHP 5 (MIS 7a) was as wet as SAHP 4 (MIS 5e: discussed below), and $\delta^{13}C_{ca}$ demonstrate a C_4 biome flourished (Fig. 40). Moreover, SAHP 5 (~205-195 ka) corresponds to lake formations in northern Arabia (Rosenberg et al., 2013), and the Sahara (Armitage et al., 2007, 2015), central ages of palaeosol formation on the Sinai Peninsula (Roskin et al., 2013) and speleothem growth in the central Negev (Vaks et al., 2010). Thus, not only did pluvial landscapes connect northern Arabia and the Levant (Breeze et al., 2016), but corridors connected northern and Southern Arabia. While archaeological evidence for such an early dispersal is currently very limited, recent dating of the Saffaqah archaeological site demonstrates hominins occupied Arabia during MIS 7, with techno-cultural similarities to Mieso (Ethiopia) archaeological assemblages (Scerri et al., 2018a). Further evidence is required, however, taken with recent findings from the Levant (Hershkovitz et al., 2018) and south-eastern Europe (Harvati et al., 2019), our data suggests MIS 7a enhancement of the monsoon domain could have facilitated *H. sapiens* range expansion into Eurasia.

Furthermore, our data shows that Southern Arabia could have facilitated occupation by *H. sapiens* shortly after their African emergence during MIS 9 (Hublin et al., 2017; Richter et al., 2017). Considering recent discussions of the pan-African origin of *H. sapiens* (Scerri et al., 2018b), we suggest that Arabia may have been frequently occupied by various *H. sapiens* lineages. The role of Green Arabia as a habitat for early *H. sapiens* may therefore add to ongoing discussions concerning localized adaptations and genetic

flow between subdivided populations (Scerri et al., 2018b). The identification of favourable conditions in MIS 7 and 9 will remain of interest if *H. sapiens* are not identified: i.e., what prevented their expansion into the region at these times?

5.4.3.3 Late Pleistocene H. sapiens dispersal

The dispersal of *H. sapiens* during the Late Pleistocene is a topic of intense debate, with models changing frequently with new fossil finds. Generally, there is an acceptance that formation of green landscapes in the Saharo-Arabian desert belt facilitated dispersals during MIS 5e (~128-121 ka), MIS 5c (~104-93 ka) and MIS 5a (85-71 ka) (Bae et al., 2017; Groucutt et al., 2018; Rabett, 2018), which is supported by the Mukalla and Hoti Cave records. During the last 130 ka, SAHP 4 (127.8 ± 0.626 to 120.3 ± 0.399 ka) was the most intense pluvial period (Fig. 42), which is in good agreement with lake records in Arabia (Rosenberg et al., 2011, 2012, 2013; Matter et al., 2015). Furthermore, $\delta^{13}C_{ca}$ values demonstrate a grassland environment flourished in the now desert areas of Yemen (Fig. 40), which is corroborated by phytolith evidence from Jabal Faya, UAE (Bretzke et al., 2013). SAHP 3 (MIS 5c) and SAHP 2 (MIS 5a) are consistent with intervals of lake formations in Arabia (Rosenberg et al., 2011, 2012, 2013; Petraglia et al., 2012) during MIS 5c and 5a and it is clear that *H. sapiens* occupied the now desert interior of Arabia within MIS 5a (e.g., Groucutt et al., 2018).

A subsequent dispersal is argued to have taken place during MIS 4-3 (Mellars, 2006a; Shea, 2008; Mellars et al., 2013; Rohling et al., 2013; Langgut et al., 2018). A growing body of archaeological evidence shows *H. sapiens* were present in Arabia during MIS 3 (Armitage et al., 2011; Delagnes et al., 2012; Jennings et al., 2016), though occupation

may have been limited to punctuated pluvial periods (Groucutt and Petraglia, 2012). Whether these could have facilitated more widespread dispersals is a subject of controversial debate (Mellars, 2006a; Groucutt et al., 2015a; Bae et al., 2017). The palaeoclimatic evidence for increased rainfall during MIS 4-3 is variable between records. It has been argued that punctuated humid intervals in northern Africa and Levant may have facilitated dispersal during MIS 4-3 (Hoffmann et al., 2016; Langgut et al., 2018). However, the lack of speleothem growth in southern Arabia during MIS 4-3 suggest that the ASM was considerably weaker and did not penetrate into the Arabian Peninsula. Our assumption is supported by more positive $\delta D_{leafwax}$ values in Core RC09-166 from the Gulf of Aden (Fig. 37), indicating lower monsoonal rainfall compared to MIS 5a or the early to middle Holocene in the Horn of Africa and Afar regions. Additional supporting evidence comes from median grain sizes in cores KL 11 (Red Sea) and KL 15 (Gulf of Aden) which are also larger and indicative of more arid climatic conditions during MIS 4-3 (Fig. 37). In contrast, palaeolake formation in the Nafud (northern Saudi Arabia) (Parton et al., 2018) and fluvial activity at Al-Quwaiayh, central Saudi Arabia (McLaren et al., 2009), Yemen (Delagnes et al., 2012), and in Oman (Blechschmidt et al., 2009; Parton et al., 2013, 2015b; Hoffmann et al., 2015) have been dated to early MIS 3. Records in Southern Arabia are not corroborated by speleothem growth at Mukalla Cave or Hoti Cave, indicating that the tropical rain-belt was suppressed. This discrepancy may stem from the potential for fluvio-lacustrine and alluvial records to record high intensity, but brief, storm and flooding events (e.g., Rosenberg et al., 2012; Hoffmann et al., 2015); whereas speleothems require prolonged and more substantial changes in regional rainfall. Moreover, brief and intense storms currently occur under modern climates during hot summers, which could mean MIS 3 alluvial records show precipitation regimes were not greatly different than current

conditions (Hoffmann et al., 2015). Taken together, MIS 3 precipitation may not have been sustained or intense enough to have substantially impacted environments in Southern Arabia. Despite archaeological evidence for MIS 3 occupation, our findings suggest that MIS 5 interstadials were 'climatic optima' for hominin dispersal; whereas *H. sapiens* dispersal opportunities during MIS 3 may have been more limited or required different behavioural adaptations. If, however, MIS 3 environments could not sustain dispersal (meaning MIS 3 populations can be related to groups that entered during MIS 5), this implies *H. sapiens* persistence during MIS 4, a time with very limited evidence for ameliorated conditions (Parton et al., 2015b).

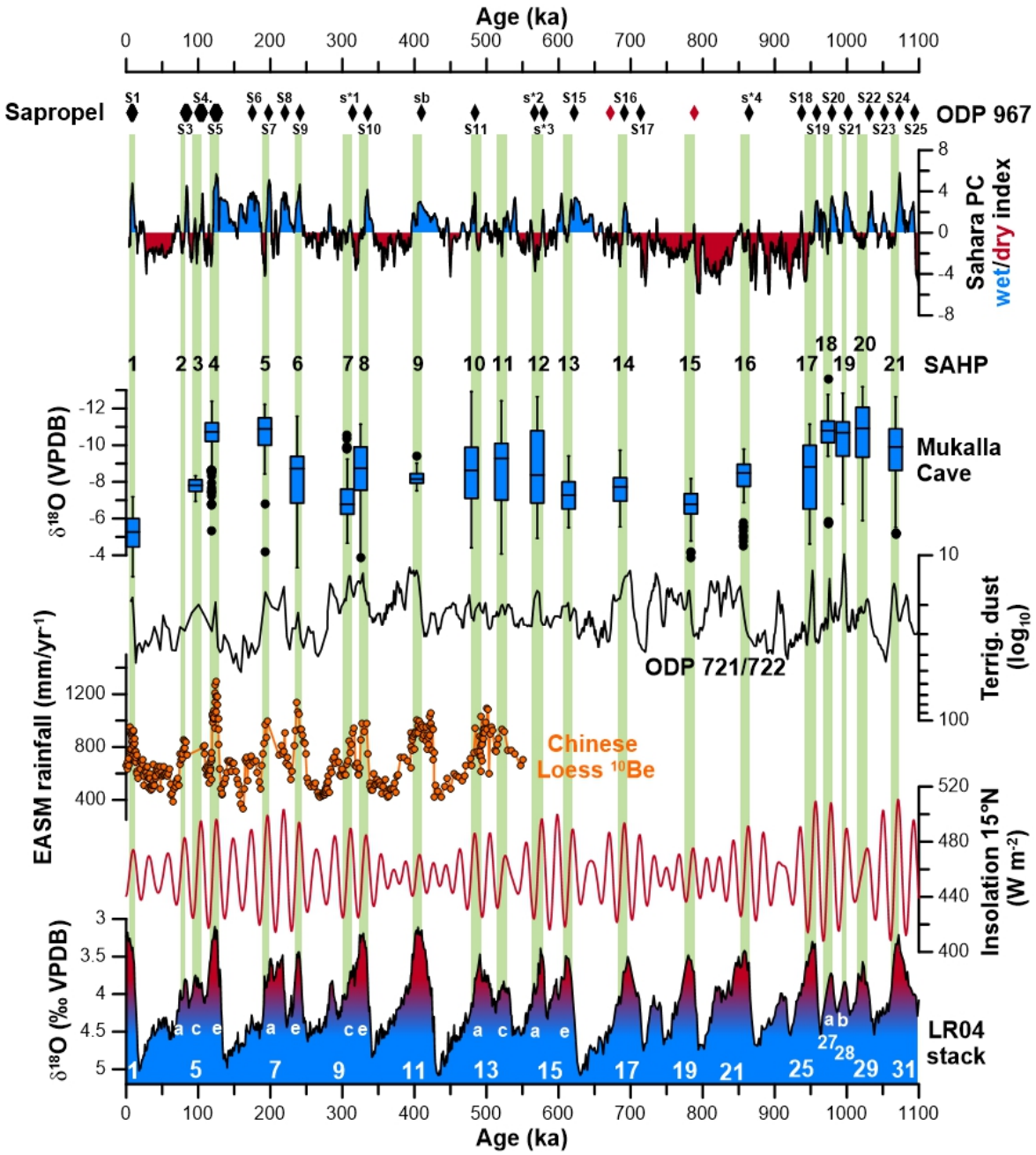

Fig. 43. SAHPs (green bars) and palaeoclimate records. (Eastern Mediterranean) ODP 967 sapropels (black = identified, red = 'ghost') and wet/dry PCA model (Grant et al., 2017); central Negev desert speleothem ages (Vaks et al., 2010); northern and Southern Arabian palaeolake ages (Rosenberg et al., 2011, 2012, 2013; Matter et al., 2015; Parton et al., 2018) and Mukalla Cave $\delta^{18}O_{ca}$ values; ODP 721/722 terrigenous dust (deMenocal, 1995); EASM reconstructed rainfall from Chinese $^{10}Be_{loess}$ (Beck et al.,

2018); NHI insolation (W m^{-2}) at 15^{o}N (Berger and Loutre, 1991, 1999) and LR04 stack foraminifera $\delta^{18}O_{benthic}$ (Lisiecki and Raymo, 2005) and Marine Isotope Stages following the taxonomy of Railsback et al. (2015).

5.5 Conclusion

New ^{230}Th and U-Pb dates for stalagmite Y99 from Mukalla Cave in Yemen allow to extend the speleothem-based record of continental wetness back to 1.1 Ma BP. In combination with previously published stalagmite records from Southern Arabia (Burns et al., 2001; Fleitmann et al., 2011), at least twenty-one humid intervals with precipitation above ~300 mm yr^{-1} developed in Southern Arabia, all them occurred during peak interglacial periods. Of all SAHPs the early to mid-Holocene humid period was the least humid period. Hydrogen and oxygen isotope measurements on water extracted from stalagmite fluid inclusions indicate that enhanced rainfall during SAHPs resulted from an intensification and greater range of the ASM and ISM. This assumption is further supported by the presence of annual laminae in some stalagmites and nearly monthly-resolved oxygen and carbon isotope measurements which indicate a strong seasonal climate during SAHP, with one rainy (monsoon) season during SAHPs. While there is restricted archaeological evidence for hominin occupation beyond 350 ka BP, these landscapes could have facilitated occupation of late *H. erectus* populations. Subsequent SAHPs may have also facilitated the dispersals of early *H. sapiens* soon after their emergence ~300 ka BP.

Acknowledgements

This work was supported by the AHRC South, West and Wales Doctoral Training Partnership (Grant AH/L503939/1) the Swiss National Science Foundation (Grant PP002-110554/1 to DF and Grant CRSI22-132646/1 to DF and ML), U.S. National Science Foundation (Grant 1702816 to RLE and HC) and the National Natural Science Foundation of China (Grant NSFC 41888101). DF acknowledges support from NERC Isotope Geosciences Facilities Steering Committee (Grant IP-1376-051). We would like to thank the editor and three anonymous reviewers for their constructive comments and suggestions.

Chapter 6

6) Plio-Pleistocene Arabian pluvial periods: initial results from Saudi Arabian speleothems

The following chapter is a work in progress manuscript. This chapter provides further answers to research questions 1-4, providing an extended chronology (beyond chapter 5) of periods of increased rainfall, a potential moisture source, differences in intensity between pluvial periods and characterisation of environmental conditions. Current authorship is as follows:

Nicholson, S.L., Pike, A.W.G., Hosfield, R., Roberts, N., Sahy, D., Woodhead, J., Affolter, S., Leuenberger, M., Pint, J., Al-Shanti, M., Groucutt, H.S., Fleitmann, D.

The author contributions are as follows: Sample collection was conducted by D.F., J.P. and M.A-S.. S.L.N. conducted the stable isotope analysis and acted as primary author for the paper under the guidance of D.F., R.H., A.W.G.P.. U-Pb dating analyses were performed by , D.S., N.R. and J.W. Laser absorption spectroscopy of speleothem fluid inclusions were performed by S.A. under the supervision of M.L and D.F.. H.S.G. provided additional review and synthesis of archaeological data. All authors contributed to the ongoing editing and refinement of the manuscript.

Abstract

The Saharo-Arabian desert belt currently acts as a vast hyper-arid ecological barrier between sub-Saharan Africa and Eurasia. Pleistocene palaeoclimate records, however, are showing that punctuated wet events activated large palaeolakes and formed savannah-type environments during peak interglacial period of the Pleistocene. However, little is known about the changing environments beyond 1 million years ago. The Pliocene is of particular interest as this was the last time in which global temperature and atmospheric CO_2 exceeded modern values. Here, we have produced speleothem derived palaeoclimate records from the Arabian Peninsula, detailing periods of enhanced precipitation throughout the Plio-Pleistocene. Speleothem growth phases were recorded at 4.38 ± 0.48 Ma, 4.08 ± 0.12 Ma, 4.099 ± 0.048 Ma, 4.11 ± 0.12 Ma, 3.776 ± 0.024 Ma, 3.51 ± 0.12 Ma and 2.57 ± 0.43 Ma. Analysis of fluid inclusion water $\delta^{18}O$ and δD shows that the monsoon domain was significantly enhanced during the early Pliocene and early Pleistocene. Speleothem $\delta^{13}C$ fell within the range expected of mixed C_3/C_4 to C_4 grasslands. The ~2.57 Ma wet period could have facilitated the earliest hominin dispersals from Africa and could show an ongoing importance of palaeoenvironmental fluctuation – particularly monsoon variability – in human distribution on evolutionary timescales.

6.1 Introduction

The vast Saharo-Arabian desert belt occupies ~12.5 million km^2 of the Earth's surface. This hyper-arid area expands from western Africa to the Thar Desert of India, and from the tropical savannah of Sahel to the Mediterranean coast of northern Africa. The Arabian Peninsula occupies a crucial centre point of the desert belt, at the interface of Africa and Eurasia. In tandem with the greater Saharan region, Arabia currently acts as a vast hyper-

arid barrier between Afrotropical and Eurasian flora and fauna. However, A growing body of evidence is showing that punctuated migrations of the tropical rain-belt and associated monsoons (African, or AM; Indian, ISM; and East Asian Monsoon, EAM) throughout the Pleistocene facilitated the activation of palaeolakes and grassland landscapes, or so called "green deserts". Current evidence shows these periods are related to low-latitude northern hemisphere insolation (NHI) maxima of peak interglacials and warm substages, with at least twenty-one south Arabian Humid Periods (SAHPs) having occurred over the last 1.1 Ma BP. The predictable nature of SAHPs means these should have occurred on much longer timescales, which could be crucial to mammal dispersal and evolutionary models throughout the Plio-Early Pleistocene (e.g., deMenocal, 2004; Dennell, 2010; Kahlke et al., 2011; O'Regan et al., 2011; Dennell and Petraglia, 2012; Larrasoaña et al., 2013; Groucutt et al., 2015a; Kuper and Kropelin, 2015; Breeze et al., 2016; Zhu et al., 2018).

Marine sediment records from the Arabian Sea (ODP 721/722, deMenocal, 1995), the Gulf of Aden (DSDP 231, Liddy et al., 2016) and the Mediterranean (ODP 967, Larrasoana et al., 2003; Grant et al., 2017) provide long and often continuous records of climate changes in the Saharo-Arabian desert belt, spanning back to the Pliocene and even, in the case of ODP 721/722, the late Miocene (~8 Ma BP). These records use terrigenous dust as a proxy for continental wetness, where reduced dust input and grain sizes, decreased hematite, changes in elemental composition or decreased $\delta^{13}C_{n\text{-}alkanoic\ acid}‰$ are related to enhanced vegetation cover during periods of higher precipitation. However, mobilisation, transport and deposition of dust is determined by multiple non-linear factors, such as production of dust, transport pathways (wind direction), wind strength, erosion and vegetation density (Zabel et al., 2001; Trauth et al., 2007), which

obscure local rainfall signatures. Terrestrial archives are thus required to test and mitigate uncertainties within marine dust records.

There are, however, few and sparsely distributed terrestrial records that fall into the Plio-Pleistocene (but see Vaks et al., 2013; Novello et al., 2015; Sniderman et al., 2016), especially in Arabia. For example, the Tertiary Sandstone and Marl (Tsm) formation (late Miocene – Pliocene) expands from ~ to ~ across Arabia (Schyfsma et al., 1978; SGS, 2007). While constituting diatomites indicate the environments were characterised by lake activation, there are no accurate ages or knowledge of spatial or temporal distribution of these wet periods. Similarly, the Barzaman Formation in UAE (and probably Oman) represents widespread alluvial activation during the late-mid Miocene (Styles et al., 2006; Lacinska et al., 2014). Reworking through erosional and incisional processes also suggests that reactivation had occurred, probably throughout the late Neogene. However, the lack of robustly dated Plio-Early Pleistocene palaeoclimate records means that current knowledge of Arabian climates at these times is mostly limited to climate simulations, which are informed by broadly dated climate records (e.g., Salzmann et al., 2011; Li et al., 2018). Providing new precisely dated palaeoclimate records are therefore of key importance to resolving these issues, especially for testing and mitigating uncertainties within palaeoclimate simulations.

Speleothems (stalagmites, stalactites and flowstones) are secondary $CaCO_3$ deposits that form in limestone caves when sufficient effective moisture is available. Unlike many terrestrial archives in deserts, speleothems are protected from desert weathering due to their sub-terranean locations. Uranium-Thorium (^{232}Th hereinafter) dating of speleothems is precise and has been used extensively to build palaeoclimate records with robust

chronologies (e.g., Burns et al., 2001; Fleitmann et al., 2003a; Shakun et al., 2007). While traditional ^{230}Th dating is chronologically limited to 700 ka, recent advances in Uranium-Lead (U-Pb, hereafter) dating techniques now offer methods to precisely date speleothem samples beyond the ^{230}Th range (e.g., Woodhead et al., 2006, 2012; Coogan et al., 2016). Previous studies have shown that the amount effect and the source effects are important controls on Arabian speleothem oxygen isotopes ($\delta^{18}O_{ca}$) (Fleitmann et al., 2003a, 2011); whereas speleothem carbon isotopes ($\delta^{13}C_{ca}$) can provide information on vegetation density and type above a cave (McDermott, 2004; Rowe et al., 2012). Additionally, fluid inclusion water hydrogen (δD_{FI}) and oxygen ($\delta^{18}O_{FI}$) can provide detailed information on past precipitation sources when compared to modern isotopes in precipitation and local meteoric waterlines (Dennis et al., 2001; Fleitmann et al., 2003b; Meckler et al., 2015).

Previously, Fleitmann et al., (2004b) reported speleothem based palaeoclimate records from the northern and central Saudi Arabian deserts. Initial ^{230}Th dating found these samples were beyond the range of ^{230}Th dating. These samples are therefore excellent candidates to extend the Arabian palaeoclimate record beyond 1 Ma BP. Here, we present new U-Pb ages for these stalagmites, which allows us to show punctuated pluvial periods occurred between 5-2 Ma BP. Additional isotope measurements performed on stalagmite calcite and fluid inclusion water allow us to track changes in the amount and source of rainfall.

6.2 Climatic and cave settings

6.2.1 Current climate

The Nefud desert dominates northern Arabian environments. Temperatures are highly variable, frequently exceeding 40°C in the summer months, while dropping below freezing during the winter. Present day climate is largely influenced by the North Atlantic/Siberian pressure system in winter. Precipitation delivered by cyclones that develop over the Eastern Mediterranean (WMCs hereinafter) during winter months measures <200 mm yr^{-1} (Glennie and Singhvi, 2002; Fick and Hijmans, 2017). This low rainfall is insufficient to overcome high evaporation, which means surface water is not a long-term or prevalent feature of the landscape and permanent waterbodies are sparsely distributed.

In southern Arabia, temperatures are variable, exceeding 40°C in the summer months, but can also reach 0°C in winter months. Present-day climate is strongly governed by two major weather systems: The North Atlantic/Siberian pressure system in winter/spring and the African/Indian monsoons in summer. Currently, the African and Indian Summer Monsoons (AM and ISM hereafter, respectively) do not penetrate further north than the highlands of Yemen and the Dhofar highlands of Oman. Though, occasional (~5-10 years) brief and intense summer storms reach the northern Oman highlands. Large scale climatic changes during the Pleistocene and Holocene were driven by incursions of the tropical rain-belt (Fleitmann et al., 2011; Rosenberg et al., 2013; Nicholson et al., 2020), which increased annual precipitation to over 300 mm yr^{-1}. These may have reached up to 28°N in the Nafud Desert (Jennings et al., 2015b) or potentially further (Petit-Maire et al., 2010; Orland et al., 2019).

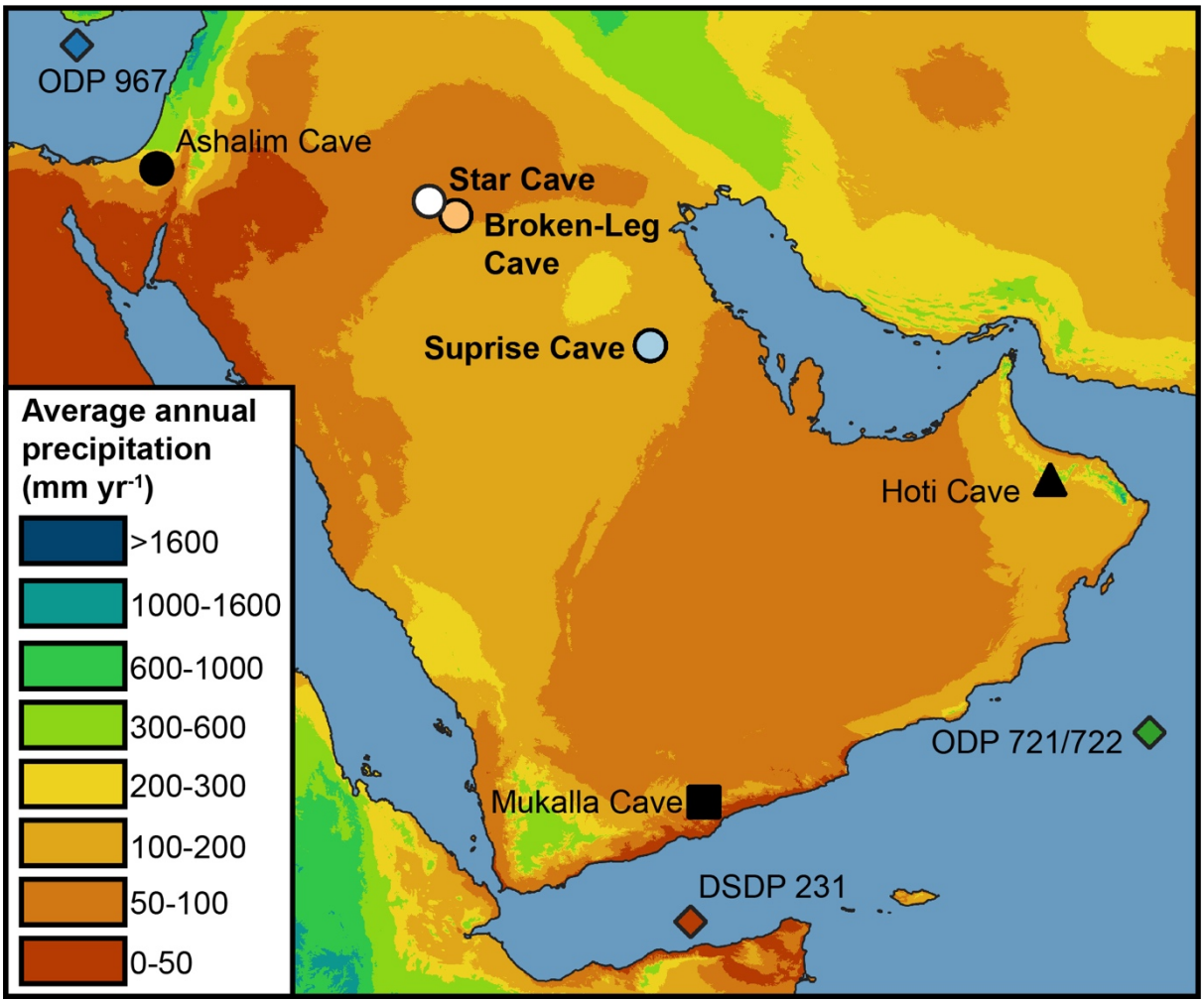

Fig. 44. Modern annual average precipitation of Arabia (available at: http://worldclim.org/; Fick and Hijmans, 2017); locations of the study sites: Star Cave, Broken-leg Cave and Surprise Cave (for extended details of the caves, see Fleitmann et al., 2004b; SGS, 2007), and locations of local Plio-Pleistocene palaeoclimate records discussed in text: Ashalim Cave (Vaks et al., 2010, 2013), Mukallah Cave (Fleitmann et al., 2011), Hoti Cave (Burns et al., 1998; Fleitmann et al., 2003b, 2011), ODP 721/722 (deMenocal, 1995) and DSDP 231 (Feakins et al., 2013; Liddy et al., 2016).

6.2.2 Samples

Speleothems were collected from Star Cave (STC; 30°07′N., 41°38′E.), Broken Leg Cave (BL; 29°45′N., 42°18′E.) and Surprise Cave (SC; 26°28′N., 47°14′E.) in the Saudi Arabian deserts from 2001-2003 (Fig. 44 and Fig. 45). The geological settings of these caves have bene made available elsewhere (SGS, 2007). No actively growing stalagmites were recorded during collection at Star Cave or Broken-Leg Cave (Fleitmann et al., 2004b; SGS, 2007), indicating that current precipitation does not recharge the aquifer above the caves. However, a few active stalactites were recorded at Surprise Cave. Stalagmites from STC range from 250 to 800 mm in size. All stalagmites collected from STC display a thick rind of white calcite on their final growth interval, often greater than 1 cm (Fleitmann et al., 2004b). Rinds throughout the stalagmites also provide clear evidence of growth discontinuities within STC stalagmites, showing their growth was reactivated multiple times. Samples STC-3 and STC-4 also include highly porous portions, indicating post-depositional alteration occurred, mostly likely due to condensation corrosion (Fleitmann et al., 2004b). As post-depositional alteration can obscure paleoclimatic signals, these areas were avoided during our analysis. Stalagmites from BL are comprised of a brown/golden calcite. BL-2 measures ~30 mm in length and shows a clear growth discontinuity (Fig. 45). Samples from SC vary in size, shape and colour. SC-2 (studied here) is comprised of a dense yellow-white calcite (Fig. 45).

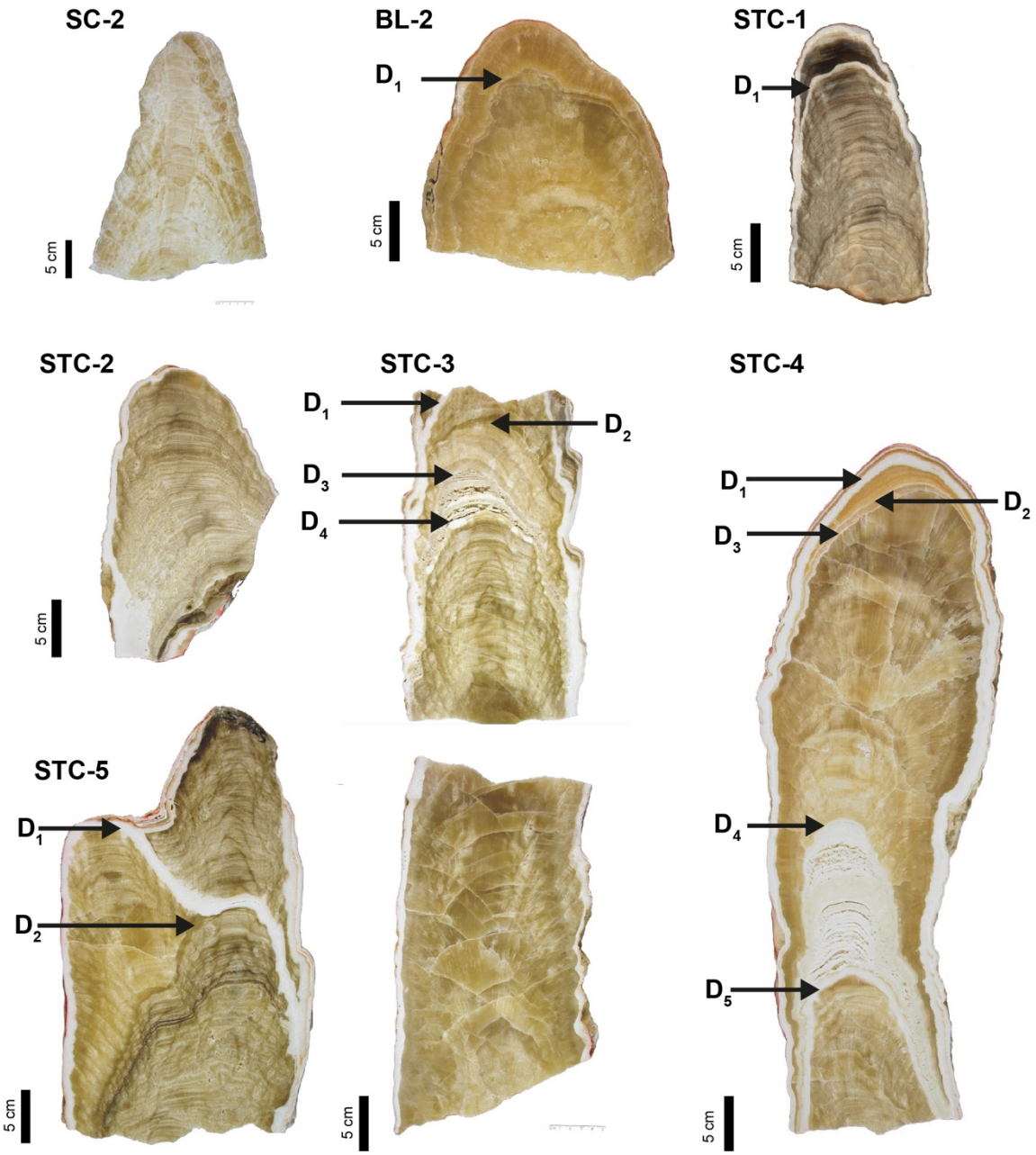

Fig. 45. Samples from BL, STC and SC. Growth discontinuities marked with 'D' numbers.

6.3 Methods

6.3.1 U-Pb dating

Initially, stalagmites were dated using Uranium-Thorium (^{230}Th) analysis (Fleitmann et al., 2004b). Samples SC-2, STC-1, STC-3, STC-4 and STC-5 and BL-2 exhibited ^{230}Th/^{234}U ratios close to 1, suggesting an age >1 Ma (Fleitmann et al., 2004b). These samples therefore offer excellent candidates to extend the terrestrial palaeoclimatic record of Arabia . U-Pb ages were then determined using both traditional solution-mode Multi-collector inductively coupled plasma mass spectrometry (MC-ICP-MS) (following the methods detailed in: Woodhead et al., 2006) along with a recently developed Laser ablation (LA-ICP-MS) method. For LA-ICP-MS, the methods and analytical protocol follows that described by Coogan et al. (2016); U/Pb ratios were normalised to WC-1 carbonate (Roberts et al., 2017) and Duff Brown carbonate (Hill et al., 2016) was run as a check on accuracy.

6.3.2 Calcite oxygen and carbon isotope analysis

A total of 228 samples for $\delta^{18}O_{ca}$ and $\delta^{13}C_{ca}$ analyses were collected at 5 mm increments from the stalagmites, following the drip track down the vertical axes. Isotope measurements were performed using a Finnigan Delta V Advantage Isotope Mass Spectrometer (IRMS) coupled to an automated carbonate preparation system (Gasbench II). Precision (1σ) is ≤0.2‰ for $\delta^{18}O$ and ≤0.1‰ for $\delta^{13}C$. Measurements were performed at the Chemical Analysis Facility (CAF), University of Reading, UK. Calcite $\delta^{18}O$ and $\delta^{13}C$ values are reported in per-mil difference to the international V-PDB standard.

6.3.3 Fluid inclusion deuterium and oxygen isotope analysis

Analysis of speleothem $\delta^{18}O_{FI}$ and δD_{FI} provide an independent method to test climate model simulations. $\delta^{18}O_{FI}$ and δD_{FI} isotopes of speleothem fluid inclusion water were analysed at the Physics institute, University of Bern, using a recently developed method (Affolter et al., 2014, 2015). Three calcite blocks of ~25 x 5 x 5 mm (L, W, H) were collected from BL-2 (n=2) and STC-3 (n=1). Samples were placed into a copper tube connecting to the line, heated to ~140°C and crushed. The liberated water is then transported to a wavelength scanned cavity ring down spectroscopy system (Picarro L1102-i analyser) under humid conditions (with standardised water of known isotopic composition) to prevent fractionation and minimize memory effects. The crushing of samples released, on average, ~1 µl of water. Precision is 1‰ for δD_{FI} and 0.2‰ for $\delta^{18}O_{FI}$. Fluid inclusion values are reported on the Vienna Standard Mean Ocean Water (V-SMOW) scale.

6.4 Results and Discussion

6.4.1 Speleothem growth ages and timing of Plio-Pleistocene wet periods

12 U-Pb ages of Saudi Arabian stalagmites indicate growth ensued at 4.38 ± 0.48 Ma (STC-1), 4.099 ± 0.058 to 2.73 ± 0.51 Ma (STC-3), 4.21 ± 0.18 to 4.03 ± 0.15 Ma (STC-5), 3.776 ± 0.024 (BL-2), 3.51 ± 0.12 (STC-4), 2.57 ± 0.43 Ma (SC-2) (Fig. 46). As previously mentioned, the samples here show clear evidence of growth discontinuities, showing that speleothem growth was reactivated multiple times. Due to overlapping age uncertainties and age reversals, individual growth phases cannot be chronologically confined. While the thick rind of STC-3 shows significant time elapsed between growth phases, the close coherence between ages, however, suggest growth phases were

deposited within quick succession, perhaps within tens of thousands of years. Although ages from SCT-1,2,4 and 5 are in close agreement these are not in perfect stratigraphic order. Additionally, one age (2.73 ± 0.51 Ma) from STC-3 was attained from the bottom of the stalagmite, yet a kernel probability density plot shows ages above cluster around 4.1 Ma (Fig. 47). Such reversals may be caused by post-depositional mobilisation of U and Pb (open-system behaviour), potential re-precipitation and small-scale dissolution of calcite (Borsato et al., 2003; Scholz et al., 2014). While post-depositional leaching of U would lead to older ages, re-precipitation of calcite could result in younger ages. Additionally, incorporation of common Pb can influence the final ages (Woodhead et al., 2006, 2012). Pb can be introduced into speleothems with sub-micron colloids or detrital particles (Fairchild and Treble, 2009); yet the methods of Pb incorporation into stalagmites are currently poorly understood. Additionally, Th mobilisation for U-Pb dating is often ignored; however, mobilisation of Th could have a significant impact on the final $^{206}Pb/^{238}U$ ratios. Further work must be conducted to understand Th mobilisation on such long timescales.

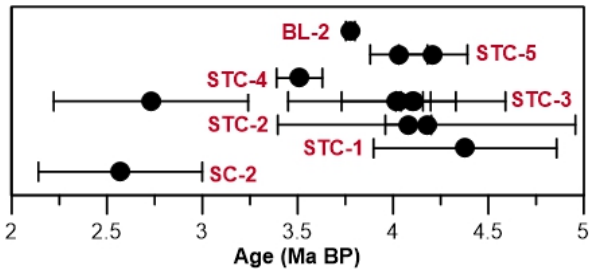

Fig. 46. U-Pb ages (Ma BP) of stalagmites from BL, SC and STC (Tab. S11-S15).

The timing of Pleistocene 'green Arabia' periods reveals that changes in glacial-boundary conditions and orbital precession have exerted strong control on monsoon rainfall in Arabia, with South Arabian Humid Periods (SAHPs) occurring within NHI maxima when

ice volume was significantly reduced (Fleitmann et al., 2011; Nicholson et al., 2020). However, glacial periods (e.g., MIS 2 and 4) and MIS 3 were characterised by lower precipitation, despite changes in precession. This shows that glacial-boundary conditions exert a strong suppressive effect on the monsoon domain. The Pliocene, however, is characterised as a period of greatly reduced or absent northern (Zachos et al., 2001) and southern (Golledge et al., 2017) hemisphere ice-sheets. Therefore, glacial-boundary conditions would have had a minimal influence over the monsoon domain; whereas, recent modelling has shown that orbital precession and NHI remained a significant control on the area of the monsoon during the Pliocene (Prescott et al., 2019). U-Pb ages attained have too large dating uncertainties to be strictly assigned to specific NHI maxima; however, a kernel probability density plot of STC-2 (4.08 ± 0.12 Ma), STC-3 (4.099 ± 0.048 Ma) and STC-5 (4.11 ± 0.12 Ma) U-Pb ages shows these centre within a distinctly warm period between ~4.146 to 4.098 Ma – Gi25 (Fig. 47). This period is characterised by both eccentricity and NHI maxima (Berger and Loutre, 1991) coupled a global ice-sheet minima (Lisiecki and Raymo, 2005). Given the previously established relationship between Arabian pluvial periods, glacial boundary conditions and insolation forcing, it is possible for us to tune these samples to Gi25 using the LR04 $\delta^{18}O_{benthic}$ stack. The younger STC-4 (3.51 ± 0.12) and SC-2 (2.57 ± 0.43) ages also fall within eccentricity peaks. While central ages of BL-2 (3.776 ± 0.024) and STC-1 (4.38 ± 0.48) fall outside of NHI peaks, the age uncertainties of these samples do fall within NHI peaks at ~3.8 Ma and 4.3-4 Ma, respectively. It is probable that analytical uncertainties, rather than a shift of the controls on monsoon dynamics, explain this slight discrepancy and thus we tentatively suggest these samples fall within NHI maxima. However, the large dating uncertainties of STC-1 and 2 and SC-2 mean these samples require additional work to fully confine their timing.

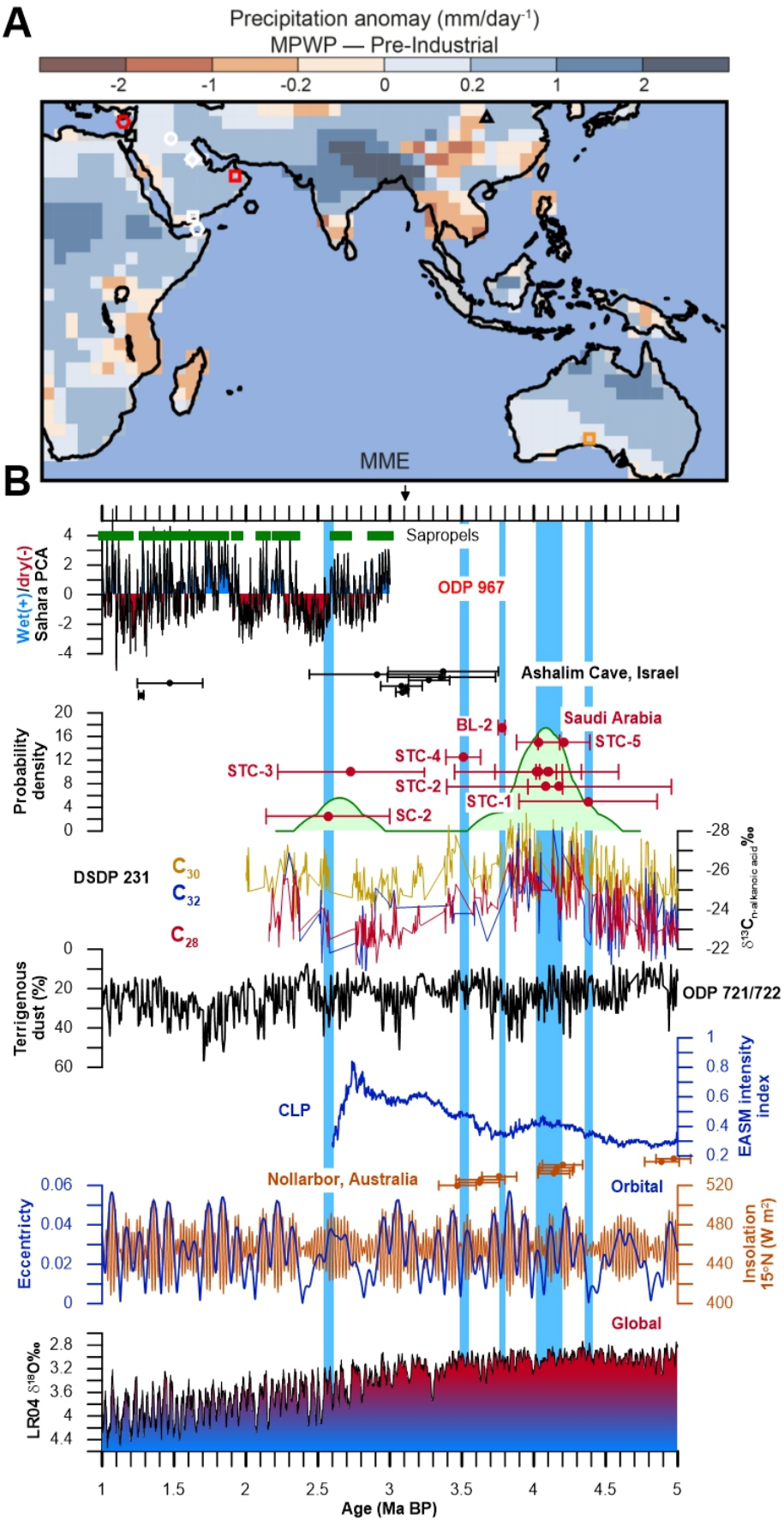
A
Precipitation anomay (mm/day-1)
MPWP — Pre-Industrial
-2
-1
-0.2
0
0.2
1
2
MME
B
Sapropels
Wet(+)/dry(-) Sahara PCA
ODP 967
Ashalim Cave, Israel
Saudi Arabia
BL-2
STC-5
STC-4
STC-3
STC-2
STC-1
SC-2
Probability density
DSDP 231
C30
C32
C28
δ13Cn-alkanoic acid ‰
Terrigenous dust (%)
ODP 721/722
CLP
EASM intensity index
Nollarbor, Australia
Orbital
Eccentricity
Insolation 15°N (W m-2)
Global
LR04 δ18O‰
Age (Ma BP)

Fig. 47. (A) Map of the Indo-Pacific region with precipitation anomaly (MPWP – pre-industrial). Location of palaeoclimate archives marked by white circle (STC and BL), white diamond (SC), white square (Mukalla Cave), red square (Hoti Cave), red hexagon (ODP 967), black square (Ashalim Cave speleothems), black hexagon (ODP 721/722), white hexagon (DSDP 231), orange square (Nullarbor Cave speleothems). (B) Ages and kernel probability density plot of Saudi Arabian speleothems compared to palaeoclimate from the aforementioned archives, EASM intensity index (Ao et al., 2016), ODP 721/722 (deMenocal, 1995), ODP 967 Sahara wet/dry PC and sapropel layers (Grant et al., 2017) orbital eccentricity and NHI (Berger and Loutre, 1991), and global ice-volume (LR04 $\delta^{18}O$) (Lisiecki and Raymo, 2005).

Speleothem ages show times at which precipitation was significantly greater than modern values and could recharge the aquifers above the caves. Absence (BL and STC) or very rare (SC) modern speleothem growth shows current rainfall (~100 mm yr^{-1}) is insufficient to overcome the high evaporation and recharge the aquifers above the caves. The size of speleothems from the study areas are similar to those of Pliocene speleothems from Ashalim Cave, Negev desert (Vaks et al., 2013), which today has comparable climates and environments to STC, BL and SC. Pliocene Negev samples exhibited similar $\delta^{18}O_{ca}$ values to those of Pleistocene speleothems, in which precipitation was estimated to have been >300 mm yr^{-1} based on the spatial distribution of actively growing samples (Vaks et al., 2010). Based on the similarities in size and shape between the samples studied here and Negev stalagmites, ~300 mm yr^{-1} or greater was required to activate speleothem growth above BL, STC and SC. This estimate is in good agreement with modelled EPWP (~4.2-4 Ma) precipitation, where precipitation estimates ranged 365-1095 mm yr^{-1} (STC and BL) and 730-1460 mm yr^{-1} (SC) over the study areas (Brierley et al., 2009). This

precipitation estimate would have been sufficient to activate fluvio-lacustrine systems across Arabia (Breeze et al., 2015). Taken together, this shows precipitation over northern Arabia was substantially increased during the early Pliocene and early Pleistocene.

6.4.1.1 Timing of wet periods

EPWP (4.2-4 Ma)

The Early Pleistocene Warm Period (EPWP) is considered to be a time of on expanded tropical domain due to reduced glacial boundary conditions and interhemispheric pressure gradient (Brierley et al., 2009). The ages of STC-1-3 fall within this period, cluster around 4.1 Ma. The timing of speleothem growth is in excellent agreement with marine archives from the Gulf of Aden and Arabian Sea. A reduction of ODP 721/722 dust occurred at ~4.45 Ma, showing increased soil humidity and denser vegetation in the Horn of Africa. This was followed by rapid fluctuations until ~4.1 Ma, suggesting climates alternated between wetter and slightly drier phases. Similarly, speleothem growth matches negative DSDP $\delta^{13}C_{\text{n-alkanoic acid}}$‰ values between 4.5 to 3.9 Ma and 3.5 to 3.4 Ma, which indicate more densely vegetated conditions as a result of increased rainfall. Increased vegetation density is also observed in phytolith records from the now desert areas of Chad at ~4.4-4.1 Ma and ~3.8-3.6 Ma (Novello et al., 2015, 2017) and are consistent with the ages STC-1-3, 5 and BL-2. The good agreement between speleothem growth ages and humid periods in Chad, Gulf of Aden and Arabian Sea suggest similar climatic influences. Indeed, current climates across Saharo-Arabia are linked by the tropical rain-belt and the annual migration of the ASM and ISM; both were considered to have undergone a northward expansion during the EPWP (Brierley et al., 2009) and could have reached northern Saharo-Arabia,

The ASM and ISM area also linked to the East Asian Summer Monsoon (EASM). A recent $\delta^{18}O_{ca}$ record from the CLP (Chinese Loess Plateau) showing EASM precipitation was intensified within the early Pliocene (Ji et al., 2017) corroborates this, as the ITCZ links the EASM to the ASM and ISM. Increased precipitation in the CLP is corroborated by pollen records, in which arboreal pollen was greater during the early Pliocene than the Middle Pliocene (Wang et al., 2006; Li et al., 2011), with Xifeng pollen showing a peak between ~4.6 to ~4.1 Ma. Similarly, a recent EASM intensity index derived from CLP magnetism showed an enhancement of the monsoon between ~4.5-3.7 Ma and another rise from 3.7 Ma onwards (Ao et al., 2016). Together, this provides further evidence that the monsoon domain underwent a northward repositioning during the EPWP.

While the monsoon domain expanded northward, records from the southern hemisphere also show that the monsoon domain expanded southwards. Speleothem growth ages of STC-1, STC-3 and STC-5 growth ages are remarkably consistent with speleothem growth recorded at Nullarbor caves, Australia (4.2-4.1 Ma). Similarly, BL-2 and STC-4 ages are also consistent with Nullarbor ages at 3.77 Ma and 3.51 Ma, respectively (Fig. 47). Pollen extracted from the Nullarbor samples demonstrate mesic environments inhabited the now xeric shrubland of southern Australia ~5.26-3.45 Ma (Sniderman et al., 2016). This was linked to a widening of the tropical rain-belt caused by a reduced interhemispheric pressure gradient and increased atmospheric water content (Brierley et al., 2009; Sniderman et al., 2016). Overall, the ages of STC-1-3, 5 and BL-2 fall into a period characterised by a drastic expansion of the monsoon domain in both hemispheres.

While speleothem age data does corroborate a particularly intense period of rainfall at 4.1 Ma, it is important to consider that speleothem ages for STC-4 (3.51 ± 0.12) and BL-2 (3.776 ± 0.024) do not fall into either the EPWP or the MPWP (discussed below). Not only does this show that there were repeated wet periods in Arabia, but that perhaps EWPW and MPWP are too restrictive when discussing the timing of Saharo-Arabian wet events during the Pliocene. This argument is corroborated by the ages of pelites from the Djurab, which show enhanced precipitation between the EPWP and MPWP (4-3.2 Ma) (Lebatard et al., 2008). We are therefore led to consider the mechanisms of monsoon variability on long timescales, outside of the Pliocene "warm" periods. Our previous analysis has shown that Arabian stalagmites grew during interglacials and warm substages throughout the later-Early to the Late Pleistocene, since ~1.1 Ma BP (Nicholson et al., 2020). These occurred at predictable intervals, during NHI peaks when glacial boundary conditions were dramatically reduced. However, during the Pliocene, the northern hemisphere ice-sheet was not as large as throughout the Pleistocene (Zachos et al., 2001; Lisiecki and Raymo, 2005) and thus glacial boundary conditions and meridional thermal contrast would have been comparatively low. Without the muting effects of glacial boundary conditions, precessional forcing (on 21 kyr cycles) of NHI could have been the primary modulator of monsoon position and intensity. This has previously been observed in climate model simulations of the MPWP, in which the position and intensity of the monsoon was regulated by precession cycles (Prescott et al., 2019). It is therefore probable that during the Pliocene, incursions of the monsoon in Arabia occurred on 21 kyr cycles. However, in the absence of both more precise dating techniques and a greater number of samples, it is not currently possible to test and confirm this hypothesis.

MPWP (3.2-3 Ma)

The Mid Pliocene Warm Period (MPWP; ~3.2-3.0 Ma) is frequently used as a representation of Pliocene climates, and, due to the high atmospheric CO_2, is often used to model future environments under high greenhouse gas conditions (Salzmann et al., 2011). Previous modelling work has identified the MPWP as a period of an expanded monsoon domain (Li et al., 2018; Prescott et al., 2018, 2019); however, no Arabian speleothem ages fell within the reputed 3.2 Ma warm period. This is inconsistent with speleothem ages from Ashalim Cave (~3.2-3.1 Ma: Vaks et al., 2013), the EASM intensity index (Ao et al., 2016) and a plethora of modelled climate simulations for the MPWP (Salzmann et al., 2011; Tindall and Haywood, 2015; Li et al., 2018). Our findings, however, are consistent with DSDP 231 $\delta^{13}C_{n\text{-alkanoic acid}}$ showing higher values (drier conditions) compared to the EPWP, suggesting the ASM and ISM were reduced in intensity ~3.2 Ma. As the ASM and ISM are connected to the EASM via ITCZ dynamics, substantial changes of climates in the horn of Africa and Arabia should be echoed in China (e.g., Fleitmann et al., 2011; Beck et al., 2018). A Chinese loess $\delta^{18}O_{ca}$ record also does not record a distinctly wet period at 3.2 Ma; a positive shift of the $\delta^{18}O_{ca}$ suggest either reduced precipitation or increased evapo-transportation (due to increased temperature) at 3.2 Ma (Ji et al., 2017). These findings are corroborated by pollen records from nearby Xifeng, showing arboreal pollen reduced from ~4.1 Ma and did not recover at 3.2 Ma as a result of reduced precipitation (Wang et al., 2006). Together, Chinese loess palaeoenvironmental records and DSDP 231 $\delta^{13}C_{n\text{-alkanoic acid}}$ suggest that the spatial extent and intensity of the monsoon domain was not as enhanced when compared to the EPWP. This is perhaps corroborated by an MPWP climate simulation, which shows precipitation was only 0.2 mm day^{-1} greater than pre-industrial over STC, BL and SC (Fig. 47; Li et al., 2018). Such a negligible increase may have not been sufficient to recharge aquifers

above the caves and could not lead to widespread stalagmite deposition. Taken together, absence of speleothem deposition and these records suggest that MPWP precipitation may not have been substantial as the EPWP. These could be explained by the fact that very few terrestrial records have been incorporated into model simulations, and the records that have been utilised are not confined exclusively to the Pliocene (e.g., Salzmann et al., 2011). Having said this, we also have to consider that only few stalagmites with large temporal distribution have been analysed here. It is therefore not possible to confidently discount the MPWP as a substantial wet period in Arabia. Further records and samples with robust chronologies are required to understand the extent of the monsoon domain at 3.2 Ma.

Plio-Pleistocene transition

Stalagmite SC-2 is dated to 2.57 ± 0.43, and falls within the Plio-Pleistocene transition and possibly MIS 103-101; however, large age uncertainties means that this assignment is rather tentative. Yet, despite large age uncertainties, the central age of SC-2 is in excellent agreement with records that show regionally enhanced precipitation around 2.6-2.4 Ma. Good agreement is seen with negative DSDP 231 $\delta^{13}C_{\text{n-alkanoic acid}}$‰ between 2.6 and 2.5 Ma, which shows precipitation was enhanced over the Horn of Africa (Liddy et al., 2016). Similarly, expansion of grasslands in Chad between ~2.5-2.3 Ma also fall into the age uncertainties of SC-2 (Novello et al., 2017). Close alignment is also seen with sapropel formations within ODP 967 (Fig. 47; Grant et al., 2017). These detail times in which increased Nile outflow and Saharan runoff led to a breakdown of deep-water circulation and anoxic conditions in the eastern Mediterranean (Rohling et al., 2015). Taken together, this shows a simultaneous increase in precipitation in the southern and northern margins of the Saharo-Arabian desert belt during the Plio-Pleistocene transition.

6.4.2 Source of moisture

Current palaeoclimatological models suggest variable sources of past precipitation to the Arabian Peninsula. Monsoon intensity was predicted to have been suppressed at around 4 Ma, due to low interhemispheric temperature gradients (Brierley et al., 2009). However, precipitation was predicted to have increased (1-2 mm/day) over the study sites, due to higher water-vapor content of the atmosphere (Brierley et al., 2009). Yet, negative $\delta^{18}O_{ca}$ and increased magnetism of the Chinese loess suggests increased EAM precipitation ~4.2-4 Ma (Ao et al., 2016; Ji et al., 2017). In either model, precipitation was derived from equatorial seas, but there is little evidence for how far this rainfall tracked into Arabia. Alternative models based on MPWP conditions have predicted that the African and Indian monsoon advanced into southern Arabia (Li et al., 2018), but have only found negligible increases in precipitation in northern Arabia of 0-0.2 mm/day (Tindall and Haywood, 2015; Prescott et al., 2018, 2019). This uncertainty is exacerbated by uncertain simulated MPWP $\delta^{18}O_{precipitation}$ values, which do not confirm a source of precipitation across Arabia (Fig. 38B). Analysis of speleothem fluid inclusion $\delta^{18}O$ and δD allows direct measurement of past groundwater $\delta^{18}O$ and δD, which can be plotted against local meteoric waterlines (LMWLs) to established changes in precipitation regimes. Fluid inclusion $\delta^{18}O$ does not undergo the kinetic isotope fractionation processes that influence $\delta^{18}O_{ca}$ during calcite precipitation (Meckler et al., 2015). $\delta^{18}O_{FI}$ is therefore preferable when comparing to local precipitation $\delta^{18}O$.

Present-day precipitation over the northern Nefud is delivered by cyclones that develop over the Mediterranean during the winter months. GNIP project GNIP/M/BH/0 (1961-

2016) provides a local meteoric waterline for Bahrain that can be related to WMCs (B-LMWL; $\delta D = 5.61\ \delta^{18}O + 9.21$). WMCs also provide the main source of rainfall in northern Oman. Though, in southern Oman precipitation is also delivered by the northern reaches of the Indian Summer Monsoon (ISM) every 5-10 years. As a result, northern Oman and have two distinct local meteoric waterlines: The Northern Local Meteoric Waterline (N-LMWL: $\delta D = 5.0\ \delta^{18}O + 10.7$) and the Southern Local Meteoric Waterline (S-LMWL; $\delta D = 7.1\ \delta^{18}O - 1.1$). The N-LMWL and B-LMWL almost match slopes and intercepts due to the shared moisture source. This is echoed by modern precipitation from northern Oman, which plots in good coherence with Bahrain precipitation (Fig. 48A); whereas precipitation delivered by the southern moisture source deviates from Bahrain precipitation, with more negative values and plot close to the GMWL ($\delta D = 8.2\ \delta^{18}O + 11.27$; Fig. 48A). Similarly, modern precipitation $\delta^{18}O$ and δD values from Addis Ababa, Ethiopia, plot close to the GMWL, in which rains are delivered by the seasonal migration of the tropical rain-belt and provides an isotopic signature for the African Summer Monsoon (ASM).

Here, we measured fluid inclusion water $\delta^{18}O$ and δD from stalagmites BL-2 and STC-3 (using the analytical protocol described by Affolter et al., 2015, 2014). BL-2 (3.7 Ma) δD_{FI} measured -82.8 to -66.7 and -10.5 to -9.5‰ for $\delta^{18}O_{FI}$. BL-2 values plot close to GMWL, in good coherence with southern Oman precipitation (Fig. 48A). BL-2 $\delta^{18}O_{FI}$ values are substantially more negative than modelled MPWP $\delta^{18}O_{precipitation}$ over the Nefud (Tindall and Haywood, 2015), suggesting either 1) an alternative moisture source at ~3.7 Ma, and/or 2) precipitation was substantially greater. This is in good agreement with simulated precipitation for 4 Ma, which shows a clear south-north precipitation decline (Brierley et al., 2009). A sample from STC-3 (~4.1 Ma: Gi25) was more positive in both

δD_{FI} (-44.7‰) and $\delta^{18}O_{FI}$ (-5.1‰) than BL-2 but plotted close to southern moisture source values (S-LMWL) and the extreme range of Bahrain precipitation. STC-3 $\delta^{18}O_{FI}$ is close to modelled MPWP $\delta^{18}O_{precipitation}$ (Fig. 48B), which is not different from modern $\delta^{18}O_{precipitation}$ delivered by WMC; however, STC-3 δD_{FI} is closely aligned to the GMWL. Combined with BL-2 data, this suggests that a southern moisture source contributed significantly to the increased precipitation during Pliocene wet periods. Overall, our δD_{FI} and $\delta^{18}O_{FI}$ data is in good agreement with palaeoclimate models of 4 Ma, in which increased precipitation was delivered from the southern moisture source (Brierley et al., 2009).

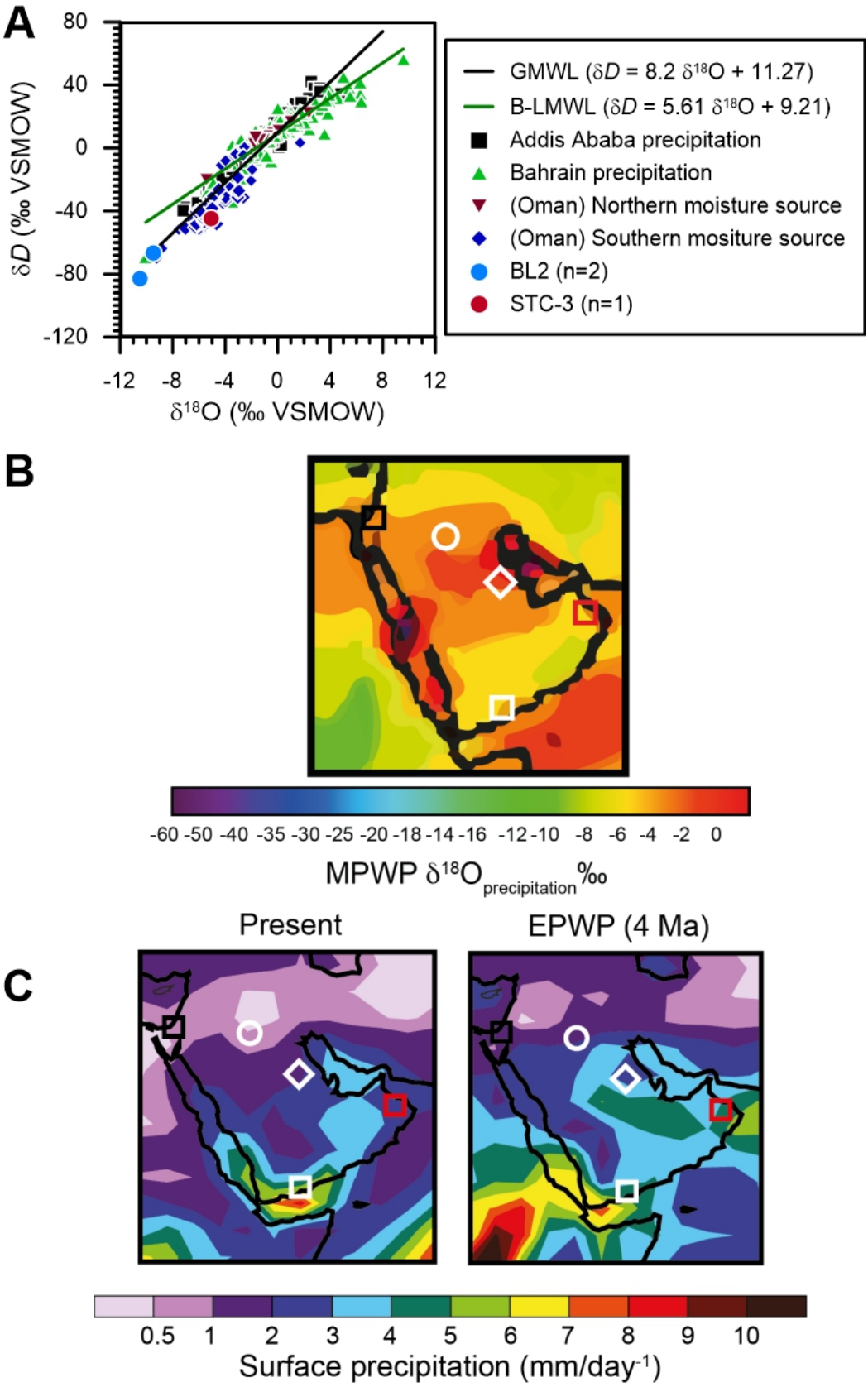
A
80
40
0
-40
-80
-120
δD (‰ VSMOW)
-12 -8 -4 0 4 8 12
δ18O (‰ VSMOW)
GMWL (δD = 8.2 δ18O + 11.27)
B-LMWL (δD = 5.61 δ18O + 9.21)
Addis Ababa precipitation
Bahrain precipitation
(Oman) Northern moisture source
(Oman) Southern mositure source
BL2 (n=2)
STC-3 (n=1)
B
-60 -50 -40 -35 -30 -25 -20 -18 -14 -16 -12 -10 -8 -6 -4 -2 0
MPWP δ18Oprecipitation ‰
C
Present
EPWP (4 Ma)
0.5 1 2 3 4 5 6 7 8 9 10
Surface precipitation (mm/day-1)

Fig. 48. (A) BL-2 and STC-3 $\delta^{18}O_{FI}$ and δD_{FI} values (Tab. S19) plotted against the GMWL and modern precipitation values from Bahrain and Addis Ababa (IAEA/WMO, 2019. Global Network of Isotopes in Precipitation. The GNIP Database. Accessible at: https://nucleus.iaea.org/wiser) and northern and southern moisture sources from Northern Oman (Weyhenmeyer et al., 2000, 2002). (B) Map of MPWP modelled $\delta^{18}O_{precipitation}$ (after Tindall and Haywood, 2015). (C) Map of model of EPWP precipitation amount (4 Ma) compared to present (after Brierley et al., 2009). Locations of BL, STC (white circle), SC (white diamond), Ashalim (black square), Hoti (red square) and Mukalla (white square) have been added to models.

6.4.3 Calcite $\delta^{18}O$ and $\delta^{13}C$

6.4.3.1 $\delta^{18}O_{ca}$

$\delta^{18}O_{ca}$ were combined with previous results from STC, BL and SC (Fleitmann et al., 2004b). $\delta^{18}O_{ca}$ values ranged -16.66‰ to -11.34‰ (STC-1), -13.94‰ to -10.14‰ (STC-3), -14.71‰ to -11.57‰ (STC-4), -12.16‰ to -5.67‰ (STC-5), -16.59‰ to -11.27‰ (BL-2) and -13.7‰ to -11.12‰ (SC-2) (

Fig. 49). With exemption of STC-5, all sample means are statistically similar to each other. STC-1 has, on average, the most negative values (-13.61‰); whereas STC-5 had the most positive average values (-10.86‰). Speleothem $\delta^{18}O_{ca}$ values can be influenced by temperature, precipitation amount, rainout and moisture source (Lachniet, 2009). Previous studies have shown that *the amount effect* (the negative correlation between $\delta^{18}O$ and precipitation amount) and *the source effect* have significant control on $\delta^{18}O_{ca}$ in Arabia (Fleitmann et al., 2003a, 2011; Shakun et al., 2007; Nicholson et al., 2020). STC-1, STC-3, STC-4, Bl-2 and SC-2 have more negative $\delta^{18}O_{ca}$ values compared to MIS 5e

speleothems from Mukalla Cave (Y99, Yemen), Hoti Cave (H13, Oman) and Wadi-Sannur Cave (WS-5d, Egypt), a time in which the spatial extent and intensity of the ASM and ISM were substantially increased across Saharo-Arabia and widespread fluvio-lacustrine systems were activated (Rosenberg et al., 2011, 2012, 2013). The different $\delta^{18}O_{ca}$ signatures of WS-5d, Y99 and H13 were related to the dominance of the ASM or ISM above each site, as well as precipitation amount, respectively (Fleitmann et al., 2011; El-Shenawy et al., 2018; Nicholson et al., 2020). Moreover, MPWP speleothem $\delta^{18}O_{ca}$ values from Ash-15 (Ashalim Cave, Negev) average -10.65‰ (Vaks et al., 2013). Differences between Saudi Arabian samples, Y99, H13 and Ash-15 are statistically significant (P = <0.05). This suggests EPWP and Plio-Pleistocene transition precipitation was enhanced compared to the MPWP and later Pleistocene wet periods. The close coherence of isotope signatures also suggests the ASM was responsible for increased Pliocene-Early Pleistocene precipitation.

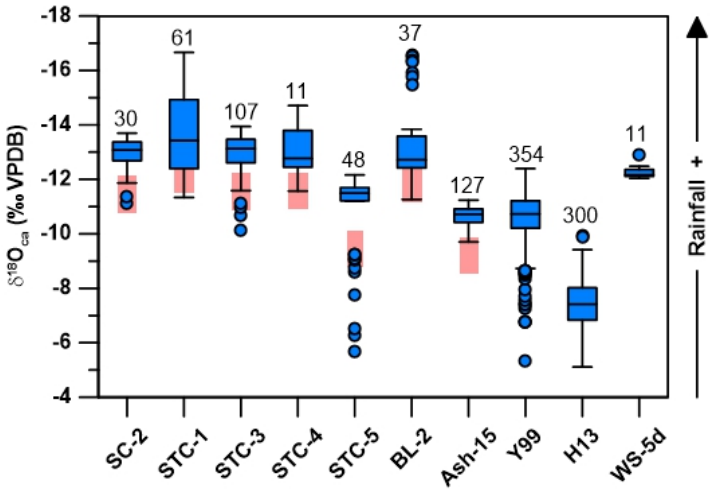

Fig. 49. Boxplot comparing $\delta^{18}O_{ca}$ from stalagmites presented in this study (Tab. S16) with $\delta^{18}O_{ca}$ of ASH-15 (Pliocene), Y99 GI-I, H13, and WS-5d (MIS 5e). Pink area highlights maximum (-2.15) and minimum (-0.74) corrections on average values for Pliocene temperature and $\delta^{18}O_{ocean}$.

However, at such an age it is also important to consider additional parameters that could influence $\delta^{18}O_{ca}$: 1) global (~2°C) and local (~3-5°C) surface air temperatures (SAT) were increased during the Pliocene (Salzmann et al., 2011; Tindall and Haywood, 2015; Prescott et al., 2018). And, 2) global ice volume was greatly reduced during the Pliocene, leading to ~0.2-1‰ more negative $\delta^{18}O_{ocean}$ values (Lisiecki and Raymo, 2005).

1. Increased SAT would be echoed by increased cave air temperature, which typically reflects average annual temperatures outside of the cave. The *cave air temperature effect* influences the temperature-dependent fraction of calcite from drip-water by ~0.18-0.23‰ per 1°C change (Kim and O'Neil, 1997). A 3-5°C increase in SAT and cave temperature should lead to ~0.54-1.15‰ decrease in $\delta^{18}O_{ca}$ values compared to present.
2. Reduced ice-sheet and decreased $\delta^{18}O_{ocean}$ would be reflected by more negative $\delta^{18}O_{vapour}$ evaporated from the moisture source. This would also be reflected by decreased $\delta^{18}O_{precipitation}$ values.

Together, these could account for -2.15 to -0.74‰ of $\delta^{18}O_{ca}$ variability. When we correct average $\delta^{18}O_{ca}$ values for these effects (

Fig. 49), the resultant values provide a record of rainfall intensity and moisture source and closely reflect those of Y99 GI-I (-10.61‰) and WS-5d (-12.26‰). This close match both suggests a similar rainfall intensity and moisture source as MIS 5e, adding credence to our previous determination of a monsoon source. However, the samples present here remain more negative than Y99 GI-I. This may be explained by either, 1) the *continental effect*: the loss of ^{18}O as an airmass travels across land, through Rayleigh distillation effects. Simulated rainfall shows a clear meridional precipitation gradient across Arabia

(Brierley et al., 2009; Tindall and Haywood, 2015; Li et al., 2018; Prescott et al., 2019), thus BL, SC and STC should be reflected by decreased rainfall and $\delta^{18}O_{ca}$ compared to Y99. Yet, without contemporaneous $\delta^{18}O_{ca}$ records from across Arabia, it is not possible to test the evolution of $\delta^{18}O$ via rainout effects; further samples are required to elucidate these issues. Or, 2) the *amount effect*, in which the negative $\delta^{18}O_{ca}$ values represent increased precipitation compared to MIS 5e.

6.4.3.2 $\delta^{13}C_{ca}$ and ecological conditions

$\delta^{13}C_{ca}$ values ranged -9.02‰ to -6.74‰ (STC-1), -8.75‰ to -2.45‰ (STC-3), -7.40‰ to -2.70‰ (STC-4), -6.38‰ to -5.20‰ (STC-5), -7.04‰ to -4.34‰ (BL-2) and -5.09‰ to -1.69‰ (SC-2) (Fig. 50). STC-4, was statistically similar to STC-5 and BL-2. The means of all other samples were different to each other. STC-1 has the most negative average value (-8.34‰); whereas SC-2 has the most positive average $\delta^{13}C_{ca}$ value (-3.80‰). These wide ranges are not uncommon in speleothems, as $\delta^{13}C_{ca}$ is influenced by a number of environmental and some counteracting parameters including: (1) density and type of vegetation (C_3/C_4), (2) soil moisture, thickness and porosity, (3) microbial and biological activity within the soil, (4) recharge conditions, (5) atmospheric CO_2 and (6) kinetic fractionation during calcite precipitation, which is influenced by cave air PCO_2 and drip rate (e.g., Baker et al., 1997; Wong and Breecker, 2015; Breecker, 2017; Mickler et al., 2019). At times of high precipitation combined with thin soils and short soil-water residence times, equilibration between soil CO_2 and percolating water may be incomplete (Bar-Matthews et al., 2003; McDermott, 2004). Under such a scenario, seepage water would have a stronger cave limestone and atmospheric CO_2 composition and thus more positive speleothem $\delta^{13}C_{ca}$ values. Furthermore, degassing along the flow path and prior

calcite precipitation can convolute the environmental signal (Mickler et al., 2019). In most cases, the most negative $\delta^{13}C_{ca}$ may provide the most robust vegetation and soil CO_2 signature.

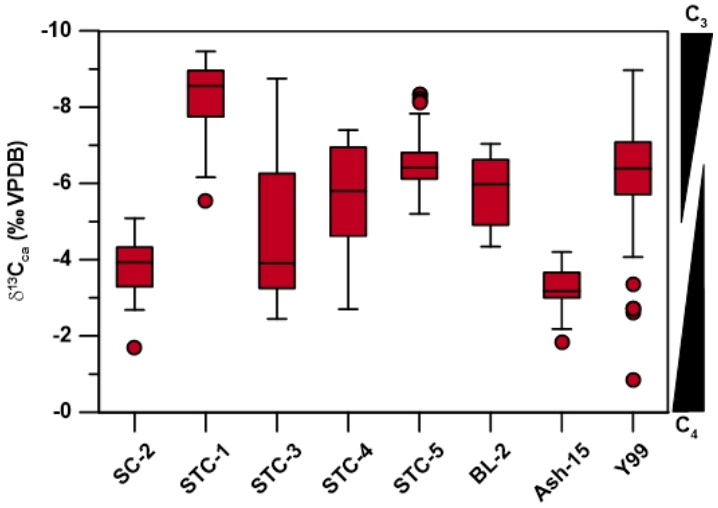

Fig. 50. $\delta^{13}C_{ca}$ values of stalagmites from this study compared to Ash-15 and Y99 (Tab. S16)

When soil CO_2 and soil water are in complete equilibrium ("open system conditions"), speleothem $\delta^{13}C_{ca}$ values represent the soil CO_2 component. Under these conditions, stalagmites growing under a C_4 dominated environment are represented by carbonate $\delta^{13}C$ values of -6‰ to +2‰ and -14‰ to -6‰ with C_3 environments. Assuming open system conditions, STC and BL $\delta^{13}C_{ca}$ values fall within mixed C_3/C_4 signatures; whereas SC $\delta^{13}C_{ca}$ values fall within the C_4 range. Relatively high $\delta^{13}C_{ca}$ may be explained by the fact that SC contains multiple entrances and greater ventilation (SGS, 2007), leading to fluctuations in cave PCO_2 and increased kinetic isotope fractionation during calcite precipitation. Nevertheless, stalagmites study here typically fall into the range of variation of MIS 5e values from Y99, which were in good coherence with

palaeontological and phytolith data showing grassland biomes formed on the Arabian Peninsula (Bretzke et al., 2013). This suggests grassland biomes were present in northern and central Arabia during the Pliocene and Early Pleistocene pluvial periods. The fact that STC-1,3-5 and BL-2 have more negative values than Ash-15 could indicate northern Arabia was characterised by increased vegetation density compared to the Negev, possibly due to greater precipitation. This argument is in good agreement with $\delta^{18}O_{ca}$ values yet requires further clarification via more robust indicators of past vegetation.

The current spatial distribution of semi-arid grasslands and bushlands allows us to further characterise Arabian palaeoenvironments. Currently, these flourish in areas receiving 300-600 mm yr^{-1} (namely the highlands of Yemen) and typically comprise a mixture of C_3 and C_4 taxa (Miller and Cope, 1996). The plains and lower slopes the Yemen highlands are dominated by drought-deciduous *Acacia-Commiphora* bushlands (Miller and Cope, 1996). This bushland is replaced by semi-evergreen and thicket bushland as altitude and annual precipitation increases. Similarly, current savanna environments of Tanzania and Kenya typically receive rainfall of 500-750 mm yr^{-1} (Lind and Morrison, 1974). While we cannot provide species level designation and anthropogenic modification of modern landscapes must be considered, $\delta^{13}C$ values suggest similar environments expanded northward with the 600-300 mm yr^{-1} isohyet. As our cave sites are located at the potential limit of the Plio-Pleistocene tropical rain-belt, large areas of Arabia to the south and west were likely to have been "green" due to increased monsoonal rainfall.

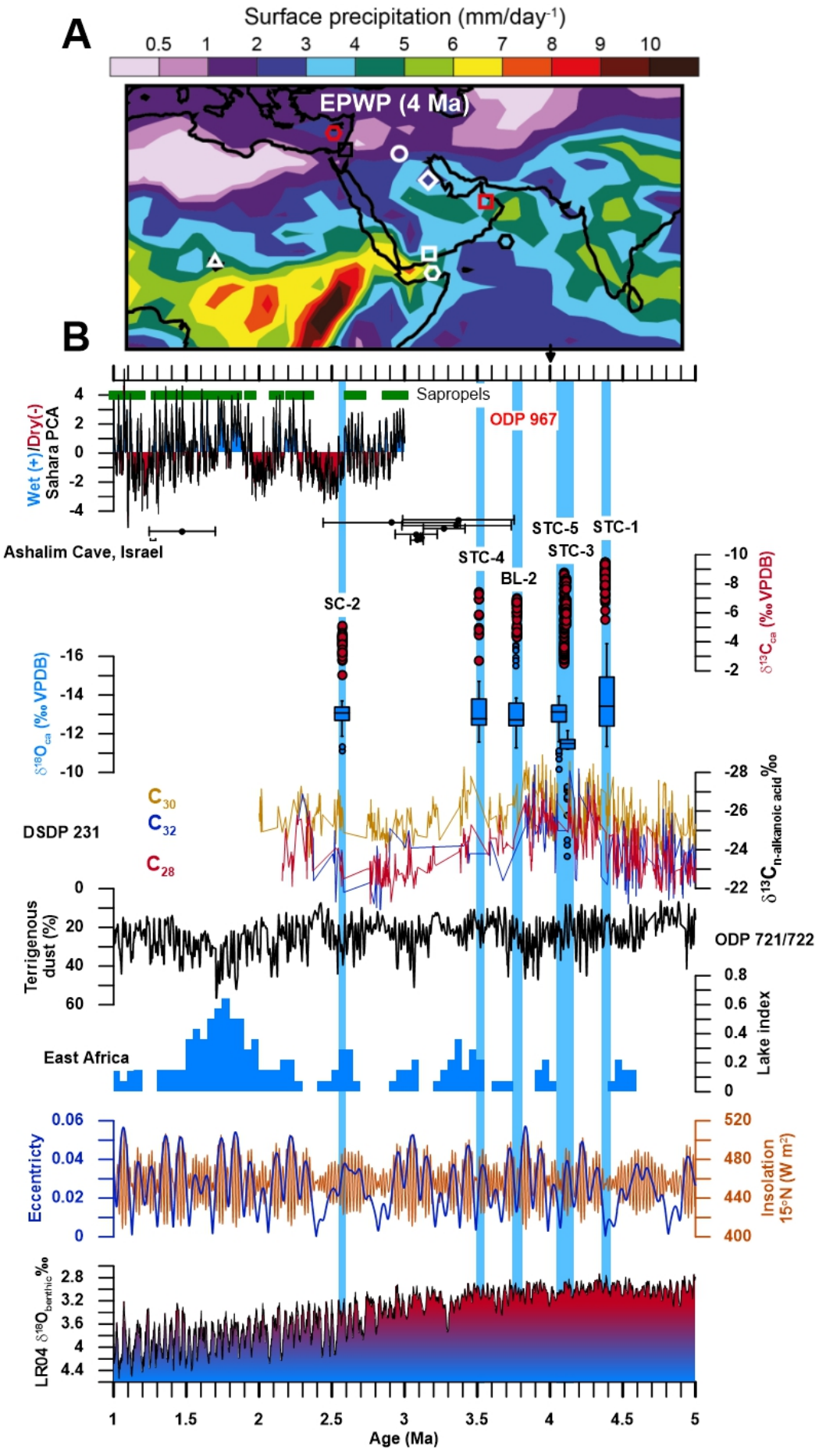
A
Surface precipitation (mm/day-1)
0.5 1 2 3 4 5 6 7 8 9 10
EPWP (4 Ma)
B
Sapropels
ODP 967
Wet (+)/Dry(-) Sahara PCA
Ashalim Cave, Israel
STC-5 STC-1
STC-4
STC-3
BL-2
SC-2
δ18Oca (‰ VPDB)
δ13Cca (‰ VPDB)
C30
C32
C28
DSDP 231
δ13Cn-alkanoic acid ‰
Terrigenous dust (%)
ODP 721/722
East Africa
Lake index
Eccentricity
Insolation 15°N (W m2)
LR04 δ18Obenthic ‰
Age (Ma)

Fig. 51. (A) Modelled early Pliocene precipitation at ~4 Ma (after Brierley et al., 2009) with location of records used here: BL and STC (white circle), SC (white diamond), Hoti Cave (red square), Mukalla cave (white square), Ashalim cave (black square), ODP 721/722 (black hexagon), DSDP 231 (white hexagon), ODP 967 (red hexagon) and Lake Chad (white triangle). (B) Boxplot of $\delta^{18}O_{ca}$ (blue) Arabian speleothems (Coloured circles mark statistically extreme values) and $\delta^{13}C_{ca}$ values compared to LR04 stack $\delta^{18}O_{benthic}$‰, eccentricity, 15°N insolation, ODP 721/722 terrigenous dust, DSDP 231 $\delta^{13}C_{n\text{-}alkanoic\ acid}$‰ (red: C_{28}; yellow: C_{30}; blue: C_{32}) (Liddy et al., 2016), Ashalim Cave speleothem ages (Vaks et al., 2013) and East African lake periods (Maslin and Trauth, 2009; Shultz and Maslin, 2013; Maslin et al., 2014).

Between ~4.3-4.0 Ma STC-1,3 and 5 $\delta^{13}C_{ca}$ values show grasslands occupied the now desert areas of Arabia in punctuated intervals. This is consistent with palaeoecological data from Chad, showing an expansion of mesic grasslands occurred ~4.4 to 4.1 Ma (Novello et al., 2015). Similarly, increased vegetation coverage in East Africa is detailed by decreased $\delta^{13}C_{n\text{-}alkanoic\ acid}$ record of the DSDP 231, Gulf of Aden (Fig. 51B; Liddy et al., 2016). Combined, this shows ameliorated conditions at 4.3-4.1 Ma were present in both the southern and northern margins of Arabia. As a southern source of moisture has been identified from BL-2 and STC-3, it is therefore likely that now arid areas of central Saharo-Arabia also experienced enhanced rainfall and vegetation during the early Pliocene. This is in good coherence with modelled data of EPWP precipitation, which shows significantly increased precipitation across Saharo-Arabia (Fig. 51A; Brierley et al., 2009).

At 3.77 ± 0.024 Ma (BL-2) and 3.5 Ma ± 0.12 (STC-4) $\delta^{13}C_{ca}$ values indicate a mixed C_3/C_4 environment was present. BL-2 and STC-4 $\delta^{13}C_{ca}$ are not significantly different from Y99 (Yemen) MIS 5e speleothem $\delta^{13}C_{ca}$ values, which were consistent with phytolith (Bretzke et al., 2013) and palaeontological data (Rosenberg et al., 2013) representing a savanna-type grassland in the Arabian interior. Based on this, it is possible that BL-2 and STC-4 $\delta^{13}C_{ca}$ values reflect similar environmental conditions at ~3.77 Ma and ~3.5 Ma. While mean $\delta^{18}O_{ca}$ of BL-2 and STC-4 are more positive (drier conditions) compared to STC-1 and STC-3, this is not reflected in the $\delta^{13}C_{ca}$ records, suggesting precipitation was sufficient to facilitate grasslands. Aquatic grasses increased at Chad at ~3.8-3.6 Ma (Novello et al., 2015), consistent with the age of BL-2, again showing good coherence between ameliorated phases in northern and southern Saharo-Arabia. Similarly, BL-2 is consistent with decreased DSDP 231 $\delta^{13}C_{n\text{-alkanoic acid}}$ values, showing increased vegetation density within the Horn of Africa. Increased precipitation exhibited by STC-4 is also synchronous to a punctuated decrease in decreased DSDP 231 $\delta^{13}C_{n\text{-alkanoic acid}}$ values and increased East African lake occurrence (Shultz and Maslin, 2013; Maslin et al., 2014), showing an interregional increase in precipitation.

Early Pleistocene (SC-2; ~2.7 Ma) $\delta^{13}C_{ca}$ values are indicative of grassland environments in central Arabia. This is in good agreement with increased grasses at lake Chad (Novello et al., 2015, 2017) and a peak in DSDP 231 $\delta^{13}C_{n\text{-alkanoic acid}}$ values (Fig. 51; Liddy et al., 2016), showing synchronous expansions of grasslands in southern margins and central Saharo-Arabia. Similarly, sapropel formation at the time indicates increased Saharan run-off and Nile outflow occurred within the early Pleistocene (Grant et al., 2017), which provides further evidence for increased precipitation within the arid interior of the Sahara. This is consistent with another peak in lake activity occurred in East Africa ~ 2.7 Ma

(Fig. 51B; Maslin and Trauth, 2009; Shultz and Maslin, 2013; Maslin et al., 2014). Not only does this show interregional simultaneous increases of precipitation, but also increased precipitation on a clear north-south transect.

6.5 Hominin occupations and dispersals?

6.5.1 Early hominins

Results provided here show that Plio-Pleistocene wet periods could have been more intense than wet periods during the Pleistocene and late-mid Holocene. Pluvial periods in the Holocene and Late Pleistocene saw significantly increased precipitation, activation of fluvial-lacustrine systems and wetlands the spread of grassland biomes across Arabia (Parker et al., 2004, 2006; Rosenberg et al., 2011, 2013; Matter et al., 2015; Parton et al., 2018). These ameliorated conditions facilitated repeated human occupations of the Arabian interior (Delagnes et al., 2012; Rosenberg et al., 2013; Hilbert et al., 2014; Groucutt et al., 2015b, 2015c, 2015d, 2018; Stimpson et al., 2016; Parton et al., 2018; Roberts et al., 2018) and show that human distribution can be linked to environmental conditions. Taken with the records provided here, this allows us to consider the timing of potential dispersals throughout the course of human evolution.

The hominin fossil record of the Pliocene to the early Pleistocene is largely limited to southern and eastern Africa. However, one of the earliest putative hominins (*Sahelanthropus tchadensis*, dated 7.24 ± 0.34 to 6.83 ± 0.45 Ma BP) was uncovered in sediments of the southern Sahara Desert of Chad (Brunet et al., 2002, 2005). The age of these fossils has been challenged due to poor stratigraphic integrity and could actually date from an earlier period within the Miocene. Regardless of the age uncertainties,

assessment of associated fauna indicate that *S. tchadensis* occupied a tropical rainforest and mesic grassland (Brunet et al., 2005). The relationship between early hominin occupation of now arid areas and environmental amelioration was recently reaffirmed by the nearby *Australopithecus bahrelghazali* fossils finds, though dating much later (3.58 ± 0.27 Ma BP: Lebatard et al., 2008). Palaeoenvironmental analyses of the surrounded environment that shows *Au. bahrelghazali* fossils were deposited during a time of increased precipitation and grassland expansion (Lebatard et al., 2008; Novello et al., 2015). These two occurrences of ameliorated conditions and hominin range expansion allows us to consider the distribution of Pliocene fossils in the context of environmental conditions. We have shown here that mixed grassland and savannah-type environments formed in northern Arabia at 3.51 ± 0.12 Ma BP (STC-4), which are coeval to ameliorated conditions in the southern Saharan margins. While further palaeoclimate and palaeontological records are required to fully comprehend the extent and nature of rainfall, grasslands and the distributions of early hominins, this evidence could demonstrate that habitable biomes existed further north than previously known. If, as our data suggests, expansion of the monsoon was responsible for increased rainfall, major fluvial-lacustrine systems and grassland environments would have activated across Saharo-Arabia. Abundance of freshwater resources and grassland environments clearly highlights the potential for early hominin distribution beyond that suggested by the scarce fossil record. Such a suggestion could lead to exciting new research questions concerning hominin distribution and Pliocene Saharo-Arabia.

6.5.2 *Early* Homo

Dispersal of *Homo* sp. during the late Pleistocene are becoming increasingly related to palaeoclimate fluctuation, particularly of the Saharo-Arabian desert belt (Groucutt et al., 2015a; Jennings et al., 2015b; Petraglia et al., 2015; Bae et al., 2017). Incursions of monsoonal rainfall saw green landscapes flourish, which facilitated occupation and dispersal of *H. sapiens*. However, currently the only known pre-Holocene hominin fossil from Arabia consists of the Al Wusta-1 intermediate phalanx from the Nefud Desert dating to ~ 95-85 ka BP (Groucutt et al., 2018). Archaeological evidence demonstrates earlier human occupations of Arabia. Currently the oldest chronometrically dated evidence for hominin occupation in Arabia consists of stone tools and modified bones from the site of T'is al Ghadah in the Nefud Desert, dating to ca. 300-500 ka (Roberts et al., 2018; Stewart et al., 2019a). But what of earlier periods?

Acheulean assemblages are widespread in Arabia (Petraglia, 2003; Petraglia et al., 2012; Jennings et al., 2015a), and their diversity probably reflects chronological differences to some extent. However, care needs to be taken in assuming that typo-technological features can be correlated with age in a straightforward way. For instance, the large and relatively crude hand-axes at the 206-76 site in the Dawadmi area have recently been dated to the end of the Acheulean period, at ca. 250-200 ka (Shipton et al., 2018).

Several claims have been made for Oldowan assemblages in Arabia (for reviews see Petraglia, 2003; Groucutt and Petraglia, 2012). These include both excavated (but undated) (Amirkhanov, 1994) and surface material (Whalen and Schatte, 1997) from Yemen, sites from Saudi Arabia (Whalen et al., 1986, 1989), and multiple sites in central Oman (Whalen, 2003). In general, the attribution simply means that a fairly simple core

and flake technology and basic shaped tools were recovered. However, in reality such technology is time transgressive and until material is recovered from well dated contexts and analysed in detail, it will be unclear if there are any Oldowan assemblages in Arabia. Some claims for Oldowan artefacts in Arabia may in fact be geofacts (e.g., Jagher, 2009). Without demonstration that humid conditions existed in Arabia around the time that the first hominins left Africa, looking or Oldowan sites in Arabia should be a focus of future research. While so far the evidence for Oldowan occupations in Arabia is not particularly convincing, this could reflect a combination of limited research in the area and a lack of targeting of deposits of the correct age. By analogy, it was only in the last few years that the first clearly Epipalaeolithic site was discovered in Arabia (Hilbert et al., 2014), so the potential for Oldowan occupations in Arabia is clear. It is interesting to point out that if we accept the claims for Oldowan assemblages in Arabia, there are in fact more sites known that in North Africa (Lahr, 2010).

More broadly, other hints of Early Pleistocene humid conditions in Arabia include the formation of pillow basalts between 2 and 1 million years ago at Al Wahbah, which are interpreted as indicating that volcanic material entered a lake (Wahab et al., 2014). Together then a picture of repeated humid periods going back millions of years is coming into focus in Arabia, for more recent periods these are demonstrably related to phases of human dispersal. Our null hypothesis is that the same applied to earlier periods. By demonstrating monsoon derived humidity in northern Arabia during the Pliocene and perhaps Early Pleistocene in northern Arabia, we can infer that much of the Peninsula would have seen improved climate at this time. Arabia has a vast palaeohydrological network, the history of which is currently poorly resolved, but if the monsoon reached at least 26°N then we can assume that all of the major river systems of Arabia would have

been activated (Breeze et al., 2015). These major west to east flowing rivers could have provided dispersal paths for hominins leaving Africa to move eastwards and occupy the rest of Asia.

The oldest documented stone tools have been found in East Africa and date to 3.3 Ma (Harmand et al., 2015). Subsequently the Oldowan dates from 2.6 million years ago (Braun et al., 2019). The origin of the genus *Homo*, and the relationship between cultural and biological aspects at the this time are debated, but some findings suggest that the genus Homo appeared broadly in sync with the origin of the Oldowan (Villmoare et al., 2015). Interestingly this occurs just before the humid period we have identified in Arabia for the first time, and therefore both biological and cultural changes may have facilitated an environmentally dispersal into Eurasia.

What about other evidence in southwest Asia? Examples from the Levant include claims for >2.4 Ma have been made from the site of Yiron (Ronen, 1991). However, there are stratigraphic complexities which do not make this secure (Scardia et al., 2019). Stronger evidence comes from the Zarqa Valley in Jordan, where recently published findings support a hominin presence from 2.5 Ma (Scardia et al., 2019). This is currently the oldest evidence for hominins outside Africa. It supplements other early indications of hominins in south (e.g., Dennell, 2008) and East Asia (Zhu et al., 2018) dating to over 2 Ma. Likewise, within Africa, evidence dating to 2.4 Ma has recently been published from Algeria (Sahnouni et al., 2018).

If the ages for first hominin presence outside of Africa are considered reliable, increased monsoon intensity at 2.57 Ma BP (SC-2) could have facilitated shifts in hominin

distribution beyond Africa. Many of the major river systems and palaeolakes would have been activated by this increase in precipitation, meaning abundant freshwater and grasslands could have facilitated hominin occupation. Although it is important to consider that 1) these environments likely differed from southern and eastern Africa, and 2) the environmental tolerances of hominins at this age are poorly understood, surely the environments of the Levant (Scardia et al., 2019) and China (Zhu et al., 2018) (and those in-between) were not exact replicas of southern or eastern Africa? With this in mind, we may deduce that some degree of environmental flexibility was part of the behavioural repertoire of early *Homo*. In this case, it is possible that early *Homo* was able to adapt to the slight environmental difference of green Arabia.

6.6 Conclusion

Preliminary data provided here indicates that the spatial extent and intensity of the monsoon domain was increased across the Arabian desert at of 4.38 ± 0.48 Ma (STC-1), 4.08 ± 0.12 Ma (STC-2), 4.099 ± 0.048 Ma (STC-3), 4.11 ± 0.12 Ma (STC-5), 3.776 ± 0.024 (BL-2), 3.51 ± 0.12 (STC-4), 2.57 ± 0.43 Ma (SC-2). Ages of STC-2,3 and 5 cluster within Gi25, suggesting this was a notably intense wet period during the early Pliocene. Within these pluvial periods, the monsoon domain expanded across most of Arabia and increased precipitation over 300 mm yr^{-1}, and was likely echoed by increased precipitation in the broader Saharo-Arabian desert belt. This facilitated the development of grasslands and probably activated vast fluvio-lacustrine systems, which may have provided habitable areas for early hominins. An Early Pleistocene wet period (2.57 ± 0.43 Ma) could be related to the earliest known hominin dispersals, allowing the distribution of (probably) early *Homo* to expand into northern Africa, the Levant and beyond. Current

evidence is limited and establishing antiquity of the Arabian Oldowan archaeological and palaeontological records should be a target for future research. Overall, we have extended the palaeoclimate record from key regions of the Arabian deserts, which demonstrate habitable biomes for hominin dispersal occurred throughout the Plio-Pleistocene.

Acknowledgments

This work was supported by the AHRC South, West and Wales Doctoral Training Partnership (Grant Number AH/L503939/1).

Chapter 7

7) Phasing between the pluvial conditions in Southern Arabia and sea-level: implications for a *H. sapiens* dispersal along the southern route during the Last Interglacial

The following chapter is a modified version of a manuscript submitted to the journal *Geophysical Research Letters*. This chapter provides further details for research questions 1 and 3; detailing the precise onset of speleothem formation, a high-resolution record of monsoonal rainfall. We use this information to provide and evaluate potential models for the dispersal of *H. sapiens* across the Bab-al-Mandab strait. This chapter has been submitted as a research paper to *Geophysical Research Letters* with the following citation:

Nicholson, S.L., Hosfield, Groucutt, H.S., R., Pike, A.W.G., Burns, S.J., Matter, A., Fleitmann, D., *Homo sapiens* dispersal via the "southern-route" out of Africa? The phase relationship between pluvial conditions in Arabia and sea-level during the last interglacial (MIS 5e).

The author contributions are as follows: S.L.N conducted the stable isotope analysis, age-model construction and acted as primary author for the paper under the supervision of

D.F., R.H., A.W.G.P. Samples were initially collected by D.F., S.J.B. and A.M.. H.S.G. provided review and support for interpretations of hominin dispersals.

Submitted to *Geophysical Research Letters*: 11th September 2020

Abstract

The Arabian Peninsula was one key area for *H. sapiens* dispersals out of Africa. Current dispersal models advocate that dispersals via the "southern route" into Arabia occurred during Glacial Termination-II (T-II), when increased monsoon precipitation and reduced sea-level and Bab-al-Mandab width increased the likelihood of crossing. The precise phasing between sea-level and monsoon precipitation is thus key to assess the likelihood of a successful crossing or the behavioural and technological capacities that facilitated crossing. Based on a precisely dated stalagmite record from Yemen we reveal a distinct phase-lag of several thousand years between sea-level rise and monsoon intensification. Pluvial conditions in southern Arabia during MIS 5e lasted from ~127.7 to ~121.1 ka BP and occurred when sea-levels were already higher than at present. We propose three models for the dispersal of *H. sapiens*; all have pertinent implications for our understanding of human technological and behavioural capacities during MIS 5e.

7.1 Introduction

Understanding how *H. sapiens* spread from Africa across the world is one of the most debated topics in human evolution (Mellars et al., 2013; Groucutt et al., 2015a; Bae et al., 2017). Two proposed main dispersal routes cross Arabia: a northern route across the Sinai into the Levant and a southern route from the Horn of Africa via the Strait of Bab-al-Mandab into Southern Arabia and beyond (Fig. 52). The accessibility of these entry

points was spatiotemporally variable and related to major climatic changes across the Saharo-Arabian deserts. During interglacial periods, both the African and Indian Summer Monsoons (ASM and ISM, respectively) were much stronger, expanded northward and transformed the Saharo-Arabian deserts into green landscapes for a few millennia (Fleitmann et al., 2003; Parton et al., 2015b). These pluvial periods, termed "Green Sahara Periods" and "Southern Arabian Humid Periods" (SAHPs) respectively, provided optimal periods for *H. sapiens* to disperse from sub-Saharan Africa into Eurasia (Fleitmann et al., 2011; Rosenberg et al., 2011; Larrasoaña et al., 2013; Nicholson et al., 2020). Over the last 130 ka BP, pluvial conditions in Southern Arabia with rainfall of more than 300 mm yr^{-1} occurred during Marine Isotope Stages (MIS) 5 and 1, and lasted from ~128-121 ka BP (MIS 5e; SAHP 4), ~104-97 ka BP (MIS 5c; SAHP 3) and ~84-71 ka BP (MIS 5a; SAHP 2) and ~10.5 to 6.2 ka BP (SAHP 1) (Fleitmann et al., 2011; Nicholson et al., 2020). In addition, there is also some evidence for a period of enhanced rainfall between approximately 60 and 50 ka BP (onset of MIS 3) (McLaren et al., 2009; Parton et al., 2015a, 2018), though the nature and timing of this period remains uncertain.

The southern dispersal route involves a maritime crossing of the Bab-al-Mandab Strait. However, its current width of approximately 27 km represents a significant challenge to dispersal and was more likely traversable at times of lower sea level, especially if sea-faring technologies were limited. One proposed timing for early *H. sapiens* dispersals is Termination-II (T-II) between 145-130 ka BP (Armitage et al., 2011; Rohling et al., 2013; Beyer et al., 2020), when sea-levels were lower and the width of the Bab-al-Mandab Strait was reduced. However, low sea-levels during glacial periods coincide with weaker ASM and ISM intensity and therefore greater aridity in the Saharo-Arabian desert belt, presenting a challenge to dispersal models during Glacial Termination-II. In contrast,

higher sea-levels prevailed during interglacial periods when the ASM and ISM were much stronger. Although abundant freshwater and food resources were available in the Saharo-Arabian deserts, crossing of the Bab-al-Mandab was more challenging due to the greater width of the Strait. Thus, the precise phasing between sea-level change and ASM/ISM intensity during T-II could be one critical factor controlling the accessibility of the southern-dispersal route - with possibly only a very narrow temporal overlap between low sea-levels and the onset of pluvial conditions in northeastern Africa and Arabia. ASM and ISM records with precise and accurate chronologies are an important prerequisite to reveal such a phasing. Here, we present a precisely dated and highly-resolved speleothem-based climate record from Mukalla Cave in Yemen, covering MIS 5e (SAHP 4; Nicholson et al., 2020). Precise Uranium-series (^{230}Th hereinafter) ages allow us to evaluate the temporal phasing between ASM/ISM rainfall and sea-level change at a possible point of entry into southern Arabia.

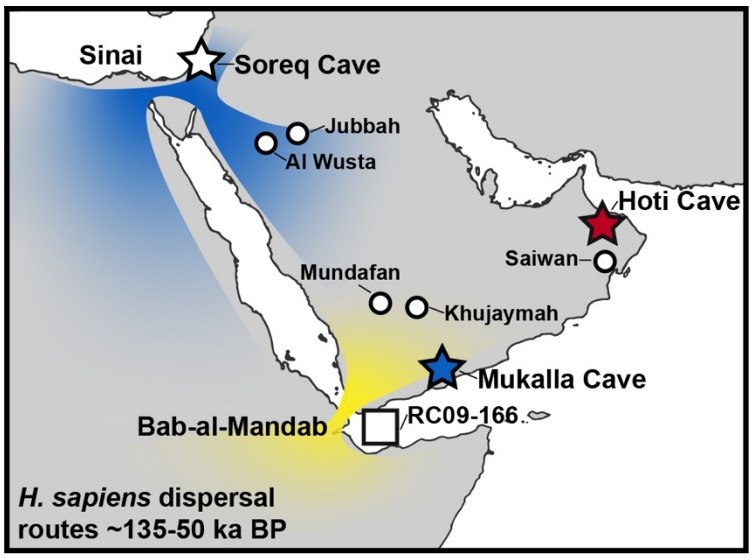

Fig. 52. Map of Arabia with locations of Mukalla Cave (blue star), Hoti Cave (red star), Soreq Cave (white star), palaeolakes (white circles), RC09-166 (white square) and proposed H. sapiens northern (blue) and southern (yellow) entry points into Arabia (Armitage et al., 2011; Rohling et al., 2013; Petraglia et al., 2019).

7.2 Materials and Methods

Stalagmite Y99 was collected from Mukalla Cave (14°55'02''N; 48°35'23'' E; ~1500 masl; Fig. 52) in southern Yemen, where climate is strongly governed by the ASM and ISM respectively. At present, both Mukalla Cave and the Bab-al-Mandab Strait are located at the northern and north-eastern margins of the ASM and ISM, with rainfall averaging <150 mm yr^{-1} (Fleitmann et al., 2011). Stalagmite Y99 covers the last 1.1 million years, during which stalagmite growth was intermittent. 17 growth intervals were identified through ^{230}Th and Uranium-lead dating, with MIS 5e being the youngest growth interval (Nicholson et al., 2020). The precise chronology of the MIS 5e growth interval is very well constrained by five ^{230}Th-ages with uncertainties of ± 500 years (Nicholson et al., 2020). The StalAge algorithm (Scholz and Hoffmann, 2011)was used to develop a robust age-depth model for previously obtained $\delta^{18}O_{ca}$ and $\delta^{13}C_{ca}$ isotope profiles (Nicholson et al., 2020). The high-resolution $\delta^{18}O_{ca}$ and $\delta^{13}C_{ca}$ profiles of stalagmite Y99 are based on 153 isotope measurements, sampled every ~1 mm along the centre of two growth axes (Fig. S4, Tab. S21). Isotope measurements were conducted at the Chemical Analysis Facility (CAF) at the University of Reading using a Thermo Fischer Delta V Advantage Mass Spectrometer (IRMS) couple to an automated preparation system (GasBench II). Precision (1σ) is <0.2‰ for $\delta^{18}O$ and <0.1‰ for $\delta^{13}C$. Isotope values are reported relative to the Vienna Peedee Belemnite (VPDB) standard.

7.3 Results and Discussion

7.3.1 Timing and Duration of SAHP 4 (MIS 5e)

The chronology of the MIS 5e section of stalagmite Y99 is based on seven ^{230}Th ages. Two ages were discarded: one ^{230}Th age at the top was not included as it is most likely

influenced by condensation corrosion and one age appears to be an outlier for unknown reasons (Fig. S4-S5). Importantly, the onset of stalagmite growth is determined by two ^{230}Th ages of 127.640 ± 0.560 ka BP and 127.811 ± 0.630 ka BP respectively, averaging 127.730 ± 0.400 ka BP. Stalagmite growth ceased at around 121.170 ± 0.500 ka BP (Fig. S6). As ~300 mm yr^{-1} of rainfall are required to trigger speleothem growth in desert caves (Vaks et al., 2010), onset of stalagmite growth reveals that monsoonal rainfall during MIS5e (SAHP 4) was at least twice as high as today. Considering the height and diameter of stalagmite Y99 and contemporaneously deposited speleothems in Hoti Cave in Northern Oman (Fleitmann et al., 2011), ASM and ISM rainfall must have been considerably higher than 300 mm yr^{-1} (Burns et al., 2001). This assumption is also supported by simulated rainfall over Arabia during MIS 5e (Otto-Bliesner, 2006; Herold and Lohmann, 2009; Jennings et al., 2015b; Gierz et al., 2017). Based on the age model for stalagmite Y99, SAHP 4 lasted for ~6.5 ka BP, which is slightly longer than the precisely-dated 4.2 kyr-long Holocene Humid period (SAHP 1; Fleitmann et al., 2007) (Fig. 53).

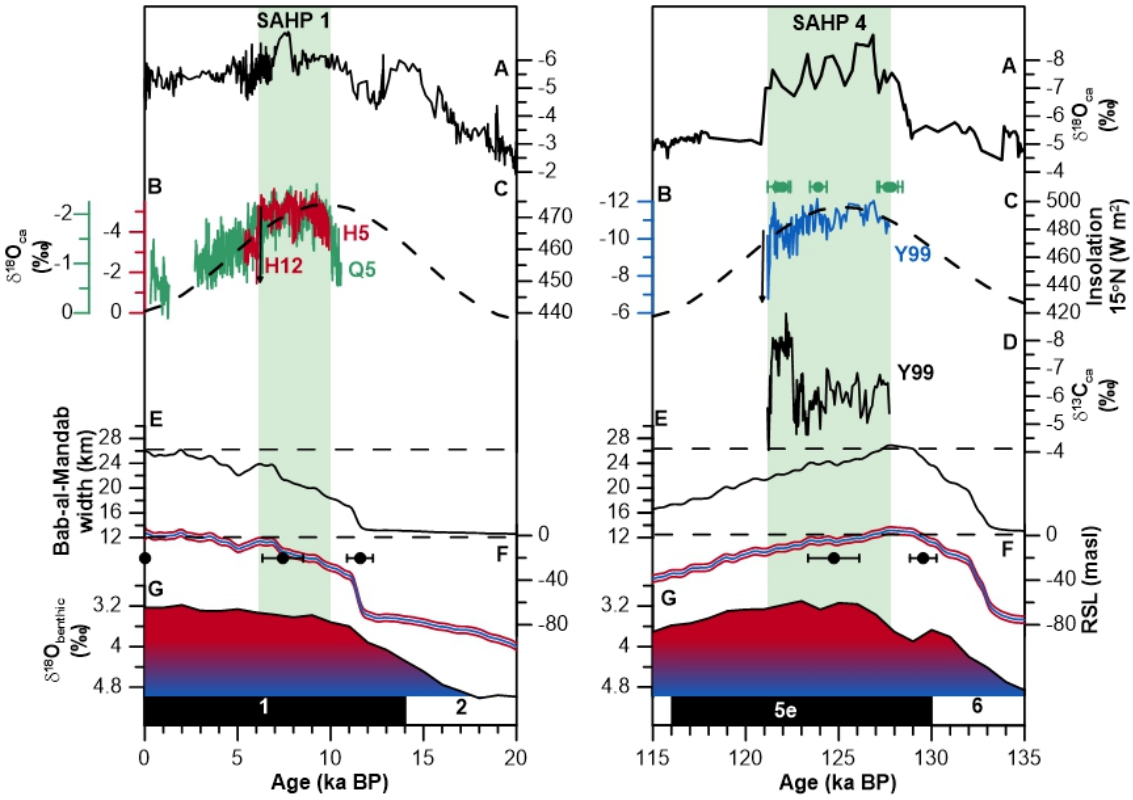

Fig. 53. Comparison of SAHP 1 and 4. (A) Soreq Cave $\delta^{18}O_{ca}$. (B) Holocene (H5, H12 and Q5) and MIS 5e (Y99) stalagmite $\delta^{18}O_{ca}$ records from Qunf Cave (green), Hoti Cave (red) and Mukalla Cave (blue). (C) July insolation (W m_2) at 15°N. (D) stalagmite Y99 $\delta^{13}C_{ca}$. Reconstructed Bab-al-Mandab width (E) using bathymetry data (GEBCO) and (F) the Relative sea-level curve and tie points. (G) global ice-volume (LR04 $\delta^{18}O_{benthic}$) and Marine Isotope Stages. Green bars denote duration of SAHP 1 and 4. Y99 ^{230}Th ages and 2σ uncertainty are given as green dots and bars.

Additional evidences support the timing and duration of SAHP 4. The onset of the MIS 5e growth interval (SAHP 4) of stalagmite Y99 at 127.730 ± 0.400 ka BP is synchronous with the onset of sapropel S5 at ~128.3 ± 2 ka BP (Grant et al., 2017) and negative shifts in speleothem δ18Oca records from Soreq and Peqiin Caves in Israel (Bar-Matthews et al., 2003). In both caves, speleothem $\delta^{18}O_{ca}$ values are influenced by the "source effect"

as $\delta^{18}O$ of (palaeo)precipitation in the Levant is directly linked to $\delta^{18}O$ of surface water in the Eastern Mediterranean. During interglacial periods, increased monsoon precipitation in the Ethiopian Highlands and higher discharge of low-$\delta^{18}O$ freshwater runoff from the Nile and North African wadi systems (Grant et al., 2012) into the Mediterranean lead to more negative $\delta^{18}O$ and sapropel formation (Rohling et al., 2015)..Thus, the sharp decrease in $\delta^{18}O_{ca}$ at ~128.3 ± 1.2 ka BP in the Soreq and Peqiin Cave $\delta^{18}O$ records is caused by an up to ~8 times higher Nile flow (compared to the pre-Aswan period; Amies et al., 2019) during MIS 5e. Taken together, the Soreq and Peqiin Cave records are in line with marked increase in ASM and ISM rainfall at onset of SAHP 4 at 127.730 ± 0.400 ka BP in stalagmite Y99, supporting the accuracy of its chronology. The termination of SAHP 4 at 121.170 ± 0.500 ka BP is also concurrent with the independently derived age estimate for the termination of sapropel S5 at ~121.5 ± 2 ka BP (Grant et al., 2017) and the distinct positive shift in $\delta^{18}O_{ca}$ in the Soreq and Peqiin Cave records (Bar-Matthews et al., 2003). Such a good correspondence between sapropel deposition in the Eastern Mediterranean and the timing of peak humidity in Southern Arabia is also observed for other SAHPs (Nicholson et al., 2020) and the (SAHP 1) between 10.5 and 6.2 ka BP (Fleitmann et al., 2007; Grant et al., 2017).

The timing of SAHP 4 also conforms with significantly higher ASM/ISM rainfall in other - albeit less precisely-dated - monsoon records. In the Gulf of Guinea, lower sea surface salinities (indicative of higher monsoon runoff) (Weldeab et al., 2007) coincide with more negative $\delta D_{leaf\text{-}wax}$ values in sediment core RC09-166 from the Gulf of Aden (Tierney et al., 2017) and high (wet) PC Sahara index values (Grant et al., 2017) (Fig. 54). Additionally, synchronous intensification of the East Asian Monsoon (EAM) is indicated by both a negative shift in stalagmite $\delta 18O_{ca}$ (Sanbao/Hulu/Linzhun) at 129.0

± 0.1 ka BP (Cheng et al., 2009a), as well as ^{10}Be-flux from the Loess Plateau (Beck et al., 2018). Overall, there is excellent agreement between the timing and duration of SAHP 4 and other records from the African and Asian monsoon domains, which suggest a significant increase in ASM and ISM strength between 129 and 127 ka BP.

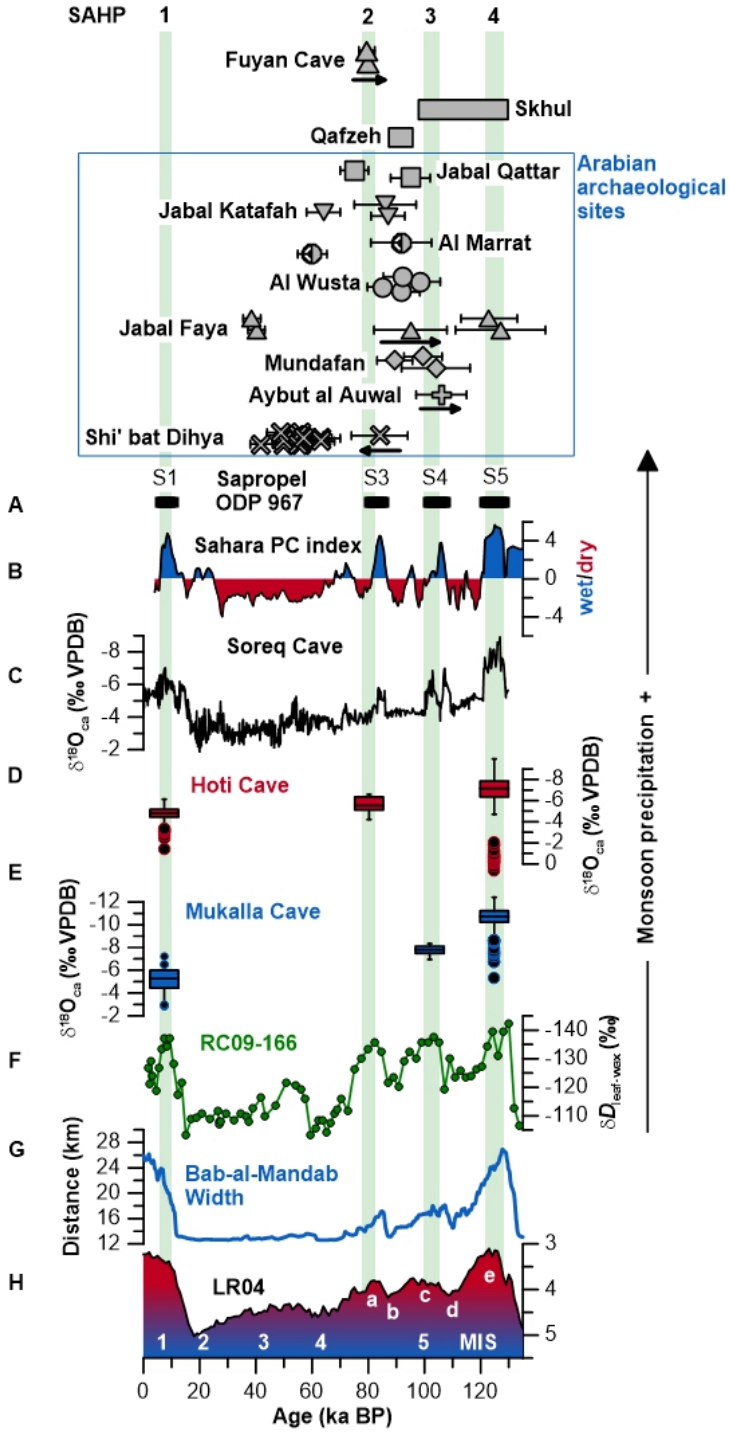

Fig. 54. Archaeological evidence for H. sapiens dispersals compared to the timing of SAHPs (green bars); sapropel layers (A) and Sahara wet/dry PC index (B) of ODP 967; Soreq Cave (C), Hoti Cave (D) and Mukalla Cave (E) stalagmite $\delta^{18}O_{ca}$ boxplots – black dots denote statistically extreme values; Gulf of Aden RC09-166 $\delta D_{leaf\text{-}wax}$ (F); Bab-al-Mandab width (G); and global ice-volume LR04 $\delta^{18}O_{benthic}$ and Marine Isotope Stages (H).

7.3.2 Climatic and environmental conditions during SAHP 4

In addition to the timing and duration of SAHP 4, $\delta^{18}O_{ca}$ and $\delta^{13}C_{ca}$ values provide useful information on the climatic and environmental conditions in southern Arabia and the Bab-al-Mandab Strait during MIS 5e. It has been shown that fluctuations in $\delta^{18}O_{ca}$ from Mukalla Cave speleothems are related to changes in the amount of ASM precipitation (Fleitmann et al., 2011; Nicholson et al., 2020), whereas the source of moisture is confirmed by isotope measurements (δD and $\delta^{18}O$) of stalagmite fluid inclusion water (Nicholson et al., 2020). The $\delta^{18}O_{ca}$ profile of stalagmite Y99 shows three distinct features. Firstly, $\delta^{18}O_{ca}$ values are lowest at onset and during the first phase of SAHP 4, indicating that ASM rainfall increased rapidly at the onset of SAHP 4, most likely within a few centuries and similar to EAM monsoon records (Cheng et al., 2009a). Secondly, ASM rainfall is highest until ~124 ka BP and decreases continuously, following summer insolation. Thirdly, the abrupt positive shift in $\delta^{18}O_{ca}$ at 121.170 ± 0.500 ka BP indicates an abrupt termination of SAHP 4, most likely within a few decades. This is a common feature of SAHPs and related to the geographical position of the cave in relation to the Intertropical Convergence Zone and monsoonal rainfall belt respectively (Fleitmann et al., 2007). The abrupt termination of speleothem growth and positive shift indicates that

the Intertropical Convergence Zone and associated monsoonal rainfall belt were located south of Mukalla Cave. In addition, $\delta^{18}O_{ca}$ values show that monsoon precipitation was substantially higher during MIS 5e (SAHP 4) compared to the Holocene period (SAHP 1). Whereas MIS 5e $\delta^{18}O_{ca}$ values (Y99) ranged from -12.4 to -5.4 ‰, Holocene values (Y97-4 and -5) ranged from -7.2 to -2.4 ‰ (Fleitmann et al., 2011; Nicholson et al., 2020). This isotopic difference is also observed at Hoti Cave (Fleitmann et al., 2011; Nicholson et al., 2020) (Fig. 56D). Similarly, MIS 5e $\delta^{18}O_{ca}$ values from both Mukalla and Hoti Cave are more negative than the averages of subsequent MIS 5c (-7.7‰) and MIS 5a (-5.56‰) SAHPs 3 and 2 respectively. Overall, Y99 $\delta^{18}O_{ca}$ values indicate that MIS 5e saw the most substantial enhancement of monsoon precipitation during the Late Pleistocene.

Stalagmite Y99 $\delta^{13}C_{ca}$ values are influenced by numerous factors, including vegetation type and density, and soil thickness and moisture above the cave (Nicholson et al., 2020). However, the various, and sometimes counteracting, controls means that stalagmite $\delta^{13}C_{ca}$ values can be difficult to interpret and that the principal factors controlling $\delta^{13}C_{ca}$ values may change over time. Y99 $\delta^{13}C_{ca}$ values vary between -4.6 and -9.0 ‰ and thus fall into a mixed C_3/C_4 vegetation signal (Clark and Fritz, 1997), suggesting that grasslands with some woody cover were present above Mukalla Cave during SAHP 4. This is consistent with a body of palaeontological records across Arabia and phytolith records from Jabal Faya (MIS 5e) and Mundafan (MIS 5c), indicating that now arid areas of Arabia were characterised by grasslands and some woody cover during humid phases (Rosenberg et al., 2011, 2013; Bretzke et al., 2013; Groucutt et al., 2015b; Stewart et al., 2020). Similar to the $\delta^{18}O_{ca}$ profile, the termination of stalagmite growth is characterised by an abrupt increase in $\delta^{13}C_{ca}$ as rainfall, drip-rate and vegetation density decreased

abruptly above Mukalla Cave. Overall, the Mukalla Cave $\delta^{13}C_{ca}$ profile indicates that increased rainfall was associated with the formation of herbaceous grasslands, with some woody cover, in the now arid interior of Yemen during MIS 5e.

7.3.3 Phasing between pluvial conditions in Southern Arabia and sea-level change during MIS 5e

Based on the stalagmite Y99 stable isotope records, climatic and environmental conditions in Southern Arabia were favourable for human dispersal along the southern dispersal route. A key-question is therefore whether the width of the Bab-al-Mandab was narrow enough for a successful crossing into Arabia. The absolute and precise age-models for the MIS 5e (SAHP 4) growth interval of stalagmite Y99 allows the comparison of the phasing between monsoonal rainfall and Bab-al-Mandab width (Fig. 53). The width of the Bab-al-Mandab Strait was reconstructed using bathymetry data and the Red Sea relative sea-level (RSL) curve, whereas the chronology of the RSL time series was developed by using the revised-series chronology of the Soreq Cave $\delta^{18}O_{ca}$ record (Grant et al., 2012, 2014). The onset of SAHP 4 at 127.730 ± 0.400 ka BP occurred when global sea-level was already 4.7 ± 3.9 m higher than today and the width of the Bab-al-Mandab Strait was >27 km, similar or even wider than today. Furthermore, at the end of SAHP 4 (121.170 ± 0.500 ka BP), global sea level was only 14.7 ± 3.1 m lower than today, yet the Bab-al-Mandab was ~22 km wide and therefore a major obstacle to the southern dispersal route. The observed phasing between the rise in monsoonal rainfall and sea-level was not unique to MIS 5e, but also repeated during the last deglaciation (Termination I) (Nicholson et al., 2020). The delayed response of the monsoons during

Terminations is related to meltwater influx of disintegrating ice-sheets into the North Atlantic and resultant weakening of the Atlantic Meridional Ocean Circulation (AMOC), which lead to colder northern hemisphere temperatures and thus dampened the effects of rising insolation forcing, thereby suppressing both the ASM/ISM and the EAM (Fleitmann et al., 2003a; Cheng et al., 2009a, 2009b; Häuselmann et al., 2015). Thus, not only did high sea-levels act as a potential barrier to dispersal during MIS 5e, a suppressed ASM/ISM throughout T-II meant that more arid conditions prevailed in Arabia and northeastern Africa when sea-levels were lower than today. This is in stark contrast to recently published models that suggest pluvial conditions prevailed as early as 135 ka BP in association with low sea-levels (Rohling et al., 2013; Beyer et al., 2020).

7.4 Models for *H. sapiens* dispersals across the southern route

With a present-day minimum width of ~27 km, the Bab-al-Mandab would represent a major obstacle for *H. sapiens* dispersals. A common suggestion is that a reduced width of the Strait facilitated a maritime crossing during Termination II (Armitage et al., 2011; Rohling et al., 2013; Bae et al., 2017). However, we have established that the intensification of the monsoon lagged behind sea-level rise during T-II and intensification occurred when the Bab-al-Mandab had reached its Late Pleistocene maximum. This instead suggests that the most optimal period of *H. sapiens* dispersal, from a palaeoclimatic perspective, was between 128-121 ka BP, when increased rainfall transformed Southern Arabia into a grassland biome. The lag between sea-level rise and the onset of pluvial conditions has potentially important implications for understanding both the route of *H. sapiens* dispersals and also the cognitive, behavioural and

technological capacities they possessed. Here, we provide three potential models for human dispersals throughout T-II and SAHP 4.

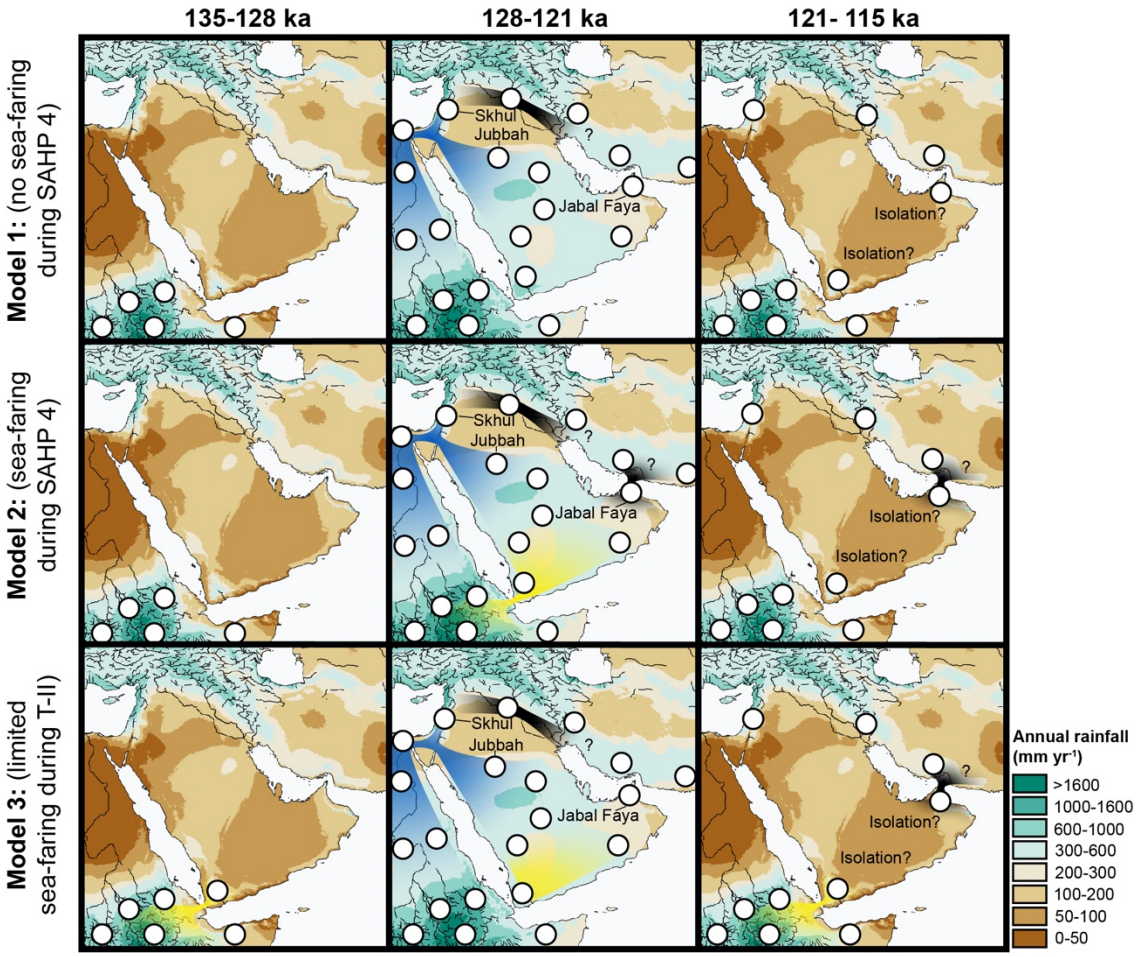

Fig. 55. Conceptual illustration of models for H. sapiens *populations (white circles) dispersals between 135-121 ka BP over northern (blue) and southern (yellow) routes. Subsequent dispersal routes via the Euphrates and Gulf of Hormuz are marked in black. Rainfall maps include simulations for MIS 5e (Otto-Bliesner, 2006) and the present-day (Fick and Hijmans, 2017) and are tuned to the chronology of Y99. All three models assume that the Sinai Peninsula (northern route) was also a likely entry point into Arabia (supported by archaeological assemblages from NE Africa, the Levant and northern Arabia).*

1) *H. sapiens* dispersed via a land-route between 128-121 ka BP. The sea-faring capabilities of *H. sapiens* prior to 70-60 ka BP are unknown (Norman et al., 2018); watercraft evidence is absent from the East African and Arabian coasts during the Late Pleistocene and high sea-levels could have acted as a barrier to alternative methods (e.g., swimming). Additionally, the earliest evidence of sea-faring is almost 70-60 kyrs later from the archipelagos of SE Asia (Norman et al., 2018), which were perhaps a more conducive environment for their development (Groucutt et al., 2015a). Thus, maritime dispersal via the Bab-al-Mandab was unlikely and dispersal was instead facilitated by crossing the green Sahara, the Sinai Peninsula and following palaeohydrological corridors into Arabia (Breeze et al., 2016) and the Levant (Shea, 2008) (Fig. 55). This model is supported by the archaeological assemblages from northeast Africa, the Nafud Desert and the Levant; these show a degree of techno-cultural similarities and suggest cultural exchange between these regions (Petraglia et al., 2012; Groucutt et al., 2019).

2) Conversely, Maritime dispersal across the Bab-al-Mandab occurred during the high sea-level period between 128-121 ka BP. Absence of relevant sea-faring technologies may be a reflection of difficult preservation conditions, but crossings of the Strait at/near its widest would have significant cognitive requirements. If sea-faring had developed, the abundant freshwater and vegetation resources at the Horn of Africa and Arabia could have stimulated successful maritime crossings and subsequent population expansions across Arabia (Fig. 55). However, archaeological support for demographic links between both sides of the Strait is unclear due to the ambiguous and heterogenous nature of stone tool assemblages from Southern Arabia at this time.

3) Maritime dispersal occurred during T-II: in this scenario, limited *H. sapiens* dispersal into Southern Arabia was aided by lower sea-levels and the reduced width of the Bab-al-Mandab Strait. These conditions might have supported less complex sea-faring or rafting compared to model 2, but also implies the development of such technologies sometime before 127 ka BP (Armitage et al., 2011; Rohling et al., 2013). However, it is possible that intermittent lower sea-levels throughout the Late Pleistocene facilitated the crossing of the Hamadryas baboon, Papio hamadryas (Kopp et al., 2014), which did not possess sea-faring capabilities such as rafting. Thus, it is not inconceivable that other fauna (including *H. sapiens*) could cross by swimming (Rohling et al., 2013). Additionally, this model suggests that H. sapiens may have been rather tolerant of arid conditions, or perhaps exploited coastal environments (Bailey et al., 2015) and/or productive microenvironments (Erlandson and Braje, 2015) in Southern Arabia. Nonetheless, we emphasise that population expansion into the inland areas of Arabia was likely restricted to the onset of pluvial conditions, when increased monsoonal rainfall transformed the desert into a mosaic of productive fluvio-lacustrine and grassland habitats (Armitage et al., 2011; Erlandson and Braje, 2015).

Overall, phase-lag between monsoon precipitation and sea-level rise highlights that, for a widespread southern dispersal into green Arabia to be successful during SAHP 4, *H. sapiens* required sea-faring capabilities, while a dispersal during T-II would have required both sea-faring and adaptive flexibility. Understanding the environmental tolerances and sea-faring capabilities of early Late Pleistocene *H. sapiens* must therefore be a key target for future research. However, we highlight that archaeological assemblages from NE Africa, the Levant and northern Arabia indicate the Sinai Peninsula (northern route) was a frequently used entry point into Arabia (Breeze et al., 2016).

Whether crossing the Bab-al-Mandab Strait was an additional route will require further archaeological investigation of coastal settings (e.g., Bailey et al., 2015) to establish clear demographic links between both sides of the Strait.

7.5 Conclusion

We have provided a new precisely dated high-resolution MIS 5e stalagmite palaeoclimate record from Mukalla Cave, Yemen. Our results indicate that the onset of increased rainfall occurred at 127.7 ka BP, after maximum deglaciation and sea-level rise. Whereas aridity prevailed throughout T-II when sea-levels were low, the Bab-al-Mandab was at its greatest width at the onset of SAHP 4. The validity of the southern dispersal route hypothesis is therefore dependent on evidence of sea-faring prior to and during MIS 5e, which is currently absent between Africa and SE Asia, and/or flexible environmental tolerances. Conversely, the northern route into Arabia was a viable route throughout SAHP 4. Our findings have pertinent impacts for understanding (1) the timings and geographies of *H. sapiens* dispersals, and (2) the potential behavioural and technological capabilities of *H. sapiens* at the onset of the Late Pleistocene.

Acknowledgments

This work was supported by the AHRC South, West and Wales Doctoral Training Partnership (Grant AH/L503939/1) the Swiss National Science Foundation (Grant PP002-110554/1to DF).

Chapter 8

8) Beyond arrows on map: the dynamics of *Homo sapiens* occupation of Arabia and dispersal during Marine Isotope Stage 5

This chapter is a modified version of a manuscript submitted to the *Journal of Anthropological Archaeology*. This chapter does not explicitly address the research questions posed in chapter 1; however, we provide a discussion of what current palaeoclimatological (including findings from this thesis) and archaeological data may inform about dispersal models. The rationale for this chapter is that *H. sapiens* dispersals – typically during MIS 5 – are frequently portrayed as simplistic arrows on a map between Arica and Eurasia. While these are useful for understanding broadscale changes in distribution, they obscure nuanced understanding of the processes of dispersal and occupation of new habitats, such as Arabia. We go beyond this approach and synthesise palaeoclimatological, archaeological and some ethnographic data to provide a more holistic understanding of the processes of Arabia occupation during MIS 5 "wet" periods. This chapter has been submitted as a research paper to *Current Anthropology* with the following citation:

Nicholson, S.L., Hosfield, R., Groucutt, H.S., Pike, A.W.G., Fleitmann, D. The palaeoclimatic conditions of the "southern route" out-of-Africa.

The author contributions are as follows: S.L.N acted as primary author for the paper with the guidance of D.F., R.H., A.W.G.P and H.S.G.. S.L.N. combined ethnographic reviews

(produced by H.S.G.) with additional ethnographic evidence and reviews of palaeoclimate, archaeological and biological literature.

Submitted to Journal of Anthropological Archaeology: 11th September 2020

Abstract

Arabia occupies a crucial central position between Africa and Eurasia. The northward expansion of the monsoonal rain-belt and the formation of grasslands during Marine Isotope Stage (MIS) 5 provided favourable conditions for *H. sapiens* to occupy and traverse now arid areas of Arabia. While Green Arabia was a crucial stepping-stone on the way to *H. sapiens* global settlement, the occupation of Arabia is an important area of study in itself and could offer vital perspectives into human-environment interactions. In particular, Green Arabia can offer a unique insight into processes of human dispersal, occupation and extirpation in an environmentally fluctuating landscape. Here we synthesise archaeological, palaeoclimate and ethnographic data to develop a holistic model for the occupation of Green Arabia and offer targets for future research. We suggest that, on broad timescales, the resource availability and carrying capacity of Green Arabia facilitated rapid population expansion and occupation across Arabia. On human time-scales, dispersal was probably a slow process due to the requirements of metapopulation structures, likely consisting of many "micro-dispersals" spanning numerous generations. Transitions to more arid conditions were probably echoed by local hominin extirpations, dispersals into surrounding regions and retraction to resource-retaining core areas.

8.1 Introduction

Homo sapiens occupation of Arabia during MIS 5 is becoming an important topic in the debate of human dispersals from Africa. Until recently, it was considered that MIS 5 *H. sapiens* dispersals were restricted to the East Mediterranean Levant; with "successful" expansions into broader Eurasia only occurring ~65-50 ka (Mellars, 2006a; Shea, 2008; Klein, 2009; Mellars et al., 2013). However, mounting evidence shows that dispersals during MIS 5 may have had a longer-term impact on human distribution than previously considered (Rabett, 2018). These dispersals were probably facilitated by substantial increases of rainfall, abundant freshwater resources and grassland environments in Saharo-Arabia during MIS 5 interstadials (MIS 5e: 130-116 ka, 5c: 104-97 ka and 5a: 84-71 ka) (Fleitmann et al., 2011; Rosenberg et al., 2011, 2012, 2013; Matter et al., 2015; Groucutt et al., 2018; Nicholson et al., 2020).

The role of Arabian environments is crucial for exploring dispersal models, given their position between sub-Saharan Africa and Eurasia (Fig. 56). Yet, owing to the early stages of research in the area, there has been a tendency to view Arabia as part of a network of prehistoric highways to the rest of Eurasia (Armitage et al., 2011; Rosenberg et al., 2011; Bae et al., 2017; Tierney et al., 2017). While useful when discussing broad changes in human distribution, this 'arrows on maps' approach obscures nuanced discussions of how *H. sapiens* dispersed, traversed and occupied landscapes on "human" timescales. Such approaches can also obscure the specific local ecological and environmental characteristics that are critical in understanding introduction, occupation and extirpation.

To stimulate new discussions, we combine palaeoenvironmental, archaeological and ethnographic data to provide new insights into human-environment interactions within Green Arabia. The aim of this paper is to review the current state of knowledge and also, and more importantly, develop a nuanced perspective and a new model for *H. sapiens* dispersal and occupation of Arabia. While the examples given are focussed towards Arabia, such discussions may be useful for understanding dispersal at broader geographical scales and in other landscape settings. In a similar fashion to White (2006) and Hosfield (2016), this paper is speculative and aims to stimulate new questions and targets for future research.

8.2 Arabian Climate and Palaeoclimate

8.2.1 Current climates and environments of Arabia

The current climates of Arabia are governed by two major weather systems: the Mediterranean frontal system in winter (December, January and February) and the African/Indian Summer Monsoon in summer (June, July and August). Precipitation over much of the peninsula measures <200 mm yr^{-1}, delivered in winter by the Winter Mediterranean Cyclonic system (WMCs). The African and Indian Summer Monsoons currently only penetrate the southernmost tips of Yemen and Oman, following the annual migration of the Inter-Tropical Convergence Zone (ITCZ) (Glennie and Singhvi, 2002; Weyhenmeyer et al., 2002). Annual precipitation is greatest in the highlands of Yemen, where rainfall may reach over 500 mm yr^{-1}. Temperatures across the Peninsula may reach in excess of 40^{o}C during summer and can fall below freezing in winter. Evaporation over much of the peninsula is close to or greater than annual precipitation. The resultant low

effective moisture (precipitation – evaporation) means that vegetation across most of the peninsula is sparsely distributed. The densest and most diverse vegetation occurs within the highlands of Yemen, Hajar, Dhofar and northern Oman, focussed around streams, valleys and the south facing slopes prone to occasional mists (Miller and Cope, 1996). However, localised rains that penetrate deep into the soils are echoed by opportunistic vegetation blooms, even in the sandy deserts. Standing waterbodies and perennial rivers are not common and usually small in size. Localised rains and low carrying capacity of sands often allow the formation of interdunal ephemeral closed lakes and streams within the endoreic basins of Arabia. These means that, while indeed there are often water sources available, they are frequently scattered and spatially variable (e.g., Petraglia et al., 2020).

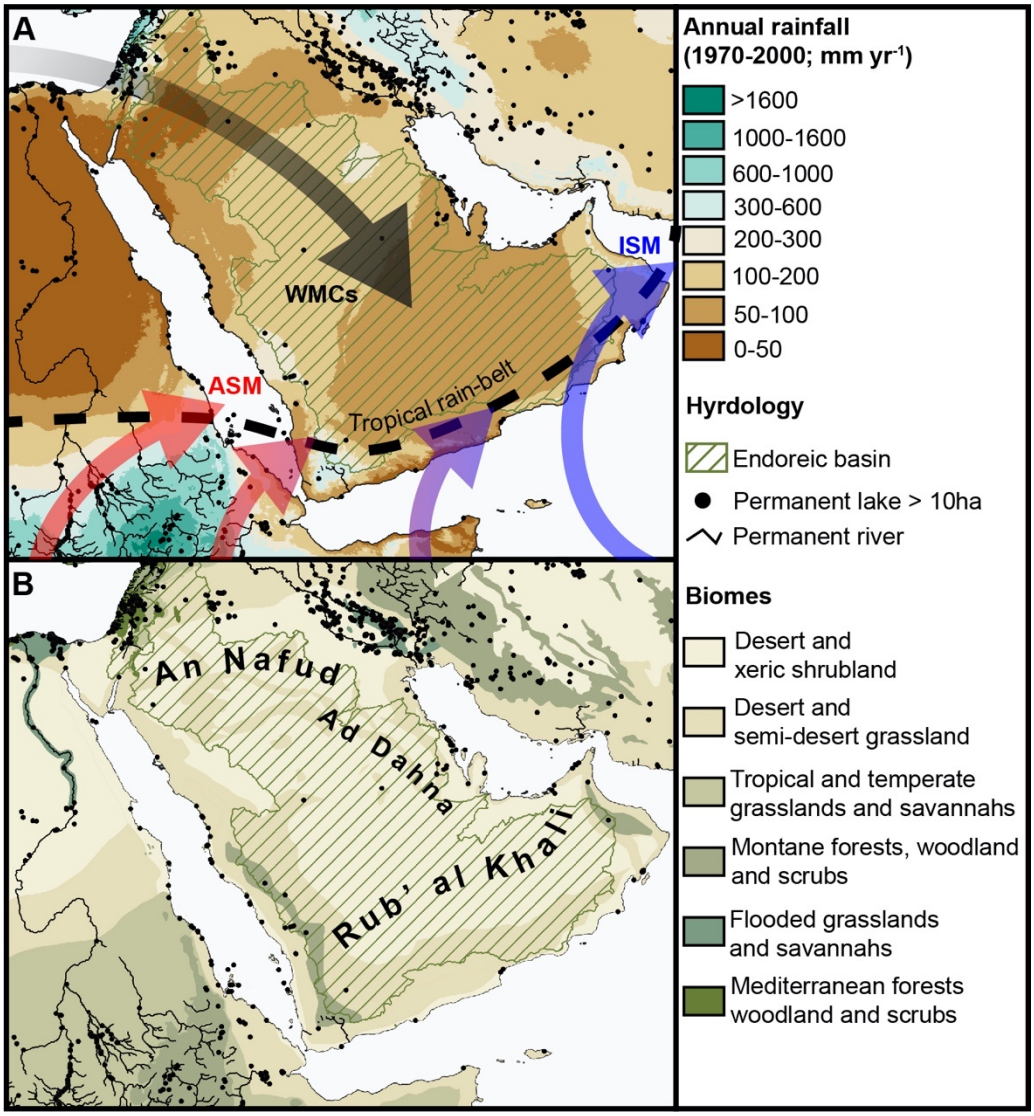

Fig. 56. (A) modern annual precipitation (1970-2000; Fick and Hijmans, 2017) map of Arabia showing permanent lakes (>10 ha; black circles: HYRDOlakes dataset), permanent rivers (HYDROlakes dataset), endoreic basins (HYDROsheds) and major weather systems. Hydrological data available at AQUASTAT. (B) map of terrestrial biomes (data available from WWF. Adapted using Miller and Cope, 1996), including rivers, lakes and endoreic basins.

8.2.2 Palaeoclimate and environments of Arabia during MIS 5 "wet" periods

Substantial increases of precipitation across the Saharo-Arabian deserts occurred during MIS 5e (~128 to 121 ka BP), 5c (~104 to 97 ka BP) and 5a (~82 to 77 ka BP). Recent analysis of speleothem fluid inclusion $\delta^{18}O$ and δD from Yemen and Oman indicate that enhanced precipitation was delivered by the ASM and ISM (Nicholson et al., 2020). Substantial enhancements of the intensity and spatial extent of the monsoonal rain-belt were a result of increased low-latitude insolation and reduced glacial-boundary conditions (Fleitmann et al., 2011; Rosenberg et al., 2013; Nicholson et al., 2020). Speleothem growth at Mukalla and Hoti Cave is coherent with the formation of Mediterranean sapropels S5 (128.3 – 121.5 ka BP), S4 (107.8 – 101.8 ka BP) and S3 (85.8 – 80.8 ka BP) and negative shifts in Soreq Cave $\delta^{18}O_{ca}$. These respond to increased precipitation in the Ethiopian Highlands and the "source effect", caused by discharge of low-$\delta^{18}O$ monsoon-driven freshwater runoff from the Nile, respectively (Bar-Matthews et al., 2003; Grant et al., 2017). Further correspondence is observed with marine sediment cores from the Gulf of Aden (RC09-166 and KL-15), the Red Sea (KL-11) and the Mediterranean (ODP 967); all records show substantial changes of Saharo-Arabian continental wetness (Fig. 57), effecting surface runoff, soil humidity (grain-sizes) and precipitation amount ($\delta D_{leaf\text{-}wax}$). While, some palaeolake deposits and alluvial records do have ages that overlap interstadial and stadial periods (e.g., Al Wusta; Groucutt et al.. 2018), the intervening periods of MIS 5d and 5b are generally characterised by a return to more arid conditions (Fleitmann et al., 2011; Grant et al., 2017; Nicholson et al., 2020).

The ASM and ISM increased annual precipitation to 600-300 mm yr^{-1} over much of Arabia (Otto-Bliesner, 2006; Fleitmann et al., 2011; Jennings et al., 2015b). The monsoon rain-belt reached as far north as the Nafud Desert, as determined by palaeolake activation

and climatic modelling (Waldmann et al., 2010; Rosenberg et al., 2013; Jennings et al., 2015b), and perhaps contributed to the catchment of palaeolake Mudawwara at 29°N during MIS 5e (Petit-Maire et al., 2010). Precipitation was lowest in the northern areas of Arabia, receiving annual rainfall of 300-200 mm yr^{-1} and in some places even less (Jennings et al., 2015b). This resulted in a distinct meridional precipitation gradient across Arabia. Similarly, a zonal precipitation gradient was caused by the incursion of the ASM into western Arabia (Rosenberg et al., 2013; Gierz et al., 2017; Nicholson et al., 2020). In combination with the aforementioned fluid inclusion $\delta^{18}O$ and δD values, sub-annual stalagmite $\delta^{18}O_{ca}$ and $\delta^{13}C_{ca}$ cycles (H13; Hoti Cave) indicate a shift to a summer-dominated precipitation regime. However, winter rains continued to deliver additional precipitation over Arabia (Gierz et al., 2017) and were enhanced in the Levant (Vaks et al., 2010). The dominance of summer rainfall across Arabia led to a distinct "wetter" summer and "drier" winter seasonality (Gierz et al., 2017; Nicholson et al., 2020). As well as increased summer precipitation, increased cloud cover of the monsoon system resulted in reduced evaporation (Herold and Lohmann, 2009) and led to increased effective moisture during the summer. The Dhofar region of Oman – which is prone to increased cloud cover, misting and vegetation blooms in the summer monsoon months, despite rainfall remaining low – is frequently used as an analogue for periods of enhanced precipitation (e.g., Rose et al. 2019).

It is important to note that there were variations in the duration and intensity of different wet periods. Speleothem $\delta^{18}O_{ca}$ (Mukalla and Hoti caves; Nicholson et al. 2020), marine sediment core $\delta D_{leaf\text{-}wax}$ (RC09-166; Tierney, deMenocal, and Zander 2017) and grainsize data (KL-15 and KL-11; Fleitmann 1997) indicate that MIS 5e saw the longest and most intense increase in precipitation. The ASM was intensified for ~6.8 kyrs as indicated by

the deposition of sapropel S5 (Grant et al. 2017) and Nile outflow was 8.8 times higher than today (Amies et al., 2019). While MIS 5c and 5a lasted for similar periods of ~6 and 5 kyrs respectively, they were reflected by more positive (i.e., reduced rainfall) $\delta^{18}O_{ca}$ and $\delta D_{leaf\text{-}wax}$ compared to MIS 5e. To place these MIS 5 sub-stages in context, speleothem $\delta^{18}O_{ca}$ from all Late Pleistocene wet periods were more negative (i.e. increased rainfall) than the Holocene Humid Period (HHP), in which increased rainfall supported human occupation in the now arid interiors of the Sahara and Arabia (Kuper and Kropelin, 2015; Petraglia et al., 2020). What these Late Pleistocene differences translated to in terms of annual precipitation and environmental response across Arabia is currently difficult to estimate.

Extensive surveys and GIS analyses of the Arabian Peninsula have shown that increased precipitation activated widespread palaeolake and river systems (Breeze et al., 2015). In southern Arabia (Tab. 5), this is exemplified by palaeolakes Mundafan, Khujaymah and Saiwan (Rosenberg et al., 2011, 2012; Groucutt et al., 2015d), further lakes and sabkhas in the central Rub' al Khali (Matter et al., 2015) and alluvial/fluvial deposits in the UAE (Parton et al., 2015a). Southern Arabian palaeolakes typically contain the ostracod *Darwinula stevensoni* and the mollusc *Unio* sp.; both show that fresh, open running water conditions persisted and diverse lacustrine flora and fauna communities were present (Rosenberg et al., 2011, 2012; Matter et al., 2015). In addition, the presence of *D. stevensoni* shows these lakes were perennial, retaining freshwater during dry seasons (Rosenberg et al., 2011, 2012). Phytolith data from Mundafan shows that grasslands, with some woody cover, were present in the nearby vicinity (Groucutt et al., 2015d).

Lake basin	*Site/core*	*Method*	*Age*	*MIS*	*Note*	*Ref*
Mundafan (Saudi Arabia)	C	TT-OSL (sands underlying lake marls)	101 ± 6 ka	MIS 5c		Rosenberg et al. (2011)
Mundafan (Saudi Arabia)	MDF-61	OSL	104.0 ± 12.2, 89.4 ± 6.3 and 99.5 ± 6.8 ka	MIS 5c		Groucutt et al. (2015d)
Khujaymah (Saudi Arabia)	B	TT-OSL (sands underlying lake marl)	Top: 136 ± 14 ka Bottom: 120 ± 10 ka	MIS 5e	Punctuated lake/sand deposits between ages	Rosenberg et al. (2011)
Khujaymah (Saudi Arabia)	D	TT-OSL (sands underlying lake marl)	99 ± 11, 96 ± 8 and 88 ± 6 ka	MIS 5c/a		Rosenberg et al. (2011)
Saiwan (Oman)	11.2	TT-OSL	108 ± 8 ka	MIS 5c		Rosenberg et al. (2012)
Saiwan (Oman)	13.6	TT-OSL	125 ± 9 ka	MIS 5e		Rosenberg et al. (2012)
Saiwan (Oman)	11.3	TT-OSL	102 ± 9 ka	MIS 5c		Rosenberg et al. (2012)
Saiwan (Oman)	11.4	TT-OSL	119 ± 14 ka	MIS 5e		Rosenberg et al. (2012)
Saiwan (Oman)	12.1	TT-OSL	Top: 102 ± 8 ka	MIS 5c		Rosenberg et al. (2012)

			Bottom: 114 ± 9 ka			
Saiwan (Oman)	12.8	TT-OSL	97 ± 12 ka	MIS 5c		Rosenberg et al. (2012)
Rub' al Khali (Saudi Arabia)	14.3	OSL	122 ± 6, 111 ± 9 and 118 ± 10 ka	MIS 5e		Matter et al. (2015)
Rub' al Khali (Saudi Arabia)	15.1	OSL (aeolian sands underlying limestone)	107 ± 13 ka	MIS 5c		Matter et al. (2015)
Rub' al Khali (Saudi Arabia)	15.3	OSL (aeolian sands underlying gypsums)	96 ± 6 ka	MIS 5c/a		Matter et al. (2015)
Rub' al Khali (Oman)	b18.1	TT-OSL	Top: 115 ± 5 ka Bottom: 82 ± 4 ka	MIS 5c/a	Sabkha	Matter et al. (2015)
Al Sibetah (UAE)		OSL	Phase IX: 88 ± 7.8 ka Phase VII: 130 ± 6.4 ka	MIS 5e, 5c and 5a	Three phases of stream activation + grassland development between 130-88 ka considered to represent MIS 5e, 5c and 5a	Parton et al. (2015)

Tab. 5 . Ages of palaeolake formations in southern Arabia.

In northern Arabia, extensive studies of the Jubbah basin have been crucial to characterising local environmental shifts in response to climate changes. Lake formation in the Jubbah basin was activated during MIS 5 (Parton et al. 2018; Tab. 6) with smaller interdunal lakes close by (Rosenberg et al., 2013). Despite a seasonal precipitation regime (Nicholson et al., 2020), rainfall was sufficient to sustain perennial freshwater lakes and riverine systems with diverse flora and fauna communities (Rosenberg et al., 2011, 2012; Breeze et al., 2015; Matter et al., 2015; Parton et al., 2018). Colder temperatures in winter months would have been echoed by reduced evaporation, perhaps aiding the perennial character of these waterbodies. Minor winter rainfall also likely contributed to maintaining year-round standing waterbodies, but most recharge would have occurred in the summer months (Rosenberg et al., 2013). Additional deep lakes in northern Arabia include Al Wusta, B'ir Hayzan and Khall Amayshan; their diatom and palaeontological records indicate environments and climates typically reflecting those of Jubbah (Rosenberg et al. 2013; Stewart et al. 2020). GIS mapping has identified further large lake basins within 100 km of Jubbah (Breeze et al., 2015, 2017) and that wetlands and lakes were probably more numerous in the western Nafud than elsewhere in northern Arabia (Breeze et al., 2017).

Lake basin	*Site/core*	*Method*	*Age*	*MIS*	*Note*	*Ref*
Jubbah (Saudi Arabia)	JB1 (zone III and IV)	OSL	<135.8 ± 23.9 and >73.4 ± 6.8 ka	MIS 5e (zone III) and MIS 5a (zone IV)		Parton et al. (2018)

Jubbah (Saudi Arabia)	JB3 (zone III)	OSL	75.3 ± 8.1 ka	MIS 5a	Age reversal (100.5 ± 20.5 ka) above considered to fall within MIS 5a.	Parton et al. (2018)
Jubbah (Saudi Arabia)	JQ1	OSL	Calcrete: 75 ± 5 ka Palaeosol: 95 ± 7 ka	MIS 5a and MIS 5c		Petraglia et al. (2011)
Khall Amayshan (Saudi Arabia)	16.4	TT-OSL (sands overlying and underlying lake diatomites)	Top: 117 ± 8 ka In lake: Bottom: 99 ± 7 ka	MIS 5e-c		Rosenberg et al. (2013)
Nafud (interdunal). Close to Khall Amayshan. (Saudi Arabia)	16.3	TT-OSL (sands underlying lake diatomites).	99 ± 7 ka	MIS 5c-a	Interdunal palaeolake	Rosenberg et al. (2013)
Nafud (interdunal). Close to Bi'r al Hayzan. (Saudi Arabia)	16.5	TT-OSL (sands overlying and underlying lake diatomites).	Top: 128 ± 9 ka Bottom: 125 ± 10 ka	MIS 5e	Interdunal palaeolake	Rosenberg et al. (2013)
Nafud (interdunal). Close to Bi'r al Hayzan. (Saudi Arabia)	17.3	TT-OSL (sands underlying lake diatomites).	99 ± 7 ka	MIS 5c-a	Interdunal palaeolake	Rosenberg et al. (2013)

Nafud (interdunal). Close to Jubbah. (Saudi Arabia)	14.3	TT-OSL (sands overlying and underlying lake diatomites).	Top: 19 ± 1 ka Bottom: 122 ± 10 ka	MIS 5e	Interdunal palaeolake	Rosenberg et al. (2013)
Nafud (interdunal). Close to Jubbah. (Saudi Arabia)	13.2	TT-OSL (sands underlying lake diatomites).	109 ± 8 ka	MIS 5c	Interdunal palaeolake.	Rosenberg et al. (2013)
Al Wusta (Saudi Arabia).		OSL (sands overlying and underlying lake diatomite). U-Series/ESR (palaeontological remains).	Top: 98.6 ± 7 ka Bottom: 85.3 ± 5.6, 92.0 ± 6.3 and 92.2 ± 6.8 ka AW1 (U-series): 87.6 ± 2.5 ka WU1601 (enamel U-series): 83.5 ± 8.1 ka WU1601 (combined U-series ESR): 103 +10/-9 ka	MIS late 5c/early 5a.	Bayesian model assigned suggests underlying sands (unit 1) were stabilised at 93.1 ± 2.6ka and unit 2 and 3 were deposited between 92.2 ± 2.6 ka and 90.4 ± 3.9 ka.	Groucutt et al. (2018)

Mudawwara (Jordan).	U-series (mollusc carbonate)	125 ± 5 121 ± 9 124 +10/-9 116 +5.5/-5.2 95.4 +3.2/-3/1 91.1 +3.4/-3.3 135 ± 6 88 ± 5 77 ± 8	MIS 5e and 5c/a	Petit-Maire et al. (2010)

Tab. 6. Ages of palaeolake activation in northern Arabia.

While palaeolakes have been (and will continue to be) vital to characterising the environments of Green Arabia, improved dating must be a target for future research. OSL dating of palaeolake sediments is particularly difficult, as environmental dose rates are difficult to estimate for the past, particularly in such dynamic environments (Clark-Balzan et al., 2017). Underlying sands are often dated as they consist of aeolian material theoretically good for OSL dating, and it can be argued that they would have become stabilised by the increased rainfall that led to lake formation shortly afterwards. While in some cases this is true (Groucutt et al., 2018), it is possible for lake deposition to occur on top of much older sands. Furthermore, compared to other records (such as speleothems), dating of palaeolakes suffers from considerable age uncertainties (often in

excess of 10%) and are often wiggle-matched to speleothem ages (e.g., Rosenberg et al., 2013). Thus, unlike speleothem records (e.g., Nicholson et al., 2020), it is very difficult to construct precise palaeoclimate records from lake sequences. The challenges include identifying major hiatuses and seasonal differences in precipitation, assessing whether lakes were diachronic, or assigning lakes to specific MISs and their substages. While Bayesian approaches can be used to mitigate uncertainties (e.g., Groucutt et al., 2018), their applicability can be limited by small sample sizes with sometimes significant inversions, which could provide artificial and misleading ages.

Nevertheless, the presence of perennial waterbodies supported large faunal communities across Arabia. Excavations at Al Wusta (late MIS 5) have yielded remains of *Hippopotamus*, *Kobus*, *Pelorovis* and *H. sapiens*, as well as ostrich eggshells (Groucutt et al., 2018). Large tooth marks on the fossils also indicate a diverse carnivore guild was present (Groucutt et al., 2018). Similar taxa have been identified at the nearby site of Khall Amayshan (117 ± 8 ka: Rosenberg et al. 2013) including, Elephantidae, Hippopotamidae, ostrich eggshell, Equidae, Bovidae and Hippotraginae (M. Stewart et al., 2020). The palaeontological records of southern Arabia match this pattern: Alcelaphinae, Bovinae, *Arabitragus jayakari*, Cervidae and Equidae have been uncovered from Late Pleistocene deposits in the Rub' Al Khali (McClure, 1984; Stewart et al., 2019b). While many of these deposits were originally dated to MIS 3, they have since been re-dated to MIS 5 (Rosenberg et al., 2011, 2012). These taxa demonstrate that temperate to semi-arid grasslands were located near to perennial waterbodies, with sufficient vegetation resources to support communities of large herbivores.

Increased effective moisture and soil humidity suggest that vegetation density was enhanced across the Saharo-Arabian deserts during MIS 5. In Arabia, grasslands were present both in close proximity to lakes (Groucutt et al., 2015c, 2018) and elsewhere (Bretzke et al., 2013; Nicholson et al., 2020). Phytolith analysis of sediments recovered from MIS 5e archaeological contexts (assemblage C) of Jebal Faya, UAE, included Pooids, Panicoids, Chloridoids and long grasses. Cyperaceae, Asteraceae, Palmae and other grasses were also present within assemblage C in small quantities – evincing mixed C_3/C_4 grassland (Bretzke et al., 2013). Speleothem growth at both Mukalla and Hoti Cave indicate that effective moisture and soil humidity were much greater in MIS 5e, and soils had formed in the now desert areas of Yemen. Calcite carbon isotope ratios ($\delta^{13}C_{ca}$) at Mukalla Cave (-8 to -2‰) fall within C_3/C_4 grassland signatures (Nicholson et al., 2020). However, there remain three key uncertainties: 1) Speleothem $\delta^{13}C_{ca}$ and phytolith analyses cannot identify species-level floral compositions. 2) Environmental records are sparsely distributed; meaning the majority of the "green" transformation of the Arabian landmass is based on interpolation or analogues with the Sahara (e.g., Larrasoaña et al., 2013). This interpretation is complicated by the archaeological and palaeontological records of northern Africa (where predicted precipitation matched northern Arabia); both records suggest a model of semi-isolated populations and show that some areas remained arid or semi-arid (Scerri et al., 2014b). And, 3) there is little knowledge of spatio-temporal environmental variability and seasonal differences in vegetation, which may have influenced seasonal survival strategies. Annual $\delta^{13}C_{ca}$ cycles of stalagmite H13 (Hoti Cave) indicate seasonal differences in drip-rate as a result of a drying of the aquifer and reduced soil moisture, which was likely echoed by a vegetation response. But there are no direct examples of seasonal vegetation variability. Understanding environmental responses to seasonal precipitation must be a target for future research.

Another issue to consider is that our discussions of Arabian environments and their suitability for dispersal have typically been limited to climate and vegetation feedback (Erlandson and Braje, 2015; Nicholson et al., 2020). Groucutt (2020b) has recently stressed the importance of other factors – with an emphasis on volcanism – on shaping both the environment and topography of Arabia. For example, while eruptions can often have negative short-term effects (contamination of water, deterioration of patch quality), there are also long-term positives, such as creating particularly fertile areas. Eruptions were fairly common throughout MIS 5, with notably high frequencies during early (~130 ka BP) and late MIS 5 (~90-80 ka BP) (Groucutt, 2020a). While the impact of these on humans in Arabia is not understood, it certainly raises questions concerning the stochastic nature of environments, the impact on human populations within "green" phases, as well as human adaption, resilience and/or localised extirpations.

In summary, pronounced shifts of Arabian environments during MIS 5 were primarily influenced by expansions and contractions of the monsoon domain on orbital cycles. These were met by expansion of grassland environments and allowed *H. sapiens* to expand into the now arid interiors. However, there remain many uncertainties and key questions for the future. For example, were lakes diachronic, or, similar to today, was there high variability in their availability? In the Arabian interior, what were environments like beyond riparian zones? How heterogenous was the landscape – both spatially and throughout the duration of these green periods – and what sort of microenvironments were present? Did other topographic features play a role in shaping the environments available to humans? All-encompassing studies of environmental and

topographic heterogeneity will be of key importance for moving beyond simplistic narratives of *H. sapiens* dispersals and occupations of Arabia.

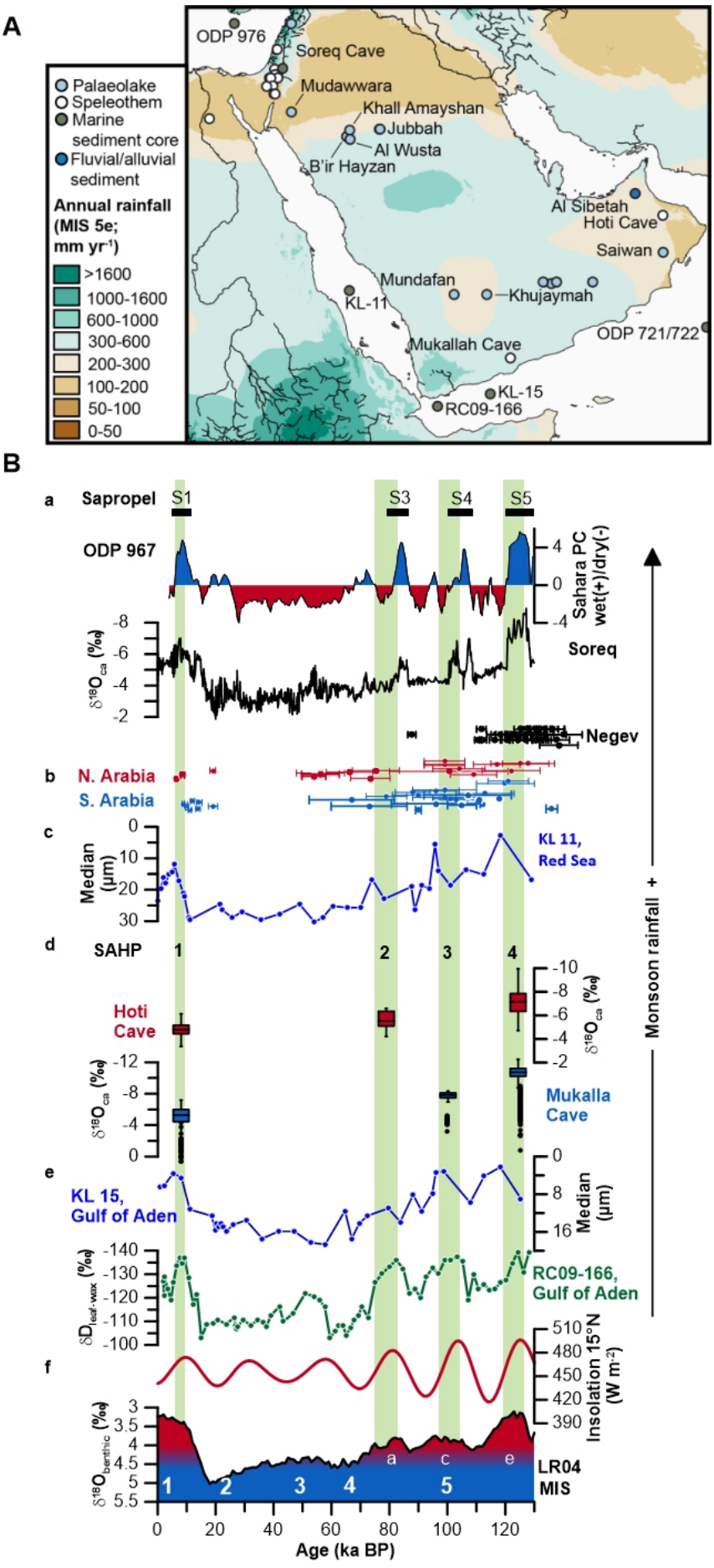
A
ODP 976
Soreq Cave
Mudawwara
Khall Amayshan
Jubbah
Al Wusta
B'ir Hayzan
Al Sibetah
Hoti Cave
Saiwan
Mundafan
Khujaymah
KL-11
Mukallah Cave
ODP 721/722
KL-15
RC09-166
Palaeolake
Speleothem
Marine sediment core
Fluvial/alluvial sediment
Annual rainfall (MIS 5e; mm yr-1)
>1600
1000-1600
600-1000
300-600
200-300
100-200
50-100
0-50
B
a Sapropel S1 S3 S4 S5
ODP 967
Sahara PC wet(+)/dry(-)
Soreq
Negev
b N. Arabia
S. Arabia
c Median (µm)
KL 11, Red Sea
d SAHP 1 2 3 4
Hoti Cave
Mukalla Cave
e KL 15, Gulf of Aden
RC09-166, Gulf of Aden
f Insolation 15°N (W m-2)
LR04 MIS
Monsoon rainfall +
Age (ka BP)

Fig. 57. (A) Precipitation map of Arabia showing locations of palaeolakes (light blue circles), speleothem cave sites (white circles), marine sediment (green circles) and fluvial/alluvial (dark blue circles). (B) Late Pleistocene climate records from Arabia. (a) ODP 967 sapropels (black rectangles) and wet/dry (blue/red line) index (Grant et al., 2017) vs. Soreq Cave stalagmite $\delta^{18}O_{ca}$ (black line) (Bar-Matthews et al., 2003; Grant et al., 2014) and Negev desert stalagmite formation (black circles) (Vaks et al., 2010). (b) lake activation (TT-)OSL ages in Northern Arabia vs. Southern Arabia (Rosenberg et al., 2011, 2012, 2013; Petraglia et al., 2012; Jennings et al., 2016; Parton et al., 2018). (c) Red Sea grain sizes (KL-11) (Fleitmann, 1997). (d) SAHP (green bars) vs. Hoti Cave $\delta^{18}O_{ca}$ values and Mukalla Cave $\delta^{18}O_{ca}$ (box-whisker plot) and $\delta^{13}C_{ca}$ (black circles) values (Nicholson et al., 2020). (e) Gulf of Aden grainsize data (KL-15) vs. $\delta D_{leaf\text{-}wax}$ values (RC09-166) (Fleitmann, 1997; Tierney et al., 2017). (f) insolation at 15°N (W m²) vs. global ice-volume (LR04 $\delta^{18}O_{benthic}$) and Marine Isotope Stages (Berger and Loutre, 1991; Lisiecki and Raymo, 2005).

8.3 Archaeology

Due to the scarcity of recovered human fossils, archaeological finds provide the main record of human activity in Arabia. Middle Palaeolithic (MP) assemblages characterise the early Late Pleistocene archaeological record of Arabia, found mostly in the now-arid interior (Fig. 3). While a large portion of these are surface finds, of those that have been excavated, most have been derived from palaeolake sediments, or deposits on the margins of palaeolakes (Groucutt et al., 2015b, 2015d, 2016), and close to fluvial channels (Breeze et al., 2015).

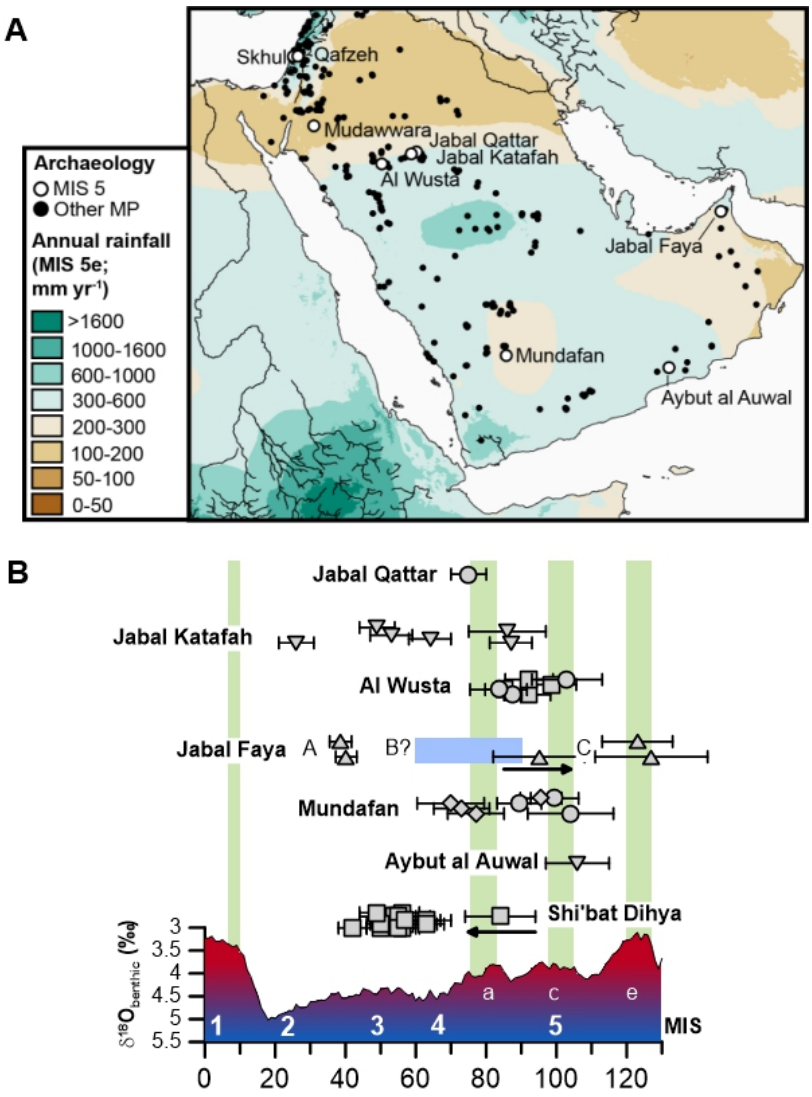

Fig. 58. (A) map showing locations of key (dated to MIS 5: white circles; undated: black circles) Arabian Middle Palaeolithic archaeological sites and annual precipitation during MIS 5e. (B) Ages of key dated Arabian archaeological sites (Armitage et al., 2011; Petraglia et al., 2011, 2012; Rose et al., 2011; Delagnes et al., 2012; Groucutt et al., 2015d, 2018). *Assemblage/unit identifiers are given for Jabal Faya and Jabal Katafah. The blue bar denotes tentative age assignment for Jabal Faya assemblage B. Different methods of age calculation are represented by difference shapes for Mundafan (diamonds: mutil-grain OSL; circles: TT-OSL) and Al Wusta (squares: OSL; circles: UTh/combined UTh-ESR).*

8.3.1 Northern Arabia

In northern Arabia, several Middle Palaeolithic assemblages have been described from the Jubbah Basin. The upper assemblage at the site of Jebel Qattar-1 (JQ-1) dates to ca. 75 ka, and features a focus on centripetal Levallois reduction, with both preferential and recurrent methods used (Petraglia et al., 2011, 2012). Other core reduction methods are present in small frequencies, such as discoidal. Retouched forms include side retouched flakes and a small retouched point. These characteristics are reminiscent of the African MSA and the Levantine MIS 5 Middle Palaeolithic (Groucutt et al., 2015b). Another site, Jebel Umm Sanman (JSM-1), consists of a surface scatter and small published excavations. Available OSL dates loosely constrain the assemblage to late MIS 5 or shortly after (Petraglia et al., 2012). The assemblage again features a focus on centripetal Levallois technology. A larger excavation was conducted at the site of JKF-1, but OSL dating the deposit again proved challenging, and resulted in a range of ca. 50-90 ka (Petraglia et al., 2012). While the core technology is rather amorphous, reflecting the frequent use of small quartz pebbles, the main reduction process involved the primarily unidirectional reduction of quartzite blocks to produce Levallois points (Groucutt et al., 2015c). JKF-1 therefore demonstrates a rather different set of characteristics to JQ-1 and JSM-1, and reflects more similarities with MIS 3 sites from the region (e.g., Jennings et al., 2016). In addition to these sites, a variety of surface Middle Palaeolithic sites have been recovered, such as JKF-12 (e.g., Groucutt et al., 2017).

Location and Site	*Assemblage*	*Age*	*Method*	*(Ref.)*

Al Wusta (Nafud Desert, Saudi Arabia)		~95-90 ka (see above)	Combined UTh-ESR, OSL and Bayesian age modelling	Groucutt et al. (2018)
Jabal Katafah (Nafud Desert, Saudi Arabia)	JKF-1; Unit H.	~90-50 ka	OSL	Petraglia et al. (2012)
Jabal Qattar (Nafud desert, Saudi Arabia(	JQ-1	75 ± 5 ka	OSL	Petraglia et al. (2011)
Khall Amayshan	KAM-1		OSL	Scerri et al. (2015)
Mundafan (Rub' al Khali, Saudi Arabia)	MDF-61	~100-80 ka	OSL and TT-OSL	Groucutt et al. (2015d)
Jabal Faya (UAE)	C	127 ± 16 123 ± 10 ka (± = 1σ).	OSL	Armitage et al. (2011)
	B	Relatively assigned to 50-90 ka based on stratigraphic position.		
	C	40.2 ± 3.0 to 38.6 ± 3.1 ka (± 1σ)		
Aybut al Auwal (Dhofar, Oman)		106 ± 9 ka (minimum age)	OSL	Rose et al. (2011)

Tab. 7. Ages of key MIS 5 archaeological sites in Arabia.

While research on the Middle Palaeolithic assemblages of Jubbah is ongoing, what can we say about the character and meaning of technological variability observed? Some aspects of this probably have a pragmatic basis. For instance, as mentioned the frequent use of small quartz pebbles at JKF-1 seems to have influenced reduction. Perhaps a wider impact, however, concerns differential reduction intensity. Groucutt et al. (2017) explored how reduction intensity (measured as the scar reduction index) varied with distance from raw material sources and found a positive relationship. This explains why the JQ-1 assemblage is so small and reduced. Such factors, however, occur within an umbrella of centripetal Levallois technology.

Quantitative comparison of Jubbah assemblages (JKF-1, JKF-12 and JSM-1) with samples from NE Africa highlighted that, while there were some similarities in core preparation techniques, high levels of technological variability mitigates against a simple interpretation (e.g., a single dispersal out of Africa echoed by a single techno-cultural complex). Instead, the variability was taken to reflect occupation by multiple populations at different times (Scerri et al., 2014a). However, given the nature of the burial contexts, current dating inaccuracies between these assemblages, as well as their temporal distribution, discussions of cultural hetero/homogeneity are not without uncertainty. Overall, while an MIS 5 occupation of the Jubbah area by hominin groups using centripetal Levallois technology is clear, further assessments are required to distinguish whether groups were present at other points, and indeed whether there were multiple occupations within MIS 5.

Similarities to Jubbah are apparent across northern Arabia. The Al Wusta archaeological assemblage (dated to late MIS 5 and the only assemblage discussed here with direct

association to a *H. sapiens* fossil) again emphasises a focus on centripetal Levallois reduction, similar to those of east and NE Africa and the Levant (Groucutt et al., 2018). Interestingly, the assemblage was mostly comprised of chert artefacts (65.05%), showing that morphological similarities with the Jubbah assemblages transcend raw material choices. Elsewhere in northern Arabia, Middle Palaeolithic assemblages of the Najd were described as rather homogenous when compared to smaller regions such as Dhofar (see below) (Groucutt et al., 2016). For example, whereas cores from sites ABY-1 and SHW-11 were characterised by preferential Levallois and centripetal reduction, AZA-2 was characterised by recurrent centripetal reduction. Additionally, QAN-1 possessed the only example of a Saudi Arabian assemblage dominated by discoidal reduction. Many of the new sites presented by Groucutt et al. (2016) lacked dating which, given that humans repeatedly occupied Arabia throughout the Pleistocene (Bailey et al., 2015; Scerri et al., 2018a), means addressing spatio-temporal variability from these assemblages is not straightforward. However, the variability does suggest that expectations of a single defining stone tool culture moving into Arabia are overly simplistic. Instead, it is apparent that different reduction strategies were employed within northern Arabia, likely reflecting differences in cultural traditions, mobility strategies or durations of individual occupations. Nevertheless, these findings present a clear indication that the Middle Palaeolithic record of northern Arabia is dominated by a focus on centripetal Levallois technology, as found with *Homo sapiens* in the Levant and northeast Africa (Groucutt et al., 2015b).

8.3.2 Southern Arabia

The archaeology of southern Arabia is somewhat more variable than northern Arabia. Artefacts uncovered at the Mundafan palaeolake (~100-80 ka) included Levallois cores characterised by recurrent centripetal (30%) and preferential with centripetal preparation (22%) strategies (Groucutt et al., 2015d). Flakes were described as standardised and typically ovoid or rectangular in shape. Additionally, a high retouch component was present, which is typically uncommon in the Arabian Middle Palaeolithic. Additional undated Middle Palaeolithic sites at Mundafan share a similar technology (Crassard et al., 2013), and lack other forms of technology such as the Nubian Levallois method.

In Dhofar, in the southwest of Oman, a rather different kind of Middle Palaeolithic technology dominates. Here numerous assemblages, particularly in western Dhofar near the spring at Mudayy, demonstrate a focus on the Nubian Levallois reduction method (Rose et al., 2011; Usik et al., 2013). The findings are virtually all surface scatters, except at the site of Aybut al Auwal where a single Nubian Levallois core and a few other lithics were found redeposited in a fluvial channel (Rose et al., 2011). To the discoverers these sites, as well as occasional hints of Nubian Levallois technology in Saudi Arabia (e.g., Crassard and Hilbert 2013), provide evidence for long distance movement between the Nile Valley and southern Arabia. However, Groucutt (2020a) has suggested an alternative explanation, that the Dhofar Middle Palaeolithic represents convergent evolution of Nubian Levallois technology, which is found from South Africa to India and over a ca. 200,000 year period. Given the minimum age of ca. 107 ka from Aybut al Auwal, it may be that MIS 5e or earlier dispersals retracted to reliable water sources in southern Arabia and developed distinctive local cultural trajectories. While currently poorly chronologically constrained, the varied Palaeolithic assemblages from southern

Arabia certainly indicate a complex demographic history (e.g., Delagnes et al. 2012; Jagher 2009; Bailey et al. 2015).

Further regional artefact variability is confirmed at Jebal Faya, UAE. This site is a notable exception to the general Arabian record, with artefacts recovered from rock shelter sediments and an occupation history spanning from MIS 5e to MIS 3 (Armitage et al., 2011; Bretzke et al., 2014). Assemblage C (127 ± 16 to 123 ± 10 ka; MIS 5e) contained artefacts with a variety of reduction strategies including the production of volumetric blades and Levallois debitage, bifaces, and retouched forms. Qualitative characteristics of this assemblage were considered similar to artefacts recovered from Muguruk, Kenya (Armitage et al., 2011), though the presence of bifaces seems to be consistent with the Huqf assemblages (Jagher, 2009). Indeed, while apparently diverse in its characteristics, the dominant characteristic of Assemblage C seems to be the focus on bifacial reduction, which is unusual for the Arabian Middle Palaeolithic. Assemblage B, however, contained little evidence of bifacial and Levallois reduction, with the exception of a few convergent flakes which are similar to Levallois points (Armitage et al., 2011). Further variability was observed in assemblage A (40.2 ± 3.0 to 38.6 ± 3.1 ka; MIS 3); assemblage A contained a diverse range of reduction strategies including the production of denticulates, side scrapers, end scrapers, and burins. Flakes were produced from platform cores, which contrasts the apparent absence of prepared platforms from Assemblage C (Armitage et al., 2011). The difference between artefact types, as well as densities, have been interpreted to relate to differences in techno-cultures (Armitage et al., 2011) and "distinct traditions in spatial behaviour" (Bretzke and Conard, 2017) between occupation phases. In summary, the assemblages of Jabal Faya are not only different from each other, but also seemingly differ from other Arabian assemblages.

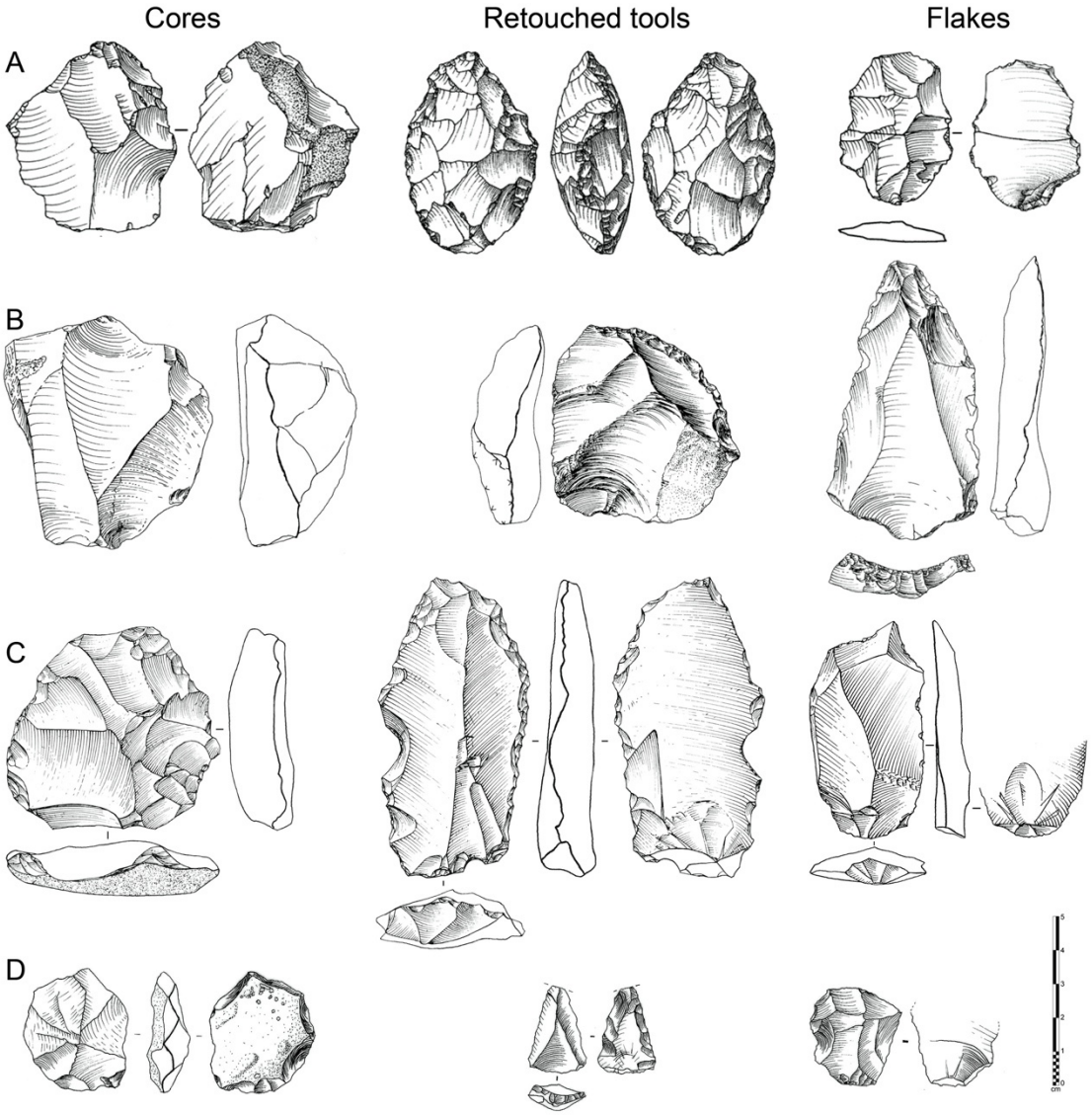

Fig. 59. Cores, retouched tools and flakes from (A) Jebel Faya assemblage C, UAE, ~125 ka, (B) Aybut Al Auwal and Mudayy As Sodh, Oman, early MIS 5, (C) Mundafan, southwest Saudi Arabia, MIS 5, (D) Jebel-Qattar 1, Nefud Desert, ~75 ka.

8.3.3 Summary

Overall, there is a high degree of spatial variability in stone tool assemblages across Arabia (e.g., Fig. 4). Ongoing analysis of the archaeological record of Arabia suggests

that sites in northern Arabia are repeatedly similar to those from Northeast Africa and the Levant (Petraglia et al., 2012; Scerri et al., 2014b; Groucutt et al., 2019), whereas those in the south repeatedly feature localised characteristics (Armitage et al., 2011; Delagnes et al., 2012). We posit two potential explanations for this: 1) multiple populations, with entirely different techno-cultures, entered Arabia during various MIS 5 substages, perhaps from different routes (via the Sinai Peninsula or the Bab al Mandab strait), or 2) Arabian assemblages, particularly those in the south, represent a high degree of localisation following an initial dispersal into northern Arabia. In terms of dispersal routes, it is important to consider that Arabian wet phases were restricted to warm substages of MIS 5 (Fleitmann et al., 2011; Nicholson et al., 2020), when sea-levels were higher than the intervening periods (Rosenberg et al., 2012; Grant et al., 2014). During the intervening stadials, an expansion of the desert likely inhibited widespread dispersals into Arabia. There is also currently no evidence from Arabia or NE Africa for relevant sea-faring technologies. We take this pattern to suggest a northern dispersal route into Arabia, followed by southward movement into Arabia following green palaeohydrological corridors (e.g., Breeze et al., 2016). We interpret the archaeological signature of the north to represent an initial dispersed population, which quickly diversified and adapted to local environments. As populations expanded southwards into Arabia, local techno-cultural characteristics developed in response to increasing distance from initial populations and local environmental and cultural factors. This pattern was likely repeated during each MIS 5 wet period, as each substage was likely represented by a new wave of settlement. However, only a handful of dated sites are currently available for analysis and few are temporally aligned. It is therefore vital to increase the spatio-temporal resolution and variability of the Arabian archaeological record to test this. The current available methods and the nature of preservation in these environments means

that producing such a database will be challenging. Furthermore, many reports from Arabian archaeological sites classify assemblages based on qualitative morphological features; there is only currently one example of inter-site quantitative morphological comparison (e.g., Scerri et al., 2014b). Further analysis comparing many assemblages are needed to generate key information on inter-assemblage morphological variability across Arabia.

It is important to note that many objects (e.g., bone tools, wood tools, eggshells) do not readily preserve but could have been crucial to surviving Green Arabia. For example, Ostrich eggs could have been used as water containers, and facilitated temporary movement away from waterbodies. Evidence for the working of eggshells has been identified at Skhul at a contemporaneous age to Arabian occupation (Groucutt et al., 2019). While ostrich eggshell fragments were uncovered at Mundafan (Groucutt et al., 2015d), it cannot be discerned whether these were used by humans. Additionally, the archaeological record of Arabia does not provide evidence of symbolic practices, which are commonly associated with rock shelters and caves in regions with dense *H. sapiens* occupation histories. Across Africa, it is clear that the MSA included specialised hunting tools, use of aquatic resources, bone tools, microlithic technologies, long distance trade, art and decoration, use of pigment, specialised hunting, structure building, social organisation and systematic processing (Mcbrearty and Brooks, 2000; Blegen, 2017; Scerri, 2017; Brooks et al., 2018). While evidence of all of these are not available from Arabia, hints of long-distance sourcing/transfer comes from occasional examples of putatively exotic raw materials in available assemblages (Petraglia et al., 2012). However, further research needs to be done on characterising raw material source, and distinguishing primary and secondary (e.g., fluvial) raw material sources. Given that *H.*

sapiens dispersed from NE Africa, it is likely that many behaviours present in Middle to Late Pleistocene Africa were key components of the behavioural repertoire of the dispersing populations. Conversely, our interpretation that *H. sapiens* were highly mobile (see below) could suggest that costly symbolising practices were not effective in these settings. Nevertheless, finding specific examples from Arabia is necessary for understanding the range of *H. sapiens* behavioural variability. This must be a target of future research.

8.4 *H. sapiens* in Green Arabia

In order to understand how humans became established, survived and retracted in Arabia, it is necessary to synthesise the environmental and archaeological records with reference to ecological, anthropological and biological datasets. Here, we address the processes of dispersal into Arabia, the dynamics of long-term survival, and population decline in the face of deteriorating climates.

8.4.1 Dispersal

Dispersal differs from migration, being defined as "a strategy to increase fitness in a heterogeneous landscape by changing the environment in which an organism lives" (Bowler and Benton 2005: 218). One of the most crucial factors when discussing the distribution of organisms and their introduction into new areas is the resources available to enhance their reproductive fitness. Both periods of increased rainfall (Shultz and Maslin, 2013; Maslin et al., 2014) and aridity (deMenocal, 1995) have been considered to influence hominin adaptation and dispersal on long time-scales through their impacts

on changing resources and population dynamics. Whereas transitions to aridity promote dispersal or extirpation due to reduced resources – namely, water, flora and fauna (deMenocal, 1995; Tierney et al., 2017) – periods of increased rainfall (and vegetation) promote population expansions within the hominin food chain, resulting in hominin population increases and, ultimately, dispersal/adaptation/extinction due to competition pressure (Shultz and Maslin, 2013; Maslin et al., 2014). The palaeoenvironmental record of Arabia clearly highlights that increased resources (water, vegetation and other animals) meant carrying capacity was greatly enhanced and offered new habitats for dispersal during wet periods. On the other hand, returns to aridity may have had a push and/or extirpating effect on resident populations. Another consideration is that shorter and stochastic events within both 'wetter' and 'drier' phases, and how these might have stimulated potentially short-lived and rapid dispersals and declines.

This is consistent with recent considerations of *source* and *sink* population dynamics (Dennell 2017; Dennell, Martinón-Torres, and Bermúdez de Castro 2011). A population sink is described as a region in which reproduction is too low to replace individuals. These are typically located in areas in which resource availability is either scarce or highly variable. On the other hand, source areas are regions in which reproduction outweighs the replacement of individuals due to resource abundance or stability. Dennell (2017: 5390) explains that "Demographic expansion thus depends greatly upon (i) extinction rates in sink populations at the edge of the inhabited range and (ii) the ability of the main source populations to support sink populations, especially those at the edge of the range. This becomes difficult when population densities are low and intergroup distances are high". With regards to Arabia, we may infer that rates of extinction were severely lowered at the edge of original habitats (such as sub-Saharan Africa and NE

Africa) in green phases such as early MIS 5e, due to increased resources promoted by monsoonal rainfall. This facilitated former sink populations to become new source populations and allowed expansion into newly habitable areas.

It must also be considered that human populations typically form metapopulations, which can be defined as "a group of spatially separated populations occupying a nexus of favourable patches" (Smith 2013: 75). Humans can be characterised by "tight" metapopulations, which maintain cohesion through kinship, ideology, culture and additional forms of identity over large distances (Dennell, 2017; Scerri et al., 2018b, 2019). The examples given above of long-distance cultural exchange throughout the MSA suggest that human metapopulations were maintained over >100s of kms (Blegen, 2017; B. A. Stewart et al., 2020). Dennell (2017) highlights the benefits of species that settle areas as part of a broader metapopulation as: 1) resilience to stochastic events and environmental/resource variability at the metapopulation level. Whereby groups comprising a metapopulation are more widely distributed in a landscape, mitigating against a metapopulation extinction. And, 2) a trial-and-error basis of settling new habitats; in which a "failing" group can be replaced or repopulated by groups from the broader metapopulation. Smith (2013) and Dennell (2017) highlight that this trial-and-error basis allows multiple groups to settle new habitats in a short space of time, where sufficient inter-group connectivity mitigates against local extinctions. If this model was relevant to Green Arabia dispersal then we should expect to see evidence that Arabian populations with cultural similarities likely maintained some contact over considerable distances. There is currently a suggestion for imported material into the Jubbah basin; however, further examples of long-distance exchange are required to understand the specific inter-connectivity of Arabian populations.

In summary, it is likely that dispersal and settlement of Arabia was a response to feedback effects between resource availability, patch carrying capacity and population pressure. Increasing rainfall across the southern limits of Saharo-Arabia, in which *H. sapiens* were likely already present, meant populations gradually expanded, resulting in increased pressure for dispersal into the new surrounding areas. We may describe this almost as a continuous dispersal, whereby populations expanded gradually into new areas with higher carrying capacities, which facilitated local population growth. Over time, local competition pressure forced expansion into additional new habitats. As rains were predominantly derived from the south-westerly monsoons, one likely aspect is that, as populations likely entered northern Arabia, the easiest expansion route was southwards, towards greater water availability and floral and faunal resources. Although the specifics of mobility were likely structured by lakes, rivers and other waterbodies (such as the Wadi Al-Batin) could have provided a corridor towards the eastern coast of Arabia (Breeze et al., 2016; Petraglia et al., 2020). As populations moved southwards, increasing differentiation due to separation from a metapopulation and autochthonous development may explain the localisation of stone tool assemblages in these regions.

Another important factor concerns whether Arabia was already occupied when humans dispersed into the area in MIS 5. Whether other human societies (or species) were already present could have had a dramatic impact on how *H. sapiens* settled Arabia (e.g., Dennell 2017). Evidence of Oldowan and Acheulean artefacts across Arabia likely suggest that pre-MIS 5 occupations had occurred (Groucutt and Petraglia, 2012). Recent dating of the Saffaqah archaeological deposits conform to this, placing an Acheulean occupation during late MIS 7 (Scerri et al., 2018a). Yet, debates on whether there were long-term

refugia in Arabia have not produced clear results (e.g., Rose 2010; Bretzke and Conard 2017). It must be considered that the majority of dated sites from Arabia have been excavated from palaeolake sediments, which are strongly aligned to interglacial periods. In other words, a failure to identify archaeological material from glacial periods is to be expected if lakes were less frequent. While indeed alluvial aggradation suggests MIS 6 was characterised by perhaps long-term, albeit less intense precipitation ~160-150 ka BP (Parton et al., 2015a), stalagmite growth in both the Negev (Vaks et al., 2010) and southern Arabia (Nicholson et al., 2020) highlight that precipitation was generally lower between ~150-130 ka BP. In this case, Arabia may have been particularly challenging for hominin occupation prior to 130 ka BP, or perhaps characterised by a low intensity occupation. For now, our working model is that Arabia was frequently occupied during Arabian green phases throughout the Middle Pleistocene (Scerri et al., 2018a; Nicholson et al., 2020); whereas returns to aridity saw depopulations (see below). Therefore, it is possible that Arabia was devoid of other humans when *H. sapiens* first entered during MIS 5e. In this case, if settlement and occupation across Green Arabia was uncontested, it was perhaps more rapid than it might have otherwise been.

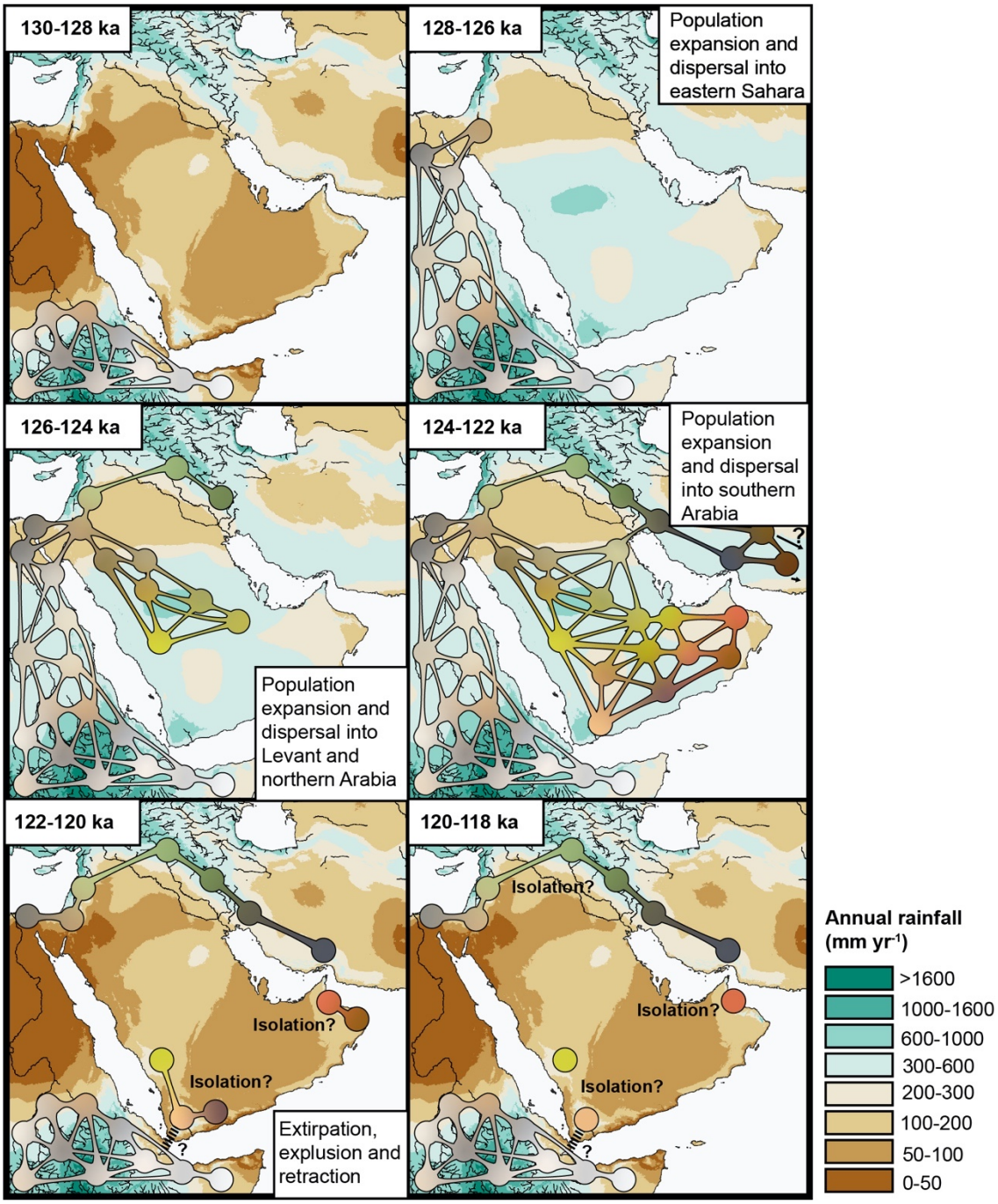

Fig. 60. Conceptual model for the dispersal of H. sapiens into Arabia and Eurasia using MIS 5e as an example. Circles denote hypothetical metapopulations, which are comprised of numerous inter-connected populations. Metapopulations are also semi-connected to other metapopulations at a much broader scale, with connectivity denoted by colour. As populations expand, they begin to differ from initial metapopulations as they adapt to new environments and develop new cultures.

8.4.2 Occupation

But what can we say about the more intricate processes of occupying Green Arabia? We have discussed the broad environmental outlines of Arabia, yet many fundamental aspects are currently not known. For example, while broad areas would have become grassland environments with water sources, the attractiveness and stability of these landscapes is currently poorly constrained. Many Arabian Palaeolithic archaeological sites are located close to palaeolakes (Petraglia et al., 2012; Groucutt et al., 2015c, 2018; Scerri et al., 2015); although Jabal Faya is a notable exception, wadis and lakes have been identified within 5 km of the site (Armitage et al., 2011; Bretzke et al., 2013). The perennial nature of the palaeolakes made these attractive habitats, which included the provision of freshwater during the drier winter months. These could have also provided rich opportunities for hunters (human and non-human) to ambush prey that are drawn to the water (Hitchcock et al., 2019). Yet, the discovery of hippo fossils and evidence of a diverse carnivore guild during late MIS 5 and other Pleistocene sites (Groucutt et al., 2018; Stewart et al., 2019b) indicate that small lakes in Arabia also came with challenges.

A further complicating factor is that we currently have little information on the character of edible plant resources for *H. sapiens* in Arabia. For example, bushed or wooded lake shores and river margins of East Africa tend to host mesophilic plants and other plants producing berries, nuts and seeds (Lind and Morrison, 1974; Sept, 1994; Marean, 1997). Drier soils, escarpments and inselbergs contain a plethora of carbohydrate rich plants with underground storage organs (USOs – including rhizomes, tubers, corns and bulbs; Vincent 1985); these are generally, nutritious, palatable and visible year-round, requiring little to no processing (Gott and Murray, 1982; Vincent, 1985). As such, these are staple

constituents of the year-round diet of traditional societies across Africa (Vincent, 1985; Marean, 1997). Their wide usage by traditional societies and identification of charred rhizomes (*Hypoxis*) at Border Cave (Wadley et al., 2020) may suggest these were a crucial source of year-round nutrition in the past. These could have been extremely useful resources during the drier seasons of Green Arabia, when other vegetation resources declined. However, the specific characteristics of the flora of Green Arabia must be a target for future research.

In any case, given the predominantly grassland character of Green Arabia during pluvial periods and the palaeontological record (Groucutt et al., 2018; Stewart et al., 2019b), it is likely that meat was also a significant component of the hominin diet. As well as the spread of animals from places such as Africa using the same semi-arid landscapes followed by humans, i.e., the 'fellow travellers', there could also have been rich animal resources already present within Arabia. As Foley (1987) noted, in important ways plants vary more than animals, and so rapid spread without significant adaptation could have occurred. Foley (1987: 263) commented that a "deer is very much like an antelope", and so for human groups moving into Arabia they would have encountered grasslands rich in bovids at least broadly similar to those with which they were familiar. It is quite possible that humans arriving during MIS 5 entered a region in which other human for tens of thousands of years due to the prevailing conditions of MIS 6. In such a situation, humans may have faced a 'naïve fauna' (e.g., Dennell, 2018), and as a result been able to expand rapidly before animals changed their behaviour.

Data compiled by Binford (2001) and Kelly (2013) illustrates clear relationships between productivity and aspects of human demography and behaviour. Ethnographic studies indicate that arid and semi-arid environments are associated with highly mobile

populations living in large ranges, with low population densities. Most hunter gatherer groups – i.e. excluding rare examples such as the sedentary groups of the north American coast – live at densities of 0.1 to 1 person per km^2 (Kelly, 2013), and sometimes at less than a tenth of this. Likewise, societies with a high reliance on meat tend to be highly mobile and live at low population densities (Grove, 2009). There are however caveats to the kinds of datasets presented in sources such as Binford (2001) and Kelly (2013). For example, most studied societies are from the Americas, with very few samples from Asia, and none from northern Africa and the Middle East. But even accounting for regional specifics, the broad pattern of how demographic and behavioural dynamics relate to the environments offers us an approximation of past patterns. It is clear from the data presented by Kelly (2013: 80-84) that low primary biomass is associated with large total areas for hunter gatherer groups and large total distances covered annually. In the more marginal areas of northern Arabia – which were at the limits of the monsoonal rains during periods such as MIS 5 – we can expect pioneering human groups to have been highly mobile and with large ranges.

Another consideration is that, while virtually all studied human groups have been expanding at a relatively rapid rate (i.e. often more than 1% a year; Gurven and Davison 2019), it is clear that hunter-gatherer populations remained relatively small in the long run. There must, therefore, have been periodic phases of catastrophic mortality (Gurven and Davison, 2019). Arabia probably exemplifies such processes, as the opening of a window of opportunity in northern Arabia could have led to rapid population expansion south- and eastwards (as above), but also environmental stochasticity (brief arid periods) were likely reflected by sudden population declines. Climate records from the HHP demonstrate that Green Arabia was prone to sudden and brief periods of aridity, which

were likely echoed by population declines (Petraglia et al., 2020). While current palaeoclimate records from MIS 5e, 5c and 5a are not of sufficient resolution to detect brief periods of aridity, it is probable that stochastic climatic factors continued to exert control on population.

The specific geological and environmental aspects of Arabia are also significant for human occupations. The deserts of Arabia are typically characterised by either rocky surfaces or deep sand (Miller and Cope, 1996). This contrasts with somewhere like Australia, where a thin sand cover means small water holes are abundant, allowing widespread occupation as long as populations are at low density and are highly mobile (e.g., Smith 2013). Current evidence suggests that in some areas of Arabia there was little occupation for broad periods of the past, due to a lack of water. Examples of this include areas in northern Arabia which were not proximal to palaeolakes and feature a very sparse archaeological record (Breeze et al., 2017), and a paucity of evidence for post-Acheulean occupation in the Dawadmi area of central Arabia (Jennings et al., 2015b; Groucutt et al., 2016; Shipton et al., 2018). It is our impression that populations in Pleistocene Arabia were relatively tethered to water sources such as lakes and rivers. These would have occurred at varying scales. It is the deep basins that contained palaeolakes, such as Jubbah in the Nafud Desert, which have produced archaeological findings covering every major period of human prehistory from the Acheulean onwards (Scerri et al., 2015, 2018a). Middle Palaeolithic sites, which mostly date to MIS 5, are significantly closer to palaeorivers than would be expected by a random distribution (Breeze et al., 2015). The connection between human demography/behaviour and the palaeohydrological structure of Arabia is therefore clear at a broad scale. The fact that Arabia is a tilted plateau – rising steeply along the entire western margin, dropping away gradually to the east – means that

during Pleistocene humid periods an extensive network of rivers formed across the peninsula (Breeze et al., 2015, 2016). What is unclear is the finer scale mechanics of this process, such as the mobility patterns which allowed survival in highly seasonal environments. This must on some level have meant retraction to perennial water sources, yet as discussed above there would have been competition for these and so the specific mobility and social strategies employed are currently unclear.

8.4.3 Decline

An important aspect for understanding *H. sapiens* occupation in Arabia is what happened following climatic optima. As climates deteriorated, reduced resources and lowered habitat carrying capacity would have increased competition pressure, resulting in population declines via dispersals, retractions and local extirpations (Bretzke and Conard, 2017). This is supported by a lack of continuity in the archaeological record at sites in the north (Groucutt et al., 2015b) and also large occupation gaps at Jabal Faya (Bretzke and Conard, 2017). However, evidence of occupation during the MIS 3 complicates this rather simplistic picture (Armitage et al., 2011; Delagnes et al., 2012; Jennings et al., 2016), suggesting either: 1) humans re-entered Arabia during MIS 4-3 (e.g., Mellars 2006); or 2) some populations survived following the return to arid conditions during the MIS 5a-4 transition (e.g., Armitage et al. 2011). Absence of prolonged, wide-spread and intense climatic amelioration across Saharo-Arabia during MIS 4-3 (Nicholson et al. 2020; Tierney, deMenocal, and Zander 2017; Grant et al. 2017) means a large-scale dispersal and sustained occupation would be surprising from a palaeoclimatic perspective. Perhaps the MIS 3 evidence represents small-scale 'pulse' dispersals and short-lived occupations associated with brief events? In the latter case, the low resource availability across much of the peninsula implies that these were probably outliers, which

survived in temporary green spots and/or in the higher productivity areas of the southern Arabian highlands (Delagnes et al., 2012, 2013). Previous hints of different land-use patterns between occupation phases have been witnessed in the Jabal Faya artefact assemblages (C: MIS 5e; B: late MIS 5 or MIS 3; and C: MIS 3), suggesting localised adaptations to changing environmental conditions (Armitage et al., 2011; Bretzke and Conard, 2017).

Others have considered that coastal regions may have provided suitable habitats for occupation following returns to aridity (e.g., Bailey et al. 2015; Erlandson and Braje 2015). The expulsion of groundwater aquifers may have transformed exposed continental shelves into high resource areas (Faure et al., 2002; Rose, 2010; Erlandson and Braje, 2015). Yet there is currently insufficient data from Arabia to understand both their specific environmental character and suitability to provide long-term habitats. Another potential issue is that where hominins have been present in coastal environments, productive inland environments were also available and exploited (e.g., Roberts et al. 2020; Reynard and Henshilwood 2019; Rector and Reed 2010). So, whether a long-term population pinned to a narrow coastal strip in an otherwise barren landscape could flourish is not without uncertainty. Further evidence of specific micro-environments, potential dispersal pathways and their suitability for occupation between wet phases are required to understand the resilience of human populations following transitions to aridity. For now, our working model is that the Late Pleistocene saw repeated population expansions into Arabia, with the largest and most sustained dispersals occurring during warm substages. This was followed by regional extirpations and population retractions during returns to aridity (e.g., MIS 5d, 5b and 4) (Bretzke and Conard, 2017).

8.5 Summary and Conclusion

Overall, we highlight that dispersal likely occurred on different rates and scales. In the first instance, we stress that dispersal could have been a rather slow process on human and ecological timescales as a) populations need time to grow, and b) it is unlikely that there was specific directionality to dispersal. As precipitation and primary productivity rose in Saharo-Arabia, populations inflated, and competition pressure forced expansion into new patches with higher carrying capacities. In order to maintain successful populations, it is highly unlikely that societies were rapidly moving across these landscapes, with a single population traversing from Africa into Eurasia. Instead, multiple semi-connected mobile metapopulations (Scerri et al., 2019) were linked across semi-arid Arabia by palaeohydrological corridors (e.g., Scerri, Drake, et al. 2014; Breeze et al. 2016). Over time, this would have included expansion towards areas of higher primary productivity and following water courses into southern Arabia (Groucutt and Petraglia, 2012; Breeze et al., 2017) and also the Levant (Shea, 2008). As populations moved into southern Arabia, it is expected that, due to both distance and ultimately due to separation, distinctive regional populations developed and came to vary from their parent populations (Fig. 5). This is potentially reflected by the localised characteristics of Middle Palaeolithic southern Arabian archaeological assemblages and autochthonous development of stone tool techno-cultures following green periods (Armitage et al. 2011; Delagnes et al. 2012). As precipitation declined and "green" environments retracted, reduced resources caused increased competition pressure, local extirpations (Bretzke and Conard, 2017), fragmentation, dispersal into remaining higher-resource areas (Delagnes et al., 2012), and group home-range size expansions. We relate these longer-term dispersals to the warm substages of MIS 5e, 5c and 5a, and perhaps MIS 3.

However, dispersal could have, at times, been rather rapid. Stochastic increases of precipitation and environmental amelioration could have facilitated very brief expansions into the now arid interiors of Arabia. These dispersals were perhaps more ephemeral and mobile in nature and perhaps subjected to local extirpations. Our current interpretation of these more ephemeral dispersals is that these were likely related to colder substages, such as MIS 5d and 5b, and perhaps MIS 4, 3 and 2. However, we emphasise that understanding these differences in environments, dispersal rates and dynamics will be key for moving away from simplistic narratives of *H. sapiens* dispersals.

8.6 Targets for future research

The conclusions drawn from this paper are based on current and limited evidences which are partly linked to theoretical expectations. We acknowledge that substantial gaps remain in both archaeological and environmental datasets, which obscure our understanding of human-environment interactions in the past. Throughout this paper we have identified challenges and targets for new research. Here, we briefly provide a few suggestions as to how these may be achieved:

1. Linking theoretical models with archaeological data can allow us to overcome simplistic narratives of how humans occupied and moved through Arabia. This includes considering macro-scale causes of dispersal, but also more micro-scale and immediate influences on human "lived" timescales. Yet, we must be cautious of interpreting archaeological data to fit our theoretical expectations: further analysis must also test expectations. For example:
    a. It is not necessarily the case that past animal migration patterns matched the present (e.g., Henton et al. 2018). If past migration patterns of prey species altered from the present, this could alter our expectations of

hominin migration and dispersal patterns. Detailed isotope (O, C and Sr) analysis of both animal and human remains could prove useful in discussions of home-range sizes and seasonal migration patterns (Pike et al., 2016; Henton et al., 2018).

b. Chemical analyses (X-Ray Fluorescence/electron probe microanalysis) of stone tool assemblages and local and distant raw material outcrops could provide information on the distance of raw material transfer (local sourcing versus imported material) (Blegen, 2017; Brooks et al., 2018). This could be used to determine how "connected" past populations may have been, and how far groups were moving.

c. Linking climate records, environmental parameters and population dynamics through numerical models (e.g., Beyer et al., 2020) could provide an additional method to visualise and test dispersal models across the Arabian Peninsula.

2. Identification and mitigation of biases within both archaeological and environmental records must be achieved to understand the full suite of *H. sapiens* behaviours and human-environment interactions in Green Arabia. For example:

a. There are very few examples of material culture beyond stone artefacts in Arabia. Further surveys of caves and open-air sites which are not raw material procurement localities on the Arabian Peninsula should be conducted to identify evidence of more permanent residency and material culture beyond stone artefacts.

b. Although it is not currently certain if a-DNA could preserve in Arabian speleothems, efforts to extract and analyse a-DNA could provide species level identification flora and fauna (Stahlschmidt et al., 2019) and improve

the current environmental record of Arabia. Additionally, more detailed considerations of the Mutual Climatic Range (MCR) of fossil fauna, diatoms, ostracods and phytolith taxa could prove useful in characterising past environments.

3. Improved dating of archaeological contexts is crucial for linking these to other palaeoclimate datasets and understanding the dynamics of *H. sapiens* occupation and dispersal. Current methods favour Bayesian statistical modelling (Groucutt et al., 2018) or "wiggle-matching" with precisely dated records (such as stalagmites, e.g., Rosenberg et al., 2013). New methods must be developed and development of current methods (e.g., OSL and single amino acids for ^{14}C dating) to provide robust and independently dated archaeological records.

Here, we have synthesised environmental, archaeological and anthropological data – and combined these with theoretical models – to understand human-environment interactions and dispersal mechanism in Arabia during MIS 5. Current evidence has allowed us to create a working model that moves beyond an "arrows on a map linking Africa to Eurasia" approach to dispersal. We emphasise that macroscale as well as microscale population dynamics must be considered when explaining human dispersal across landscapes.

Acknowledgments

This work was supported by the AHRC South, West and Wales Doctoral Training Partnership (Grant AH/L503939/1). HSG thanks the Max Planck Society for funding.

Chapter 9

9) Conclusion: Going Global

9.1 Introduction

The aim of this thesis has been to explore the potential long-term impact of Arabian palaeoclimate on hominin dispersals and occupations of Arabia. While the changing climatic conditions of the Arabian palaeoclimate are increasingly well studied, current records are influenced by factors which are difficult to account for. For example, the deposition of terrigenous material in marine sediment core records are influenced by dust production, wind strength and direction etc. (Zabel et al., 2001; Trauth et al., 2009); whereas current terrestrial records are limited to ~450 ka BP and do not provide evidence on moisture source (e.g., Rosenberg et al., 2013; Parton et al., 2018). Both of these archives have been exploited by both palaeoclimate and archaeological research initiatives but information from an independent archive is required to test and mitigate these uncertainties. This thesis has therefore produced stalagmite-based palaeoclimate records from key locations on the Arabian Peninsula in order to answer four main research questions:

1. *Timing of wet periods*: Are substantial increases of precipitation are related to interglacial periods and warm substages throughout the Pliocene and the Pleistocene?
2. *Past moisture source*: Can stalagmites confirm whether the African Summer Monsoon and Indian Summer Monsoon become the dominant source of precipitation over Southern Arabia during pluvial periods?

3. *Nature of wet periods*: Are there substantial differences in rainfall between pluvial periods? And how does rainfall very within pluvial periods?
4. *Environmental character*: Can speleothem records serve as a palaeoecological archive by confirming the development of grasslands during pluvial periods?

This thesis has been structured around three papers, presented as a results papers detailing the palaeoclimate conditions of Southern Arabia over the past 1.1 million-years (chapter 5); followed by a chapter providing initial results of Plio-Pleistocene stalagmites (chapter 6); a results paper presenting a high-resolution stalagmite used to address *H. sapiens* dispersal routes ~130-120 ka BP (chapter 7); and a discussion piece, which aimed to provide a more nuanced discussion of human-environment interactions during green Arabia periods (chapter 8). The following sections summarise the key conclusions from each results chapter, reviews the key scientific advances presented in this thesis, and discuss potential for future work.

9.2 Key conclusions and scientific advances

.

9.2.1 Question and Objective 1: Timing of wet periods

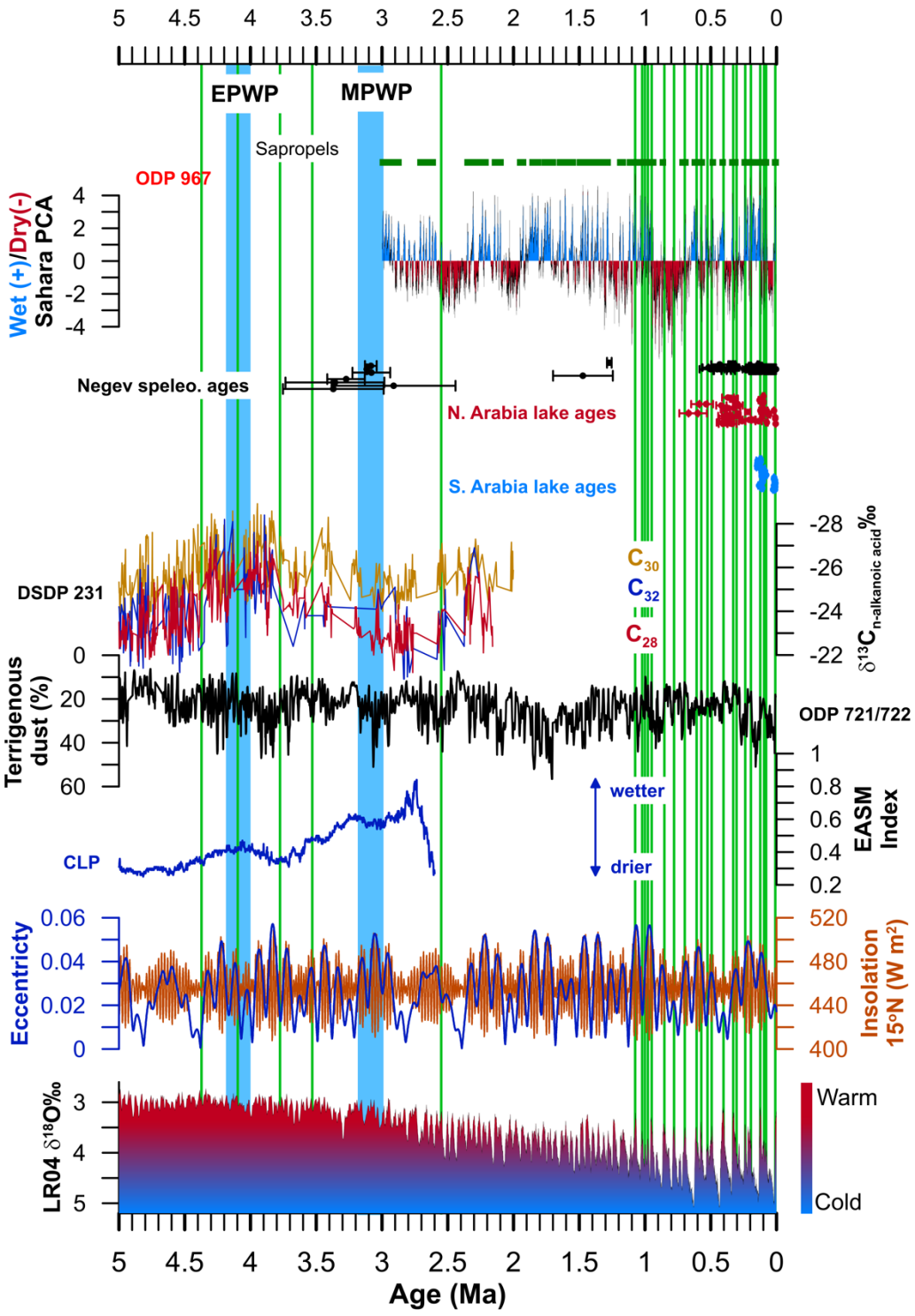

Fig. 61. Timing of wet events in Arabia (green bars) compared to local and regional records including OD 976 PC2 and sapropels, Negev speleothem ages, DSDP 231

$\delta^{13}C_{n\text{-}alkonoic\ acid}$‰, ODP 721/722, CLP EASM intensity index, orbital eccentric and NHI and global ice-volume (LR04 $\delta^{18}O$‰).

Identification and timing of wet periods have been provided throughout the results papers of this thesis. Chapters 5, 6 and 7 presented new speleothem-based climate reconstructions, which, due to the activation threshold of >300 mm yr^{-1} rainfall, provides timings of substantial changes in annual rainfall.

Results from chapter 5 extended timing of wet periods to 1.1 Ma BP, approximately 700-600 kyrs beyond the range of many terrestrial palaeoclimate records from Arabia (e.g., Rosenberg et al., 2013; Parton et al., 2018; Fig. 60). Using evidence from both Mukalla and Hoti Cave, South Arabian Humid Periods (SAHPs) were assigned to detail the timing of increased rainfall over the last 1.1 Ma BP. SAHPs were related to insolation maxima, showing that orbital precession has strong control over the position and intensity of the monsoon rain-belt. This was also confirmed in Chapter 7, in which the high-resolution Y99 $\delta^{18}O_{ca}$ record shows a clear relationship to the July insolation (15°N) curve. It is important to note, however, that glacial periods were not represented by speleothem growth, despite changes in precession. This indicates that glacial-boundary conditions had a suppressive effect on the tropical rain-belt, which is supported by numerous records throughout the monsoon domain at both local and inter-regional scales (e.g., Ehrmann et al., 2017; Grant et al., 2017; Tierney et al., 2017; Beck et al., 2018). While indeed some terrestrial records perhaps a more minor increase in rainfall during MIS 3 (e.g., Parton et al., 2013, 2018; Jennings et al., 2016), absence of speleothem growth or detection in a plethora of palaeoclimate records suggests these increases were not protracted (or

intense) periods of increased rainfall. The discrepancy between might be a result of the suppressive effects of glacial boundary conditions and activation thresholds. Whereas "climatic optima" (e.g., MIS 5e) were characterised by reduced glacial-boundary conditions and high NHI, the suppressive effects of glacial-boundary conditions muted the effects of low precession during colder periods (such as MIS 3). Despite high glacial-boundary conditions, enhanced NHI facilitated moderate increases of precipitation during glacial phases that are undetectable at Mukalla and Hoti Cave but present in alluvial fan and some lake records (e.g., Parton et al. 2015b, 2018). Nevertheless, the clear relationship between SAHPs, orbital precession and glacial-boundary conditions means speleothem growth occurs at predicted intervals over the last 1.1 million-years. Overall, the speleothem records of Yemen and Oman record substantial increases in rainfall during a key period of human range expansions.

The initial results presented in chapter 6 provide an insight into the timing of wet periods beyond 1.1 Ma BP. An important finding was that many speleothem ages cluster around the so-called "Early Pliocene Warm Period", yet none were dated to the frequently studied "Mid Pliocene Warm Period". Additionally, wet periods continued to occur between these "warm periods" and into the Early Pleistocene. Age uncertainties are too large to assess the relationship between insolation forcing and expansions of the monsoon domain from these samples alone. Yet, the relationship detected throughout the Pleistocene (as described above), low Pliocene glacial coverage and the simulated impact of precession during the Middle Pliocene Warm Period (Ji et al., 2017; Li et al., 2018; Prescott et al., 2019) certainly raises the likelihood that frequent incursions of the monsoon occurred throughout the Pliocene. Finding further examples of Pliocene

speleothem growth from Arabia, over a broad temporal range of the Pliocene, should be a target of future research

In summary, the timing of speleothem growth in Arabia adds to the mounting evidence that the expansions and contractions of the monsoon domain are influenced by three major factors:

1. Glacial-boundary conditions; which supresses the monsoon domain during periods of increase ice-sheet coverage and leads to expansions during reduced ice-sheet coverage.
2. Orbital eccentricity; which, throughout the Middle-Late Pleistocene, regulates changes in glacial-boundary conditions on ~100 ka cycles (Fig. 62).
3. Orbital precession and low latitude northern hemisphere insolation; which acts as a key control on the interhemispheric pressure gradient that drives monsoon position and intensity on ~21 ka cycles (Fig. 62).

This provides a framework for understanding the timing of green Arabia periods and potential hominin dispersals throughout the Pleistocene. One final point to note, that, despite current (low) glacial-boundary conditions, low orbital eccentricity and high precession means the monsoon is currently in a weakened state (e.g., Fig. 61). We may therefore speculate that – while glacial-boundary conditions appear to have a strong suppressive effect on the spatial extent of the tropical rain belt – low latitude NHI (determined by eccentricity and precession) is a key control on the intensity of monsoon rainfall.

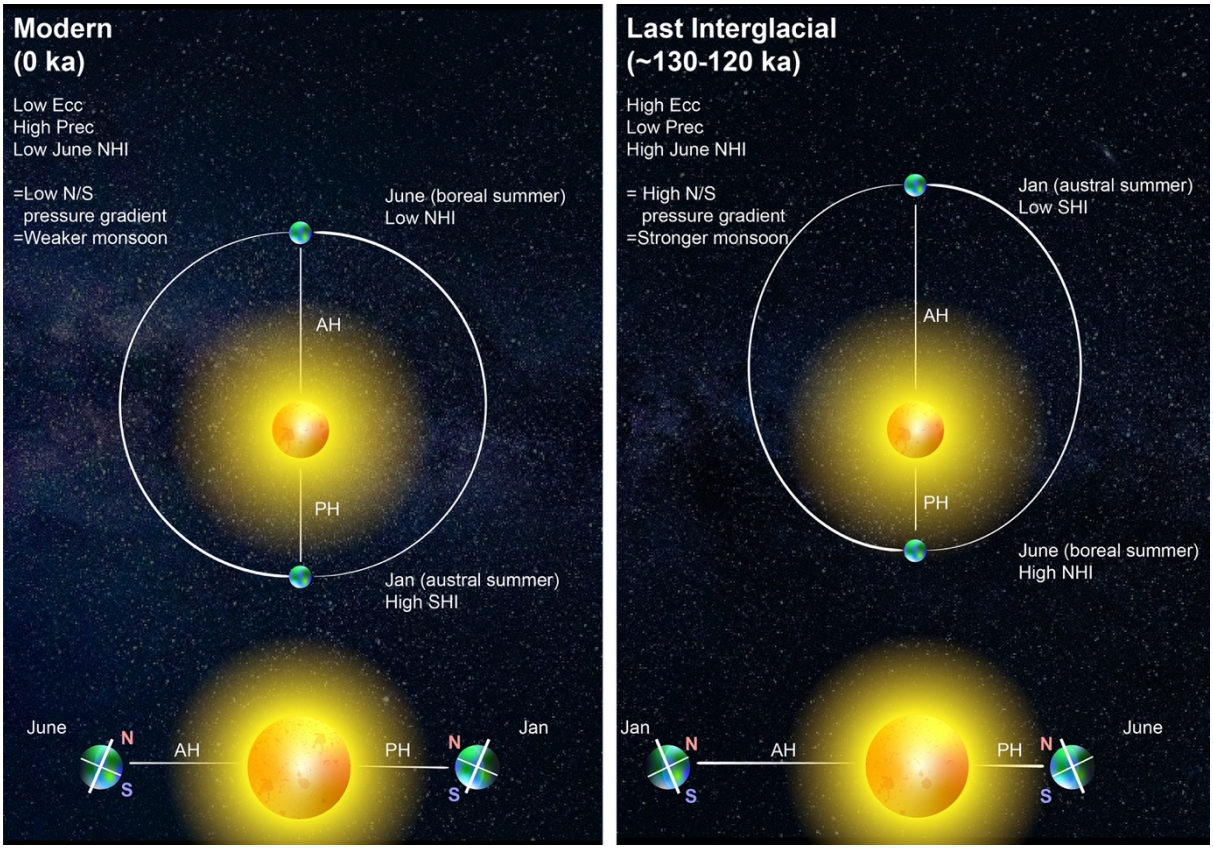

Fig. 62. Illustration of orbital forcing effects on the monsoon.

9.2.2 Question and Objective 2: Past moisture source

To understand the nature of wet periods, it has been necessary to clarify which moisture source was responsible for bringing increased precipitation to Arabia. This can be used to understand precipitation gradients across Arabia, which could have played crucial roles in human dispersal patterns (e.g., Chapter 8). Speleothem fluid inclusion data generated in this thesis demonstrates that the ISM expanded to at least 23°N during the Holocene and MIS 5e, becoming the dominant source of moisture in northern Oman (chapter 4). Similarly, a zonal incursion of the ASM brought increased precipitation to Yemen during MIS 5e and MIS 7e (chapter 5). Linking these findings with speleothem $\delta^{18}O_{ca}$ values shows that the tropical rain-belt remained the dominant source of moisture during Pleistocene speleothem growth periods (chapter 5). While the northward expansion of

the ISM has been confirmed previously (Fleitmann et al., 2003b), the incursion of the ASM has only been confirmed by climate simulations (Herold and Lohmann, 2009; Gierz et al., 2017). Findings from this thesis provide confirmation that a zonal incursion of the ASM increased precipitation to Arabia. This means that not only does the speleothem record of Yemen provide a climatic record of southern Arabia, it also provides a palaeoclimate record of the eastern Sahara.

9.2.3 Question and Objective 3: Nature of wet periods

A simplistic "wet" or "dry" dichotomy is a pertinent issue within discussions of Arabian palaeoclimate. Due to the activation threshold for stalagmite growth (>300 mm yr^{-1}), it has not been possible to show how climates varied during "drier" phases. However, stalagmite $\delta^{18}O_{ca}$ values provide a record of varying monsoon intensity during "wet" periods. Prior to this thesis, there has been very little quantification of inter-wet period variability (but see Burns et al., 1998; Fleitmann et al., 2011; Parton et al., 2015a, 2018) and even fewer Pleistocene high-resolution records from Arabia.

Inter-wet period variability

Stalagmite $\delta^{18}O_{ca}$ values have been used to show the changing intensity of the ASM and ISM at Mukalla Cave and Hoti Cave, with more negative $\delta^{18}O_{ca}$ reflecting increased precipitation (chapter 5). Previous work by Burns et al. (1998) and Fleitmann et al. (2011) have shown the varying intensities of wet periods over the last 350 ka BP; whereas the results from this thesis have expanded the knowledge of inter-wet period climatic variability up to 1.1 Ma BP. While $\delta^{18}O_{ca}$ of all Pleistocene SAHPs were significantly

more negative than SAHP 1 (the early-mid Holocene), SAHP(MIS) 4 (5e), 5 (7a) and 18-20 (27a-29) stand out as periods characterised by more negative $\delta^{18}O_{ca}$ (increased rainfall). Within the last 130 ka BP, SAHP 4 stands out as the period characterised by the most rainfall, which is supported by numerous palaeoclimate records from the monsoon domain (Weldeab et al., 2007; Grant et al., 2017; Tierney et al., 2017; Beck et al., 2018). This increased monsoon rainfall can be explained by the lowest ice-sheet coverage and highest insolation values over the last 130 ka BP, which resulted in greater interhemispheric pressure contrast and the most pronounced shift in the monsoon domain.

Intra-wet period variability

A high resolution $\delta^{18}O_{ca}$ record from Y99 GI-I was produced using a precise StalAge age-depth model (chapter 7). The $\delta^{18}O_{ca}$ record showed relatively stable climates persisted between 127.7 to ~124 ka, after which precipitation gradually declined and became more variable following the insolation curve. The termination of the event was characterised by an abrupt shift to reduced precipitation. This can be related to a breach in the threshold for stalagmite growth, in which the 300 mm yr^{-1} isohyet returned to a southwestern position. The precision of this record allowed both confinement of the timing of SAHP 4 (which can reduce the large age uncertainties of current palaeolake records) and provided an insight into the climatic variability throughout SAHP 4, both key information for restricting timings and for understanding human-climate interactions during wet periods.

Sub-annual $\delta^{18}O_{ca}$ and $\delta^{13}C_{ca}$ records were produced from an annually laminated stalagmite (H13). The cyclical increase and decrease of these proxies within annual layer demonstrate that Arabia was characterised by highly seasonal precipitation regimes, with

distinct “wetter” and “drier” seasons (chapter 5). This, combined with the identification of a southern source of precipitation, indicates that summer monsoon precipitation became the dominant source of rainfall during MIS 5e. While the vegetation responses of seasonal rainfall are not known for green Arabia, it is likely that reduced rainfall during winter months was echoed by reduced vegetation density (Nemani, 2003). This information could be pertinent when discussing human-environment interactions in Arabia but providing specific examples should be a priority of future research.

9.2.4 Question and Objective 4: Environmental character

Analysis of speleothem $\delta^{13}C_{ca}$ within this thesis has provided an insight into the environmental character of SAHPs. $\delta^{13}C_{ca}$ of speleothems fell into a mixed C_3 and C_4 signature. While explaining $\delta^{13}C_{ca}$ variability is not straightforward (see Chapters 4 and 5), this provides evidence that vegetation, most likely grasslands, were present above the caves during SAHPs. These findings are in good agreement with palaeontological (Rosenberg et al., 2013; Stimpson et al., 2016; Groucutt et al., 2018; Roberts et al., 2018) and phytolith (Bretzke et al., 2013; Jennings et al., 2016) studies across Arabia, suggesting that SAHPs were characterised by widespread grasslands. This adds to the growing body of evidence that increased rainfall and abundant freshwater resources created habitable biomes for hominin occupations. However, this information is limited as it does not provide detailed evidence of both the constituent taxa nor evidence of broader landscape variability (Chapter 8). Further analyses (see below) must be conducted in order to elucidate these issues, which may assist discussions of human-environment interactions in green Arabia.

Another key finding is that climates were highly seasonal. In Chapter 5, sub-annual analysis of a sample from Hoti Cave (H13) showed that climates were defined by a wetter (summer) and drier (winter) seasonality. This potentially opens new questions for understanding shifting climates on annual cycles and what this might mean for human occupation (e.g., Chapter 8). While lakes were perennial, were they seasonally more brackish/fresh? Did vegetation density have a seasonal component? If so, what might this mean for survival strategies and mobility patterns of hominins?

9.3 Timing of Hominin dispersals and demographic shifts

The Arabian Deserts sit at a crucial centre point between Eurasia and Africa, forming a vast geographic barrier between Afrotropical and Eurasian fauna. However, the evidence provided in this thesis and elsewhere demonstrates that formation of "green" deserts provided habitats for the northward (Afrotropical) and southward (Eurasian) dispersal of fauna, including extinct and extant hominins (Rosenberg et al., 2013; Stimpson et al., 2016; Groucutt et al., 2018; Roberts et al., 2018; Scerri et al., 2018a; Stewart et al., 2019; Stewart et al., 2020). These so-called "windows of opportunity" can be linked to the timing of human dispersals into Eurasia.

9.3.1 Pliocene

There is extremely limited evidence for hominin presence beyond eastern and southern Africa during the Pliocene; however, isolated *Au. bahrelghazali* remains in the Djurab Desert indicate hominin presence beyond eastern or southern Africa at ~3.56 ± 0.27 Ma (Brunet et al., 1996; Lebatard et al., 2008). Importantly, these remains were associated with a period of enhanced precipitation and expansion of grasslands in Chad (Novello et

al., 2015, 2017), which allows us to consider the distribution of early hominins with respect to environmental conditions. The northward expansion of the monsoon domain means that the Saharo-Arabian desert would have received considerably higher precipitation and been characterised by increased vegetation (Chapter 6). Despite the absence of direct fossil evidence, formation of these environments could have provided new habitats for early hominins in Saharo-Arabia, which could have initiated dispersal. While finding such ancient fossils from these regions is challenging, data provided in this thesis could support the formation of new hypotheses concerning the relationship of green periods to the distribution of early hominins. For example, did climatic optima initiate northward expansions of early hominins and other mammals (e.g., Hughes et al., 2008; O'Regan et al., 2011; Sen, 2013)? Could hominins have reached Eurasia? If so, what does this mean for the environmental tolerances of early hominins?

9.3.2 Early Pleistocene

The earliest known hominin dispersals occurred with the Early Pleistocene (2.7-0.78 Ma BP). Within the late Pliocene to Early Pleistocene, the addition of Oldowan stone tool technologies from 2.9 Ma (Braun et al., 2019) provides an indicator of hominin presence independent from the fragile and scarce fossil record. The appearance of the Oldowan is also remarkably close to the earliest candidates of *Homo* species at ~2.8 Ma (Villmoare et al., 2015). While there is a lack of absolute dating, surface Oldowan assemblages have been recovered in Yemen (Amirkhanov, 1994; Whalen and Schatte, 1997), Saudi Arabia (Whalen et al., 1986, 1989) and central Oman (Whalen, 2003). The designations of these were based on simple core and flake technology and basic shapes and it should be noted that similar morphologies are present in Holocene contexts (Groucutt and Petraglia,

2012) and some may be geofacts (Jagher, 2009). Thus, directly associating these remains to hominin occupations of Arabia during the Early Pleistocene is not straightforward. Targeted exploration of deposits over 1 Ma should be conducted to explore the potential for Oldowan occupations of the Arabian Peninsula. However, taken at face value, current Oldowan data suggests a much deeper occupation history of the Arabian Peninsula.

Further afield, Oldowan assemblages have been uncovered in China (~2.1 Ma: Zhu et al., 2018) and the Levant (2.5-2.1 Ma: Scardia et al., 2019), predating the earliest fossil evidence for hominin presence outside of Africa at Dmanisi, Georgia (~1.85 Ma: Messager et al., 2011; Lordkipanidze et al., 2013). Oldowan tools uncovered in Algeria have also recently been dated to 2.4 Ma (Sahnouni et al., 2018). It is important to note that the assemblages from Algeria and the Levant only provide a *terminus ante quem* for dispersal and are only slightly younger than the central age of SC-2 (2.57 ± 0.4 Ma). Taken together with the results generated in this thesis, an Oldowan occupation of "Green Arabia" is not necessarily a farfetched proposition. It is possible that palaeoenvironmental fluctuations – particularly monsoon variability – of the Saharo-Arabian desert belt had a much deeper and long-term impact on hominin dispersals and demography. Producing further palaeoclimate records between 3-1 Ma could be used to confine the timings of any Oldowan occupations.

Following the Oldowan, Acheulean technologies developed approximately 1.76 Ma (Turkana, Kenya; Lepre et al., 2011) and have been uncovered outside of Africa by 1.6-1.4 Ma (Belmaker et al., 2002). Acheulean tools have also been recovered from across Arabia; however, very few ages for these have been attained. Those that have been dated range between 0.8 Ma to 0.2 Ma BP (Bailey et al., 2015; Scerri et al., 2018a). The central

position of Arabia between Africa and the Levant, and the long duration of the Acheulean tradition, may indicate SAHPs (MIS) 21(31)-16(21) provided opportunities for Acheulean hominin occupations. Furthermore, the established relationship between orbital parameters, glacial boundary conditions and SAHPs suggests that SAHPs perhaps occurred beyond 1.1 Ma and throughout the Early Pleistocene. In this case, there may have been numerous opportunities for hominin occupations throughout the Early Pleistocene. However, both extending the palaeoclimate record and further archaeological data are required to truly understand any occupations Acheulean hominins throughout the earlier portion of the Early Pleistocene. Specific targeting of Early Pleistocene deposits for archaeological analysis will be required to understand the influence of climate on human distribution in Arabia.

9.3.3 Middle Pleistocene

As stated in the last section, two Arabian Acheulean tool assemblages have been dated to the Middle Pleistocene (Bailey et al., 2015; Scerri et al., 2018a). Ages ranged 0.8-0.3 Ma (Bailey et al., 2015) to ~0.2 Ma (Scerri et al., 2018a), meaning the Acheulean has a potentially broad temporal distribution (and potentially broader when the Early Pleistocene is considered; section 9.3.2). The earliest potentially Middle Pleistocene stone tools were uncovered and described by Bailey et al. (2015) on the Saudi Arabian Red Sea coast. These were broadly dated between 0.8-0.3 Ma and also broadly assigned to the ESA (early stone age). Regardless, these provide good evidence for hominin occupation of Arabia sometime during the earlier portion of the Middle Pleistocene and could be confined to SAHP 16-7.

Flint scatters have been uncovered at the palaeolake deposits of T'is al Ghada (Stimpson et al., 2016), dated between ~500 (MIS 13) and ~300 (MIS 9) ka (Stimpson et al., 2016; Roberts et al., 2018). While Y99 growth indicates precipitation likely exceeded 300 mm yr^{-1}, the comparatively high and wide ranging $\delta^{18}O_{ca}$ of these periods suggests greater climatic variability and perhaps overall drier conditions when compared to SAHP 4 (MIS 5e). Having said this, it is crucial to note that these values are not dissimilar from SAHP 2 (MIS 5a) $\delta^{18}O_{ca}$, a time in which perennial waterbodies and grasslands were present in northern Arabia (Groucutt et al., 2018). It is therefore likely that northward migration of the tropical rain-belt during MIS 13-9 could have supported hominin occupation of Arabia. However, due to the lack of archaeological data, there are limited details on the lasting impacts of occupations/dispersals during these periods.

Scerri et al. (2018) provided another Acheulean assemblage from the Saffaqah site, Saudi Arabia, finding techno-cultural affinities with African assemblages from Mieso (presence of cleavers and large flakes). While age uncertainties of the bracketing deposits were large, they indicate the archaeological layer (layer E) dated to MIS 7, which could be related to SAHP 6 or 5. For SAHP 5, $\delta^{18}O_{ca}$ values were not dissimilar from SAHP 4, and suggest a similar intensity of the monsoon. Taken with recent findings from Misliya Cave, Israel (Hershkovitz et al., 2018), and Apidima, Greece (Harvati et al., 2019), it is possible that the migration of the tropical rain-belt during MIS 7a facilitated the northward dispersal of African *H. sapiens* populations into the Levant and perhaps southern Europe. However, further evidence is required to 1) confine the age of the archaeological deposits at Saffaqah, 2) provide more robust evidence of population links between Saffaqah and Africa (or Levantine assemblages), and 3) fully understand the age

of the Misliya Cave sample (Hershkovitz et al., 2018; Sharp and Paces, 2018) and the age and taxonomy of the Apidima remains (Harvati et al., 2019; Wade, 2019).

In summary, Middle Pleistocene wet periods likely facilitated the introduction of Acheulean-bearing hominins (*H. erectus*/*heidelbergensis*/early *H. sapiens*) into Arabia. While the overall impact of these occupations on broader evolutionary changes is not understood, linking archaeological and fossil data to SAHPs could confine the timing of any dispersals and Arabian occupations. Having said this, targeted dating of deposits containing Acheulean artefacts is required to provide insights into the broad timing of these occupations.

9.3.4 Late Pleistocene

The dispersal of *H. sapiens* is one of the most debated topics in palaeoanthropology. Chapter 7 aimed to clarify the timings of Late Pleistocene dispersals along the "southern route". To do this, the timing of SAHPs were compared to the width of the Bab-al-Mandab strait. It was found that during SAHP 4 (MIS 5e), the Bab-al-Mandab was wider than at present due to increased sea-level. While the increased rainfall made southern Arabia an attractive landscape, characterised by abundant freshwater and vegetation, without open-sea-faring capabilities it is unlikely that *H. sapiens* populations could disperse across the strait. We therefore posited three potential models to explain *H. sapiens* dispersals during SAHP 4. 1) *H. sapiens* dispersed into Arabia from the north, following a dispersal via the Sinai Peninsula. This is seemingly consistent with the archaeological signature from succeeding wet periods, which show a degree of cultural exchange between NE Africa, Arabia and the Levant (Groucutt et al., 2019). 2) *H. sapiens*

had sea-faring capabilities and dispersed into southern Arabia during SAHP 4. 3) *H. sapiens* had some (perhaps more limited) sea-faring capabilities and cross during the sea-level low-stand during T-II (prior to the onset of SAHP 4). However, this model emphasis that population expansion into the Arabian interior was likely restricted to the onset of pluvial conditions. It is not possible to use this record to rule out either model; yet, the key finding, that the onset of pluvial conditions lagged sea-level rise, has pertinent implications for our understanding of dispersal at the onset of the Late Pleistocene.

Chapter 8 explored *H. sapiens* dispersals at both "macro-scales" and "micro-scales" to provide a more nuanced discussion of how humans lived in and moved across the Arabian landscape. Considerations of the biological motivators of dispersal and recent discussions of population structure suggests that dispersal was likely to be, on human timescales, a rather slow and protracted process comprising of numerous "micro-dispersals" over thousands of years (Chapter 8). It is likely that populations expanded across the landscape in predetermined directions but were reacting to a variety of population and environmental pressures, expressed simply as push and pull factors.

9.4 Future work

9.4.1 Integration with (and refinement of) palaeoclimate models

U-Pb and ^{230}Th ages attained during this thesis have been used to identify the precise timing of pluvial conditions. This precision has the power to increase the accuracy of computer-based palaeoclimate simulations, especially those that are informed by broadly dated or asynchronous palaeoclimate records (e.g., the Pliocene). Current EPWP and MPWP climate simulations are frequently supplemented by Quaternary records (e.g.,

Salzmann et al., 2011), which may not be accurately represent Pliocene climates due to differences in orbital configurations and global parameters. The records produced within this thesis can be used to improve those models, by providing a representation of the timing and nature of wet periods at a contemporaneous (or near contemporaneous) age.

The temporal resolution achieved in this thesis may also improve the resolution of palaeoclimate models. For example, the resolution of MIS 5e precipitation simulations is currently limited to 5 kyr intervals (130, 125 and 120 ka; Jennings et al., 2015; Gierz et al., 2017). The StalAge model for Y99 GI-I, however, achieved a resolution ranging from 0.9 to 91.8 yrs per mm, with one $\delta^{18}O_{ca}$ measurement per mm. Y99 GI-I $\delta^{18}O_{ca}$ therefore represents a sub-centennial record of Arabian palaeoclimate, and can be used to study variability at a much greater resolution than current models. Integration of these data with climate simulations could be used to increase the knowledge of monsoon variability throughout MIS 5e. This could lead to both increased understanding of the temporal variability of precipitation throughout MIS 5e and provide new hypotheses for climate-human interactions within green Arabia.

9.4.2 Independent proxies (to test current proxies)

This thesis has provided high resolution $\delta^{18}O$ and $\delta^{13}C$ palaeoclimate records, which have allowed comparison of monsoon intensity between interglacial periods throughout the Pleistocene. Yet, the use of $\delta^{18}O$ within palaeoclimate reconstructions has been questioned (Gierz et al., 2017) due to the numerous factors that affect $\delta^{18}O$, including both climatological (e.g., source water $\delta^{18}O$, precipitation amount, rainout, air temperature), and karst system (e.g., cave temperature, drip rate, degassing) processes.

While the relationship between $\delta^{18}O$ and modern precipitation in Arabia is well established, this should be tested with independent proxies. Sr/Ca and Mg/Ca values have shown promise as additional precipitation proxies. Unlike rainfall $\delta^{18}O$, these are derived from the soils above the cave and they are not affected by airmass history. Initial Sr, Mg and Ca measurements were attained for Y99 growth phase I-V via ICP-OES analyses and are provided in appendices (Tab. S22-S28). One striking finding was that neither Sr/Ca or Mg/Ca from GI-I were correlated to each other, $\delta^{18}O_{ca}$ or $\delta^{13}C_{ca}$, perhaps suggesting some cave-specific controls on each record.

9.4.3 Temporal distribution

Palaeoclimate records provided in this thesis detail wet events in Arabia over the last 4.3 Ma. The most profound observation is the relationship between speleothem growth ages and northern hemisphere insolation (NHI) maxima. As discussed in chapter 2, during boreal summer insolation maxima, the increased low-latitude interhemispheric pressure gradient enhanced the monsoons in the Indo-Pacific (Beck et al., 2018). Periods of high orbital eccentricity and low precession result in greater northern hemisphere insolation, which in turn intensify Indian ocean monsoons. While there is good coherence between Y99 growth ages, eccentricity maxima and precession minima for the last 1.1 million years, we have recorded no speleothem growth between ~2.5-1.1 Ma. The aforementioned processes suggest this may be due to an absence of samples, rather than a difference of precipitation regimes. Indeed, within this time interval sapropel layers within ODP 967 suggests that the Sahara continued to undergo punctuated green periods, as a result of enhanced humidity (Grant et al., 2017). Sapropel deposition is particularly frequent between 2-1.3 Ma, which is a crucial time for the proposed initial hominin

dispersals from Africa (Lordkipanidze et al., 2007b; Messager et al., 2011). However, the Mediterranean has a broad catchment and is influenced by a number of climatological and environmental factors, wet Saharo-Arabia periods interpreted from Mediterranean sediment cores must be corroborated by terrestrial records. It is therefore vital that future work must provide precisely dated palaeoclimate records that span this period.

Improving the absolute chronology of Y99 could be another important aim of future work. In chapter 5, three U-Pb ages extended the chronology of Y99 to ~1.1 Ma BP, beyond the range of ^{230}Th dating. No absolute ages were attained between Growth Intervals XIII (0.85 ± 0.069 Ma: MIS 21) and XVIII (1.072 ± 0.048 to 1.073 ± 0.042: MIS 31). While the intermediate growth phases could be assigned to the remaining peak interglacial periods and warm substages, an absolute chronology ought to be developed. This may be achieved by further U-Pb dating using both MC-ICP-MS and LA-ICP-MS techniques, and was suggested in initial reviews. The growth phases likely date to the lower limits of U-Pb dating and upper limits of ^{230}Th dating, meaning that ages attained from these growth phases would be characterised by large dating uncertainties (e.g., Woodhead et al., 2006, 2012; Cheng et al., 2013). A recent study has used a combination of multiple aliquot and single aliquot U-Pb measurements and age modelling software to construct a robust age-model for a stalagmite from Corichia Cave (Italy), with age uncertainties of <10 kyrs between 965-950 and 885-865 ka BP (Bajo et al., 2020). Applying this method to the growth intervals between GI XIII and GI XVIII could provide some clarity on their ages.

9.4.4 Spatial distribution

Within this thesis, palaeoclimate reconstructions have been developed over a broad latitudinal transect from 30.13°N to 14.92°N. This distribution has allowed the latitudinal migration of the tropical rain-belt to be precisely tracked on broad interglacial-glacial timescales. Yet, the extent of Pleistocene rain-belt migrations has mostly relied the on palaeoclimate records situated further to the north (e.g., Rosenberg et al., 2013; Parton et al., 2018), which may have lower activation thresholds and cannot currently determine moisture source. Moreover, while speleothems are indeed excellent 'master' records, showing large-scale regional climate changes, the current distribution of speleothem records means it is not possible to show more local climate signatures and 'micro-climates' (see Chapter 8). Micro-climates and micro-environments could be key for understanding climatic variability and human-environment interactions during green Arabia, as well as their spatio-temporal variability. For example, to what extent did climatic variation create more or less "attractive" habitats and could these have been reflected by increased/decreased population densities? Increasing the spatial distribution of palaeoclimate records (including speleothems) is therefore key to building a robust representation of Arabian palaeoenvironments. These may then be used to explore key issues concerning the 'lived' experience of *H. sapiens* populations during these wet phases.

A Saudi Geological Survey report provided locations and surveys of caves across Saudi Arabia. These were clustered in southwestern, eastern and northern Saudi Arabia (Fig. 63). Many of these sites contained fossil speleothems; analyses of speleothems from these caves, following the methods outlined throughout this thesis, could provide further

evidence for the extent of tropical rain-belt migration and the palaeoenvironments of Arabia.

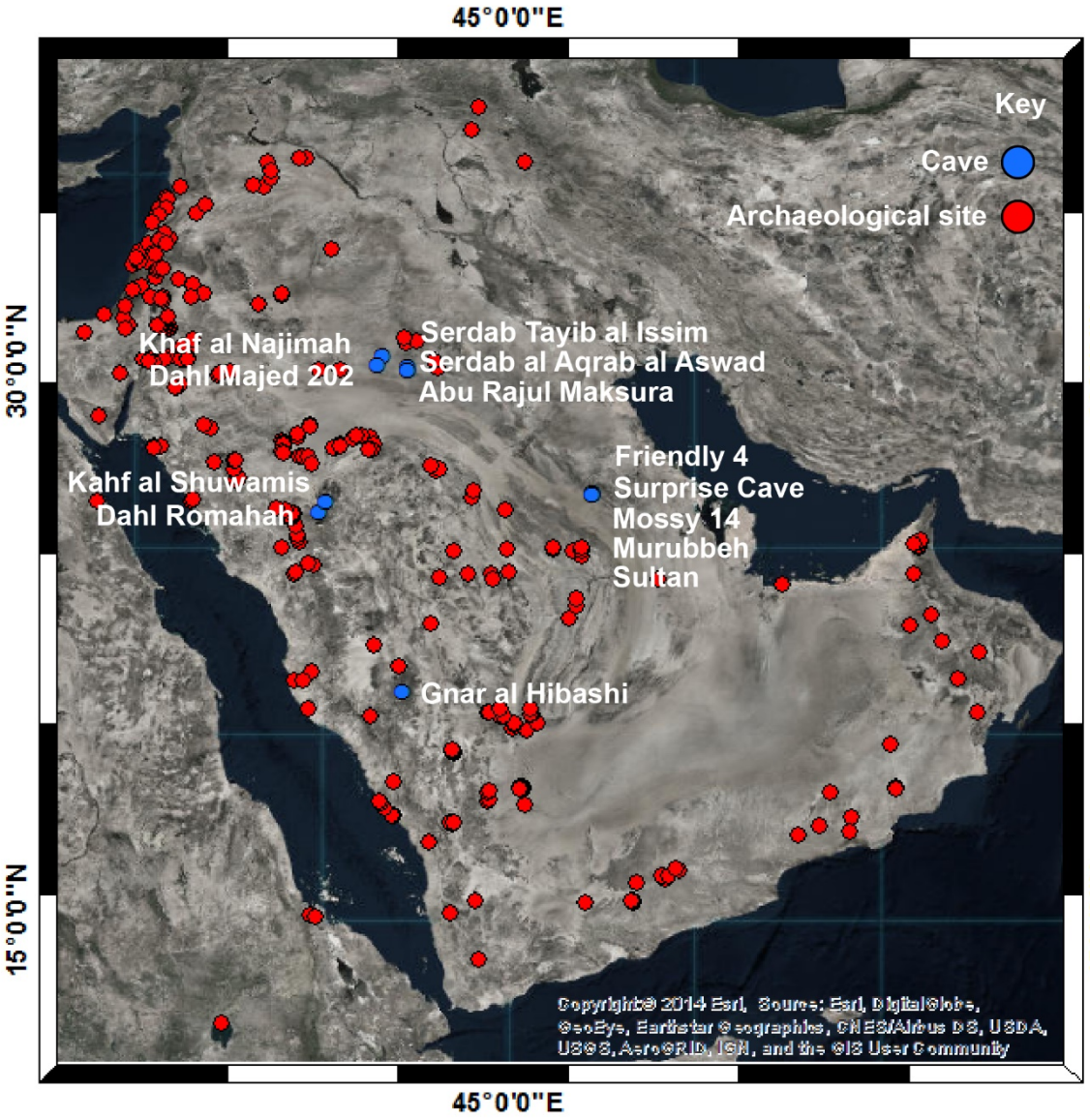

Fig. 63. Map of stalagmite caves (blue circles) in Arabia with MSA archaeological sites (red circles). Locations of caves are provided in Forti et al. (2003), Fleitmann et al. (2004) and SGS (2007).

9.4.5 Environmental character

A pertinent issue for the study of green Arabia is that current descriptions of the landscape have been simplistically limited to "green", "grassland" or "savannah-type". As discussed in chapters 2 and 8, the modern landscape of Arabia is highly heterogenous, with environments varying by annual precipitation, topography, soil type etc (Miller and Cope, 1996). It is therefore important to ask why should "green" Arabia be characterised simply as a "grassland"? Indeed, East Africa, a potential analogue for green Arabia, is a highly heterogenous landscape, containing numerous environments (e.g., savannahs, semi-arid grasslands, coastal mangroves, mountain forests), each with different flora and faunal constituents from the other (Lind and Morrison, 1974). These, again, vary by altitude, annual precipitation, topography etc. This variation also continues on a local level, in which micro-environments play a key role in local biodiversity. The role of such landscape variability at regional and local levels in Arabia (both spatiality and temporally) have yet to be identified and included in environmental models; however, this is key for understanding human-environment interactions throughout Arabia and dispersal mechanisms. For example, were there areas that supported human occupation in glacial periods? Or did each climate optima see a new wave of dispersal?

It has not been possible to resolve these issues within this thesis as the relationship between $\delta^{13}C_{ca}$ and vegetation is complicated by a variety of signals (e.g., atmospheric/soil/cave limestone CO_2 contribution, vegetation density, soil humidity, soil temperature, drip-rate, prior calcite precipitation and degassing along the flow path). Without close monitoring of the evolution of $\delta^{13}C_{drip\text{-}water}$ from soil end members above the cave, it is difficult to directly relate $\delta^{13}C_{ca}$ variation to changes in vegetation (e.g., Mickler et al., 2019). Even when an environmental signature can be established, $\delta^{13}C_{ca}$

provides extremely limited detail on taxonomic composition of vegetation above the cave. Moreover, current flora records are predominantly based on phytoliths (e.g., Bretzke et al., 2013; Jennings et al., 2016), which only provide family-level identification. In order to fully comprehend landscape variability – and understand how human populations survived these landscapes – it is crucial to provide more detailed information on the constituent species of 'Green Arabia'.

Speleothems may be used to achieve this. As mixing of precipitation water with CO_2 predominantly occurs within the soil zone, organic components can be incorporated into the groundwater and resultant speleothem. These can include amino acids, fossil pollen, lipid biomarkers (particularly *n*-alkanes) and ancient DNA. Advances in the extraction of ancient DNA from speleothems have successfully allowed identification of Quaternary flora and fauna above Solkota Cave, Georgia (Stahlschmidt et al., 2019). This exciting new technique could be applied to Arabian speleothems, as their subterranean location is perhaps more likely to preserve aDNA than more exposed locations (e.g., palaeolake deposits). The information that aDNA provides would substantially increase the knowledge of Arabian palaeoenvironments and could be used to model human-environment interactions in Arabia.

9.4.6 Relationship between palaeoclimate records and human records

Apart from palaeolake sediments, there are virtually no palaeoclimate records from Arabia that bare contextual relationship to Pleistocene human remains of any sort. While thesis has produced a variety of palaeoclimate data, it lacks contextual association with archaeological material. In other words, while this can provide broad regional climatic

signals, they do not provide precise details on the "lived" environments of human populations and can only provide a limited understanding of human-environment interactions. Thus, it is imperative to provide further precisely-dated palaeoclimate records with close relationships to archaeological material.

A recent SGS report provided initial surveys of numerous caves with fossil and active speleothem growth. Many of the sites contained a mixture of animal remains (SGS, 2007), yet extensive analyses have not been conducted. The random assortment of faunal composition raises questions as to whether human remains may be present. If the stratigraphic and depositional history of these fossils can be linked to cave speleothems, the combination of speleothem and palaeontological analyses could accurately associate fauna (and potentially humans) to specific wet periods.

Another method to achieve this would be to produce high-resolution records from deposits of which archaeological material has already been uncovered. Many of the dated Pleistocene archaeological assemblages from Arabia have been derived from palaeolake sediments, and the Al Wusta palaeolake provided the only current example of a Pleistocene *H. sapiens* fossil. Freshwater molluscs (including gastropods and bivalves) are common within palaeolake deposits and offer a unique palaeoclimate archive. Similarly, to speleothems, mollusc shells are formed of calcium carbonate ($CaCO_3$) polymorphs, including calcite but mostly aragonite that are formed in consecutive growth layers. Identification of growth regular growth layers and knowledge of growth rates permit the construction of ultra-high-resolution $\delta^{18}O_{shell}$ and $\delta^{13}C_{shell}$ palaeoclimate records. In freshwater molluscs $\delta^{18}O_{shell}$ tends to represent salinity of water at the time of formation (changes in salinity are diagnostic of freshwater input and therefore reflect an

amount effect); whereas $\delta^{13}C_{shell}$ is reflected by ambient CO_2 and dissolved inorganic carbon in the lake environment (Leng and Lewis, 2016). Moreover, as the molluska class is highly specious with specific ecological niches, their identification alone provides a great deal of palaeoclimatic and palaeoenvironmental environmental information including temperature, rainfall and humidity, soil type and chemistry, water salinity and chemistry (Twaddle et al., 2016). Identification of mollusc species and analysis of $\delta^{18}O/\delta^{13}C_{shell}$ offer a unique method to produce high-resolution palaeoclimate records with contextual relationships to archaeological material.

9.5 Conclusion

In summary, this thesis has provided new palaeoclimate records from key times and locations for hominin dispersals. Data shows that South Arabian Humid Periods were caused by northward migration of the tropical rain-belt during periods of low glacial-coverage and increased northern hemisphere insolation. The expansion of the monsoon domain created landscapes characterised by abundant freshwater and ample vegetation resources, which provided habitats to facilitate hominin occupations and dispersal over the last 1.1 million years. Not only does this highlight the potential for an older archaeological record of Arabia than previously thought, this also highlights the role that Saharo-Arabian palaeoenvironment fluctuations – driven by monsoon domain variability – had on long-term hominin distribution and dispersals.

Bibliography

Abotalib, A.Z., Sultan, M., Jimenez, G., Crossey, L., Karlstrom, K., Forman, S., Krishnamurthy, R. V., Elkadiri, R., Polyak, V., 2019. Complexity of Saharan paleoclimate reconstruction and implications for modern human migration. Earth and Planetary Science Letters. 508, 74–84.

Affolter, S., Fleitmann, D., Leuenberger, M., 2014. New online method for water isotope analysis of speleothem fluid inclusions using laser absorption spectroscopy (WS-CRDS). Climate of the Past. 10, 1291–1304.

Affolter, S., Häuselmann, A.D., Fleitmann, D., Häuselmann, P., Leuenberger, M., 2015. Triple isotope (δD, δ17O, δ18O) study on precipitation, drip water and speleothem fluid inclusions for a Western Central European cave (NW Switzerland). Quaternary Science Reviews. 127, 73–89.

Agustí, J., Lordkipanidze, D., 2011. How " African" was the early human dispersal out of Africa? Quaternary Science Reviews. 30, 1338–1342.

Al-ameri, A., Schneider, M., Abu Lohom, N., Sprenger, C., 2014. The Hydrogen (δD) and Oxygen (δ18O) Isotopic Composition of Yemen's Rainwater. Arabian Journal for Science and Engineering. 39, 423–436.

Allen, J., O'Connell, J., 2014. Both half right:Updating the evidence for dating first human arrivals in Sahul. Australian Archaeology. 79, 86–108.

Allen, M.B., Armstrong, H.A., 2008. Arabia-Eurasia collision and the forcing of mid-Cenozoic global cooling. Palaeogeography, Palaeoclimatology, Palaeoecology. 265, 52–58.

Almazroui, M., 2011. Sensitivity of a regional climate model on the simulation of high

intensity rainfall events over the Arabian Peninsula and around Jeddah (Saudi Arabia). Theoretical and Applied Climatology. 104, 261–276.

Almazroui, M., Islam, M.N., Jones, P.D., Athar, H., Rahman, M.A., 2012. Recent climate change in the Arabian Peninsula: Seasonal rainfall and temperature climatology of Saudi Arabia for 1979-2009. Atmospheric Research. 111, 29–45.

Almogi-Labin, A., Schmiedl, G., Hemleben, C., Siman-Tov, R., Segl, M., Meischner, D., 2000. The influence of the NE winter monsoon on productivity changes in the Gulf of Aden, NW Arabian Sea, during the last 530 ka as recorded by foraminifera. Marine Micropaleontology. 40, 295–319.

Amies, J.D., Rohling, E.J., Grant, K.M., Rodríguez-Sanz, L., Marino, G., 2019. Quantification of African Monsoon Runoff During Last Interglacial Sapropel S5. Paleoceanography and Paleoclimatology. 34, 1487–1516.

Amirkhanov, H., 1994. Research on the Palaeolithic and Neolithic of Hadramaut and Mahra. Arabian Archaeology and Epigraphy. 5, 217–228.

An, Z.S., Zhang, P.Z., Wang, E., Wang, S.M., Qiang, X.K., 2006. Changes of the monsoon-arid environment in China and growth of the Tibetan Plateau since the Miocene. Quaternary Science. 26, 678–693.

Ao, H., Roberts, A.P., Dekkers, M.J., Liu, X., Rohling, E.J., Shi, Z., An, Z., Zhao, X., 2016. Late Miocene-Pliocene Asian monsoon intensification linked to Antarctic ice-sheet growth. Earth and Planetary Science Letters. 444, 75–87.

Armitage, S.J., Bristow, C.S., Drake, N.A., 2015. West African monsoon dynamics inferred from abrupt fluctuations of Lake Mega-Chad. Proceedings of the National Academy of Sciences. 112, 8543–8548.

Armitage, S.J., Drake, N.A., Stokes, S., El-Hawat, A., Salem, M.J., White, K., Turner, P., McLaren, S.J., 2007. Multiple phases of North African humidity recorded in

lacustrine sediments from the Fazzan Basin, Libyan Sahara. Quaternary Geochronology. 2, 181–186.

Armitage, S.J., Jasim, S.A., Marks, A.E., Parker, A.G., Usik, V.I., Uerpmann, H.P., 2011. The southern route "out of Africa": Evidence for an early expansion of modern humans into Arabia. Science. 331, 453–456.

Arsuaga, J.L., Martínez, I., Gracia, A., Lorenzo, C., 1997. The Sima de los Huesos crania (Sierra de Atapuerca, Spain). A comparative study. Journal of Human Evolution. 33, 219–281.

Ascenzi, A., Biddittu, I., Cassoli, P.F., Segre, A.G., Segre-Naldini, E., 1996. A calvarium of late Homo erectus from Ceprano, Italy. Journal of Human Evolution. 31, 409–423.

Asrat, A., Baker, A., Leng, M.J., Hellstrom, J., Mariethoz, G., Boomer, I., Yu, D., Jex, C.N., Gunn, J., 2018. Paleoclimate change in Ethiopia around the last interglacial derived from annually-resolved stalagmite evidence. Quaternary Science Reviews. 202, 197–210.

Ayalon, A., Bar-Matthews, M., Kaufman, A., 2002. Climatic conditions during marine oxygen isotope stage 6 in the eastern Mediterranean region from the isotopic composition of speleothems of Soreq Cave, Israel. Geology. 30, 303–306.

Ayalon, A., Bar-Matthews, M., Sass, E., 1998. Rainfall-recharge relationships within a karstic terrain in the Eastern Mediterranean semi-arid region, Israel: δ 18O and δD characteristics. Journal of Hydrology. 207, 18–31.

Backeberg, B.C., Penven, P., Rouault, M., 2012. Impact of intensified Indian Ocean winds on mesoscale variability in the Agulhas system. Nature Climate Change. 2, 608–612.

Badertscher, S., Borsato, A., Frisia, S., Cheng, H., Edwards, R.L., Tüysüz, O.,

Fleitmann, D., 2014. Speleothems as sensitive recorders of volcanic eruptions – the Bronze Age Minoan eruption recorded in a stalagmite from Turkey. Earth and Planetary Science Letters. 392, 58–66.

Bae, C.J., Douka, K., Petraglia, M.D., 2017. On the origin of modern humans: Asian perspectives. Science. 358, eaai9067.

Bailey, G., 2010. The Red Sea, Coastal Landscapes, and Hominin Dispersals. In: Petraglia, M.D., Rose, J.I. (Eds.), The Evolution of Human Populations in Arabia. Springer, Dordrecht, pp. 15–37.

Bailey, G.N., Devès, M.H., Inglis, R.H., Meredith-Williams, M.G., Momber, G., Sakellariou, D., Sinclair, A.G.M., Rousakis, G., Al Ghamdi, S., Alsharekh, A.M., 2015. Blue Arabia: Palaeolithic and underwater survey in SW Saudi Arabia and the role of coasts in Pleistocene dispersals. Quaternary International. 382, 42–57.

Bajo, P., Drysdale, R.N., Woodhead, J.D., Hellstrom, J.C., Hodell, D., Ferretti, P., Voelker, A.H.L., Zanchetta, G., Rodrigues, T., Wolff, E., Tyler, J., Frisia, S., Spötl, C., Fallick, A.E., 2020. Persistent influence of obliquity on ice age terminations since the Middle Pleistocene transition. Science. 367, 1235–1239.

Bajo, P., Hellstrom, J., Frisia, S., Drysdale, R., Black, J., Woodhead, J., Borsato, A., Zanchetta, G., Wallace, M.W., Regattieri, E., Haese, R., 2016. "Cryptic" diagenesis and its implications for speleothem geochronologies. Quaternary Science Reviews. 148, 17–28.

Baker, A., Ito, E., Smart, P.L., McEwan, R.F., 1997. Elevated and variable values of 13C in speleothems in a British cave system. Chemical Geology. 136, 263–270.

Bar-Matthews, M., Ayalon, A., Gilmour, M., Matthews, A., Hawkesworth, C.J., 2003. Sea - land oxygen isotopic relationships from planktonic foraminifera and speleothems in the Eastern Mediterranean region and their implication for

paleorainfall during interglacial intervals. Geochimica et Cosmochimica Acta. 67, 3181–3199.

Bar-Matthews, M., Ayalon, A., Kaufman, A., 2000. Timing and hydrological conditions of Sapropel events in the Eastern Mediterranean, as evident from speleothems, Soreq cave, Israel. Chemical Geology. 169, 145–156.

Bar-Matthews, M., Ayalon, A., Matthews, A., Sass, E., Halicz, L., 1996. Carbon and oxygen isotope study of the active water-carbonate system in a karstic Mediterranean cave: Implications for paleoclimate research in semiarid regions. Geochimica et Cosmochimica Acta. 60, 337–347.

Bar-Matthews, M., Matthews, A., Ayalon, A., 1991. Environmental Controls of Speleothem Mineralogy in a Karstic Dolomitic Terrain (Soreq Cave, Israel). The Journal of Geology. 99, 189–207.

Bar-Yosef, O., 1994. The lower paleolithic of the Near East. Journal of World Prehistory. 8, 211–265.

Bar-Yosef, O., Belmaker, M., 2011. Early and Middle Pleistocene Faunal and hominins dispersals through Southwestern Asia. Quaternary Science Reviews. 30, 1318–1337.

Bard, E., Delaygue, G., Rostek, F., Antonioli, F., Silenzi, S., Schrag, D.P., 2002. Hydrological conditions over the western Mediterranean basin during the deposition of the cold Sapropel 6 (ca. 175 Kyr BP). Earth and Planetary Science Letters. 202, 481–494.

Basha, G., Kishore, P., Venkat Ratnam, M., Ouarda, T.B.M.J., Velicogna, I., Sutterley, T., 2015. Vertical and latitudinal variation of the intertropical convergence zone derived using GPS radio occultation measurements. Remote Sensing of Environment. 163, 262–269.

Bassinot, F.C., Labeyrie, L.D., Vincent, E., Quidelleur, X., Shackleton, N.J., Lancelot, Y., 1994. The astronomical theory of climate and the age of the Brunhes-Matuyama magnetic reversal. Earth and Planetary Science Letters. 126, 91–108.

Beauvilain, A., 2008. The contexts of discovery of Australopitheucs bahrelghazalie (Abel) and of Sahelnathropus tchadensis (Tourmaï): unearthed, embedded in sandstone, or surface collected? South Africa Journal of Science. 104, 165–168.

Beck, J.W., Zhou, W., Li, C., Wu, Z., White, L., Xian, F., Kong, X., An, Z., 2018. A 550,000-year record of East Asian monsoon rainfall from 10Be in loess. Science. 360, 877–881.

Belmaker, M., 2011. On the Road to China: The Environmental Landscape of the Early Pleistocene in Western Eurasia and Its Implication for the Dispersal of Homo. In: Norton, C.J., Braun, D.R. (Eds.), Asian Paleoanthropology. Springer, Dordrecht, pp. 31–40.

Belmaker, M., Tchernov, E., Condemi, S., Bar-Yosef, O., 2002. New evidence for hominid presence in the Lower Pleistocene of the Southern Levant. Journal of Human Evolution. 43, 43–56.

Berger, A., Li, X.S.S., Loutre, M.F.F., 1999. Modelling northern hemisphere ice volume over the last 3 Ma. Quaternary Science Reviews. 18, 1–11.

Berger, A., Loutre, M.F., 1991. Insolation values for the climate of the last 10 million years. Quaternary Science Reviews. 10, 297–317.

Berger, A., Loutre, M.F., 1999. Parameters of the Earths orbit for the last 5 Million years in 1 kyr resolution. Supplement to: Berger, A; Loutre, M F (1991): Insolation values for the climate of the last 10 million of years. Quaternary Science Reviews, 10(4), 297-317, doi:10.1016/0277-3791(91)90033-Q.

Berger, W.H., Jansen, E., 1994. Mid-Pleistocene Climate Shift—The Nansen

Connection. In: Johannessen, O.M., Muench, R.D., Overland, J.E. (Eds.), The Polar Oceans and Their Role in Shaping the Global Environment, Volume 84. American Geophysical Union, Washington DC, pp. 295–311.

Bergström, A., McCarthy, S.A., Hui, R., Almarri, M.A., Ayub, Q., Danecek, P., Chen, Y., Felkel, S., Hallast, P., Kamm, J., Blanché, H., Deleuze, J.-F., Cann, H., Mallick, S., Reich, D., Sandhu, M.S., Skoglund, P., Scally, A., Xue, Y., Durbin, R., Tyler-Smith, C., 2020. Insights into human genetic variation and population history from 929 diverse genomes. Science. 367, eaay5012.

Bermúdez de Castro, J.M., Martinón-Torres, M., Gómez-Robles, A., Prado-Simón, L., Martín-Francés, L., Lapresa, M., Olejniczak, A., Carbonell, E., 2011. Early Pleistocene human mandible from Sima del Elefante (TE) cave site in Sierra de Atapuerca (Spain): A comparative morphological study. Journal of Human Evolution. 61, 12–25.

Bettis, E.A., Milius, A.K., Carpenter, S.J., Larick, R., Zaim, Y., Rizal, Y., Ciochon, R.L., Tassier-Surine, S.A., Murray, D., Suminto, Bronto, S., 2009. Way out of Africa: Early Pleistocene paleoenvironments inhabited by Homo erectus in Sangiran, Java. Journal of Human Evolution. 56, 11–24.

Beyer, R.M., Krapp, M., Eriksson, A., Manica, A., 2020. Windows out of Africa: A 300,000-year chronology of climatically plausible human contact with Eurasia. bioRxiv. 2020.01.12.901694.

Binford, L., 2001. Constructing Frames of Reference. An analytical method for archaeological theory building using ethnographic and environmental data. University of California Press, London.

Blain, H.A., Agustí, J., Lordkipanidze, D., Rook, L., Delfino, M., 2014. Paleoclimatic and paleoenvironmental context of the Early Pleistocene hominins from Dmanisi

(Georgia, Lesser Caucasus) inferred from the herpetofaunal assemblage. Quaternary Science Reviews. 105, 136–150.

Blechschmidt, I., Matter, A., Preusser, F., Rieke-Zapp, D., 2009. Monsoon triggered formation of Quaternary alluvial megafans in the interior of Oman. Geomorphology. 110, 128–139.

Blegen, N., 2017. The earliest long-distance obsidian transport: Evidence from the ~200 ka Middle Stone Age Sibilo School Road Site, Baringo, Kenya. Journal of Human Evolution. 103, 1–19.

Blinkhorn, J., Achyuthan, H., Ajithprasad, P., 2015. Middle Palaeolithic point technologies in the Thar Desert, India. Quaternary International. 382, 237–249.

Blinkhorn, J., Achyuthan, H., Petraglia, M., Ditchfield, P., 2013. Middle Palaeolithic occupation in the Thar Desert during the Upper Pleistocene: the signature of a modern human exit out of Africa? Quaternary Science Reviews. 77, 233–238.

Blinkhorn, J., Ajithprasad, P., Mukherjee, A., Kumar, P., Durcan, J., Roberts, P., 2019. The first directly dated evidence for Palaeolithic occupation on the Indian coast at Sandhav, Kachchh. Quaternary Science Reviews. 224, 105975.

Blome, M.W., Cohen, A.S., Tryon, C.A., Brooks, A.S., Russell, J., 2012. The environmental context for the origins of modern human diversity: A synthesis of regional variability in African climate 150,000-30,000 years ago. Journal of Human Evolution. 62, 563–592.

Bond, G.C., Lotti, R., 1995. Iceberg discharges into the North Atlantic on millennial time scales during the last glaciation. Science. 267, 1005–1010.

Borsato, A., Frisia, S., Fairchild, I.J., Somogyi, A., Susini, J., 2007. Trace element distribution in annual stalagmite laminae mapped by micrometer-resolution X-ray

fluorescence: Implications for incorporation of environmentally significant species. Geochimica et Cosmochimica Acta. 71, 1494–1512.

Borsato, A., Quinif, Y., Bini, A., Dublyansky, Y. V., 2003. Open-system alpine speleothems: implications for U-series dating and palaeoclimate reconstructions. Studi Trentini di Scienze Naturali – Acta Geologica. 80, 71–83.

Bowler, D.E., Benton, T.G., 2005. Causes and consequences of animal dispersal strategies: relating individual behaviour to spatial dynamics. Biological Reviews. 80, 205–225.

Bowler, J.M., Johnston, H., Olley, J.M., Prescott, J.R., Roberts, R.G., Shawcross, W., Spooner, N.A., 2003. New ages for human occupation and climatic change at Lake Mungo, Australia. Nature. 421, 837–840.

Braun, D.R., Aldeias, V., Archer, W., Arrowsmith, J.R., Baraki, N., Campisano, C.J., Deino, A.L., DiMaggio, E.N., Dupont-Nivet, G., Engda, B., Feary, D.A., Garello, D.I., Kerfelew, Z., McPherron, S.P., Patterson, D.B., Reeves, J.S., Thompson, J.C., Reed, K.E., 2019. Earliest known Oldowan artifacts at >2.58 Ma from Ledi-Geraru, Ethiopia, highlight early technological diversity. Proceedings of the National Academy of Sciences. 116, 201820177.

Breecker, D.O., 2017. Atmospheric pCO2 control on speleothem stable carbon isotope compositions. Earth and Planetary Science Letters. 458, 58–68.

Breeze, P.S., Drake, N.A., Groucutt, H.S., Parton, A., Jennings, R.P., White, T.S., Clark-Balzan, L., Shipton, C., Scerri, E.M.L., Stimpson, C.M., Crassard, R., Hilbert, Y., Alsharekh, A., Al-Omari, A., Petraglia, M.D., 2015. Remote sensing and GIS techniques for reconstructing Arabian palaeohydrology and identifying archaeological sites. Quaternary International. 382, 98–119.

Breeze, P.S., Groucutt, H.S., Drake, N.A., Louys, J., Scerri, E.M.L., Armitage, S.J.,

Zalmout, I.S.A., Memesh, A.M., Haptari, M.A., Soubhi, S.A., Matari, A.H., Zahir, M., Al-Omari, A., Alsharekh, A.M., Petraglia, M.D., 2017. Prehistory and palaeoenvironments of the western Nefud Desert, Saudi Arabia. Archaeological Research in Asia. 10, 1–16.

Breeze, P.S., Groucutt, H.S., Drake, N.A., White, T.S., Jennings, R.P., Petraglia, M.D., 2016. Palaeohydrological corridors for hominin dispersals in the Middle East ~250-70,000 years ago. Quaternary Science Reviews. 144, 155–185.

Bretzke, K., Armitage, S.J., Parker, A.G., Walkington, H., Uerpmann, H.P., 2013. The environmental context of Paleolithic settlement at Jebel Faya, Emirate Sharjah, UAE. Quaternary International. 300, 83–93.

Bretzke, K., Conard, N.J., 2017. Not just a crossroad population dynamics and changing material culture in southwestern asia during the late pleistocene. Current Anthropology. 58, S449–S462.

Bretzke, K., Conard, N.J., Uerpmann, H.P., 2014. Excavations at jebel faya - the FAY-NE1 shelter sequence. Proceedings of the Seminar for Arabian Studies. 44, 69–81.

Bretzke, K., Yousif, E., Jasim, S., 2018. Filling in the gap – The Acheulean site Suhailah 1 from the central region of the Emirate of Sharjah, UAE. Quaternary International. 466, 23–32.

Brierley, C.M., Fedorov, A. V, Liu, Z., Herbert, T.D., Lawrence, Ki.T., LaRiviere, J.P., 2009. Greatly Expanded Tropical Warm Pool and Weakened Hadley Circulation in the Early Pliocene. Science. 323, 1714–1718.

Brooks, A.S., Yellen, J.E., Potts, R., Behrensmeyer, A.K., Deino, A.L., Leslie, D.E., Ambrose, S.H., Ferguson, J.R., D'Errico, F., Zipkin, A.M., Whittaker, S., Post, J., Veatch, E.G., Foecke, K., Clark, J.B., 2018. Long-distance stone transport and pigment use in the earliest Middle Stone Age. Science. 360, 90–94.

Brown, F., Harris, J., Leakey, R., Walker, A., 1985. Early Homo erectus skeleton from west Lake Turkana, Kenya. Nature. 316, 788–792.

Brown, G.E., Schmidt, D.L., Huffman Jr, A.C., 1989. Geology of the Arabian Peninsula; shield area of western Saudi Arabia.(No. 560-A). U.S. Geological Survey Professional Paper. 199.

Brunet, M., Guy, F., Pilbeam, D., Lieberman, D.E., Likius, A., Mackaye, H.T., Ponce De León, M.S., Zollikofer, C.P.E., Vignaud, P., 2005. New material of the earliest hominid from the Upper Miocene of Chad. Nature. 434, 752–755.

Brunet, M., Guy, F., Pilbeam, D., Mackaye, H.T., Likius, A., Ahounta, D., Beauvilain, A., Blondel, C., Bocherens, H., Boisserie, J.-R., De Bonis, L., Coppens, Y., Dejax, J., Denys, C., Duringer, P., Eisenmann, V., Fanone, G., Fronty, P., Geraads, D., Lehmann, T., Lihoreau, F., Louchart, A., Mahamat, A., Merceron, G., Mouchelin, G., Otero, O., Campomanes, P.P., De Leon, M.P., Rage, J.-C., Sapanet, M., Schuster, M., Sudre, J., Tassy, P., Valentin, X., Vignaud, P., Viriot, L., Zazzo, A., Zollikofer, C., 2002. A new hominid from the Upper Miocene of Chad, Central Africa. Nature. 418, 145–151.

Burns, S.J., Fleitmann, D., Matter, A., Kramers, J., Al-Subbary, A.A., 2003. Indian Ocean Climate and an Absolute Chronology over Dansgaard/Oeschger Events 9 to 13. Science. 301, 1365 LP – 1367.

Burns, S.J., Fleitmann, D., Matter, A., Neff, U., Mangini, A., 2001. Speleothem evidence from Oman for continental pluvial events during interglacial periods. Geology. 29, 623–626.

Burns, S.J., Matter, A., Frank, N., Mangini, A., 1998. Speleothem-based paleoclimate record from northern Oman. Geology. 26, 499–502.

Caseldine, C.J., McGarry, S.F., Baker, A., Hawkesworth, C., Smart, P.L., 2008. Late

Quaternary speleothem pollen in the British Isles. Journal of Quaternary Science. 23, 193–200.

Cerling, T.E., Wynn, J.G., Andanje, S.A., Bird, M.I., Korir, D.K., Levin, N.E., MacE, W., MacHaria, A.N., Quade, J., Remien, C.H., 2011. Woody cover and hominin environments in the past 6-million years. Nature. 476, 51–56.

Chan, E.K.F., Timmermann, A., Baldi, B.F., Moore, A.E., Lyons, R.J., Lee, S., Kalsbeek, A.M.F., Petersen, D.C., Rautenbach, H., Förtsch, H.E.A., Bornman, M.S.R., Hayes, V.M., 2019. Human origins in a southern African palaeo-wetland and first migrations. Nature. 575, 185–189.

Chauhan, P.R., 2009. Early Homo Occupation Near the Gate of Tears: Examining the Paleoanthropological Records of Djibouti and Yemen. In: Hovers, E., Braun, D.R. (Eds.), Interdisciplinary Approaches to the Oldowan. Springer, Dordrecht, pp. 49–59.

Chen, H., Xu, Z., Clift, P.D., Lim, D., Khim, B.K., Yu, Z., 2019. Orbital-scale evolution of the Indian summer monsoon since 1.2 Ma: Evidence from clay mineral records at IODP Expedition 355 Site U1456 in the eastern Arabian Sea. Journal of Asian Earth Sciences. 174, 11–22.

Cheng, H., Edwards, R.L., Broecker, W.S., Denton, G.H., Kong, X., Wang, Y., Zhang, R., Wang, X., 2009a. Ice age terminations. Science. 326, 248–252.

Cheng, H., Edwards, R.L., Hoff, J., Gallup, C.D., Richards, D.A., Asmerom, Y., 2000. The half-lives of uranium-234 and thorium-230. In: Chemical Geology.

Cheng, H., Edwards, R.L., Sinha, A., Spötl, C., Yi, L., Chen, S., Kelly, M., Kathayat, G., Wang, X., Li, X., Kong, X., Wang, Y., Ning, Y., Zhang, H., 2016. The Asian monsoon over the past 640,000 years and ice age terminations. Nature. 534, 640–646.

Cheng, H., Edwards, R.L., Wang, Y., Kong, X., Ming, Y., Kelly, M.J., Wang, X., Gallup, C.D., Liu, W., 2006. A penultimate glacial monsoon record from Hulu Cave and two-phase glacial terminations. Geology. 34, 217–220.

Cheng, H., Fleitmann, D., Edwards, R.L., Wang, X., Cruz, F.W., Auler, A.S., Mangini, A., Wang, Y., Kong, X., Burns, S.J., Matter, A., 2009b. Timing and structure of the 8.2. kyr B.P. event inferred from δ 18O records of stalagmites from China, Oman, and Brazil. Geology. 37, 1007–1010.

Cheng, H., Lawrence Edwards, R., Shen, C.C., Polyak, V.J., Asmerom, Y., Woodhead, J., Hellstrom, J., Wang, Y., Kong, X., Spötl, C., Wang, X., Calvin Alexander, E., 2013. Improvements in ^{230}Th dating, ^{230}Th and ^{234}U half-life values, and U-Th isotopic measurements by multi-collector inductively coupled plasma mass spectrometry. Earth and Planetary Science Letters. 371–372, 82–91.

Chiang, J.C.H., Fung, I.Y., Wu, C.H., Cai, Y., Edman, J.P., Liu, Y., Day, J.A., Bhattacharya, T., Mondal, Y., Labrousse, C.A., 2015. Role of seasonal transitions and westerly jets in East Asian paleoclimate. Quaternary Science Reviews. 108, 111–129.

Clark-Balzan, L., Parton, A., Breeze, P.S., Groucutt, H.S., Petraglia, M.D., 2017. Resolving problematic luminescence chronologies for carbonate- and evaporite-rich sediments spanning multiple humid periods in the Jubbah Basin, Saudi Arabia. Quaternary Geochronology. 45, 50–73.

Clark, I., Fritz, P., 1997. Environmnetal Istopes in Hydrogeology. Lewis Publishers, New York.

Clark, P.U., Archer, D., Pollard, D., Blum, J.D., Rial, J.A., Brovkin, V., Mix, A.C., Pisias, N.G., Roy, M., 2006. The middle Pleistocene transition: characteristics, mechanisms, and implications for long-term changes in atmospheric pCO2.

Quaternary Science Reviews. 25, 3150–3184.

Clark, R.J., 1976. New cranium of Homo erectus from Lake Ndutu, Tanzania. Nature. 262, 485–487.

Clarke, R.J., 1990. The Ndutu cranium and the origin ofHomo sapiens. Journal of Human Evolution. 19, 699–736.

Clarkson, C., Jacobs, Z., Marwick, B., Fullagar, R., Wallis, L., Smith, M., Roberts, R.G., Hayes, E., Lowe, K., Carah, X., Florin, S.A., McNeil, J., Cox, D., Arnold, L.J., Hua, Q., Huntley, J., Brand, H.E.A., Manne, T., Fairbairn, A., Shulmeister, J., Lyle, L., Salinas, M., Page, M., Connell, K., Park, G., Norman, K., Murphy, T., Pardoe, C., 2017. Human occupation of northern Australia by 65,000 years ago. Nature. 547, 306–310.

Clarkson, C., Petraglia, M., Korisettar, R., Haslam, M., Boivin, N., Crowther, A., Ditchfield, P., Fuller, D., Miracle, P., Harris, C., Connell, K., James, H., Koshy, J., 2009. The oldest and longest enduring microlithic sequence in India : 35 000 years of modern human occupation and change at the Jwalapuram Locality 9 rockshelter. Antiquity. 83, 326–348.

Clemens, S.C., Prell, W.L., 2003. A 350,000 year summer-monsoon multi-proxy stack from the Owen Ridge, Northern Arabian Sea. In: Marine Geology. pp. 35–51.

Coogan, L.A., Parrish, R.R., Roberts, N.M.W., 2016. Early hydrothermal carbon uptake by the upper oceanic crust: Insight from in situ U-Pb dating. Geology. 44, 147–150.

Crassard, R., Hilbert, Y.H., 2013. A Nubian Complex Site from Central Arabia: Implications for Levallois Taxonomy and Human Dispersals during the Upper Pleistocene. PLoS ONE. 8.

Crassard, R., Petraglia, M.D., Drake, N.A., Breeze, P., Gratuze, B., Alsharekh, A.,

Arbach, M., Groucutt, H.S., Khalidi, L., Michelsen, N., Robin, C.J., Schiettecatte, J., 2013. Middle Palaeolithic and Neolithic Occupations around Mundafan Palaeolake, Saudi Arabia: Implications for Climate Change and Human Dispersals. PLoS ONE. 8, e69665.

Crémière, A., Lepland, A., Chand, S., Sahy, D., Condon, D.J., Noble, S.R., Martma, T., Thorsnes, T., Sauer, S., Brunstad, H., 2016. Timescales of methane seepage on the Norwegian margin following collapse of the Scandinavian Ice Sheet. Nature Communications. 7, 11509.

Currat, M., Excoffier, L., 2004. Modern Humans Did Not Admix with Neanderthals during Their Range Expansion into Europe. PLoS Biology. 2, e421.

Dabbagh, A., Emmermann, R., Hötzl, H., Jado, A., Lippolt, H., Kollmann, W., Moser, H., Rauert, W., Zötl, J., 1984. The development of Tihamat Asir during the Quaternary. In: Jado, A.R., Zötl, J.G. (Eds.), Quaternary Period in Saudi Arabia Volume 2: Sedimentological, Hydrogeological, Hydrochemical, Geomorphological, Geochronological and Climatological Investigations in Western Saudi Arabia. Springer, Vienna, pp. 150–173.

Dai, Y.W., Zhang, C.C., Zhao, H.X., Wan, J.Z., Deng, L.L., Zhou, Z.Y., Dun, Y.Y., Liu, C.Q., Yuan, D., Wang, T., 2016. Chikusetsusaponin V attenuates lipopolysaccharide-induced liver injury in mice. Immunopharmacology and Immunotoxicology. 38, 167–174.

Dansgaard, W., 1964. Stable isotopes in precipitation. Tellus. 16, 436–468.

de Lumley, M.-A., 1981. L'Homme de Tautavel. Critères morphologiques et stade évolutif. In: de Lumley, H., Labeyri, J. (Eds.), Absolute Dating and Isotope Analysis in Prehistory – Methods and Limits. Prétirage, CNRS, Paris, pp. 43–73.

de Lumley, M.-A., 2015. L'homme de Tautavel. Un Homo erectus européen évolué.

Homo erectus tautavelensis. L'Anthropologie. 119, 303–348.

De Vries, A.J., Tyrlis, E., Edry, D., Krichak, S.O., Steil, B., Lelieveld, J., 2013. Extreme precipitation events in the Middle East: Dynamics of the Active Red Sea Trough. Journal of Geophysical Research Atmospheres. 118, 7087–7108.

Delagnes, A., Crassard, R., Bertran, P., Sitzia, L., 2013. Cultural and human dynamics in southern Arabia at the end of the Middle Paleolithic. Quaternary International.

Delagnes, A., Tribolo, C., Bertran, P., Brenet, M., Crassard, R., Jaubert, J., Khalidi, L., Mercier, N., Nomade, S., Peigné, S., Sitzia, L., Tournepiche, J.F., Al-Halibi, M., Al-Mosabi, A., MacChiarelli, R., 2012. Inland human settlement in southern Arabia 55,000 years ago. New evidence from the Wadi Surdud Middle Paleolithic site complex, western Yemen. Journal of Human Evolution. 63, 452–474.

deMenocal, P.B., 1995. Plio-Pleistocene African Climate. Science. 270, 53–59.

deMenocal, P.B., 2004. African climate change and faunal evolution during the Pliocene-Pleistocene. Earth and Planetary Science Letters. 220, 3–24.

Demuro, M., Arnold, L.J., Aranburu, A., Sala, N., Arsuaga, J.L., 2019. New bracketing luminescence ages constrain the Sima de los Huesos hominin fossils (Atapuerca, Spain) to MIS 12. Journal of Human Evolution. 131, 76–95.

Dennell, R., 2017. Human colonization of Asia in the late pleistocene the history of an invasive species. Current Anthropology. 58, S383–S396.

Dennell, R., Martinón-Torres, M., Bermúdez de Castro, J.M., 2011. Hominin variability, climatic instability and population demography in Middle Pleistocene Europe. Quaternary Science Reviews. 30, 1511–1524.

Dennell, R.W., 2008. The Palaeolithic Settlement of Asia. Cambridge University Press, Cambridge.

Dennell, R.W., 2010. "Out of Africa I": Current Problems and Future Prospects. In: Out

of Africa. pp. 247–273.

Dennell, R.W., 2011. The Colonization of "Savannahstan": Issues of Timing(s) and Patterns of Dispersal Across Asia in the Late Pliocene and Early Pleistocene. In: Norton, C.J., Braun, D.R. (Eds.), Asian Paleoanthropology. Springer, Dordrecht, pp. 7–30.

Dennell, R.W., 2013. Hominins, deserts, and the colonisation and settlement of continental Asia. Quaternary International. 300, 13–21.

Dennell, R.W., 2018. Pleistocene hominin dispersals, naïve faunas and social networks. In: Bovin, N., Crassard, R., Petraglia, M.D. (Eds.), Human Dispersal and Species Movement: From Prehistory to the Present. Cambridge University Press, Cambridge, pp. 62–89.

Dennell, R.W., Petraglia, M.D., 2012. The dispersal of Homo sapiens across southern Asia: How early, how often, how complex? Quaternary Science Reviews. 47, 15–22.

Dennell, R.W., Roebroeks, W., 2005. An Asian perspective on early human dispersal from Africa. Nature. 438, 1099–1104.

Dennis, P.F., Rowe, P.J., Atkinson, T.C., 2001. The recovery and isotopic measurement of water from fluid inclusions in speleothems. Geochimica et Cosmochimica Acta. 65, 871–884.

Drake, N., Breeze, P., 2016. Climate Change and Modern Human Occupation of the Sahara from MIS 6-2. In: Jones, S.C., Stewart, B.A. (Eds.), Africa from MIS 6-2, Vertebrate Paleobiology and Paleoanthropology. Springer, Dordrecht, pp. 103–122.

Drake, N.A., Blench, R.M., Armitage, S.J., Bristow, C.S., White, K.H., 2011. Ancient watercourses and biogeography of the Sahara explain the peopling of the desert.

Proceedings of the National Academy of Sciences. 108, 458–462.

Drake, N.A., Breeze, P., Parker, A., 2013. Palaeoclimate in the Saharan and Arabian Deserts during the Middle Palaeolithic and the potential for hominin dispersals. Quaternary International. 300, 48–61.

Dreybrodt, W., 2011. Comments on processes contributing to the isotope composition of 13C and 18O in calcite deposited to speleothems. Acta Carsologica. 40, 233–238.

Dublyansky, Y. V., Spötl, C., 2009. Hydrogen and oxygen isotopes of water from inclusions in minerals: design of a new crushing system and on-line continuous-flow isotope ratio mass spectrometric analysis. Rapid Communications in Mass Spectrometry. 23, 2605–2613.

Dünkeloh, A., Jacobeit, J., 2003. Circulation dynamics of Mediterranean precipitation variability 1948-98. International Journal of Climatology. 23, 1843–1866.

Edgell, H.S., 2006. Arabian Deserts: Nature, Origin and Evolution. Springer, Dordrecht.

Ehrmann, W., Schmiedl, G., Beuscher, S., Krüger, S., 2017. Intensity of African Humid Periods Estimated from Saharan Dust Fluxes. PLOS ONE. 12, e0170989.

El-Shenawy, M.I., Kim, S.-T., Schwarcz, H.P., Asmerom, Y., Polyak, V.J., 2018. Speleothem evidence for the greening of the Sahara and its implications for the early human dispersal out of sub-Saharan Africa. Quaternary Science Reviews. 188, 67–76.

Engel, M., Matter, A., Parker, A.G., Parton, A., Petraglia, M.D., Preston, G.W., Preusser, F., 2017. Lakes or wetlands? A comment on 'The middle Holocene climatic records from Arabia: Reassessing lacustrine environments, shift of ITCZ in Arabian Sea, and impacts of the southwest Indian and African monsoons' by

Enzel et al. Global and Planetary Change. 148, 258–267.

Enzel, Y., Kushnir, Y., Quade, J., 2015. The middle Holocene climatic records from Arabia: Reassessing lacustrine environments, shift of ITCZ in Arabian Sea, and impacts of the southwest Indian and African monsoons. Global and Planetary Change. 129, 69–91.

Epstein, S., Buchsbaum, R., Lowenstam, H., Urey, H.C., 1953. Revised carbonate–water isotopic temperature scale. Geological Society of America Bulletin. 64, 1315–1325.

Erlandson, J.M., Braje, T.J., 2015. Coasting out of Africa: The potential of mangrove forests and marine habitats to facilitate human coastal expansion via the Southern Dispersal Route. Quaternary International. 382, 31–41.

Fairchild, I.J., Borsato, A., Tooth, A.F., Frisia, S., Hawkesworth, C.J., Huang, Y., McDermott, F., Spiro, B., 2000. Controls on trace element (Sr–Mg) compositions of carbonate cave waters: implications for speleothem climatic records. Chemical Geology. 166, 255–269.

Fairchild, I.J., McMillan, E.A., 2007. Speleothems as indicators of wet and dry periods. International Journal of Speleology. 36, 69–74.

Fairchild, I.J., Smith, C.L., Baker, A., Fuller, L., Spötl, C., Mattey, D., McDermott, F., 2006. Modification and preservation of environmental signals in speleothems. Earth-Science Reviews. 75, 105–153.

Fairchild, I.J., Treble, P.C., 2009. Trace elements in speleothems as recorders of environmental change. Quaternary Science Reviews. 28, 449–468.

Falguères, C., Shao, Q., Han, F., Bahain, J.J., Richard, M., Perrenoud, C., Moigne, A.M., Lumley de, H., 2015. New ESR and U-series dating at Caune de l'Arago, France: A key-site for European Middle Pleistocene. Quaternary Geochronology.

30, 547–553.

Falguères, C., Yokoyama, Y., Shen, G., Bischoff, J.L., Ku, T.L., de Lumley, H., 2004. New U-series dates at the Caune de l'Arago, France. Journal of Archaeological Science. 31, 941–952.

Faure, H., Walter, R.C., Grant, D.R., 2002. The coastal oasis: Ice age springs on emerged continental shelves. Global and Planetary Change. 33, 47–56.

Feakins, S.J., Levin, N.E., Liddy, H.M., Sieracki, A., Eglinton, T.I., Bonnefille, R., 2013. Northeast African vegetation change over 12 m.y. Geology. 41, 295–298.

Fernandes, C.A., Rohling, E.J., Siddall, M., 2006. Absence of post-Miocene Red Sea land bridges: biogeographic implications. Journal of Biogeography. 33, 961–966.

Fick, S.E., Hijmans, R.J., 2017. WorldClim 2: new 1-km spatial resolution climate surfaces for global land areas. International Journal of Climatology. 37, 4302–4315.

Fisher, M., Membery, D.A., 1998. Climate. In: Ghazanfar, S.A., Fisher, M. (Eds.), Vegetation of the Arabian Peninsula. Springer, Dordrecht, pp. 5–38.

Fleitmann, D., 1997. Klastischer Eintrag in das Rote Meer und den Golf von Aden durch den Arabischen Monsun-Untersuchungen an Kolbenlot-Kernen. Diplom-Arbeit, Institut und Museum für Geologie und Paläontologie der Georg-August-Universität zu Göttingen.

Fleitmann, D., Burns, S.J., Mangini, A., Mudelsee, M., Kramers, J., Villa, I., Neff, U., Al-Subbary, A.A., Buettner, A., Hippler, D., Matter, A., 2007. Holocene ITCZ and Indian monsoon dynamics recorded in stalagmites from Oman and Yemen (Socotra). Quaternary Science Reviews. 26, 170–188.

Fleitmann, D., Burns, S.J., Mudelsee, M., Neff, U., Kramers, J., Mangini, A., Matter, A., 2003a. Holocene forcing of the Indian monsoon recorded in a stalagmite from

Southern Oman. Science. 300, 1737–1739.

Fleitmann, D., Burns, S.J., Neff, U., Mangini, A., Matter, A., 2003b. Changing moisture sources over the last 330,000 years in Northern Oman from fluid-inclusion evidence in speleothems. Quaternary Research. 60, 223–232.

Fleitmann, D., Burns, S.J., Neff, U., Mudelsee, M., Mangini, A., Matter, A., 2004a. Palaeoclimatic interpretation of high-resolution oxygen isotope profiles derived from annually laminated speleothems from Southern Oman. Quaternary Science Reviews. 23, 935–945.

Fleitmann, D., Burns, S.J., Pekala, M., Mangini, A., Al-Subbary, A., Al-Aowah, M., Kramers, J., Matter, A., 2011. Holocene and Pleistocene pluvial periods in Yemen, southern Arabia. Quaternary Science Reviews. 30, 783–787.

Fleitmann, D., Matter, A., 2009. The speleothem record of climate variability in Southern Arabia. Comptes Rendus - Geoscience. 341, 633–642.

Fleitmann, D., Matter, A., Pint, J.J., Al-Shanti, M.A., 2004b. The speleothem record of climate change in Saudi Arabia, Saudi Geological Survey.

Foley, R.A., 1987. Another Unique Species. Patterns in human evolutionary ecology. Harlow.

Frisia, S., Borsato, A., Fairchild, I.J., Susini, J., 2005. Variations in atmospheric sulphate recorded in stalagmites by synchrotron micro-XRF and XANES analyses. Earth and Planetary Science Letters. 235, 729–740.

Frumkin, A., Ford, D.C., Schwarcz, H.P., 1999. Continental oxygen isotopic record of the last 170,000 years in Jerusalem. Quaternary Research. 51, 317–327.

Gabunia, L., Vekua, A., Lordkipanidze, D., Swisher, C.C., Ferring, R., Justus, A., Nioradze, M., Tvalchrelidze, M., Antón, S.C., Bosinski, G., Jöris, O., Lumley, M.A.D., Majsuradze, G., Mouskhelishvili, A., 2000. Earliest Pleistocene hominid

cranial remains from Dmanisi, Republic of Georgia: Taxonomy, geological setting, and age. Science. 288, 1019–1025.

Gaillardet, J., Viers, J., Dupré, B., 2013. Trace Elements in River Waters. In: Treatise on Geochemistry: Second Edition.

Gallotti, R., 2016. The East African origin of the Western European Acheulean technology: Fact or paradigm? Quaternary International. 411, 9–24.

Garcea, E.A.A., 2016. Dispersals Out of Africa and Back to Africa: Modern origins in North Africa. Quaternary International. 408, 79–89.

Garrard, A.N., Harvey, C.P.D., Switsur, V.R., 1981. Environment and settlement during the Upper Pleistocene and Holocene at Jubba in the Great Nefud, northern Arabia. Atlal. 5, 137–148.

Gasse, F., Vidal, L., Van Campo, E., Demory, F., Develle, A.-L., Tachikawa, K., Elias, A., Bard, E., Garcia, M., Sonzogni, C., Thouveny, N., 2015. Hydroclimatic changes in northern Levant over the past 400,000 years. Quaternary Science Reviews. 111, 1–8.

Genty, D., Baker, A., Massault, M., Proctor, C., Gilmour, M., Pons-Branchu, E., Hamelin, B., 2001. Dead carbon in stalagmites: carbonate bedrock paleodissolution vs. ageing of soil organic matter. Implications for 13 C variations in speleothems. Geochimica et Cosmochimica Acta. 65, 3443–3457.

Genty, D., Vokal, B., Obelic, B., Massault, M., 1998. Bomb 14C time history recorded in two modern stalagmites - importance for soil organic matter dynamics and bomb 14C distribution over continents. Earth and Planetary Science Letters. 160, 795–809.

Geraads, D., Blondel, C., Likius, A., Mackaye, H.T., Vignaud, P., Brunet, M., 2008. New hippotragini (Bovidae, Mammalia) from the Late Miocene of Toros-Menalla

(Chad). Journal of Vertebrate Paleontology. 28, 231–242.

Geyh, M.A., Thiedig, F., 2008. The Middle Pleistocene Al Mahrúqah Formation in the Murzuq Basin, northern Sahara, Libya evidence for orbitally-forced humid episodes during the last 500,000 years. Palaeogeography, Palaeoclimatology, Palaeoecology. 257, 1–21.

Ghoneim, E., 2008. Optimum groundwater locations in the northern United Arab Emirates. International Journal of Remote Sensing. 29, 5879–5906.

Gierz, P., Werner, M., Lohmann, G., 2017. Simulating climate and stable water isotopes during the Last Interglacial using a coupled climate-isotope model. Journal of Advances in Modeling Earth Systems. 9, 2027–2045.

Glennie, K.W., Singhvi, A.K., 2002. Event stratigraphy, paleoenvironment and chronology of SE Arabian deserts. Quaternary Science Reviews. 21, 853–869.

Goede, A., McCulloch, M., McDermott, F., Hawkesworth, C., 1998. Aeolian contribution to strontium and strontium isotope variations in a Tasmanian speleothem. Chemical Geology. 149, 37–50.

Golledge, N.R., Thomas, Z.A., Levy, R.H., Gasson, E.G.W., Naish, T.R., McKay, R.M., Kowalewski, D.E., Fogwill, C.J., 2017. Antarctic climate and ice sheet configuration during a peak-warmth Early Pliocene interglacial. Climate of the Past Discussions. 13, 959–975.

Gonfiantini, R., Roche, M.-A., Olivry, J.-C., Fontes, J.-C., Zuppi, G.M., 2001. The altitude effect on the isotopic composition of tropical rains. Chemical Geology. 181, 147–167.

Gott, B., Murray, L., 1982. Ecology of root use by the Aborigines of southern Australia. Archeology of Oceania. 17, 59–67.

Graham, N.E., Barnett, T.P., 1987. Sea Surface Temperature, Surface Wind

Divergence, and Convection over Tropical Oceans. Science. 238, 657–659.

Grant, K.M., Grimm, R., Mikolajewicz, U., Marino, G., Ziegler, M., Rohling, E.J., 2016. The timing of Mediterranean sapropel deposition relative to insolation, sea-level and African monsoon changes. Quaternary Science Reviews. 140, 125–141.

Grant, K.M., Rohling, E.J., Bar-Matthews, M., Ayalon, A., Medina-Elizalde, M., Ramsey, C.B., Satow, C., Roberts, A.P., 2012. Rapid coupling between ice volume and polar temperature over the past 50,000 years. Nature. 491, 744–747.

Grant, K.M., Rohling, E.J., Ramsey, C.B., Cheng, H., Edwards, R.L., Florindo, F., Heslop, D., Marra, F., Roberts, A.P., Tamisiea, M.E., Williams, F., 2014. Sea-level variability over five glacial cycles. Nature Communications. 5, 5076.

Grant, K.M., Rohling, E.J., Westerhold, T., Zabel, M., Heslop, D., Konijnendijk, T., Lourens, L., 2017. A 3 million year index for North African humidity/aridity and the implication of potential pan-African Humid periods. Quaternary Science Reviews. 171, 100–118.

Grootes, P.M., Stuiver, M., White, J.W.C., Johnsen, S., Jouzel, J., 1993. Comparison of oxygen isotope records from the GISP2 and GRIP Greenland ice cores. Nature. 366, 552–554.

Groucutt, H.S., 2020a. Volcanism and human prehistory in Arabia. Journal of Volcanology and Geothermal Research. 402, 107003.

Groucutt, H.S., 2020b. Culture and Convergence: The Curious Case of the Nubian Complex. In: Groucutt, H.S. (Ed.), Culture History and Convergent Evolution: Can We Detect Populations in Prehistory? Springer, Cham, pp. 55–86.

Groucutt, H.S., Breeze, P., Drake, N.A., Jennings, R.P., Parton, A., White, T., Shipton, C., Clark-Balzan, L., Al-Omari, A., Cuthbertson, P., Wedage, O.M.C., Bernal, M.A., Alsharekh, A., Petraglia, M.D., 2016. The middle palaeolithic of the Nejd,

Saudi Arabia. Journal of Field Archaeology. 41, 131–147.

Groucutt, H.S., Grün, R., Zalmout, I.A.S., Drake, N.A., Armitage, S.J., Candy, I., Clark-Wilson, R., Louys, J., Breeze, P.S., Duval, M., Buck, L.T., Kivell, T.L., Pomeroy, E., Stephens, N.B., Stock, J.T., Stewart, M., Price, G.J., Kinsley, L., Sung, W.W., Alsharekh, A., Al-Omari, A., Zahir, M., Memesh, A.M., Abdulshakoor, A.J., Al-Masari, A.M., Bahameem, A.A., Al Murayyi, K.M.S., Zahrani, B., Scerri, E.M.L., Petraglia, M.D., 2018. Homo sapiens in Arabia by 85,000 years ago. Nature Ecology & Evolution. 2, 800–809.

Groucutt, H.S., Petraglia, M.D., 2012. The prehistory of the Arabian peninsula: Deserts, dispersals, and demography. Evolutionary Anthropology. 21, 113–125.

Groucutt, H.S., Petraglia, M.D., Bailey, G., Scerri, E.M.L., Parton, A., Clark-Balzan, L., Jennings, R.P., Lewis, L., Blinkhorn, J., Drake, N.A., Breeze, P.S., Inglis, R.H., Devès, M.H., Meredith-Williams, M., Boivin, N., Thomas, M.G., Scally, A., 2015a. Rethinking the dispersal of Homo sapiens out of Africa. Evolutionary Anthropology. 24, 149–164.

Groucutt, H.S., Scerri, E.M.L., Amor, K., Shipton, C., Jennings, R.P., Parton, A., Clark-Balzan, L., Alsharekh, A., Petraglia, M.D., 2017. Middle Palaeolithic raw material procurement and early stage reduction at Jubbah, Saudi Arabia. Archaeological Research in Asia. 9, 44–62.

Groucutt, H.S., Scerri, E.M.L., Lewis, L., Clark-Balzan, L., Blinkhorn, J., Jennings, R.P., Parton, A., Petraglia, M.D., 2015b. Stone tool assemblages and models for the dispersal of Homo sapiens out of Africa. Quaternary International. 382, 8–30.

Groucutt, H.S., Scerri, E.M.L., Stringer, C., Petraglia, M.D., 2019. Skhul lithic technology and the dispersal of Homo sapiens into Southwest Asia. Quaternary International. 515, 30–52.

Groucutt, H.S., Shipton, C., Alsharekh, A., Jennings, R.P., Scerri, E.M.L., Petraglia, M.D., 2015c. Late Pleistocene lakeshore settlement in northern Arabia: Middle Palaeolithic technology from Jebel Katefeh, Jubbah. Quaternary International. 382, 215–236.

Groucutt, H.S., White, T.S., Clark-Balzan, L., Parton, A., Crassard, R., Shipton, C., Jennings, R.P., Parker, A.G., Breeze, P.S., Scerri, E.M.L., Alsharekh, A., Petraglia, M.D., 2015d. Human occupation of the Arabian Empty Quarter during MIS 5: Evidence from Mundafan Al-Buhayrah, Saudi Arabia. Quaternary Science Reviews. 119, 116–135.

Grove, M., 2009. Hunter-gatherer movement patterns: Causes and constraints. Journal of Anthropological Archaeology. 28, 222–233.

GrüN, R., Spooner, N.A., Thorne, A., Mortimer, G., Simpson, J.J., Mcculloch, M.T., Taylor, L., Curnoe, D., 2000. Age of the Lake Mungo 3 skeleton, reply to Bowler & Magee and to Gillespie & Roberts. Journal of Human Evolution. 38, 733–741.

Grün, R., Stringer, C., McDermott, F., Nathan, R., Porat, N., Robertson, S., Taylor, L., Mortimer, G., Eggins, S., McCulloch, M., 2005. U-series and ESR analyses of bones and teeth relating to the human burials from Skhul. Journal of Human Evolution. 49, 316–334.

GRÜN, R., STRINGER, C.B., 1991. ELECTRON SPIN RESONANCE DATING AND THE EVOLUTION OF MODERN HUMANS. Archaeometry. 33, 153–199.

Gurven, M.D., Davison, R.J., 2019. Periodic catastrophes over human evolutionary history are necessary to explain the forager population paradox. Proceedings of the National Academy of Sciences. 116, 12758–12766.

Harmand, S., Lewis, J.E., Feibel, C.S., Lepre, C.J., Prat, S., Lenoble, A., Boës, X.,

Quinn, R.L., Brenet, M., Arroyo, A., Taylor, N., Clément, S., Daver, G., Brugal, J.P., Leakey, L., Mortlock, R.A., Wright, J.D., Lokorodi, S., Kirwa, C., Kent, D. V., Roche, H., 2015. 3.3-million-year-old stone tools from Lomekwi 3, West Turkana, Kenya. Nature. 521, 310–315.

Harmon, R.S., 1979. An isotopic study of groundwater seepage in the central Kentucky Karst. Water Resources Research. 15, 476–480.

Hartland, A., Fairchild, I.J., Lead, J.R., Borsato, A., Baker, A., Frisia, S., Baalousha, M., 2012. From soil to cave: Transport of trace metals by natural organic matter in karst dripwaters. Chemical Geology. 304–305, 68–82.

Hartley, A.J., Chong, G., 2002. Late Pliocene age for the Atacama Desert: Implications for the desertification of western South America. Geology. 30, 43.

Harvati, K., Röding, C., Bosman, A.M., Karakostis, F.A., Grün, R., Stringer, C., Karkanas, P., Thompson, N.C., Koutoulidis, V., Moulopoulos, L.A., Gorgoulis, V.G., Kouloukoussa, M., 2019. Apidima Cave fossils provide earliest evidence of Homo sapiens in Eurasia. Nature. 571, 500–504.

Haslam, M., Clarkson, C., Roberts, R.G., Bora, J., Korisettar, R., Ditchfield, P., Chivas, A.R., Harris, C., Smith, V., Oh, A., Eksambekar, S., Boivin, N., Petraglia, M., 2012. A southern Indian Middle Palaeolithic occupation surface sealed by the 74 ka Toba eruption: Further evidence from Jwalapuram Locality 22. Quaternary International. 258, 148–164.

Häuselmann, A.D., Fleitmann, D., Cheng, H., Tabersky, D., Günther, D., Edwards, R.L., 2015. Timing and nature of the penultimate deglaciation in a high alpine stalagmite from Switzerland. Quaternary Science Reviews. 126, 264–275.

Haywood, A.M., Hill, D.J., Dolan, A.M., Otto-Bliesner, B.L., Bragg, F., Chan, W.-L., Chandler, M.A., Contoux, C., Dowsett, H.J., Jost, A., Kamae, Y., Lohmann, G.,

Lunt, D.J., Abe-Ouchi, A., Pickering, S.J., Ramstein, G., Rosenbloom, N.A., Salzmann, U., Sohl, L., Stepanek, C., Ueda, H., Yan, Q., Zhang, Z., 2013. Large-scale features of Pliocene climate: results from the Pliocene Model Intercomparison Project. Climate of the Past. 9, 191–209.

Hellstrom, J.., McCulloch, M.., 2000. Multi-proxy constraints on the climatic significance of trace element records from a New Zealand speleothem. Earth and Planetary Science Letters. 179, 287–297.

Hendy, C.H., 1971. The isotopic geochemistry of speleothems-I. The calculation of the effects of different modes of formation on the isotopic composition of speleothems and their applicability as palaeoclimatic indicators. Geochimica et Cosmochimica Acta. 35, 801–824.

Henton, E., Ruben, I., Palmer, C., Martin, L., Garrard, A., Thirlwall, M., Jourdan, A.L., 2018. The Seasonal Mobility of Prehistoric Gazelle Herds in the Azraq Basin, Jordan: Modelling Alternative Strategies Using Stable Isotopes. Environmental Archaeology. 23, 187–199.

Herold, M., Lohmann, G., 2009. Eemian tropical and subtropical African moisture transport: An isotope modelling study. Climate Dynamics. 33, 1075–1088.

Hershkovitz, I., Marder, O., Ayalon, A., Bar-Matthews, M., Yasur, G., Boaretto, E., Caracuta, V., Alex, B., Frumkin, A., Goder-Goldberger, M., Gunz, P., Holloway, R.L., Latimer, B., Lavi, R., Matthews, A., Slon, V., Mayer, D.B.Y., Berna, F., Bar-Oz, G., Yeshurun, R., May, H., Hans, M.G., Weber, G.W., Barzilai, O., 2015. Levantine cranium from Manot Cave (Israel) foreshadows the first European modern humans. Nature. 520, 216–219.

Hershkovitz, I., Weber, G.W., Quam, R., Duval, M., Grün, R., Kinsley, L., Ayalon, A., Bar-Matthews, M., Valladas, H., Mercier, N., Arsuaga, J.L., Martinón-Torres, M.,

Bermúdez de Castro, J.M., Fornai, C., Martín-Francés, L., Sarig, R., May, H., Krenn, V.A., Slon, V., Rodríguez, L., García, R., Lorenzo, C., Carretero, J.M., Frumkin, A., Shahack-Gross, R., Bar-Yosef Mayer, D.E., Cui, Y., Wu, X., Peled, N., Groman-Yaroslavski, I., Weissbrod, L., Yeshurun, R., Tsatskin, A., Zaidner, Y., Weinstein-Evron, M., 2018. The earliest modern humans outside Africa. Science. 359, 456–459.

Higham, T., Compton, T., Stringer, C., Jacobi, R., Shapiro, B., Trinkaus, E., Chandler, B., Gröning, F., Collins, C., Hillson, S., O'Higgins, P., FitzGerald, C., Fagan, M., 2011. The earliest evidence for anatomically modern humans in northwestern Europe. Nature. 479, 521–524.

Hilbert, Y.H., White, T.S., Parton, A., Clark-Balzan, L., Crassard, R., Groucutt, H.S., Jennings, R.P., Breeze, P., Parker, A., Shipton, C., Al-Omari, A., Alsharekh, A.M., Petraglia, M.D., 2014. Epipalaeolithic occupation and palaeoenvironments of the southern Nefud Desert, saudi arabia, during the terminal Pleistocene and Early Holocene. Journal of Archaeological Science. 50, 460–474.

Hill, C.A., Polyak, V.J., Asmerom, Y., P. Provencio, P., 2016. Constraints on a Late Cretaceous uplift, denudation, and incision of the Grand Canyon region, southwestern Colorado Plateau, USA, from U-Pb dating of lacustrine limestone. Tectonics. 35, 896–906.

Hitchcock, R.K., Crowell, A.L., Brooks, A.S., Yellen, J.E., Ebert, J.I., Osborn, A.J., 2019. The Ethnoarchaeology of Ambush Hunting: A Case Study of ǂGi Pan, Western Ngamiland, Botswana. African Archaeological Review. 36, 119–144.

Hodell, D.A., Venz-Curtis, K.A., 2006. Late Neogene history of deepwater ventilation in the Southern Ocean. Geochemistry, Geophysics, Geosystems. 7, 1–6.

Hoffmann, D.L., Rogerson, M., Spötl, C., Luetscher, M., Vance, D., Osborne, A.H., Fello, N.M., Moseley, G.E., 2016. Timing and causes of North African wet phases during the last glacial period and implications for modern human migration. Scientific Reports. 6, 36367.

Hoffmann, G., Rupprechter, M., Rahn, M., Preusser, F., 2015. Fluvio-lacustrine deposits reveal precipitation pattern in SE Arabia during early MIS 3. Quaternary International. 382, 145–153.

Hopley, P.J., Marshall, J.D., Latham, A.G., 2009. Speleothem preservation and diagenesis in South African hominin sites: Implications for paleoenvironments and geochronology. Geoarchaeology. 24, 519–547.

Hopley, P.J., Marshall, J.D., Weedon, G.P., Latham, A.G., Herries, A.I.R., Kuykendall, K.L., 2007. Orbital forcing and the spread of C4 grasses in the late Neogene: stable isotope evidence from South African speleothems. Journal of Human Evolution. 53, 620–634.

Hosfield, R., 2016. Walking in a Winter Wonderland? Strategies for Early and Middle Pleistocene Survival in Midlatitude Europe. Current Anthropology. 57, 653–682.

Hosfield, R., Cole, J., 2018. Early hominins in north-west Europe: A punctuated long chronology? Quaternary Science Reviews. 190, 148–160.

Huang, Y., Fairchild, I.J., Borsato, A., Frisia, S., Cassidy, N.J., McDermott, F., Hawkesworth, C.J., 2001. Seasonal variations in Sr, Mg and P in modern speleothems (Grotta di Ernesto, Italy). Chemical Geology. 175, 429–448.

Hublin, J.J., Ben-Ncer, A., Bailey, S.E., Freidline, S.E., Neubauer, S., Skinner, M.M., Bergmann, I., Le Cabec, A., Benazzi, S., Harvati, K., Gunz, P., 2017. New fossils from Jebel Irhoud, Morocco and the pan-African origin of Homo sapiens. Nature. 546, 289–292.

Hughes, J.K., Elton, S., O'Regan, H.J., 2008. Theropithecus and 'Out of Africa' dispersal in the Plio-Pleistocene. Journal of Human Evolution. 54, 43–77.

Hurrell, J.W., Kushnir, Y., Visbeck, M., 2001. An overview of the north atlantic oscillation. Science. 291, 603–605.

Jaffey, A.H., Flynn, K.F., Glendenin, L.E., Bentley, W.C., Essling, A.M., 1971. Precision Measurement of Half-Lives and Specific Activities of <math display="inline"> <mrow> <mmultiscripts> <mrow> <mi mathvariant="normal">U</mi> </mrow> <mprescripts/> <mrow/> <mrow> <mn>235</mn> </mrow> <mrow/> <mrow/> </mmultiscripts> </mrow> </math. Physical Review C. 4, 1889–1906.

Jagher, R., 2009. The Central Oman Paleolithic Survey: Recent Research in Southern Arabia and Reflection on the Prehistoric Evidence. In: Petraglia, M.D., Rose, J.I. (Eds.), The Evolution of Human Populations in Arabia: Paleoenvironments, Prehistory and Genetics (Vertebrate Paleobiology and Paleoanthropology). Springer, Dordrecht, pp. 139–150.

Jennings, R.P., Parton, A., Clark-Balzan, L., White, T.S., Groucutt, H.S., Breeze, P.S., Parker, A.G., Drake, N.A., Petraglia, M.D., 2016. Human occupation of the northern Arabian interior during early Marine Isotope Stage 3. Journal of Quaternary Science. 31, 953–966.

Jennings, R.P., Shipton, C., Al-Omari, A., Alsharekh, A.M., Crassard, R., Groucutt, H., Petraglia, M.D., 2013. Rock art landscapes beside the Jubbah palaeolake, Saudi Arabia. Antiquity. 87, 666–683.

Jennings, R.P., Shipton, C., Breeze, P., Cuthbertson, P., Bernal, M.A., Wedage, W.M.C.O., Drake, N.A., White, T.S., Groucutt, H.S., Parton, A., Clark-Balzan, L., Stimpson, C., al Omari, A.A., Alsharekh, A., Petraglia, M.D., 2015a. Multi-scale

Acheulean landscape survey in the Arabian Desert. Quaternary International. 382, 58–81.

Jennings, R.P., Singarayer, J., Stone, E.J., Krebs-Kanzow, U., Khon, V., Nisancioglu, K.H., Pfeiffer, M., Zhang, X., Parker, A., Parton, A., Groucutt, H.S., White, T.S., Drake, N.A., Petraglia, M.D., 2015b. The greening of Arabia: Multiple opportunities for human occupation of the Arabian Peninsula during the Late Pleistocene inferred from an ensemble of climate model simulations. Quaternary International. 382, 181–199.

Ji, S., Nie, J., Breecker, D.O., Luo, Z., Song, Y., 2017. Intensified aridity in northern China during the middle Piacenzian warm period. Journal of Asian Earth Sciences. 147, 222–225.

Jochum, K.P., Scholz, D., Stoll, B., Weis, U., Wilson, S.A., Yang, Q., Schwalb, A., Börner, N., Jacob, D.E., Andreae, M.O., 2012. Accurate trace element analysis of speleothems and biogenic calcium carbonates by LA-ICP-MS. Chemical Geology. 318–319, 31–44.

Jordan, T.E., Kirk-Lawlor, N.E., Blanco, N.P., Rech, J.A., Cosentino, N.J., 2014. Landscape modification in response to repeated onset of hyperarid paleoclimate states since 14 Ma, Atacama Desert, Chile. Geological Society of America Bulletin. 126, 1016–1046.

Kahlke, R.-D., García, N., Kostopoulos, D.S., Lacombat, F., Lister, A.M., Mazza, P.P.A., Spassov, N., Titov, V. V., 2011. Western Palaearctic palaeoenvironmental conditions during the Early and early Middle Pleistocene inferred from large mammal communities, and implications for hominin dispersal in Europe. Quaternary Science Reviews. 30, 1368–1395.

Kaya, F., Bibi, F., Eronen, J.T., Žliobaitė, I., Hui, T., Fortelius, M., 2018. The rise and

fall of the Old World savannah fauna and the origins of the African savannah biome. Nature Ecology & Evolution. 2, 241–246.

Kealy, S., Louys, J., O'Connor, S., 2017. Reconstructing Palaeogeography and Inter-island Visibility in the Wallacean Archipelago During the Likely Period of Sahul Colonization, 65–45 000 Years Ago. Archaeological Prospection. 24, 259–272.

Kelly, R.L., 2013. The Lifeways of Hunter-Gatherers: The Foraging Spectrum. Cambridge University Press, Cambridge.

Kelly, S.D., Newville, M.G., Cheng, L., Kemner, K.M., Sutton, S.R., Fenter, P., Sturchio, N.C., Spötl, C., 2003. Uranyl incorporation in natural calcite. Environmental Science and Technology. 37, 1284–1287.

Kelly, S.D., Rasbury, E.T., Chattopadhyay, S., Kropf, A.J., Kemner, K.M., 2006. Evidence of a stable uranyl site in ancient organic-rich calcite. Environmental Science and Technology. 40, 2262–2298.

Kim, S.-T., O'Neil, J.R., 1997. Equilibrium and nonequilibrium oxygen isotope effects in synthetic carbonates. Geochimica et Cosmochimica Acta. 61, 3461–3475.

Kimbel, W.H., Villmoare, B., 2016. From Australopithecus to Homo : the transition that wasn't. Philosophical Transactions of the Royal Society B: Biological Sciences. 371, 2–8.

Klein, R.G., 2009. The Human Career: Human Biological and Cultural Origins, 3rd ed. University of Chicago Press.

Koehler, G., Wassenaar, L.I., 2012. Determination of the hydrogen isotopic compositions of organic materials and hydrous minerals using thermal combustion laser spectroscopy. Analytical Chemistry. 84, 3640–3645.

Kuhlwilm, M., Gronau, I., Hubisz, M.J., De Filippo, C., Prado-Martinez, J., Kircher, M., Fu, Q., Burbano, H.A., Lalueza-Fox, C., De La Rasilla, M., Rosas, A., Rudan,

P., Brajkovic, D., Kucan, Ž., Gušic, I., Marques-Bonet, T., Andrés, A.M., Viola, B., Pääbo, S., Meyer, M., Siepel, A., Castellano, S., 2016. Ancient gene flow from early modern humans into Eastern Neanderthals. Nature. 530, 429–433.

Kuper, R., Kropelin, S., 2015. Holocene Occupation Motor of in Africa ' s the Sahara : Evolution. 313, 803–807.

Kutzbach, J.E., Chen, G., Cheng, H., Edwards, R.L., Liu, Z., 2014. Potential role of winter rainfall in explaining increased moisture in the Mediterranean and Middle East during periods of maximum orbitally-forced insolation seasonality. Climate Dynamics. 42, 1079–1095.

Kvamstø, N.G., Skeie, P., Stephenson, D.B., 2004. Impact of Labrador sea-ice extent on the North Atlantic oscillation. International Journal of Climatology. 24, 603–612.

Lachniet, M.S., 2009. Climatic and environmental controls on speleothem oxygen-isotope values. Quaternary Science Reviews. 28, 412–432.

Lachniet, M.S., Patterson, W.P., 2006. Use of correlation and stepwise regression to evaluate physical controls on the stable isotope values of Panamanian rain and surface waters. Journal of Hydrology. 324, 115–140.

Lacinska, A.M., Styles, M.T., Farrant, A.R., 2014. Near-surface diagenesis of ophiolite-derived conglomerates of the Barzaman Formation, United Arab Emirates: a natural analogue for permanent CO 2 sequestration via mineral carbonation of ultramafic rocks. Geological Society, London, Special Publications. 392, 343–360.

Lahr, M.M., 2010. Saharan Corridors and Their Role in the Evolutionary Geography of 'Out of Africa I.' In: Fleagle, J.G., Shea, J.J., Grine, F.E., Baden, A.L., Leakey, R.E. (Eds.), Out of Africa I: The First Hominin Colonization of Eurasia (Vertebrate Paleobiology and Paleoanthropology). pp. 27–46.

Lambeck, K., Purcell, A., Flemming, N.C., Vita-Finzi, C., Alsharekh, A.M., Bailey, G.N., 2011. Sea level and shoreline reconstructions for the Red Sea: isostatic and tectonic considerations and implications for hominin migration out of Africa. Quaternary Science Reviews. 30, 3542–3574.

Langgut, D., Almogi-Labin, A., Bar-Matthews, M., Pickarski, N., Weinstein-Evron, M., 2018. Evidence for a humid interval at ~56–44 ka in the Levant and its potential link to modern humans dispersal out of Africa. Journal of Human Evolution. 124, 75–90.

Langmuir, D., 1978. Uranium solution-mineral equilibria at low temperatures with applications to sedimentary ore deposits. Geochimica et Cosmochimica Acta. 42, 547–569.

Larrasoaña, J.C., Roberts, A.P., Rohling, E.J., 2013. Dynamics of Green Sahara Periods and Their Role in Hominin Evolution. PLoS ONE. 8, e76514.

Larrasoana, J.C., Roberts, A.P., Rohling, E.J., Winklhofer, M., Wehausen, R., 2003. Three million years of monsoon variability over the northern Sahara. Climate Dynamics. 21, 689–698.

Lebatard, A.-E., Bourles, D.L., Duringer, P., Jolivet, M., Braucher, R., Carcaillet, J., Schuster, M., Arnaud, N., Monie, P., Lihoreau, F., Likius, A., Mackaye, H.T., Vignaud, P., Brunet, M., 2008. Cosmogenic nuclide dating of Sahelanthropus tchadensis and Australopithecus bahrelghazali: Mio-Pliocene hominids from Chad. Proceedings of the National Academy of Sciences. 105, 3226–3231.

LeGrande, A.N., Schmidt, G.A., 2006. Global gridded data set of the oxygen isotopic composition in seawater. Geophysical Research Letters. 33, L12604.

Leng, M.J., Lewis, J.P., 2016. Oxygen isotopes in molluscan shell: Applications in

environmental archaeology. Environmental Archaeology. 21, 295–306.

Leppard, T.P., Runnels, C., 2017. Maritime hominin dispersals in the Pleistocene: advancing the debate. Antiquity. 91, 510–519.

Lepre, C.J., Roche, H., Kent, D. V., Harmand, S., Quinn, R.L., Brugal, J.P., Texier, P.J., Lenoble, A., Feibel, C.S., 2011. An earlier origin for the Acheulian. Nature. 477, 82–85.

Li, X., Fang, X., Wu, F., Miao, Y., 2011. Pollen evidence from Baode of the northern Loess Plateau of China and strong East Asian summer monsoons during the Early Pliocene. Chinese Science Bulletin. 56, 64–69.

Li, X., Jiang, D., Tian, Z., Yang, Y., 2018. Mid-Pliocene global land monsoon from PlioMIP1 simulations. Palaeogeography, Palaeoclimatology, Palaeoecology. 512, 56–70.

Liddy, H.M., Feakins, S.J., Tierney, J.E., 2016. Cooling and drying in northeast Africa across the Pliocene. Earth and Planetary Science Letters. 449, 430–438.

Lind, E.M., Morrison, M.E.S., 1974. East African Vegatation. Longman, London.

Lippmann, F., 1973. Sedimentary Carbonate Minerals. Springer-Verlag, Berlin.

Lisiecki, L.E., Raymo, M.E., 2005. A Pliocene-Pleistocene stack of 57 globally distributed benthic δ 18O records. Paleoceanography. 20, 1–17.

Liu, W., Martinón-Torres, M., Cai, Y.J., Xing, S., Tong, H.W., Pei, S.W., Sier, M.J., Wu, X.H.X.J., Edwards, R.L., Cheng, H., Li, Y.Y., Yang, X.X., De Castro, J.M.B., Wu, X.H.X.J., 2015. The earliest unequivocally modern humans in southern China. Nature. 526, 696–699.

Liu, X., Dong, B., Yin, Z.-Y., Smith, R.S., Guo, Q., 2019. Continental drift, plateau uplift, and the evolutions of monsoon and arid regions in Asia, Africa, and Australia during the Cenozoic. Science China Earth Sciences. 62, 1053–1075.

Lolis, C.J., Bartzokas, A., Katsoulis, B.D., 2002. Spatial and temporal 850 hPa air temperature and sea-surface temperature covariances in the Mediterranean region and their connection to atmospheric circulation. International Journal of Climatology. 22, 663–676.

Loosdrecht, M. Van De, Bouzouggar, A., Humphrey, L., Posth, C., Barton, N., Aximu-petri, A., Nickel, B., Nagel, S., Talbi, E.H., Abdeljalil, M., Hajraoui, E., Amzazi, S., Hublin, J., Pääbo, S., Schiffels, S., Meyer, M., Haak, W., Jeong, C., Krause, J., 2018. Pleistocene North African genomes. Science. 552, 548–552.

Lordkipanidze, D., De Ponce León, M.S., Margvelashvili, A., Rak, Y., Rightmire, G.P., Vekua, A., Zollikofer, C.P.E., 2013. A complete skull from Dmanisi, Georgia, and the evolutionary biology of early Homo. Science. 342, 326–331.

Lordkipanidze, D., Jashashvili, T., Vekua, A., de León, M.S.P., Zollikofer, C.P.E., Rightmire, G.P., Pontzer, H., Ferring, R., Oms, O., Tappen, M., Bukhsianidze, M., Agusti, J., Kahlke, R., Kiladze, G., Martinez-Navarro, B., Mouskhelishvili, A., Nioradze, M., Rook, L., 2007. Postcranial evidence from early Homo from Dmanisi, Georgia. Nature. 449, 305–310.

Lordkipanidze, D., Vekua, A., Ferring, R., Rightmire, G.P., Agusti, J., Kiladze, G., Mouskhelishvili, A., Nioradze, M., de León, M.S.P., Tappen, M., Zollikofer, C.P.E., 2005. The earliest toothless hominin skull. Nature. 434, 717–718.

Malaspinas, A.-S., Westaway, M.C., Muller, C., Sousa, V.C., Lao, O., Alves, I., Bergström, A., Athanasiadis, G., Cheng, J.Y., Crawford, J.E., Heupink, T.H., Macholdt, E., Peischl, S., Rasmussen, S., Schiffels, S., Subramanian, S., Wright, J.L., Albrechtsen, A., Barbieri, C., Dupanloup, I., Eriksson, A., Margaryan, A., Moltke, I., Pugach, I., Korneliussen, T.S., Levkivskyi, I.P., Moreno-Mayar, J.V., Ni, S., Racimo, F., Sikora, M., Xue, Y., Aghakhanian, F.A., Brucato, N., Brunak,

S., Campos, P.F., Clark, W., Ellingvåg, S., Fourmile, G., Gerbault, P., Injie, D., Koki, G., Leavesley, M., Logan, B., Lynch, A., Matisoo-Smith, E.A., McAllister, P.J., Mentzer, A.J., Metspalu, M., Migliano, A.B., Murgha, L., Phipps, M.E., Pomat, W., Reynolds, D., Ricaut, F.-X., Siba, P., Thomas, M.G., Wales, T., Wall, C.M., Oppenheimer, S.J., Tyler-Smith, C., Durbin, R., Dortch, J., Manica, A., Schierup, M.H., Foley, R.A., Lahr, M.M., Bowern, C., Wall, J.D., Mailund, T., Stoneking, M., Nielsen, R., Sandhu, M.S., Excoffier, L., Lambert, D.M., Willerslev, E., 2016. A genomic history of Aboriginal Australia. Nature. 538, 207–214.

Mallick, S., Li, H., Lipson, M., Mathieson, I., Gymrek, M., Racimo, F., Zhao, M., Chennagiri, N., Nordenfelt, S., Tandon, A., Skoglund, P., Lazaridis, I., Sankararaman, S., Fu, Q., Rohland, N., Renaud, G., Erlich, Y., Willems, T., Gallo, C., Spence, J.P., Song, Y.S., Poletti, G., Balloux, F., Van Driem, G., De Knijff, P., Romero, I.G., Jha, A.R., Behar, D.M., Bravi, C.M., Capelli, C., Hervig, T., Moreno-Estrada, A., Posukh, O.L., Balanovska, E., Balanovsky, O., Karachanak-Yankova, S., Sahakyan, H., Toncheva, D., Yepiskoposyan, L., Tyler-Smith, C., Xue, Y., Abdullah, M.S., Ruiz-Linares, A., Beall, C.M., Di Rienzo, A., Jeong, C., Starikovskaya, E.B., Metspalu, E., Parik, J., Villems, R., Henn, B.M., Hodoglugil, U., Mahley, R., Sajantila, A., Stamatoyannopoulos, G., Wee, J.T.S., Khusainova, R., Khusnutdinova, E., Litvinov, S., Ayodo, G., Comas, D., Hammer, M.F., Kivisild, T., Klitz, W., Winkler, C.A., Labuda, D., Bamshad, M., Jorde, L.B., Tishkoff, S.A., Watkins, W.S., Metspalu, M., Dryomov, S., Sukernik, R., Singh, L., Thangaraj, K., Paäbo, S., Kelso, J., Patterson, N., Reich, D., 2016. The Simons Genome Diversity Project: 300 genomes from 142 diverse populations. Nature. 538, 201–206.

Manzi, G., Magri, D., Milli, S., Palombo, M.R., Margari, V., Celiberti, V., Barbieri, Mario, Barbieri, Maurizio, Melis, R.T., Rubini, M., Ruffo, M., Saracino, B., Tzedakis, P.C., Zarattini, A., Biddittu, I., 2010. The new chronology of the Ceprano calvarium (Italy). Journal of Human Evolution. 59, 580–585.

Marcos, S.A., 1970. Physical and chemical oceanography of the Red Sea. Oceanography and Marine Biology - An Annual Review. 8, 73–202.

Marean, C.W., 1997. Hunter-Gatherer Foraging Strategies in Tropical Grasslands: Model Building and Testing in the East African Middle and Later Stone Age. Journal of Anthropological Archaeology. 16, 189–225.

Martínez-Garcia, A., Rosell-Melé, A., Jaccard, S.L., Geibert, W., Sigman, D.M., Haug, G.H., 2011. Southern Ocean dust-climate coupling over the past four million years. Nature. 476, 312–315.

Maslin, M.A., Brierley, C.M., 2015. The role of orbital forcing in the Early Middle Pleistocene Transition. Quaternary International. 389, 47–55.

Maslin, M.A., Brierley, C.M., Milner, A.M., Shultz, S., Trauth, M.H., Wilson, K.E., 2014. East African climate pulses and early human evolution. Quaternary Science Reviews. 101, 1–17.

Maslin, M.A., Trauth, M.H., 2009. Plio-Pleistocene East African Pulsed Climate Variability and Its Influence on Early Human Evolution. In: The First Humans – Origin and Early Evolution of the Genus Homo. pp. 151–158.

Matter, A., Neubert, E., Preusser, F., Rosenberg, T., Al-Wagdani, K., 2015. Palaeo-environmental implications derived from lake and sabkha deposits of the southern Rub' al-Khali, Saudi Arabia and Oman. Quaternary International. 382, 120–131.

Matthews, A., Ayalon, A., Bar-Matthews, M., 2000. D/H ratios of fluid inclusions of Soreq cave (Israel) speleothems as a guide to the Eastern Mediterranean Meteoric

Line relationships in the last 120 ky. Chemical Geology. 166, 183–191.

McBrearty, S., 1988. The Sangoan-Lupemban and middle stone age sequence at the Muguruk site, western Kenya. World Archaeology. 19, 388–420.

Mcbrearty, S., Brooks, A.S., 2000. The revolution that wasn't: A new interpretation of the origin of modern human behavior. Journal of Human Evolution. 39, 453–563.

McClure, H.A., 1976. Radiocarbon chronology of late Quaternary lakes in the Arabian Desert. Nature. 263, 755–756.

McClure, H.A., 1984. Late Quaternary palaeoenvironments of the Rub' Al Khali. University College London.

McDermott, F., 2004. Palaeo-climate reconstruction from stable isotope variations in speleothems: a review. Quaternary Science Reviews. 23, 901–918.

McDonald, J., Drysdale, R., Hill, D., 2004. The 2002-2003 El Niño recorded in Australian cave drip waters: Implications for reconstructing rainfall histories using stalagmites. Geophysical Research Letters. 31, 1–4.

McDougall, I., Brown, F.H., Vasconcelos, P.M., Cohen, B.E., Thiede, D.S., Buchanan, M.J., 2012. New single crystal 40 Ar/ 39 Ar ages improve time scale for deposition of the Omo Group, Omo–Turkana Basin, East Africa. Journal of the Geological Society. 169, 213–226.

McGarry, S., Bar-Matthews, M., Matthews, A., Vaks, A., Schilman, B., Ayalon, A., 2004. Constraints on hydrological and paleotemperature variations in the Eastern Mediterranean region in the last 140ka given by the δD values of speleothem fluid inclusions. Quaternary Science Reviews. 23, 919–934.

McGarry, S.F., Caseldine, C., 2004. Speleothem Palynology: an undervalued tool in Quaternary studies. Quaternary Science Reviews. 23, 2389–2404.

McLaren, S.J., Al-Juaidi, F., Bateman, M.D., Millington, A.C., 2009. First evidence for episodic flooding events in the arid interior of central Saudi Arabia over the last 60 ka. Journal of Quaternary Science. 24, 198–207.

McMillan, E.A., Fairchild, I.J., Frisia, S., Borsato, A., McDermott, F., 2005. Annual trace element cycles in calcite-aragonite speleothems: Evidence of drought in the western Mediterranean 1200-1100 yr BP. Journal of Quaternary Science. 20, 423–433.

Meckler, A.N., Affolter, S., Dublyansky, Y. V., Krüger, Y., Vogel, N., Bernasconi, S.M., Frenz, M., Kipfer, R., Leuenberger, M., Spötl, C., Carolin, S., Cobb, K.M., Moerman, J., Adkins, J.F., Fleitmann, D., 2015. Glacial-interglacial temperature change in the tropical West Pacific: A comparison of stalagmite-based paleo-thermometers. Quaternary Science Reviews. 127, 90–116.

Meece, D.E., Benninger, L.K., 1993. The coprecipitation of Pu and other radionuclides with CaCO3. Geochimica et Cosmochimica Acta. 57, 1147–11458.

Mellars, P., 2006a. Why did modern human populations disperse from Africa ca. 60,000 years ago? A new model. Proceedings of the National Academy of Sciences. 103, 9381–9386.

Mellars, P., 2006b. Going East: New Genetic and Archaeological Perspectives on the Modern Human Colonization of Eurasia. Science. 313, 796–800.

Mellars, P., Gori, K.C., Carr, M., Soares, P.A., Richards, M.B., 2013. Genetic and archaeological perspectives on the initial modern human colonization of southern Asia. Proceedings of the National Academy of Sciences. 110, 10699–10704.

Messager, E., Lordkipanidze, D., Delhon, C., Ferring, C.R., 2010a. Palaeoecological implications of the Lower Pleistocene phytolith record from the Dmanisi Site (Georgia). Palaeogeography, Palaeoclimatology, Palaeoecology. 288, 1–13.

Messager, E., Lordkipanidze, D., Kvavadze, E., Ferring, C.R., Voinchet, P., 2010b. Palaeoenvironmental reconstruction of Dmanisi site (Georgia) based on palaeobotanical data. Quaternary International. 223–224, 20–27.

Messager, E., Nomade, S., Voinchet, P., Ferring, R., Mgeladze, A., Guillou, H., Lordkipanidze, D., 2011. 40Ar/39Ar dating and phytolith analysis of the Early Pleistocene sequence of Kvemo-Orozmani (Republic of Georgia): Chronological and palaeoecological implications for the hominin site of Dmanisi. Quaternary Science Reviews. 30, 3099–3108.

Meyer, M., Arsuaga, J.-L., de Filippo, C., Nagel, S., Aximu-Petri, A., Nickel, B., Martínez, I., Gracia, A., de Castro, J.M.B., Carbonell, E., Viola, B., Kelso, J., Prüfer, K., Pääbo, S., 2016. Nuclear DNA sequences from the Middle Pleistocene Sima de los Huesos hominins. Nature. 531, 504–507.

Mgeladze, A., Lordkipanidze, D., Moncel, M.-H., Despriee, J., Chagelishvili, R., Nioradze, M., Nioradze, G., 2011. Hominin occupations at the Dmanisi site, Georgia, Southern Caucasus: Raw materials and technical behaviours of Europe's first hominins. Journal of Human Evolution. 60, 571–596.

Mickler, P.J., Carlson, P., Banner, J.L., Breecker, D.O., Stern, L., Guilfoyle, A., 2019. Quantifying carbon isotope disequilibrium during in-cave evolution of drip water along discreet flow paths. Geochimica et Cosmochimica Acta. 244, 182–196.

Millard, A.R., 2008. A critique of the chronometric evidence for hominid fossils: I. Africa and the Near East 500-50 ka. Journal of Human Evolution. 54, 848–847.

Miller, A.G., Cope, T.A., 1996. Flora of the Arabian Peninsula and Socotra. Edinburgh University Press, Edinburgh.

Mitchell, T.D., Jones, P.D., 2005. An improved method of constructing a database of monthly climate observations and associated high-resolution grids. International

Journal of Climatology. 25, 693–712.

Moncel, M.H., Ashton, N., Lamotte, A., Tuffreau, A., Cliquet, D., Despriée, J., 2015. The Early Acheulian of north-western Europe. Journal of Anthropological Archaeology. 40, 302–331.

Mturi, A.A., 1976. New hominid from Lake Ndutu, Tanzania. Nature. 262, 484–485.

Muttoni, G., Scardia, G., Kent, D. V., 2010. Human migration into Europe during the late Early Pleistocene climate transition. Palaeogeography, Palaeoclimatology, Palaeoecology. 296, 79–93.

Neff, U., Burns, S.J., Mangini, A., Mudelsee, M., Fleitmann, D., Matter, A., 2001. Strong coherence between solar variability and the monsoon in Oman between 9 and 6 kyr ago. Nature. 411, 290–293.

Nehme, C., Verheyden, S., Noble, S.R., Farrant, A.R., Sahy, D., Hellstrom, J., Delannoy, J.J., Claeys, P., 2015. Reconstruction of MIS 5 climate in the central Levant using a stalagmite from Kanaan Cave, Lebanon. Climate of the Past. 11, 1785–1799.

Nemani, R.R., 2003. Climate-Driven Increases in Global Terrestrial Net Primary Production from 1982 to 1999. Science. 300, 1560–1563.

Nicholson, S.E., 2009. A revised picture of the structure of the “monsoon” and land ITCZ over West Africa. Climate Dynamics. 32, 1155–1171.

Nicholson, S.E., 2018. The ITCZ and the Seasonal Cycle over Equatorial Africa. Bulletin of the American Meteorological Society. 99, 337–348.

Nicholson, S.L., Pike, A.W.G., Hosfield, R., Roberts, N., Sahy, D., Woodhead, J., Cheng, H., Edwards, R.L., Affolter, S., Leuenberger, M., Burns, S.J., Matter, A., Fleitmann, D., 2020. Pluvial periods in Southern Arabia over the last 1.1 million-years. Quaternary Science Reviews. 229, 106112.

Norman, K., Inglis, J., Clarkson, C., Faith, J.T., Shulmeister, J., Harris, D., 2018. An early colonisation pathway into northwest Australia 70-60,000 years ago. Quaternary Science Reviews. 180, 229–239.

Novello, A., Barboni, D., Sylvestre, F., Lebatard, A.-E., Paillès, C., Bourlès, D.L., Likius, A., Mackaye, H.T., Vignaud, P., Brunet, M., 2017. Phytoliths indicate significant arboreal cover at Sahelanthropus type locality TM266 in northern Chad and a decrease in later sites. Journal of Human Evolution. 106, 66–83.

Novello, A., Lebatard, A.-E., Moussa, A., Barboni, D., Sylvestre, F., Bourlès, D.L., Paillès, C., Buchet, G., Decarreau, A., Duringer, P., Ghienne, J.-F., Maley, J., Mazur, J.-C., Roquin, C., Schuster, M., Vignaud, P., 2015. Diatom, phytolith, and pollen records from a 10Be/9Be dated lacustrine succession in the Chad basin: Insight on the Miocene–Pliocene paleoenvironmental changes in Central Africa. Palaeogeography, Palaeoclimatology, Palaeoecology. 430, 85–103.

O'Connell, J.F., Allen, J., 2004. Dating the colonization of Sahul (Pleistocene Australia-New Guinea): A review of recent research. Journal of Archaeological Science. 31, 835–853.

O'Connell, J.F., Allen, J., Williams, M.A.J., Williams, A.N., Turney, C.S.M., Spooner, N.A., Kamminga, J., Brown, G., Cooper, A., 2018. When did Homo sapiens first reach Southeast Asia and Sahul? Proceedings of the National Academy of Sciences. 115, 8482–8490.

O'Regan, H.J., Turner, A., Bishop, L.C., Elton, S., Lamb, A.L., 2011. Hominins without fellow travellers? First appearances and inferred dispersals of Afro-Eurasian large-mammals in the Plio-Pleistocene. Quaternary Science Reviews. 30, 1343–1352.

Orland, I.J., He, F., Bar-Matthews, M., Chen, G., Ayalon, A., Kutzbach, J.E., 2019.

Resolving seasonal rainfall changes in the Middle East during the last interglacial period. Proceedings of the National Academy of Sciences. 116, 24985–24990.

Otto-Bliesner, B.L., 2006. Simulating Arctic Climate Warmth and Icefield Retreat in the Last Interglaciation. Science. 311, 1751–1753.

Pagani, L., Lawson, D.J., Jagoda, E., Mörseburg, A., Eriksson, A., Mitt, M., Clemente, F., Hudjashov, G., DeGiorgio, M., Saag, Lauri, Wall, J.D., Cardona, A., Mägi, R., Sayres, M.A.W., Kaewert, S., Inchley, C., Scheib, C.L., Järve, M., Karmin, M., Jacobs, G.S., Antao, T., Iliescu, F.M., Kushniarevich, A., Ayub, Q., Tyler-Smith, C., Xue, Y., Yunusbayev, B., Tambets, K., Mallick, C.B., Saag, Lehti, Pocheshkhova, E., Andriadze, G., Muller, C., Westaway, M.C., Lambert, D.M., Zoraqi, G., Turdikulova, S., Dalimova, D., Sabitov, Z., Sultana, G.N.N., Lachance, J., Tishkoff, S., Momynaliev, K., Isakova, J., Damba, L.D., Gubina, M., Nymadawa, P., Evseeva, I., Atramentova, L., Utevska, O., Ricaut, F.-X., Brucato, N., Sudoyo, H., Letellier, T., Cox, M.P., Barashkov, N.A., Škaro, V., Mulahasanovic´, L., Primorac, D., Sahakyan, H., Mormina, M., Eichstaedt, C.A., Lichman, D. V., Abdullah, S., Chaubey, G., Wee, J.T.S., Mihailov, E., Karunas, A., Litvinov, S., Khusainova, R., Ekomasova, N., Akhmetova, V., Khidiyatova, I., Marjanović, D., Yepiskoposyan, L., Behar, D.M., Balanovska, E., Metspalu, A., Derenko, M., Malyarchuk, B., Voevoda, M., Fedorova, S.A., Osipova, L.P., Lahr, M.M., Gerbault, P., Leavesley, M., Migliano, A.B., Petraglia, M., Balanovsky, O., Khusnutdinova, E.K., Metspalu, E., Thomas, M.G., Manica, A., Nielsen, R., Villems, R., Willerslev, E., Kivisild, T., Metspalu, M., 2016. Genomic analyses inform on migration events during the peopling of Eurasia. Nature. 538, 238–242.

Pagani, M., Liu, Z., LaRiviere, J., Ravelo, A.C., 2010. High Earth-system climate sensitivity determined from Pliocene carbon dioxide concentrations. Nature

Geoscience. 3, 27–30.

Palombo, M.R., 2013. What about causal mechanisms promoting early hominin dispersal in Eurasia? A research agenda for answering a hotly debated question. Quaternary International. 295, 13–27.

Parker, A.G., Eckersley, L., Smith, M.M., Goudie, A.S., Stokes, S., Ward, S., White, K., Hodson, M.J., 2004. Holocene vegetation dynamics in the northeastern Rub' al-Khali desert, Arabian Peninsula: a phytolith, pollen and carbon isotope study. Journal of Quaternary Science. 19, 665–676.

Parker, A.G., Manning, M., Goudie, A.S., Kennet, D., Stokes, S., White, K., Hodson, M.J., 2006. A Record of Holocene Climate Change from Lake Geochemical Analyses in Southeastern Arabia. Quaternary Research. 66, 465–476.

Parker, A.G., Rose, J.I., 2008. Climate change and human origins in southern Arabia. Proceedings of the Seminar for Arabian Studies. 38, 25–42.

Parton, A., Clark-Balzan, L., Parker, A.G., Preston, G.W., Sung, W.W., Breeze, P.S., Leng, M.J., Groucutt, H.S., White, T.S., Alsharekh, A., Petraglia, M.D., 2018. Middle-late quaternary palaeoclimate variability from lake and wetland deposits in the Nefud Desert, Northern Arabia. Quaternary Science Reviews. 202, 78–97.

Parton, A., Farrant, A.R., Leng, M.J., Schwenninger, J.L., Rose, J.I., Uerpmann, H.P., Parker, A.G., 2013. An early MIS 3 pluvial phase in Southeast Arabia: Climatic and archaeological implications. Quaternary International. 300, 62–74.

Parton, A., Farrant, A.R., Leng, M.J., Telfer, M.W., Groucutt, H.S., Petraglia, M.D., Parker, A.G., 2015a. Alluvial fan records from southeast Arabia reveal multiple windows for human dispersal. Geology. 43, 295–298.

Parton, A., White, T.S., Parker, A.G., Breeze, P.S., Jennings, R., Groucutt, H.S., Petraglia, M.D., 2015b. Orbital-scale climate variability in Arabia as a potential

motor for human dispersals. Quaternary International. 382, 82–97.

Pedgley, D.E., 1969. Cyclones along the Arabian coast. Weather. 24, 456–470.

Peigné, S., de Bonis, L., Likius, A., Mackaye, H.T., Vignaud, P., Brunet, M., 2008. Late Miocene Carnivora from Chad: Lutrinae (Mustelidae). Zoological Journal of the Linnean Society. 152, 793–846.

Perdikouri, C., Kasioptas, A., Geisler, T., Schmidt, B.C., Putnis, A., 2011. Experimental study of the aragonite to calcite transition in aqueous solution. Geochimica et Cosmochimica Acta. 75, 6211–6224.

Petit-Maire, N., Carbonel, P., Reyss, J.L., Sanlaville, P., Abed, A.M., Bourrouilh, R., Fontugne, M.R., Yasin, S., 2010. A vast Eemian palaeolake in Southern Jordan (29°N). Global and Planetary Change. 72, 368–373.

Petraglia, M., Clarkson, C., Boivin, N., Haslam, M., Korisettar, R., Chaubey, G., Ditchfield, P., Fuller, D., James, H., Jones, S., Kivisild, T., Koshy, J., Lahr, M.M., Metspalu, M., Roberts, R., Arnold, L., 2009. Population increase and environmental deterioration correspond with microlithic innovations in South Asia ca. 35,000 years ago. Proceedings of the National Academy of Sciences. 106, 12261–12266.

Petraglia, M.D., 2003. The Lower Paleolithic of the Arabian Peninsula: Occupations, adaptations, and dispersals. Journal of World Prehistory. 17, 141–180.

Petraglia, M.D., Alsharekh, A., Breeze, P., Clarkson, C., Crassard, R., Drake, N.A., Groucutt, H.S., Jennings, R.P., Parker, A.G., Parton, A., Roberts, R.G., Shipton, C., Matheson, C., Al-Omari, A., Veall, M.A., 2012. Hominin Dispersal into the Nefud Desert and Middle Palaeolithic Settlement along the Jubbah Palaeolake, Northern Arabia. PLoS ONE. 7, e49840.

Petraglia, M.D., Alsharekh, A.M., Crassard, R., Drake, N.A., Groucutt, H., Parker,

A.G., Roberts, R.G., 2011. Middle Paleolithic occupation on a Marine Isotope Stage 5 lakeshore in the Nefud Desert, Saudi Arabia. Quaternary Science Reviews. 30, 1555–1559.

Petraglia, M.D., Breeze, P.S., Groucutt, H.S., 2019. Blue Arabia, Green Arabia: Examining Human Colonisation and Dispersal Models. In: Rasul, N.M.A., Stewart, I.C.F. (Eds.), Geological Setting, Palaeoenvironment and Archaeology of the Red Sea. Springer International Publishing, Cham, pp. 675–683.

Petraglia, M.D., Groucutt, H.S., Guagnin, M., Breeze, P.S., Boivin, N., 2020. Human responses to climate and ecosystem change in ancient Arabia. Proceedings of the National Academy of Sciences. 117, 8263–8270.

Petraglia, M.D., Korisettar, R., Boivin, N., Clarkson, C., Ditchfield, P., Jones, S., Koshy, J., Lahr, M.M., Oppenheimer, C., Pyle, D., Roberts, R., Schwenninger, J.-L.J.-L., Arnold, L., White, K., 2007. Middle Paleolithic Assemblages from the Indian Subcontinent Before and After the Toba Super-Eruption. Science. 317, 114–116.

Petraglia, M.D., Parton, A., Groucutt, H.S., Alsharekh, A., 2015. Green Arabia: Human prehistory at the Crossroads of Continents. Quaternary International. 382, 1–7.

Petraglia, M.D., Rose, J.I., 2010. The Evolution of Human Populations in Arabia, Vertebrate Paleobiology and Paleoanthropology. Springer, Dordrecht.

Pickarski, N., Kwiecien, O., Langgut, D., Litt, T., 2015. Abrupt climate and vegetation variability of eastern Anatolia during the last glacial. Climate of the Past. 11, 1491–1505.

Pike, A.W.G., Angelucci, D.E., Cooper, M.J., Linscott, B., Matias, H., Zilhão, J., 2016. Reconstructing Neanderthal mobility and range at Gruta de Oliveira, Portugal, using high resolution laser ablation Sr isotope analysis. In: Proceedings of the

European Society for the Study of Human Evolution 5. p. 188.

Poage, M.A., Chamberlain, C.P., 2001. Empirical relationships between elevation and the stable isotope composition of precipitation and surface waters: Considerations for studies of paleoelevation change. American Journal of Science. 301, 1–15.

Pontzer, H., Rolian, C., Rightmire, G.P., Jashashvili, T., Ponce de León, M.S., Lordkipanidze, D., Zollikofer, C.P.E., 2010. Locomotor anatomy and biomechanics of the Dmanisi hominins. Journal of Human Evolution. 58, 492–504.

Potts, R., 1996. Evolution and climate variability. Science. 273, 922–923.

Potts, R., 1998a. Environmental hypotheses of hominin evolution. American Journal of Physical Anthropology. 107, 93–136.

Potts, R., 1998b. Variability selection in hominid evolution. Evolutionary Anthropology. 7, 81–96.

Prescott, C.L., Dolan, A.M., Haywood, A.M., Hunter, S.J., Tindall, J.C., 2018. Regional climate and vegetation response to orbital forcing within the mid-Pliocene Warm Period: A study using HadCM3. Global and Planetary Change. 161, 231–243.

Prescott, C.L., Haywood, A.M., Dolan, A.M., Hunter, S.J., Tindall, J.C., 2019. Indian monsoon variability in response to orbital forcing during the late Pliocene. Global and Planetary Change. 173, 33–46.

Profico, A., di Vincenzo, F., Gagliardi, L., Piperno, M., Manzi, G., 2016. Filling the gap. Human cranial remains from Gombore II (Melka kunture, Ethiopia; ca. 850 ka) and the origin of Homo heidelbergensis. Journal of Anthropological Sciences. 94, 41–63.

Qu, T., Bar-Yosef, O., Wang, Y., Wu, X., 2013. The Chinese Upper Paleolithic:

Geography, Chronology, and Techno-typology. Journal of Archaeological Research. 21, 1–73.

Quade, J., Dente, E., Armon, M., Ben Dor, Y., Morin, E., Adam, O., Enzel, Y., 2018. Megalakes in the Sahara? A Review. Quaternary Research. 90, 253–275.

Rabett, R.J., 2018. The success of failed Homo sapiens dispersals out of Africa and into Asia. Nature Ecology and Evolution. 2, 212–219.

Railsback, L.B., Gibbard, P.L., Head, M.J., Voarintsoa, N.R.G., Toucanne, S., 2015. An optimized scheme of lettered marine isotope substages for the last 1.0 million years, and the climatostratigraphic nature of isotope stages and substages. Quaternary Science Reviews. 111, 94–106.

Rasbury, E.T., Cole, J.M., 2009. Directly dating geologic events: U-Pb dating of carbonates. Reviews of Geophysics. 47, 1–27.

Raymo, M.E., 1997. The timing of major climate terminations. Paleoceanography. 12, 577–585.

Rector, A.L., Reed, K.E., 2010. Middle and late Pleistocene faunas of Pinnacle Point and their paleoecological implications. Journal of Human Evolution. 59, 340–357.

Reynard, J.P., Henshilwood, C.S., 2019. Environment versus behaviour: Zooarchaeological and taphonomic analyses of fauna from the Still Bay layers at Blombos Cave, South Africa. Quaternary International. 500, 159–171.

Richter, D., Grün, R., Joannes-Boyau, R., Steele, T.E., Amani, F., Rué, M., Fernandes, P., Raynal, J.P., Geraads, D., Ben-Ncer, A., Hublin, J.J., McPherron, S.P., 2017. The age of the hominin fossils from Jebel Irhoud, Morocco, and the origins of the Middle Stone Age. Nature. 546, 293–296.

Risi, C., Bony, S., Vimeux, F., 2008. Influence of convective processes on the isotopic composition (δ18O and δD) of precipitation and water vapor in the tropics: 2.

Physical interpretation of the amount effect. Journal of Geophysical Research Atmospheres. 113, 1–12.

Roberts, A.P., Rohling, E.J., Grant, K.M., Larrasoaña, J.C., Liu, Q., 2011. Atmospheric dust variability from Arabia and China over the last 500,000 years. Quaternary Science Reviews. 30, 3537–3541.

Roberts, N.M.W., Rasbury, E.T., Parrish, R.R., Smith, C.J., Horstwood, M.S.A., Condon, D.J., 2017. A calcite reference material for LA-ICP-MS U-Pb geochronology. Geochemistry, Geophysics, Geosystems. 18, 2807–2814.

Roberts, P., Prendergast, M.E., Janzen, A., Shipton, C., Blinkhorn, J., Zech, J., Crowther, A., Sawchuk, E.A., Stewart, M., Ndiema, E., Petraglia, M., Boivin, N., 2020. Late Pleistocene to Holocene human palaeoecology in the tropical environments of coastal eastern Africa. Palaeogeography, Palaeoclimatology, Palaeoecology. 537, 109438.

Roberts, P., Stewart, M., Alagaili, A.N., Breeze, P., Candy, I., Drake, N., Groucutt, H.S., Scerri, E.M.L., Lee-Thorp, J., Louys, J., Zalmout, I.S., Al-Mufarreh, Y.S.A., Zech, J., Alsharekh, A.M., al Omari, A., Boivin, N., Petraglia, M., 2018. Fossil herbivore stable isotopes reveal middle Pleistocene hominin palaeoenvironment in 'Green Arabia.' Nature Ecology and Evolution. 2, 1871–1878.

Roberts, R., Yoshida, H., Galbraith, R., 1998. Single-aliquot and single-grain optical dating confirm thermoluminescence age estimates at Malakunanja II rock shelter in northern Australia. Ancient TL. 16, 19–24.

Roberts, R.G., Jones, R., Smith, M.A., 1990. Thermoluminescence dating of a 50,000-year-old human occupation site in northern Australia. Nature. 345, 153–156.

Roberts, R.G., Jones, R., Spooner, N.A., Head, M.J., Murray, A.S., Smith, M.A., 1994. The human colonisation of Australia: optical dates of 53,000 and 60,000 years

bracket human arrival at Deaf Adder Gorge, Northern Territory. Quaternary Science Reviews. 13, 575–583.

Rohling, E.J., Grant, K.M., Roberts, A.P., Larrasoaña, J.-C., 2013. Paleoclimate Variability in the Mediterranean and Red Sea Regions during the Last 500,000 Years. Current Anthropology. 54, S183–S201.

Rohling, E.J., Marino, G., Grant, K.M., 2015. Mediterranean climate and oceanography, and the periodic development of anoxic events (sapropels). Earth-Science Reviews. 143, 62–97.

Ronen, A., 1991. The Yiron-Gravel lithic assemblage: Artifacts older than 2.4 My in Israel. Archäologisches Korrespondenzblatt. 21, 159–165.

Ronen, A., 2006. The oldest human groups in the Levant. Comptes Rendus - Palevol.

Rose, J.I., 2010. New light on human prehistory in the Arabo-Persian Gulf Oasis. Current Anthropology. 51, 849–883.

Rose, J.I., Hilbert, Y.H., Usik, V.I., Marks, A.E., Jaboob, M.M.A., Černý, V., Crassard, R., Preusser, F., 2019. 30,000-Year-Old Geometric Microliths Reveal Glacial Refugium in Dhofar, Southern Oman. Journal of Paleolithic Archaeology. 2, 338–357.

Rose, J.I., Usik, V.I., Marks, A.E., Hilbert, Y.H., Galletti, C.S., Parton, A., Geiling, J.M., Černý, V., Morley, M.W., Roberts, R.G., 2011. The Nubian complex of Dhofar, Oman: An African Middle Stone Age industry in Southern Arabia. PLoS ONE. 6, e28239.

Rosenberg, T.M., Preusser, F., Blechschmidt, I., Fleitmann, D., Jagher, R., Matter, A., 2012. Late Pleistocene palaeolake in the interior of Oman: A potential key area for the dispersal of anatomically modern humans out-of-Africa? Journal of Quaternary Science. 27, 13–16.

Rosenberg, T.M., Preusser, F., Fleitmann, D., Schwalb, A., Penkman, K.E.H., Schmid, T.W., Al-Shanti, M.A., Kadi, K.A., Matter, A., 2011. Humid periods in southern Arabia: Windows of opportunity for modern human dispersal. Geology. 39, 1115–1118.

Rosenberg, T.M., Preusser, F., Risberg, J., Plikk, A., Kadi, K.A., Matter, A., Fleitmann, D., 2013. Middle and Late Pleistocene humid periods recorded in palaeolake deposits of the Nafud desert, Saudi Arabia. Quaternary Science Reviews. 70, 109–123.

Roskin, J., Katra, I., Porat, N., Zilberman, E., 2013. Evolution of Middle to Late Pleistocene sandy calcareous paleosols underlying the northwestern Negev Desert Dunefield (Israel). Palaeogeography, Palaeoclimatology, Palaeoecology. 387, 134–152.

Rowe, P.J., Mason, J.E., Andrews, J.E., Marca, A.D., Thomas, L., Van Calsteren, P., Jex, C.N., Vonhof, H.B., Al-Omari, S., 2012. Speleothem isotopic evidence of winter rainfall variability in northeast Turkey between 77 and 6 ka. Quaternary Science Reviews. 45, 60–72.

Rozanski, K., Araguas-Araguas, L., Gonfiantini, R., 1993. Isotopic patterns in modern global precipitation. In: Swart, P.K., Lohmann, K.L., McKenzie, J., Savin, S. (Eds.), Climate Change in Continental Isotopic Records. American Geophysical Union, Washington DC, pp. 1–37.

Sahnouni, M., Parés, J.M., Duval, M., Cáceres, I., Harichane, Z., Van Der Made, J., Pérez-González, A., Abdessadok, S., Kandi, N., Derradji, A., Medig, M., Boulaghraif, K., Semaw, S., 2018. 1.9-million- and 2.4-million-year-old artifacts and stone tool–cutmarked bones from Ain Boucherit, Algeria. Science. 362, 1297–1301.

Salzmann, U., Williams, M., Haywood, A.M., Johnson, A.L.A., Kender, S., Zalasiewicz, J., 2011. Climate and environment of a Pliocene warm world. Palaeogeography, Palaeoclimatology, Palaeoecology. 309, 1–8.

Scally, A., Durbin, R., 2012. Revising the human mutation rate: implications for understanding human evolution. Nature reviews. Genetics. 13, 745–753.

Scardia, G., Parenti, F., Miggins, D.P., Gerdes, A., Araujo, A.G.M., Neves, W.A., 2019. Chronologic constraints on hominin dispersal outside Africa since 2.48 Ma from the Zarqa Valley, Jordan. Quaternary Science Reviews. 219, 1–19.

Scerri, E.M.L., 2017. The North African Middle Stone Age and its place in recent human evolution. Evolutionary Anthropology. 26, 119–135.

Scerri, E.M.L., Breeze, P.S., Parton, A., Groucutt, H.S., White, T.S., Stimpson, C., Clark-Balzan, L., Jennings, R.P., Alsharekh, A., Petraglia, M.D., 2015. Middle to Late Pleistocene human habitation in the western Nefud Desert, Saudi Arabia. Quaternary International. 382, 200–214.

Scerri, E.M.L., Chikhi, L., Thomas, M.G., 2019. Beyond multiregional and simple out-of-Africa models of human evolution. Nature Ecology & Evolution. 3, 1370–1372.

Scerri, E.M.L., Drake, N.A., Jennings, R.P., Groucutt, H.S., 2014a. Earliest evidence for the structure of Homo sapiens populations in Africa. Quaternary Science Reviews. 101, 207–216.

Scerri, E.M.L., Groucutt, H.S., Jennings, R.P., Petraglia, M.D., 2014b. Unexpected technological heterogeneity in northern Arabia indicates complex Late Pleistocene demography at the gateway to Asia. Journal of Human Evolution. 75, 125–142.

Scerri, E.M.L., Shipton, C., Clark-Balzan, L., Frouin, M., Schwenninger, J.-L., Groucutt, H.S., Breeze, P.S., Parton, A., Blinkhorn, J., Drake, N.A., Jennings, R.P., Cuthbertson, P., Omari, A. Al, Alsharekh, A.M., Petraglia, M.D., 2018a. The

expansion of later Acheulean hominins into the Arabian Peninsula. Scientific Reports. 8, 17165.

Scerri, E.M.L., Thomas, M.G., Manica, A., Gunz, P., Stock, J.T., Stringer, C., Grove, M., Groucutt, H.S., Timmermann, A., Rightmire, G.P., D'Errico, F., Tryon, C.A., Drake, N.A., Brooks, A.S., Dennell, R.W., Durbin, R., Henn, B.M., Lee-Thorp, J., DeMenocal, P., Petraglia, M.D., Thompson, J.C., Scally, A., Chikhi, L., 2018b. Did Our Species Evolve in Subdivided Populations across Africa, and Why Does It Matter? Trends in Ecology & Evolution. 33, 582–594.

Scheidegger, Y., Baur, H., Brennwald, M.S., Fleitmann, D., Wieler, R., Kipfer, R., 2010. Accurate analysis of noble gas concentrations in small water samples and its application to fluid inclusions in stalagmites. Chemical Geology. 272, 31–39.

Schimpf, D., Kilian, R., Kronz, A., Simon, K., Spötl, C., Wörner, G., Deininger, M., Mangini, A., 2011. The significance of chemical, isotopic, and detrital components in three coeval stalagmites from the superhumid southernmost Andes (53°S) as high-resolution palaeo-climate proxies. Quaternary Science Reviews. 30, 443–459.

Scholz, D., Hoffmann, D.L., 2011. StalAge - An algorithm designed for construction of speleothem age models. Quaternary Geochronology. 6, 369–382.

Scholz, D., Hoffmann, D.L., Jochum, K.P., Spötl, C., Riechelmann, D.F.C., 2014. Diagenesis of speleothems and its effects on the accuracy of 230Th/U-ages. Chemical Geology. 387, 74–86.

Schuster, M., Duringer, P., Ghienne, J.F., Vignaud, P., Mackaye, H.T., Likius, A., Brunet, M., 2006. The age of the Sahara desert. Science. 311, 821.

Schyfsma, E., Felber, H., Hötzl, H., Moser, H., Rauert, W., Zötl, J.G., 1978. As Sulb Plateau. In: Al-Sayari, S.S., Zötl, J.G. (Eds.), Quaternary Period in Saudi Arabia. Springer, Vienna, pp. 163–172.

Scoffin, T.P., 1987. An Introlduction to Carbonate Sediments and Rocks. Chapman and Hall, New York.

Sen, S., 2013. Dispersal of African mammals in Eurasia during the Cenozoic: Ways and whys. Geobios. 46, 159–172.

Sept, J.M., 1994. Beyond bones: Archaeological sites, early hominid subsistence, and the costs and benefits of exploiting wild plant foods in east African riverine landscapes. Journal of Human Evolution. 27, 295–320.

SGS, 2007. Maps of Caves Surveyed By Saudi Geological Survey, Kingdom of Saudi Arabia., Saudi Geological Survey Cave Unit.

Shakun, J.D., Burns, S.J., Fleitmann, D., Kramers, J., Matter, A., Al-Subary, A., 2007. A high-resolution, absolute-dated deglacial speleothem record of Indian Ocean climate from Socotra Island, Yemen. Earth and Planetary Science Letters. 259, 442–456.

Sharp, W.D., Paces, J.B., 2018. Comment on "The earliest modern humans outside Africa." Science. 362, eaat6598.

Sharp, Z. (The U. of N.M., 2007. Principles of Stable Isotope Geochemistry. In: Principles of Stable Isotope Geochemistry. Pearson.

Shea, J.J., 2008. Transitions or turnovers? Climatically-forced extinctions of Homo sapiens and Neanderthals in the east Mediterranean Levant. Quaternary Science Reviews. 27, 2253–2270.

Shipton, C., Blinkhorn, J., Breeze, P.S., Cuthbertson, P., Drake, N., Groucutt, H.S., Jennings, R.P., Parton, A., Scerri, E.M.L., Alsharekh, A., Petraglia, M.D., 2018. Acheulean technology and landscape use at Dawadmi , central Arabia. PLoS ONE. 13, 1–36.

Shultz, S., Maslin, M., 2013. Early Human Speciation, Brain Expansion and Dispersal

Influenced by African Climate Pulses. PLoS ONE. 8, e76750.

Siddall, M., Rohling, E.J., Almogi-Labin, A., Hemleben, C., Meischner, D., Schmelzer, I., Smeed, D.A., 2003. Sea-level fluctuations during the last glacial cycle. Nature. 423, 853–858.

Simpson, J.J., Grün, R., 1998. Non-destructive gamma spectrometric U-series dating. Quaternary Science Reviews. 17, 1009–1022.

Smith, J.R., Hawkins, A.L., Asmerom, Y., Polyak, V., Giegengack, R., 2007. New age constraints on the Middle Stone Age occupations of Kharga Oasis, Western Desert, Egypt. Journal of Human Evolution. 52, 690–701.

Smith, M., 2013. The Archaeology of Australia's Deserts. Cambridge University Press, Cambridge.

Sniderman, J.M.K., Woodhead, J.D., Hellstrom, J., Jordan, G.J., Drysdale, R.N., Tyler, J.J., Porch, N., 2016. Pliocene reversal of late Neogene aridification. Proceedings of the National Academy of Sciences. 113, 1999–2004.

Soares, P., Alshamali, F., Pereira, J.B., Fernandes, V., Silva, N.M., Afonso, C., Costa, M.D., Musilová, E., MacAulay, V., Richards, M.B., Černý, V., Pereira, L., 2012. The expansion of mtDNA haplogroup L3 within and out of Africa. Molecular Biology and Evolution. 29, 915–927.

Spoor, F., 2013. Palaeoanthropology: Small-brained and big-mouthed. Nature.

Spoor, F., Leakey, M.G., Gathogo, P.N., Brown, F.H., Antón, S.C., McDougall, I., Kiarie, C., Manthi, F.K., Leakey, L.N., 2007. Implications of new early Homo fossils from Ileret, east of Lake Turkana, Kenya. Nature. 448, 688–691.

Stahlschmidt, M.C., Collin, T.C., Fernandes, D.M., Bar-Oz, G., Belfer-Cohen, A., Gao, Z., Jakeli, N., Matskevich, Z., Meshveliani, T., Pritchard, J.K., McDermott, F., Pinhasi, R., 2019. Ancient Mammalian and Plant DNA from Late Quaternary

Stalagmite Layers at Solkota Cave, Georgia. Scientific Reports. 9, 6628.

Stepanov, V.I., 1997. Notes on Mineral Growth from the Archive of V.I. Stepanov (1924-1988). Proceedings of the University of Bristol Spelaeological Society. 21, 25–42.

Stewart, B.A., Zhao, Y., Mitchell, P.J., Dewar, G., Gleason, J.D., Blum, J.D., 2020. Ostrich eggshell bead strontium isotopes reveal persistent macroscale social networking across late Quaternary southern Africa. Proceedings of the National Academy of Sciences. 201921037.

Stewart, M., Louys, J., Breeze, P.S., Clark-Wilson, R., Drake, N.A., Scerri, E.M.L., Zalmout, I.S., Al-Mufarreh, Y.S.A., Soubhi, S.A., Haptari, M.A., Alsharekh, A.M., Groucutt, H.S., Petraglia, M.D., 2020. A taxonomic and taphonomic study of Pleistocene fossil deposits from the western Nefud Desert, Saudi Arabia. Quaternary Research. 95, 1–22.

Stewart, M., Louys, J., Groucutt, H.S., Candy, I., Clark-Wilson, R., Breeze, P.S., Drake, N.A., Price, G.J., Al-Mufarreh, Y.S.A., Soubhi, S.A., Zalmout, I.S., Alsharekh, A.M., al Omari, A., Petraglia, M.D., 2019a. Taphonomy of the Pleistocene faunal assemblages from Ti's al Ghadah. Quaternary Science Reviews. 218, 228–253.

Stewart, M., Louys, J., Price, G.J., Drake, N.A., Groucutt, H.S., Petraglia, M.D., 2019b. Middle and Late Pleistocene mammal fossils of Arabia and surrounding regions: Implications for biogeography and hominin dispersals. Quaternary International. 515, 12–29.

Stimpson, C.M., Lister, A., Parton, A., Clark-Balzan, L., Breeze, P.S., Drake, N.A., Groucutt, H.S., Jennings, R.P., Scerri, E.M.L., White, T.S., Zahir, M., Duval, M., Grün, R., Al-Omari, A., Al Murayyi, K.S.M., Zalmout, I.S., Mufarreh, Y.A., Memesh, A.M., Petraglia, M.D., 2016. Middle Pleistocene vertebrate fossils from

the Nefud Desert, Saudi Arabia: Implications for biogeography and palaeoecology. Quaternary Science Reviews. 143, 13–36.

Stringer, C., 2000. Coasting out of Africa. Nature. 405, 24–27.

Stringer, C., 2012. The status of Homo heidelbergensis (Schoetensack 1908). Evolutionary Anthropology. 21, 101–107.

Styles, M., Ellison, R., Arkley, S., Crowley, Q.G., Farrant, A., Goodenough, K.M., McKervey, J., Pharaoh, T., Phillips, E., Schofield, D., Thomas, R.J., 2006. The Geology and Geophysics of the United Arab Emirates, Volume 2: Geology. United Arab Emirates, Ministry of Energy, Petroleum and Minerals Sector, Minerals Department, Abu Dhabi, United Arab Emirates.

Suwa, G., Asfaw, B., Kono, R.T., Kubo, D., Owen Lovejoy, C., White, T.D., 2009. The ardipithecus ramidus skull and its implications for hominid origins. Science. 326, 68–68.

Svensson, A., Andersen, K.K., Bigler, M., Clausen, H.B., Dahl-Jensen, D., Davies, S.M., Johnsen, S.J., Muscheler, R., Parrenin, F., Rasmussen, S.O., Röthlisberger, R., Seierstad, I., Steffensen, J.P., Vinther, B.M., 2008. A 60 000 year Greenland stratigraphic ice core chronology. Climate of the Past. 4, 47–57.

Templeton, A., 2002. Out of Africa again and again. Nature. 416, 45–51.

Thomas, H., Geraads, D., Janjou, D., Vaslet, D., Memesh, A., Billiou, D., Bocherens, H., Dobigny, G., Eisenmann, V., Gayet, M., Lapparent de Broin, F., Petter, G., Halawani, M., 1998. First Pleistocene faunas from the Arabian peninsula: an Nafud desert, Saudi Arabia. Comptes Rendus de l'Académie des Sciences - Series IIA - Earth and Planetary Science. 326, 145–152.

Thorne, A., Grün, R., Mortimer, G., Spooner, N.A., Simpson, J.J., McCulloch, M., Taylor, L., Curnoe, D., 1999. Australia's oldest human remains: Age of the Lake

Mungo 3 skeleton. Journal of Human Evolution. 36, 591–612.

Tierney, J.E., deMenocal, P.B., Zander, P.D., 2017. A climatic context for the out-of-Africa migration. Geology. 45, 1023–1026.

Timmermann, A., Friedrich, T., 2016. Late Pleistocene climate drivers of early human migration. Nature. 538, 92–95.

Tindall, J.C., Haywood, A.M., 2015. Modeling oxygen isotopes in the Pliocene: Large-scale features over the land and ocean. Paleoceanography. 30, 1183–1201.

Torfstein, A., Goldstein, S.L., Kushnir, Y., Enzel, Y., Haug, G., Stein, M., 2015. Dead Sea drawdown and monsoonal impacts in the Levant during the last interglacial. Earth and Planetary Science Letters. 412, 235–244.

Toro-Moyano, I., Martínez-Navarro, B., Agustí, J., Souday, C., Bermúdez de Castro, J.M., Martinón-Torres, M., Fajardo, B., Duval, M., Falguères, C., Oms, O., Parés, J.M., Anadón, P., Julià, R., García-Aguilar, J.M., Moigne, A.-M., Espigares, M.P., Ros-Montoya, S., Palmqvist, P., 2013. The oldest human fossil in Europe, from Orce (Spain). Journal of Human Evolution. 65, 1–9.

Trauth, M.H., Larrasoaña, J.C., Mudelsee, M., 2009. Trends, rhythms and events in Plio-Pleistocene African climate. Quaternary Science Reviews. 28, 399–411.

Trauth, M.H., Maslin, M.A., Deino, A.L., Strecker, M.R., Bergner, A.G.N., Dühnforth, M., 2007. High- and low-latitude forcing of Plio-Pleistocene East African climate and human evolution. Journal of Human Evolution. 53, 475–486.

Treble, P., Shelley, J.M.G., Chappell, J., 2003. Comparison of high resolution sub-annual records of trace elements in a modern (1911-1992) speleothem with instrumental climate data from southwest Australia. Earth and Planetary Science Letters. 216, 141–153.

Treble, P.C., Fairchild, I.J., Griffiths, A., Baker, A., Meredith, K.T., Wood, A.,

McGuire, E., 2015. Impacts of cave air ventilation and in-cave prior calcite precipitation on Golgotha Cave dripwater chemistry, southwest Australia. Quaternary Science Reviews. 127, 61–72.

Turney, C.S.M., Bird, M.I., Fifield, L.K., Roberts, R.G., Smith, M., Dortch, C.E., Grün, R., Lawson, E., Ayliffe, L.K., Miller, G.H., Dortch, J., Cresswell, R.G., 2001. Early Human Occupation at Devil's Lair, Southwestern Australia 50,000 Years Ago. Quaternary Research. 55, 3–13.

Twaddle, R.W., Ulm, S., Hinton, J., Wurster, C.M., Bird, M.I., 2016. Sclerochronological analysis of archaeological mollusc assemblages: methods, applications and future prospects. Archaeological and Anthropological Sciences. 8, 359–379.

Tzedakis, P.C., Andrieu, V., de Beaulieu, J.-L., Crowhurst, S., Follieri, M., Hooghiemstra, H., Magri, D., Reille, M., Sadori, L., Shackleton, N.J., Wijmstra, T.A., 1997. Comparison of terrestrial and marine records of changing climate of the last 500,000 years. Earth and Planetary Science Letters. 150, 171–176.

Tzedakis, P.C., Crucifix, M., Mitsui, T., Wolff, E.W., 2017. A simple rule to determine which insolation cycles lead to interglacials. Nature. 542, 427–432.

Tziperman, E., Gildor, H., 2003. On the mid-Pleistocene transition to 100-kyr glacial cycles and the asymmetry between glaciation and deglaciation times. Paleoceanography. 18, 1–8.

Usik, V.I., Rose, J.I., Hilbert, Y.H., Van Peer, P., Marks, A.E., 2013. Nubian Complex reduction strategies in Dhofar, southern Oman. Quaternary International. 300, 244–266.

Vaks, A., Bar-Matthews, M., Ayalon, A., Matthews, A., Frumkin, A., 2018. Pliocene-Pleistocene palaeoclimate reconstruction from Ashalim Cave speleothems, Negev

Desert, Israel. Geological Society Special Publication. 466, 201–216.

Vaks, A., Bar-Matthews, M., Ayalon, A., Matthews, A., Frumkin, A., Dayan, U., Halicz, L., Almogi-Labin, A., Schilman, B., 2006. Paleoclimate and location of the border between Mediterranean climate region and the Saharo-Arabian Desert as revealed by speleothems from the northern Negev Desert, Israel. Earth and Planetary Science Letters. 249, 384–399.

Vaks, A., Bar-Matthews, M., Matthews, A., Ayalon, A., Frumkin, A., 2010. Middle-Late Quaternary paleoclimate of northern margins of the Saharan-Arabian Desert: Reconstruction from speleothems of Negev Desert, Israel. Quaternary Science Reviews. 29, 2647–2662.

Vaks, A., Woodhead, J., Bar-Matthews, M., Ayalon, A., Cliff, R.A., Zilberman, T., Matthews, A., Frumkin, A., 2013. Pliocene-Pleistocene climate of the northern margin of Saharan-Arabian Desert recorded in speleothems from the Negev Desert, Israel. Earth and Planetary Science Letters. 368, 88–100.

Veizer, J., Clayton, R.N., Hinton, R.W., 1992. Geochemistry of precambrian carbonates: IV. Early paleoproterozoic (2.25 ± 0.25 ga) seawater. Geochimica et Cosmochimica Acta. 56, 875–885.

Villmoare, B., 2018. Early *Homo* and the role of the genus in paleoanthropology. American Journal of Physical Anthropology. 165, 72–89.

Villmoare, B., Kimbel, William H, Seyoum, C., Campisano, Christopher J, DiMaggio, Erin N, Rowan, John, Braun, D.R., Arrowsmith, J Ramón, Reed, Kaye E, Leakey, L.S.B., Tobias, P. V., Napier, J.R., Antón, S.C., Potts, R., Aiello, L.C., DiMaggio, E. N., Campisano, C. J., Rowan, J., G. Dupont-Nivet, Deino, A.L., Bibi, F., Lewis, M.E., Souron, A., Werdelin, L., Reed, K. E., Arrowsmith, J. R., Campisano, C. J., Feibel, C.S., Kimbel, W. H., Delezene, L.K., White, T.D., Johanson, D.C.,

Kimbel, W. H., Suwa, G., Wood, B.A., White, T.D., Guatelli-Steinberg, D., Irish, J.D., Leakey, M.G., Spoor, F., Dean, M.C., Feibel, C.S., Antón, S.C., Kiarie, C., Leakey, L.N., Weidenreich, F., Wood, B.A., Noten, F.L. Van, Montagu, M.F.A., Suwa, G., White, T.D., Howell, F.C., Kimbel, W. H., Johanson, D.C., Rak, Y., Boisserie, J.-R., Guy, F., Delagnes, A., Hlukso, L.J., Bibi, F., Beyene, Y., Guillemot, C., Leakey, R.E., Walker, A.C., McDougall, I., Brown, F.H., Vasconcelos, P.M., Cohen, B.E., Thiede, D.S., Buchanan, M.J., Asfaw, B., White, T., Lovejoy, O., Latimer, B., Simpson, S., Suwa, G., White, T.D., Asfaw, B., Suwa, G., Strait, D.S., Grine, F.E., Wood, B.A., Baker, J., Spoor, F., Berger, L.R., Ruiter, D.J. de, Churchill, S.E., Schmid, P., Carlson, K.J., Dirks, P.H., Kibii, J.M., DeMenocal, P.B., Potts, R., Berger, L., Irish, J.D., Guatelli-Steinberg, D., Legge, S.S., Ruiter, D.J. de, Berger, L.R., Kimbel, W. H., Carter, K., Worthington, S., Smith, T.M., Skelton, R.R., McHenry, H.M., Strait, D.S., Grine, F.E., Moniz, M.A., Leakey, M.G., Spoor, F., Brown, F.H., Gathogo, P.N., Kiarie, C., Leakey, L.N., McDougall, I., Spoor, F., Leakey, M.G., Leakey, L.N., Delezene, L.K., Kimbel, W. H., Moggi-Cecchi, J., Grine, F.E., Tobias, P. V., Kaifu, Y., Baba, H., Aziz, F., Indriati, E., Schrenk, F., Jacob, T., White, T.D., Johanson, D.C., White, T.D., Suwa, G., Simpson, S., Asfaw, B., 2015. Paleoanthropology. Early Homo at 2.8 Ma from Ledi-Geraru, Afar, Ethiopia. Science. 347, 1352–5.

Vincent, A.S., 1985. Plant foods in savanna environments: A preliminary report of tubers eaten by the Hadza of northern Tanzania. World Archaeology. 17, 131–148.

Visbeck, M.H., Hurrell, J.W., Polvani, L., Cullen, H.M., 2001. The North Atlantic Oscillation: Past, present, and future. Proceedings of the National Academy of Sciences of the United States of America. 98, 12876–12877.

Vonhof, H.B., van Breukelen, M.R., Postma, O., Rowe, P.J., Atkinson, T.C., Kroon, D.,

2006. A continuous-flow crushing device for on-lineδ2H analysis of fluid inclusion water in speleothems. Rapid Communications in Mass Spectrometry. 20, 2553–2558.

Wade, L., 2019. Was our species in Europe 210,000 years ago? Science. 365, 111.

Wadley, L., Backwell, L., D'Errico, F., Sievers, C., 2020. Cooked starchy rhizomes in Africa 170 thousand years ago. Science. 367, 87–91.

Wahab, A.A., Abul Maaty, M.A., Stuart, F.M., Awad, H., Kafafy, A., 2014. The geology and geochronology of Al Wahbah maar crater, Harrat Kishb, Saudi Arabia. Quaternary Geochronology. 21, 70–76.

Waldmann, N., Torfstein, A., Stein, M., 2010. Northward intrusions of low- and mid-latitude storms across the Saharo-Arabian belt during past interglacials. Geology. 38, 567–570.

Walker, A., Leakey, R., 1993. The Nariokotome Homo erectus Skeleton. Springer, Berlin.

Wang, F., Michalski, G., Seo, J.H., Granger, D.E., Lifton, N., Caffee, M., 2015. Beryllium-10 concentrations in the hyper-arid soils in the Atacama Desert, Chile: Implications for arid soil formation rates and El Niño driven changes in Pliocene precipitation. Geochimica et Cosmochimica Acta. 160, 227–242.

Wang, L., Lü, H.Y., Wu, N.Q., Li, J., Pei, Y.P., Tong, G.B., Peng, S.Z., 2006. Palynological evidence for Late Miocene-Pliocene vegetation evolution recorded in the red clay sequence of the central Chinese Loess Plateau and implication for palaeoenvironmental change. Palaeogeography, Palaeoclimatology, Palaeoecology. 241, 118–128.

Wang, Y.J., Cheng, H., Edwards, R.L., An, Z.S., Wu, J.Y., Shen, C.C., Dorale, J.A., 2001. A high-resolution absolute-dated late pleistocene monsoon record from Hulu

Cave, China. Science. 294, 2345–2348.

Weldeab, S., Lea, D.W., Schneider, R.R., Andersen, N., 2007. Supporting Online Material for 155,000 Years of West African Monsoon and Ocean Thermal Evolution. Science. 316, 0–9.

Welker, F., Hajdinjak, M., Talamo, S., Jaouen, K., Dannemann, M., David, F., Julien, M., Meyer, M., Kelso, J., Barnes, I., Brace, S., Kamminga, P., Fischer, R., Kessler, B.M., Stewart, J.R., Pääbo, S., Collins, M.J., Hublin, J.-J., 2016. Palaeoproteomic evidence identifies archaic hominins associated with the Châtelperronian at the Grotte du Renne. Proceedings of the National Academy of Sciences. 113, 11162–11167.

Weyhenmeyer, C.E., Burns, S.J., Waber, H.N., Aeschbach-Hertig, W., Kipfer, R., Loosli, H.H., Matter, A., 2000. Cool glacial temperatures and changes in moisture source recorded in Oman groundwaters. Science. 287, 842–845.

Weyhenmeyer, C.E., Burns, S.J., Waber, H.N., Macumber, P.G., Matter, A., 2002. Isotope study of moisture sources, recharge areas, and groundwater flow paths within the eastern Batinah coastal plain, Sultanate of Oman. Water Resources Research. 38, 2-1-2–22.

Whalen, N.M., 2003. Lower Palaeolithic sites of the Huqf area of Central Oman. The Journal of Oman Studies. 13, 175–182.

Whalen, N.M., Ali, J.S., Sindi, H.O., Pease, D.W., 1986. A Lower Pleistocene site near Shuwayhitiyah in northern Saudi Arabia. Atlal. 10, 94–101.

Whalen, N.M., Davis, W.P., Pease, D.W., 1989. Early Pleistocene migrations into Saudi Arabia. Atlal. 12, 59–75.

Whalen, N.M., Schatte, K.E., 1997. Pleistocene sites in southern Yemen. Arabian Archaeology and Epigraphy. 8, 1–10.

White, M.J., 2006. Things to do in Doggerland when you're dead: Surviving OIS3 at the northwestern-most fringe of Middle Palaeolithic Europe. World Archaeology. 38, 547–575.

White, T.D., Asfaw, B., Beyene, Y., Haile-Selassie, Y., Lovejoy, C.O., Suwa, G., Woldegabriel, G., 2009. Ardipithecus ramidus and the paleobiology of early hominids. Science. 326, 75–86.

White, T.D., Asfaw, B., DeGusta, D., Gilbert, H., Richards, G.D., Suwa, G., Clark Howell, F., Howell, F.C., 2003. Pleistocene Homo sapiens from Middle Awash, Ethiopia. Nature. 423, 742–747.

White, T.D., WoldeGabriel, G., Asfaw, B., Ambrose, S., Beyene, Y., Bernor, R.L., Boisserie, J.R., Currie, B., Gilbert, H., Haile-Selassie, Y., Hart, W.K., Hlusko, L.J., Howell, F.C., Kono, R.T., Lehmann, T., Louchart, A., Lovejoy, C.O., Renne, P.R., Saegusa, H., Vrba, E.S., Wesselman, H., Suwa, G., 2006. Asa Issie, Aramis and the origin of Australopithecus. Nature. 440, 883–889.

White, W.., 1981. Reflectance Spectra and Color in Speleothems. National Speleological Society Bulletin. 43, 20–26.

Wickens, L.B., 2013. Geochemistry and Petrography of Speleothems From Turkey and Iran: Palaeoclimate and Diagenesis. University of East Anglia.

Williams, M.A.J., Duller, G.A.T., Williams, F.M., Woodward, J.C., Macklin, M.G., El Tom, O.A.M., Munro, R.N., El Hajaz, Y., Barrows, T.T., 2015. Causal links between Nile floods and eastern Mediterranean sapropel formation during the past 125 kyr confirmed by OSL and radiocarbon dating of Blue and White Nile sediments. Quaternary Science Reviews. 130, 89–108.

Wolpoff, M.H., Senut, B., Pickford, M., Hawks, J., 2002. Palaeoanthropology: Sahelanthropus or 'Sahelpithecus'? Nature. 419, 581–582.

Wong, C.I., Breecker, D.O., 2015. Advancements in the use of speleothems as climate archives. Quaternary Science Reviews. 127, 1–18.

Wood, B., Boyle, E.K., 2016. Hominin taxic diversity: Fact or fantasy? American Journal of Physical Anthropology. 159, S37–S78.

Woodhead, J., Hellstrom, J., Maas, R., Drysdale, R., Zanchetta, G., Devine, P., Taylor, E., 2006. U-Pb geochronology of speleothems by MC-ICPMS. Quaternary Geochronology. 1, 208–221.

Woodhead, J., Hellstrom, J., Pickering, R., Drysdale, R., Paul, B., Bajo, P., 2012. U and Pb variability in older speleothems and strategies for their chronology. Quaternary Geochronology. 14, 105–113.

WorldClim, 2015. WorldClim - Global Climate Data: Free climate data for ecological modeling and GIS. Very high resolution interpolated climate surfaces for global land areas.

Wynn, P.M., Borsato, A., Baker, A., Frisia, S., Miorandi, R., Fairchild, I.J., 2013. Biogeochemical cycling of sulphur in karst and transfer into speleothem archives at Grotta di Ernesto, Italy. Biogeochemistry. 114, 255–267.

Yonge, C.J., 1982. Stable Isotope Studies of Water Extracted from Speleothems. McMaster University, Hamilton, ON, Canada.

Zabel, M., Schneider, R.R., Wagner, T., Adegbie, A.T., De Vries, U., Kolonic, S., 2001. Late quaternary climate changes in central Africa as inferred from terrigenous input to the Niger fan. Quaternary Research. 56, 207–217.

Zachos, J., Pagani, H., Sloan, L., Thomas, E., Billups, K., 2001. Trends, rhythms, and aberrations in global climate 65 Ma to present. Science. 292, 686–693.

Zhang, J.F., Wang, X.Q., Qiu, W.L., Shelach, G., Hu, G., Fu, X., Zhuang, M.G., Zhou, L.P., 2011. The paleolithic site of Longwangchan in the middle Yellow River,

China: Chronology, paleoenvironment and implications. Journal of Archaeological Science. 38, 1537–1550.

Zhang, Z., Ramstein, G., Schuster, M., Li, C., Contoux, C., Yan, Q., 2014. Aridification of the Sahara desert caused by Tethys Sea shrinkage during the Late Miocene. Nature. 513, 401–404.

Zhu, Y., 2012. Variations of the summer Somali and Australia cross-equatorial flows and the implications for the Asian summer monsoon. Advances in Atmospheric Sciences. 29, 509–518.

Zhu, Z., Dennell, R.W., Huang, W., Wu, Y., Qiu, S., Yang, S., Rao, Z., Hou, Y., Xie, J., Han, J., Ouyang, T., 2018. Hominin occupation of the Chinese Loess Plateau since about 2.1 million years ago. Nature. 559, 608–612.